Erasing the eraser. The synthesis and biological evaluation of some novel epigenetic inhibitors.

School of Pharmacy

Adam Lee

Supervisor: Prof. A. Ganesan
Second Supervisor: Prof. M. Searcey

A thesis submitted in partial fulfilment for the degree of
Doctor of Philosophy
July 2020

The most fruitful basis for the discovery of a new drug is to start with an old drug.
Sir James Black

Abstract

Epigenetic abnormalities have been implicated in a wide variety of disorders and as such are of increasing interest as potential drug targets. Histone deacetylases (HDACs) and Lysine Specific Demethylase 1 (LSD1) are two such targets that have received significant attention in recent times. Although both enzymes have been found to be crucial in several regulatory roles, their overexpression has been observed in a number of cancers. Several HDAC inhibitors are already approved for use in various cancers and a number of LSD1 inhibitors are currently in clinical trials.

The lack of approved inhibitors for LSD1 and the lack of isoform specific inhibitors of the HDACs suggests a need for further research and development in both of these key areas of epigenetic drug discovery. In addition, the ability of cancer as a disease to become resistant to treatment is a major hurdle.

Evidence is now emerging that combining both HDAC and LSD1 inhibitors can have a synergistic effect in cancer. To that end, we have developed a dual LSD1/HDAC inhibitor based upon the structure of GSK2879552, the clinical candidate of GlaxoSmithKline. This dual inhibitor aims to take advantage of any synergistic effect between LSD1 and HDAC, as well as addressing the problem of drug resistance through the mode of dual target engagement.

Further, we have developed a novel, potent, LSD1 inhibitor with good in cell activity. This was followed up with the synthesis of several analogues with the aim of working towards further structure optimisation.

Work on our dual inhibitor, led to the development of two novel HDAC6 inhibitors with promising activity both in and out of cell. Again, the series was extended in order to determine if this activity could be further improved.

Finally, a novel HDAC inhibitor comprising a carboxylic acid zinc binding motif, and low μM levels of activity is presented.

Access Condition and Agreement

Each deposit in UEA Digital Repository is protected by copyright and other intellectual property rights, and duplication or sale of all or part of any of the Data Collections is not permitted, except that material may be duplicated by you for your research use or for educational purposes in electronic or print form. You must obtain permission from the copyright holder, usually the author, for any other use. Exceptions only apply where a deposit may be explicitly provided under a stated licence, such as a Creative Commons licence or Open Government licence.

Electronic or print copies may not be offered, whether for sale or otherwise to anyone, unless explicitly stated under a Creative Commons or Open Government license. Unauthorised reproduction, editing or reformatting for resale purposes is explicitly prohibited (except where approved by the copyright holder themselves) and UEA reserves the right to take immediate ‘take down’ action on behalf of the copyright and/or rights holder if this Access condition of the UEA Digital Repository is breached. Any material in this database has been supplied on the understanding that it is copyright material and that no quotation from the material may be published without proper acknowledgement.

Acknowledgments

I would first like to thank my supervisor and mentor of the last four years, Prof. Ganesan. Thank you for giving me the opportunity to work on this project and for all your help, advice, encouragement and endless ideas, as well as for allowing me the freedom to explore the topic.

I would also like to extend my gratitude to my second supervisor, Prof. Searcey, for always being available should I need his help. In addition, I would like to thank him for the use of the equipment in his lab and also thank his post docs, and in particular Dr. Marco Cominetti, for their help and advice over the course of my project.

I would like to thank all of our collaborators for their considerable contributions to this project, particularly Ipek Bulut of the Acilan Ayhan group, Koc university for her considerable work on the biological evaluation of several of our compounds. Also, Dusan Ruzic of the Nikolic group, University of Belgrade for his work on both the HDAC assays and virtual docking studies.

Thank you to all my fellow PhD students both in the Ganesan group and throughout both the School of Pharmacy and Chemistry for their help and friendship over the last four years and I wish them all the best of luck with their respective projects and future endeavours.

Finally, I would most like to thank my family, and in particular my wife Rebecca, without whose considerable support this PhD would not have been possible.

Contents

Abstract iv

Acknowledgments vi

Contents vii

List of Figures x

List of Schemes xv

List of Tables xvii

Declaration of Authorship xx

Chapter One 2

1. Introduction 2

1.1. Epigenetics, a quick look at the past. 2

1.2. A more modern view. 4

1.3. Methylation of lysine 8

1.4. Demethylation of Lysine 10

1.5. Irreversible inhibition of LSD1, the beginning. 14

1.6. Irreversible inhibition of LSD1, beyond the first generation. 18

1.7. Irreversible LSD1 inhibitors in clinical trials. 23

1.8. The zinc dependent histone deacetylases (HDACs). 27

1.9. Inhibitors of the zinc dependent HDACs 30

1.10. Introduction summary and thesis aims. 39

Chapter Two 40

2. A series of novel LSD1 inhibitors based on GSK2879552. 40

2.1. Introduction 40

2.2. The synthesis of GSK2879552. 41

2.3. The synthesis of a novel LSD1 inhibitor (compound 2.8a). 46

2.4. The biological evaluation of compound 2.8a. 47

2.4.1. LSD1 Inhibition. 47

2.4.2. Cellular Thermal Shift Assay (CETSA) 48

2.4.3. Leukaemia cell viability 50

2.4.4. Methylation fold change in response to inhibition. 52

2.4.5. Gene expression changes. 54

2.4.6. Synergy of 2.8a with other known anti-cancer drugs. 56
2.4.7. Inducing apoptosis. 58
2.4.8. Repair of doxorubicin induced damage 63
2.5. The synthesis of further GSK2879552 analogues. 72
2.5.1. Biological activity. 74
2.6. Conclusion and future work. 77
2.7. Chapter two experimental. 79
2.7.1. Experimental procedures. 79
2.7.2. *trans*-GSK2879552 synthesis....81
2.7.3. Amide analogues.....89
Chapter Three 94
3. The design, synthesis and biological activity of a dual LSD1/HDAC inhibitor and control compounds. 94
3.1. Introduction. 94
3.1.1. Chapter aims. 97
3.2. The synthesis of a dual LSD1/HDAC inhibitor (compound 3.8). 98
3.3. The synthesis of our control compounds. 99
3.4. The biological activity of dual inhibitor 3.8. 101
3.4.1. Cell free assays. 101
3.4.2. Cellular Thermal Shift Assay (CETSA). 105
3.4.4. Methylation and acetylation fold change in response to inhibition.....110
3.4.5. Gene expression changes. 113
3.4.6. Synergy of 3.8 with other known anti-cancer compounds 117
3.4.7. Inducing apoptosis. 119
3.4.8. Repair of doxorubicin induced damage 124
3.5. Virtual docking study. 128
3.6. Conclusion and future work. 131
3.7. Chapter three experimental. 133
3.7.1. Experimental procedures 133
Chapter Four 138
4. A series of novel zinc dependent HDAC inhibitors. 138
4.1. Introduction 138
4.1.1. Chapter aims. 139
4.2. The synthesis of four series of potential HDAC inhibitors. 139
4.3.2. Cell viability assay. 148

4.4 Virtual docking study. ... **152**
4.5. Conclusion and future works. ... **154**
4.6. Chapter four experimental ... **155**
4.6.1. Experimental procedures ... **155**
4.6.2. General procedure for synthesis of methyl ester precursors. ... **155**
4.6.3. General procedure for the synthesis of hydroxamic acids. ... **155**
4.6.4. *Para*-series ... **156**
4.6.5. *Meta*-series ... **161**
4.6.6. *Ortho*-series ... **167**
4.6.7. Alkene-series ... **174**
Chapter Five ... 180
5. The design and synthesis of a novel HDAC inhibitor with a carboxylic acid ZBG. ... 180
5.1. Introduction ... **180**
5.2. The synthesis of a HDAC inhibitor comprising a carboxylic acid ZBG. ... **181**
5.3. The enzymatic evaluation of 5.13a. ... **187**
5.4. The synthesis of further analogues of 5.13a ... **189**
5.5. Conclusion and future works. ... **191**
5.6. Chapter five experimental. ... **192**
5.6.1. Experimental procedures ... **192**
Appendix ... 203
Chapter two NMR. ... **203**
Chapter two HPLC data ... **217**
Chapter three NMR ... **221**
Chapter three HPLC data ... **226**
Chapter four NMR. ... **228**
Chapter five NMR ... **274**
References ... 290

List of Figures

Figure 1.1. Waddington's Epigenetic landscape. **3**

Figure 1.2. *The effect of histone modification on gene activation.* **6**

Figure 1.3. *Ribbon diagram of LSD1.* **13**

Figure 1.4. *The differentiation pathway for the formation of blood cells.* **14**

Figure 1.5. *Some of the first MAO inhibitors trialled against LSD1 and the second-generation analogue of phenelzine.* **16**

Figure 1.6. *Examples of para substituted tranylcypromine analogues.* **19**

Figure 1.7. *Examples of more specific LSD1 inhibitors developed around the TCP scaffold.*[49,54] **21**

Figure 1.8. *Example of TCP analogues substituted at position C1 and C2 of the cyclopropyl ring.*[57,58] **22**

Figure 1.9. *(A) The synthetic route for the synthesis of spirocyclic TCP derivatives and (B) examples of N-alkylated analogues.*[59] **23**

Figure 1.10. *(1.31-1.36) Structures of TCP derived LSD1 inhibitors that have taken part in clinical trials. (1.37-1.38) Additional TCP derived LSD1 inhibitors developed by GSK alongside their clinical candidate.* **27**

Figure 1.11. *Acetyl Coenzyme A.* **28**

Figure 1.12. *The analogous nature of a typical HDAC inhibitor (SAHA) and its natural acetyllysine substrate.* **31**

Figure 1.13. *Clinically approved HDAC inhibitors.* **32**

Figure 1.14. *An example of how modification of a HDAC inhibitor cap can increase selectivity.*[83,84] **33**

Figure 1.15 *Structure of ricolinostat.* **33**

Figure 1.16. *An example of how linker modification can increase HDAC isoform selectivity.*[86] **34**

Figure 1.17. *Examples of HDAC inhibitors with a benzamide ZBG.*[84] **35**

Figure 1.18. *The structure of the depsipeptide, romidepsin and the thioester, largazole along with their reduced/hydrolysed structures.*[96] **37**

Figure 1.19. *Examples of HDAC inhibitors containing a carboxylic acid ZBG.* **38**

Figure 2.1. *Retrosynthetic analysis of GSK2879552.* **41**

Figure 2.2. *Graphical representation of the LSD1 cell free assay results for **2.8a** along with control compounds.* **47**

Figure 2.3. *Graphical representation of the effect of ligand binding on the thermal degradation of proteins.* **49**

Figure 2.4. *Western blot of CETSA on **2.8a** controls.* **49**

Figure 2.5. *Graphs of cell viability in fused and non-fused cell lines, comparing GSK2879552 and 2.8a.* **51**

Figure 2.6. *Western blot of H3K4me2 levels measured at 18 and 24 hours in response to inhibition with GSK2879552 and **2.8a** in THP-1 and MOLM-13 cells.* **52**

Figure 2.7. *H3K4me2 levels measured over 18 and 24 hours in response to inhibition with GSK2879552 and **2.8a** in THP-1 and MOLM-13 cells.* **53**

Figure 2.8. *Graphical representation of CD86 and CD11b expression levels in THP-1 cells in response to inhibition with GSK2879552, **2.8a** and a negative control.* **55**

Figure 2.9. *Cell viability of THP-1 cells inhibited with combinations of **2.8a** and other known anti-cancer agents.* **57**

Figure 2.10. *Apoptosis profiles for 2.8a and doxorubicin in THP-1 cells.* **60**

Figure 2.11. *Graphical representation of apoptosis data for doxorubicin and **2.8a** in THP-1 cells.* **60**

Figure 2.12. *Apoptosis profiles for **2.8a** and doxorubicin in THP-1 cells.* **62**

Figure 2.13. *Graphical representation of apoptosis data for doxorubicin and **2.8a** in THP-1 cells using Annexin V binding assay.* **62**

Figure 2.14. *The molecular structure of the anthracyclines, daunorubicin and doxorubicin.* **63**

Figure 2.15. *Population profiles of phosphorylation vs H2AX expression in THP-1 cells treated with doxorubicin and **2.8a**.* **65**

Figure 2.16. *Graphical representation of γ-H2AX activation in THP-cells treated with doxorubicin and **2.8a**.* **66**

Figure 2.17. *ROS profiles for THP-1 cells treated with doxorubicin and **2.8a**.* **68**

Figure 2.18. *Graphical representation of THP-1 cells containing ROS upon treatment with doxorubicin and **2.8a**.* **69**

Figure 2.19. *The expression of 12 different damage repair genes in response to LSD1 inhibition with **2.8a**.* **71**

Figure 2.20. *General structure of our series of potential LSD1 inhibitors based on the structure of GSK2879552.* **72**

Figure 2.21. *All analogues of GSK2879552.* **73**

Figure 2.22. *Cell viability assay results of all compounds **2.8a-g** with doxorubicin as a control in THP-1 cells at 100 and 10 μM concentrations of inhibitors.* **74**

Figure 2.23. *Cell viability assay to determine the IC50 of all compounds **2.8a-g** in THP-1 cells.* **76**

Figure 3.1. *Examples of dual LSD1/HDAC inhibitors.*[137] **96**

Figure 3.2. *The tranylcypromine analogue of bizine and the corresponding LSD1/HDAC inhibitor hybrid.*[138] **97**

Figure 3.3. *The structure of our dual LSD1/HDAC inhibitor and control compounds.* **100**

Figure 3.4. *Graphical representation of the LSD1 assay results for our dual inhibitor and control compounds.* **102**

Figure 3.5. *Graphical representation of the HDAC assays recorded for dual inhibitor **3.8** and positive HDAC control **3.12**.* **104**

Figure 3.6. *Western blot of CETSA on dual inhibitor **3.8** and control compounds.* **105**

Figure 3.7. *Comparison of the effect of changing the R-group at the end of GSK2879552 on activity in cancer cells.* **107**

Figure 3.8. *Graphical representation of cell viability assays in THP-1 and MOLM-13 cells.* **108**

Figure 3.9. *Graphical representation of cell viability assays in K562 and JURKAT cells.* **109**

Figure 3.10. *Western blot of methylation and acetylation levels in THP-1 cells in response to inhibition of LSD1 and HDACs.* **110**

Figure 3.11. *Graphical representation of methylation and acetylation levels in THP-1 cells in response to LSD1 and HDAC inhibition.* **111**

Figure 3.12. *Ac-Tub levels in THP-1 cells after treatment with LSD1 and HDAC inhibitors.* **112**

Figure 3.13. *Graphical representation of data from Table 3.6.* **114**

Figure 3.14. *Graphical representation of the data from Table 3.7.* **115**

Figure 3.15. *Graphical representation of the data from Table 3.8.* **117**

Figure 3.16. *Cell viability of THP-1 cells inhibited with combinations of our inhibitors and other known anti-cancer compounds.* **118**

Figure 3.17. *Cell viability graph of **3.8** and **3.12** in combination with alternative Top2 inhibitor, etoposide. Cell viability graph of doxorubicin and HDAC inhibitor ricolinostat.* **119**

Figure 3.18. *Apoptosis profiles for **3.8, 3.12** and doxorubicin in THP-1 cells.* **121**

Figure 3.19. *Graphical representation of apoptosis data presented in Table 3.9.* **121**

Figure 3.20. *Apoptosis profiles for **3.8, 3.12** and doxorubicin in THP-1 cells.* **123**

Figure 3.21. *Graphical representation of apoptosis data presented in Table 3.10.* **123**

Figure 3.22. *Population profiles of phosphorylation vs H2AX expression in THP-1 cells treated with doxorubicin, **3.8** and **3.12**.* **125**

Figure 3.23. *Graphical representation of γ-H2AX activation in THP-cells treated with doxorubicin, **3.8** and **3.12**.* **125**

Figure 3.24. *ROS profiles for THP-1 cells treated with doxorubicin, **3.8** and **3.12**.* **127**

Figure 3.25. *Graphical representation of ROS (+) profile data for THP-1 cells treated with doxorubicin, **3.8** and **3.12**.* **127**

Figure 3.26. *Position of ligand 3.8 inside the binding site of the HDAC6 seen from the extracellular side (left) and 2D presentation of important interactions with amino acid residues in the active pocket of HDAC6 (right).* **128**

Figure 3.27. *Position of ligand MH-25 inside the binding site of the HDAC6 seen from the extracellular side (left) and 2D presentation of important interactions with amino acid residues in the active pocket of HDAC6 (right).* **129**

Figure 4.1. Para series of potential HDAC inhibitors and the methyl ester precursors. **141**

Figure 4.2. Meta series of potential HDAC inhibitors and the methyl ester precursors. **142**

Figure 4.3. Ortho series of potential HDAC inhibitors and the methyl ester precursors. **143**

Figure 4.4. Alkene series of potential HDAC inhibitors and the methyl ester precursors. **144**

Figure 4.5. *Graphical representation of the HDAC assay data for **4.2a** and **4.2b**.* **147**

Figure 4.6. *THP-1 cell viability assay results at an inhibitor concentration of 100 μM.* **149**

Figure 4.7. *THP-1 cell viability assay results at an inhibitor concentration of 10 μM.* **150**

Figure 4.8. *THP-1 cell viability assay IC_{50} graphs for active compounds from the alkene series.* **151**

Figure 4.9. *Position of ligand 4.2a inside the binding site of the HDAC6 seen from the extracellular side (left) and 2D presentation of important interactions with amino acid residues in the active pocket of HDAC6 (right).* **153**

Figure 4.10. *Position of ligand 4.2b inside the binding site of the HDAC6 seen from the extracellular side (left) and 2D presentation of important interactions with amino acid residues in the active pocket of HDAC6 (right).* **153**

Figure 5.1. *The tert-butyl peak ratio, as determined by NMR, from a diastereomeric mixture of compound 5.3 following synthesis via the tosylhydrazone method.* **183**

Figure 5.2. Graphical representation of the HDAC inhibition data presented in Table 5.1. ..... **188**

Figure 5.3. *Compound 5.13a showing the cap, linker and ZBG sections of the molecule.* **189**

List of Schemes

Scheme 1.1. *A mechanism for the methylation of cytosine in which SAM acts as co-factor.*[12] **8**

Scheme 1.2. *Methylation of H3K27 via mechanism proposed by Fortin et al.* .. **10**

Scheme 1.3. *Fe(II) mediated mechanism employed by JHDMs.*[24] **11**

Scheme 1.4. *FAD dependent demethylation mechanism of LSD1.*[24] **12**

Scheme 1.5. *Inhibition of LSD1 by TCP via adduct formation with its FAD cofactor.*[49,50] **18**

Scheme 1.6. *Possible positions for the modification of tranylcypromine.* **19**

Scheme 1.7. *Deacteylation mechanism as put forward by Finnin et al.*[75] **30**

Scheme 2.1. *Possible synthetic routes to the target product, trans-GSK2879552 (**1.35**).* **42**

Scheme 2.2. *Mechanism for Ti(IV) isopropoxide promoted reductive amination.* **43**

Scheme 2.3. *The synthesis of novel LSD1 inhibitor **2.8** from GSK2879552.* ... **46**

Scheme 2.4. *One and two-electron metabolic pathways of doxorubicin.* **67**

Scheme 3.1. *The synthesis of dual inhibitor, **3.8**, from the GSK2879552 methyl ester precursor.* **98**

Scheme 3.2. *The synthesis of 4-bromomethylbenzhydroxylamine.*[139] **99**

Scheme 3.3. *The conversion of carboxylic acid **3.14** to amine **3.15** via the Curtius rearrangement.* **100**

Scheme 3.4. *Reductive amination step with tranylcypromine analogue **3.15** to give the precursor compound to both **3.12** and **3.13**.* **101**

Scheme 4.1. *The initial development of test molecules **4.2a** and **4.2b**.* **138**

Scheme 4.2. *General synthetic method including the alternative route via the carboxylic acid.* **140**

Scheme 4.3. *Deprotection with H_2/Pd and the resulting undesired cleavage of the N-benzyl group.* **140**

Scheme 5.1. *Original synthesis of the LSD1 inhibitor **5.8** by Borrello et al.*[151] **182**

Scheme 5.2. *Alternative tosylhydrazone method of cyclopropane ring formation.* **182**

Scheme 5.3. *The anticipated, but unobserved, cis/trans equilibration of* ***5.3*** *under basic conditions.* **.....183**

Scheme 5.4. *The conversion of alkene* ***5.2*** *to cyclopropane* ***5.3*** *via the stereospecific JCC reaction.* **.....184**

Scheme 5.5. *The proposed mechanism of the alkene by-product* ***5.10*** *during the JCC reaction.* **.....185**

Scheme 5.6. *The mechanism of the Curtius rearrangement in both the presence and absence of water.* **.....186**

Scheme 5.7. *The modified Borrello synthesis used in this work.* **.....186**

Scheme 5.8. *The synthetic route of* ***5.13a*** *along with analogues* ***5.13b, 5.13c, 5.16*** *and* ***5.19****.* **.....190**

List of Tables

Table 1.1. *Phenelzine and bizine selectivity profile for LSD1 vs MAOA, MAOB and LSD2.* **15**

Table 1.2. *The Inhibition of tranylcypromine derivatives against LSD1, LSD2 and MAO.* **17**

Table 1.3. *Classification of the zinc dependent HDACs, their cellular function and their known inhibitors.* **29**

Table 1.4. *IC_{50} values of FDA/CFDA approved HDAC inhibitors.*[87–90] **36**

Table 2.1. *Relative yields achieved in each oxidation reaction on primary alcohol **2.10**.* **44**

Table 2.2. *pIC_{50} data recorded for **2.8a** and control compounds.* **48**

Table 2.3. *Cell viability data of **2.8a** in examples of fused and non-fused cell lines.* **50**

Table 2.4. *Tabulated data of H3K4me2 levels in response to LSD1 inhibition with GSK2879552 and **2.8a** in THP-1 and MOLM-13 cells.* **53**

Table 2.5. *CD86 expression levels in THP-1 cells on inhibition of LSD1.* **54**

Table 2.6. *CD11b expression levels in THP-1 cells on inhibition of LSD1.* **55**

Table 2.7. *The apoptosis profile data of doxorubicin and **2.8a** both individually and in combination in THP-1 cells measured using caspase activation.* **59**

Table 2.8. *The apoptosis profile data of doxorubicin and **2.8a** both individually and in combination in THP-1 cells measured using Annexin V.* **61**

Table 2.9. *% population of H2AX levels in THP-1 cells in response to treatment with doxorubicin and **2.8a**.* **65**

Table 2.10. *ROS data for THP-1 cells treated with doxorubicin and **2.8a**.* **68**

Table 2.11. *Fold change in the expression of 12 damage repair genes in response to inhibition of LSD1 with **2.8a**.* **70**

Table 2.12. *IC_{50} values of compounds **2.8a-g** in a cell viability assay in THP-1 cells.* **77**

Table 3.1. *pIC_{50} data recorded for dual inhibitor **3.8** and control compounds.* **102**

Table 3.2. *HDAC assay data recorded for dual inhibitor **3.8** and control compounds. TSA used as a standard. na = not available.* **103**

Table 3.3. *Tabulated cell viability data gathered for **3.8** and control compounds in MLL and non-MLL cell lines.* **106**

Table 3.4. Tabulated data of methylation and acetylation levels in THP-1 cells in response to LSD1 and HDAC inhibition. **112**

Table 3.5. *CD86 expression change in response to LSD1 and HDAC inhibitor treated THP-1 cells.* **114**

Table 3.6. *CD11b expression change in response to LSD1 and HDAC inhibitor treated THP-1 cells.* **115**

Table 3.7. *p21 expression change in response to LSD1 and HDAC inhibitor treated THP-1 cells.* **116**

Table 3.8. *The apoptosis profile data of **3.8** and **3.12** both individually and in combination with doxorubicin in THP-1 cells measured using caspase activation.* **120**

Table 3.9. *The apoptosis profile data of **3.8** and **3.12** both individually and in combination with doxorubicin in THP-1 cells measured using Annexin V.* **122**

Table 3.10. *Tabulated % population data for γ-H2AX levels in THP-1 cells treated with doxorubicin, **3.8** and **3.12**.* **124**

Table 3.11. *ROS data for THP-1 cells treated with doxorubicin, 3.8 and **3.12**.* **126**

Table 3.12. *Correlation between IC_{50} and Gold ChemScore values.* **130**

Table 4.1. *HDAC assay data for compounds **4.2a** and **4.2b** along with positive and negative control compounds.* **145**

Table 4.2. *Tabulated IC_{50} data from a THP-1 cell viability assay.* **152**

Table 5.1. Results of the HDAC assays carried out on compound **5.13a**. **187**

Declaration of Authorship

I, Adam Lee, declare that the thesis entitled “Erasing the eraser. The synthesis and biological evaluation of some novel epigenetic inhibitors” submitted by me for the degree of Doctor of Philosophy at the School of Pharmacy is my original work, derived by the results of my own research, except where due reference is made to other authors or researchers.

I also certify that it has not been previously submitted by me for a degree at this or any other university.

Signed

……..

Date

……..

Chapter One

1. Introduction

1.1. Epigenetics, a quick look at the past.

Although epigenetics is seen as a relatively modern branch of science, the concept of epigenetics has been around for some time. As far back as Hippocrates and Aristotle the idea of inheritance of acquired characteristics is put forward.[1] Sometimes referred to as 'soft inheritance,' this is the theory that offspring may inherit traits acquired by their parents. In the early 19th century this school of thought became widely associated with a French naturalist by the name of Jean Baptiste Lamarck, and the idea of inheritance of acquired characteristics became known as Lamarckism.[2]

The term 'epigenetic' itself, was not coined until 1939. In his book: An Introduction to Modern Genetics, developmental biologist Conrad Waddington, used the term to link the classical embryological theories of preformation and epigenesis.[3] Preformation is the belief that the organism is somehow preformed in its embryonic state and that development is simply the miniature form unfolding into its adult form. Epigenesis is a competing theory in which the organism is not fully formed as an embryo but develops gradually over time by the addition of parts. Waddington suggested that although development proceeds on the 'preformed' qualities of the fertilised egg, its constituents interact to give rise to new types of tissue and organ not originally present, saying that this development must be considered 'epigenetic'. He later introduced the idea of canalisation, as a way of explaining why it may be that some acquired traits persist into offspring while others do not.[4] This led to his, now famous, epigenetic landscape illustration (Figure 1.1).[5] This illustration is of an undulating landscape that represents the developmental pathway from genotype to phenotype. Marbles are shown to be rolling down this landscape from the highest point, representing the genotype, through a series of forks and slopes, before finally coming to rest at various phenotypic outcomes. The idea is to show that by manipulating the landscape, i.e. changing the environmental

conditions of the organism, one could change the phenotypic outcome without the need to change the genotype. He experimentally showed that by selectively breeding organisms with a desired characteristic, within a few generations' offspring would display that characteristic without the need for environmental stimulation.

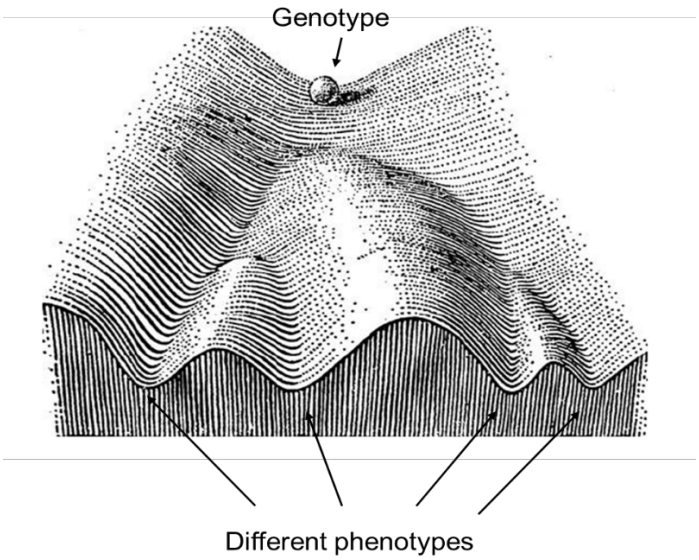

Figure 1.1. Waddington's Epigenetic landscape.
(Used with permission)[5]

The single groove at the top of the hill represents the genotype of the organism while the marble, when at the top, represents an undifferentiated cell (zygote). As the marble rolls down the landscape it makes 'choices' at various forks thus denoting the cell becoming more specialised as it does so. The troughs at the bottom denote specific phenotypes at which the differentiated cell comes to rest. The nature of the illustration implies the marble cannot go back up the hill or over to a different trough without outside interference, thus showing that once a cell has become specialised it cannot revert back to a less specialised state, or, become a cell of a different type.

In 1958 Nanney published a paper giving a slightly different view on the use of the term 'epigenetic'.[6] The differences between the use of the term by Waddington and that by Nanney are summed up nicely by Haig who says; "Waddington introduced 'epigenetics' to refer to the study of the causal mechanisms by which genes of the genotype bring about phenotypic effects."

Nanney chose ‘epigenetic’ to refer to mechanisms of cellular heredity that were not based on the semi-conservative replication of DNA.[7]

Although both descriptions could perhaps be interpreted as being correct in terms of the modern understanding of epigenetics, it is Nanney’s interpretation which is more in keeping with the modern view.

Modern day definitions of epigenetics are numerous, albeit many of them alluding to the same meaning. But perhaps the best way of looking at the subject should be based on one’s need of the description. In everyday life epigenetics could mean simply the differences observed in ‘identical’ (or more correctly, monozygotic) twins, or the difference between a caterpillar and a butterfly. If a deeper explanation is required then a molecular description defining epigenetics as the biological mechanism by which genes are either activated or silenced through reversible changes to genetic material, without any change to the DNA sequence itself, may be used. As will become apparent, it is this second description which is most appropriate to this work.

1.2. A more modern view.

Deoxyribonucleic acid (DNA) is the blueprint of all life. In human somatic cells, DNA is composed of approximately 3 billion base pairs making up 23 pairs of chromosomes. Of those only around 1.5% make up genes, sections of DNA which code for proteins, and it is these genes which are responsible for all life. Any changes to the genomic sequence of these genes can therefore have devastating effects. One example of this is sickle cell anaemia, a disease which affects the shape of red blood cells thus inhibiting their proper function. Red blood cells consist of four proteins bound together in a quaternary structure, two alpha-chains and two beta-chains. The beta-chains are coded for by the HBB gene, found on chromosome 11 and made up of 1605 base pairs. A single point mutation of this gene, in which adenine is substituted for thymine, leads to a glutamic acid residue being replaced by valine at position 6 in the protein.[8] The result of this is a decrease in the hydrophilicity in that region of the beta-chain which thus enables adjacent chains to associate via hydrophobic interactions. This has the effect of aggregation between the beta-chains of affected cells thus

deforming the cells and inhibiting their function. A second example is Tay-Sachs syndrome, a condition in which a deficiency of beta-hexosaminidase A leads to the toxic build-up of GM2 gangliosides in the cells of the spinal cord and brain. Beta-hexosaminidase A is an enzyme of which one sub-unit is coded for by the HEXA gene. According to the Human Gene Mutation Database (HGMD) there have been 169 different mutations to the HEXA gene reported to date, with 148 of those resulting in Tay-Sachs[9], many of which are due to single point mutations.

These examples are two among many and illustrate the importance of keeping the genome safe from damage. In order to accomplish this, nature has come up with a number of ways to both protect and repair DNA. The double helix structure of DNA itself is one such method. By having two strands bound to one another, exposure of the base pairs is limited and hence less prone to damage. It also ensures that following cell division, each cell has one original copy of DNA therefore ensuring faithful replication and reducing the chance of mutation due to error. A further protective measure is seen in the way DNA is packaged within the nucleus. DNA is wound around proteins called histones. This histone-DNA complex, called a nucleosome, consists of an octamer of eight histone proteins along with a section of 146 base pairs of DNA. The nucleosomes are in turn linked by a section of DNA called linker DNA, made up of various lengths of non-coding base pairs.[10] The sugar phosphate backbone of DNA is anionic at physiological pH and can therefore bind electrostatically to the cationic lysine and arginine residues found on the tail like structures of the histone proteins. When DNA is bound like this, the genetic material is inaccessible and hence less prone to damage. However, this inaccessibility also means the coding parts of the DNA, the genes, are unavailable for transcription. The system which has evolved to remedy this is an epigenetic one.

In order for genes to become accessible, the section of DNA containing the required gene must dissociate from the histone. This mean that either the DNA must become less anionic or the histone must become less cationic so as to decrease their affinity for one another. The latter is one solution chosen by nature and is accomplished by post-translational modification of the histone tails.

Functionalisation of certain residues, such as acetylation of lysine, has the effect of neutralising the charge on that residue and hence the histone. This allows the DNA at that point to unwind and become transcriptionally active. This process is reversible and with the functionalised residue restored, the affinity of the histone for the DNA returns and the gene is once again made inaccessible and inactive (Figure 1.2).

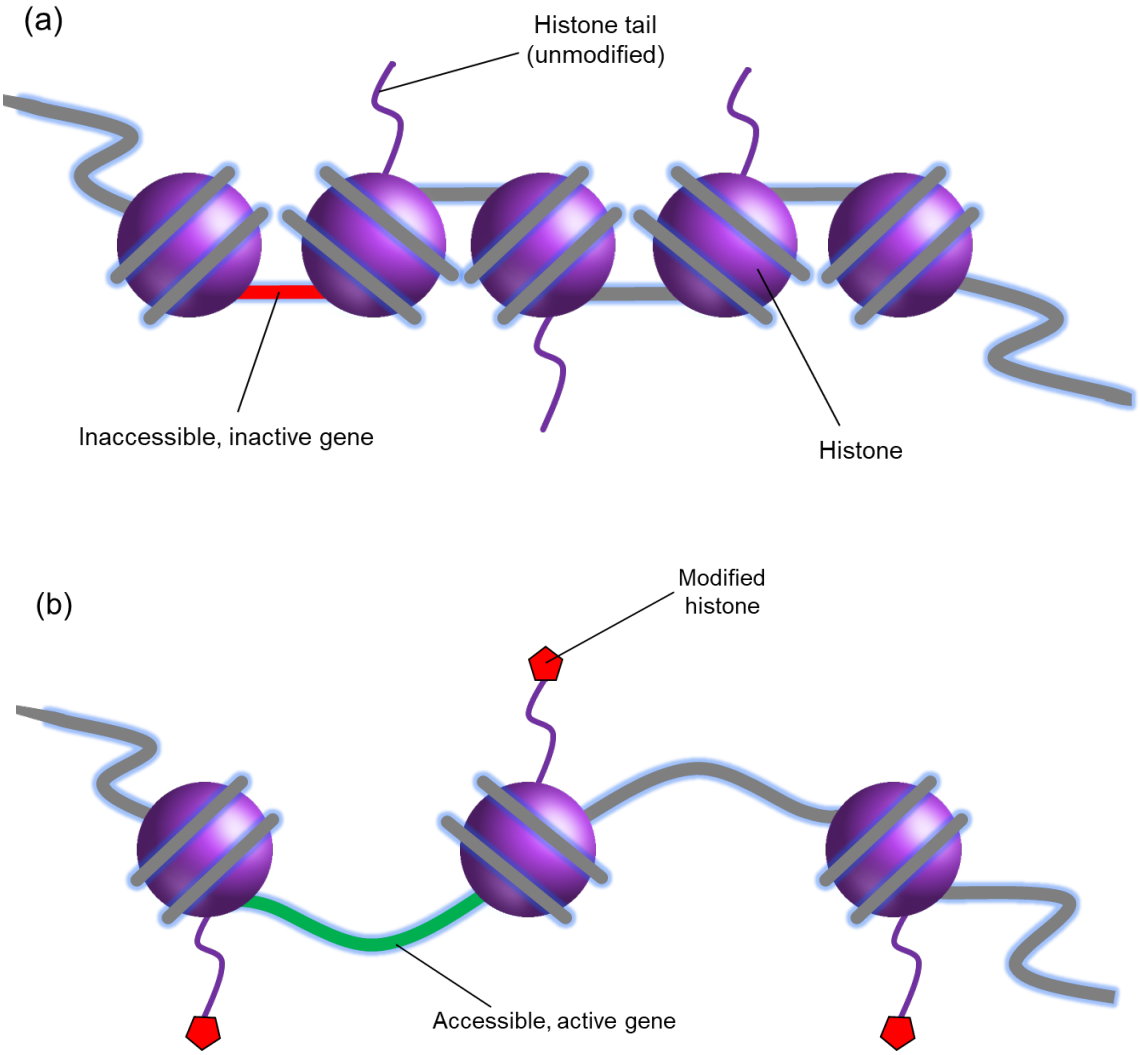

Figure 1.2. *The effect of histone modification on gene activation.*

(a) DNA tightly bound to histones and hence the genes are inaccessible and silenced. (b) Acetylation of the lysine residues on the histone tails results in a loss of affinity between the DNA and the histone. The DNA unwinds from the histone and the gene becomes activated and open to transcription.

This dynamic regulation is carried out by three groups of proteins commonly known as ‘writers’, ‘erasers’ and ‘readers’. The writers functionalise macromolecules susceptible to epigenetic change. These changes include methylation (Arg and Lys), acetylation (Lys), phosphorylation (Ser and Thr), ubiquitination (Lys) and sumoylation (Lys). The erasers remove these groups and the readers recognise the marks that make up this ‘epigenetic code’ and help facilitate various processes such as transcription.

Probably the most studied epigenetic modification, and one focus of this work, is methylation, which cannot only occur at the arginine and lysine residues of histones, but can also occur on DNA itself, as well as at many other proteins. Methylation of DNA occurs at the C5 position of cytosine to give 5-methylcytosine (5mC). The change is considered epigenetic as no accompanying change to the base sequence is observed. The ‘writers’ in terms of DNA methylation are DNA methyltransferases (DNMTs). They are a family of five enzymes, Dnmt1, Dnmt2, Dnmt3a, Dnmt3b and Dnmt3l. All methylate cytosine, (Dnmt2 methylates cytosine at position 38 in aspartic acid tRNA),[11] through the recruitment of co-factor, S-adenosyl methionine (SAM), which donates a methyl group to cytosine, becoming S-adenosyl homocytesine (SAH) (Scheme 1.1).[12]

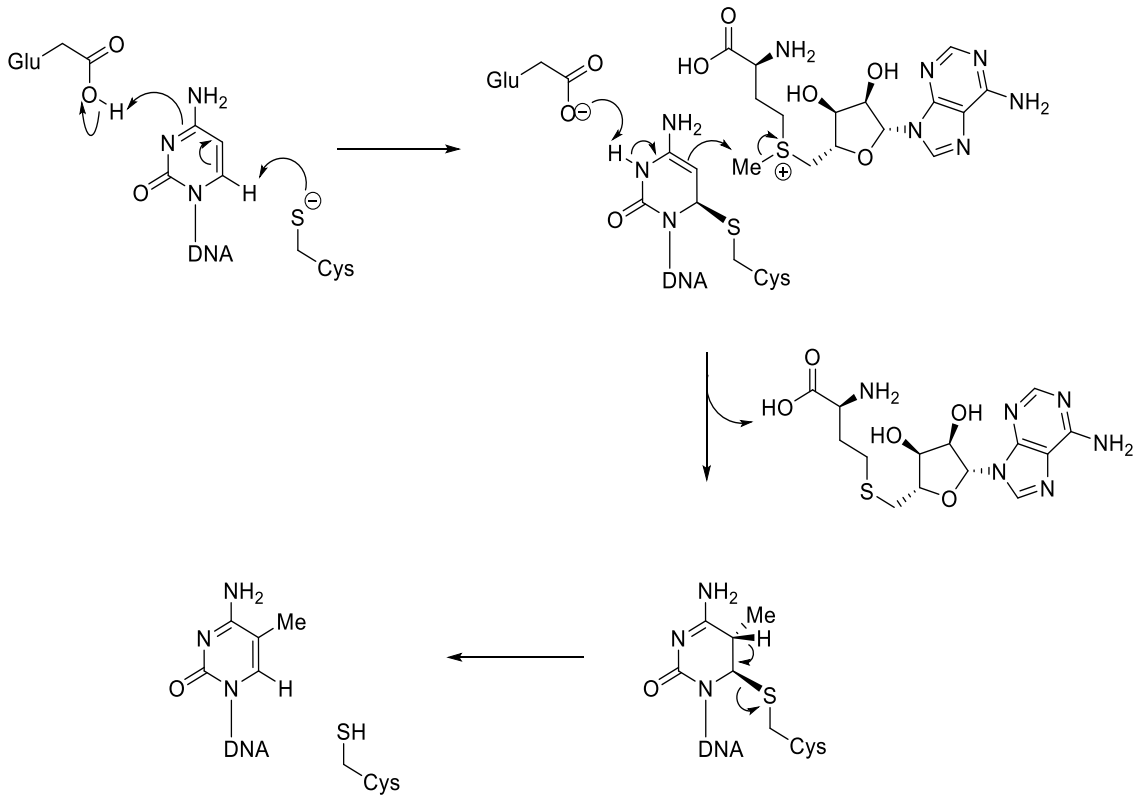

Scheme 1.1. *A mechanism for the methylation of cytosine in which SAM acts as co-factor.*[12]

Methylation of cytosine occurs at CpG sites, regions of the genome in which cytosine and guanine are linked by a phosphate group. The CpG notation distinguishes this from cytosine-guanine base paring (CG) between which there is no phosphate. When CpG sites in promotor regions are methylated, proteins containing methyl binding domains (MBDs) are able to bind to them, thus preventing the necessary transcription factors from making contact and so silencing the gene.[13] Gene silencing by methylation is a normal and required part of mammalian development[14] but it can also be a source of disease, specifically, cancer. Hypermethylation of the CpG promotor regions of tumour suppressor genes, for example, can cause unwanted gene suppression and ultimately lead to the development of cancer.[15]

1.3. Methylation of lysine

There are currently six known sites of lysine methylation on histones: H3K4, H3K9, H3K27, H3K36, H3K79 and H4K20. Although all can lead to both

activation and deactivation of genes depending on their methylation state, each is generally associated with one or the other. For example, H3K4 is strongly linked to gene activation in both methylated and acetylated states. It does this via the promotion of postitive transcription factors in place of negative ones, and so H3K4me3 will promote the binding of chromodomain-helicase-DNA binding protein 1 (CHD1)[16] for example, while blocking the binding of nucleosome remodelling and deacetylase (NuRD) complex.[17] Each can exist as an unmodified lysine or can be mono, di or tri-methylated and although long believed to be irreversible, the reversibility of lysine methylation was established in 2004 with the first reported lysine demethylase, Lysine Specific Demethylase 1 (LSD1).[18] This reversibility established lysine methylation as being able to take part in the dynamic process of gene activation and silencing. If the process were an irreversible one, then methylation would simply result in the permanent activation or repression of genes which is often seen in faulty systems resulting in disease.

Methylation of lysine is facilitated by a range of enzymes collectively known as lysine methyltransferases (KMTs). There are currently more than thirty KMTs and all but one (DOT1L) contain the SET domain. All these SET-domain KMTs have a structurally conserved SAM binding pocket which facilitates the catalytic transfer of a methyl group to the lysine residue. One example is that of Ezh2, the catalytic subunit of Polycomb Repressive Complex 2 (PCR2). Ezh2 is non-catalytic as a single entity, but in complex with two other non-catalytic subunits, it gains KMT function via its SET domain.[19] Ezh2 is capable of mono, bi and trimethylation of H3K27 with trimethylation considered its primary function *in vivo*.[20] It acts as a transcriptional repressor,[20,21] although variants have also been implicated in transcriptional activation in a wide variety of cancers.[22] As with all SET domain containing KMTs, methylation occurs via transfer of a methyl group from SAM, to give the corresponding H3K27me/me2/me3 residue, (Scheme 1.2).[23]

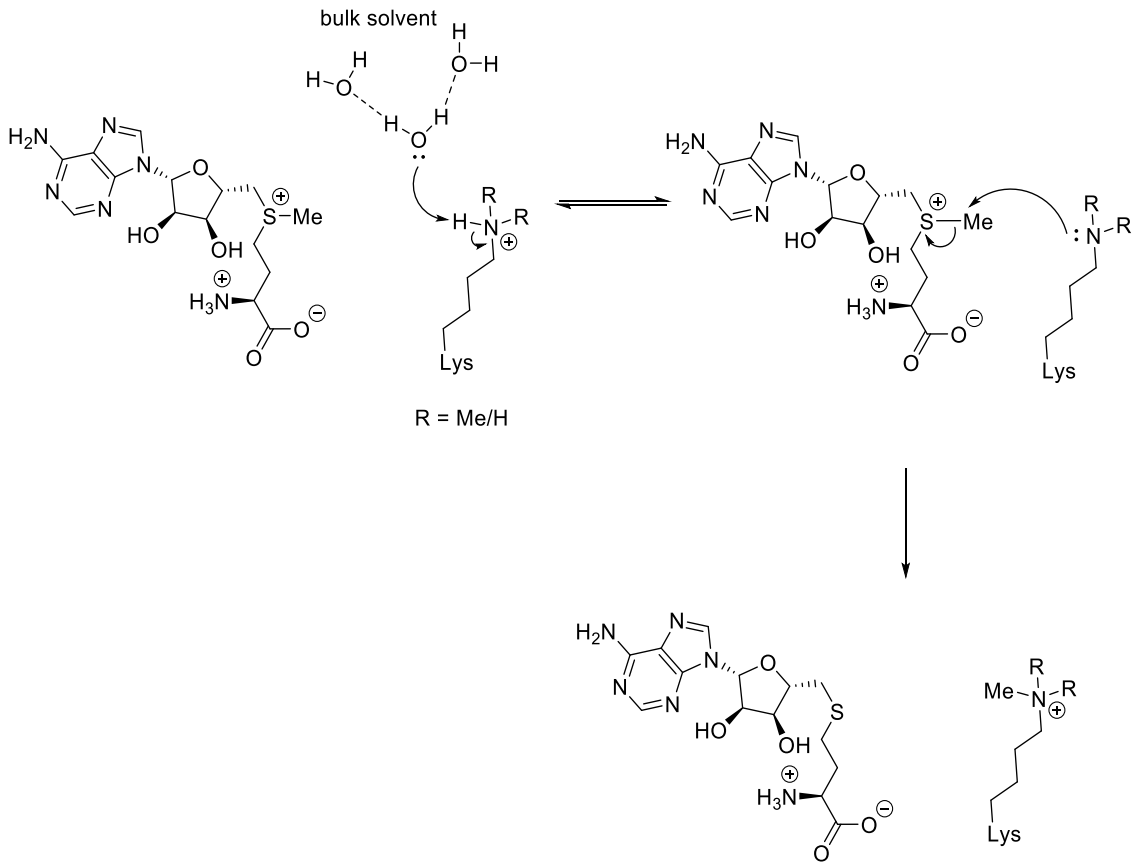

Scheme 1.2. *Methylation of H3K27 via mechanism proposed by Fortin et al.*

Evidence supporting the proposal that H3K27 is deprotonated by bulk solvent, which has access via a channel to the active site, is given. This shows that lysine deprotonation is enzyme-dependent and rate limiting and is unlikely to occur prior to binding.[23]

1.4. Demethylation of Lysine

There are two families of lysine demethylases (KDMs) comprising of more than 25 enzymes. The bulk of those are the Jumonji C domain containing histone demethylases (JHDMs) which can demethylate all three lysine methylation states. This is achieved through the use of both α-ketoglutarate (αKG) and Fe(II) co-factors. Fe(II) coordinates both αKG and molecular oxygen thus allowing nucleophilic attack of O_2 on αKG and releasing CO_2 to give succinate and a highly reactive Fe(IV)=O species. Fe(IV)=O then hydroxylates the methylated lysine which then spontaneously decomposes into formaldehyde and demethylated lysine (scheme 1.3).[24]

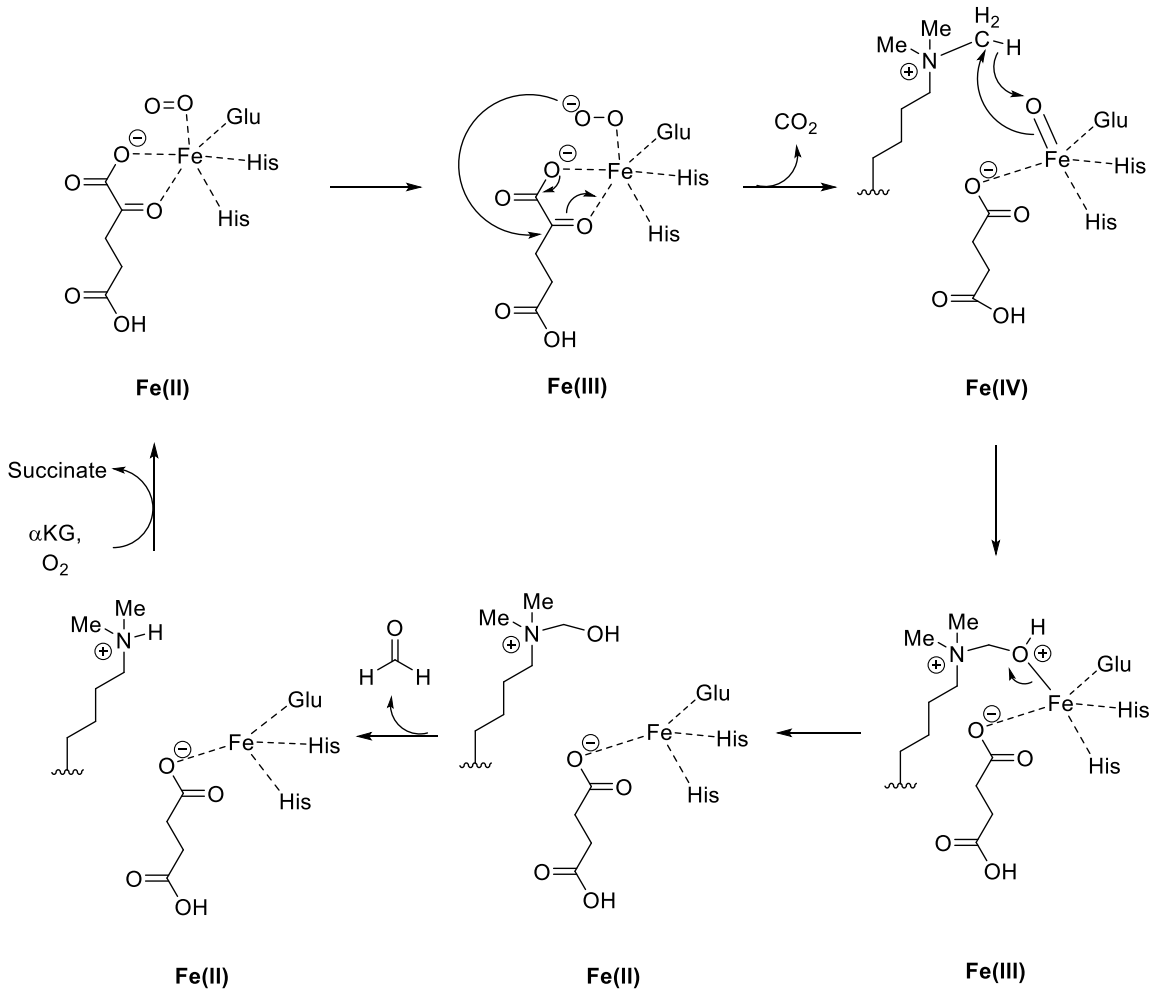

Scheme 1.3. *Fe(II) mediated mechanism employed by JHDMs.*[24]

In contrast, the second family of KDMs which contains only two members, LSD1/KDM1A and LSD2/KDM1B, are incapable of removing methyl groups from trimethylated substrates. The reason is that the mechanism used requires the presence of a lone pair of electrons in order to facilitate the demethylation process. LSD1/2 do not use iron cofactors but instead rely on flavin adenine dinucleotide (FAD) for their catalytic activity. Hydride transfer between this FAD cofactor and the lysine nitrogen lone pair is the most likely pathway taken and hence with the nitrogen lone pair tied up in trimethyl-lysine, this pathway would be unavailable. Reduced $FADH_2$ is then oxidised with molecular oxygen to give hydrogen peroxide, while the imine is hydrolysed with water to give the same carbinolamine intermediate seen in the Fe mediated reaction above. This then collapses as before to give the demethylated lysine and formaldehyde by-product (scheme 1.4).[24]

In LSD1 the FAD cofactor is embedded in the amine oxidase domain, the largest part of the 852 amino acid chain, made up of 457 residues. In addition, LSD1 also consists of a 99 residue SWIRM domain and a 105 residue long Tower domain which splits the amine oxidase domain (Figure 1.3).[25] It is this Tower domain, along with a lack of two zinc finger domains, which distinguish LSD1 from LSD2. The Tower domain is an important feature, as it facilitates binding to several interacting proteins such as CoREST, CtBP1, HDAC1/2, snail and metastasis-associated protein (MTA).[26, 27] These binding partners have been shown to be important in the demethylase activity of LSD1 by mutational deletion of the Tower domain.[26]

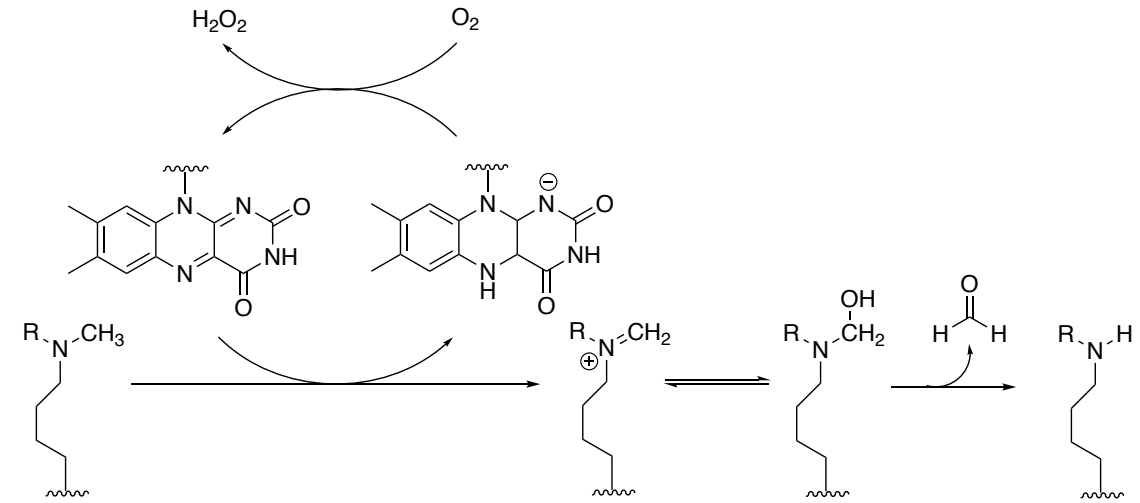

Scheme 1.4. *FAD dependent demethylation mechanism of LSD1.*[24]

The main histone substrates of LSD1 are mono and di-methylated lysine 4 and 9 on histone 3 (H3K4me/me2 and H3K9me/me2). Demethylation of H3K4 has been linked to transcriptional repression while demethylation of H3K9 has been shown to aid transcriptional activation.[28] In addition, LSD1 has also been reported to act upon a number of non-histone substrates. The tumor-suppressor p53 is one such target, specifically K370me2 of p53. By demethylating K370me2 to k370me, p53 has a decreased affinity for the coactivator binding protein, 53BP1. This lack of interaction with its coactivator means that mono-methylated p53 becomes transcriptionally repressed in terms of its pro-apoptotic function.[29] Furthermore, this LSD1-p53 complex results in an increased specificity of LSD1

for histone substrate H3K4me2.[30] This suggests that p53 may well recruit LSD1 in order to aid chromatin moderated gene regulation.

A second example of a non-histone substrate of LSD1 is DNMT1. As discussed above, DNMT1 is a writer responsible for the methylation of DNA at the C5 positon of cytosine. Its function is the maintenance of methylation patterns on DNA following DNA replication. Methylation at K1096 of DNMT1 can lead to degradation of this protein, but LSD1 mediated demethylation stabilises the protein and hence allows it to carry out its function.[31] An interesting point of note is the lack of similarity shown between these non-histone substrates and their histone counterparts given the high level of specificity LSD1 seems to show for histone position. A greater understanding of this substrate recognition could therefore be useful when attempting to therapeutically target LSD1. It should be noted at this point that although there are numerous literature examples of non-histone proteins as LSD1 substrates,[29,32–39] there is yet to be given sufficient evidence given which confirms these as true LSD substrates.[40]

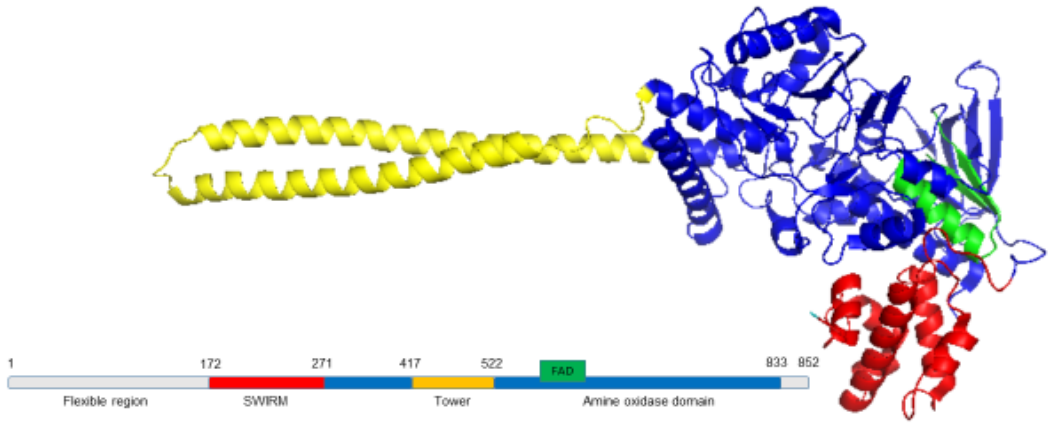

Figure 1.3. *Ribbon diagram of LSD1.*

Showing the SWIRM domain in red, the Tower domain in yellow and the amine oxidase domain (AOD) in blue with the FAD binding site in the AOD shown in green. Adapted from PDB entry 2HKO using PyMOL software.

LSD1 appears to be required for the regulation of many biological processes. One such process which exemplifies this is the key role played in the formation

of blood cells. In conjunction with the methyltransferase, mixed-lineage leukemia 1 (MLL), LSD1 has been shown to be essential in the maintenance of several blood cell types through the stages of differentiation from hematopoietic stem cells right through to granulocytes and possibly B cells, T cells and NK cells (Figure 1.4). Studies in which bone marrow contained LSD1 deficient cells, showed an inability to produce both myeloid and lymphoid progenitor cells, thus highlighting the critical role of LSD1 in this process.[41]

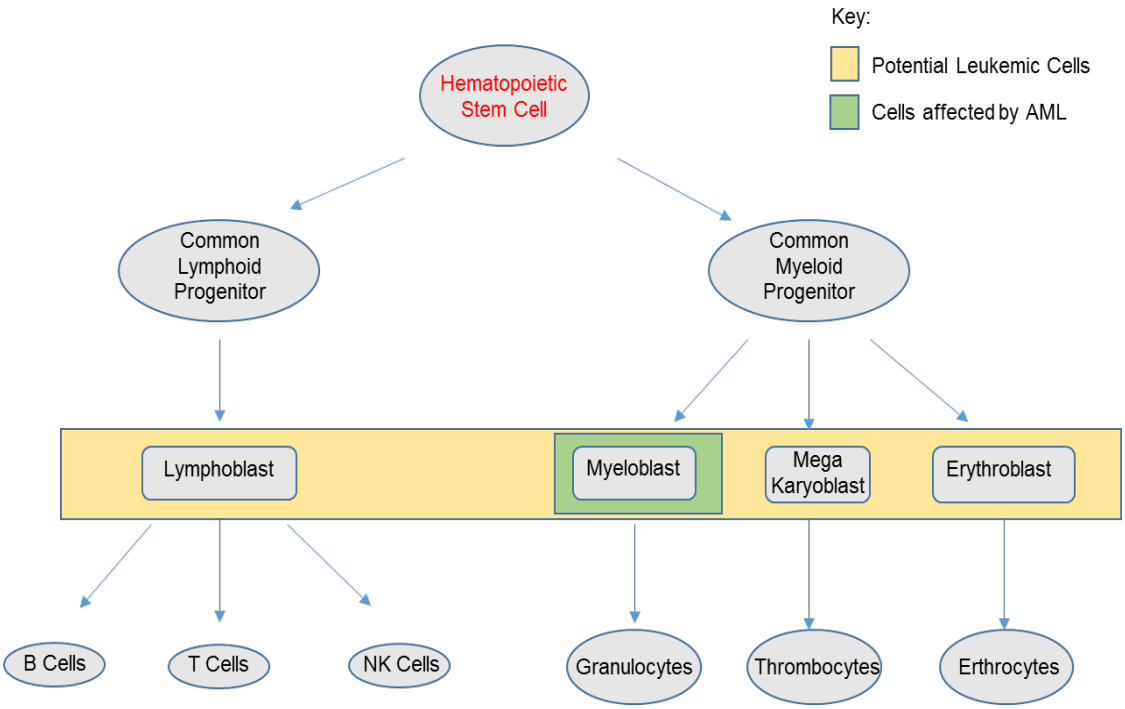

Figure 1.4. *The differentiation pathway for the formation of blood cells.*

The process begins with pluripotent hematopoietic stem cells, which are themselves maintained by MLL and LSD1. They then differentiate into common myeloid and lymphoid progenitor cells via a pathway in which LSD1 is required. These progenitor cells then give rise to all other blood cells. LSD1 is believed to be required in the formation of erythrocytes, granulocytes and perhaps the B,T and NK cells of the immune system.[41]

1.5. Irreversible inhibition of LSD1, the beginning.

Monoamine oxidase (MAO) are a family of enzymes which, as their name suggests, catalyse the oxidation of monoamine substrates. They are found in the outer membrane of mitochondria and, amongst other things, metabolise certain neurotransmitters such as dopamine, serotonin and noradrenaline. Like LSD1, MAOs have a covalently bound FAD cofactor which features in its catalytic mechanism, converting amine substrates to the corresponding imine

prior to hydrolysis to the appropriate carbonyl compound. Of course, the difference is the substrate and so while MAO converts its amine substrate into a carbonyl, LSD1 removes methyl groups from methylamines with the corresponding loss of carbonyl by product, formaldehyde.

The amine oxidase domain of LSD1 gives it an homology with MAO and hence, known MAO inhibitors (MAOIs) were the first to be tried in an inhibitory role against LSD1. Phenelzine (**1.1**), tranylcypromine (**1.2**) and pargyline (**1.3**) were some of the first small molecules studied in this way (figure 1.5), but due to their high affinity for MAO and in the case of pargyline their relatively weak inhibition of LSD1,[42] they were unlikely to ever be marketed as LSD1 inhibitors. Inevitably, second generation analogues followed. Bizine (**1.4**, figure 1.5), was reported in 2014 with an increased selectivity for LSD1 over MAO-A, MAO-B and LSD2 of 23-fold, 63-fold and >100-fold respectively (table 1.1). Bizine also showed good cancer cell antiproliferation effects, slowing the rate of cellular proliferation in LNCaP and H460 with an IC_{50} of 16 and 14μM respectively. This was an improvement on phenelzine which showed less than a 50% reduction of ^{3}H-thymidine incorporation in H560 cells with 80 μM.[43]

Enzyme Tested	Inhibitor	K_i (μM)	Selectivity for LSD1 vs Enzyme Tested
MAOA	Phenelzine	0.8±0.4	0.2
	Bizine	2.6±2.3	22.7
MAOB	Phenelzine	3.9±1.7	1.2
	Bizine	6.5±4.6	62.5
LSD2	Phenelzine	N/A	N/A
	Bizine	N/A	>100

Table 1.1. *Phenelzine and bizine selectivity profile for LSD1 vs MAOA, MAOB and LSD2.*

Adapted from cole et al. supplementary table 1.[43]

However, bizine is still the only real example of an irreversible LSD1 inhibitor based on the phenelzine structure. In contrast, compounds developed around the cyclopropane containing tranylcypromine (TCP) structure are abundant throughout the literature.

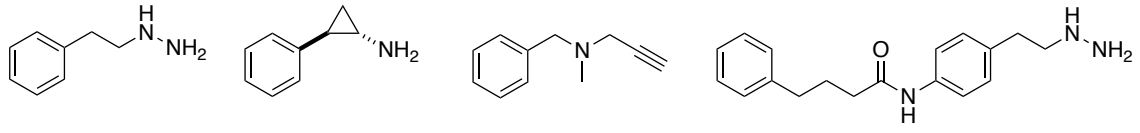

Figure 1.5. *Some of the first MAO inhibitors trialled against LSD1 and the second-generation analogue of phenelzine.*

trans-2-Phenylcyclopropylamine (t-PCPA), also known by its trade name Parnate and perhaps most commonly as tranylcypromine (TCP), is a clinically approved drug for the treatment of various neurological disorders such as depression.[44] TCP inhibits MAO, resulting in an increase in the level of certain mood elevating neurotransmitters, thus alleviating the condition. In 2006 TCP was reported as an inhibitor of LSD1 with an IC_{50} of less than 2μM in addition to showing a global increase in H3K4me2 levels and reduced transcriptional activity within cells.[45] Unlike both phenelzine and pargyline, TCP contains two stereocenters. This begs the question, which stereoconfiguration is the most active and or specific? A study carried out in 2010 by Binda *et al.* compared the activity of racemic trans TCP with both the (1S, 2R) and (1R, 2S) enantiomers.[46] The group also looked at the activity of the *cis* (1R, 2R) and (1S, 2S) configurations (Table1.2). They found both *trans* enantiomers and the racemic *trans* diastereoisomer to be the more active than either of the *cis* enantiomers. In addition, the (1R, 2S) configuration was found to be the superior enantiomer with a K_i of 168 μM. All compounds were, as expected, clearly more specific to MAO-B, including the *cis* enantiomers, and also much more potent. MAO-B activity was not determined in this study but other studies such as that by Hong *et al.* show both MAO-A and MAO-B to have similar activity in both *cis* and *trans* configurations, with *trans* having an IC_{50} of 23 and 4 μM and *cis* of 29 and 8 μM against MAO-A and MAO-B respectively.[47] Interestingly, it seems that TCP also inhibits LSD2 with a comparative level of potency as for LSD1. Karytinos *et al.* reported a K_i of 242 and 180 μM for LSD1 and LSD2 respectively.[48] This was backed up by Binda *et al.* in 2010 who reported a K_i of 271 and 186 μM (Table 1.2). Binda *et al.* also showed that the *cis* diastereoisomer was superior to the *trans* with both (1*R*, 2*R*) and (1*S*, 2*S*)

showing a K_i of 131 and 68 μM respectively in LSD2. This is far superior to that of the same compounds in LSD1 which show a K_i of 364 and 506 μM (table 1.2).[46]

		K_i (μM)			
Compound	**Stereoconfiguration**	**LSD1**	**LSD2**	**MAO-A**	**MAO-B**
t-PCPA	Racemic *trans*	271	186	19	16
t-PCPA	(1R, 2S)	168	127	nd	89
t-PCPA	(1S, 2R)	284	137	nd	4.4
c-PCPA	(1R, 2R)	364	131	nd	39
c-PCPA	(1S, 2S)	506	68	nd	50

Table 1.2. *The Inhibition of tranylcypromine derivatives against LSD1, LSD2 and MAO.*

All compounds were in the form of a HCl salt. nd = not determined. Table adapted from Binda et al. Table 1.[46]

As discussed in section 1.4, the LSD1 mechanism of action involves the FAD cofactor within it's active site. TCPs inhibitory action occurs via the formation of a covalent adduct between itself and the FAD cofactor.[49,50] With the FAD cofactor tied up in this adduct, its catalytic function becomes inert and the enzyme thus ceases to function. The mechanism by which this occurs is thought to be via a single electron transfer (SET) mechanism in which a single electron is transferred from the TCP amine to one of the FAD nitrogens. This drives the homolytic bond cleavage, which opens up the cyclopropyl ring before the reactive intermediate covalently bonds to FAD (Scheme 1.5).

A second competing theory is that of a hydride transfer mechanism. This would seem plausible as it would seem this is the most likely pathway by which the demethylation mechanism of LSD1 is thought to proceed (scheme1.4). However, X-ray crystal structures showing covalent adducts between the radical intermediates and FAD, consistent with a SET mechanism, would seem to make SET more likely.[46,51,50] In addition, it stands to reason that a hydride transfer mechanism of action would lead to reversible inhibition of LSD1 and this has not as yet been observed.

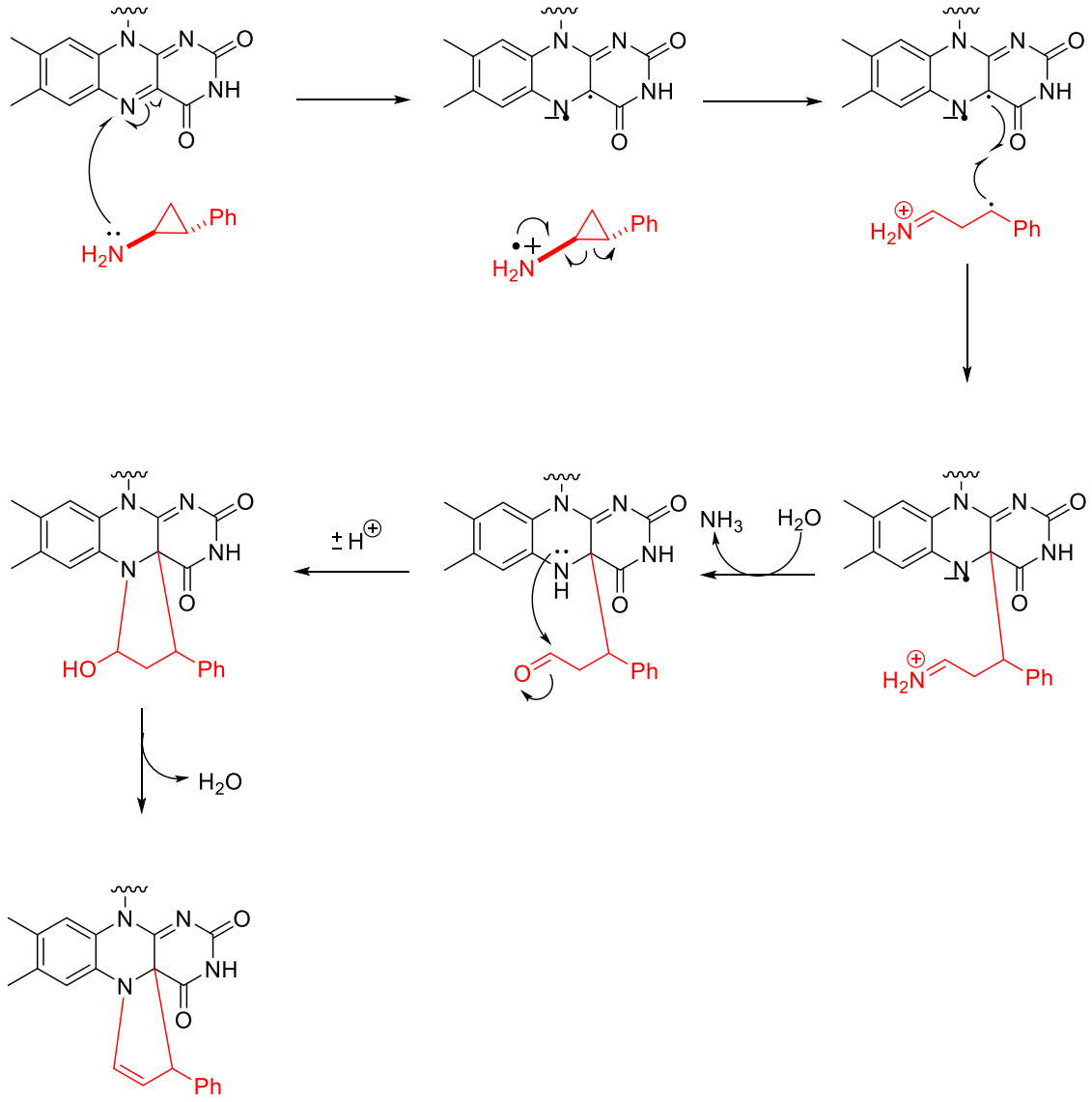

Scheme 1.5. *Inhibition of LSD1 by TCP via adduct formation with its FAD cofactor.*[49,50]

1.6. Irreversible inhibition of LSD1, beyond the first generation.

The relatively weak inhibition and poor selectivity of TCP created an opportunity for the development of more potent, selective inhibitors. TCP was indeed a good starting point for the development of such inhibitors having been in use for a number of years as a treatment for depression and had been found to be relatively safe.[52] It was also, importantly, known to inhibit LSD1.

Three possibilities for the modification of TCP exist. Substitution of the aryl ring, alkylation of the amine and further substitution of the cyclopropyl ring (Scheme 1.6). Some of the first modified compounds were introduced by Binda *et al.* in 2010. By modifying the *para* position of the aryl ring, a decrease in K_i from 271

μM in TCP to 1-2 μM (**1.5-1.7**) was observed. In addition, several compounds also showed reduced MAO-B affinity from k_i = 16μM in TCP to no observed inhibition. However, LSD2 and MAO-A were still inhibited with low μM K_i making these first inhibitors lack complete specificity for LSD1 (Figure 1.6).

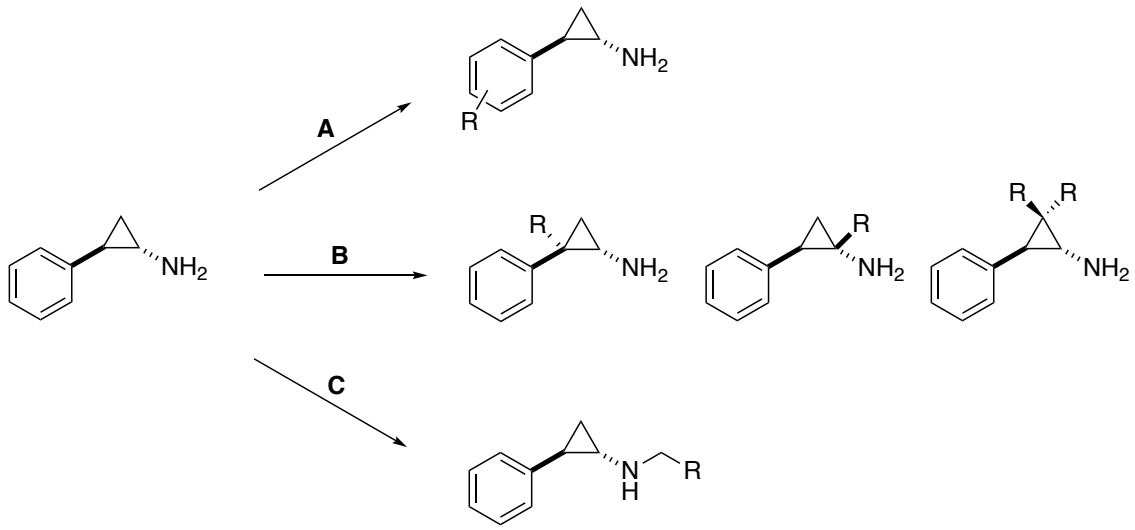

Scheme 1.6. *Possible positions for the modification of tranylcypromine.*

***A**. Substitution of the aryl ring. **B**. Substitution of the cyclopropane ring. **C**. Alkylation of the amine.*

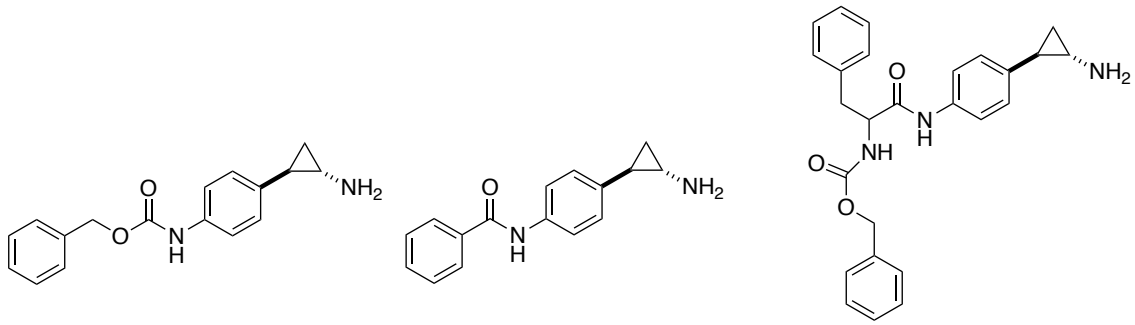

1.5
LSD1 K_i = 1.9 μM
LSD2 K_i = 20 μM
MAO-A K_i = 0.5 μM
MAO-B K_i = 7.4 μM

1.6
LSD1 K_i = 1.1 μM
LSD2 K_i = 61 μM
MAO-A K_i = 2.3 μM
MAO-B K_i = 3.5 μM

1.7
LSD1 K_i = 1.3 μM
LSD2 K_i = 38 μM
MAO-A K_i = 1.2 μM
MAO-B *not active at maximum 267 μM*

Figure 1.6. *Examples of para substituted tranylcypromine analogues.*

Compounds show increased affinity for both LSD1 and LSD2 and reduced affinity for MAO-B.[46]

Functionalisation of the benzene ring was also the target of many other groups, predominantly at the *para* position, with a variety functional groups. Benelkebir *et*

al. showed that simple *para*-bromination of TCP decreased K_i to 3.7 μM from 25.0 μM in TCP, while in LNCaP prostate cancer cell lines IC_{50} decreased from >100,000 μM in TCP down to 111 μM.[53]

The large size of the LSD1 cavity allows for the development of relatively large inhibitors. Ueda *et al.* designed inhibitors based on the superimposition of the x-ray crystal structures of an FAD-TCP adduct and an FAD-*N*-propargyl lysine peptide adduct, both in the active site of LSD1. These compounds consisted of the amino acid side chain linked to the benzene ring of TCP through an ether bond. It was hoped that this group would bind sufficiently to LSD1 while also being unable to bind MAO due to the large groups inability to fit into the MAO active site. The result was 2 compounds (Figure 1.7, **1.8**, **1.9**) which showed both increased inhibition of LSD1 and decreased inhibition of both MAO-A and B.[49] The *meta* isomer was later modified by the same group (Figure 1.7, **1.10**) by *N*-alkylation to afford an inhibitor 6 times more potent than its unalkylated counterpart. However it was also reported to show 8 times less activity as an antiproliferative agent in HeLa cell lines. The reasoning put forward for the poor performance in cell was that binding proteins may have changed the conformation of the protein and therefore the shape of the active site.[54] This compound was not reported as being tested against LNCaP cell lines.

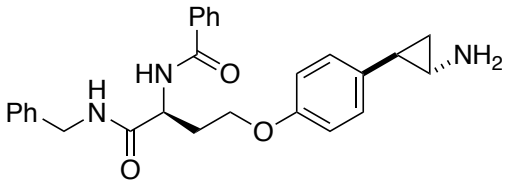

1.8
LSD1 IC_{50} = 1.9 μM
MAO-A IC_{50} = 290 μM
MAO-B IC_{50} = >1000 μM

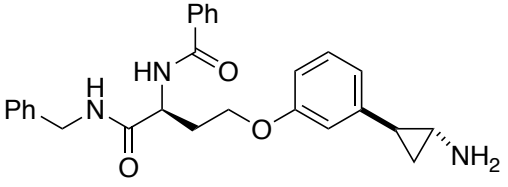

1.9
LSD1 IC_{50} = 2.5 μM
MAO-A IC_{50} = 230 μM
MAO-B IC_{50} = 500 μM

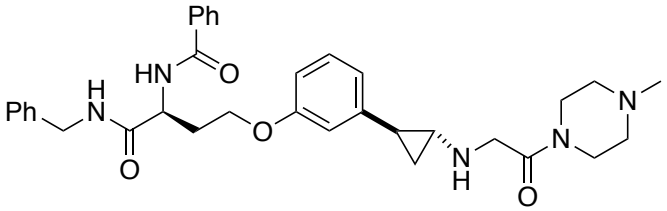

1.10
LSD1 IC_{50} = 0.38 μM

Figure 1.7. *Examples of more specific LSD1 inhibitors developed around the TCP scaffold.*[49,54]

Substitution of the benzene ring of TCP is perhaps the most common substitution in the academic literature and there are several reviews covering many of these.[26,55,56] Less common are examples of substitutions on the cyclopropyl group. Vianello *et al.* reported a series of novel compounds in which TCP was substituted with a number of functional groups around the cyclopropyl ring.[57] Most of the compounds reported increased potency as a LSD1 inhibitor relative to TCP but none showed any significant increase in specificity for LSD1 over MAO and many in fact showed an increased potency for both MAO-A and MAO-B. As an example of this compound **1.11** is modified by the addition of a phenyl group at the C1 position of the cyclopropane ring (Figure 1.8). LSD1 inhibition is increased from an IC_{50} of 11.6 μM in TCP to 0.2 μM but MAO-A inhibition also increased from 1.19 μM to 83 nm. Later the same compound was modified further to **1.12** by Borrello *et al.* with the addition of a fluorine at the C2 position of the cyclopropyl group (Figure 1.8).[58] This also increased affinity for LSD1 with a decrease in IC_{50} to 2.1 μM from 25 μM in the TCP reference. Both MAO-A and MAO-B also saw modest increases to 18 and 37 μM respectively. However, when the phenyl substituent at C1 is removed (**1.13**) a loss of LSD1 affinity is observed with an IC_{50} > 25 μM. This affinity can however be regained, and in some cases improved upon, by small additional substitutions to the aryl ring. Substituting in the *para* position (**1.14-1.16**) with $-CF_3$, $-SF_5$ and Cl resulted in improved IC_{50} of 2.1, 0.8 and 6.7 μM respectively, while replacing the *meta* -H (**1.17-1.20**) with $-CF_3$, SF_5, -OMe or -F resulted in an IC_{50} of 8.2, 8.4, 1.2 and 6.7 μM respectively. **1.19** and **1.20** also showed good activity in THP-1and MV4-11 cells with respective IC_{50} values of 8.5 and 1.6 μM in THP-1 and 1.9 and 4.9 μM in MV4-11.

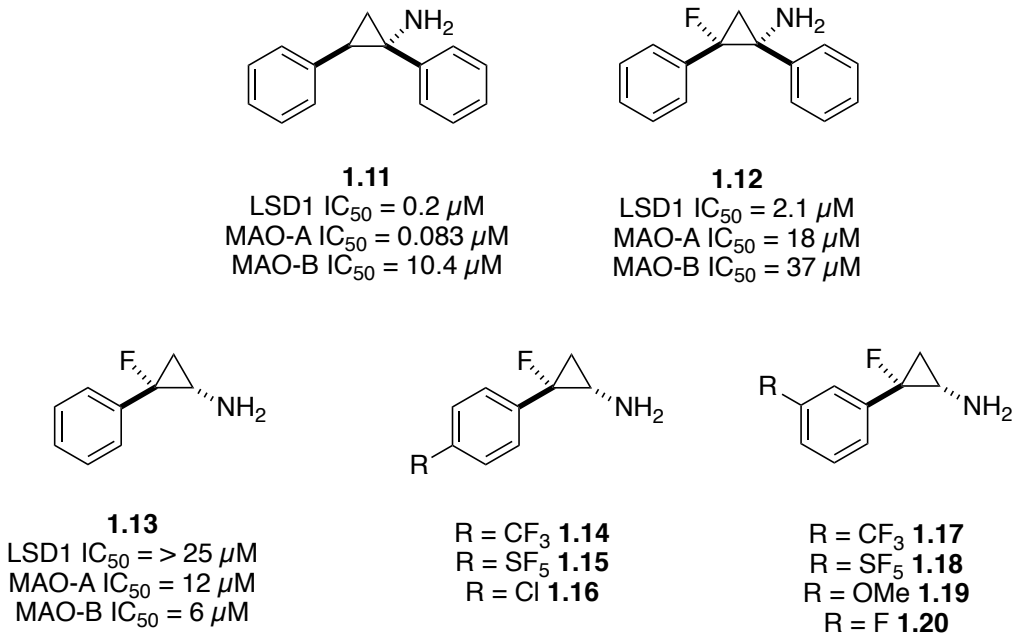

Figure 1.8. *Example of TCP analogues substituted at position C1 and C2 of the cyclopropyl ring.*[57,58]

A second approach to substitution of the cyclopropyl ring in TCP, is the formation of a spirocyclic group at the C2 position. Shi *et al.* recently published a series of such spirocyclic TCP derivatives.[59] Synthesis starts with 1-indanone (**1.21**) which undergoes conversion of the carbonyl to terminal alkene **1.22** in a Wittig reaction, before cyclopropanation with ethyl diazoacetate and a rhodium(II)acetate catalyst to give a mixture of *trans* and *cis* ethyl esters **1.23-*R*** and **1.23-*S***. The esters were then hydrolysed to the respective carboxylic acids **1.24-*R*** and **1.24-*S*** which could then be converted to the corresponding carbamates **1.25-*R*** and **1.25-*S*** via Curtius rearrangement (Figure 1.9A). The respective *R* and *S* enantiomers were then separated via flash chromatography before deprotection to give **1.25-*R*** and **1.25-*S*** as the HCl salts. Both **1.25-*R*** and **1.25-*S*** showed improved LSD1 inhibition, IC_{50} 0.17 and 0.78 μM respectively, and reduced MAO-A inhibition of >100 μM. This suggests that the conformational lock acts to enhance the inhibition of LSD1 and further increases selectivity over MAO-A. Further modification via *N*-alkylation resulted in LSD1 inhibitors with very low nm potency and good selectivity (Figure 1.9B).

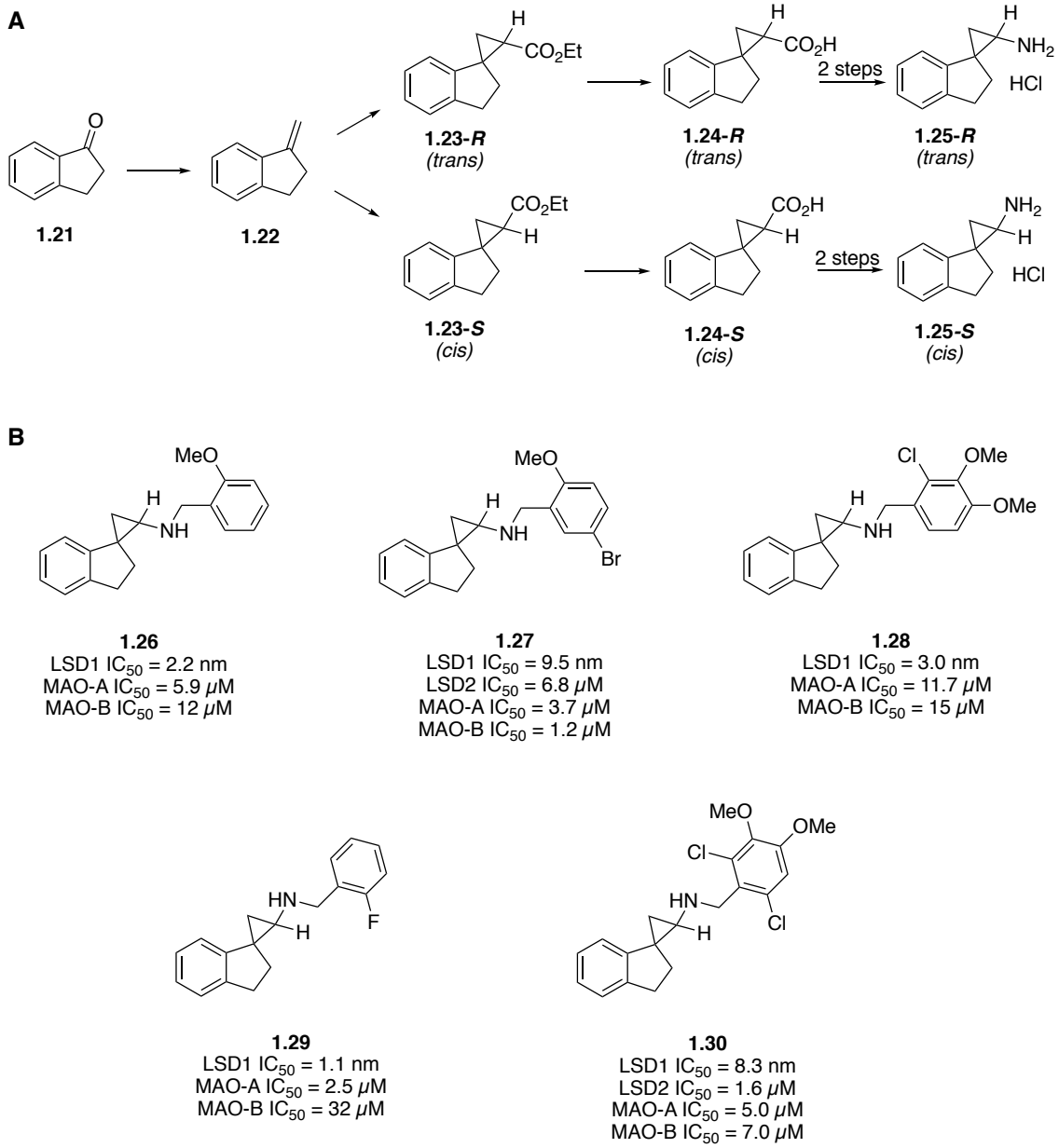

Figure 1.9. *(A) The synthetic route for the synthesis of spirocyclic TCP derivatives and (B) examples of N-alkylated analogues.*[59]

1.7. Irreversible LSD1 inhibitors in clinical trials.

Unlike the histone deacetylases (HDACs), LSD1 does not have a clinically approved drug available. There are however several clinical candidates presently undergoing clinical trials, mainly for the treatment of cancer. Clinicaltrials.gov (accessed January 2020) currently lists nine different LSD1 inhibitors in eighteen different studies. Five of these inhibitors are TCP derived inhibitors (including TCP itself), one is phenelzine, and two are reversible LSD1 inhibitors. In addition,

the EU Clinical Trials Register (accessed January 2020) currently lists two TCP derived irreversible LSD1 inhibitors in seven separate studies.

TCP itself is, at present, the subject of three clinical studies. All three studies are in combination with all-trans retinoic acid (ATRA) and one also incorporates the chemotherapy drug cytarabine. The vitamin A derivative, ATRA, has been used in cancer therapy for some time, mainly in the treatment of acute promyelocytic leukaemia (APL).[60] For the treatment of non-APL AML, ATRA alone has not seen much success, but in combination with other chemotherapy agents however, it showed some promise.[60,61] It was found that by inhibiting LSD1, H3K4me2 is upregulated which may reactivate the ATRA differentiation pathway in AML.[60,62] As a result, ATRA is commonly found being trialled in combination with many LSD1 inhibitors.

Phenelzine is listed in one recently completed study for the treatment of metastatic breast cancer in combination with chemotherapy drug paclitaxel.

Interestingly, all six TCP derived irreversible LSD1 inhibitors are *N*-alkylated (Figure 1.10, **1.31-1.35**). Of these six, two are also substituted at the benzene ring (Figure 1.10, **1.32** and **1.34**) but none are substituted at the cyclopropyl group. One of these five is quite unique in that the benzene ring itself has been substituted with a thiophene group (**1.36**).

The first LSD1 inhibitor to enter clinical trials was Oryzons so called ORY-1001 (**1.31**) in 2014 for the treatment of AML. In 2018 Oryzon published details of the structure and pharmacology of ORY-1001.[63] The compound is comprised of four stereocentres, the TCP moiety has *trans* (1*R*, 2*S*) stereochemistry with the amine *N*-alkylated to *trans-4*-cyclohexylamine. ORY-1001 inhibits LSD1 with an IC_{50} of 18 nM, SMOX at 7.4 μM and IL4I1, LSD2, MAO-A and MAO-B IC_{50} >100 μM. In cell, a THP-1 differentiation assay returned an EC_{50} <1 nM and also engaged enzymatically active LSD1 in THP-1 cells with an EC_{50} of 0.63 and 0.55 nM after 24 and 96 hours respectively. It is also claimed that ORY-1001 performs well *in vivo,* reducing tumor growth in MV(4;11) xenographs and increasing survival in rodent xenograft models of acute leukemia. In addition to ORY-1001, Oryzon also have a dual LSD1/MAO-B inhibitor in clinical trials, ORY-2001 (**1.32**) which they also identify as Vafidemstat. Unlike ORY-1001, Oryzon have not published the structure or pharmacological data for this compound but the structure is thought to be **1.32** (Figure 1.10), however the chirality is unclear.[64] Oryzen have put some

limited data on their website, oryzon.com (accessed January 2020), in which they disclose ORY-2001 to inhibit LSD1 and MAO-B with an IC_{50} of 100 and 75 nM respectively. They claim they have had positive results in 7 different animal models and *in-vitro* models and that ORY-2001 corrects the lack of sociability of aged SAMP8 mice. Studies outside Oryzon have also suggested the prevention of the development of cognitive impairment in SAMP8 mice[65] as well as complete rescue of memory in SAMP8 mice achieved at low doses.[66]

Imago BioSciences currently have INCB059872 listed in 3 trials. A terminated study for sickle cell disease, a second study recruiting for Relapsed Ewing Sarcoma and a third study in combination with ATRA, Azacitidine and Nivolumab for solid tumours and hematologic malignancy. Again, the structure is not clear but believed to be similar to **1.33**. No LSD1 inhibition data has yet been reported but at the 2016 AACR Annual Meeting, Lee *et al*. reported INCB059872 to be a potent, selective and orally bioavailable inhibitor of LSD1 through the formation covalent FAD-adducts. They also reported that a panel of SCLC cell lines was inhibited by INCB059782 with EC_{50} values between 47-377 nM but non-tumorigenic cells, such as IL-2 stimulated T cells from normal donors were much less sensitive with IC_{50} values >10 μM.[67] Imago BioSciences have a second compound also taking part in three clinical studies. IMG-7289 also identified as Bomedemstat, is listed as not yet recruiting in a study against thrombocythemia, recruiting for a second study against myelofibrosis, PPV-MF, PET-MF and PMF and a third complete study in combination with ATRA against AML and myelodysplastic syndrome. The exact structure has not as yet been divulged but is listed by the National Institute of Health website (nih.gov) as **1.34**. As expected of a TCP derived compound, IMG-7289 is an irreversible inhibitor of LSD1 which increases both H3K4 and H3K9 methylation. In addition IMG-7289 treated mice showed decreased platelet count, reticulocytes, monocytes and neutrophils as well as increased global H3K9me2 levels in bone marrow compared to control mice.[64]

TAK-418 is a compound developed by Takeda Pharmaceutical and currently is listed as recruiting for a study on healthy volunteers. The structure is undisclosed but possibly takes the form of **1.36** based on information from the National Institute of Health website (nih.gov). If this structure is accurate, then this compound is unique as a TCP derived LSD1 inhibitor as the benzene ring has

been replaced by a thiophene group. A patent taken out by Takeda lists **1.36** as inhibiting LSD1 with an IC_{50} value of <0.1 μM and an MAO-A and MAO-B IC_{50} >100 μM.[68]

In 2015, GlaxoSmithKline (GSK) published the structure and pharmacological data for three TCP derived compounds.[51] GSK2879552 (**1.35**), GSK-LSD1 (**1.37**) and GSK2699537 (**1.38**). Although they have not explicitly disclosed the chirality of the compounds it is assumed from the figures published that all three have (1*R*, 2*S*) chirality. GSK-LSD1 and GSK2699537 have not undergone clinical trials but GSK2879552 is currently listed in three studies. All three classed as terminated with results. The conditions studied included SCLC, AML in combination with ATRA and Myelodysplastic syndrome in combination with Azacitidine. GSK2879552 inhibits LSD1 with a K_i^{app} value of 1.7 μM and is also reported to be 280-fold selective over D-amino acid oxidase. In addition, inhibition of MAO-A and MAO-B was too weak to calculate either K_i^{app} or K_{inact} values. *In vitro,* GSK2879552 was tested against a panel of 165 human cancer cell lines. Although several different cancers showed sensitivity to growth inhibition, antiproliferation was mainly seen in SCLC and AML cell lines with 9/28 SCLC and 20/29 AML cell lines during the 6-day proliferation assay. In the sensitive cell lines, growth inhibition had EC_{50} values in the range 2-240 nM. Tumor growth inhibition (TGI) was measured in xenograph bearing mice to determine *in vivo* effects. H526, NCI-H1417, NCI-H510 and NCI-H69 tumor bearing mice showed TGI of 57, 83, 38 and 49 % repectively. In addition, one non-sensitive SCLC cell line, NCI-H2171, also showed partial TGI *in vivo*, suggesting broader activity profiles in SCLC *in vivo* than *in vitro.*[51]

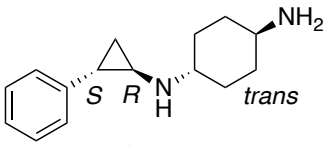

ORY-1001

1.31

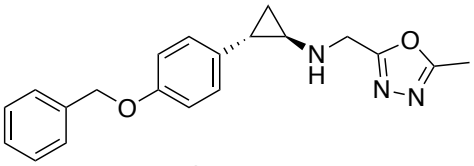

ORY-2001

1.32

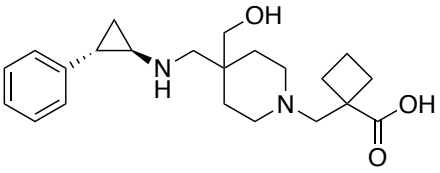

INCB059872

1.33

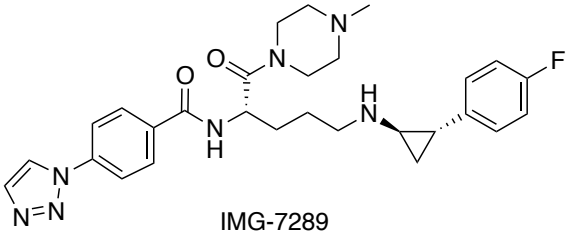

IMG-7289

1.34

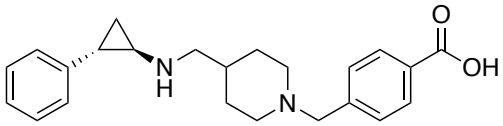

GSK2879552

1.35

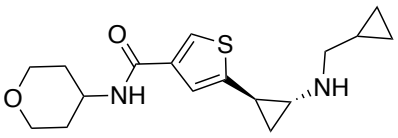

TAK-418

1.36

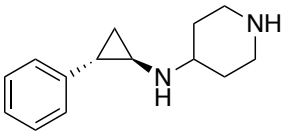

GSK-LSD1

1.37

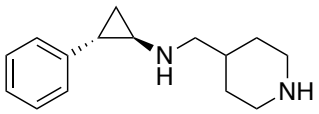

GSK2699537

1.38

Figure 1.10. *(1.31-1.36) Structures of TCP derived LSD1 inhibitors that have taken part in clinical trials. (1.37-1.38) Additional TCP derived LSD1 inhibitors developed by GSK alongside their clinical candidate.*

1.8. The zinc dependent histone deacetylases (HDACs).

As discussed, the reversible nature of lysine methylation was not established until 2004.[18] In contrast, the reversible enzymatic acetylation of histones was apparent over three decades earlier.[69,70,71] Acetylation of histones is carried out by the so called histone acetylases (HATs) which act by transferring an acetyl group to the histone from acetyl Coenzyme A (Figure 1.11). In addition, acetyl CoA can acetylate histones directly with no involvement from HATs. The reverse of this

process is carried out by a family of enzymes collectively known as histone deacetylases (HDACs). The level of acetylation within the cell is therefore due to the balance between these two opposing processes.

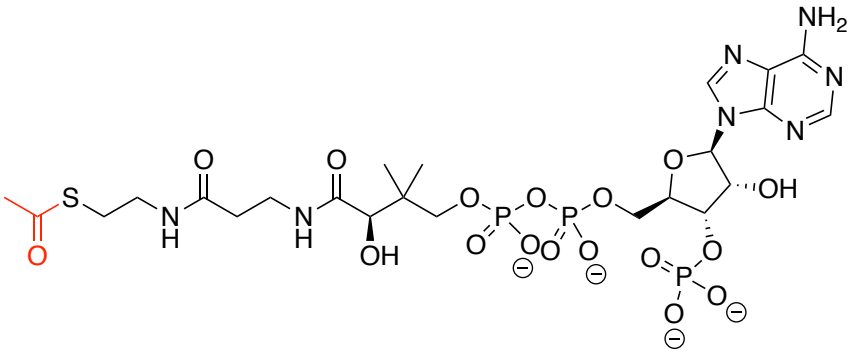

Figure 1.11. *Acetyl Coenzyme A.*

The acetyl group, highlighted in red, is transferred to the histone proteins by HDAC enzymes.

HDACs are part of an ancient protein superfamily comprised of the histone deacetylases, acetylpolyamine amidohydrolases and the acetoin utilisation proteins.[72] The eighteen known HDACs are then divided further into the sirtuins, which contain the cofactor NAD^+ in their active site, and the zinc-dependent HDACs. The latter is identified by the presence of a zinc(II) cation within the active site. The zinc-dependent HDACs are then classified further, into four classes based on their cellular function and DNA sequence similarity (Table 1.3).[73,74]
Various proposals for the catalytic mechanism of the zinc dependent HDACs has been in the literature for some time. In 1999, Finnin *et al.* proposed their model based on crystal structures of histone deacetylase-like protein (HDLP), HDLP-Zn^{2+} trichostatin A and HDLP-ZN^{2+}-SAHA complexes (Scheme 1.7).[75] This was followed with proposals by Vanommeslaeghe *et al.* and Corminboeuf *et al.* in 2005 and 2006 respectively.[76,77] In 2010, Bertrand reviewed these proposals and concluded that the available evidence supported the Vanommeslaeghe model.[78] However, Bertrand revisited this in 2016[79] and reviewed several other mechanistic studies that had since being carried out[80,81] thus showing that the details of the true mechanism have not yet being fully agreed on. That said, these mechanistic studies are more than sufficient models to allow the design of some highly potent inhibitors.

Class	Protein	Amino acids	Cellular function	Known Inhibitors
I	HDAC1	482	Cell survival and proliferation	Vorinostat, Panobinostat, belinostat, ITF2357, PCI-24781, FK288, entinostat, MGCD0103, trichostatin A, LAQ824, mocetinostat, pracinostat
I	HDAC2	488	Cell proliferation and insulin resistance	
I	HDAC3	428	Cell survival and proliferation	
I	HDAC8	377	Cell proliferation	
IIA	HDAC4	1084	Regulation of skeletogenesis and gluconeogenesis	Vorinostat, Panobinostat, belinostat, ITF2357, PCI-24781, trichostatin A, LAQ824, pracinostat
IIA	HDAC5	1122	Cellular development and differentiation, cardiovascular growth and function, gluconeogenesis.	
IIA	HDAC7	952	Thymocyte differentiation, endothelial function and glucogenesis.	
IIA	HDAC9	1011	HR, thymocyte differentiation, cardiovascular growth and function.	
IIB	HDAC6	1215	Cell motility and control of cytoskeletal dynamics.	Vorinostat, Panobinostat, belinostat, ITF2357, PCI-24781, trichostatin A, LAQ824, pracinostat
IIB	HDAC10	673	HR, autophagy mediated cell survival.	
IV	HDAC11	347	Immunomodulators-DNA replication.	Vorinostat, trichostatin, LAQ824, belinostat, IFT2357, mocetinostat, pracinostat

Table 1.3. *Classification of the zinc dependent HDACs, their cellular function and their known inhibitors.*

Table adapted from Suraweera et al. Table 1.[74]

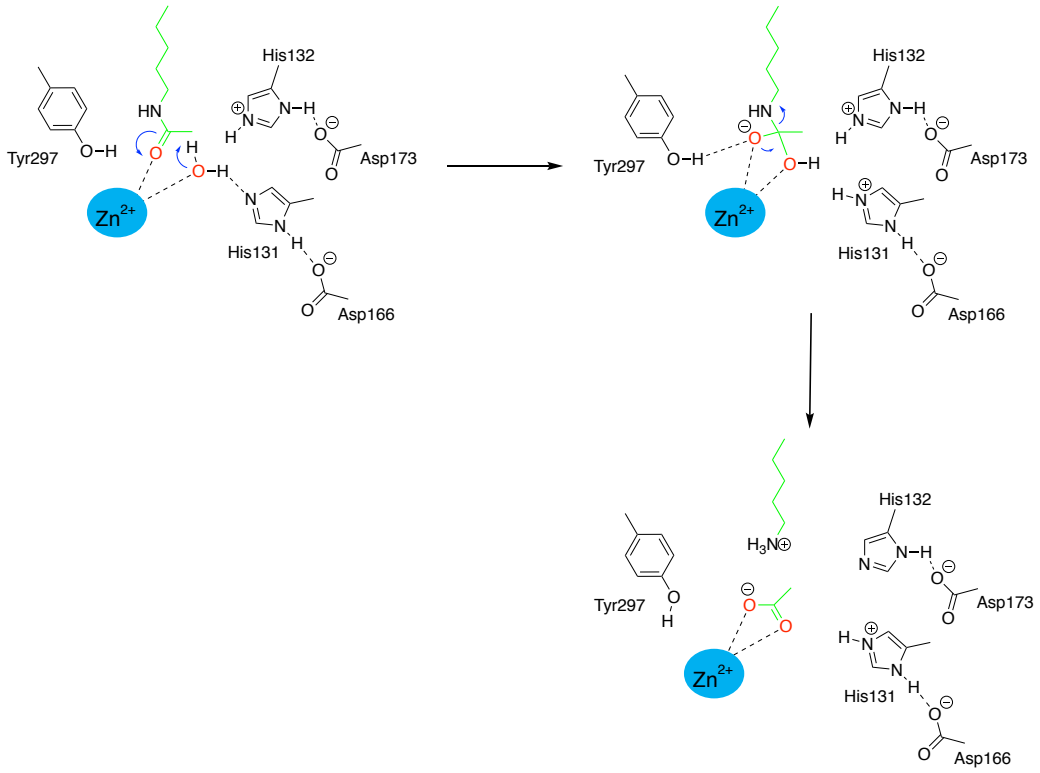

Scheme 1.7. *Deacteylation mechanism as put forward by Finnin et al.*[75]

1.9. Inhibitors of the zinc dependent HDACs.

X-ray structures of the HDAC active site have identified the structure as consisting of a deep, narrow tube-like pocket, ~11Å long. The walls of the pocket are covered with mainly hydrophobic and aromatic residues and the Zn cation cofactor is positioned at the bottom of the pocket. In addition, there is a cavity adjacent to this pocket which may provide a space for the diffusion of the removed acetate molecule away from the active site.[75] As such, the structure of HDAC inhibitors tend to consist of three main parts. A cap, which sits in a solvent exposed region, outside the narrow channel like pocket. A linker, that occupies the channel itself and a zinc binding group (ZBG), which chelates to the zinc cofactor at the heart of the active site (Figure 1.12). This model was studied further via HDAC-inhibitor crystal structures. Both suberoylanilide hydroxamic acid (SAHA) and the more potent trichostatin A (TSA), were studied in complex with HDLP. They found that both compounds form bidentate coordination to the zinc cofactor, make multiple van der Waals contacts along the tube-like hydrophobic portion of the pocket and the phenyl caps make contacts at the

entrance. The higher affinity of TSA over SAHA was attributed to the increased number of contacts in the hydrophobic channel and the better fitting cap. In addition, the reduced affinity of the SAHA cap may be due to the longer carbon chain of the linker making the separation between ZBG and cap larger. Also, reduced interaction between the linker and the pocket may be down to a lack of methyl group branches and the increased flexibility of the saturated chain.[75]

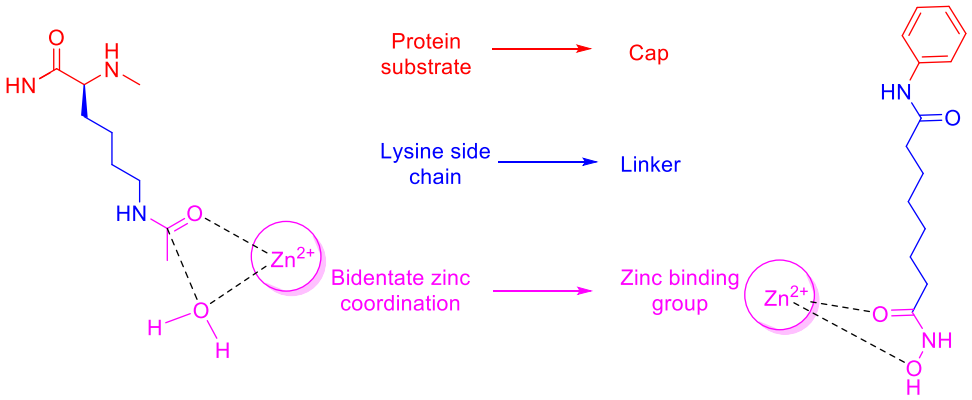

Figure 1.12. *The analogous nature of a typical HDAC inhibitor (SAHA) and its natural acetyllysine substrate.*

The early identification of HDACs as a drug target, relative to the demethylases, has led to the advanced development of their inhibitors. As such, there are currently five FDA approved inhibitors on the market as well as an additional inhibitor approved for use in china (Figure 1.13). An interesting feature of these approved inhibitors is the variety of both the zinc binding group and linker. Three of the six have a hydroxamate ZBG in addition to one thiol, one benzamide and one carboxylic acid. The hydroxamate is the most popular ZBG found in HDAC inhibitors throughout the literature due to its strong binding affinity with the HDAC zinc cation cofactor. However this strong binding interaction can also result in poor selectivity and off target side-effects due to the presence of other zinc dependent enzymes.[82]

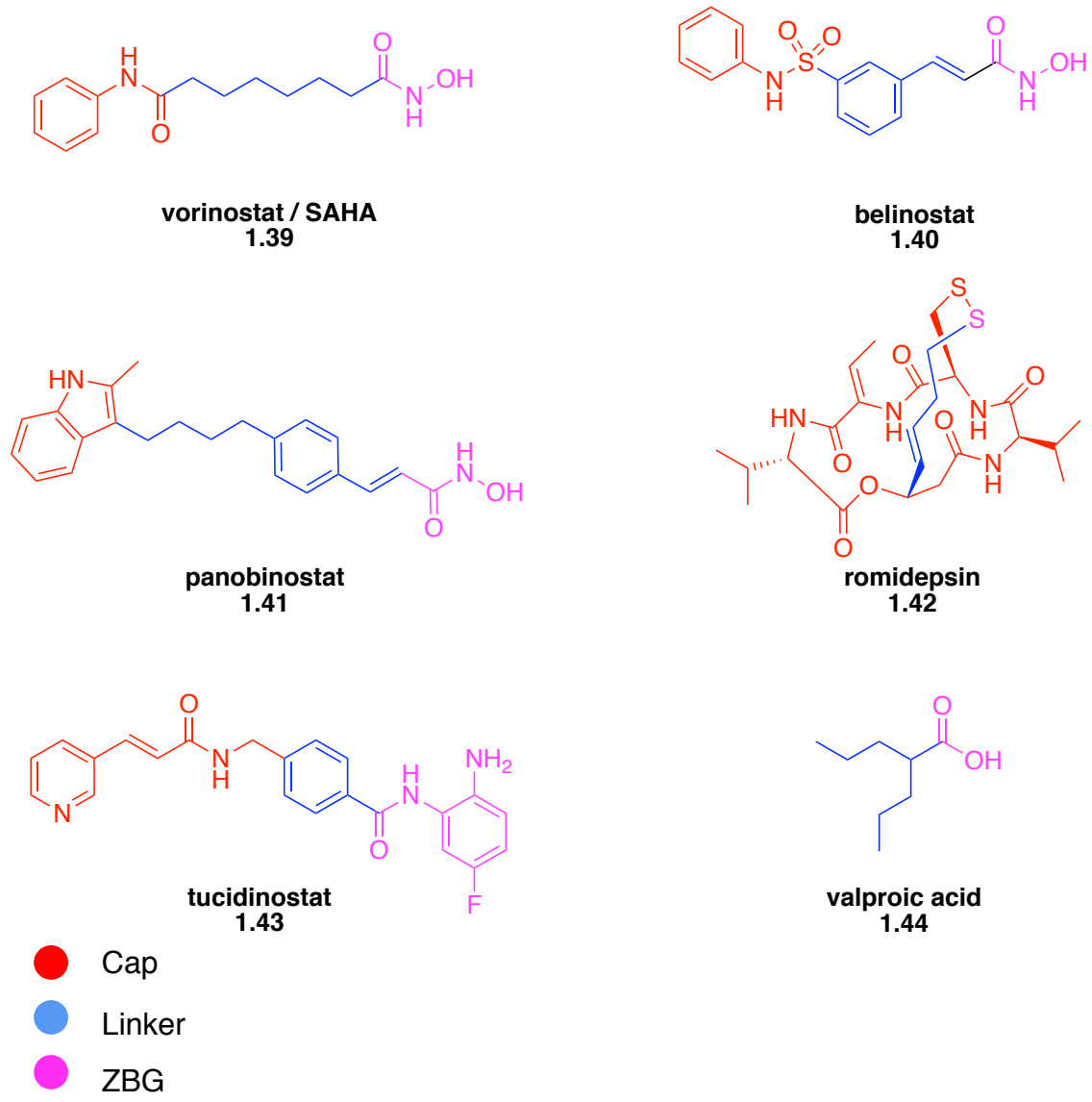

Figure 1.13. *Clinically approved HDAC inhibitors.*

Vorinostat, belinostat, panobinostat and romidepsin are FDA approved HDAC inhibitors. In addition, valproic acid is FDA approved for seizures but, although not approved for use as such, has been shown to weakly inhibit HDACs. Tucidinostat (formerly chidamide) is not FDA approved but is approved for use in China.

One way to address this selectivity issue is through modification of the linker/cap. This approach has seen success through the development of a number of isoform selective HDAC inhibitors. Tubacin is one such example. Reported by Haggarty *et al.* in 2003,[83] the structure is an analogue of SAHA with the addition of a large substituent to the *para* position of the benzene cap. This large cap is a mimic of the HDAC6 natural substrate, α-tubulin, and as such gives good selectivity over other HDAC isoforms (Figure 1.14).[84]

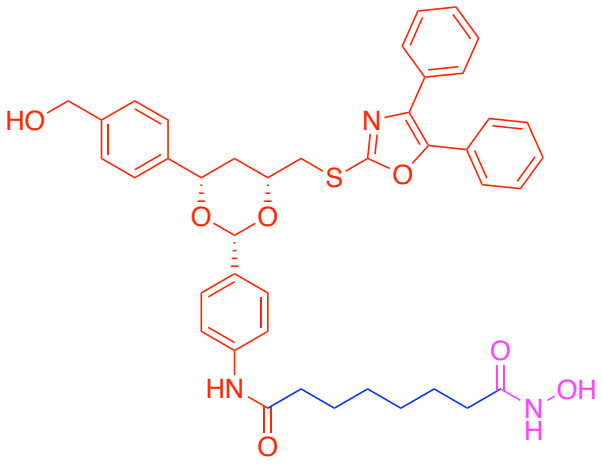

tubacin
1.45
HDAC6 IC_{50} = 0.004 μM
HDAC1-5, 7-11 IC_{50} = > 1.27 μM

Figure 1.14. *An example of how modification of a HDAC inhibitor cap can increase selectivity.*[83,84]

One further HDAC inhibitor of note is the clinical candidate ricolinostat (Figure 1.15), also known as ACY-1215 (**1.46)**. Ricolinostat has been the subject many of clinical trials for a number of different cancers including multiple myeloma, breast carcinoma, lymphoma and ovarian cancer. It is described as a potent HDAC6 inhibitor with an IC_{50} value of 4.7 nM in cell free enzymatic assays and shows more than 10-fold selectivity over the other class 1 HDACs, HDAC1, 2 and 3 with IC_{50} values of 58, 48 and 51 nM respectively. In addition, HDAC8 has an IC_{50} value of 100 nM and the remaining zinc dependent HDACs, 4, 5, 7, 9 and 11 > 1μM.[85]

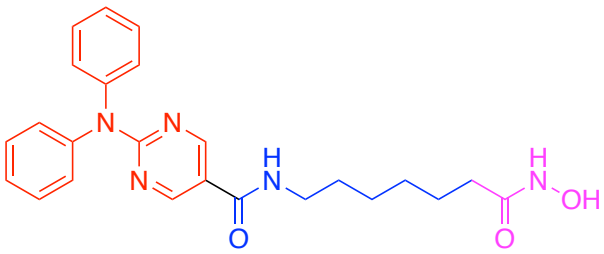

ricolinostat
1.46

HDAC1 IC_{50} = 58 nM
HDAC2 IC_{50} = 48 nM
HDAC3 IC_{50} = 51 nM
HDAC6 IC_{50} = 4.7 nM
HDAC8 IC_{50} = 100 nM
HDAC4, 5, 7, 9, 11 IC_{50} = > 1 μM

Figure 1.15 *Structure of ricolinostat.*

An additional example of improving isoform selectivity was reported by Balasubramaniam *et al.* in 2008 with their compound, PCI-34051 (**1.47**). The linker was modified from the long, chain like structure of SAHA and TSA to a short, planar aromatic linker. The result was > 200-fold selectivity for HDAC8 over HDAC1 and 6, and >1000 fold selectivity over HDAC2, 3 and 10 (Figure 1.16).[86]

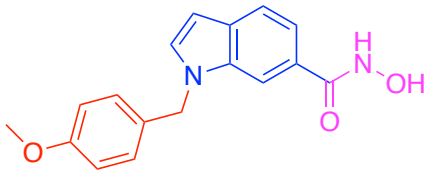

PCI-34051
1.47
HDAC8 IC_{50} = 0.01 μM
HDAC1 IC_{50} = 4 μM
HDAC2, 3 IC_{50} = > 50 μM
HDAC10 IC_{50} = 13 μM

Figure 1.16. *An example of how linker modification can increase HDAC isoform selectivity.*[86]

While these modifications to the cap and linker address selectivity between HDAC isoforms, they do not solve the problem of off-target effects due to the strong affinity of hydroxamic acids for metal ions. The obvious solution to this is to change the ZBG, although this comes with the penalty of weaker binding to the zinc ion and therefore a potentially less potent inhibitor. Common substitutions include benzamides and thiols. In addition, several examples of carboxylic acids can be found but due to the relatively weak binding of the carboxylic acid to the HDAC zinc cofactor, these are less prevalent.

The benzamide group are the most common choice after the hydroxamic acids. They have the advantage of being largely selective for class 1 HDACs and the increase in selectivity would also suggest a decrease in off-target effects. Tucidinostat (**1.43**) is currently approved for use against relapsed and refractory PTCL by the Chinese Food and Drug Administration (CFDA) but not yet by the FDA (Figure 1.13, Table 1.4). However, at the time of writing, tucidinostat is listed in 59 clinical studies (ClinicalTrials.gov). In addition, there are several analogues of tucidinostat also taking part in clinical trials (Figure 1.17). Entinostat (**1.48**), mocetinostat (**1.49**) and tacedinaline (**1.50**) are currently listed in 67, 22 and 3 clinical studies respectively.

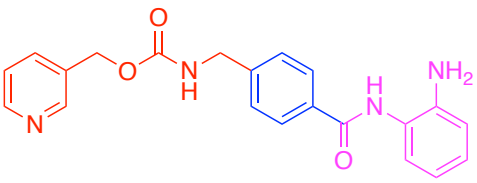

entinostat
1.48
HDAC1 IC_{50} = 0.022 μM
HDAC2 IC_{50} = 0.065 μM
HDAC3 IC_{50} = 0.36 μM

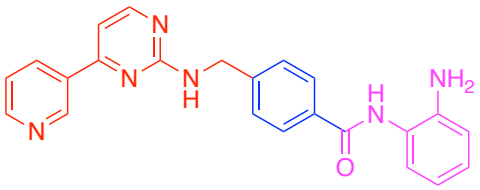

mocetinostat
1.49
HDAC1 IC_{50} = 0.009 μM
HDAC2 IC_{50} = 0.034 μM
HDAC3 IC_{50} = 0.265 μM

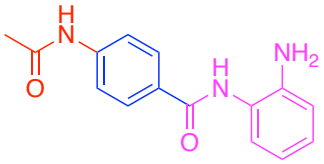

tacedinaline
1.50
HDAC1 IC_{50} = 0.09 μM
HDAC2 IC_{50} = 0.09 μM
HDAC3 IC_{50} = 0.120 μM
HDAC8 IC_{50} = > 20 μM

Figure 1.17. *Examples of HDAC inhibitors with a benzamide ZBG.*[84]

Isoform	IC_{50} (μM)					Valproic acid (mM)
	Vorinostat	Belinostat	Panobinostat	Romidepsin	Chidamide	
1	76	18	3	0.8	95	0.7
2	360	34	13	1.0	160	0.8
3	58	21	2	1.3	67	1
8	>1000	160	280	26	733	-
4	>1000	>1000	200	470	>30000	1.5
5	160	76	8	>1000	>30000	1
7	>1000	600	530	>1000	>30000	1.3
9	78	44	6	>1000	>30000	-
6	27	15	11	330	>30000	>20
10	88	31	2	0.9	78	>20
11	110	44	3	0.3	432	-

Table 1.4. *IC_{50} values of FDA/CFDA approved HDAC inhibitors.*[87–90]

The thiol zinc binding motif is somewhat less explored and many of the examples found in the literature are centred around replacement of the hydroxamic acid of SAHA with a thiol group and then modifying the cap to increase selectivity.[91–93] A more original use of thiols as ZBGs are found in the depsipeptides. Romidepsin, also known as FK228 and FR901228, is one such example of this class of inhibitor. A natural product isolated from the *Chromobacterium violaceum* bacterium, romidepsin was first reported in 1994 as a novel anti-tumor agent.[94] In 1998 it was reported as the first example of a class 1 natural product HDAC inhibitor.[95] Later, it was shown by Cole *et al.* using the x-ray structure of a HDAC8-largazole thiol complex, that the disulfide romidepsin is in fact the pro-drug and the inhibitory species is the free thiol which is reached following reduction of the disulphide bridge (Figure 1.18).[96] In 2009, romidepsin was given FDA approval for use in CTCL and then PTCL in 2011. It remains the only approved depsipeptide HDAC inhibitor and is currently listed in 99 clinical studies (ClinicalTrials.gov).

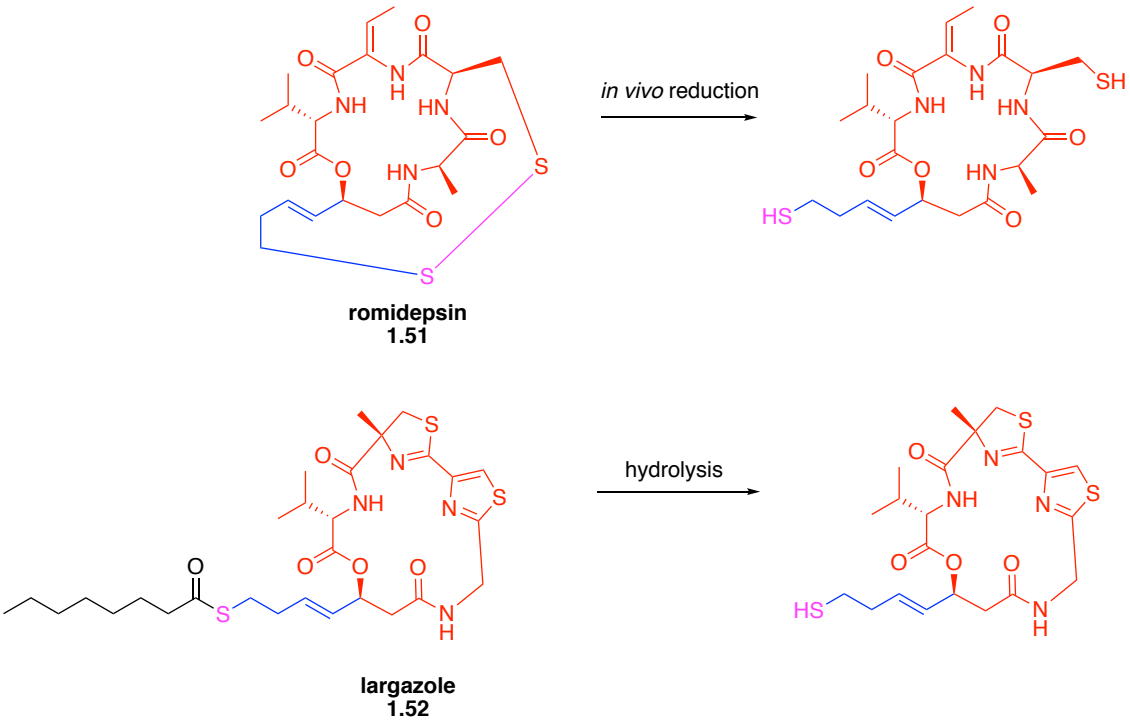

Figure 1.18. *The structure of the depsipeptide, romidepsin and the thioester, largazole along with their reduced/hydrolysed structures.*[96]

Largazole is a cyclic depsipetide isolated from Symploca sp. It shares a portion of its core structure with romidepsin and hydrolysis in vivo releases the free thiol which acts as a ZBG in HDACs. Largazole is a potent HDAC inhibitor in its own right and a number of analogues with impressive potency and antiproliferative effects have been developed.[97,98]

The relatively weak binding affinity of carboxylic acids as a ZBG has resulted in little investigation of carboxylic acids as potential HDAC inhibitors. The most studied are the short chain fatty acids, Valproic acid (**1.44**), butyric acid (**1.53**) and phenylbutyrate (**1.54**) (Figure 1.19). All have been identified as weak HDAC inhibitors (mM levels of activity) but due to their anti-proliferative/anti-cancer effects they have been well studied for a number of years.[99] Other carboxylic acids identified include the natural products chlorogenic acid (**1.55**) and caffeic acid (**1.56**) (Figure 1.19). HDAC inhibition activity In HeLa nuclear extracts revealed IC_{50} values of 375 μM and 2.54 mM for **1.55** and **1.56** respectively.[100]

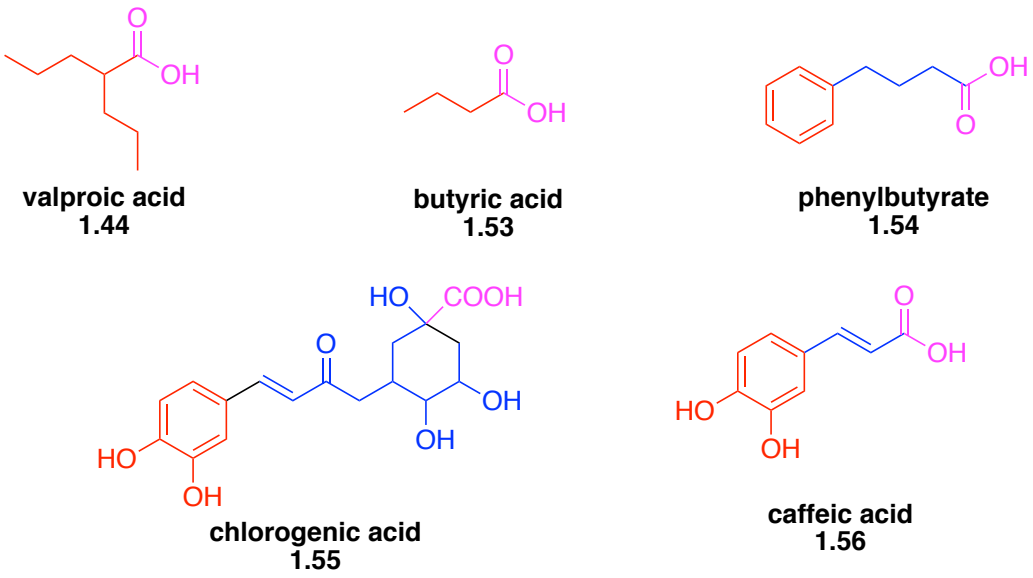

Figure 1.19. *Examples of HDAC inhibitors containing a carboxylic acid ZBG.*

1.10. Introduction summary and thesis aims.

This introduction has given an overview of the topic of epigenetics as well as the enzymes responsible for lysine demethylation and histone deacetylation. It has also given a brief summary of the main inhibitors of these enzymes developed to date and details of any current clinical activity.

The following chapters will describe the design, synthesis and biological activity of some novel epigenetic inhibitors of both LSD1 and the zinc dependent HDACs. Each chapter will comprise a brief introduction covering any required detail not covered above.

The synthesis of all compounds was carried out in large part by myself, the author, and those that were not, were carried out by undergraduate project students under my supervision. The biological data was gathered in collaboration with several other researchers. All HDAC assays and virtual docking studies were carried out by Dusan Ruzic of the Nikolic group, University of Belgrade. The LSD1 assays were run by Roman Belle of the Kawamura group at the university of Oxford. The THP-1 cell viability assays presented in Chapter two (compounds **2.8a-g**) and all compounds in Chapter four were carried out by Gabriela Burianova of the O'Connell group, UEA. All other biological testing was carried out by Ipek Bulut of the Acilan Ayhan group, Koc University, Istanbul.

The aim of this work is to contribute to and broaden the understanding of the field of epigenetic drug development in the area of LSD1 and HDAC inhibition.

Chapter Two

2. A series of novel LSD1 inhibitors based on GSK2879552.

2.1. Introduction

In 2015, GlaxoSmithKline (GSK) reported a series of three LSD1 inhibitors (**1.35**, **1.37**, **1.38**, Figure 1.10), disclosing both structure and biological activity data. Amongst them was GSK2879552 (**1.35**), described by GSK as a potent, selective, orally available, bioactive, mechanism based inactivator of LSD1. Following an extensive cell proliferation assay on 165 different cancer cell lines it was determined that both AML and SCLC cell lines displayed the highest sensitivity.[51] Subsequently, GSK2879552 has been the subject of several clinical trials for both AML and SCLC along with high risk myelodysplastic syndromes. The structure of GSK2879552 includes a carboxylic acid functional group. This carboxylic acid allows for simple, one step conversion to other functional groups and, along with its strong biological profile, makes GSK2879552 a good starting point for the development of a novel LSD1 inhibitor.

The LSD1 active site is a large cavity, ~23 Å from its entrance to the core of the catalytic site, and 1245 $Å^3$ in volume. The left-hand side of the cavity consists of mostly hydrophobic residues while the right-side is much more acidic and lined with backbone carbonyl oxygen atoms. The FAD cofactor is found in the catalytic core, the N5 nitrogen atom of which is hydrogen bound to lysine residue K661 by a conserved water molecule. A point mutation of K661 eliminates all demethylation activity of LSD1, thus demonstrating its vital role.[101]

The large size of the LSD1 active site gives plenty of scope for the design of its inhibitors. Given both the potency and selectivity of GSK2879552 it stands to reason that any changes should be minor in order to conserve/improve upon these features. To this end, we have designed and synthesised a series of seven potential LSD1 inhibitors based on GSK2879552 by modifying the carboxylic acid functional group to an alkylated amide. The following chapter presents the synthesis and biological activity data gathered thus far.

2.2. The synthesis of GSK2879552.

Before any modification could be made to GSK2879552, it first needed to be synthesised in sufficient quantity. GSK2879552 can be purchased commercially but the high cost made this option inaccessible. In order to determine a synthetic route, the original patent containing GSK2879552[102] was consulted and in conjunction with a retrosynthetic analysis (Figure 2.1), two routes were selected to try. Route **A** (Scheme 2.1) is the longest of the two, containing six steps in total. The first is a reductive amination with commercially purchased tranylcypromine (**1.2**) and Boc-protected carboxaldehyde **2.1** to give **2.2**. Protection of the secondary amine to form a trifluoroacetamide affords **2.3** before removal of the Boc group to allow the resulting **2.4** to undergo S_N2 displacement with **2.5** to give ester **2.6**. Removal of the trifluoroacetamide group restores the secondary amine, **2.7a**. Finally, ester hydrolysis affords the target product, racemic *trans*-GSK2879552, **1.35**.

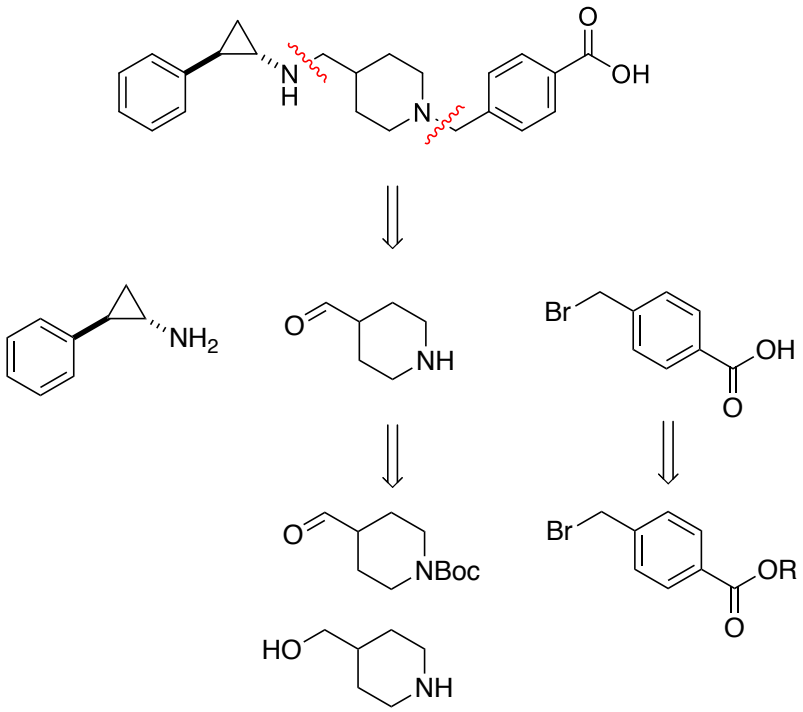

Figure 2.1. *Retrosynthetic analysis of GSK2879552.*

GSK2879552 can be disconnected into three smaller subunits which, in turn, can be further amended to give the desired commercially available synthons.

Route **B** (Scheme 2.1) is a shorter, four step synthesis starting with an S_N2 reaction between bromomethyl ester **2.5** and piperidinemethanol **2.9** to give **2.10**.

Oxidation of the primary alcohol to an aldehyde then affords **2.11**, before reductive amination with TCP gives the methyl ester **2.7** which is then hydrolysed to the target product, **1.35**.

Route A

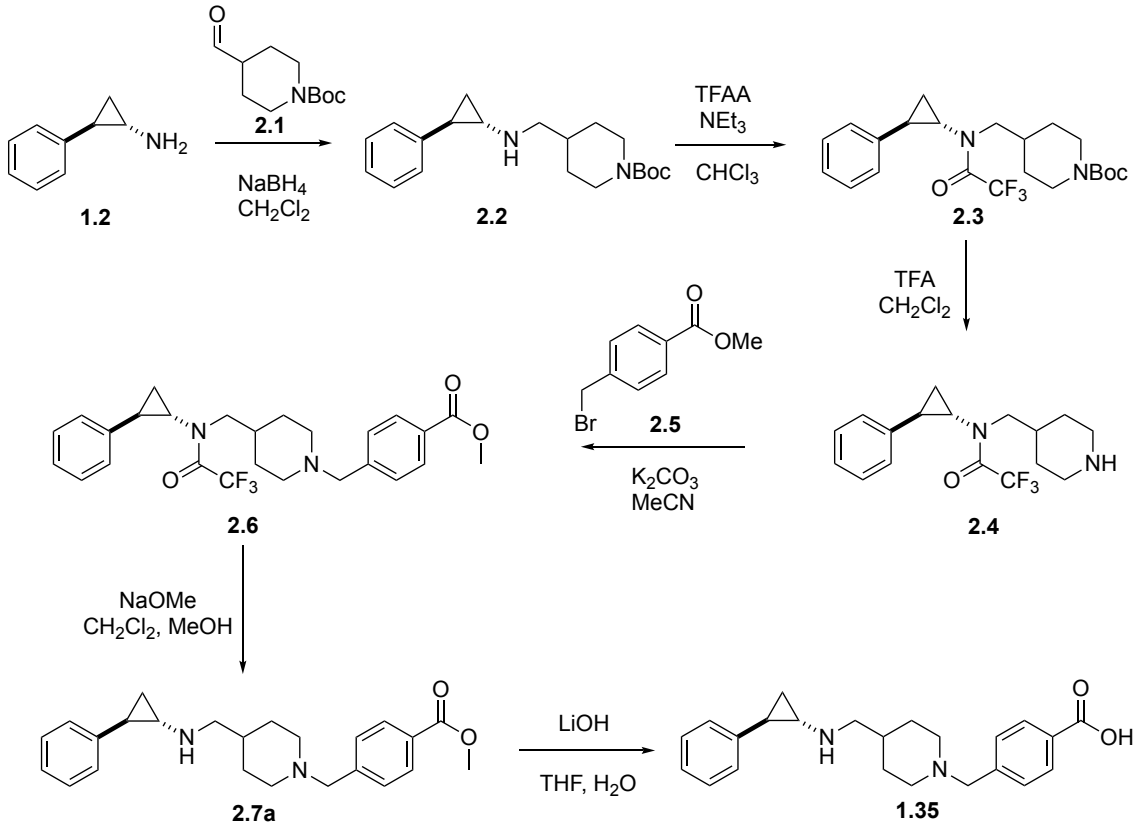

Route B

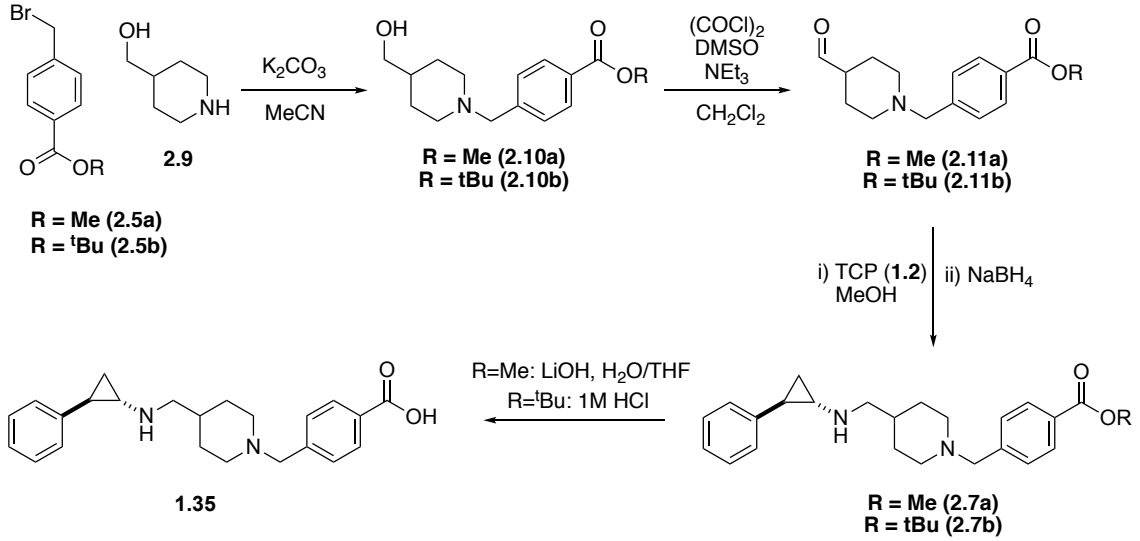

Scheme 2.1. *Possible synthetic routes to the target product, trans-GSK2879552 (**1.35**).*

Although route **A** is two steps longer than route **B**, two of those steps are deprotections which are expected to give high yields. In addition, the potentially low yielding reductive amination step is at the beginning of the synthesis and as such, allows for a larger scale reaction to negate that loss. There is also no need to carry out the oxidation of the primary alcohol to an aldehyde which was identified as another potentially low yielding step.

The positives to route **B** are the reduced number of reactions required and although the reductive amination is late in the synthesis, this would mean less TCP which is by far the most expensive reagent.

The first steps of both these routes were carried out in parallel. Initially, reductive amination was attempted using the HCl salt of TCP however, solubility issues ultimately led to the reaction being unsuccessful. Subsequently, TCP.HCl was neutralised with 4M NaOH and the solution extracted with dichloromethane to give the free base TCP in almost quantitative yield. Reductive amination was again attempted with the free base TCP and **2.1**. Three fractions were isolated following workup and purification by flash chromatography, but none of them were consistent with the expected product **2.2**. The literature was consulted for an alternative method which resulted in the trial of reductive amination in the presence of Titanium(IV) isopropoxide.[103] $Ti(O^iPr)_4$ acts as a Lewis acid, coordinating to the aldehyde, activating it and promoting imine formation. The imine is then reduced with an appropriate hydride (Scheme 2.2). The reaction was carried out on a 600 mg scale, with respect to TCP and afforded a 36% yield.

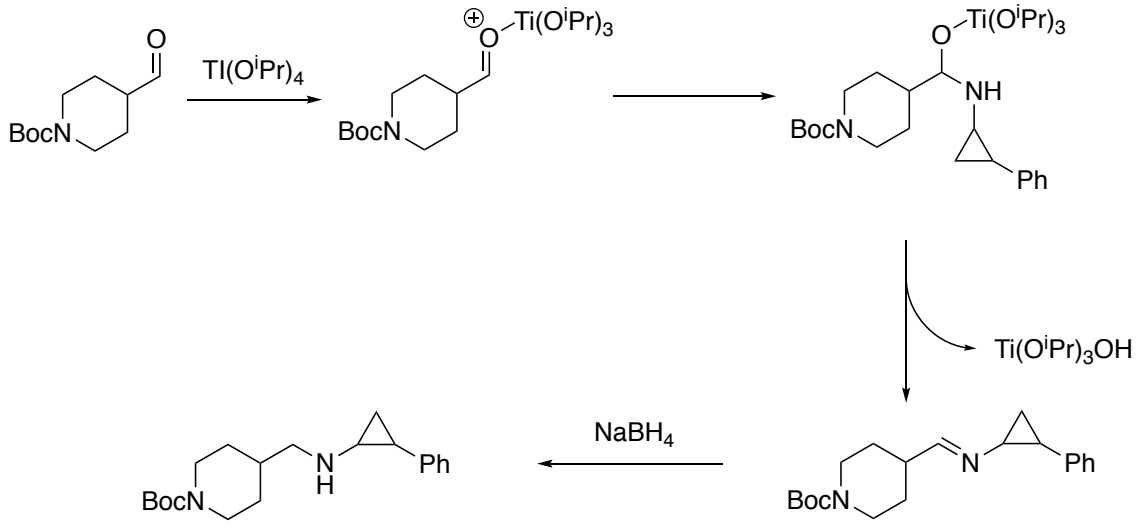

Scheme 2.2. *Mechanism for Ti(IV) isopropoxide promoted reductive amination.*

In contrast to the first step of route **B**, the S_N2 reaction between **2.5** and **2.9** worked very well. The reaction is carried out in acetonitrile in the presence of potassium carbonate at reflux over 2 hours. Following a simple acid-base work-up, **2.10** was isolated in 83% yield and can be used in subsequent steps without further purification. Given the large disparity in yield of this first step, the reduced number of overall steps and the relative expense of using TCP in the large quantities required, it was decided to follow route **B** only from this point on.

The second step of Route **B** is the oxidation of primary alcohol **2.10** to aldehyde **2.11**. The method used in the GSK patent was Swern oxidation and has an associated yield of 55%. Given the moderate yield we decided to try some other methods of oxidation in an attempt to improve it (Table 2.1). Three other methods were trialled; pyridinium dichromate (PDC), tetrapropylammonium perruthenate (TPAP) and Dess-Martin periodinane (DMP). These reactions resulted in 5, 30 and 55 % yields respectively. As the best yield, using DMP, was equal to the reported yield using Swern oxidation and the relatively high expense of DMP as a reagent, we decided that Swern oxidation should be tried. The result was the expected 55% yield which was improved in subsequent reactions to consistently > 80%. The improvement was found by ensuring each reagent was dissolved in dichloromethane and cooled to -78 °C prior to addition to the reaction mixture.

Reagent	Yield (%)
PDC	5
TPAP/NMO	30
DMP	55
Swern oxidation	>80

Table 2.1. *Relative yields achieved in each oxidation reaction on primary alcohol **2.10**.*

The next step was reductive amination of TCP to aldehyde **2.11**, but on small scales (<1 g) we struggled to get this step to work following the patent method. This method requires that, following imine formation and reduction, the diluted reaction mixture is extracted with dichloromethane and the combined extracts washed with a 10 % solution of aqueous acetic acid. Brine is then poured slowly

into the resulting organic phase and ester **2.7** should precipitate out of the solution. On the scales described this was never observed and **2.7** had to be painstakingly isolated by other methods. However, on larger scales the method worked well and **2.7** was isolated in low to moderate yields of ~35 %. This was lower than the 62 % yield stated in the patent, but it was noted that the patent method uses the *tert*-butyl ester. Our choice to use the methyl ester was based on cost and it was not anticipated that a change in ester would affect the yield so considerably. Given the high cost of TCP it seemed counterproductive to save a small amount of money on the ester only to lose more on the loss of TCP and so we switched to the *tert*-butyl analogue in subsequent reactions. The change had the desired effect and the reductive amination step realised an improved yield of 66 %. In addition, the subsequent base catalysed hydrolysis of the methyl ester, to afford carboxylic acid **1.35**, resulted in a 41 % yield and required purification via flash chromatography. However, removal of the *tert*-butyl group by heating in 1M aqueous HCl gives the dihydrochloride salt of **1.35** in 69 % yield, high purity and no requirement for additional purification steps.

2.3. The synthesis of a novel LSD1 inhibitor (compound 2.8a).

Once the synthesis of GSK2879552 is complete, the modification to the novel LSD1 inhibitor, **2.8a**, can be achieved in a single step (Scheme 2.3). Amide coupling is a common method for the conversion of a carboxylic acid to an amide and there are a range of coupling agents available to facilitate this reaction.[104] The reagent of choice in this case was 1-Ethyl-3-(3dimethyl aminopropyl)carbodiimide (EDC) catalysed by hydroxybenzotriazole (HOBt), based on previous successes with this reagent in coupling reactions. **2.8a** was isolated in 32% yield following purification on both silica and C18 reverse phase columns. It should also be noted that prep-HPLC was used subsequent to this in order to achieve the desired level of purity, and yield following this was not calculated.

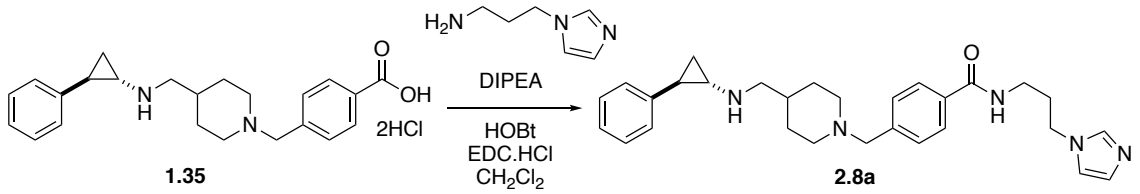

Scheme 2.3. *The synthesis of novel LSD1 inhibitor **2.8** from GSK2879552.*

2.4. The biological evaluation of compound 2.8a.

2.4.1. LSD1 Inhibition.

The enzymatic activity of compound **2.8a** was evaluated in a cell free assay in order to determine the level of LSD1 inhibitory activity. The activity was determined alongside GSK2879552, as a positive control, and **3.13** (described in chapter 3) as a negative control (Figure 2.2, Table 2.2).

Compound **2.8a** was found to have an IC_{50} value of 0.063 μM (pIC_{50}: 7.20). This compares favourably to the positive control, GSK2879552, which had an IC_{50} value of 1.80 μM (pIC50: 5.74±0.23). Negative control **3.13** performed as expected and was not active at these concentrations (< 5 μM). It should be noted that **2.8a** was only evaluated over one replicate and hence these results should be treated with caution until such time that a repeat assay can be performed.

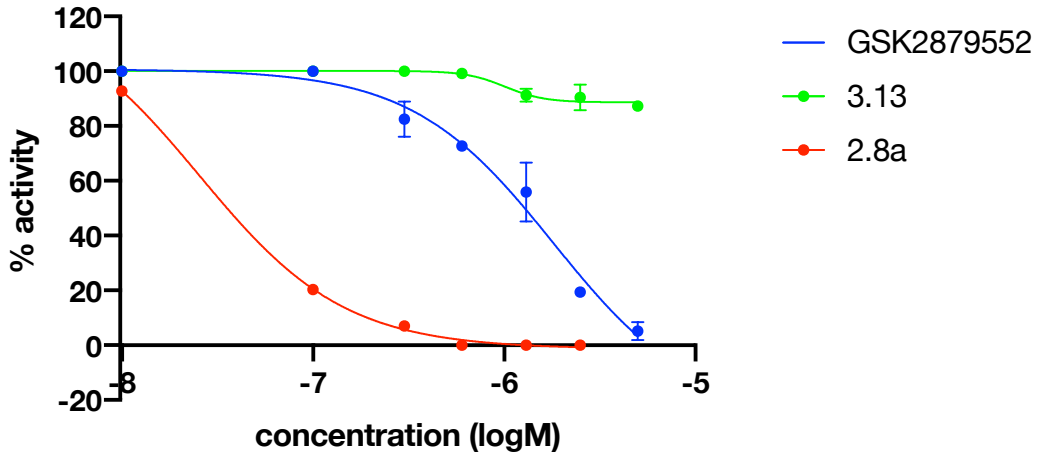

Figure 2.2. *Graphical representation of the LSD1 cell free assay results for **2.8a** along with control compounds.*

GSK2879552: Data shown as % activity ± Std. Error, n=3.
*Compound **2.8a**: Data shown as % activity, n=1.*
*Data for GSK2879552 and **3.13** generated by Belle et al., Oxford University (unpublished).*
*Data for **2.8a** generated by Bulut et al., Koc University (unpublished).*

Compound	LSD1 pIC_{50}
2.8a	7.20
GSK2879552	5.74±0.23
3.13	< 5.30

Table 2.2. *pIC_{50} data recorded for **2.8a** and control compounds.*

2.4.2. Cellular Thermal Shift Assay (CETSA)

Protein stability is the thermodynamic equilibrium in which a protein reversibly and rapidly unfolds and folds. This stability is the difference in the Gibbs free energy (ΔG) of the proteins folded (G_f) and unfolded (G_u) states.

$$\Delta G_u = G_u - G_f$$

The larger the difference between the folded and unfolded states, i.e. the larger and more positive ΔG_u, the more stable the protein.

As Gibbs free energy can be defined as:

$$\Delta G = \Delta H - T\Delta S$$

where H is the enthalpy of the system, S is the entropy and T the temperature, an increase in temperature will lead to a decrease in ΔG and hence the protein will become unstable and denature.

CETSA[105] takes advantage of this property of proteins and uses it to directly measure the target engagement of drugs within the cellular environment. Cells are treated with the appropriate drug and then heated. If the drug binds effectively to the target protein, the stability of the protein is increased and hence the higher the temperature required to destabilise and denature that protein (Figure 2.3).

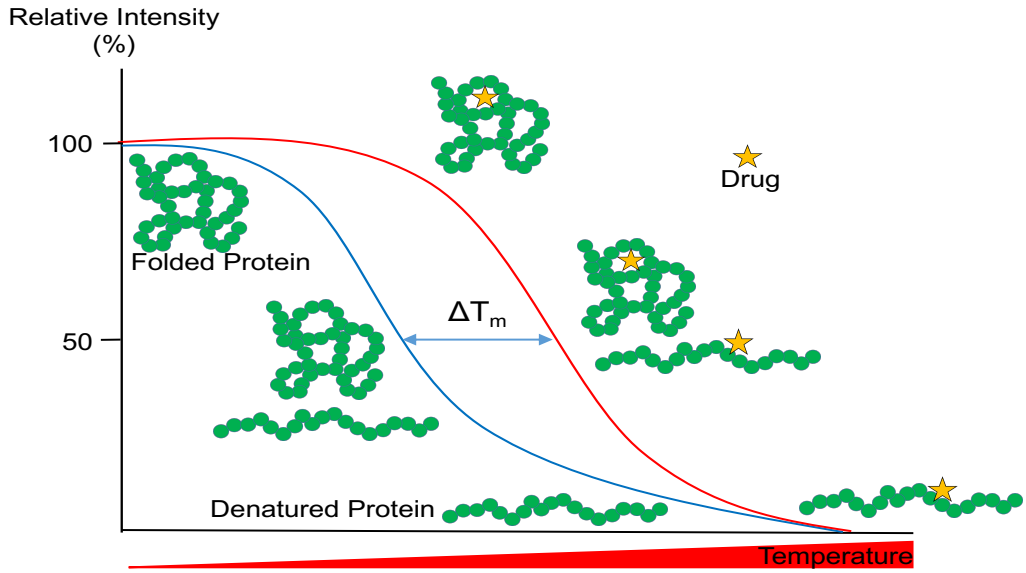

Figure 2.3. *Graphical representation of the effect of ligand binding on the thermal degradation of proteins.*

THP-1 cells were treated with 500 nM of compound **2.8a** and the response measured using western blot (Figure 2.4). Increased stability was noted in both GSK2879552 and compound **2.8a** relative to no inhibitor, with **2.8a** showing slightly better target engagement than GSK2879552.

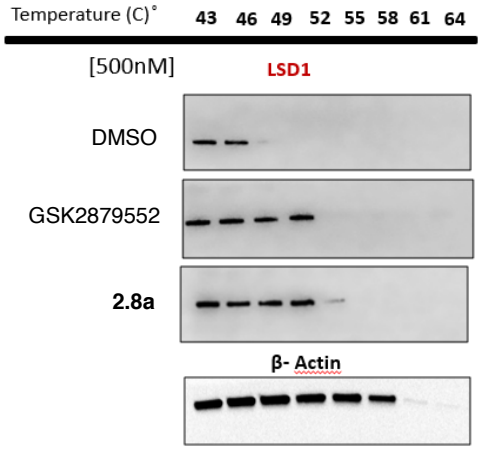

Figure 2.4. *Western blot of CETSA on **2.8a** controls.*
Data generated by Bulut et al., Koc University (unpublished).

These data are consistent with good target engagement between LSD1 and our inhibitor **2.8a**.

2.4.3. Leukaemia cell viability.

Given the promising response of compound **2.8a** in a cell free assay and evidence of target engagement, the next step was to test the pharmacological effect in cell. As discussed in section 1.7, GSK2879552 was assessed by GSK in 29 AML cell lines and found to be sensitive in 20. Given this high ratio of sensitivity it was logical to test compound **2.8a** activity in leukaemia cell lines. Two MLL fusion cell lines, THP-1 and MOLM-13, along with two non-fusion cell lines, K-562 and JURKAT, were tested in a cell viability assay. GSK2879552 was used as a control.

The results of this assay (Table 2.2, Figure 2.5) showed that although all cell lines displayed sensitivity to compound **2.8a**, it showed superior activity in the fused cell lines over the non-fused and in particular, MOLM-13. MLL is known to be a member of a much larger protein supercomplex of which LSD1 is also a component.[106] It is also a member of an elongation factor RNA polymerase II (ELL) complex which contains positive transcription elongation factor (p-TEFb) components that are known to interact with both AF9 and AF4 fusion partners.[107] In addition, LSD1 has been shown to act on genomic loci bound by MLL-AF9 to sustain expression of the onco gene and preventing differentiation and apoptosis.[108] This gives a good clue as to why these fused cell lines seem to show sensitivity to LSD1 inhibition.

Another point of note is the activity of compound **2.8a** relative to GSK2879552. Compound **2.8a** outperformed GSK2879552 in all cells showing >10 fold better activity in THP-1 and almost 90 fold increase in MOLM-13.

	MLL-AF9 Fused		**Non-MLL Fused**	
	THP-1 IC_{50} (μM)	**MOLM-13** IC_{50} (μM)	**K-562** IC_{50} (μM)	**JURKAT** IC_{50} (μM)
GSK2879552	>20	15.0 ± 3.5	>20	>20
2.8a	1.8 ± 0.4	0.17 ± 0.01	7.6 ± 0.3	10.2 ± 1.7

Table 2.3. *Cell viability data of **2.8a** in examples of fused and non-fused cell lines.*

Data shown as % cell viability ± stdp, n=3
Data generated by Bulut et al., Koc University (unpublished).

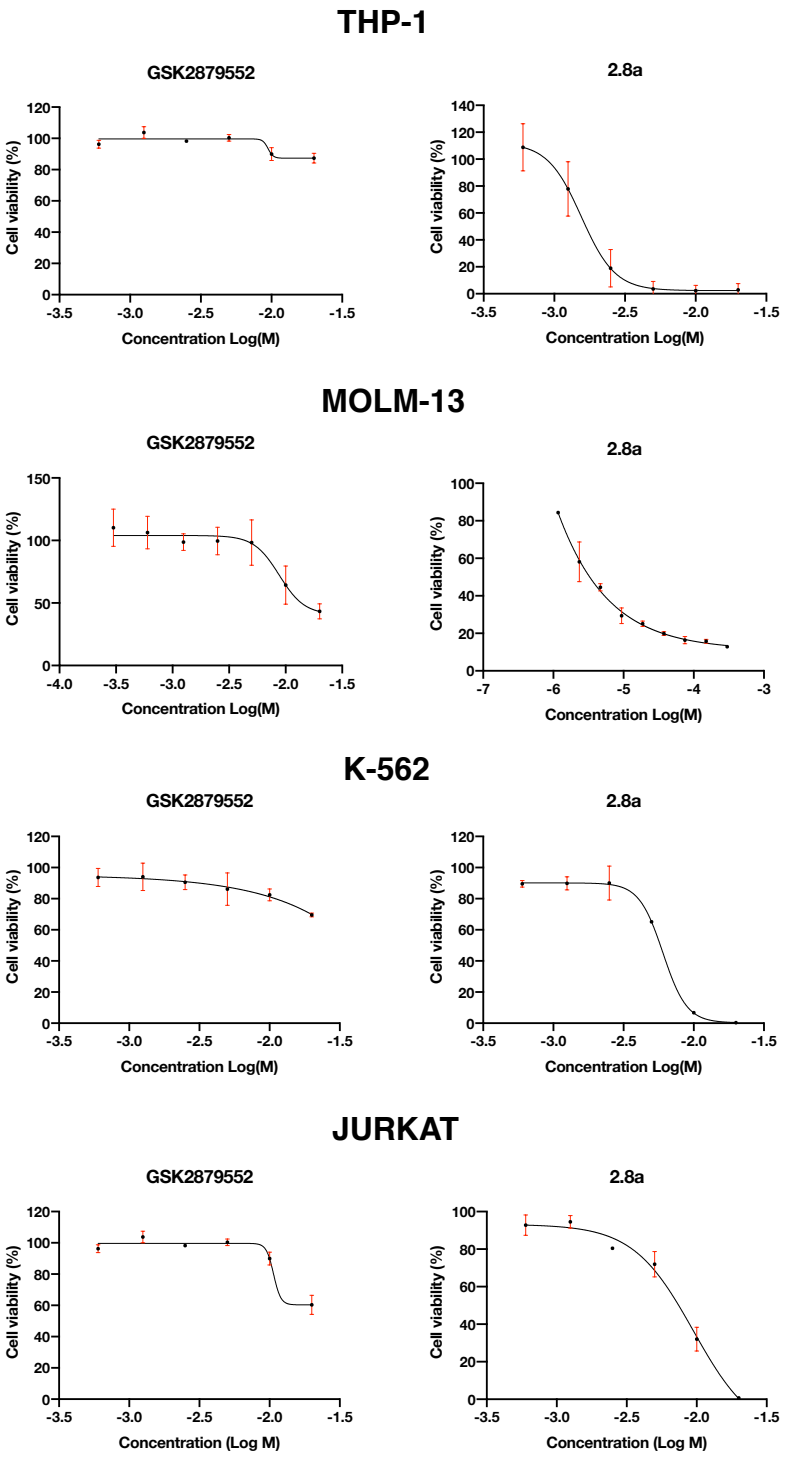

Figure 2.5. *Graphs of cell viability in fused and non-fused cell lines, comparing GSK2879552 and 2.8a.*

Data shown as % cell viability ± stdp, n=3
Data generated by Bulut et al., Koc University (unpublished).

2.4.4. Methylation fold change in response to inhibition.

As the overexpression of LSD1 would be predicted to decrease histone methylation levels, its inhibition would therefore be expected to cause an increase. To this end, H3K4me2 levels were measured using western analysis in both THP-1 and MOLM-13 cells over 24 hours using a 2 μM dose of the appropriate inhibitor and total histone H3 as a control (Figure 2.6).

In THP-1 cells both GSK2879552 and **2.8a** seeded cells showed highest H3K4me2 levels at 18 hours before decreasing back to baseline levels after 24 hours. In contrast, H3K4me2 levels peaked after 24 hours in MOLM-13 cells seeded with **2.8a** and showed a 2.8-fold increase, slightly better than GSK2879552 which showed a 2.2-fold increase (Figure 2.7, Table 2.3).

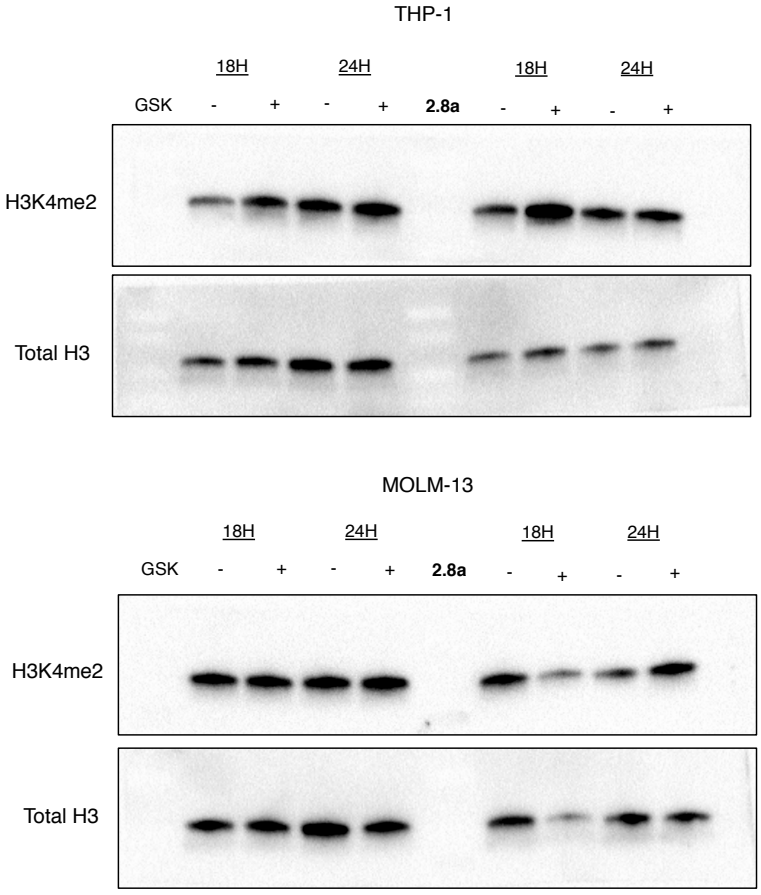

Figure 2.6. *Western blot of H3K4me2 levels measured at 18 and 24 hours in response to inhibition with GSK2879552 and **2.8a** in THP-1 and MOLM-13 cells.*
Data generated by Bulut et al., Koc University (unpublished).

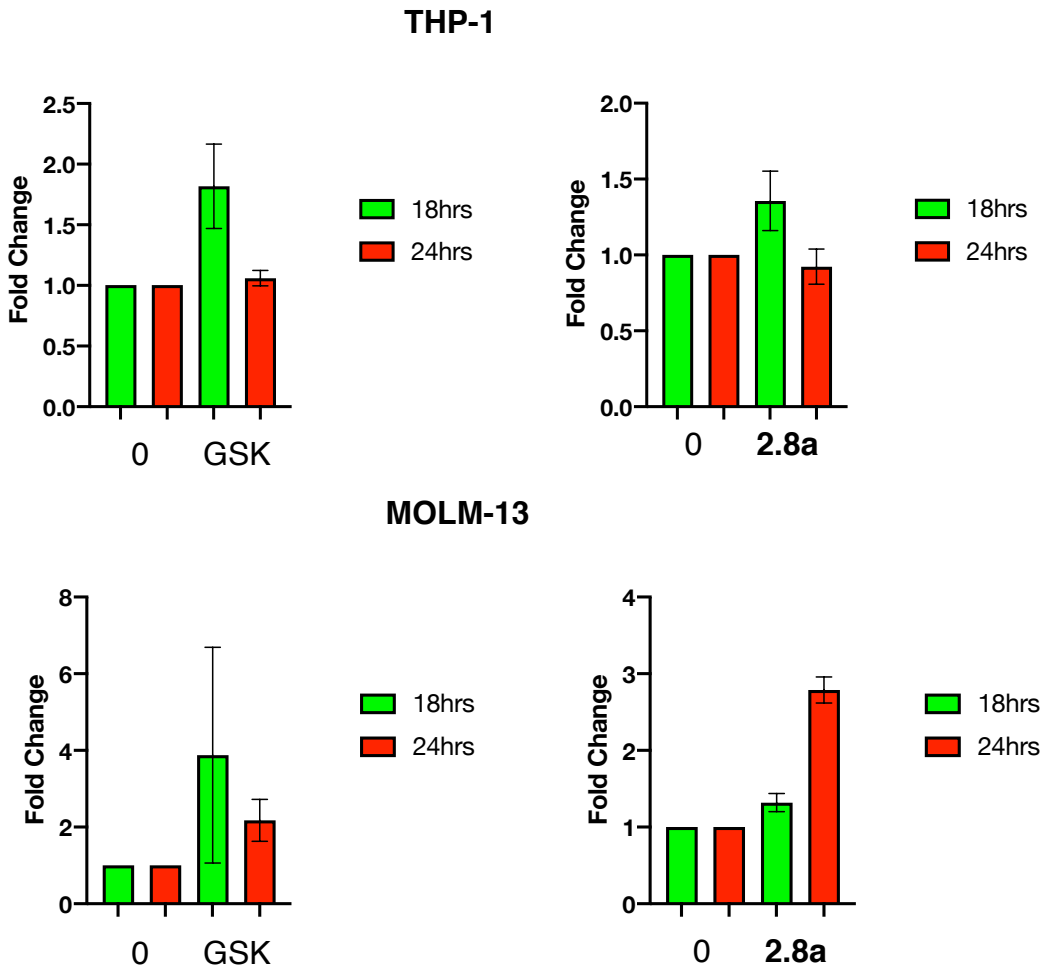

Figure 2.7. *H3K4me2 levels measured over 18 and 24 hours in response to inhibition with GSK2879552 and **2.8a** in THP-1 and MOLM-13 cells.*

Data shown as H3K4me2 fold change ± stdp, n=2
Data generated by Bulut et al., Koc University (unpublished).

Time (hrs)	THP-1		MOLM-13	
	GSK2879552	**2.8a**	GSK2879552	**2.8a**
18	1.81±0.34	1.35±0.19	3.87±2.81	1.31±0.11
24	1.06±0.06	0.92±0.11	2.17±0.54	2.78±0.16

Table 2.4. *Tabulated data of H3K4me2 levels in response to LSD1 inhibition with GSK2879552 and **2.8a** in THP-1 and MOLM-13 cells.*

Data shown as H3K4me2 fold change ± SD, n=2
Data generated by Bulut et al., Koc University (unpublished).

2.4.5. Gene expression changes.

To further investigate the effect of out inhibitor, compound **2.8a**, on the inhibition of LSD1, the expression of biomarkers CD86 and CD11b was measured in THP-1 cells. Both CD86 and CD11b gene expression are repressed in the presence of LSD1 and it has been shown that when LSD1 expression is inhibited, both CD86 and CD11b are upregulated. As such, they can be used as biomarkers to demonstrate LSD1 inhibition in cell.[109,110]

The expression of CD86 and CD11b were measured in THP-1 cells in the presence of 0.5 and 1.0 μM concentrations of GSK2879552 and **2.8a** relative to unexposed cells (Table 2.4, Table 2.5, Figure 2.8).

As expected, the exposure of both GSK2879552 and **2.8a** to THP-1 cells resulted in elevated levels of both CD86 and CD11b in all concentrations. CD86 expression increased around 25-fold in the presence of both GSK2879552 and **2.8a** at a concentration of 0.5 μM and a 43 and 57-fold increase was seen from GSK2879552 and **2.8a** respectively at 1.0 μM. CD11b expression increased 6-fold and 9-fold at concentrations of 0.5 and 1.0 μM respectively in the presence of GSK2879552 and increased a further 10-fold at both concentrations on exposure to **2.8a**.

Compound	**CD86 Fold Change**		
	0 μM	**0.5 μM**	**1.0 μM**
Neg Ctrl (**3.13**)	1.0±0.0	1.1±0.4	1.0±0.6
GSK2879552	1.0±0.0	27.2±3.5	43.4±16.8
2.8a	1.0±0.0	25.3±31.6	57.1±22.3

Table 2.5. *CD86 expression levels in THP-1 cells on inhibition of LSD1.*

Data shown as CD86 level fold change ± stdp, n=2
Data generated by Bulut et al., Koc University (unpublished).

Compound	CD11b Fold Change		
	0 μM	**0.5 μM**	**1.0 μM**
Neg Ctrl (**3.13**)	1.0±0.0	2.1±1.6	2.7±1.3
GSK2879552	1.0±0.0	6.8±3.9	9.3±5.0
2.8a	1.0±0.0	16.9±6.6	19.1±5.8

Table 2.6. *CD11b expression levels in THP-1 cells on inhibition of LSD1.*

Data shown as CD11b level fold change ± stdp, n=2
Data generated by Bulut et al., Koc University (unpublished).

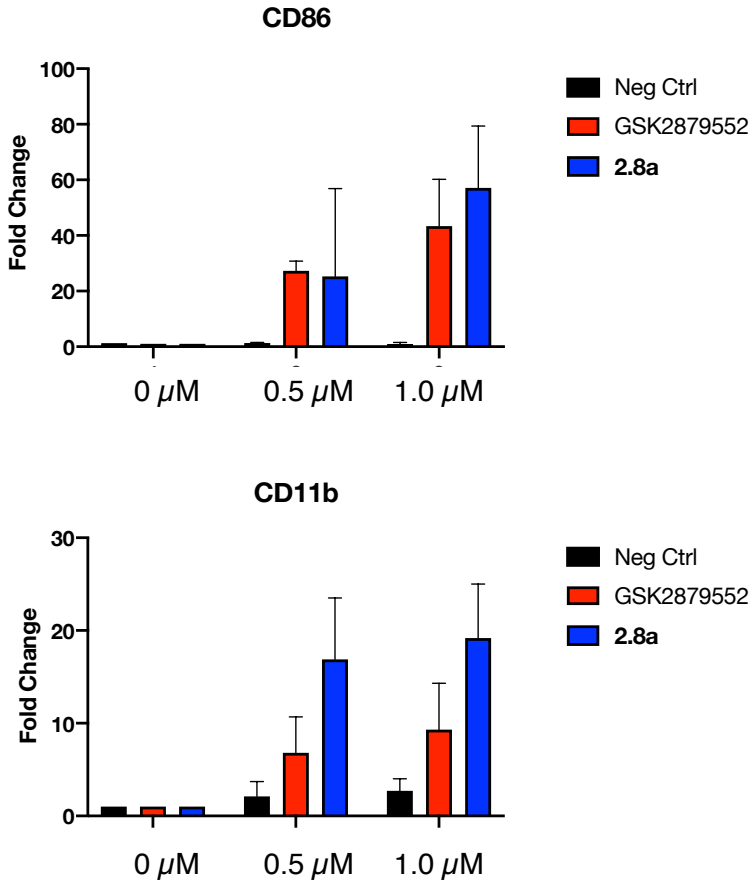

Figure 2.8. *Graphical representation of CD86 and CD11b expression levels in THP-1 cells in response to inhibition with GSK2879552, **2.8a** and a negative control.*

Data shown as CD86 and CD86 level fold change ± stdp, n=2
Data generated by Bulut et al., Koc University (unpublished).

2.4.6. Synergy of 2.8a with other known anti-cancer drugs.

The treatment of cancer via combination therapy is an important and well-established tool in modern cancer therapy.[111] Cancer drugs are often highly toxic and the development of resistance to treatment is a common problem. Combining drugs therefore has a number of advantages. They can improve efficacy and delay the onset of drug resistance.[112] In addition, there are examples of drug combinations reducing toxicity such as those that act by being antagonistic for normal cells and protecting them, while still exhibiting a toxic affect in cancerous cells.[113] One further advantage is that the cost of treatments can be reduced through combining new drugs with cheaper, already approved ones.

However, the effect is not always a positive one and it is important to note that while the additive effects of combining drugs can have a positive result, for example through the antagonistic effect mentioned, this additive effect can also act to increase toxicity.[114] For example both trastuzumab and doxorubicin are cardiotoxic and their synergistic effects translate into increased cardiotoxicity relative to each individual drug. The aim then is to find a combination with a high therapeutic index in which the toxicity to cancer cells is much greater than to normal cells.

Compound **2.8a** was tested in combination with four known anti-cancer drugs; cytarabine, cisplatin, paclitaxel and doxorubicin (Figure 2.9) all of which have been used in the treatment of leukaemia. Synergy was tested by investigating the effect of each drug both individually and in combination with **2.8a** in a cell viability assay.

THP-1 cells were treated with **2.8a** (1.25 μM) over 72 hours followed by co-treatment with the additional anti-cancer agents over 48 hours. Co-treatment with cytarabine (0.6 μM) and cisplatin (1.25 μM) showed no synergistic effects with **2.8a**. However, both paclitaxel (3 μM) and doxorubicin (0.06 μM) showed good synergistic effects, reducing cell numbers by 50 and 70 % respectively at this dose.

For comparison, the effect of GSK2879552 was also tested in combination with doxorubicin and also showed good synergistic effect, reducing the number of live cells by 87 %. This suggests that in terms of synergistic effects with doxorubicin, our modification of GSK2879552 is of no additional benefit. Testing with

GSK2879552 in combination with the other anti-cancer agents should now be carried out to determine if the modification made is stopping synergy.

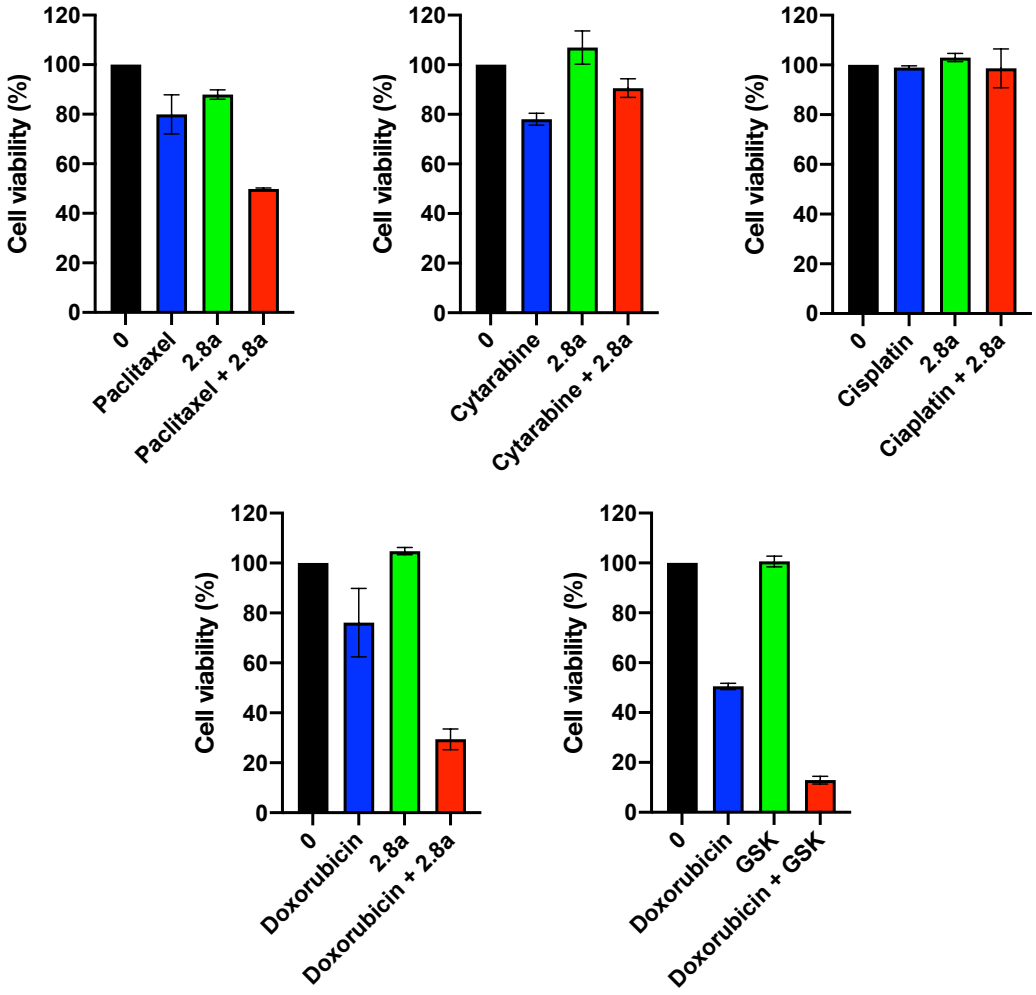

Figure 2.9. *Cell viability of THP-1 cells inhibited with combinations of **2.8a** and other known anti-cancer agents.*

Data shown as % cell viability ± stdp, n=2
Data generated by Bulut et al., Koc University (unpublished).

2.4.7. Inducing apoptosis.

The term apoptosis was coined in 1972 in a paper by Kerr *et al.* to describe the mechanism of programmed cell death.[115] It is the cells natural response to damage and prevents the proliferation of faulty cell's and the legacy of mutated DNA. The process of apoptosis is complex, involving multiple signalling pathways, proteins and protein regulators, including the caspases. The caspases are a family of proteases which take part in the process of apoptosis. The classic apoptosis pathway consists of a cascade of these caspase enzymes ending with the downstream 'effector' or 'executioner' caspases, caspase-3, -6 and -7.[116] As such, the activation of both caspase-3 and caspase-7 can be used a tool for the detection of apoptosis.

A further method of apoptosis recognition is the Annexin V binding assay. Cell membranes contain the phospholipid, phosphatidylserine (PS), which faces into the cytosol of the cell. During early apoptosis, the asymmetry of the cell membrane is lost, and PS is exposed to the outer surface of the cell in order to facilitate recognition and removal of the dying cell via phagocytosis. In the presence of Ca^{2+}, hapten labelled annexin V has a high affinity for PS and hence allows for the detection of apoptotic cells.[117] This cell labelling is again a good tool for identifying cells which are undergoing apoptosis.

The deregulation of the apoptosis pathway is considered to be one of the hallmarks of cancer.[118] It is the goal therefore of many cancer treatments to reinstate this pathway and trigger apoptosis in tumour cells.

To test whether our compound, **2.8a**, induces apoptosis in cancer cells, THP-1 cells were exposed to **2.8a** both on its own and in combination with doxorubicin and the apoptosis profiles determined using both caspase-3/7 (Table 2.6, Figure2.10, Figure 2.11) and annexin V assays (Table 2.7, Figure 2.12, Figure 2.13).

Caspase-3/7 assay

At a concentration of 1.25 μM, **2.8a** did not show any significant change in the apoptosis profile relative to uninhibited cells while doxorubicin, at a concentration of 60 nM, induced apoptosis in around 17% of cells. The largest difference was seen when a combination of **2.8a** and doxorubicin was used, showing the proportion of apoptotic cells to be around 60 %.

Inhibitor	% Population			
	Live	Apoptotic	Apoptotic/Dead	Dead
No Inhibitor	95.65±0.9	0.30±0.05	3.48±1.03	0.58±0.18
doxorubicin	66.63±8.58	7.06±4.46	22.85±5.55	3.14±1.43
GSK2879552	95.20±0.00	1.00±0.05	3.62±0.07	0.17±0.12
GSK + dox	54.05±0.85	14.62±0.77	31.00±0.05	0.32±0.02
2.8a	96.08±0.88	0.40±0.20	2.40±0.40	1.13±0.68
2.8a + dox	26.90±8.15	7.04±5.94	62.30±3.25	3.76±1.04

Table 2.7. *The apoptosis profile data of doxorubicin and **2.8a** both individually and in combination in THP-1 cells measured using caspase activation.*

Data shown as %population ± stdp, n=2.
Data generated by Bulut et al., Koc University (unpublished).

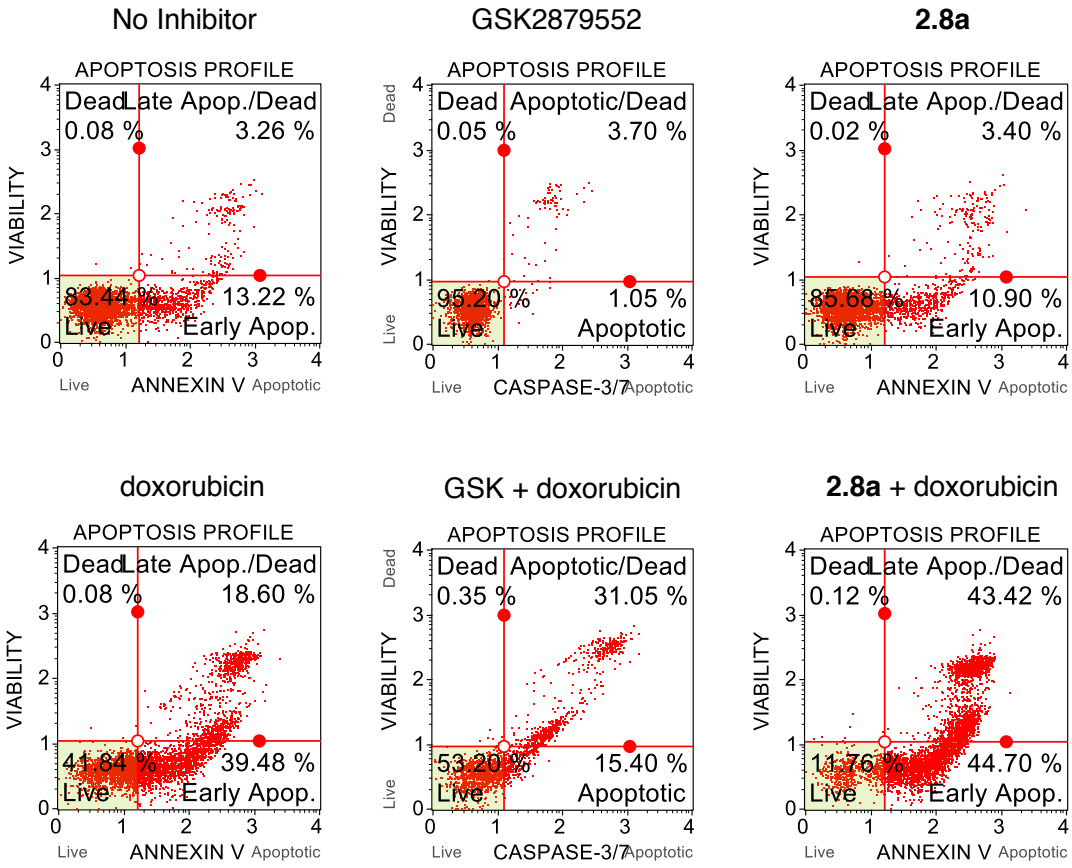

Figure 2.10. *Apoptosis profiles for 2.8a and doxorubicin in THP-1 cells.*

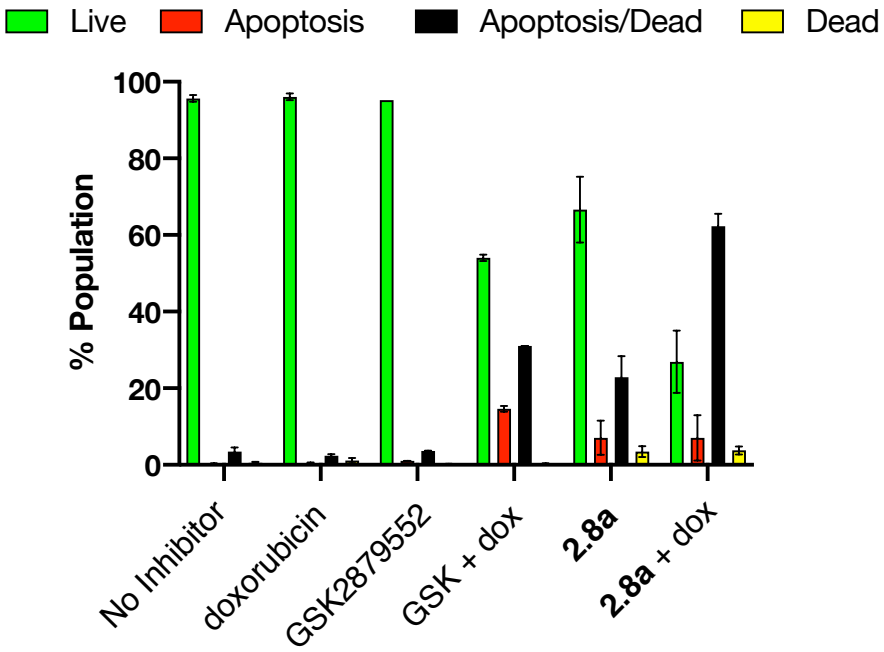

Figure 2.11. *Graphical representation of apoptosis data for doxorubicin and **2.8a** in THP-1 cells.*

Data shown as %population ± stdp, n=2.
Data generated by Bulut et al., Koc University (unpublished).

Annexin V

Again, there was no change in the levels of apoptosis seen between cells inhibited with **2.8a**, at a concentration of 1.25 μM, and uninhibited cells. Cells inhibited with 60 nM doxorubicin however showed around 40 and 20% of cells in early and late apoptosis respectively. Once again, combining **2.8a** and doxorubicin showed the largest increase in apoptotic cells with 45% of cells in early apoptosis and around 45% in late apoptosis.

Inhibitor	% Population			
	Live	Early apoptosis	Late apoptosis/Dead	Dead
No Inhibitor	78.40±5.05	16.44±3.22	4.93±1.67	0.24±0.16
doxorubicin	39.77±2.07	41.32±1.84	18.7±0.10	0.22±0.14
GSK2879552	93.16±0.92	3.43±0.71	3.07±0.17	0.34±0.04
GSK + dox	70.38±0.62	10.25±1.11	18.11±0.39	1.26±0.10
2.8a	80.94±4.74	15.20±4.30	3.58±0.18	0.29±0.27
2.8a + dox	12.93±1.17	47.33±2.63	39.24±4.19	0.51±0.39

Table 2.8. *The apoptosis profile data of doxorubicin and **2.8a** both individually and in combination in THP-1 cells measured using Annexin V.*

Data shown as %population ± stdp, n=2.
Data generated by Bulut et al., Koc University (unpublished).

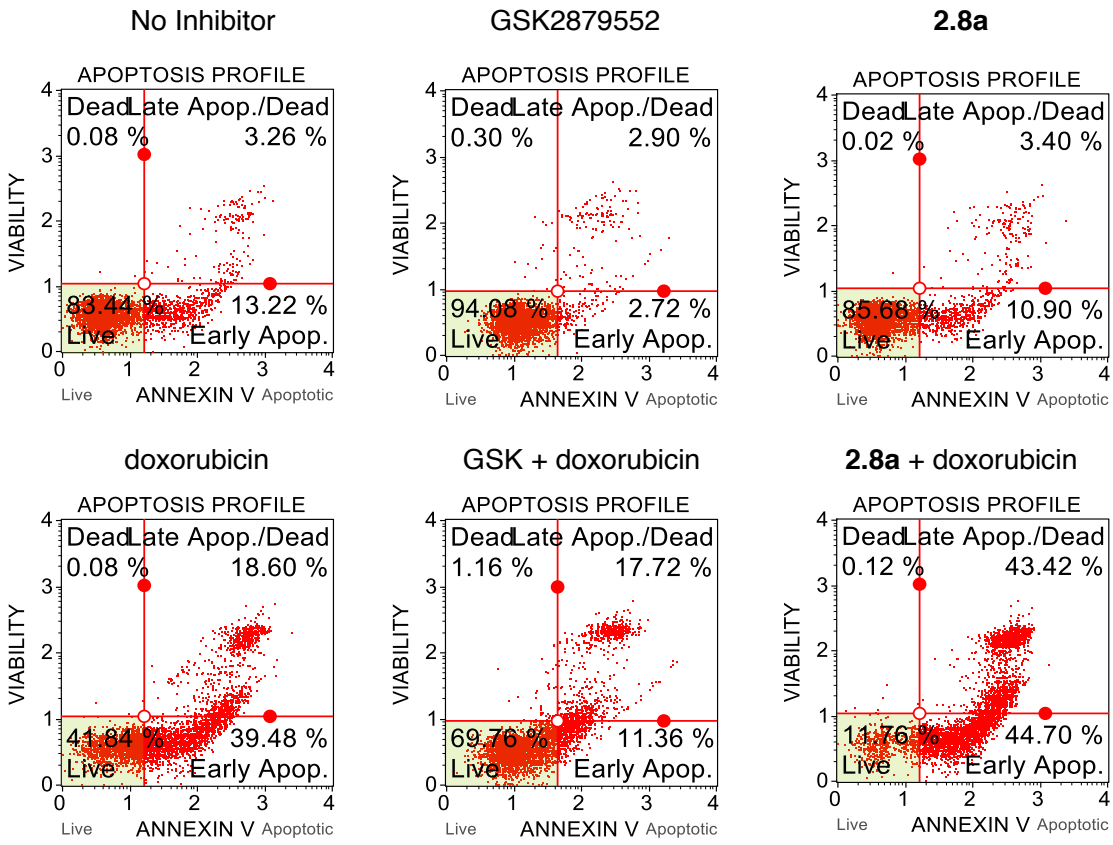

Figure 2.12. *Apoptosis profiles for **2.8a** and doxorubicin in THP-1 cells. Data generated by Bulut et al., Koc University (unpublished).*

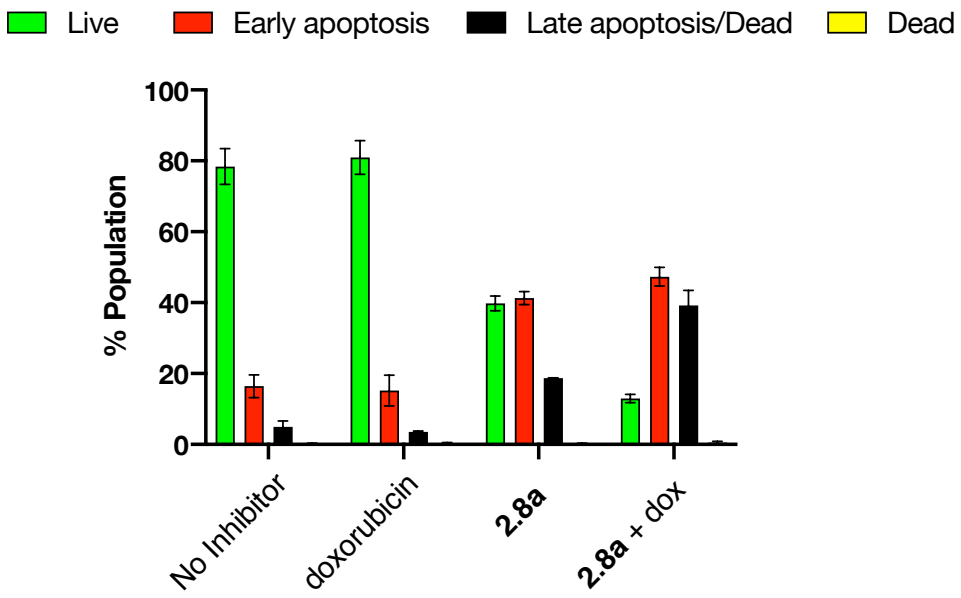

Figure 2.13. *Graphical representation of apoptosis data for doxorubicin and **2.8a** in THP-1 cells using Annexin V binding assay.*

Data shown as %population ± stdp, n=2.
Data generated by Bulut et al., Koc University (unpublished).

These results are consistent with the findings presented in section 2.4.6. which show **2.8a** to have good synergy with doxorubicin. Measurement using caspase-3 and 7 are predominantly late apoptotic cells whilst measurement via Annexin V assay shows a larger proportion of early apoptosis. These data are consistent with both methods and when total apoptosis (early + late) is examined it shows consistently high proportions of apoptotic cells.
Further work should include the apoptosis profiles of GSK2879552 to determine if the modifications made have any bearing on the results.

2.4.8. Repair of doxorubicin induced damage

Anthracyclines are a family of antitumor antibiotics. The first anthracycline, daunorubicin (Figure 2.14), was isolated independently from strains of *Streptomyces caeroleorubidus*, in 1962 in France and then from *Streptomyces peucetius* in 1963 and 1964 in Italy and the Soviet Union respectively.[119] In 1969, its 14-hydroxy analogue, doxorubicin (Figure 2.14), was reported[120] and in 1974 marketed as Adriamycin® for the treatment of carcinomas and soft tissue sarcomas and is now listed as being associated with over 24 different cancers (DrugBank.ca).

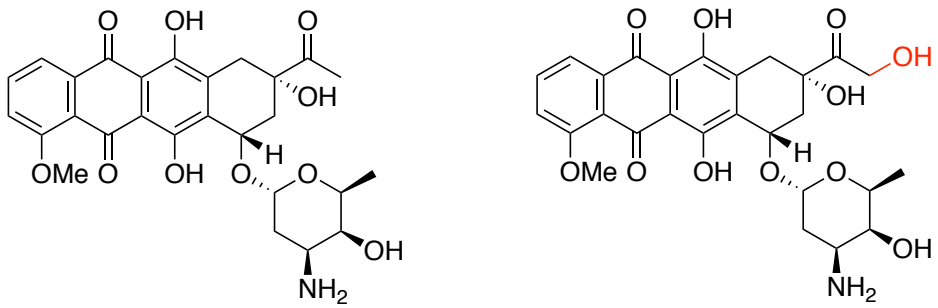

daunorubicin doxorubicin

Figure 2.14. *The molecular structure of the anthracyclines, daunorubicin and doxorubicin.*

Doxorubicins mechanism of action involves intercalculation with DNA base pairs, causing breakage of the DNA strands. It also inhibits type II topoisomerase, a DNA repair enzyme, thus preventing DNA repair and inducing apoptosis as well as acting to cause free radical-mediated oxidative damage to DNA.

It was hypothesised that our inhibitors would sensitize cells to DNA damage and so upon treatment with doxorubicin, cells would no longer be able to compensate and die. To this end, the effect of our inhibitor **2.8a**, on the damage induced by doxorubicin was investigated in several ways: the non-repair of DNA double strand breaks (DSBs) due to topoisomerase type II (Top2) inhibition, the oxidative damage caused by the generation of reactive oxygen species (ROS) and the potential regulation of gene repair pathways.

The repair of DSBs

The topoisomerases are enzymes which play an important role in DNA replication. Top2 essentially plays a role in changing the topology of DNA, which may have become knotted or catenated, by the cleavage and subsequent re-ligation of double stranded DNA.[121] The anthracyclines act by stabilising the Top2-DNA intermediate in which a DNA strand is cut and then covalently bind to the enzyme forming a DNA-Top2 cleavage complex.[122] Because the DNA cuts go unrepaired this becomes lethal for the cell. As the breakage of double stranded DNA is such a dangerous event for a cell, they have mechanisms in place to repair the DNA in the event of DSBs which are initiated by an epigenetic reaction. In response to a break, rapid phosphorylation of histone variant H2AX at serine-139 generates γ-H2AX. γ-H2AX then facilitates a number of functions in response to DSBs.[123,124] It is this early cellular response, generating γ-H2AX, which can be used to detect damage to DNA in the form of DSBs.

THP-1 cells were treated with 1.25 μM **2.8a** and/or 62.5 nM doxorubicin. Cells in which γ-H2AX had been activated were then counted to determine the level of cell damage (Table 2.8, Figure 2.15, Figure 2.16). Cells treated with **2.8a** showed no change in γ-H2AX levels relative to untreated cells and as expected, cells treated with doxorubicin only showed higher levels of γ-H2AX activation at 37%. Cells treated with both doxorubicin and **2.8a** showed slightly higher activation at 44%, although this change is not significant when statistical error is accounted for. These data suggest that the THP-1 cell line is not sensitised to DNA damage by **2.8a**.

Inhibitor	% population
No inhibitor	8.15±0.55
Doxorubicin	36.83±4.42
2.8a	4.60±0.50
2.8a + doxorubicin	44.32±6.67

Table 2.9. *% population of H2AX levels in THP-1 cells in response to treatment with doxorubicin and **2.8a**.*

Data shown as %population ± stdp, n=2.
Data generated by Bulut et al., Koc University (unpublished).

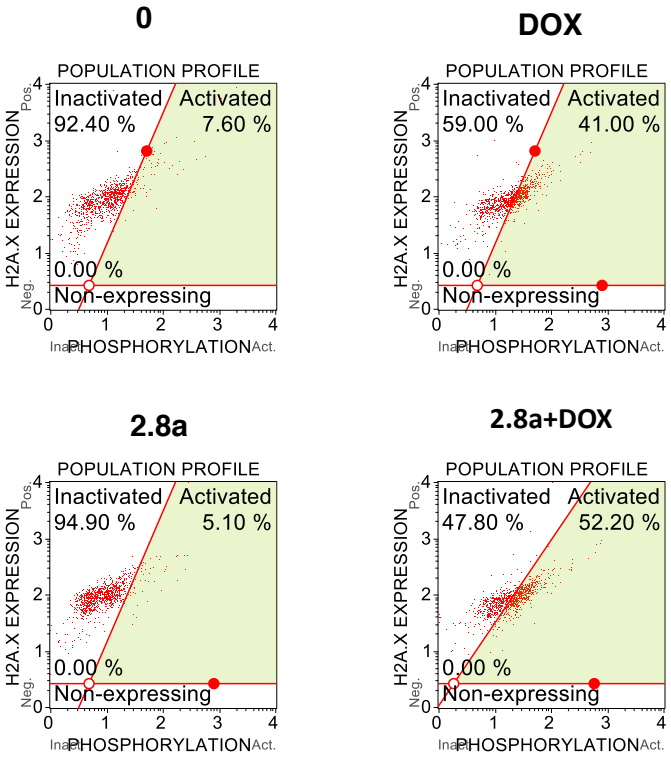

Figure 2.15. *Population profiles of phosphorylation vs H2AX expression in THP-1 cells treated with doxorubicin and **2.8a**.*
Data generated by Bulut et al., Koc University (unpublished).

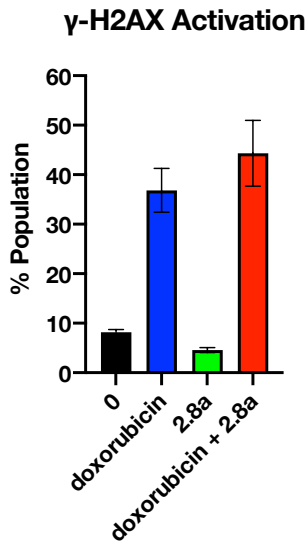

Figure 2.16. *Graphical representation of γ-H2AX activation in THP-cells treated with doxorubicin and **2.8a**.*

Data shown as %population ± stdp, n=2.
Data generated by Bulut et al., Koc University (unpublished).

The formation of ROS

Cancer treatment with doxorubicin is now well known to come with the risk of developing cardiomyopathy, which sits at around 50-60% for patients on high doses.[125] One of the reasons for this is down to how doxorubicin is metabolised. Doxorubicin can follow one of three metabolic pathways, one-electron reduction, two-electron reduction and deglycosidation. Deglycosidation is the minor pathway, accounting for only around 1-2% of doxorubicin metabolism. Two-electron transfer converts the carbonyl at C13 to a secondary alcohol and one-electron reduction, results in the formation of ROS $O_2^{\cdot-}$ and toxic H_2O_2 (Scheme 2.4). Due to the lower levels of anti-oxidants and detoxifying enzymes in cardiomyocytes, the effect of these toxic by-products on the cells becomes amplified.[126]

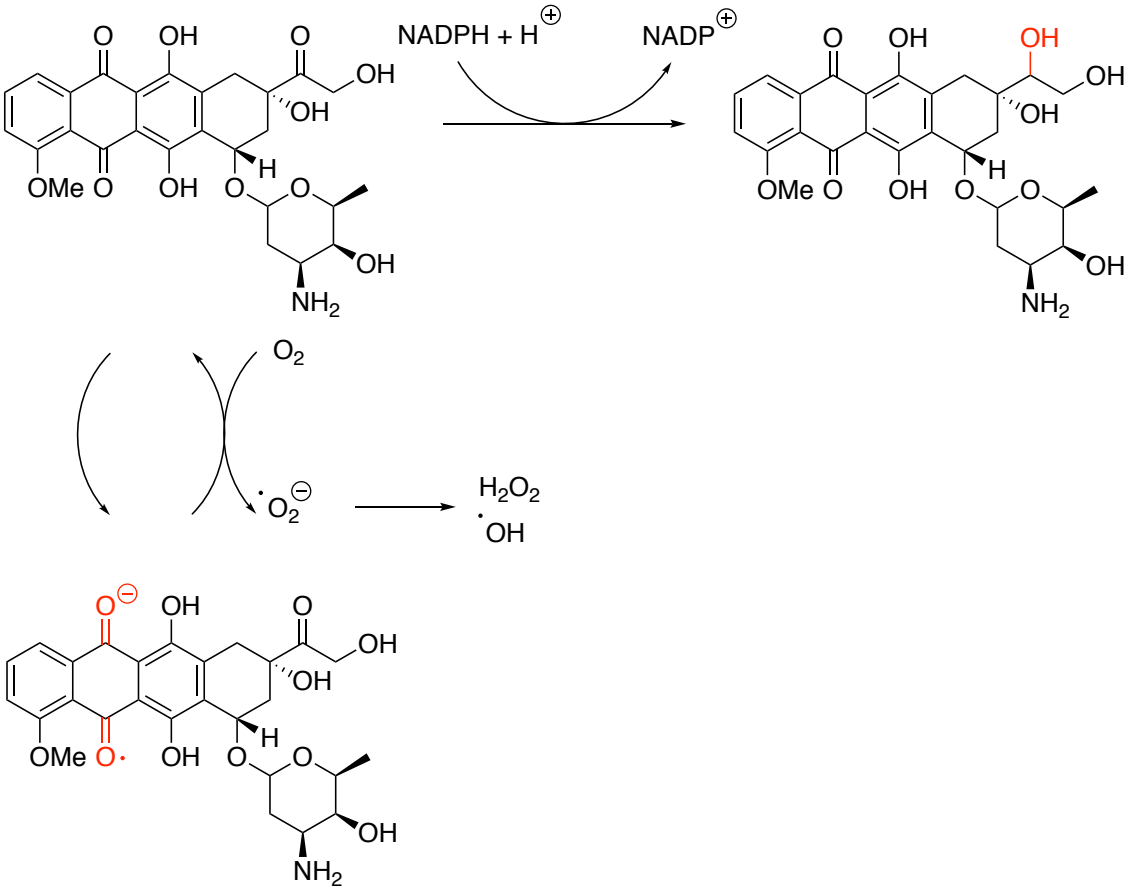

Scheme 2.4. *One and two-electron metabolic pathways of doxorubicin.*

Again, the hypothesis is that cells sensitised to damage by our inhibitors will be unable to compensate upon treatment with doxorubicin and so cells treated with doxorubicin and **2.8a** should show a high population of ROS containing cells. THP-1 cells were treated with 1.25 μM **2.8a** and/or 62.5 nM doxorubicin. Cells treated with **2.8a** only, showed no increase in the presence of ROS relative to untreated cells. Cells treated with doxorubicin only, showed the highest population at 43 % of ROS containing cells whilst those treated with both doxorubicin and **2.8a** showed a lower population of ROS containing cells at 20 % (Table 2.9, Figure 2.17, Figure 2.18). This data suggests that **2.8a** decreases the sensitivity of cells to the production of ROS due to the presence of doxorubicin metabolites. This could be a positive result as by reducing the production of ROS in cells, the risk of developing cardiomyopathy may also be reduced.

Inhibitor	% Population	
	ROS (-)	ROS (+)
No inhibitor	95.15±0.65	4.49±0.41
Doxorubicin	56.35±3.65	43.50±3.50
2.8a	94.75±0.55	5.09±0.49
2.8a + doxorubicin	79.35±3.65	19.90±3.90

Table 2.10. *ROS data for THP-1 cells treated with doxorubicin and **2.8a**.*

Data shown as %population ± stdp, n=2.
Data generated by Bulut et al., Koc University (unpublished).

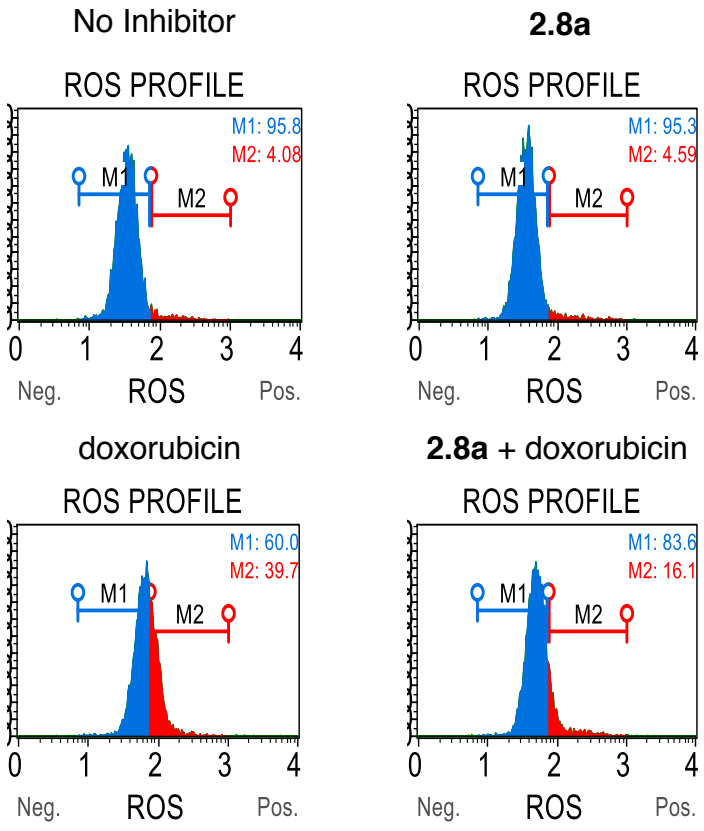

Figure 2.17. *ROS profiles for THP-1 cells treated with doxorubicin and **2.8a**.*
Data generated by Bulut et al., Koc University (unpublished).

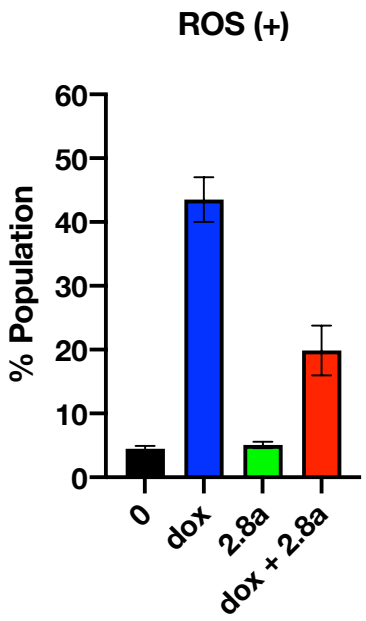

Figure 2.18. *Graphical representation of THP-1 cells containing ROS upon treatment with doxorubicin and **2.8a**.*

Data shown as %population ± stdp, n=2.
Data generated by Bulut et al., Koc University (unpublished).

Expression change in damage repair genes.

Because it is known that doxorubicin is a cause of DNA damage, the type of genes and pathways activated can be estimated. By screening the expression of these genes in the presence of **2.8a**, we can see if our inhibitor has any effect on these pathways. It was hypothesised that if LSD1 regulates any of these repair genes, upon inhibition of LSD1, the repair mechanism would collapse and result in cell death.

Twelve genes from four mechanistic groups were screened for changes in expression levels on inhibition with **2.8a** (Table 2.10, Figure 2.19). Of these four groups, only the homology directed repair (HDR) pathway genes showed any increase in expression levels and in particular ATM which showed an almost 2-fold increase. This suggests that there may be a degree of LSD1 regulation within this pathway although further investigation is required. Further work into this area will use RNA-sequencing to find any further hit genes with higher levels of expression and give us a better idea of how this mechanism works.

Mechanism	Gene	Fold Change	
		DMSO	2.8a
Base Excision Repair (BER)	OGG1	1	0.74±0.31
	MUTYH	1	0.90±0.18
	GADD45A	1	0.62±0.17
Nucleotide Excision Repair (NER)	XPA	1	0.97±0.16
	ERCC1	1	0.75±0.13
	ERCC3	1	0.97±0.07
Homology Directed Repair (HDR)	RAD51	1	1.39±0.03
	RAD52	1	1.40±0.29
	ATM	1	1.88±0.29
	ATR	1	1.45±0.11
Non-Homologous End Joining (NHEJ)	XRCC5	1	0.72±0.12
	LIG4	1	0.92±0.03

Table 2.11. *Fold change in the expression of 12 damage repair genes in response to inhibition of LSD1 with **2.8a**.*

Data shown as gene fold change ± stdp, n=2. Data normalised to DMSO = 1. Data generated by Bulut et al., Koc University (unpublished).

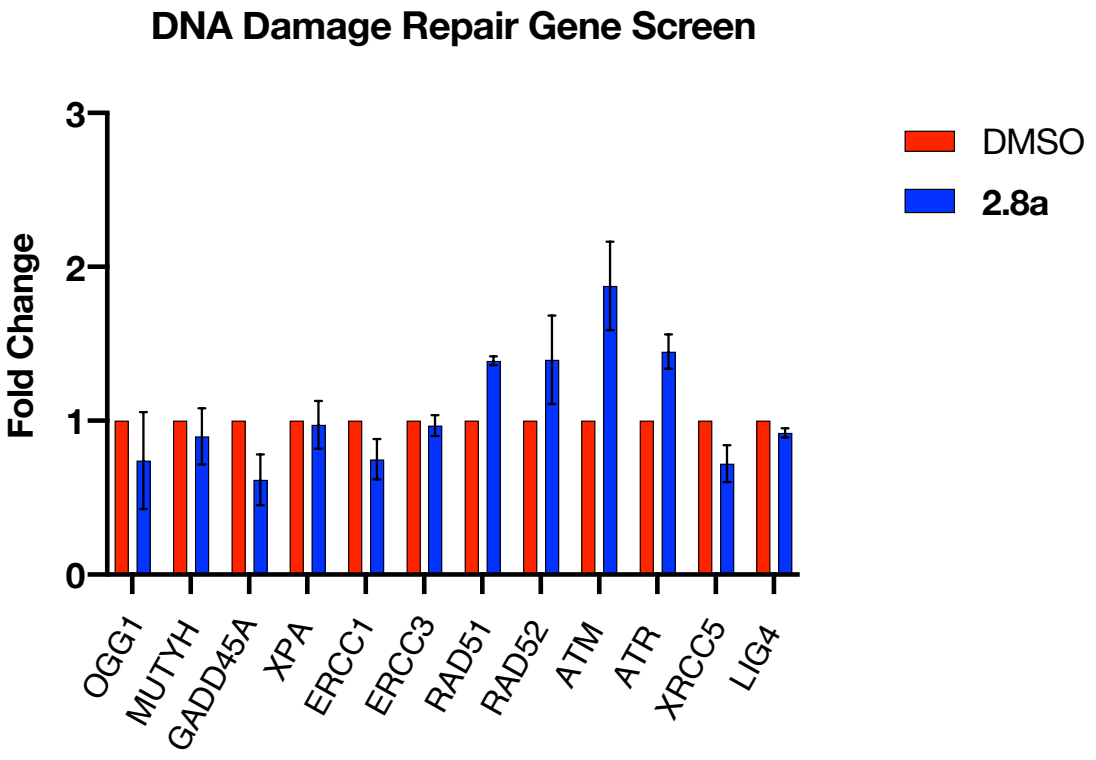

Figure 2.19. *The expression of 12 different damage repair genes in response to LSD1 inhibition with **2.8a**.*

Data shown as gene fold change ± stdp, n=2.
Data generated by Bulut et al., Koc University (unpublished).

2.5. The synthesis of further GSK2879552 analogues.

Having shown that our compound **2.8a** is a potent inhibitor of LSD1, with good in cell activity, the next logical step was to expand the series. To this end, we modified the amide R group (Figure 2.19) to try and identify which features are important and to see if any improvement could be made. There are three main changes which can be made to the amide R group. Carbon chain length, carbon chain rigidity and the functional group at the end of the chain. To this end, six further compounds were synthesised (Figure 2.20).

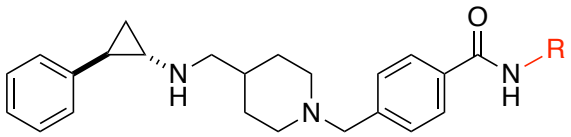

2.8

Figure 2.20. *General structure of our series of potential LSD1 inhibitors based on the structure of GSK2879552.*

The first change was to reduce the carbon chain length in order to determine if chain length is important. **2.8b** has the same imidazole group at the end of the saturated chain, but two carbons in place of three. Following this, because the region that the amide R group is thought to be occupying in the LSD1 functional site is understood to be acidic,[127] and imidazole is expected to be positively charged at physiological pH, the presence of the nitrogen's should be important for affinity. To test this, imidazole was replaced with an aromatic ring which retains aromaticity but loses polarity. Compounds **2.8c**, **2.8d** and **2.8e** incorporate this change while also consisting of a varied carbon chain length of 3, 2 and 1 carbon respectively.

Compound **2.8f** was modified by replacing the imidazole ring with a *N*-alkylated piperidine ring. This change retains a certain amount of polarity but loses aromaticity.

The final compound, **2.8g**, contains tranylcypromine as the amide R group. This retains the 3-carbon chain length but provides rigidity as well as conserving aromaticity.

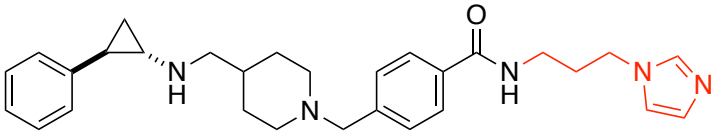

2.8a

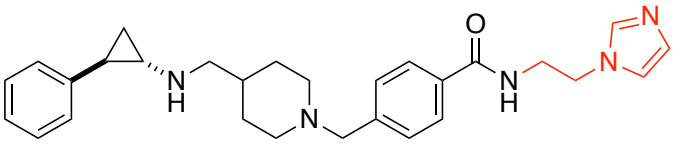

2.8b

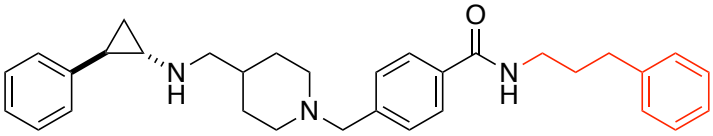

2.8c

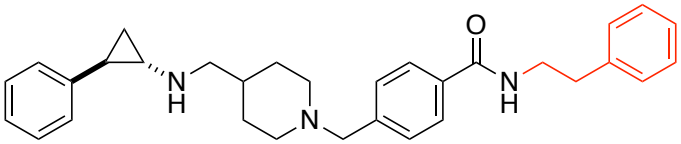

2.8d

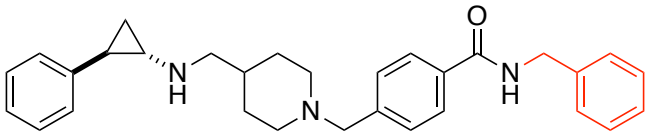

2.8e

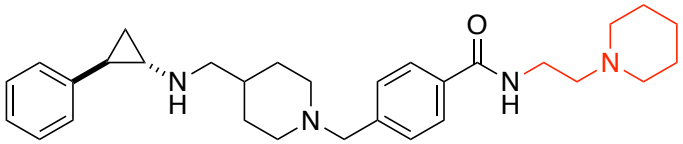

2.8f

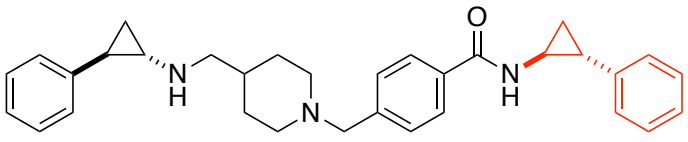

2.8g

Figure 2.21. *All analogues of GSK2879552.*

2.5.1. Biological activity.

The first test available to us was a cell viability test in THP-1 cells. THP-1 cells show high expression of LSD1 and compound **2.8a** performed well in a previous assay with an IC_{50} of 1.8 μM in THP-1 (section 2.4.3.).

The anti-proliferative effect of all compounds **2.8a-g** was first tried at a concentration of 100 μM (Figure 2.22) to gauge activity, using doxorubicin as a control. All compounds showed strong anti-proliferative activity at this concentration and so the assay was repeated, for all compounds, at a concentration of 10 μM (Figure 2.21). The results of the 10 μM assay indicated that all compounds in which the amide R-group carbon chain contained three carbons, **2.8a**, **2.8c** and **2.8g**, had strong anti-proliferative activity at this concentration, while all compounds with less than three carbons had poor activity. The anti-proliferative effect held regardless of functional group on the end of the chain and also irrespective of whether the chain was in a free or restricted conformation.

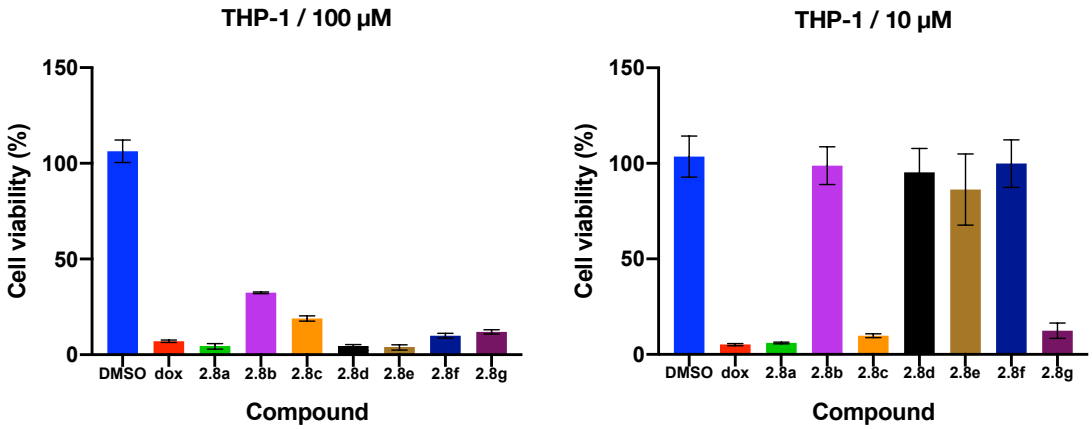

Figure 2.22. *Cell viability assay results of all compounds **2.8a-g** with doxorubicin as a control in THP-1 cells at 100 and 10 μM concentrations of inhibitors.*

Data shown as cell viability % ± std, n=3.
Data generated by Burianova et al., UEA (unpublished).

Finally, the IC_{50} of all compounds **2.8a-g** were determined (Figure 2.23, Table 2.11), and the results gave some interesting insights. The importance of carbon

chain length, highlighted in the 10 μM assay, was reiterated. Compounds **2.8a**, **2.8c** and **2.8g** displayed the lowest IC_{50}'s of 0.7, 9.5 and 5.9 μM respectively. Further significance to chain length is demonstrated by compounds **2.8c-e**. These compounds all have the same functional group at the end of the chain and only chain length is varied. This emphasised the trend, as chain length is reduced the IC_{50} increases. Future work should add a compound with a fourth carbon in the chain in order to ascertain if three carbons is indeed the optimum, or if the optimum is yet to be found.

The difference in functional groups at the end of the carbon chain can be compared by looking at compounds **2.8b**, **2.8d** and **2.8f** which all have two carbons in the chain and so keeps this variable constant. **2.8d** and **2.8f** returned IC_{50} values of 28.4 and 29.9 μM respectively suggesting that aromaticity is not important. In addition, **2.8b** had the highest IC_{50} of all compounds at 70.1 μM again suggesting that neither aromaticity nor basicity is important to affinity. Again, future work should incorporate compounds with no R-group at the end of the chain to establish the necessity of this feature.

Finally, comparing compounds **2.8c** and **2.8g** allows us to determine if incorporating rigidity into the carbon chain has any significant effect on affinity. These have IC_{50} values of 9.5 and 5.9 μM respectively suggesting that restricting the conformation of the chain is not of substantial benefit. One further feature which could be explored in terms of chain rigidity is to replace the saturated chain with double bonds. In the case of **2.8b** and **2.8d** this would add conjugation throughout the entire R-group.

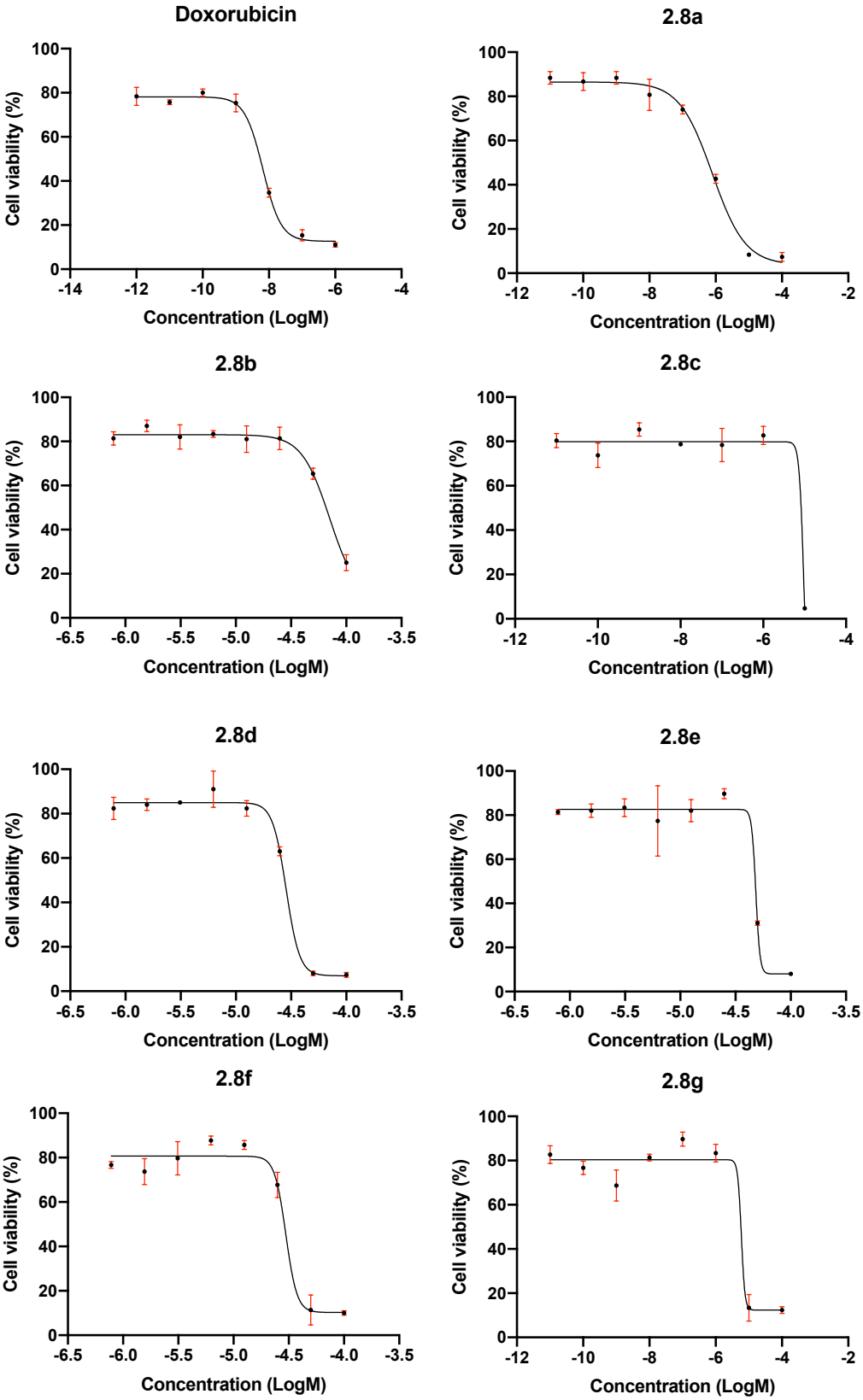

Figure 2.23. *Cell viability assay to determine the IC50 of all compounds **2.8a-g** in THP-1 cells.*

Data shown as cell viability % ± std, n=3.
Data generated by Burianova et al., UEA (unpublished).

Compound	R-group	IC_{50} ± std (μM)
2.8a	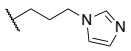	0.79±0.03
2.8b	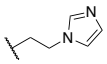	69.14±2.86
2.8c	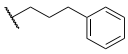	4.77±0.32
2.8d	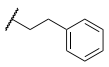	30.84±0.70
2.8e		41.90±0.57
2.8f	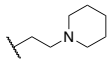	32.86±2.71
2.8g	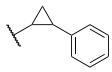	5.29±0.62

Table 2.12. *IC_{50} values of compounds **2.8a-g** in a cell viability assay in THP-1 cells.*

Data shown as cell viability % ± std, n=3.
Data generated by Burianova et al., UEA (unpublished).

2.6. Conclusion and future work.

In this chapter we have presented the synthesis and biological activity of a novel LSD1 inhibitor, **2.8a**. This inhibitor is synthesised in one step from GSKs clinical candidate, GSK2879552.

Using CETSA, **2.8a** was shown to have good target engagement in THP-1 cells demonstrating a significant increase in thermal degradation temperature relative to untreated cells and a small increase relative to GSK2879552.

2.8a demonstrated good in cell activity, particularly in MLL fused cell lines and more specifically MOLM-13. In addition, non-fused cell lines also proved susceptible at low μM concentrations and performed significantly better than control compound, GSK2879552.

The activity of **2.8a** as a LSD1 inhibitor was further supported through the analysis of molecular markers, CD86 and CD11b. Both markers showed a considerable increase in expression levels in the presence of **2.8a** as well as higher expression levels than those seen for GSK2879552.

One further area of exploration was to investigate the synergistic effects between **2.8a** and other known anti-cancer agents. Of these, doxorubicin showed excellent synergistic activity in combination with **2.8a** and a significant increase in the level of apoptotic cells were seen on exposure to a combination of **2.8a** and doxorubicin relative to doxorubicin alone.

A deeper investigation into this synergy revealed that while γ-H2AX levels showed no significant change, the levels of ROS did drop relative to treatment with doxorubicin alone suggesting possible benefits through the reduction of cardiomyopathy.

A screen of DNA damage repair genes suggested a possible link to the HDR gene repair pathway but not at any significant level. Further work will investigate these pathways further with the aim of identifying any link between LSD1 regulation of these gene repair pathways.

A further six analogues were synthesised in an effort to optimise the structure. Initial cell viability testing in THP-1 cells suggests that carbon chain length is the most important feature with three carbons showing better performance than one or two. Chain rigidity and the functional group at the end of the chain had less of an impact on in-cell activity. Future work should now look to investigate if further lengthening the carbon chain would serve to increase activity and also the effect of removing the terminal functional group altogether.

2.7. Chapter two experimental.

2.7.1. Experimental procedures.

All commercially available chemicals and reagents were purchased from Fluorochem, Fisher Scientific, Sigma Aldrich, Acros Organics, Alfa Aesar or VWR and used as provided, including all anhydrous solvents.

All glassware used was flame dried under vacuum or oven dried prior to use. All reactions were carried out under a nitrogen atmosphere unless otherwise stated. Any reference made to solvent being removed *in vacuo* refers to its removal by evaporation, under reduced pressure, on a rotary evaporator at 40°C and if required, dried further under high vacuum at room temperature.

All thin layer chromatography (TLC) was carried out on Merck TLC Silica Gel 60 F_{254} aluminium backed TLC plates from Merck. Plates were visualised under UV (254 nm) light or, when appropriate, stained with ninhydrin and heated. All chromatography was carried out on a Teledyne ISCO Combi*Flash* Rf 150 using pre-packed, disposable silica columns purchased from Kinesis or pre-packed, reusable C18 reverse phase columns purchased direct from Teledyne ISCO.

Melting points were determined using a Stuart SMP10 melting point apparatus.

Infrared spectra were recorded using a Spectrum Two FT-IR Spectrometer from PerkinElmer. Data is given wavenumbers (cm^{-1}).

All NMR were carried out on Brucker Ultrashield 400 Plus spectrometer. All samples were dissolved in an appropriate deuterated solvent. ^{1}H NMR was recorded at 400 MHz, ^{13}C at 101 MHz and ^{19}F at 376 MHz unless otherwise stated. All NMR spectral data was processed using Mnova software from Mestrelab Research and calibrated using the appropriate deuterated solvent peak. Multiplicity splitting patterns are reported as s (singlet), d (doublet), t (triplet), q (quartet), m (multiplet), brd (broad) and combinations thereof. Coupling

constants (*J*) are reported in Hz and the number of protons determined via integration, calibrated from a peak of known origin.

High Resolution Mass Spectometry (HRMS) was carried out at the John Innis Centre, Norwich Research Park. Samples were run by direct flow injection, without chromatography, on a Shimadzu IT-ToF mass spectrometer with an Acquity/Prominence UHPLC as front end. Samples were run in 50% MeCN at a flow rate of 0.6 ml min^{-1} for 2 minutes. The Photo Diode Array (PDA) collected UV/visible spectra from 200-600 nm and the Mass spectrometer collected both positive and negative full MS from *m/z* 200-2000.
LC-ToF spectra was carried out on an Agilent 6220 ToF-MS fitted with a hybrid Agilent 1100/1200 LC system. LC conditions consisted of a 10-100 % gradient of acetonitrile in water, 0.1 % formic acid additive and a flow rate of 0.5 ml min^{-1}. The column was a Thermo Accucore 100 x 2.1 mm C-18 column with 2.4 µM pore size fitted with a C-18 column guard. Data was typically collected over a range of *m/z* 200-2000. All data was processed using ACD Spectrus Processor software from ACD Labs.

Purity was determined using HPLC analysis on an Agilent Technologies 1200 series HPLC fitted with a ZORBAX Eclipse C18 reverse phase column. A gradient of 95:5 water:MeOH with 0.05% TFA to 5:95 water:MeOH with 0.05% TFA was used over a run time of 25 minutes and a typical flow rate of 1 ml min^{-1}. UV/visible spectra were recorded at 254 and 214 nm and purity determined by % peak area.

Some minor characterisation data has been omitted as university services, and therefore data collection, was interrupted by the COVID-19 outbreak.

2.7.2. *trans*-GSK2879552 synthesis

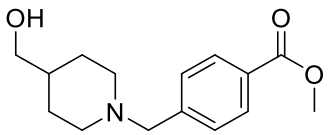

Methyl 4-{[4-(hydroxymethyl)piperidin-1-yl]methyl}benzoate, (2.10a).

This compound was prepared by a modified version of the procedure for **2.10b**.[102]

A flame dried flask was charged with **2.5a** (3.00 g, 13.11 mmol) and 4-piperidinemethanol (1.51 g, 13.09 mmol). Anhydrous acetonitrile (60 ml) was then added, making a white suspension. Potassium carbonate (5.43 g, 39.29 mmol) was added and the mixture refluxed under a nitrogen atmosphere for 2 hrs. The mixture was allowed to cool to room temperature before being filtered and concentrated under reduced pressure. The concentrate was dissolved in EtOAc (50 ml) and to it added 1M HCl (50 ml). The aqueous layer was separated and washed with EtOAc (50 ml) and then basified with 4M NaOH to pH 10. The aqueous mixture was then twice extracted with EtOAc (50 ml) and the combined organic layers washed with brine (50ml) and dried over $MgSO_4$. Removing the solvent *in vacuo* gave **2.10a** (2.86 g, 83 %) as a white solid. Mp 57-58ºC, ^{1}H NMR (400 MHz, Chloroform-*d*) δ 7.98 (d, *J* = 8.3 Hz, 2H), 7.39 (d, *J* = 8.4 Hz, 2H), 3.90 (s, 3H), 3.55 (s, 2H), 3.48 (d, *J* = 6.4 Hz, 2H), 2.88 (d, *J* = 11.5 Hz, 2H), 1.99 (td, *J* = 11.7, 2.4 Hz, 2H), 1.74 – 1.68 (m, 2H), 1.55 – 1.45 (m, 2H), 1.31 (qd, *J* = 12.3, 12.0, 12.0, 3.9 Hz, 2H); 13C NMR (101 MHz, Chloroform-*d*) δ 167.1, 143.8, 129.6, 129.1, 129.0, 67.8, 63.0, 53.6, 52.1, 38.5, 28.7; HMRS (ESI) *m/z* calcd for $C_{15}H_{21}NO_3$ $[M^+H]^+$ 264.1594, found 264.1596.

This compound has been reported in the literature but no data given.[128]

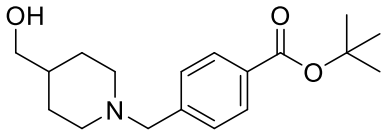

***tert*-Butyl 4-{[4-(hydroxymethyl)piperidin-1-yl]methyl}benzoate, (2.10b).**

Made using the procedure for **2.10a**.

Isolated as a yellow solid. (5.65 g, 84 %)

Mp 70-71 ºC, ^{1}H NMR (400 MHz, Chloroform-*d*) δ 7.91 (d, *J* = 8.3 Hz, 2H), 7.36 (d, *J* = 8.3 Hz, 2H), 3.52 (s, 2H), 3.46 (t, *J* = 5.4 Hz, 2H), 2.86 (dt, *J* = 11.1, 3.2 Hz, 2H), 2.10 (t, *J* = 5.3 Hz, 1H), 1.96 (td, *J* = 11.7, 2.5 Hz, 2H), 1.75 – 1.64 (m, 2H), 1.57 (s, 9H), 1.53 – 1.40 (m, 1H), 1.34 – 1.21 (m, 2H); ^{13}C NMR (101 MHz, Chloroform-*d*) δ 165.8, 143.3, 130.8, 129.4, 128.9, 80.9, 67.7, 63.0, 53.5, 53.5, 38.5, 28.8, 28.2; HRMS (ESI) *m/z* calcd for $C_{18}H_{27}NO_3$ $[M^+H]^+$ 306.2064, found 306.2064.

These data are consistent with that reported in the literature.[102]

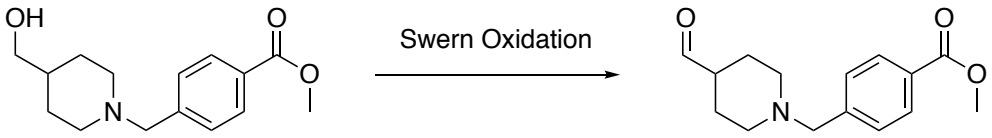

Methyl 4-[(4-formylpiperidin-1-yl)methyl]benzoate, (2.11a).

This compound was prepared by a modified version of the procedure for **2.11b**.[102] DMSO (4.4 ml, 61.9 mmol) was dissolved in dry dichloromethane (100 ml) and cooled to -78ºC. Oxalyl chloride (3.4 ml, 39.6 mmol) was then also dissolved in dry dichloromethane (38 ml) and cooled to -78 ºC before being slowly added to the DMSO solution. The mixture was then stirred for 30 minutes at -78 ºC under a nitrogen atmosphere before **2.10a** (7.01 g, 26.6 mmol) was dissolved in dry dichloromethane (40 ml), cooled to -78 ºC and added slowly to the DMSO/oxalyl chloride solution. The resulting mixture was stirred at -78 ºC under nitrogen for 3 hours. After this time, trimethylamine (19 ml, 136.3 mmol) was dissolved in dry dichloromethane (20 ml) and cooled to -78 ºC before being added to the benzoate mixture. This mixture was stirred at -78 ºC for a further 20 minutes, before water (50 ml) was added and the mixture allowed to warm to room temperature. The aqueous layer was separated, and the pH adjusted to ~7 with 2M HCl. The aqueous layer was then extracted with dichloromethane (20

ml) and all organic layers combined and washed with water and brine (50 ml), dried over $MgSO_4$ and concentrated. The concentrate was then purified on a silica column eluting with a gradient of 0-100 % EtOAc in petroleum ether to give **2.11a** (4.9 g, 71 %) as a yellow oil which solidified to a crystalline solid under high vacuum. Mp 49-50ºC, ^{1}H NMR (400 MHz, Chloroform-*d*) δ 9.64 (d, *J* = 1.2 Hz, 1H), 7.97 (d, *J* = 8.4 Hz, 2H), 7.37 (d, *J* = 8.5 Hz, 2H), 3.89 (s, 3H), 3.53 (s, 2H), 2.80-2.75 (m, 2H), 2.28-2.20 (m, 1H), 2.11 (td, *J* = 11.1, 2.7 Hz, 2H), 1.90-1.85 (m, 2H), 1.73-1.63 (m, 2H); ^{13}C NMR (101 MHz, Chloroform-*d*) δ 203.9, 167.1, 144.0, 129.6, 129.0, 128.8, 62.9, 52.68, 52.1, 47.9, 25.5; HMRS (ESI) *m/z* calcd for $C_{15}H_{19}NO_3$ $[M^+H]^+$ 262.1438, found 262.1441.

This compound has been reported in the literature but no data given.[128]

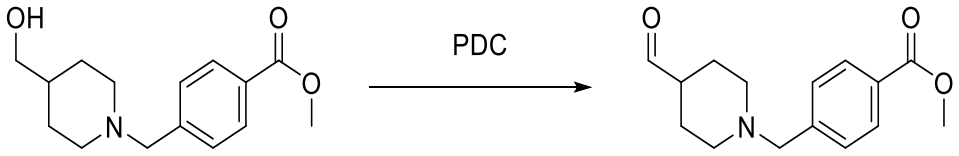

Methyl 4-[(4-formylpiperidin-1-yl)methyl]benzoate, (2.11a).

Alternative oxidation procedure.

Anhydrous dichloromethane was added to a flask was charged with **2.10a** (323 mg, 1.22 mmol) and stirred until all solid had dissolved. To it was added silica and ground up 4Å molecular sieves (567 mg). Pyridinium dichromate (PDC) (668 mg, 1.76 mmol) was added and the mixture stirred at room temperature under a nitrogen atmosphere for 16hrs. The reaction mixture was then diluted with Et_2O and filtered through a pad of silica. The filtrate was then concentrated and purified via silica column chromatography (0 – 100 % EtOAc:PE) to give **2.11a** (16mg, 5%) as a yellow oil.

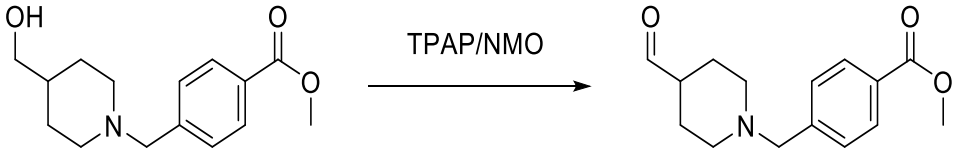

Methyl 4-[(4-formylpiperidin-1-yl)methyl]benzoate, (2.11a).

Alternative oxidation procedure.

2.10a (142 mg, 0.54 mmol) was dissolved in anhydrous dichloromethane (4ml). Tetrapropylammonium perruthenate (TPAP) (18.7 mg, 0.05 mmol) and *N*-Methylmorpholine-*N*-Oxide (NMO) (124 mg, 1.06 mmol) were then added and the mixture stirred at room temperature for 3 hrs. The mixture was then filtered through celite and the filtrate concentrated *in vacuo*. The concentrate was purified via flash chromatography (0 – 100 % EtOAc:PE) to give **2.11a** (42 mg, 30 %) as a yellow oil.

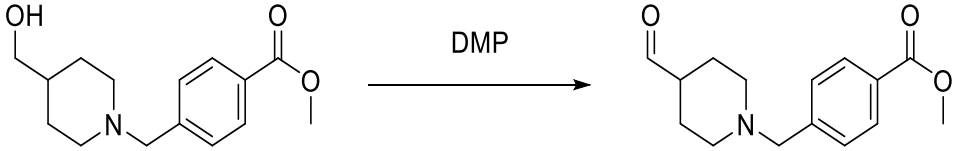

Methyl 4-[(4-formylpiperidin-1-yl)methyl]benzoate, (2.11a).

Alternative oxidation procedure.

2.10a (143 mg, 0.54 mmol) was dissolved in anhydrous dichloromethane (4 ml) and cooled to 0 ºC. Dess-Martin periodinane (DMP) (453 mg, 1.07 mmol) was added and the mixture stirred at 0 ºC under a nitrogen atmosphere for 20 minutes. The mixture was then allowed to warm to room temperature and stirring continued for a further 30 minutes. 2M Na_2SO_4 (10 ml) was added followed by saturated $NaCO_3$ (10 ml) and dichloromethane (10 ml) the organic layer was removed and the aqueous layer further extracted with dichloromethane (15 ml). The combined organic layers were then washed with brine and dried over $MgSO_4$ before being concentrated and purified via flash chromatography (0 – 100 % EtOAc:PE) to give **2.11a** (76 mg, 55 %) as a yellow oil.

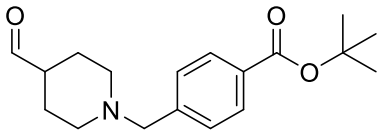

***tert*-Butyl 4-[(4-formylpiperidin-1-yl)methyl]benzoate, (2.11b).**

Made using the Swern oxidation procedure for **2.11a**.

Isolated as a yellow solid. (72%)

Mp = 72-73 ºC, ^{1}H NMR (400 MHz, Chloroform-*d*) δ 9.64 (d, *J* = 1.2 Hz, 1H), 7.93 (d, *J* = 8.3 Hz, 2H), 7.38 (d, *J* = 8.1 Hz, 2H), 3.57 (s, 2H), 2.85 – 2.75 (m, 2H), 2.31 – 2.09 (m, 3H), 1.91 (d, *J* = 13.3 Hz, 2H), 1.74 (t, *J* = 11.6 Hz, 2H), 1.58 (s, 9H); ^{13}C NMR (101 MHz, Chloroform-*d*) δ 203.8, 165.7, 131.2, 129.6, 129.0, 81.0, 62.8, 52.5, 47.7, 28.3, 25.3; HRMS (ESI) *m/z* calcd for $C_{18}H_{25}NO_3$ $[M^+H]^+$ 304.1907, found 304.1918.

These data are consistent with that reported in the literature.[102]

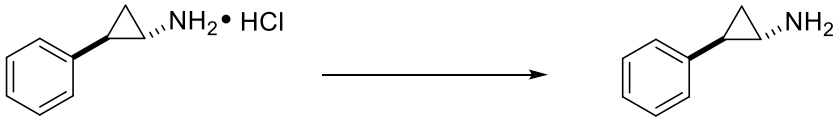

***trans*-2-Phenylcyclopropylamine, (1.2).**

trans-2-Phenylcyclopropylamine hydrochloride (2.00 g, 11.79 mmol) was dissolved in water (30 ml). 4M NaOH (10 ml) was added slowly then the mixture stirred for 30 minutes. The mixture was extracted three times with dichloromethane (30 ml) and the combined organic layers dried over $MgSO_4$ and filtered. The filtrate was evaporated *in vacuo* to give **1.2** (1.50 g, 96 %) as an off white solid. ^{1}H NMR (400MHz, Chloroform-*d*) δ 7.26-7.23 (m, 2H), 7.16-7.12 (m, 1H), 7.03-7.01 (m, 2H), 2.55 (ddd, *J* = 7.3, 4.3, 3.1Hz, 1H), 1.86 (ddd, *J* = 9.1, 5.8, 3.1Hz, 1H), 1.66 (s, 2H), 1.04 (ddd, *J* = 9.4, 5.2, 4.3Hz, 1H), 0.98 (dt, *J* = 7.1, 5.5Hz, 1H).

These data are consistent with that reported in the literature.[129]

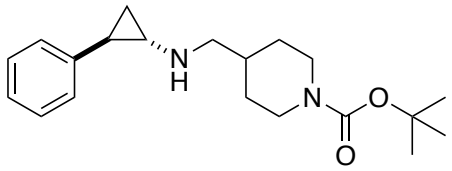

***tert*-Butyl-4-{[(2-phenylcyclopropyl)amino]methyl}piperidine-1-carboxylate, (2.2).**

This compound was prepared by a modified version of a general procedure reported by Bhattacharyya.[103]

A flame dried, round bottom flask was charged with **1.2** (667 mg, 5.01 mmol) Titanium (iv) isopropoxide (3.4 ml, 11.48 mmol) was added followed by 1-Boc-piperidine-4-carboxylate (838 mg, 3.93 mmol) and the mixture stirred at room temperature under a nitrogen atmosphere for 3 hrs. Methanol (4 ml) was then added and the flask was cooled to 0 ºC. Sodium borohydride (311 mg, 8.22 mmol) was added slowly before warming the flask back up to room temperature and stirring continued for 1 hr. 1M NaOH (10 ml) was added followed by water (10 ml) and dichloromethane (20 ml). The organic layer was recovered and dried over $MgSO_4$ before being concentrated under reduced pressure and purified via flash chromatography (0–100% EtOAc:PE) to give **2.2** (468 mg, 36 %) as a yellow oil. ^{1}H NMR (400 MHz, Methanol-*d*$_4$) δ 7.21 (t, *J* = 7.5Hz, 2H), 7.11 (t, *J* = 7.4Hz, 1H), 7.04 (d, *J* = 7.2Hz, 2H), 4.10-4.04 (m, 2H), 2.77-2.70 (m, 2H), 2.59-2.57 (m, 2H), 2.29 (ddd, *J* = 7.4, 4.4, 3.4Hz, 1H), 1.90 (ddd, *J* = 9.2, 5.8, 3.3Hz, 1H), 1.74-1.64 (m, 3H), 1.45 (s,9H), 1.10-0.97 (m, 4H); ^{13}C NMR (101 MHz, Methanol-*d*$_4$) δ 156.4, 143.4, 129.2, 126.7, 126.5, 80.8, 61.5, 56.1, 42.6, 36.9, 31.4, 28.7, 25.2, 20.8, 16.7, 14.4, 11.0.

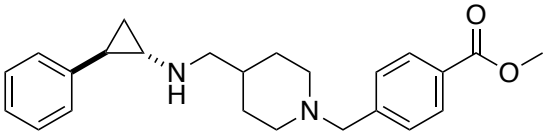

Methyl4-{[4-({[(trans)-2-phenylcyclopropyl]amino}methyl)piperidin-1-yl]methyl} benzoate, (2.7a).

To a solution of **2.11a** (4.10 g, 15.70 mmol) in dry methanol (33 ml) was added *trans*-2-phenylcyclopropanamine (2.50 g, 18.78 mmol). The mixture was heated to reflux for 10 minutes before cooling back to room temperature. Sodium borohydride (0.89 g, 23.53 mmol) was then slowly added and the mixture stirred

at room temperature for 1 hour. Water was added (50 ml) followed by dichloromethane (50 ml) and the organic layer separated and washed with a solution of 10 % acetic acid (50 %). Brine (50 ml) was then slowly added allowing the precipitation of a white solid. The solid was filtered and then suspended in propan-2-ol and sonicated before being filtered again to give **2.7a** (2.06 g, 35 %) as a white solid. ^{1}H NMR (400 MHz, Methanol-d_4) δ 8.11 (d, J = 8.3 Hz, 2H), 7.71 (d, J = 8.4 Hz, 2H), 7.33 – 7.27 (m, 2H), 7.25 – 7.16 (m, 3H), 4.37 (s, 2H), 3.93 (s, 3H), 3.46 (d, J = 12.8 Hz, 2H), 3.17 (d, J = 6.9 Hz, 2H), 3.07 (t, J = 12.5 Hz, 2H), 2.98 (ddd, J = 7.9, 4.4, 3.6 Hz, 1H), 2.58 (ddd, J = 10.3, 6.6, 3.6 Hz, 1H), 2.23 – 2.02 (m, 3H), 1.70 (q, J = 12.9 Hz, 2H), 1.59 (ddd, J = 10.4, 6.7, 4.4 Hz, 1H), 1.36 (dt, J = 7.8, 6.6 Hz, 1H); ^{13}C NMR (101 MHz, DMSO-d_6) δ 165.8, 138.9, 134.9, 131.9, 130.4, 129.3, 128.4, 126.4, 126.4, 58.1, 52.3, 51.6, 50.6, 37.9, 30.5, 26.5, 20.3, 12.4; HRMS (ESI) *m/z* calcd for $C_{24}H_{30}N_2O_2$ $[M^+H]^+$ 379.2380, found 379.2380.

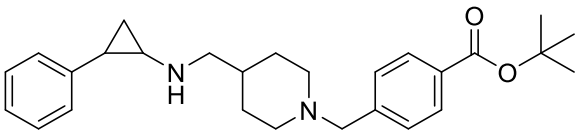

***tert*-Butyl 4-[(4-{[(2-phenylcyclopropyl)amino]methyl}piperidin-1-yl)methyl] benzoate, (2.7b).**

Made using the procedure for **2.7a**.

Isolated as a white solid. (5.58 g, 66 %)

^{1}H NMR (400 MHz, Methanol-d_4) δ 8.02 (d, J = 8.3 Hz, 2H), 7.63 (d, J = 8.3 Hz, 2H), 7.31 – 7.26 (m, 2H), 7.23 – 7.14 (m, 3H), 4.25 (s, 2H), 3.38 (d, J = 12.8 Hz, 2H), 3.09 (d, J = 6.7 Hz, 2H), 2.97 – 2.86 (m, 3H), 2.49 (ddd, J = 10.2, 6.5, 3.5 Hz, 1H), 2.13 – 2.00 (m, 3H), 1.70 – 1.63 (m, 2H), 1.60 (s, 9H), 1.52 (ddd, J = 10.6, 6.5, 4.4 Hz, 1H), 1.31 (dt, J = 7.8, 6.5 Hz, 1H); ^{13}C NMR (101 MHz, Methanol-d_4) δ 175.9, 166.6, 139.9, 136.6, 134.1, 132.2, 130.8, 129.6, 127.7, 127.3, 82.8, 61.2, 53.7, 52.9, 40.1, 32.8, 28.3, 22.8, 21.2, 13.9; HRMS *m/z* calcd for $C_{27}H_{36}N_2O_2$ $[M^+H]^+$ 421.2850, found 421.2868.

These data are consistent with that reported in the literature.[102]

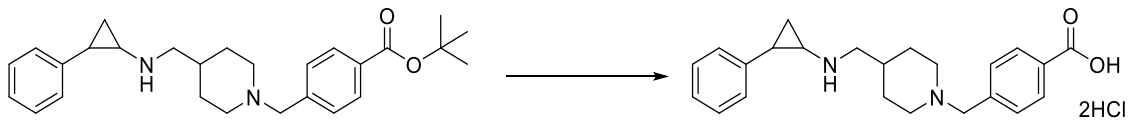

4-[(4-{[(2-phenylcyclopropyl)amino]methyl}piperidin-1-yl)methyl]benzoic acid dihydrochloride, (1.35).

A suspension of **2.7b** (3.00 g, 7.13 mmol) in 1M HCl (40 ml) was heated to 89 ºC for 3 hrs. The reaction mixture was allowed to cool to room temperature and then placed in an ice bath overnight. The resulting white precipitate was filtered and dried *in vacuo* to give **1.35** (0.85 g, 27 %) as a white solid. ^{1}H NMR (400 MHz, Methanol-d_4) δ 8.12 (d, J = 8.3 Hz, 2H), 7.70 (d, J = 8.4 Hz, 2H), 7.33 – 7.28 (m, 2H), 7.26 – 7.16 (m, 3H), 4.43 (s, 2H), 3.54 (d, J = 12.3 Hz, 2H), 3.26 – 3.07 (m, 4H), 3.02 (dt, J = 7.9, 4.1 Hz, 1H), 2.61 (ddd, J = 10.3, 6.6, 3.6 Hz, 1H), 2.27 – 2.06 (m, 3H), 1.81 – 1.57 (m, 3H), 1.38 (dt, J = 7.9, 6.7 Hz, 1H); ^{13}C NMR (101 MHz, Methanol-d_4) δ 167.3, 137.9, 133.5, 132.3, 131.2, 130.0, 128.3, 126.6, 126.0, 59.6, 52.0, 51.5, 38.3, 30.8, 26.7, 21.0, 12.0; HRMS (ESI) *m/z* calcd for $C_{23}H_{28}N_2O_2$ $[M^+H]^+$ 365.2224, found 365.2228.

These data are consistent with that reported in the literature.[51,102]

2.7.3. Amide analogues.

Amide coupling general procedure.

To a suspension of **1.35** (1 eq) in dichloromethane was added DIPEA (4 eq) and the resulting mixture stirred until clear. HOBt.H_2O (0.2 eq) and EDC.HCl (1.5eq) was added and the mixture stirred at room temperature for 30 mins. The appropriate amine (1.2 eq) was then added in one portion and stirred at room temperature under a nitrogen atmosphere overnight. After confirming completion with TLC, the reaction mixture was diluted with dichloromethane before concentrating. The resulting concentrate was then purified via chromatography, first on silica eluting with 9:1 CH_2Cl_2:MeOH followed by a C18 functionalised reverse phase column eluting with a gradient of 5-100 % MeOH in H_2O.

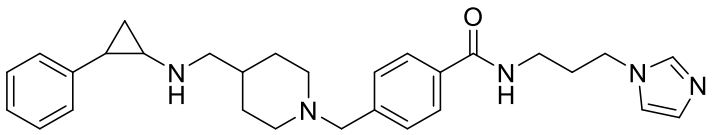

***N*-[3-(1*H*-imidazol-1-yl)propyl]-4-[(4-{[(2-phenylcyclopropyl)amino]methyl}piperidin-1-yl)methyl]benzamide, (2.8a).**

Isolated as a colourless oil, (174 mg, 32 %).

^{1}H NMR (400 MHz, Methanol-d_4) δ 7.78 (d, *J* = 8.4 Hz, 2H), 7.70 (s, 1H), 7.43 (d, *J* = 8.4 Hz, 2H), 7.25 – 7.18 (m, 2H), 7.18 (t, *J* = 1.3 Hz, 1H), 7.13 – 7.07 (m, 1H), 7.03 (dd, *J* = 8.2, 1.1 Hz, 2H), 6.97 (t, *J* = 1.1 Hz, 1H), 4.11 (t, *J* = 7.0 Hz, 2H), 3.56 (s, 2H), 3.39 (t, *J* = 6.8 Hz, 2H), 2.89 (brd-d, *J* = 11.4 Hz, 2H), 2.58 (d, *J* = 6.8 Hz, 2H), 2.30 – 2.26 (m, 1H), 2.10 (p, *J* = 6.9 Hz, 2H), 2.06 – 1.97 (m, 2H), 1.89 (ddd, *J* = 9.3, 5.9, 3.3 Hz, 1H), 1.79 – 1.69 (m, 2H), 1.59 – 1.45 (m, 1H), 1.32 – 1.18 (m, 2H), 1.10 – 1.02 (m, 1H), 1.01 – 0.95 (m, 1H); ^{13}C NMR (101 MHz, Methanol-d_4) δ 170.1, 143.4, 142.7, 138.5, 134.5, 130.7, 129.2, 129.1, 128.2, 126.7, 126.5, 120.6, 63.7, 56.2, 54.5, 45.7, 42.6, 38.1, 36.5, 32.0, 31.2, 25.2, 16.6; HRMS (ESI) *m/z* calcd for $C_{29}H_{37}N_5O$ $[M^+H]^+$ 472.3071, found 472.3088, calcd for $C_{29}H_{37}N_5O$ $[M+Na]^+$ 494.2890, found 494.2897; Purity 95.6%.

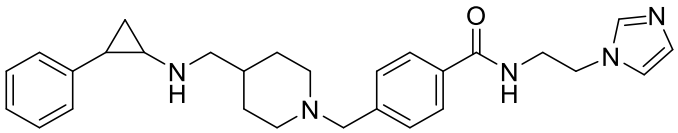

***N*-[2-(1*H*-imidazol-1-yl)ethyl]-4-[(4-{[(2-phenylcyclopropyl)amino]methyl} piperidin-1-yl)methyl]benzamide (2.8b).**

Isolated as a colourless oil, (155 mg, 30 %).

IR (cm^{-1}) 3277, 3026, 2919, 2807, 1639; ^{1}H NMR (400 MHz, Methanol-d_4) δ 7.74 (d, *J* = 8.4 Hz, 2H), 7.61 (t, *J* = 1.0 Hz, 1H), 7.39 (d, *J* = 8.3 Hz, 2H), 7.20 (t, *J* = 7.5 Hz, 2H), 7.13 – 7.07 (m, 2H), 7.05 – 7.00 (m, 2H), 6.96 (t, *J* = 1.1 Hz, 1H), 4.23 (t, *J* = 6.0 Hz, 2H), 3.69 (t, *J* = 6.0 Hz, 2H), 3.51 (s, 2H), 2.85 (brd-d, *J* = 11.4 Hz, 2H), 2.56 (dd, *J* = 6.8, 1.5 Hz, 2H), 2.26 (ddd, *J* = 7.5, 4.4, 3.3 Hz, 1H), 1.98 (t, *J* = 11.7 Hz, 2H), 1.89 (ddd, *J* = 9.2, 5.8, 3.2 Hz, 1H), 1.76 – 1.66 (m, 2H), 1.56 – 1.43 (m, 1H), 1.23 (qd, *J* = 12.2, 3.7 Hz, 2H), 1.11 – 1.01 (m, 1H), 1.00 – 0.93 (m, 1H); ^{13}C NMR (101 MHz, Methanol-d_4) δ 170.0, 143.3, 142.9, 138.6, 134.1, 130.6, 129.2, 129.1, 128.2, 126.7, 126.5, 120.8, 63.7, 56.2, 54.5, 46.9, 42.6, 41.8, 36.5, 31.2, 25.2, 16.7; HRMS (ESI) *m/z* calcd for $C_{28}H_{35}N_5O$ $[M^+H]^+$ 458.2915 found, ; Purity 99.2%.

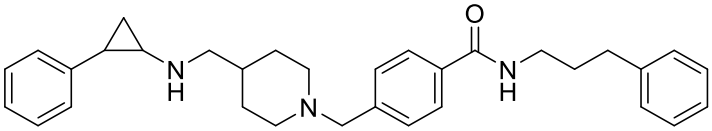

4-[(4-{[(2-phenylcyclopropyl)amino]methyl}piperidin-1-yl)methyl]-*N*-(3-phenylpropyl)benzamide (2.8c).

Isolated as a white solid, (147 mg, 26 %).

Mp 213-215ºC (DC); IR (cm^{-1}) 3348, 2542, 1650; ^{1}H NMR (400 MHz, Methanol-d_4) δ 7.91 (d, *J* = 8.3 Hz, 2H), 7.68 (d, *J* = 8.3 Hz, 2H), 7.35 – 7.12 (m, 10H), 4.40 (s, 2H), 3.54 (d, *J* = 12.6 Hz, 2H), 3.42 (t, *J* = 7.2 Hz, 2H), 3.18 (d, *J* = 6.8 Hz, 2H), 3.16 – 3.06 (m, 2H), 3.01 (dt, *J* = 7.9, 4.1 Hz, 1H), 2.73 – 2.67 (m, 2H), 2.59 (ddd, *J* = 10.3, 6.6, 3.6 Hz, 1H), 2.22 – 2.01 (m, 3H), 1.95 (p, *J* = 7.6 Hz, 2H), 1.76 – 1.55 (m, 3H), 1.38 (q, *J* = 6.8 Hz, 1H); ^{13}C NMR (101 MHz, Methanol-d_4) δ 169.1, 143.0, 139.2, 137.5, 133.3, 132.7, 129.7, 129.4, 129.1, 128.0, 127.4, 126.9, 61.0, 53.4, 52.8, 40.8, 39.7, 34.3, 32.3, 32.2, 28.1, 22.4, 13.4; HRMS (ESI) *m/z* calcd for $C_{32}H_{39}N_3O$ $[M^+H]^+$ 482.3166, found 482.3182; Purity 100%.

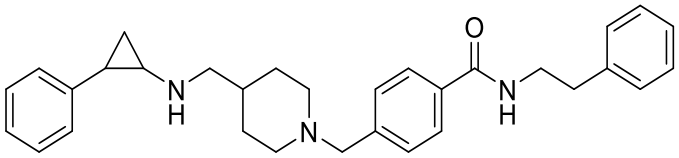

4-[(4-{[(2-phenylcyclopropyl)amino]methyl}piperidin-1-yl)methyl]-*N*-(2-phenylethyl) benzamide (2.8d).

Isolated as a yellow oil, (76 mg, 14 %).

IR (cm^{-1}) 3301, 3026, 2919, 2808, 1633; ^{1}H NMR (400 MHz, Chloroform-*d*) δ 7.66 (d, *J* = 8.0 Hz, 2H), 7.38 (d, *J* = 8.3 Hz, 2H), 7.34 (d, *J* = 6.9 Hz, 2H), 7.31 – 7.23 (m, 5H), 7.21 – 7.12 (m, 1H), 7.05 (d, *J* = 7.1 Hz, 2H), 6.23 (brd-s, 1H), 3.73 (q, *J* = 6.7 Hz, 2H), 3.53 (s, 2H), 2.95 (t, *J* = 6.9 Hz, 2H), 2.88 (brd-d, *J* = 11.3 Hz, 2H), 2.64 (d, *J* = 6.7 Hz, 2H), 2.34 (ddd, *J* = 7.2, 4.3, 3.2 Hz, 1H), 1.98 (t, *J* = 11.0 Hz, 2H), 1.90 (ddd, *J* = 9.1, 5.8, 3.1 Hz, 1H), 1.76 – 1.65 (m, 2H), 1.57 – 1.41 (m, 1H), 1.28 (qd, *J* = 12.2, 3.6 Hz, 2H), 1.07 (dt, *J* = 9.4, 4.8 Hz, 1H), 0.99 (dt, *J* = 6.8, 5.5 Hz, 1H); ^{13}C NMR (101 MHz, Chloroform-*d*) δ 167.4, 142.4, 139.0, 133.4, 129.3, 128.9, 128.8, 128.8, 128.3, 126.8, 126.6, 125.8, 125.5, 63.0, 55.5, 53.7, 41.8, 41.2, 35.9, 35.8, 30.5, 25.3, 17.1; HRMS (ESI) *m/z* calcd for $C_{31}H_{37}N_3O$ $[M^+H]^+$ 468.3010, found 468.3011; Purity 99.2%.

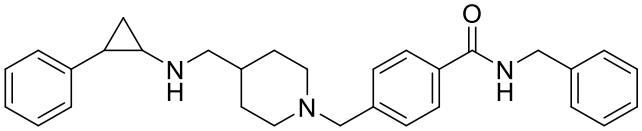

***N*-benzyl-4-[(4-{[(2-phenylcyclopropyl)amino]methyl}piperidin-1-yl)methyl]benzamide (2.8e).**

Isolated as a yellow oil, (159 mg, 31 %).

IR (cm^{-1}) 3298, 3027, 2917, 2808, 1634; ^{1}H NMR (400 MHz, Chloroform-*d*) δ 7.76 (d, *J* = 8.0 Hz, 2H), 7.44 – 7.23 (m, 9H), 7.16 (t, *J* = 7.3 Hz, 1H), 7.05 (d, *J* = 8.0 Hz, 2H), 6.57 (brd-s, 1H), 4.66 (s, 1H), 3.54 (s, 1H), 2.88 (brd-d, *J* = 11.0 Hz, 2H), 2.64 (d, *J* = 6.7 Hz, 2H), 2.34 (dt, *J* = 7.1, 3.6 Hz, 1H), 1.98 (t, *J* = 11.3 Hz, 2H), 1.90 (ddd, *J* = 8.9, 5.6, 3.0 Hz, 1H), 1.71 (brd-s, 2H), 1.56 – 1.42 (m, 1H), 1.28 (q, *J* = 11.5 Hz, 2H), 1.07 (dt, *J* = 9.3, 4.7 Hz, 1H), 0.99 (q, *J* = 5.9 Hz, 1H); ^{13}C NMR (101 MHz, Chloroform-*d*) δ 167.3, 142.6, 142.5, 138.4, 133.1, 129.2, 128.8, 128.3, 128.0, 127.6, 127.0, 125.8, 125.5, 63.0, 55.5, 53.7, 44.1, 41.8, 35.9, 30.6, 30.6, 25.3; HRMS (ESI) *m/z* calcd for $C_{30}H_{35}N_3O$ $[M^+H]^+$ 454.2853, found 454.2871; Purity 99.2%.

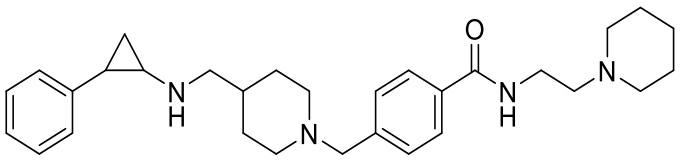

4-[(4-{[(2-phenylcyclopropyl)amino]methyl}piperidin-1-yl)methyl]-*N*-[2-(piperidin-1-yl)ethyl]benzamide (2.8f).

Isolated as a yellow oil, (52 mg, 10 %).

IR (cm^{-1}) 3312, 3026, 2930, 2851, 2803, 1635; ^1H NMR (400 MHz, Methanol-d_4) δ 7.79 (d, *J* = 8.4 Hz, 2H), 7.43 (d, *J* = 8.3 Hz, 2H), 7.25 – 7.17 (m, 2H), 7.13 – 7.07 (m, 1H), 7.06 – 7.00 (m, 2H), 3.59 – 3.50 (m, 4H), 2.95 – 2.84 (m, 2H), 2.62 – 2.55 (m, 4H), 2.52 (brd-s, 4H), 2.27 (ddd, *J* = 7.5, 4.4, 3.4 Hz, 1H), 2.08 – 1.96 (m, 2H), 1.89 (ddd, *J* = 9.3, 5.9, 3.3 Hz, 1H), 1.78 – 1.69 (m, 2H), 1.63 (p, *J* = 5.5 Hz, 4H), 1.56 – 1.43 (m, 3H), 1.25 (qd, *J* = 12.4, 3.7 Hz, 2H), 1.11 – 0.94 (m, 2H); ^{13}C NMR (101 MHz, Methanol-d_4) δ 169.8, 143.4, 142.6, 134.5, 130.7, 129.2, 128.2, 126.7, 126.5, 63.8, 58.9, 56.2, 55.5, 54.5, 42.6, 37.8, 31.2, 30.5, 26.5, 25.2, 25.1, 16.6; HRMS (ESI) *m/z* calcd for $C_{30}H_{42}N_4O$ $[M^+H]^+$ 475.3432, found 475.3435; Purity 96.1%.

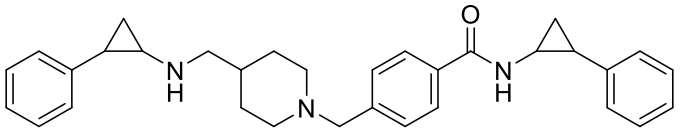

***N*-(2-phenylcyclopropyl)-4-[(4-{[(2-phenylcyclopropyl)amino]methyl}piperidin-1-yl)methyl]benzamide (2.8g).**

Isolated as a colourless oil, (105 mg, 19 %).

IR (cm^{-1}) 3287, 3026, 2917, 2795, 1633; ^1H NMR (400 MHz, Chloroform-*d*) δ 7.75 (d, *J* = 8.2 Hz, 2H), 7.40 (d, *J* = 8.2 Hz, 2H), 7.34 – 7.14 (m, 8H), 7.05 (d, *J* = 7.1 Hz, 2H), 6.63 (d, *J* = 2.1 Hz, 1H), 3.55 (s, 2H), 3.09 (dq, *J* = 7.5, 3.4 Hz, 1H), 2.88 (d, *J* = 11.3 Hz, 2H), 2.64 (d, *J* = 6.8 Hz, 2H), 2.34 (ddd, *J* = 7.2, 4.3, 3.2 Hz, 1H), 2.19 (ddd, *J* = 9.6, 6.3, 3.4 Hz, 1H), 2.05 – 1.94 (m, 2H), 1.90 (ddd, *J* = 9.1, 5.8, 3.1 Hz, 1H), 1.78 – 1.66 (m, 2H), 1.56 – 1.44 (m, 1H), 1.38 – 1.22 (m, 4H), 1.08 (dt, *J* = 9.4, 5.0 Hz, 1H), 0.99 (dt, *J* = 6.9, 5.5 Hz, 1H); ^{13}C NMR (101 MHz, Methanol-d_4) δ 168.6, 142.5, 142.4, 140.5, 133.0, 129.3, 128.4, 128.3, 126.9, 126.6, 126.2, 125.8, 125.5, 62.9, 55.5, 53.7, 41.8, 35.9, 32.6, 30.5, 30.5, 25.2, 24.9, 17.1, 16.3; HRMS (ESI) *m/z* calcd for $C_{32}H_{37}N_3O$ $[M^+H]^+$ 480.3010, found 480.3024; Purity 97.1%.

Chapter Three

3. The design, synthesis and biological activity of a dual LSD1/HDAC inhibitor and control compounds.

3.1. Introduction.

'One drug, one target, one disease' is a common phrase found in the academic literature regarding the philosophy of many drug producers. This is in principle a logical approach, as designing a drug for a single target allows the researcher to develop a potent, highly selective drug with minimal off-target effects. However, single target drugs have their limitations. Diseases such as cancer are often complex conditions for which there is no single treatment. In addition, the development of resistance to treatment is a common occurrence frequently making a single treatment ineffective. Often, the solution is combination therapy in which a number of drugs are used in an effort to overcome these hurdles, but multiple drugs increase the risk of adverse side effects, drug-drug interactions and other complications.

While drugs that unintentionally hit multiple targets can be problematic, drugs that are designed to do so can have great advantages. In the same way that a single target drug can be designed to be both specific and potent, a dual mechanism drug can be just as specific for its intended targets while also having high potency. It can reduce the need for combination therapy, reducing the risk of drug-drug interaction as well as making drug resistance less likely.

There are a number of so-called multi-target drugs already FDA approved, primarily for the treatment of cancers. In addition, there are a number of further drugs which are approved for use in combination. However the term 'multi-target' is used throughout the literature to refer to drugs which simply lack specificity rather than drugs which target truly different proteins. For example, Li *et al.* claims that the first approved multi-target drug was imatinib in 2001 for chronic myeloid leukaemia and was followed by sorafenib in 2005 for renal cell carcinoma.[130] In reality, both of these drugs simply inhibit more than one kinase making them unselective rather than multi-target.

There are currently no single-target LSD1 inhibitors approved for use, neither are there any approved multi-target inhibitors of LSD1. To this end, the focus of this work is the synthesis and biological evaluation of a dual LSD1/HDAC inhibitor.

LSD1 has a close association with HDACs and along with HDAC1 and 2 is a subunit of the corepressor complexes, RE1 silencing transcription factor (CoREST)[131] and nucleosome remodelling and deacetylating complex (NURD).[132] Dhanusha *et al.* identified LSD1 itself as a substrate of HDAC1, which deacetylates LSD1 at K374 resulting in altered histone 3 binding and gene expression activity of LSD1.[133] The inhibition of HDAC1 therefore has the effect of increasing LSD1 acetylation and hence reducing LSD1 activity. This in turn increases H3K4 methylation leading to gene repression.[133–135] What's more, inhibiting LSD1 and HDAC in combination has been shown to synergistically lead to apoptosis in glioblastoma cells but not in normal human astrocytes.[136] This serves to validate dual LSD1-HDAC inhibition and hence the need for dual inhibitors of the same.

There are now many literature examples of dual LSD1/HDAC inhibitors available. Duan *et al.* reported several examples of tranylcypromine derivatives with an additional HDAC inhibiting pharmacophore (Figure 4.1). Their most potent inhibitor is one such compound (**3.1**) in which a SAHA analogue is modified by adding TCP to the para position of the benzene ring. **3.1** is specific for LSD1 over MAOA and B, inhibiting LSD1 with an IC_{50} value of 1.20 μM. It also has very potent class I HDAC activity, inhibiting HDAC1, 2 and 5 at 0.015, 0.023 and 16.84 μM respectively. **3.1** also showed good in cell activity in a number of cancer cell lines through antiproliferation assays and apoptosis profiles.[137] Other examples included TCP analogues modified to include a HDAC inhibiting constituent incorporating both hydroxamic acid and benzamide zinc binding groups (Figure 3.1, **3.2 – 3.5**).

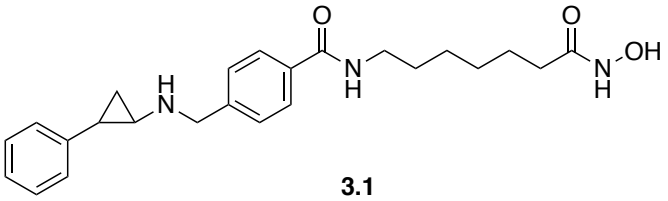

3.1
LSD1 IC_{50} = 1.20 μM
MAOA IC_{50} = 21.11 μM
MAOB IC_{50} = 87.09 μM
HDAC1 IC_{50} = 0.015 μM
HDAC2 IC_{50} = 0.023 μM
HDAC5 IC_{50} = 16.84 μM

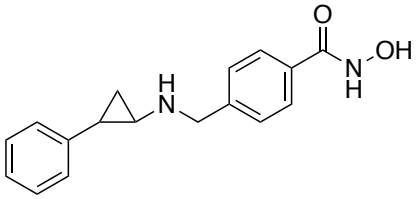

3.2
LSD1 IC_{50} = 4.09 μM
MAOA IC_{50} = 45.84 μM
MAOB IC_{50} = >100 μM
HDAC1 IC_{50} = 1.44 μM
HDAC2 IC_{50} = 3.10 μM

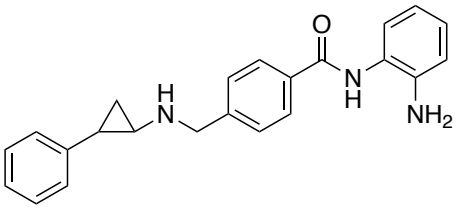

3.3
LSD1 IC_{50} = 7.16 μM
MAOA IC_{50} = 50.07 μM
MAOB IC_{50} = 87.09 μM
HDAC1 IC_{50} = 0.218 μM
HDAC2 IC_{50} = 0.413 μM

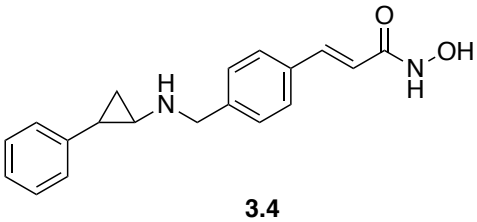

3.4
LSD1 IC_{50} = 2.21 μM
MAOA IC_{50} = 39.41 μM
MAOB IC_{50} = >100 μM
HDAC1 IC_{50} = 0.012 μM
HDAC2 IC_{50} = 0.025 μM
HDAC5 IC_{50} = 2.97 μM

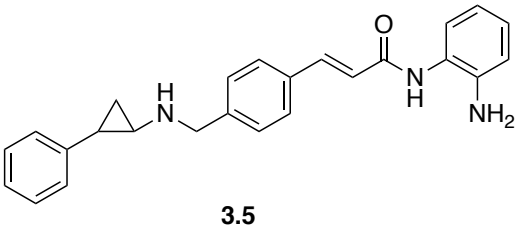

3.5
LSD1 IC_{50} = 3.85 μM
MAOA IC_{50} = 36.89 μM
MAOB IC_{50} = >100 μM
HDAC1 IC_{50} = 0.314 μM
HDAC2 IC_{50} = 0.491 μM

Figure 3.1. *Examples of dual LSD1/HDAC inhibitors.*[137]

A further example of a dual LSD1/HDAC inhibitor was described recently by Kalin. A series of hybrid compounds based on the known HDAC inhibitors vorinostat (**1.39**), panbinostat (**1.41**) and entinostat (**1.47**) together with the tranylcypromine analogue (Figure 3.2, **3.6**) of the LSD1 inhibitor bizine (**1.4**). These compounds were designed to target the CoREST complex and hence, inhibit LSD1, HDAC1 and 2. Their best example was a hybrid of **3.6** and **1.47** which they called corin (Figure 3.2, **3.7**). Corin was a potent inhibitor of LSD1 with a K_i value of 0.10 μM and inhibited HDAC1 with an IC_{50} of 0.147 μM. In addition, LSD1 and HDAC1

were inhibited as part of the CoREST ternary complex with IC_{50} values of 0.33 and 0.206 μM respectively. For comparison, GSK2879552 inhibited LSD1 as part of this complex with an IC_{50} of 0.38 μM.[138]

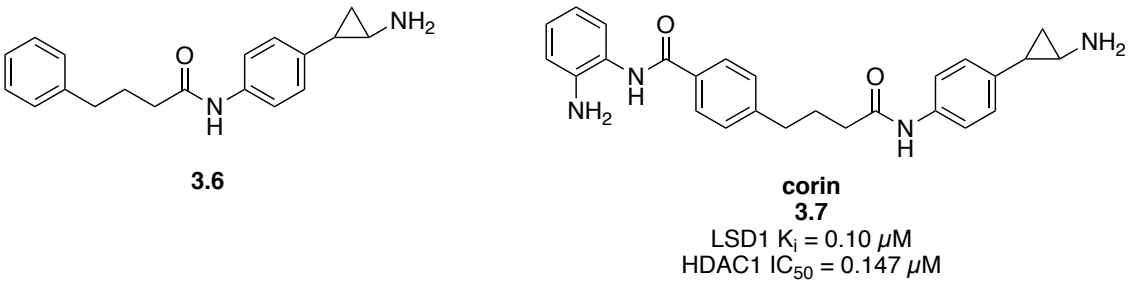

Figure 3.2. *The tranylcypromine analogue of bizine and the corresponding LSD1/HDAC inhibitor hybrid.*[138]

3.1.1. Chapter aims.

In this chapter we will present the synthesis and biological activity of a dual action LSD1/HDAC inhibitor (**3.8**). Like the novel LSD1 inhibitors presented in the previous chapter, our dual inhibitor is also based on the structure of the GSK clinical candidate, GSK2879552. The carboxylic acid functional group on GSK2879552, which was subsequently converted to an amide, is now converted to a hydroxamic acid. The change is minimal, adding only one nitrogen and one hydrogen but in doing so creates a hybrid compound with two modes of action. In addition, we have created a series of control compounds (**1.35**, **3.9**, **3.10**) to help us evaluate the biological activity of **3.8**.

3.2. The synthesis of a dual LSD1/HDAC inhibitor (compound 3.8).

There are two conventional methods of hydroxamic acid synthesis. The first is activation of the carboxylic acid by conversion to the acid chloride, followed by nucleophilic substitution with the appropriate *O*-protected hydroxamate. Deprotection then affords the hydroxamic acid. The second route is direct nucleophilic substitution of an ester with hydroxylamine.

As our synthetic route to GSK2879552 (section 2.2) features the synthesis of an ester prior to the final carboxylic acid it seemed logical to go directly from the ester to the hydroxamic acid. Synthesis of the methyl ester was carried out as previously described (section 2.2). The methyl ester was then dissolved in anhydrous methanol before adding a solution of hydroxylamine in methanol and stirring at room temperature overnight. The pH of the mixture is then adjusted to ~7 before filtering and purifying to give **3.8** as a white solid in around 25% yield with no starting material recovery (Scheme 3.1).

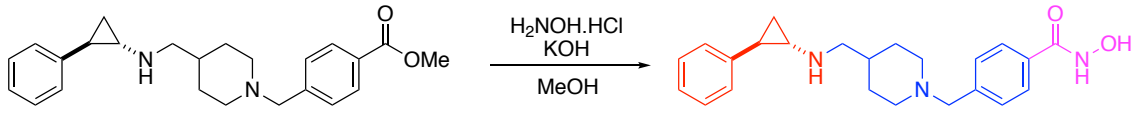

2.7a **3.8**

Scheme 3.1. *The synthesis of dual inhibitor, **3.8**, from the GSK2879552 methyl ester precursor.*

The low yield prompted us to explore a second approach to the synthesis of **3.8**. Amitai *et al.* described a method for the synthesis of 4-bromomethyl benzhydroxamic acid[139] (**3.11**). This method starts with bromomethylbenzoic acid (**3.9**) which is activated by conversion to the acid chloride (**3.10**) before substitution with hydroxylamine to give **3.11** in 79% yield (Scheme 3.2). In principle, **3.9** can then be used in place of **2.5a** in the rest of the synthesis (Scheme 2.1, route B). In practice however, the solubility of **3.11** made the subsequent reactions difficult and this route was abandoned in favour of the original method.

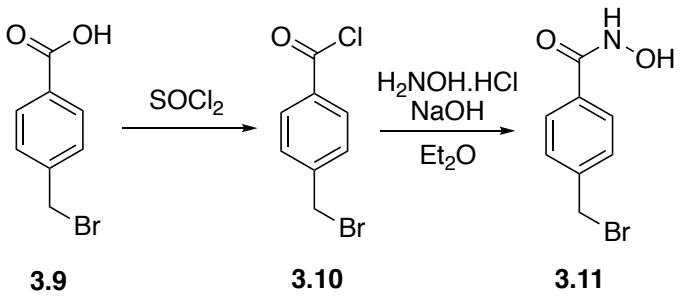

3.9 **3.10** **3.11**

Scheme 3.2. *The synthesis of 4-bromomethylbenzhydroxylamine.*[139]

3.3. The synthesis of our control compounds.

In order to effectively evaluate the biological activity of **3.8**, we needed controls against which **3.8** could be compared. These control compounds would ideally be similar in structure to **3.8** but lacking either one or both pharmacophores so that any difference in activity could be attributed to the relevant feature.

The positive control for LSD1 inhibition is GSK2879552. This should effectively inhibit LSD1 and hence provide a good benchmark against which to compare **3.8** but is not expected to inhibit HDACs.

The positive control for HDAC inhibition is compound **3.12**. **3.12** has the same structure as **3.8** with the exception of the regiochemistry around the cyclopropyl ring. By placing both substitutions on the same carbon in place of adjacent carbons, LSD1 inhibitory activity was observed to be lost (See Section 3.4) and hence **3.12** should inhibit HDACs but not LSD1.

Finally, we made negative control **3.13** which retains the carboxylic acid functional group of GSK2879552 but also contains the altered regiochemistry of the cyclopropyl group, thus rendering **3.13** inert to both LSD1 and HDAC activity.

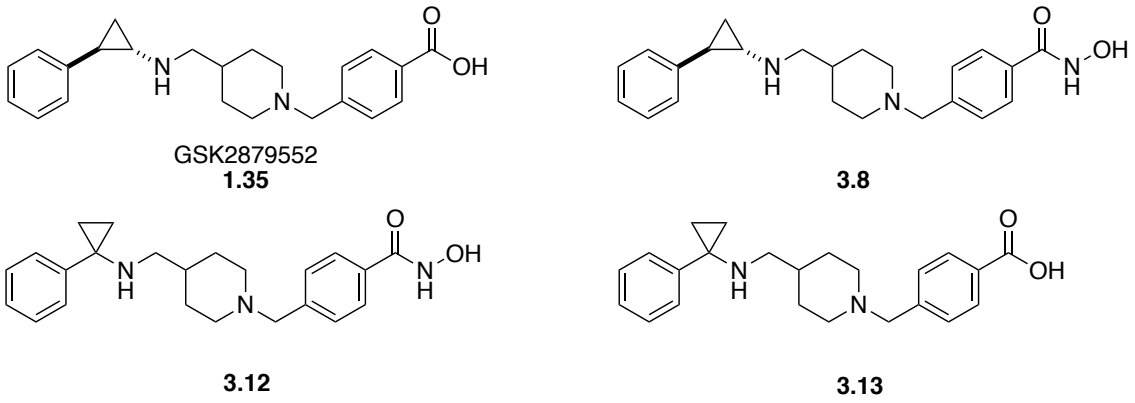

Figure 3.3. *The structure of our dual LSD1/HDAC inhibitor and control compounds.*

The synthesis of both **3.12** and **3.13** was carried out via the same route as for **3.8** and **1.35** but using 1-phenyl-1-cyclopropylamine (**3.15**) in place of tranylcypromine. **3.15** was not commercially available but its synthesis could be achieved in one step via Curtius rearrangement from the carboxylic acid **3.14** (scheme 3.3).

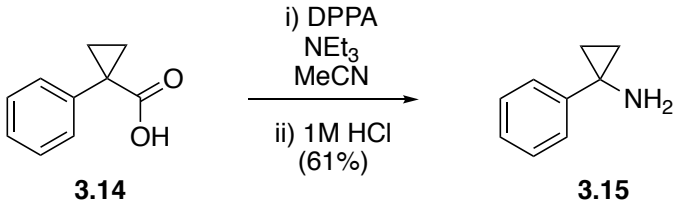

Scheme 3.3. *The conversion of carboxylic acid **3.14** to amine **3.15** via the Curtius rearrangement.*

3.4. The biological activity of dual inhibitor 3.8.

3.4.1. Cell free assays.

LSD1 Inhibition.

The first step was to test dual inhibitor **3.8** along with all control compounds for LSD1 inhibition in a cell free assay. Along with these compounds we also tested two further compounds for LSD1 activity, **3.15** and **3.16**. **3.15** is the analogue of tranylcypromine and its status in terms of LSD1 inhibition has never been reported. **3.16**, the precursor to **3.12** and **3.13**, was also tested as again, the LSD1 activity of the 1-phenyl-1-cyclopropylamine containing compounds was hitherto unknown.

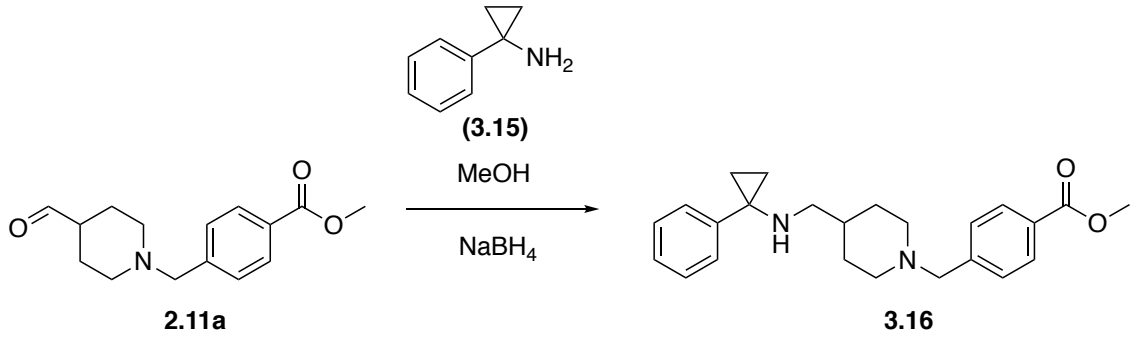

2.11a **3.16**

Scheme 3.4. *Reductive amination step with tranylcypromine analogue **3.15** to give the precursor compound to both **3.12** and **3.13**.*

Assay results showed that both dual inhibitor **3.8** and GSK2879552 were the only active compounds thus showing that the regiochemistry of the cyclopropyl ring is important to LSD1 activity. **3.8** was found to have an IC_{50} value of 0.53 μM (pIC_{50}: 6.27±0.02). This was observed to be more potent than GSK2879552, which had an IC_{50} value of 1.54 μM (pIC_{50}: 5.81±0.10).

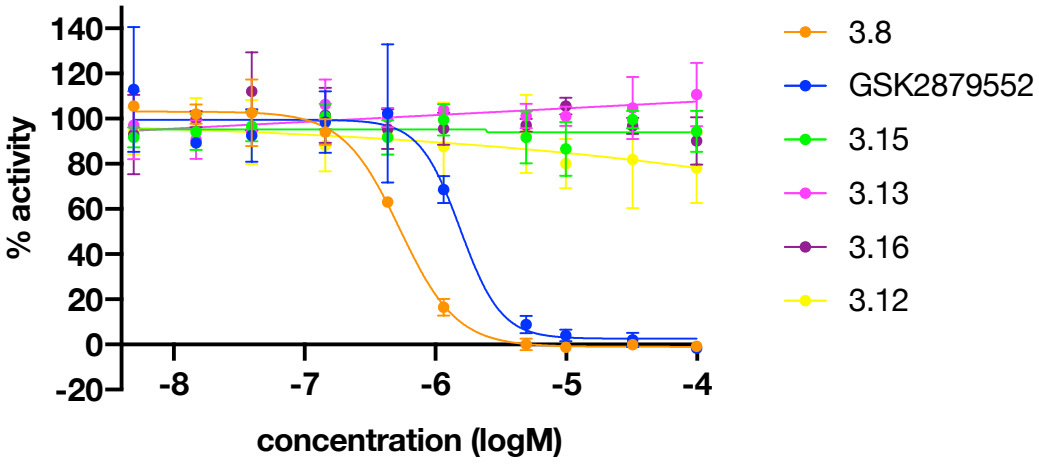

Figure 3.4. *Graphical representation of the LSD1 assay results for our dual inhibitor and control compounds.*

Data shown as % activity ± Std. Error, n=3.
Data generated by Belle et al., Oxford University (unpublished).

Compound	LSD1 pIC_{50}
GSK2879552	5.81±0.10
3.8	6.27±0.02
3.12	< 4
3.13	< 4
3.15	< 4
3.16	< 4

Table 3.1. *pIC_{50} data recorded for dual inhibitor **3.8** and control compounds.*

Data shown as pIC_{50} ± Std. Error, n=3.
Data generated by Belle et al., Oxford University (unpublished).

HDAC inhibition study.

Having found that our dual inhibitor **3.8** inhibits LSD1 with a good level of potency, the next step was to test HDAC inhibitory activity. **3.8** along with control compounds GSK2879552, **3.12** and **3.13** were each tested for activity in HDAC 1, 3, 6 and 8. Both the negative control **3.13** and GSK2879552 showed no activity at the levels tested. Both these compounds have a carboxylic acid functional

group and the lack of activity suggests that the rest of the molecule does not have sufficient binding affinity in the HDACs tested to hold the compound in place and allow the carboxylic acid to bind to the zinc cofactor. This result also shows that **3.13** makes a good negative control for **3.8**.

Dual inhibitor **3.8** showed activity in all HDACs tested but was particularly potent in HDAC6 and to a slightly lesser extent HDAC8 with IC_{50} values of 5.04 (pIC_{50}: 5.27±0.01), 2.28 (pIC_{50}: 5.64±0.02), 0.140 (pIC_{50}: 6.85±0.22) and 0.287 μM (pIC_{50}: 6.54±0.04) in HDAC1, 3, 6 and 8 respectively.

Positive HDAC control **3.12** also showed good activity across the range and again showing higher specificity in HDAC6. IC_{50} values were 7.57 (pIC_{50}: 5.12±0.01), 4.09 (pIC_{50}: 5.38±0.02), 0.248 (pIC_{50}: 6.60±0.09), 0.449 μM (pIC_{50}: 6.34±0.06), in HDAC1, 3, 6 and 8 respectively. This result is interesting as dual inhibitor **3.8** is around twice as potent as **3.12** in all HDAC isoforms and suggests that the regiochemistry around the cyclopropyl ring is not only important for LSD1 inhibition, but also affects HDAC affinity. One further point is that as well as being a good positive control compound, **3.12** is also a good, novel HDAC inhibitor in its own right.

	pIC_{50}			
	HDAC1	**HDAC3**	**HDAC6**	**HDAC8**
GSK2879552	< 4	< 4	< 4	< 4
3.8	5.27±0.01	5.64±0.02	6.85±0.22	6.54±0.04
3.12	5.12±0.01	5.38±0.02	6.60±0.09	6.34±0.06
3.13	< 4	< 4	< 4	< 4
TSA	7.00±na	8.71±0.05	8.66±0.14	6.52±0.10

Table 3.2. *HDAC assay data recorded for dual inhibitor **3.8** and control compounds. TSA used as a standard. na = not available.*

Data shown as pIC_{50} ± Std. Error, n=3.
Data generated by Ruzic et al., University of Belgrade (unpublished).

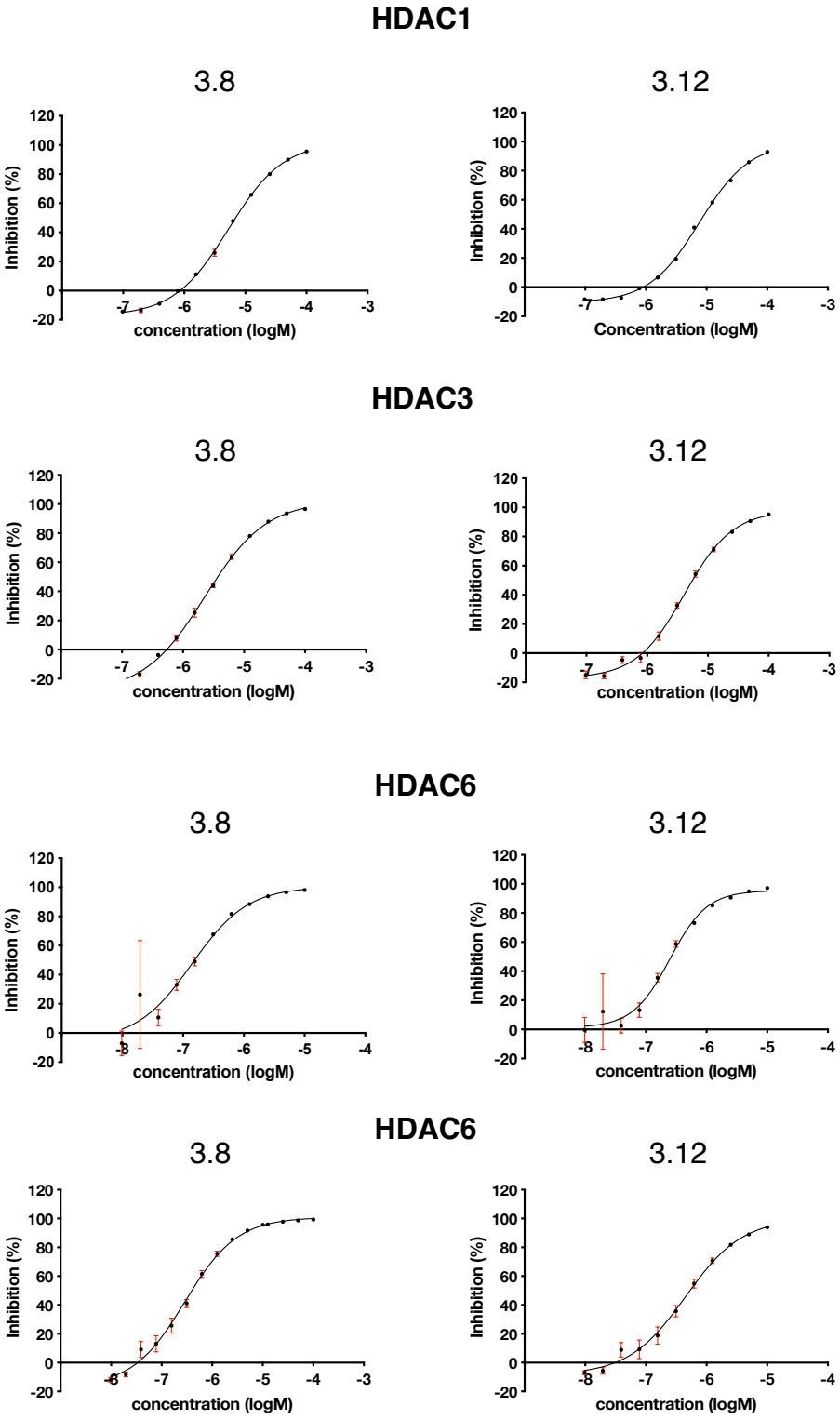

Figure 3.5. *Graphical representation of the HDAC assays recorded for dual inhibitor **3.8** and positive HDAC control **3.12**.*

Data shown as % inhibition ± Std.Error, n=3.
Data generated by Ruzic et al., University of Belgrade (unpublished).

It should be noted that in November 2017, dual inhibitor **3.8** was reported in a patent filed by Jubilant Biosys Ltd.[140] **3.8** is listed as one of 160 compounds and has limited data attached. However, the patent does state the IC_{50} values for LSD1 and HDAC6 as 0.011 and 0.235 μM respectively. The stereochemistry of the patent compound is not disclosed and hence it is difficult to directly compare these data to the data we have collected for **3.8**.

3.4.2. Cellular Thermal Shift Assay (CETSA).

CETSA was used to assess the thermal stability of the target enzymes, LSD1 and HDAC 6, upon ligand binding in THP-1 cells. Cells were treated with 500 nM of each compound and the response measured using western blot (Figure 3.6). In terms of binding to LSD1, **3.8** was found to bind as well as GSK2879552 whilst both the positive HDAC control **3.12** and negative control **3.13** performed no better than untreated cells. These data are consistent with good engagement between dual inhibitor **3.8** and LSD1 and poor engagement between LSD1 and control compounds **3.12** and **3.13**.

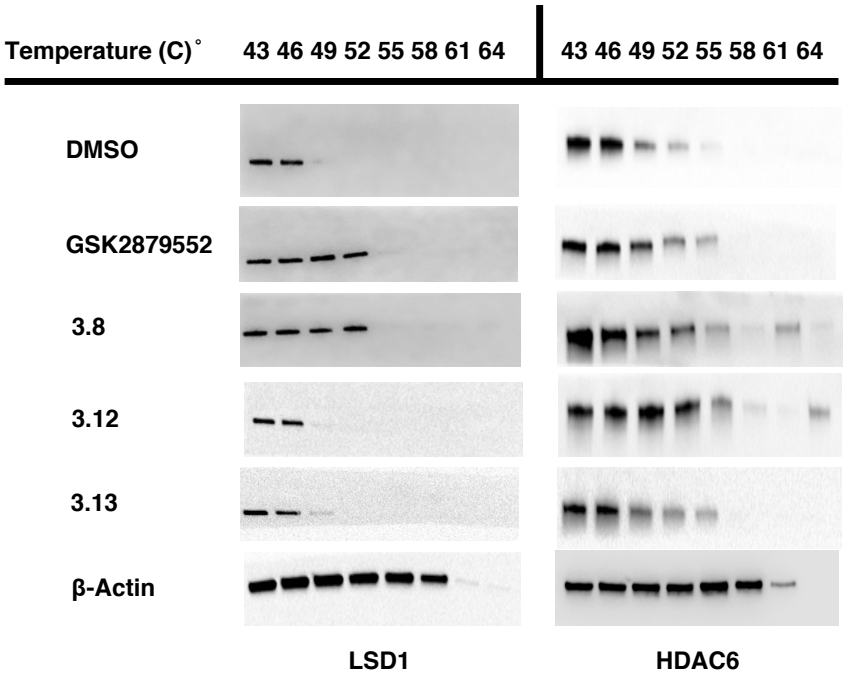

Figure 3.6. *Western blot of CETSA on dual inhibitor **3.8** and control compounds.*
Data generated by Bulut et al., Koc University (unpublished).

Binding to HDAC6 was observed in both **3.8** and positive HDAC control **3.12**. GSK2879552 and negative control **3.13** both performed no better than untreated cells. Again, these data are consistent with good engagement between **3.8** and HDAC6 and taken together, these data support **3.8** as being a dual LSD1 HDAC inhibitor.

3.4.3. Leukaemia cell viability.

In cell activity was investigated by analysing dual inhibitor **3.8** and control compounds in both fused MLL and non-MLL fused cell lines (Table 3.4, Figure 3.8, Figure 3.9). All cells showed sensitivity to **3.8** with IC_{50} values below 20 μM in all cells but in particular MOLM-13 in which **3.8** outperformed all controls with an IC_{50} of 1.3 μM. Negative control **3.13** behaved as anticipated with IC_{50} values above the maximum dose of 20 μM in all cells whilst positive LSD1 control, GSK2879552, only showed activity in MOLM-13. Positive HDAC control **3.12** showed activity in all cell lines and again in particular MOLM-13. It is tempting to say this data may suggest a greater sensitivity to the HDAC inhibiting function of **3.8** however, if this data is taken together with that for **2.8a-g** (chapter 2) it shows that compounds based on GSK2879552 which inhibit LSD1 and not HDAC can be just as if not more active in these cell lines.

Compound	MLL-AF9 Fused		Non-MLL Fused	
	THP-1 IC_{50} (μM)	**MOLM-13** IC_{50} (μM)	**K562** IC_{50} (μM)	**JURKAT** IC_{50} (μM)
GSK2879552	>20	15.0±3.5	>20	>20
3.8	16.3±5.4	1.3±0.4	16.6±2.6	15.5±1.4
3.12	9.7±2.4	6.7±1.6	17.6±1.6	10.7±0.8
3.13	>20	>20	>20	>20

Table 3.3. *Tabulated cell viability data gathered for **3.8** and control compounds in MLL and non-MLL cell lines.*

Data shown as % cell viability ± stdp, THP-1 n=3, MOLM-13 n=4, K562 and JURKAT n=2.
Data generated by Bulut et al., Koc University (unpublished).

Looking at THP-1 cell viability data for all these compounds thus builds up a slightly bigger picture of functional groups that show high activity in THP-1 (Figure 3.7). Compounds with a carboxylic acid show poor activity in all cases. Compounds in which the carboxylic acid is substituted with an amide improves activity but not in all cases. Amides functionalised with a hydroxyl group show good activity in all tested cell lines, whilst amides functionalised with a carbon chain in which three carbons have also shown good activity in THP-1 but poor activity when the number of carbons is reduced.

Regiochemistry around the cyclopropyl ring does not seem to have any significant effect. Comparing **3.8** and **3.12** shows that **3.8** has better activity in MOLM-13 and **3.12** is more active in THP-1 and JURKAT. Both have similar activity in K562.

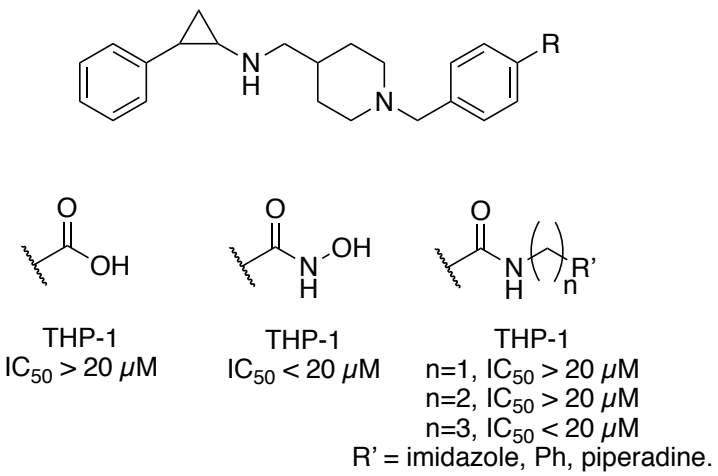

Figure 3.7. *Comparison of the effect of changing the R-group at the end of GSK2879552 on activity in cancer cells.*

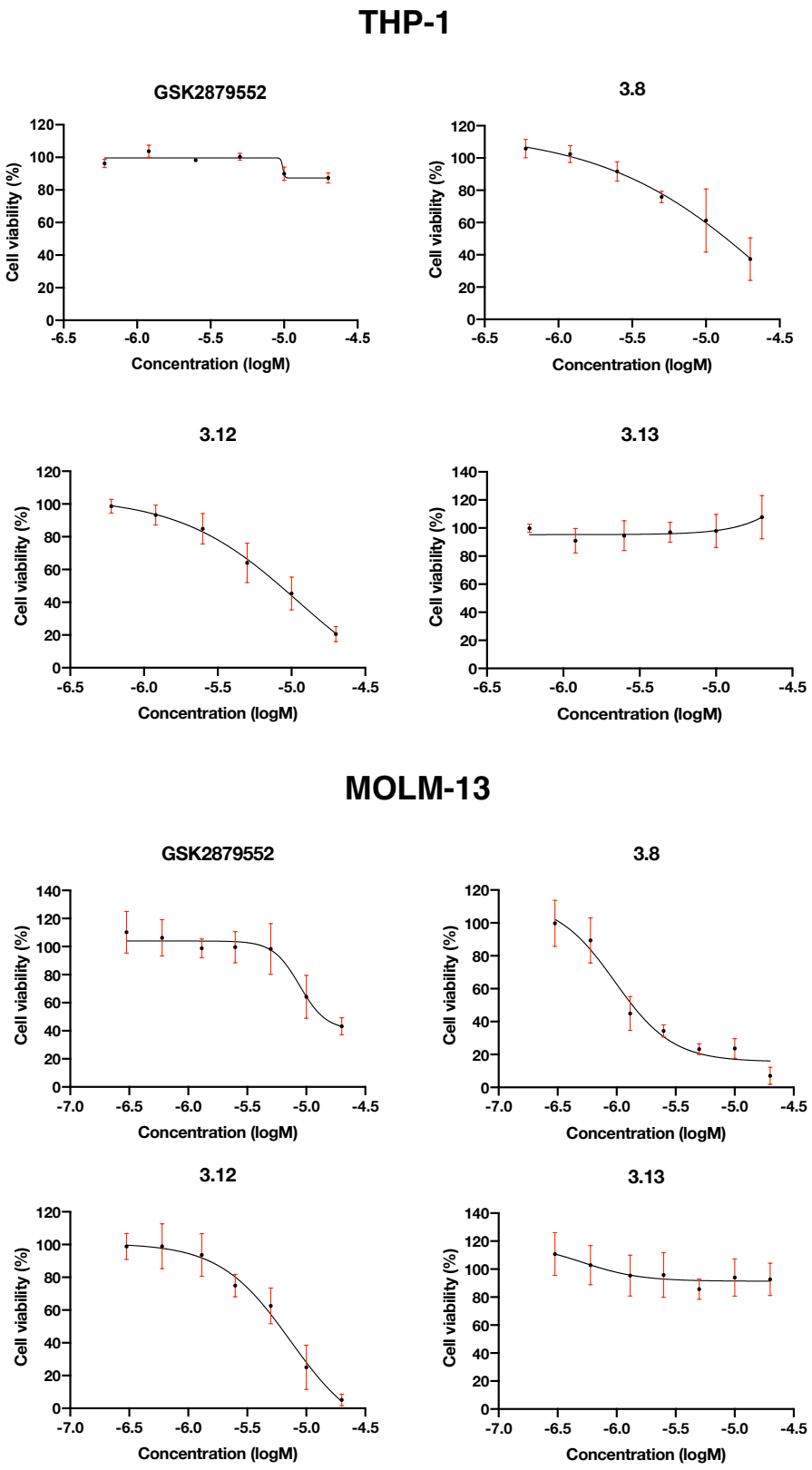

Figure 3.8. *Graphical representation of cell viability assays in THP-1 and MOLM-13 cells.*

Data shown as % cell viability ± stdp, THP-1 n=3, MOLM-13 n=4.
Data generated by Bulut et al., Koc University (unpublished).

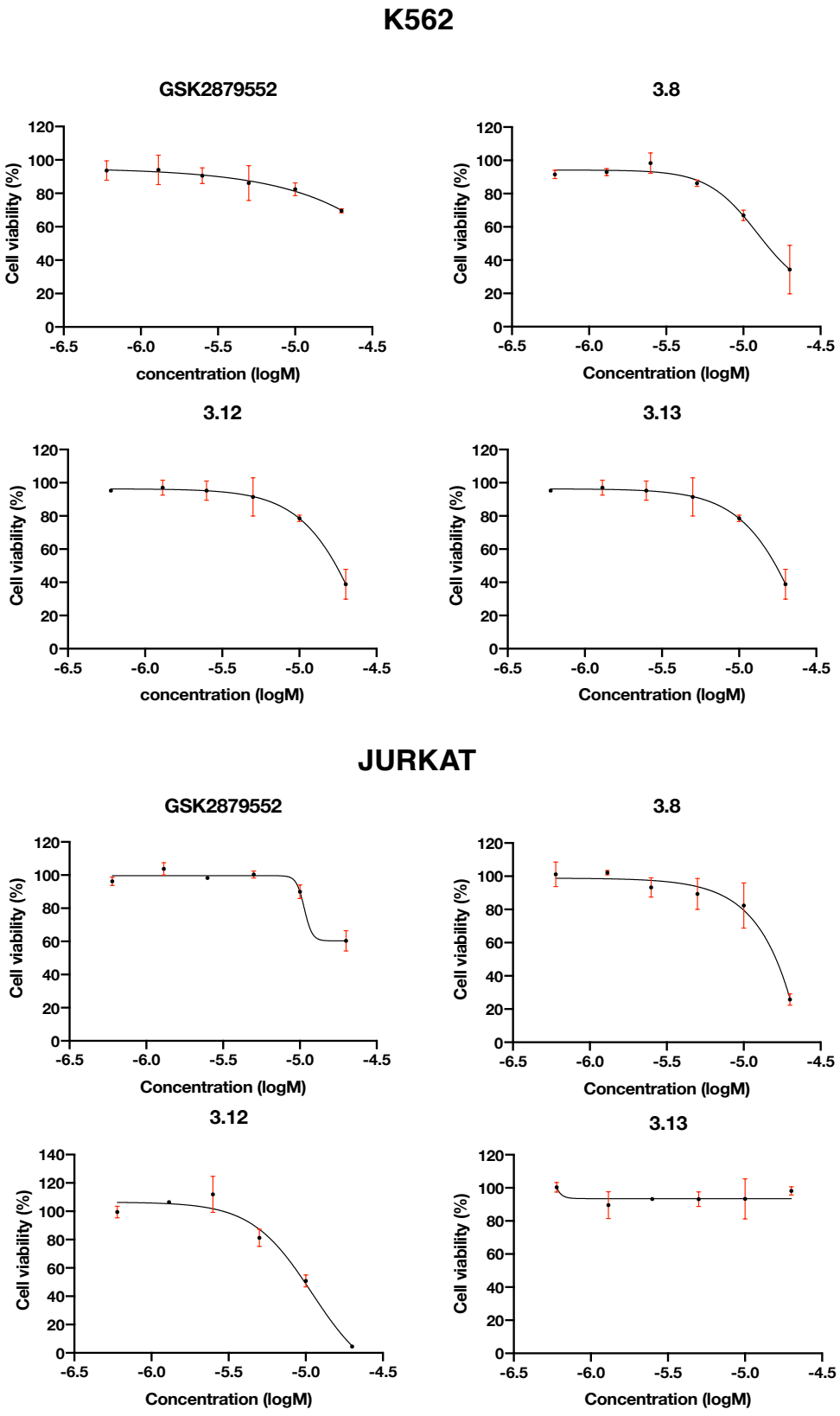

Figure 3.9. *Graphical representation of cell viability assays in K562 and JURKAT cells.*

Data shown as % cell viability ± stdp, n=2.
Data generated by Bulut et al., Koc University (unpublished).

3.4.4. Methylation and acetylation fold change in response to inhibition.

As a dual inhibitor to both LSD1 and HDAC, an increase in both methylation and acetylation levels would be expected in cells treated with **3.8**. H3K4me and H3K9me levels in THP-1 cells were analysed by western blot over 24 hours using a 5 μM dose of the appropriate inhibitor (Figure 3.10).

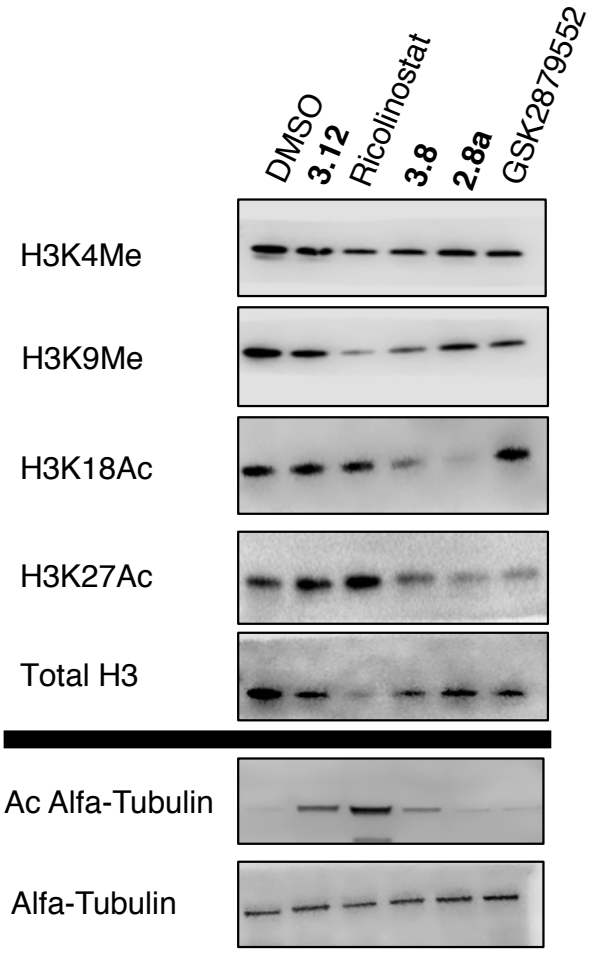

Figure 3.10. *Western blot of methylation and acetylation levels in THP-1 cells in response to inhibition of LSD1 and HDACs.*
Data generated by Bulut et al., Koc University (unpublished).

No significant change was seen in either H3K4me or H3K9me levels in response to **3.8**. In contrast, LSD1 inhibitors GSK2879552 and **2.8a** both showed 1.5-fold changes in H3K4me levels. All HDAC inhibitors showed no change in methylation levels relative to untreated cells as expected.

An observed 1.8-fold increase in H3K27Ac levels was seen in cells treated with **3.8**, lower than both control compounds, **3.12** and ricolinostat which showed 2 and 6-fold increases respectively. Positive HDAC control **3.12** also showed a 1.9-fold increase in H3K18Ac levels relative to just 1.1-fold for **3.8** (Figure 3.11, Table 3.5).

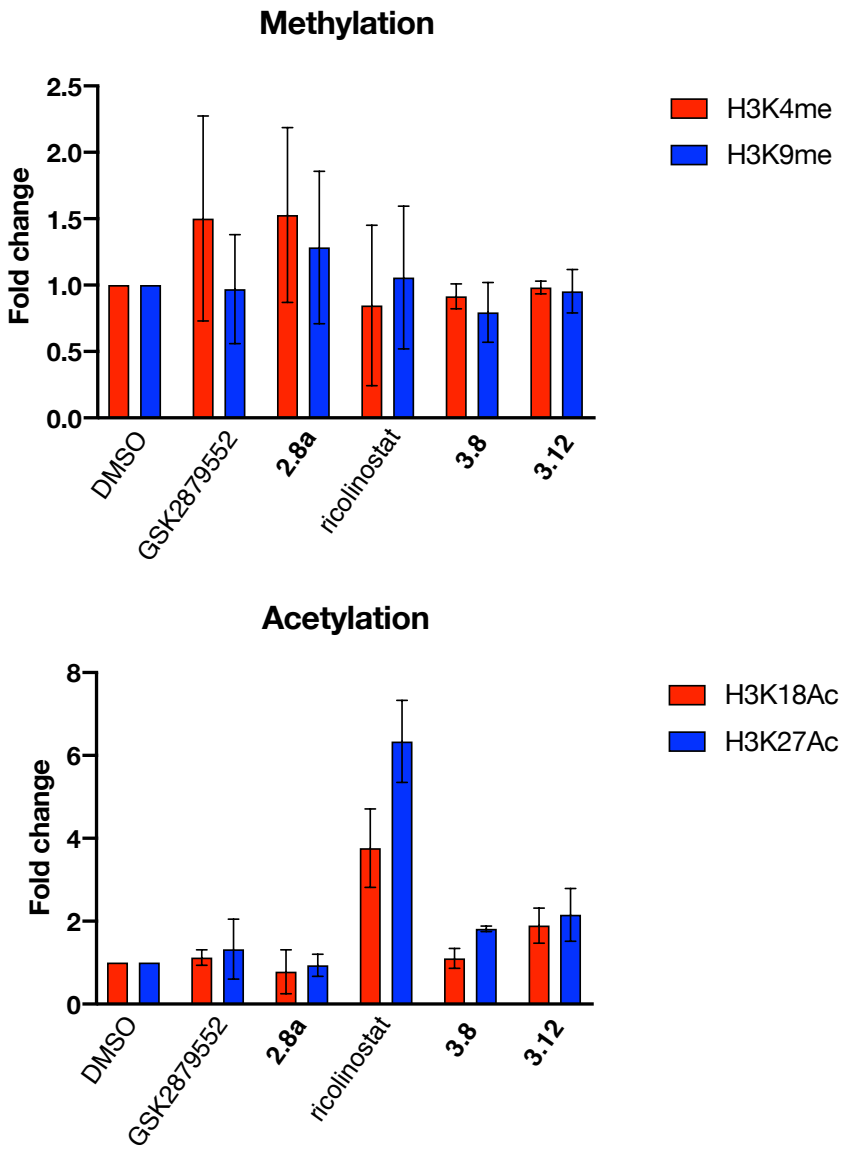

Figure 3.11. *Graphical representation of methylation and acetylation levels in THP-1 cells in response to LSD1 and HDAC inhibition.*

Data shown as fold change ± stdp, n=2.
Data generated by Bulut et al., Koc University (unpublished).

As a further control, levels of acetylated α-tubulin (Ac-Tub) were monitored. Both LSD1 inhibitors, GSK2879552 and **2.8a** showed no change in Ac-Tub levels. Dual inhibitor **3.8** increased Ac-Tub levels over 3-fold compared to HDAC controls ricolinostat and **3.12** which increased levels around 14 and 7-fold respectively (Table 3.5, Figure 3.12).

Substrate	Fold Change					
	DMSO	GSK	2.8a	Ric	3.8	3.12
H3K4me	1	1.50±0.77	1.53±0.66	0.85±0.60	0.92±0.09	0.98±0.05
H3K9me	1	0.97±0.41	1.28±0.57	1.06±0.54	0.80±0.23	0.95±0.16
H3K18Ac	1	1.12±0.19	0.78±0.53	3.77±0.95	1.10±0.24	1.89±0.43
H3K27Ac	1	1.33±0.73	0.94±0.27	6.34±0.99	1.82±0.07	2.15±0.64
Ac-Tub	1	0.99±0.13	1.01±0.24	14.62±1.68	3.37±0.53	6.80±1.10

Table 3.4. Tabulated data of methylation and acetylation levels in THP-1 cells in response to LSD1 and HDAC inhibition.

Data shown as fold change ± stdp, n=2.
Data generated by Bulut et al., Koc University (unpublished).

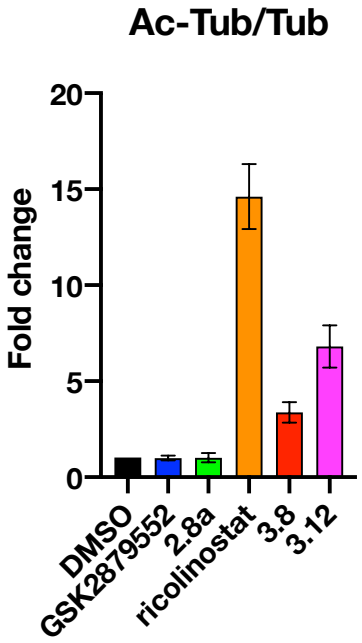

Figure 3.12. *Ac-Tub levels in THP-1 cells after treatment with LSD1 and HDAC inhibitors.*

Data shown as fold change ± stdp, n=2.
Data generated by Bulut et al., Koc University (unpublished).

3.4.5. Gene expression changes.

Just as CD86 and CD11b are downstream molecular markers for LSD1, HDAC inhibition is complicit in the upregulation of cyclin-dependent kinase inhibitor, p21. As such, just as the expression of CD86 and CD11b can be used to support a connection to LSD1 inhibition, p21 expression can be used as a tool to investigate if the activity of a drug is related to HDAC inhibition. As **3.8** is designed to be an inhibitor of both LSD1 and HDAC, its effect on all the aforementioned molecular markers has been explored.

CD86 and CD11b expression.

THP-1 cells were treated with 0.5 and 1.0 μM doses of dual inhibitor **3.8**, along with all our control compounds and the HDAC6 inhibitor ricolinostat (Table 3.6, Figure 3.13, Table 3.7, Figure 3.14). The expectation is that the HDAC inhibitors and the negative control should not significantly increase CD86/CD11b expression but LSD1 inhibitors should. This pattern was observed in both the expression of CD86 and CD11b. HDAC controls, ricolinostat and **3.12** and negative control **3.13**, all showed no significant change relative to untreated cells. In contrast, cells treated with a 0.5 μM dose of dual inhibitor **3.8** showed an increased CD86 and CD11b expression by 21 and 9-fold respectively. This was a similar fold change to that observed in GSK2879552 treated cells at this dose however at a dose of 1.0 μM, **3.8** revealed a 95 and 34-fold increase in CD86 and CD11b expression respectively, relative to 43 and 9-fold respectively for GSK2879552. This is good evidence that **3.8** is acting as an LSD1 inhibitor.

Compound	CD86 Fold Change		
	0 µM	**0.5 µM**	**1.0 µM**
GSK2879552	1.0±0.0	27.25±3.53	43.42±16.80
3.8	1.0±0.0	21.14±1.65	95.63±9.64
3.12	1.0±0.0	0.19±0.16	0.14±0.04
3.13	1.0±0.0	1.13±0.47	0.95±0.59
ricolinostat	1.0±0.0	9.19±12.36	0.20±0.07

Table 3.5. *CD86 expression change in response to LSD1 and HDAC inhibitor treated THP-1 cells.*

Data shown as fold change ± stdp, n=2.
Data generated by Bulut et al., Koc University (unpublished).

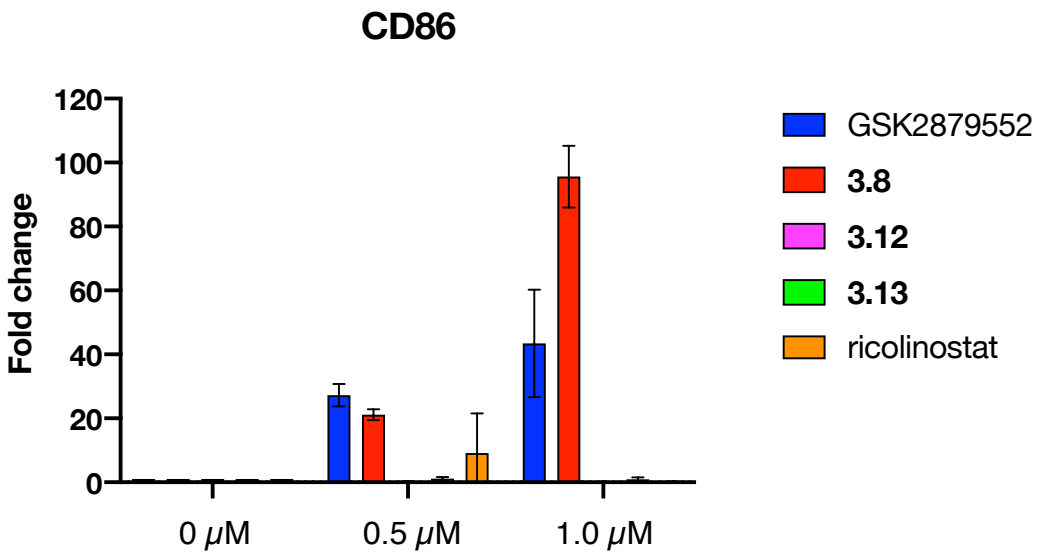

Figure 3.13. *Graphical representation of data from Table 3.6.*

Data shown as fold change ± stdp, n=2.
Data generated by Bulut et al., Koc University (unpublished).

Compound	CD11b Fold Change		
	0 μM	0.5 μM	1.0 μM
GSK2879552	1.0±0.0	6.82±3.89	9.30±4.97
3.8	1.0±0.0	9.31±2.50	34.57±10.43
3.12	1.0±0.0	2.12±1.64	9.06±4.87
3.13	1.0±0.0	0.82±1.13	2.69±1.34
ricolinostat	1.0±0.0	1.99±0.89	10.45±3.15

Table 3.6. *CD11b expression change in response to LSD1 and HDAC inhibitor treated THP-1 cells.*

Data shown as fold change ± stdp, n=2.
Data generated by Bulut et al., Koc University (unpublished).

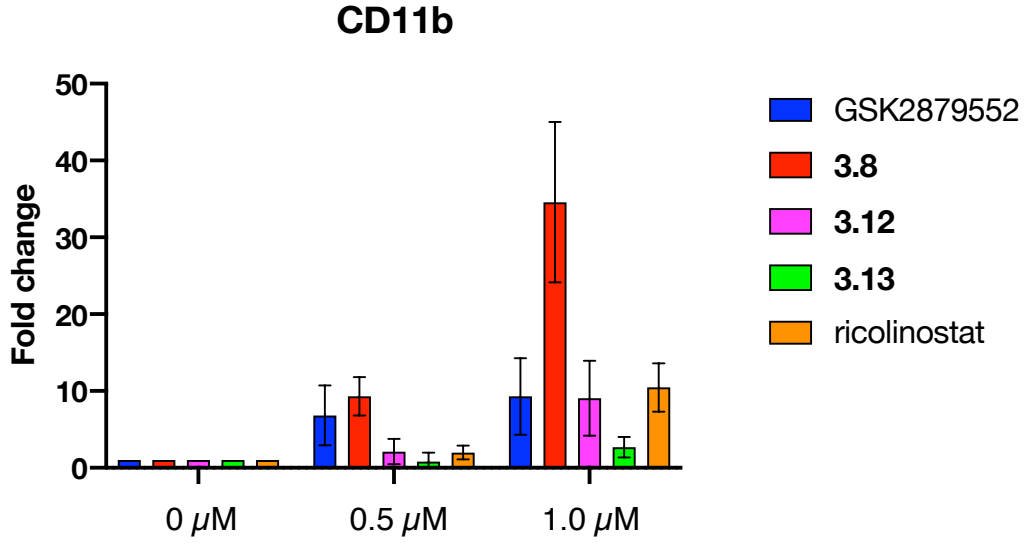

Figure 3.14. *Graphical representation of the data from Table 3.7.*

Data shown as fold change ± stdp, n=2.
Data generated by Bulut et al., Koc University (unpublished).

p21 expression.

THP-1 cells were again treated with 0.5 and 1.0 μM doses of **3.8** and control compounds over 72 hours. Levels of p21 were then determined (Table 3.8, Figure 3.15) with the expectation that LD1 inhibitors would present as no change in p21 expression levels but HDAC inhibitors would cause an increase. At a dose of 0.5 μM, none of the compounds resulted in any significant increase in p21 expression although it was noted that the negative control **3.13** showed a 0.56-fold decrease in expression. At the increased dose of 1.0 μM, all compounds lead to an increase in p21 expression. Single target HDAC inhibitors, **3.12** and ricolinostat both showed the largest increase of 3.7 and 8.8-fold respectively. In addition, LSD1 inhibitor GSK2879552 presented a 1.7-fold increase and negative control **3.13** showed a 2.5-fold increase. Dual inhibitor **3.8** increased p21 expression 3.8-fold but with a large error margin. The error means that p21 expression change due to treatment with **3.8** could lie anywhere between a 1.8 and 5.8-fold increase which may still be significant. However, given the high fold change observed in negative control **3.13**, these results should be treated with caution.

In summary, the only effect of note is in response to the control compound ricolinostat. The lack of effect in response to **3.8** and **3.12** may be due to time or the effect could be cell dependent. Further work is required to determine if **3.8** has any effect on p21 in a cellular environment.

Compound	p21 Fold Change		
	0 μM	**0.5 μM**	**1.0 μM**
GSK2879552	1.0±0.0	1.20±0.40	1.73±0.20
3.8	1.0±0.0	2.38±2.22	3.84±2.04
3.12	1.0±0.0	1.41±0.43	3.72±0.09
3.13	1.0±0.0	0.44±0.00	2.58±0.71
ricolinostat	1.0±0.0	1.11±0.02	8.86±2.20

Table 3.7. *p21 expression change in response to LSD1 and HDAC inhibitor treated THP-1 cells.*

Data shown as fold change ± stdp, n=2.
Data generated by Bulut et al., Koc University (unpublished).

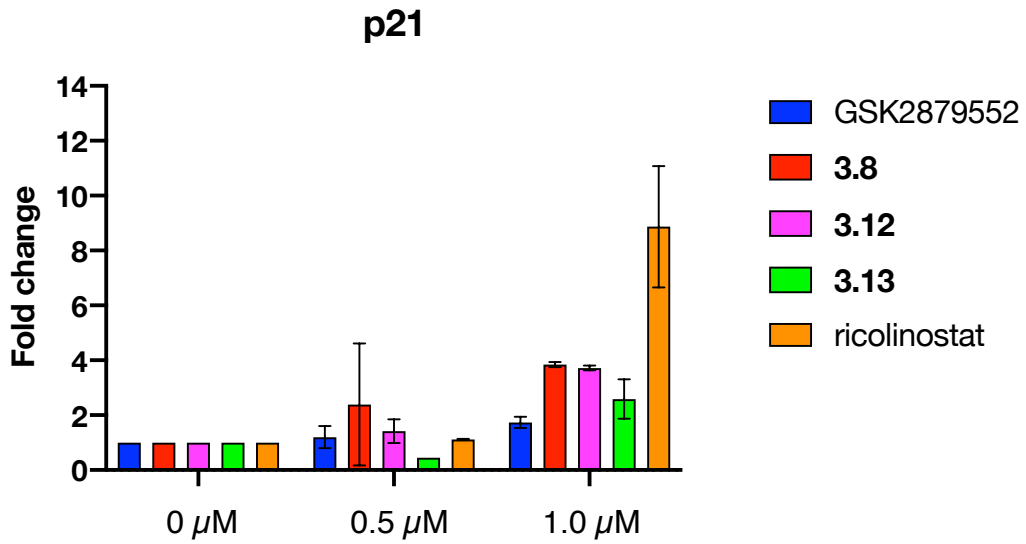

Figure 3.15. *Graphical representation of the data from Table 3.8.*

Data shown as fold change ± stdp, n=2.
Data generated by Bulut et al., Koc University (unpublished).

3.4.6. Synergy of 3.8 with other known anti-cancer compounds

Compound **3.8** along with positive HDAC control **3.12** were tested for synergy with a series of known anti-cancer agents. This comprised testing in combination with either paclitaxel, cytarabine, cisplatin and doxorubicin and synergy was determined in a cell viability assay in THP-1 cells (Figure 3.16). Cells were treated with either **3.8** (5 μM) or **3.12** (5 μM) over 72 hours followed by co-treatment with additional anti-cancer agents over a further 48 hours.

3.8 and **3.12** were first tested in combination with paclitaxel (3 μM) and both **3.8** and **3.12** appeared to show a weak synergistic effect killing around half of cells in each case. In combination with cytarabine (0.6 μM), **3.8** had no additional effect relative to either cytarabine or **3.8** alone. **3.12** performed slightly better killing half of all cells when in combination. Neither **3.8** nor **3.12** showed any effect in combination with cisplatin (1.25 μM). Like **2.8a**, both **3.8** and **3.12** showed the best synergy in combination with doxorubicin (0.06 μM) killing around 80 and 70 % of cells respectively.

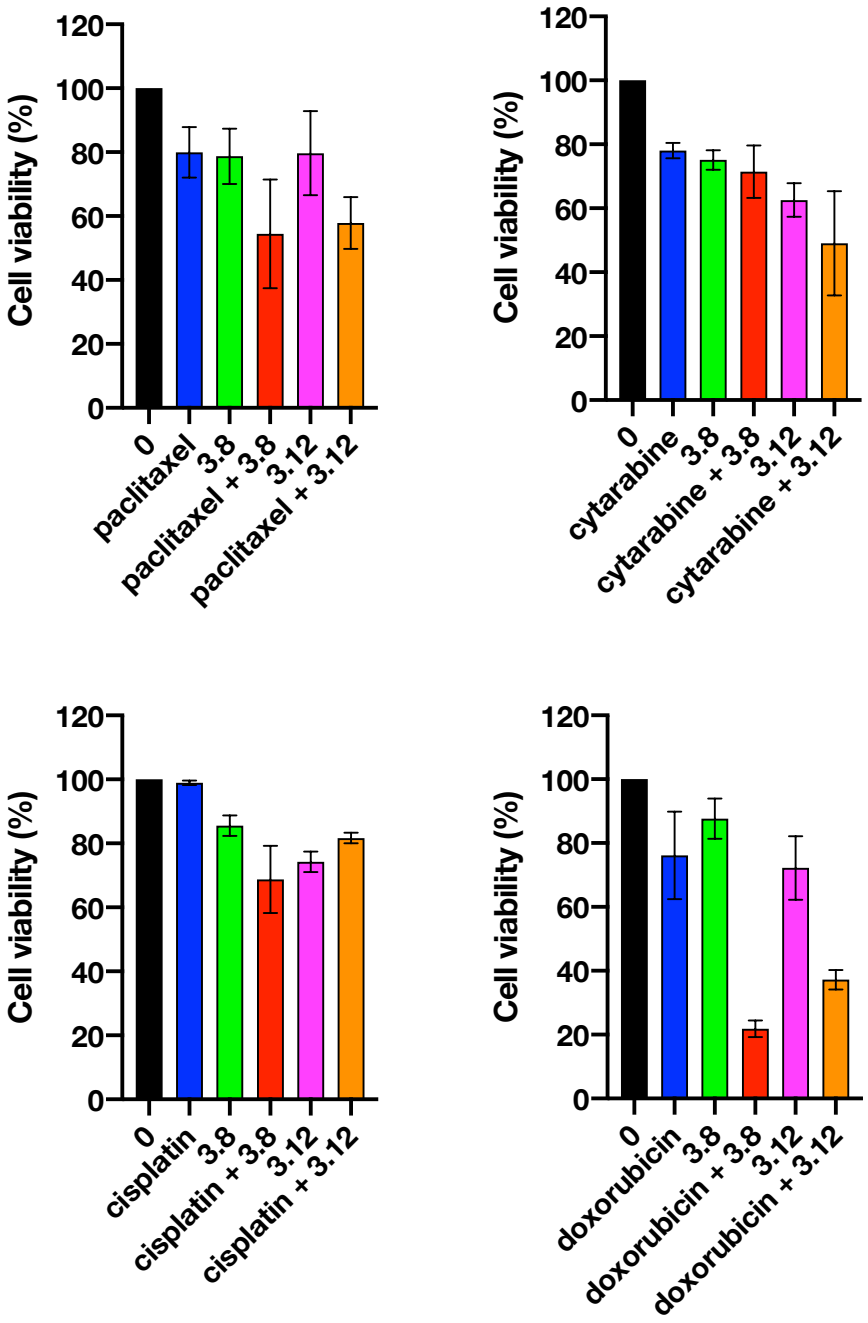

Figure 3.16. *Cell viability of THP-1 cells inhibited with combinations of our inhibitors and other known anti-cancer compounds.*

Data shown as % cell viability ± stdp, n=2.
Data generated by Bulut et al., Koc University (unpublished).

Having established that dual LSD1/HDAC inhibitor **3.8** and HDAC inhibitor **3.12** all have good synergy with doxorubicin, it raises the questions, do these compounds show synergy with other topoisomerase inhibitors and does doxorubicin act synergistically with all HDAC inhibitors. To investigate this, both

3.8 and **3.12** were tested in combination with an additional topoisomerase type II inhibitor, etoposide.[141] The results of the assay showed that neither **3.8** nor **3.12** had any significant synergistic effect relative to lone treatment. In addition, doxorubicin was tested in combination with HDAC inhibitor, ricolinostat. Again, no significant synergistic effect was seen relative to doxorubicin alone (Figure 3.7).

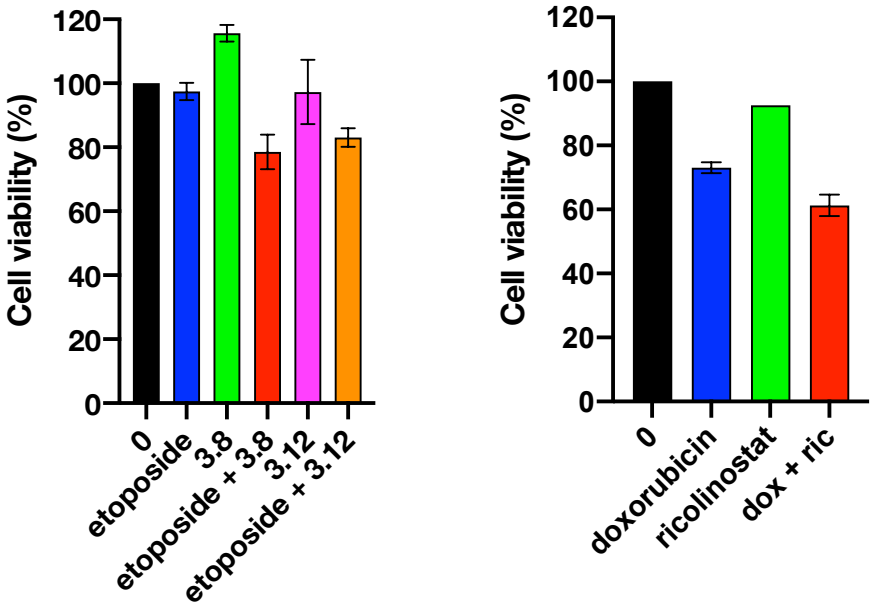

Figure 3.17. *Cell viability graph of **3.8** and **3.12** in combination with alternative Top2 inhibitor, etoposide. Cell viability graph of doxorubicin and HDAC inhibitor ricolinostat.*

Data shown as % Cell viability ± stdp, n=2.
Data generated by Bulut et al., Koc University (unpublished).

3.4.7. Inducing apoptosis.

Caspase-3/7 assay.

To further ascertain the synergistic effects of **3.8** with doxorubicin, as well as investigate if **3.8** has any apoptotic effect in cancer cells, THP-1 cells were treated with **3.8**, both alone and in combination with doxorubicin. Like LSD1 inhibitor **2.8a**, the apoptotic effect of these compounds was measured in a caspase-3/7 assay. In addition, positive HDAC and LSD1 controls, **3.12** and GSK2879552 were also tested under the same conditions.

At a concentration of 5 μM, nether **3.8** nor controls **3.12** and GSK2879552 displayed any apoptotic effect in THP-1 cells when used alone. In combination with doxorubicin however, **3.8** and **3.12** demonstrated an excellent response. Over 80% of cells where observed to be in apoptosis or dead following treatment with **3.8** and 70% for **3.12**, relative to just 20% in response to doxorubicin alone. In addition, GSK2879552 also showed a synergistic effect although less significant at around 50% of cells observed to be in apoptosis or dead.

Inhibitor	**% Population**			
	Live	**Apoptotic**	**Apoptotic/Dead**	**Dead**
No Inhibitor	95.65±0.90	0.30±0.05	3.47±1.02	0.57±0.17
doxorubicin	66.62±8.57	7.05±4.45	22.85±5.55	3.47±1.43
GSK2879552	95.30±0.25	1.22±0.17	3.27±0.37	0.22±0.07
GSK + dox	38.82±0.47	12.60±0.05	48.27±0.42	0.30±0.10
3.8	95.85±0.55	0.25±0.20	2.75±0.15	1.15±0.60
3.8 + dox	10.07±2.37	6.20±4.80	81.60±0.90	2.12±1.52
3.12	93.62±0.07	0.45±0.30	4.62±0.52	1.30±0.90
3.12 + dox	22.69±0.45	5.27±2.47	68.66±0.68	3.50±1.20

Table 3.8. *The apoptosis profile data of **3.8** and **3.12** both individually and in combination with doxorubicin in THP-1 cells measured using caspase activation.*

Data shown as % population ± stdp, n=2.
Data generated by Bulut et al., Koc University (unpublished).

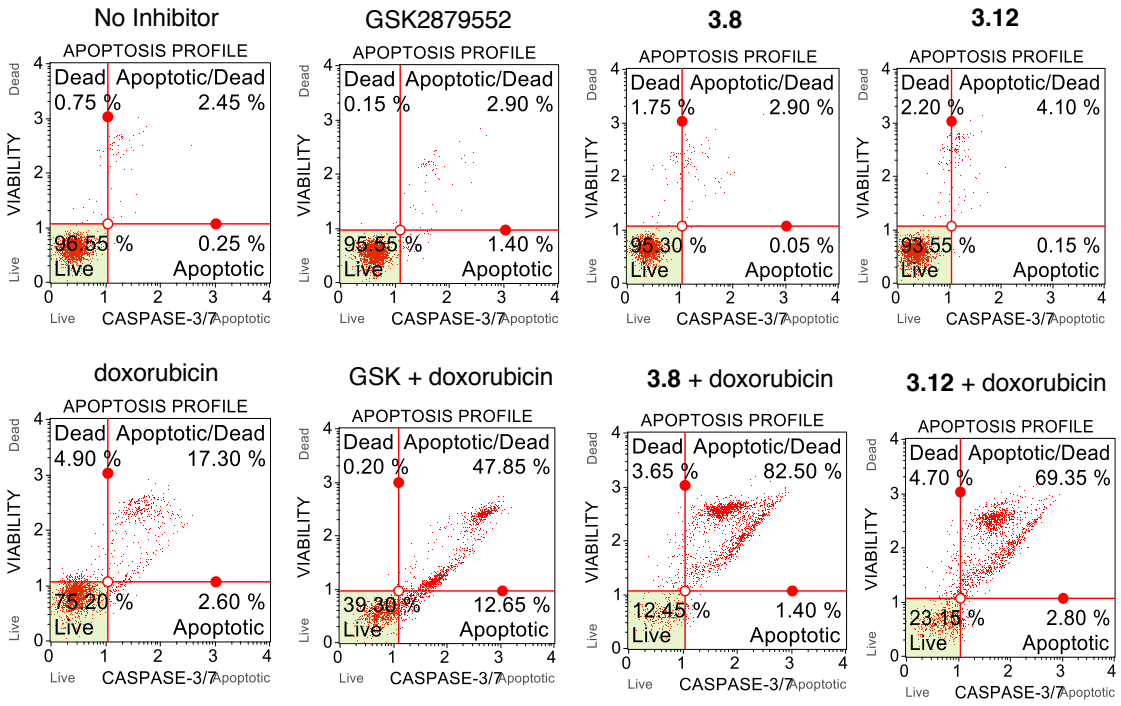

Figure 3.18. *Apoptosis profiles for **3.8**, **3.12** and doxorubicin in THP-1 cells.*
Data generated by Bulut et al., Koc University (unpublished).

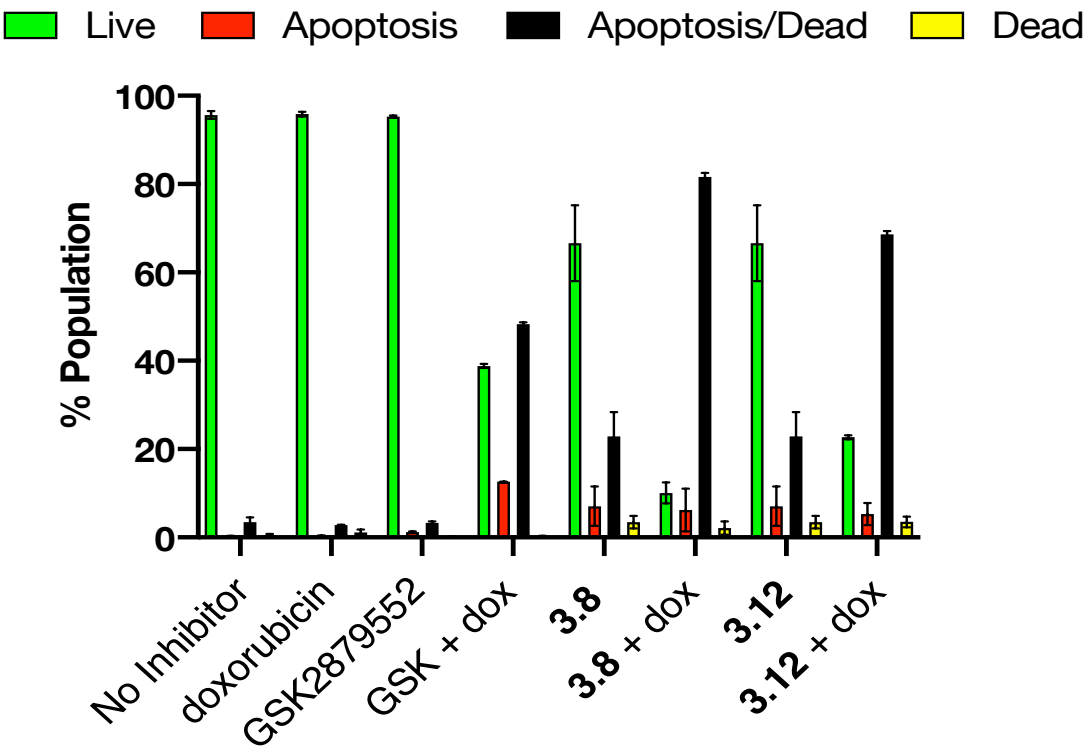

Figure 3.19. *Graphical representation of apoptosis data presented in Table 3.9.*

Data shown as % population ± stdp, n=2.
Data generated by Bulut et al., Koc University (unpublished).

Annexin V binding assay.

The results of the annexin V binding assay where found to be largely consistent with that of the caspase assay. At a concentration of 5μM, both **3.8** and **3.12** alone had little apoptotic effect relative to untreated cells at this concentration. However, both once again showed a large increase when in combination with doxorubicin. Following treatment of THP-1 cells with **3.8** and doxorubicin, around 30% of cells were observed to be in early apoptosis and over 50% in late apoptosis/dead. A combination of **3.12** and doxorubicin led to around 50% of cells being found in early apoptosis and 25% in late apoptosis/dead. The annexin V assay did show a higher proportion of cells in apoptosis upon treatment with doxorubicin alone relative to the caspase assay, but even so, the effect seemed to be amplified upon co-treatment with our inhibitors.

In addition, both **3.8** and **3.12** showed higher levels of cells in apoptosis both alone and in co-treatment with doxorubicin.

Inhibitor	**% Population**			
	Live	**Early apoptosis**	**Late apoptosis/Dead**	**Dead**
No Inhibitor	78.39±5.04	16.43±3.21	4.93±1.67	0.24±0.16
doxorubicin	39.77±2.07	41.31±1.83	18.70±0.10	0.21±0.13
GSK2879552	93.73±0.09	3.05±0.01	2.84±0.06	0.38±0.04
GSK + dox	55.01±2.69	11.14±1.06	31.50±3.68	2.35±0.07
3.8	79.96±4.86	15.09±4.61	4.66±0.04	0.29±0.21
3.8 + dox	16.87±8.67	31.07±10.12	51.70±1.20	0.35±0.25
3.12	71.33±6.93	19.32±3.38	7.53±1.81	0.31±0.23
3.12 + dox	23.57±3.72	50.42±4.77	25.65±8.60	0.35±0.10

Table 3.9. *The apoptosis profile data of **3.8** and **3.12** both individually and in combination with doxorubicin in THP-1 cells measured using Annexin V.*

Data shown as % population ± stdp, n=2.
Data generated by Bulut et al., Koc University (unpublished).

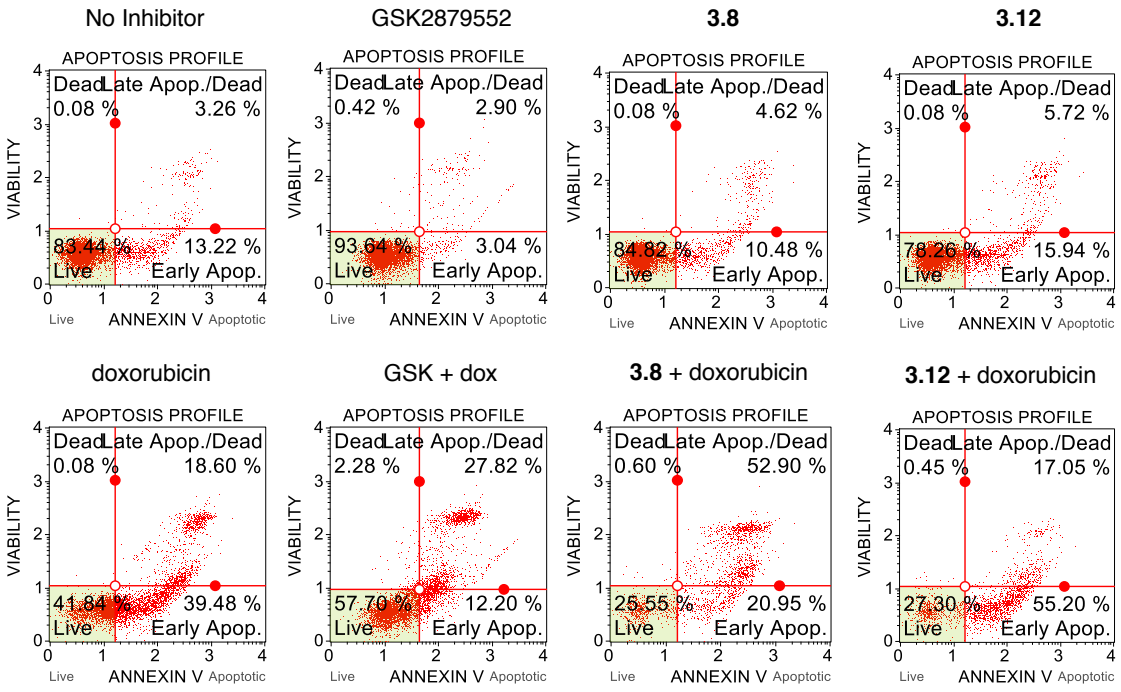

Figure 3.20. *Apoptosis profiles for **3.8**, **3.12** and doxorubicin in THP-1 cells. Data generated by Bulut et al., Koc University (unpublished).*

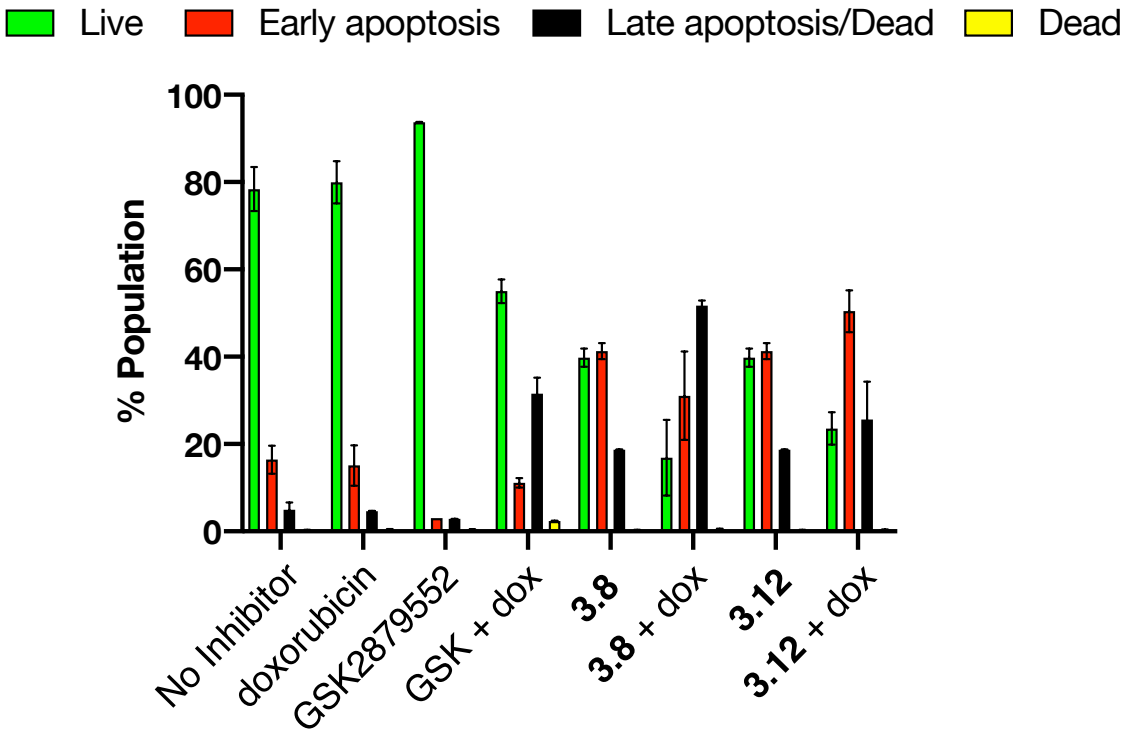

Figure 3.21. *Graphical representation of apoptosis data presented in Table 3.10.*

Data shown as %population ± stdp, n=2.
Data generated by Bulut et al., Koc University (unpublished).

3.4.8. Repair of doxorubicin induced damage

THP-1 cells were treated with 5 μM doses of **3.8** and **3.12**, both alone and in combination with doxorubicin (60 nM) (Table 3.11, Figure 3.22, Figure 3.23). Cells treated with either **3.8** or **3.12** alone showed no increase in γ-H2AX levels relative to untreated cells. However, they both showed an increase in levels when in combination with doxorubicin, relative to doxorubicin alone. **3.8** revealed just short of a 50% rise in γ-H2AX levels and **3.12** just over 50%, both better than the 36% increase observed in cells treated with doxorubicin alone. This is further evidence that **3.8** acts synergistically with doxorubicin. In addition, the low γ-H2AX levels observed in cells treated with **3.8** and **3.12** alone shows that cell damage in the form of DSBs are not caused by **3.8** or **3.12**. But the increased γ-H2AX levels in co-treated cells supports the hypothesis that **3.8** and **3.12** sensitises cells to DNA damage and hence when doxorubicin induces this damage the cell is unable to recover.

Inhibitor	% population
No inhibitor	8.15±0.55
doxorubicin	36.83±4.42
3.8	6.70±2.80
3.8 + doxorubicin	47.34±2.35
3.12	9.35±1.85
3.12 + doxorubicin	53.95±2.35

Table 3.10. *Tabulated % population data for γ-H2AX levels in THP-1 cells treated with doxorubicin, **3.8** and **3.12**.*

Data shown as %population ± stdp, n=2.
Data generated by Bulut et al., Koc University (unpublished).

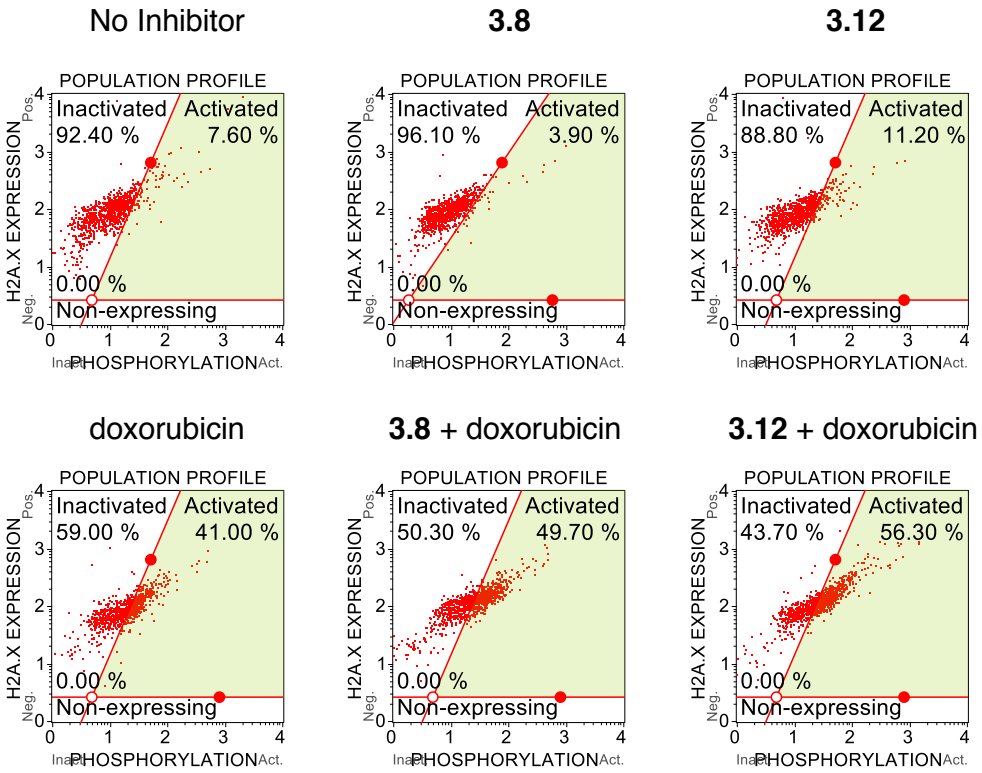

Figure 3.22. *Population profiles of phosphorylation vs H2AX expression in THP-1 cells treated with doxorubicin, **3.8** and **3.12**.*
Data generated by Bulut et al., Koc University (unpublished).

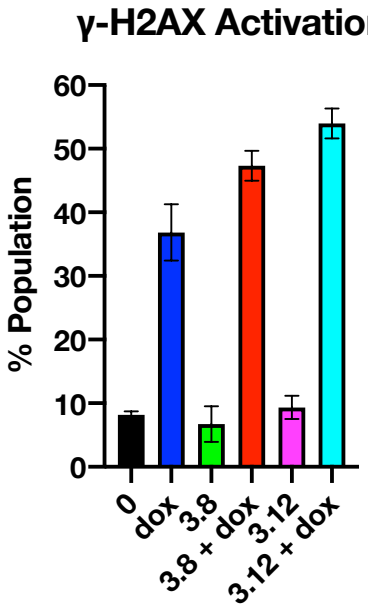

Figure 3.23. *Graphical representation of γ-H2AX activation in THP-cells treated with doxorubicin, **3.8** and **3.12**.*

Data shown as %population ± stdp, n=2.
Data generated by Bulut et al., Koc University (unpublished).

The formation of ROS.

THP-1 cells were again treated with 5 μM doses of **3.8** and **3.12** both alone and in combination with a 60 nM dose of doxorubicin (Table 3.12, Figure 3.24, Figure 3.25). Cells treated with **3.8** and **3.12** only revealed no increase in ROS relative to untreated cells suggesting that **3.8** and **3.12** do not generate ROS. When in combination with doxorubicin, neither **3.8** nor **3.12** displayed any significant change in ROS relative to doxorubicin alone. This suggests that co-treatment with doxorubicin and either **3.8** or **3.12** does not have any effect on the production of ROS relative to treatment with doxorubicin alone.

Inhibitor	**% Population**	
	ROS (-)	**ROS (+)**
No inhibitor	95.15±0.65	4.49±0.41
doxorubicin	56.35±3.65	43.5±3.50
3.8	93.90±0.30	5.92±0.25
3.8 + doxorubicin	48.75±3.75	49.95±3.05
3.12	94.55±0.55	5.15±0.29
3.12 + doxorubicin	55.50±6.50	43.75±6.25

Table 3.11. *ROS data for THP-1 cells treated with doxorubicin, 3.8 and **3.12**.*

Data shown as % population ± stdp, n=2.
Data generated by Bulut et al., Koc University (unpublished).

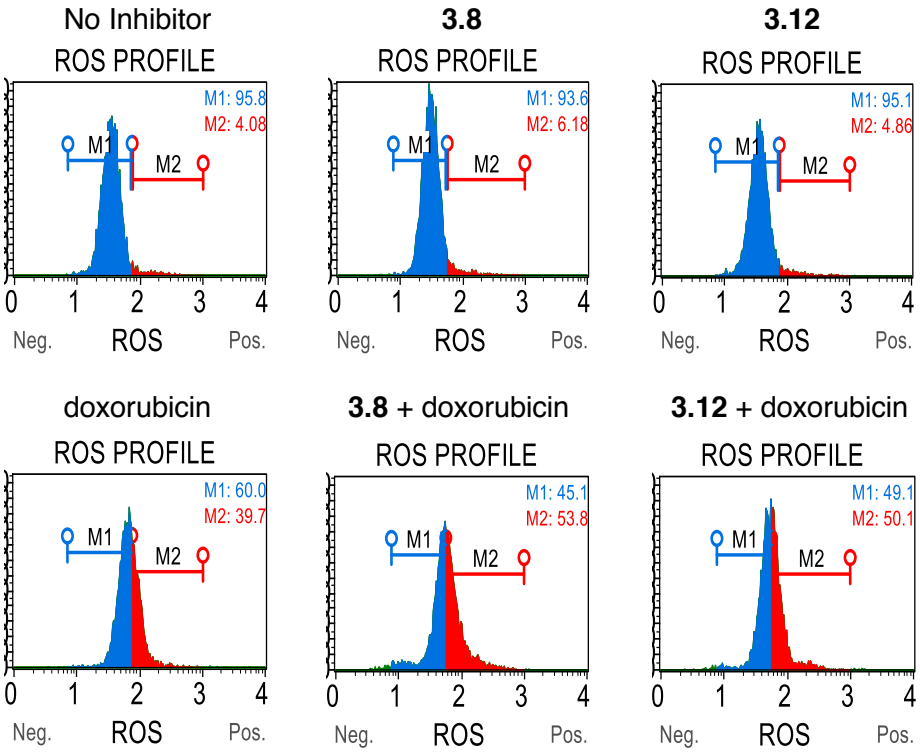

Figure 3.24. *ROS profiles for THP-1 cells treated with doxorubicin, **3.8** and **3.12**.*
Data generated by Bulut et al., Koc University (unpublished).

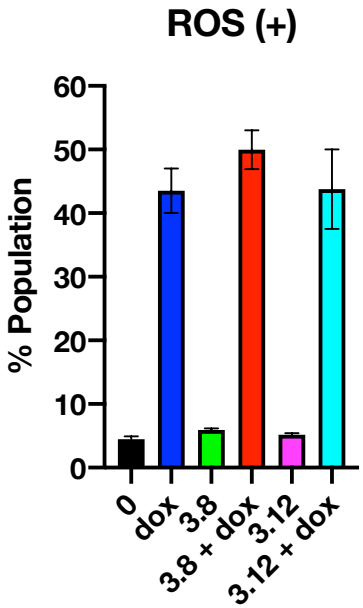

Figure 3.25. *Graphical representation of ROS (+) profile data for THP-1 cells treated with doxorubicin, **3.8** and **3.12**.*

Data shown as % population ± stdp, n=2.
Data generated by Bulut et al., Koc University (unpublished).

3.5. Virtual docking study.

Both **3.8** and **3.12** were modelled in a virtual docking (VD) study (Figure 3.26, Figure 3.27), carried out in order to determine the most likely binding position and mode of these compounds within the HDAC6 active site. VD was carried out in collaboration with Dusan Ruzic and Katarina Nikolic at the University of Belgrade, Serbia. Docking was performed using GOLD Software 5.6.0 (DOI: 10.1006/jmbi.1996.0897). The HDAC6 crystal structure (human isoform, second catalytic domain) was taken from the Protein Data Bank, entry PDB:5EDU, prepared via PlayMolecule online platform (playmolecule.org/) and the number of docking runs set to 100. The ChemScore scoring function (doi.org/10.1002/prot.10465) was used to estimate the free energy of binding, as it additionally takes into consideration metal-ligand coordination important for Zn^{2+}-hydroxamic acid binding.

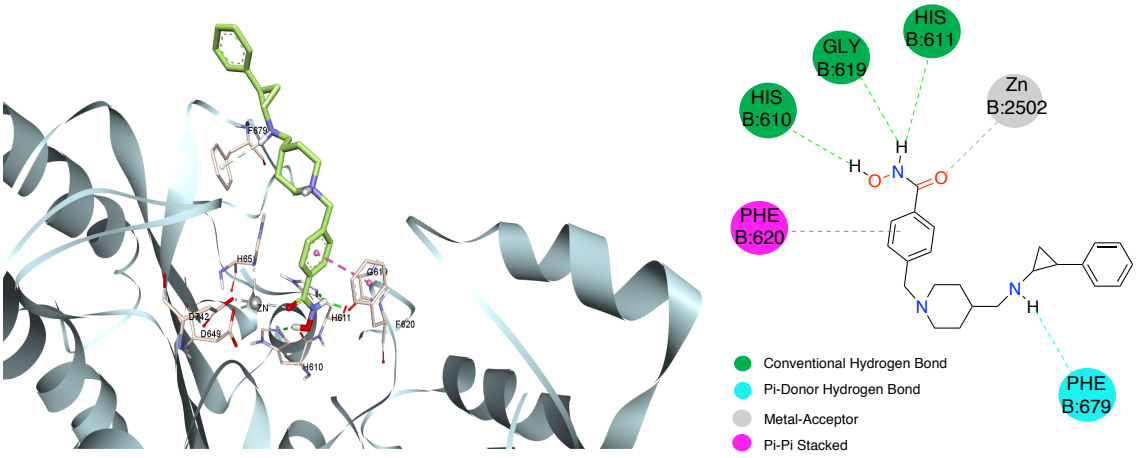

Figure 3.26. *Position of ligand 3.8 inside the binding site of the HDAC6 seen from the extracellular side (left) and 2D presentation of important interactions with amino acid residues in the active pocket of HDAC6 (right).*

The most interesting feature to come out of the VD study of **3.8** was the unusual monodentate binding mode to the zinc co-factor of HDAC6. Whilst monodentate binding is not unheard of, it is quite rare. In 2017, Porter *et al.* reported the crystal structures of the HDAC6 inhibitors HPB, HPOB and ACY1083, along with minor conformers of both ricolinostat and TSA, showing monodentate binding to Zn^{2+}.

They put forward evidence that phenylhydroxamates with bulky substituents, are able to exploit this mode of binding in the HDAC6 active site by coordinating with Zn^{2+} through a monodentate hydroxamate N-O^- group while the C=O group accepted a hydrogen bond from a Zn^{2+} bound water molecule.[142] Although **3.8** has the phenylhydroxamate moiety, the monodentate binding mode predicted in our study suggests that it is the hydroxamate C=O that is bound in a monodentate fashion to Zn^{2+} with the N-H and O-H groups forming hydrogen bonds to HIS611, Gly619 and HIS610.

In contrast, **3.12** is predicted to comprise a bidentate binding mode in which the hydroxamic acid is coordinated to the Zn^{2+} ion via both the C=O and N-O groups. The structure of **3.8** and **3.12** are identical with the exception of the regiochemistry around the cyclopropyl ring. Although this is a minor change it has the effect of shifting the π-donor hydrogen bond between Phe679 and the tranylcypromine amine in **3.8** to a π-π stacking interaction between Phe679 and the cyclopropylamine phenyl group of **3.12**. The hydrogen bond between His610 to the hydroxamic acid O-H group remains but the hydrogen bonds between the hydroxamic acid N-H of **3.8** and Gly619 and His611 are lost.

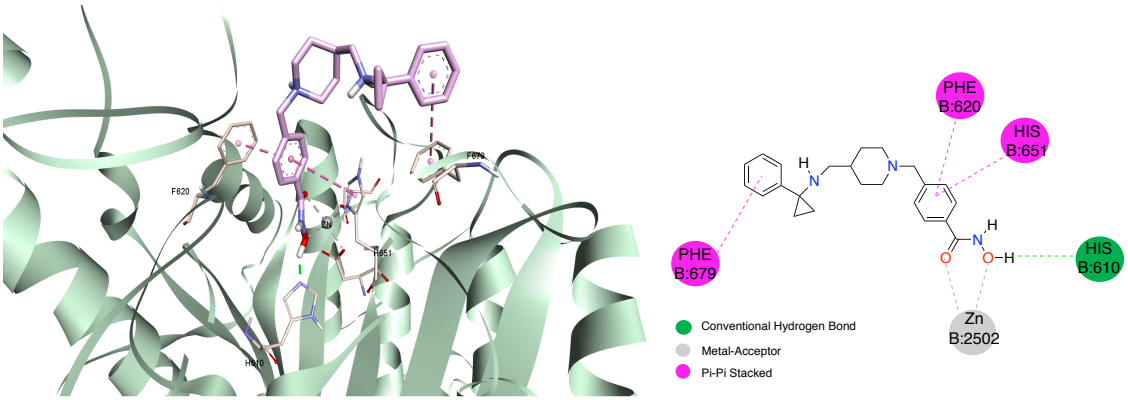

Figure 3.27. *Position of ligand MH-25 inside the binding site of the HDAC6 seen from the extracellular side (left) and 2D presentation of important interactions with amino acid residues in the active pocket of HDAC6 (right).*

Analysis of the IC_{50} values and the corresponding ChemScore values of both **3.8** and **3.12** shows a good correlation between the two. In a given set of compounds, the lower the IC_{50} value the higher the respective ChemScore value should be relative to other compounds modelled under the same conditions. **3.8** has an IC_{50}

value of 0.140 μM and a ChemSore value of 36.147 whist compound **3.12** has an IC_{50} of 0.248 μM and a ChemScore value of 34.961 (Table 3.13). This is a logical result as the compound with the lower IC_{50} also has the higher ChemScore value.

Compound	HDAC6 IC_{50} (μM)	Gold ChemScore
3.8	0.140	36.147
3.12	0.248	34.961

Table 3.12. *Correlation between IC_{50} and Gold ChemScore values.*

Data generated by Ruzic et al., University of Belgrade (unpublished).

3.6. Conclusion and future work.

This chapter has covered the synthesis and biological activity of a dual LSD1/HDAC inhibitor **3.8** along with a series of control compounds GSK2879552, **3.12** and **3.13**.

In a cell free LSD1 assay, **3.8** showed good sub-micromolar activity (IC_{50} = 0.55 μM) and was 3 times as potent as its precursor GSK2879552 (IC_{50} = 1.68 μM). In addition, **3.8** showed good sub-micromolar activity in in both HDAC6 and 8 (IC_{50} = 0.248 and 0.449 μM respectively). Positive HDAC control **3.12** also showed good activity in HDAC6 and 8 but not in LSD1. Negative control **3.13** was not observed to have any activity in either the LSD1 or any of the HDAC assays. CETSA was used to determine if **3.8** showed target engagement to both LSD1 and HDAC6 in THP-1 cells. This was indeed found to be the case, suggesting that **3.8** has affinity for both LSD1 and HDAC6. In addition, all controls behaved as expected. This is all good evidence, not only that **3.8** has affinity for both targets, but also that the control compounds can be used as a reliable measure of activity of **3.8**. Future work will determine if target engagement is extended beyond HDAC6 to HDAC1 and 8. **3.8** has shown low μM activity in HDAC1 and nM activity in HDAC8, therefore good target engagement would be expected.

Cell viability assays in both fused and non-fused leukaemia cell lines showed that **3.8** is active in THP-1, K562 and JURKAT with an IC_{50} value around 15 μM in each and 1.3 μM in MOLM-13. **3.12** also performed best in MOLM-13 (~6 μM) and <20 μM in all others. In contrast positive LSD1 control GSK2879552 only had an IC_{50} <20 μM in MOLM-13 and negative control **3.13** was not active in any. Future work could extend this panel of cells, not only to other leukaemia cells but also to other cancer cell lines, to get a much deeper understanding of the activity of **3.8**.

Both methylation and acetylation levels were monitored in response to inhibition with our compounds. Both H3K4me and H3K9me levels showed no change relative to untreated cells, following treatment with either **3.8** or GSK2879552. However, there was a 2-fold increase H3K27Ac levels in response to **3.8** as well as ~2-fold increase in H3K18Ac and H3K27Ac levels in response to **3.12**.

Performance of **3.8** as a LSD1 inhibitor was further supported by examining molecular markers, CD86 and CD11b. **3.8** showed much higher fold changes

than GSK2879552 whilst both **3.12** and **3.13** displayed no change as anticipated. The HDAC6 molecular marker, p21, was also studied in response to treatment with **3.8** and **3.12** but no significant change in levels was observed. It is thought this could be a time or cell dependence issue and future work could extend this assay into different cells to determine if this is indeed the case.

Synergy of **3.8** with other anti-cancer compounds was investigated. A cell viability assay in THP-1 cells found both **3.8** and **3.12** to have good synergy with doxorubicin. This activity was further investigated through analysis of caspase-3/7 and annexin V assays. Both supported good synergistic behaviour with both **3.8** and **3.12** showing increased levels of apoptosis relative to both doxorubicin alone and a combination of GSK2879552 and doxorubicin.

An investigation of **3.8** and **3.12** in combination with doxorubicin on the effect of ROS produced in response to treatment with doxorubicin, showed that neither **3.8** nor **3.12** had any effect on ROS levels.

VD was carried out on the structures of both **3.8** and **3.12** and found them to have monodentate and bidentate binding modes respectively within the HDAC6 active site. In addition, **3.8** and **3.12** had ChemScore values of 36.147 and 34.961 respectively which is in support of their respective IC_{50} values.

3.7. Chapter three experimental.

3.7.1. Experimental procedures

All experimental procedures are the same as for those described in Chapter two, section 2.7.1.

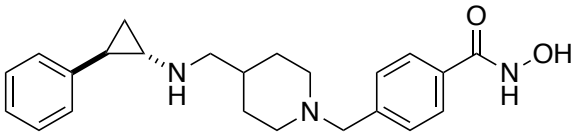

N-hydroxy-4-[(4-{[(2-phenylcyclopropyl)amino]methyl}piperidin-1-yl)methyl]benzamide (3.8)

In separate flasks, **2.7a** (1.00 g, 2.64 mmol), hydroxylamine hydrochloride (0.97 g, 13.96 mmol) and potassium hydroxide (1.52 g, 27.09 mmol) were dissolved in dry methanol (25 ml, 5 ml, 8 ml) respectively. The potassium hydroxide solution was then slowly added to the hydroxylamine solution and the resulting mixture stirred at room temperature for 30 minutes. This mixture was then filtered, and the filtrate added to the benzoate solution, which was then stirred at room temperature overnight. Reaction completion was confirmed via TLC and then the reaction mixture pH adjusted to 7 with 6M HCl. The reaction mixture was filtered and concentrated. The concentrate was purified using a C18 reverse phase column, eluting with a gradient of 10-100 % methanol in water to give **3.8** (0.25 g, 25 %), as a white solid. IR (cm^{-1}) 2915, 1611; ^{1}H NMR (400 MHz, DMSO-d_6) δ 7.69 (d, J = 8.3 Hz, 2H), 7.34 (d, J = 8.2 Hz, 2H), 7.21 (t, J = 7.5 Hz, 2H), 7.13 – 7.06 (m, 1H), 7.03 – 6.99 (m, 2H), 3.45 (s, 2H), 2.82 – 2.70 (m, 2H), 2.46 (dd, J = 6.6, 2.2 Hz, 2H), 2.17 (ddd, J = 7.3, 4.4, 3.0 Hz, 1H), 1.88 (tdd, J = 11.5, 4.5, 2.3 Hz, 2H), 1.74 (ddd, J = 9.0, 5.4, 2.7 Hz, 1H), 1.70 – 1.59 (m, 2H), 1.36 (ddt, J = 11.1, 7.5, 3.9 Hz, 1H), 1.11 (dddd, J = 15.5, 11.8, 7.6, 3.6 Hz, 2H), 0.97 – 0.87 (m, 2H); ^{13}C NMR (101 MHz, Methanol-d_4) δ 175.3, 143.4, 140.5, 138.2, 130.2, 130.1, 129.2, 126.7, 126.5, 64.0, 56.2, 54.5, 49.8, 42.6, 36.5, 31.1, 25.1, 16.6; HRMS m/z calcd for $C_{23}H_{29}N_3O_2$ [M+H]+ 380.2333, found 380.2334; Purity 97.5%.

These data are consistent with that reported in the literature.[140]

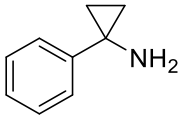

1-Phenyl-1-cyclopropylamine (3.15).[133]

1-Phenyl-1-cyclopropanecarboxylic acid (1.00 g, 6.14 mmol) was dissolved in anhydrous acetonitrile (40 ml). Triethylamine (0.85 ml, 6.14 mmol) was then added followed by diphenylphosphoryl azide (1.33 ml, 6.14 mmol) and the mixture heated to 50ºC for 2 hrs. After cooling to room temperature, 1M HCl (40 ml) was added and the mixture refluxed for 16 hrs. The acetonitrile was removed under reduced pressure and the pH of the remaining aqueous mixture raised to 13-14 with 1M NaOH. The aqueous phase was then extracted with dichloromethane (3 x 100 ml) and the combined organic extracts dried over $MgSO_4$, filtered and concentrated. The concentrate was purified on a silica column eluting with a gradient of 10-100 % EtOAc in Hexanes to give **3.15** (0.64 g, 61 %) as a yellow oil. ^{1}H NMR (400 MHz, DMSO-*d*$_6$) δ 7.32 – 7.23 (m, 4H), 7.15 – 7.10 (m, 1H), 2.27 (brd-s, 2H), 0.98 – 0.93 (m, 2H), 0.92 – 0.86 (m, 2H); ^{13}C NMR (101 MHz, Chloroform-*d*) δ 147.0, 128.5, 126.0, 125.5, 36.8, 17.9; LC-ToF (ESI) m/z calcd for $C_9H_{11}N$ $[M+H]^+$ 134.10, found 134.10.

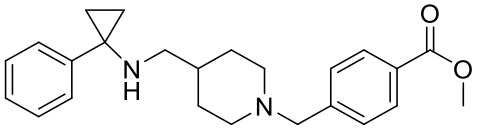

Methyl 4-{[4-({[1-phenylcyclopropyl]amino}methyl) piperidin-1-yl]methyl} benzoate (3.16).

3.15 (0.50 g, 2.95 mmol) and **2.11a** (0.68 g, 2.46 mmol) were dissolved in anhydrous methanol (5 ml) and placed under reflux for 1 hour. The mixture was then allowed to cool to room temperature before slowly adding $NaBH_4$ (0.13 g, 3.69 mmol) and stirring at ambient temperature for 1 hour. The mixture was quenched with water (50 ml) then extracted with dichloromethane (3 x 50ml), dried over $MgSO_4$ and filtered. The filtrate was concentrated and purified on a silica column eluting with a gradient of 0-10 % MeOH in dichloromethane to give **3.16** (0.81 g, 87 %) as a yellow oil. ^{1}H NMR (400 MHz, Chloroform-*d*) δ 7.89 (d, J = 8.3 Hz, 2H), 7.30 (d, J = 8.0 Hz, 2H), 7.26 – 7.18 (m, 4H), 7.15 – 7.10 (m, 1H), 3.83 (s, 3H), 3.43 (s, 2H), 2.74 (d, J = 11.4 Hz, 2H), 2.34 (d, J = 6.5 Hz, 2H),

1.85 (td, J = 11.5, 2.5 Hz, 2H), 1.57 (dd, J = 13.1, 2.9 Hz, 2H), 1.29 – 1.16 (m, 1H), 1.14 – 1.11 (m, 2H), 0.90 – 0.85 (m, 1H), 0.85 – 0.80 (m, 1H); ^{13}C NMR (101 MHz, Chloroform-*d*) δ 167.2, 143.8, 129.6, 129.0, 128.9, 128.3, 127.4, 126.3, 63.1, 53.9, 52.4, 52.1, 42.5, 36.6, 30.7, 15.9; LC-ToF (ESI) m/z calcd for $C_{24}H_{30}N_2O_2$ [M+H]+ 379.24, found 379.24.

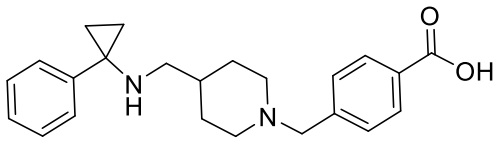

4-[(4-{[(1-phenylcyclopropyl)amino]methyl}piperidin-1-yl)methyl]benzoic acid (3.13).

3.16 (0.40 g, 1.06 mmol) was dissolved in a 3:1 mixture of THF:H_2O and to it added LiOH (0.08 g, 3.17 mmol) and stirred at 50 ºC for 16 hrs. The mixture was then allowed to cool to room temperature before adjusting to pH 2 with saturated $KHSO_4$. It was then concentrated under reduced pressure and the concentrate purified on an amine functionalized silica column eluting with a gradient of 10-100 % EtOAc in Petroleum ether to give **3.13** (0.81 g, 87 %) as a white solid. ^{1}H NMR (400 MHz, Methanol-d_4) δ 7.90 (d, J = 8.3 Hz, 2H), 7.36 – 7.26f (m, 6H), 7.21 – 7.16 (m, 1H), 3.56 (s, 1H), 2.89 (d, J = 12.0 Hz, 2H), 2.36 (d, J = 6.7 Hz, 2H), 2.03 (td, J = 11.9, 2.6 Hz, 2H), 1.73 – 1.65 (m, 2H), 1.43 – 1.32 (m, 1H), 1.20 – 1.09 (m, 2H), 0.99 – 0.92 (m, 2H), 0.92 – 0.84 (m, 2H); ^{13}C NMR (101 MHz, Methanol-d_4) δ 175.1, 144.1, 139.9, 138.3, 130.2, 129.2, 128.9, 127.5, 63.8, 54.3, 53.2, 43.5, 36.9, 31.0, 15.2; HRMS (ESI) m/z calcd for $C_{23}H_{28}N_2O_2$ [M+H]+ 365.2224, found 365.2218; Purity 98.3%.

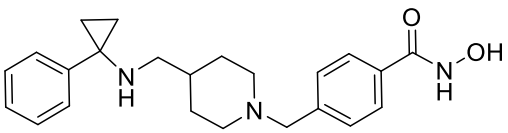

***N*-hydroxy-4-[(4-{[(1-phenylcyclopropyl)amino]methyl}piperidin-1-yl) methyl]benzamide (3.12).**

In separate flasks, **3.16** (1.00 g, 2.64 mmol), hydroxylamine hydrochloride (0.85, 13.21 mmol) and potassium hydroxide (1.54 g, 26.42 mmol) were dissolved in dry methanol (15 ml, 10 ml, 10 ml) respectively. The potassium hydroxide solution was then slowly added to the hydroxylamine solution and the resulting mixture stirred at room temperature for 30 minutes. This mixture was then filtered, and the filtrate added to the benzoate solution and stirred at room temperature overnight. Reaction completion was confirmed by TLC and then the reaction mixture pH adjusted to 7 with 6M HCl. The reaction mixture was filtered and concentrated. The concentrate was then dissolved in cold ethanol and again filtered and concentrated. The concentrate was purified using an amine-functionalised column, eluting with a gradient of 0-10 % methanol in dichloromethane to give **3.12** (0.30 g, 30 %) as a white solid. ^{1}H NMR (400 MHz, Methanol-d_4) δ 7.69 (d, J = 8.3 Hz, 2H), 7.39 (d, J = 8.4 Hz, 2H), 7.36 – 7.24 (m, 4H), 7.21 – 7.14 (m, 1H), 3.53 (s, 2H), 2.83 (d, J = 11.8 Hz, 2H), 2.35 (d, J = 6.7 Hz, 2H), 1.98 (td, J = 11.8, 2.5 Hz, 2H), 1.71 – 1.63 (m, 2H), 1.41 - 1.30 (m, 1H), 1.20 – 1.06 (m, 2H), 1.00 – 0.91 (m, 2H), 0.91 – 0.84 (m, 2H); ^{13}C NMR (101 MHz, Methanol-d_4) δ 196.1, 172.2, 170.7, 160.7, 159.0, 158.5, 157.4, 157.1, 157.1, 156.2, 155.7, 91.9, 82.6, 81.4, 71.7, 65.1, 59.3, 43.3; HRMS (ESI) m/z calcd for $C_{23}H_{29}N_3O_2$ [M+H]+ 380.2333, found 380.2330; Purity 98.1%.

Chapter Four

4. A series of novel zinc dependent HDAC inhibitors.

4.1. Introduction

The synthesis, structures, testing and clinical use of some zinc dependent HDAC inhibitors has been extensively explored in both chapters 1 and 3 of these theses. As such, the increasing number of clinically approved HDAC inhibitors and the continued efforts of pharmaceutical companies to develop further inhibitors of the HDACs suggests an ongoing need for further research within this area.

During the synthesis of dual inhibitor **3.8**, various methods for the synthesis of hydroxamic acids were explored. To facilitate this, two compounds were used as test molecules, **2.10a** and **4.2** (scheme 4.1). These were precursors to GSK2879552 and chosen so as to have a structure similar to that of the target compound whilst still being easy and cheap to make. The resulting hydroxamic acid analogues, **4.1a** and **4.3a** (scheme 4.1), were subsequently submitted for *in vitro* testing and found to be inhibitors of HDAC6 with nano-molar levels of potency. As such, we have developed four series of novel compounds comprising small linker and cap groups for the inhibition of HDAC6.

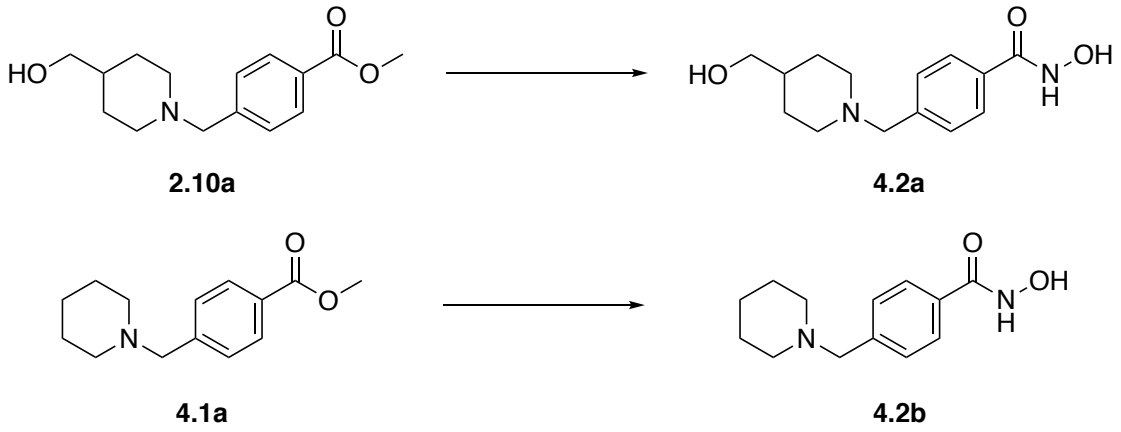

2.10a **4.2a**

4.1a **4.2b**

Scheme 4.1. *The initial development of test molecules **4.2a** and **4.2b**.*

4.1.1. Chapter aims.

Four series of compounds containing the hydroxamic functional group have been synthesised based on the structure and subsequent *in vitro* activity of **4.1a** and **4.3a**. The aim is to determine if the structure of these compounds can be further modified to give increased potency and selectivity for HDAC6.

4.2. The synthesis of four series of potential HDAC inhibitors.

The synthesis of these compounds is a simple one and each compound can be reached in just two steps. The first step is identical to that used in the first step of the synthesis of GSK2879552 (Chapter 2, Section 2.2), and is nucleophilic substitution between methyl-4-(bromomethyl)benzoate and the appropriate secondary amine. The resulting methyl ester is then converted to a hydroxamic acid (Scheme 4.2). The method for this conversion is that described in chapter 3 section 3.2.

Occasionally, for reasons not completely understood, this method would result in the formation of the carboxylic acid in place of the hydroxamic acid. This may be due to the presence of water in the reagents used but it only seemed to affect a small number of reactions and persisted on repeated experiments. Therefore, when this occurred, an alternative method was employed in which the methyl ester is hydrolysed to give the carboxylic acid followed by amide coupling with *O*-benzyl hydroxylamine. This is then followed by a deprotection step with BCl_3, to give the corresponding hydroxamic acid (Scheme 4.2). The more traditional method of benzyl deprotection with H_2/Pd was initially tried but was found to additionally attack the *N*-benzyl group of the piperazine, thus breaking the molecule in half (Scheme 4.3). The yield for substitution of the methyl ester with benzyl protected hydroxylamine followed by deprotection of the hydroxamic acid with BCl_3 carried an overall yield of around 11 % for these reactions. This is much lower than the standard method which has a yield of anything from ~10-90 % but often over 50 %. This method was therefore only used when necessary.

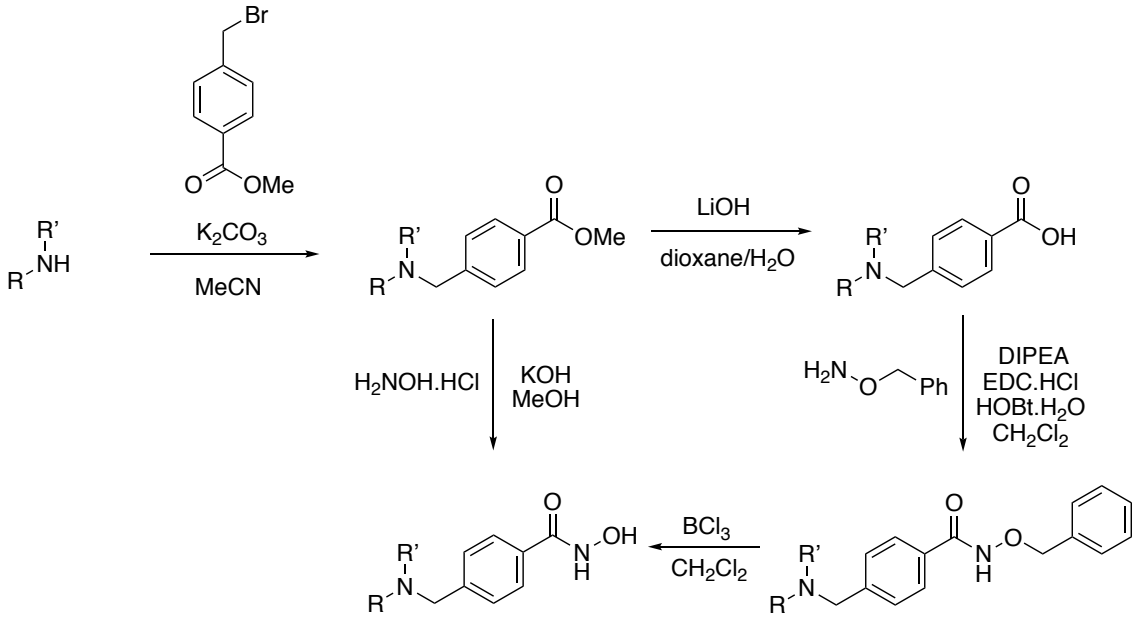

Scheme 4.2. *General synthetic method including the alternative route via the carboxylic acid.*

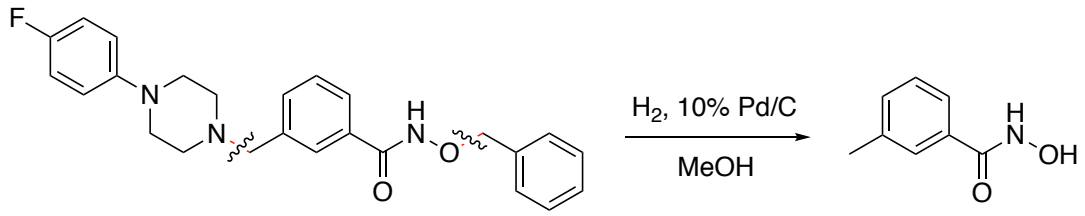

Scheme 4.3. *Deprotection with H_2/Pd and the resulting undesired cleavage of the N-benzyl group.*

The initial series of compounds followed on from **4.2a** and **4.2b** giving further analogues in which the phenylhydroxymate is substituted in the *para* position (Figure 4.1). These analogues were then repeated with the substitution in the *meta* (Figure 4.2) and *ortho* (Figure 4.3) position. Finally, a series comprising an additional *trans*-alkene linker adjacent to the hydroxymate group was developed (Figure 4.4).

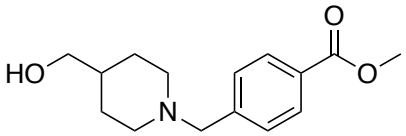

2.10a

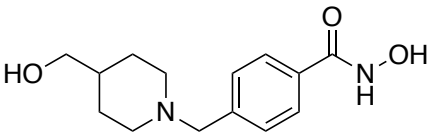

4.2a

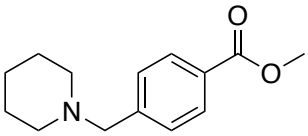

4.1a

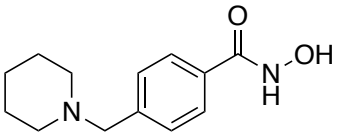

4.2b

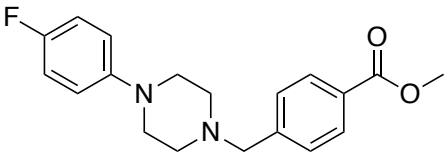

4.1b

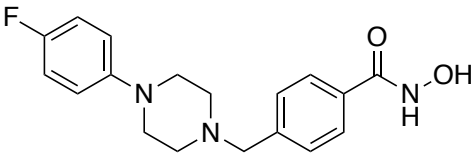

4.2c

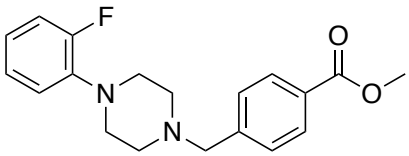

4.1c

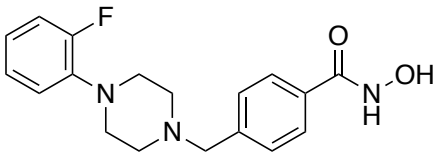

4.2d

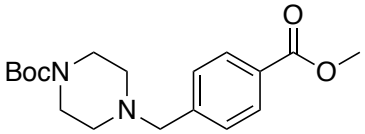

4.1d

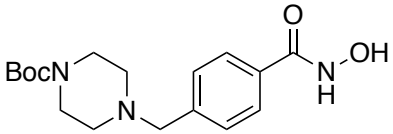

4.2e

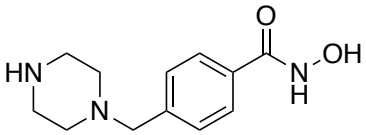

4.2f

Figure 4.1. Para series of potential HDAC inhibitors and the methyl ester precursors.

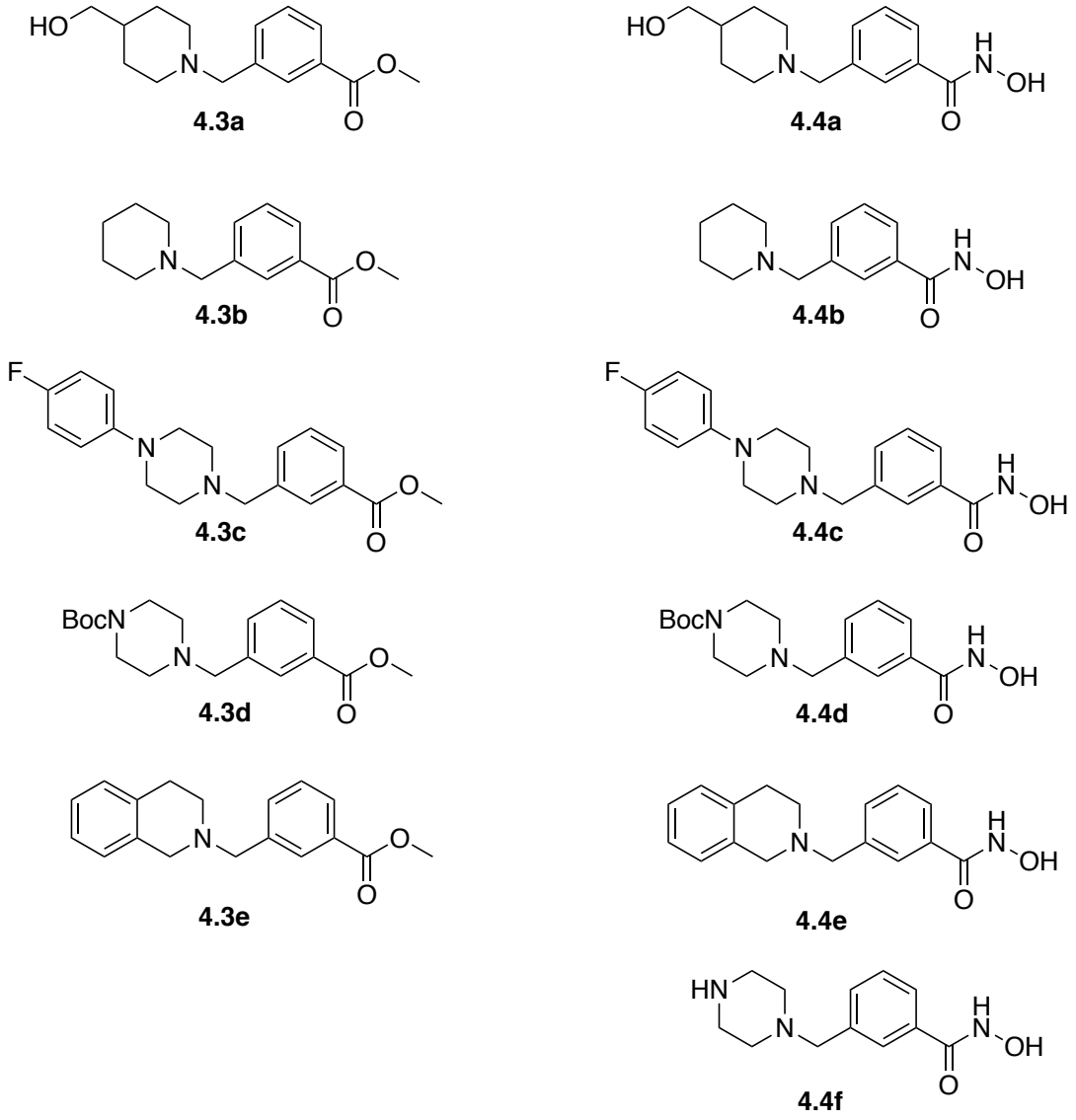

Figure 4.2. Meta series of potential HDAC inhibitors and the methyl ester precursors.

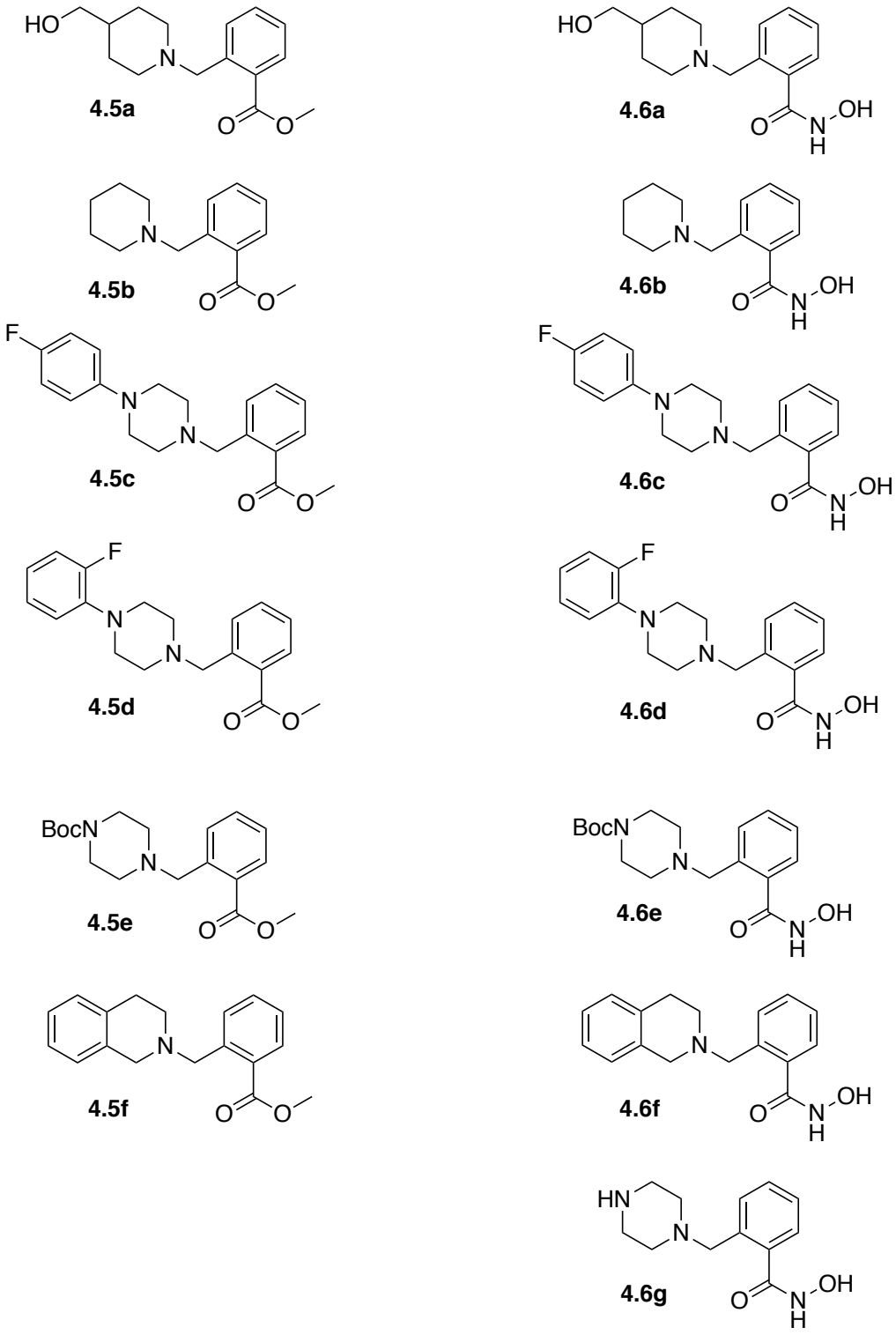

Figure 4.3. Ortho series of potential HDAC inhibitors and the methyl ester precursors.

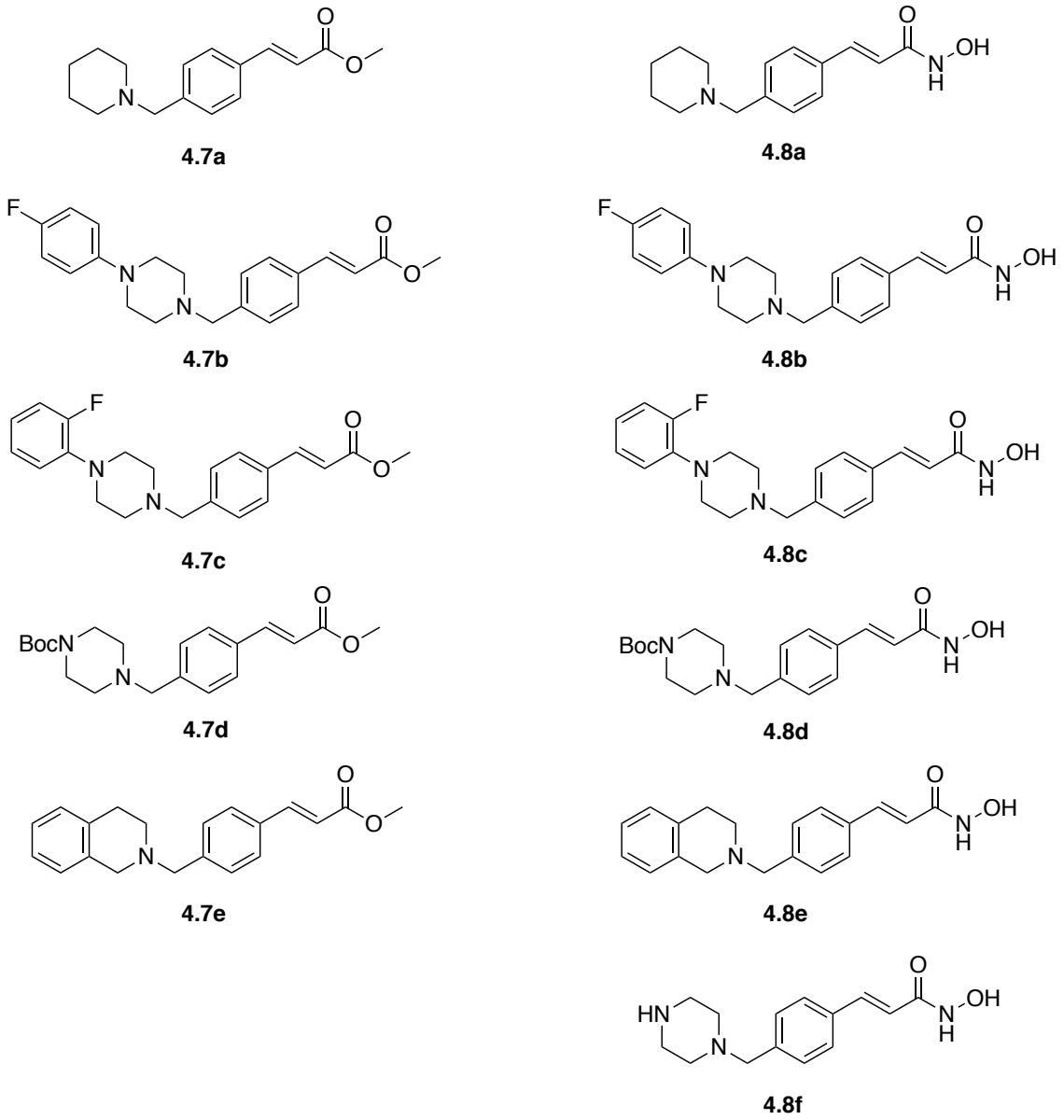

Figure 4.4. Alkene series of potential HDAC inhibitors and the methyl ester precursors.

4.3. Biological activity.

4.3.1. Cell free HDAC assays.

Compounds **4.2a** and **4.2b**, along with **2.10a** and trichostatin A (TSA) as positive and negative reference compounds, were subjected to *in vitro* screening against HDAC1, 3, 6 and 8 (Table 4.1, Figure 4.4). These were carried out in collaboration with Dusan Ruzic of the University of Belgrade and carried out at the Fraunhofer Institute, Freiburg.

Both **4.2a** and **4.2b** showed low μM activity in both HDAC1 and 3 and nM activity in both HDAC6 and 8. Of these both performed particularly well in HDAC6 with IC_{50} values of 0.30 (pIC_{50}: 6.51±0.06) and 0.35 μM (pIC_{50}: 6.44±0.05) for **4.2a** and **4.2b** respectively, more than 2-fold more active than in HDAC8. This suggests a certain amount of isoform specificity for the inhibition of HDAC6. Negative control **2.10a** was not active at concentrations of less than 100 μM in any of the isoforms tested.

Isoform	**pIC_{50}**			
	4.2a	**4.2b**	TSA	**2.10a**
HDAC1	4.79±0.03	4.73±0.03	7.00±0.06	< 4
HDAC3	4.98±0.04	4.91±0.03	8.71±0.05	< 4
HDAC6	6.51±0.06	6.44±0.05	8.66±0.14	< 4
HDAC8	6.14±0.04	6.09±0.05	6.52±0.10	< 4

Table 4.1. *HDAC assay data for compounds **4.2a** and **4.2b** along with positive and negative control compounds.*

Data generated by Ruzic et al., University of Belgrade (unpublished).

These results seem to follow the same pattern as for both **3.8** and **3.12** which also both showed strongest activity in HDAC6 and were in turn about 2-fold more active than in HDAC8. This is not unexpected given the similarities in structure, but both **3.8** and **3.12** were more active across all tested HDAC isoforms suggesting that these compounds, which comprise a shorter linker, may be

limited in the level of potency as the number of interactions with the HDAC active site is naturally reduced. The extended linker in the alkene series of compounds (**4.8a-f**) should address this and it would be interesting to see if potency is increased when these are tested in the future.

Further to this, selectivity should not be impacted by linker length and so it will also be interesting to see if any of the changes made do anything to improve selectivity for the HDAC6 isoform.

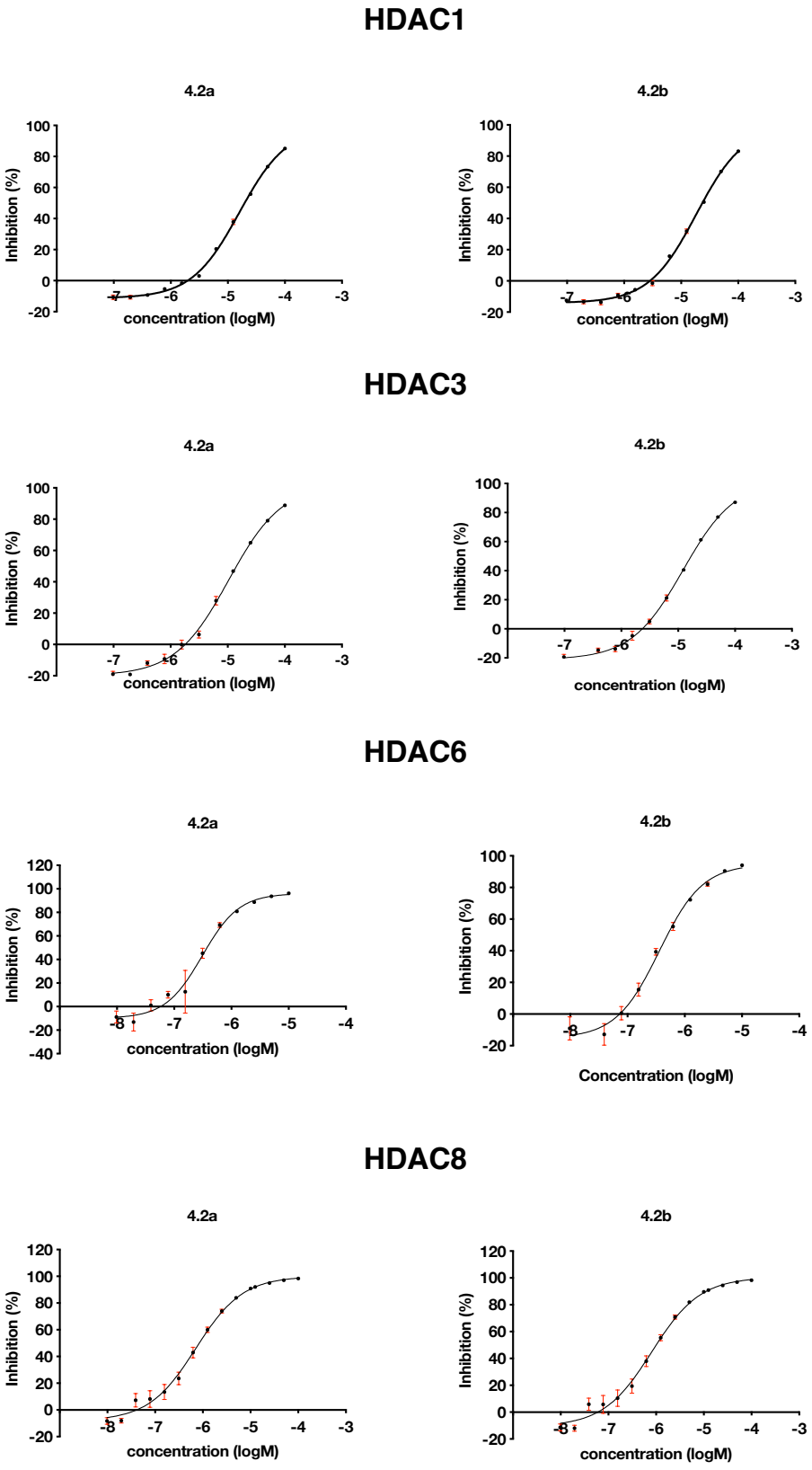

Figure 4.5. *Graphical representation of the HDAC assay data for **4.2a** and **4.2b**. Data generated by Ruzic et al., University of Belgrade (unpublished).*

4.3.2. Cell viability assay.

A THP-1 cell viability assay became immediately available for the testing of these compounds and was used to get an indication of the activity levels of these compounds in the absence of an available *in vitro* HDAC assay.

Testing was initially carried out at an inhibitor concentration of 100 μM. Any compounds that showed activity were then tested at a concentration of 10 μM and the IC_{50} of compounds active at this concentration were subsequently determined. Doxorubicin was used as a positive control.

All inhibitors, **4.2a-f**, **4.4a-f**, **4.6a-f** and **4.8a-f** were analysed in a MTS cell viability assay in THP-1 cells at an inhibitor concentration of 100 μM (Figure 4.5). Only two compounds from the *para*-series showed sufficient activity to justify testing at a lower concentration, **4.2c** and **4.2d**. Compounds **4.2a** and **4.2b**, which are the only compounds from these series to have assessed for activity against HDACs in a cell free assay, both showed barely any activity within this particular cell line. No compounds from the *meta*-series of compounds showed any significant activity and again only two compounds in the *ortho*-series, compounds **4.6d** and **4.6f**.

In contrast however, the alkene series of compounds demonstrated much better activity within the THP-1 cell line. Five of the six tested were found to have sufficient activity to warrant testing at lower concentrations with only **4.8b** not showing much activity.

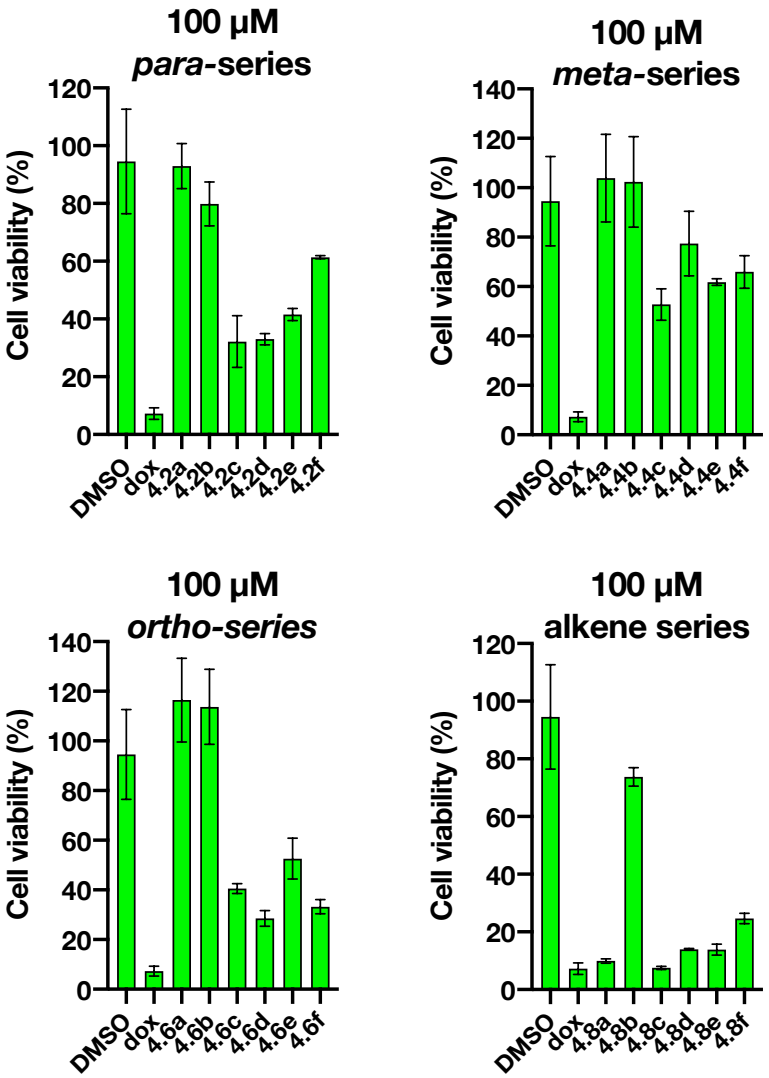

Figure 4.6. *THP-1 cell viability assay results at an inhibitor concentration of 100 µM.*

Data shown as % cell viability ± std, n=3.
Data generated by Burianova et al., UEA (unpublished).

Compounds that showed activity were then tested at the reduced concentration of 10 µM (Figure 4.6). The two compounds brought forward from the *para*-series both showed no activity at this concentration. The same was found for the two compounds tested from the *ortho*-series. Again, the majority of compounds from the alkene series showed good levels of activity and only **4.8f** was not submitted for IC_{50} determination.

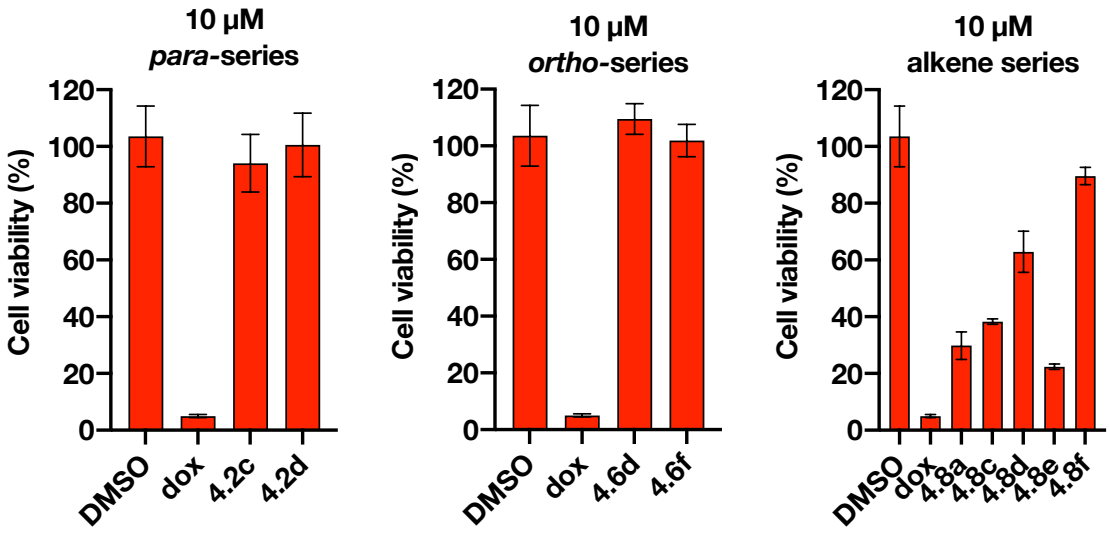

Figure 4.7. *THP-1 cell viability assay results at an inhibitor concentration of 10 µM.*

Data shown as % cell viability ± std, n=3.
Data generated by Burianova et al., UEA (unpublished).

Only four of the original twenty-four compounds were assessed for an IC_{50} value and all four were from the alkene series of compounds. These were **4.8a**, **4.8c**, **4.8d** and **4.8e** and were found to have IC_{50} values of 6.27, 8.68, 22.70 and 4.01 µM respectively (Figure 4.7).

Two compounds of note within these four are **4.8c** and **4.8d**. Both of these compounds have close analogues that did not show strong activity in the THP-1 cell line. This may give a little insight into the features of these compounds which are important. **4.8b** and **4.8c** are *para* and *ortho* fluorophenyl piperazine analogues respectively. *Para* analogue **4.8b** showed no activity at a concentration of 100 µM, whilst *ortho* analogue **4.8c** has an IC_{50} value of 8.68 µM. In addition, the comparative fluorophenyl compounds from the *para*-series, **4.2c** and **4.2d** were both active at 100 µM but not at 10 µM. Therefore, with the additional alkene linker, the 4-fluorophenyl analogue is the more active compound but in the absence of the alkene linker the 2-fluorophenyl analogue is superior, within the THP-1 cell line.

Compound **4.8d** and **4.8f** are the respective Boc-protected and free base analogues of the piperazine substituted alkene series compounds. Boc-protected **4.8d** has an IC_{50} value of 22.70 μM whilst free base **4.8f** was only active at a concentration of 100 μM. In addition, the comparative *para*-series compounds, **4.2e** and **4.2f** also showed slightly better activity in the Boc-protected piperazine, suggesting that having a free amine at the cap end of the molecule is not beneficial in this cell line.

The most active compound was found to be **4.8e** which has an IC_{50} value of 4.01 μM. The *para*-series analogue was not available so no direct comparison could be made to determine the impact of the additional alkene linker on this activity. The *meta*-series analogue **4.4e** was moderately active at a concentration of 100 μM as was the *ortho*-series analogue **4.6f** but not active at 10 μM.

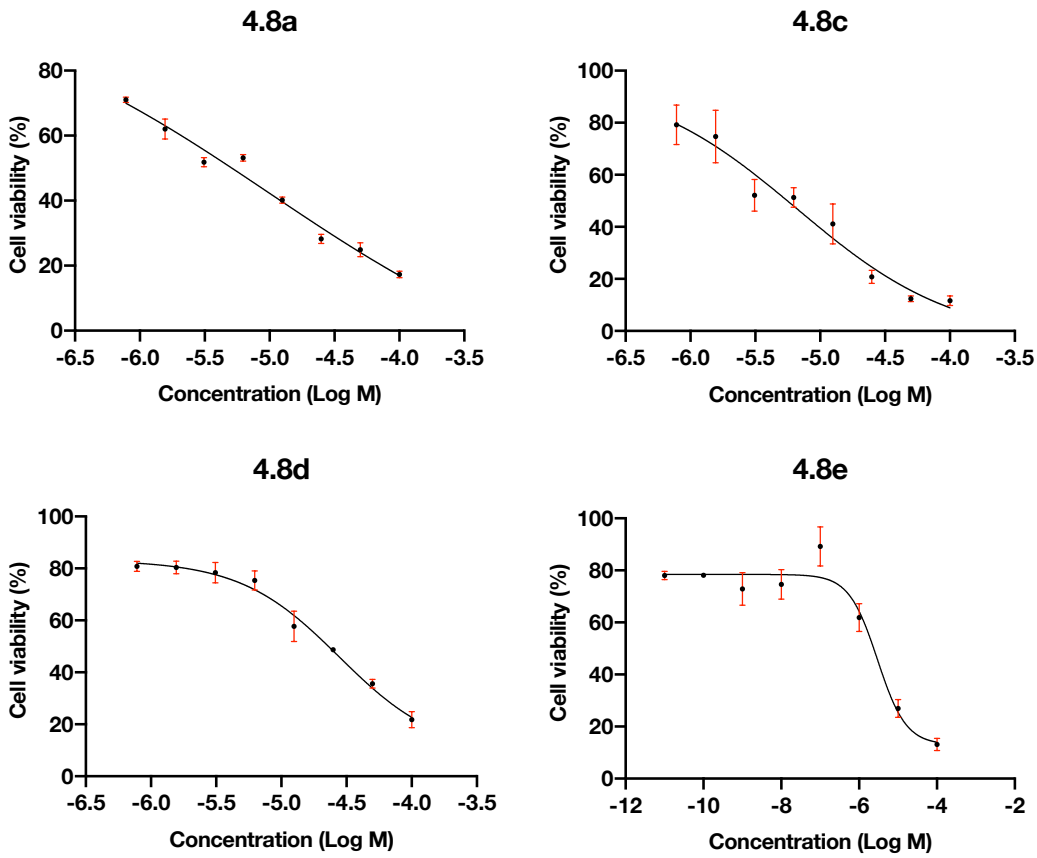

Figure 4.8. *THP-1 cell viability assay IC_{50} graphs for active compounds from the alkene series.*

Data shown as % cell viability ± std, n=3.
Data generated by Burianova et al., UEA (unpublished).

Compound	IC_{50} (μM)
4.8a	6.27±0.46
4.8c	8.68±1.99
4.8d	22.70±1.14
4.8e	4.01±1.24

Table 4.2. *Tabulated IC_{50} data from a THP-1 cell viability assay.*

Data shown as % cell viability ± std, n=3.
Data generated by Burianova et al., UEA (unpublished).

4.4 Virtual docking study.

Both **4.2a** and **4.2b** were modelled in a VD study (Figure 4.8, Figure 4.9), carried out in order to determine the most likely binding position and mode of these compounds within the HDAC6 active site. VD was carried out in collaboration with Dusan Ruzic and Katarina Nikolic at the University of Belgrade, Serbia. Docking was performed using GOLD Software 5.6.0 (DOI: 10.1006/jmbi.1996.0897). The HDAC6 crystal structure (human isoform, second catalytic domain) was taken from the Protein Data Bank, entry PDB:5EDU, prepared via PlayMolecule online platform (playmolecule.org/) and the number of docking runs set to 100. The ChemScore scoring function (doi.org/10.1002/prot.10465) was used to estimate the free energy of binding, as it additionally takes into consideration metal-ligand coordination important for Zn^{2+}-hydroxamic acid binding.

The only difference in structure between **4.2a** and **4.2b** is the additional hydroxymethyl group at position 4 on the piperidine ring. The hydroxy group itself did not show any significant interactions in our model but several additional interactions between the HDAC6 active site residues and **4.2a** were apparent. These included two additional pi-pi stacking interactions with Phe680 and His 651 as well as a carbon hydrogen bond interaction with Ser568. Both **4.2a** and **4.2b** had predicted bidentate binding modes between the oxygen atoms of their respective hydroxamate groups and the Zn^{2+} cofactor.

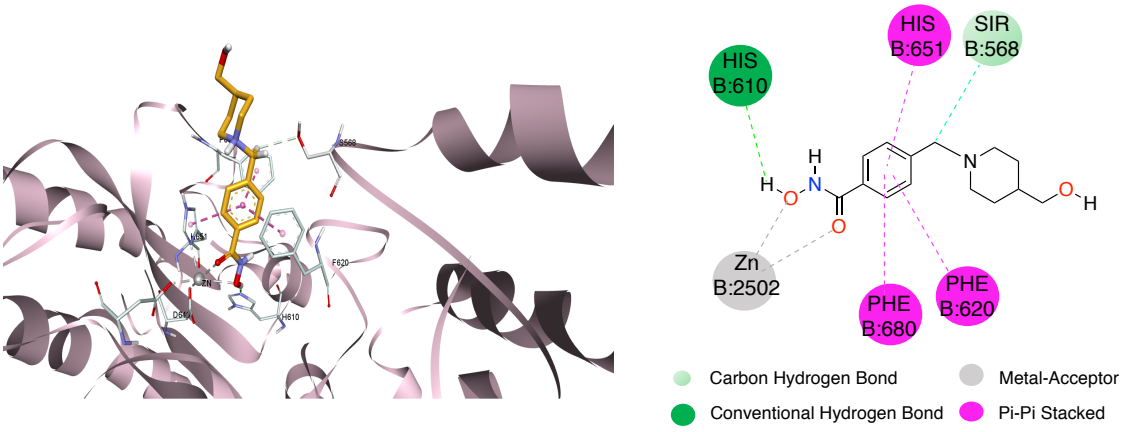

Figure 4.9. *Position of ligand 4.2a inside the binding site of the HDAC6 seen from the extracellular side (left) and 2D presentation of important interactions with amino acid residues in the active pocket of HDAC6 (right).*

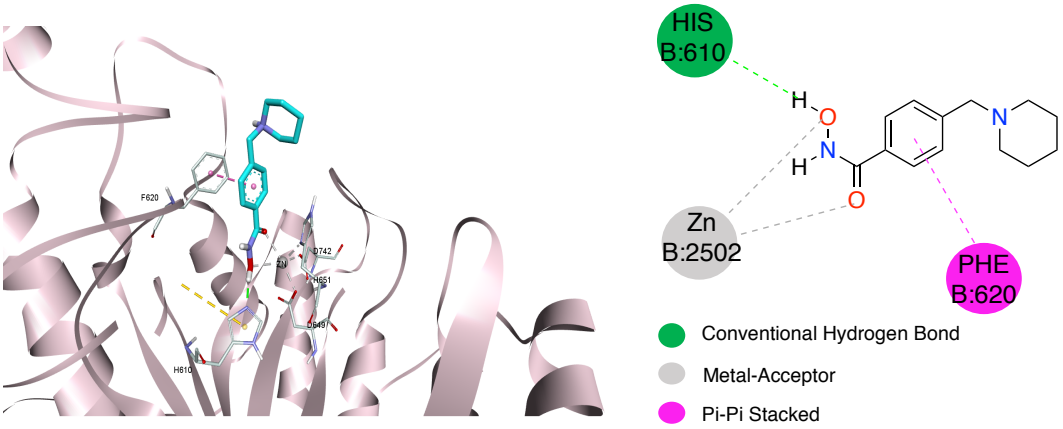

Figure 4.10. *Position of ligand 4.2b inside the binding site of the HDAC6 seen from the extracellular side (left) and 2D presentation of important interactions with amino acid residues in the active pocket of HDAC6 (right).*

4.5. Conclusion and future works.

Four series of compounds comprising the hydroxamic acid functional group have been synthesised. Two of these compounds, **4.2a** and **4.2b**, have been shown to inhibit HDAC6 with nano-molar potency. Future work should extend this testing to all other compounds synthesised in order to determine how the structural changes made to each compound affect both potency and selectivity.

All synthesised compounds were subjected to a cell viability assay using the THP-1 cell line. Results suggested that the *para, meta* and *ortho* series did not show strong activity. The alkene series of compounds however, showed much stronger activity particularly compounds **4.8a**, **4.8c** and **4.8e**. Of course, this is only one cell line and response can be cell line specific and hence future work should incorporate additional cell lines so as to better evaluate the in-cell pharmacological effects of these compounds.

A virtual docking study was carried out on compounds **4.2a** and **4.2b**. Both compounds were predicted to have a bidentate binding mode between their respective hydroxamic acid functional groups and the HDAC6 Zn^{2+} cofactor. Future work could extend this study to other compounds in these series to determine how the differing structural changes affect binding and thus help to guide the structure of further analogues.

4.6. Chapter four experimental

4.6.1. Experimental procedures

All experimental procedures are the same as for those described in Chapter two, section 2.7.1.

4.6.2. General procedure for synthesis of methyl ester precursors.

A dry flask was charged with Methyl 4-(bromomethyl)benzoate (1 eq), followed by the appropriate piperazine/piperadine (1 eq). Acetonitrile (5 ml $mmol^{-1}$) was added and stirred until all solids are dissolved. Potassium carbonate (3 eq) was added and the resulting mixture stirred at reflux under a nitrogen atmosphere for 2 hrs. The mixture was then cooled to room temperature before filtering and concentrating. The concentrate was dissolved in EtOAc and washed with water and brine. The organics were dried over $MgSO_4$ before drying *in vacuo.* If purity was deemed sufficient the resulting product was used in the subsequent step, if further purification was required this was carried out via column chromatography on silica in an appropriate mixture of EtOAc and hexanes.
All reactions were carried out on either a 1 or 2 g scale with respect to methyl 4-(bromomethyl)benzoate.

4.6.3. General procedure for the synthesis of hydroxamic acids.

In separate flasks, the appropriate methyl ester (1 eq), hydroxylamine hydrochloride (5 eq) and potassium hydroxide (8 eq) were dissolved in anhydrous methanol. The potassium hydroxide solution was then slowly added to the hydroxylamine solution and the resulting mixture stirred at room temperature for 30 minutes. The mixture was then filtered, and the filtrate added to the benzoate solution, which was then stirred at room temperature overnight. The pH of the mixture was adjusted to ~7 with 6M HCl and subsequently filtered and concentrated. Purification was carried out on a C-18 reverse phase column, eluting with a gradient of 10-100 % methanol in water.

4.6.4. *Para*-series

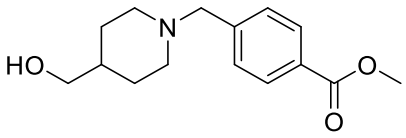

Methyl 4-{[4-(hydroxymethyl)piperidin-1-yl]methyl}benzoate (2.10a).

Isolated as a white solid, (83%).

Mp 57ºC; IR (cm^{-1}) 3497, 2937, 2905, 2794, 2755, 1718, 1694; ^{1}H NMR (400 MHz, Chloroform-*d*) δ 7.97 (d, *J* = 8.3 Hz, 2H), 7.40 (d, *J* = 8.7 Hz, 2H), 3.90 (s, 3H), 3.55 (s, 2H), 3.48 (t, *J* = 5.4 Hz, 2H), 2.89 (d, *J* = 11.6 Hz, 1H), 2.00 (td, *J* = 11.7, 2.5 Hz, 1H), 1.76 – 1.67 (m, 3H), 1.56 – 1.43 (m, 1H), 1.37 – 1.23 (m, 2H); ^{13}C NMR (101 MHz, Chloroform-*d*) δ 167.2, 144.3, 129.6, 129.0, 128.9, 67.9, 63.1, 53.6, 52.1, 38.6, 28.9; HMRS (ESI) *m/z* calcd for $C_{15}H_{21}NO_3$ $[M+H]^+$ 264.1594, found 264.1593.

These data are consistent with that reported in the literature.[102]

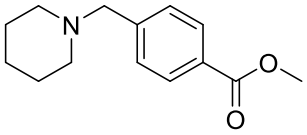

Methyl 4-[(piperidin-1-yl)methyl]benzoate (4.1a).

Isolated as a colourless oil, (79%).

^{1}H NMR (400 MHz, Chloroform-*d*) δ 7.97 (d, *J* = 8.2 Hz, 2H), 7.39 (d, *J* = 8.0 Hz, 2H), 3.90 (d, *J* = 1.0 Hz, 3H), 3.50 (s, 2H), 2.36 (brd-s, 4H), 1.56 (p, *J* = 5.6 Hz, 4H), 1.46 – 1.37 (m, 2H); ^{13}C NMR (101 MHz, Chloroform-*d*) δ 167.2, 144.5, 129.5, 129.0, 128.8, 63.5, 54.7, 52.0, 26.1, 24.4; No HRMS was obtained for this compound.

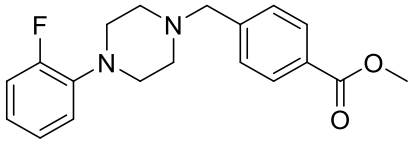

Methyl 4-{[4-(2-fluorophenyl)piperazin-1-yl]methyl}benzoate (4.1c).

Isolated as a white solid, (65%).

IR (cm^{-1}) 3070, 3007, 2957, 2945, 2834, 2804, 2767, 1715; ^{1}H NMR (400 MHz, Chloroform-*d*) δ 8.01 (d, *J* = 8.3 Hz, 2H), 7.45 (d, *J* = 8.0 Hz, 2H), 7.08 – 6.89 (m, 3H), 3.92 (s, 3H), 3.63 (s, 2H), 3.12 (brd-s, 4H), 2.65 (brd-s, 4H); ^{13}C NMR (101 MHz, Chloroform-*d*) δ 167.1, 157.1, 154.6, 129.7, 129.1, 124.6, 124.5, 122.5, 119.1, 119.0, 116.3, 116.1, 62.8, 53.3, 52.2, 50.6; ^{19}F NMR (376 MHz, Chloroform-*d*) δ -122.72; HRMS (ESI) *m/z* calcd for $C_{19}H_{21}FN_2O_2$ $[M+H]^+$ 329.1660, found 329.1654.

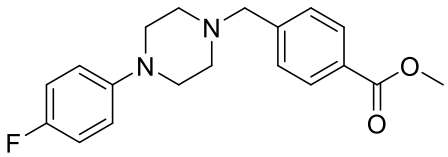

Methyl 4-{[4-(4-fluorophenyl)piperazin-1-yl]methyl}benzoate (4.1b).

Isolated as a white solid, (51%).

IR (cm^{-1}) 2818, 1721; ^{1}H NMR (400 MHz, Chloroform-*d*) δ 8.01 (d, *J* = 8.4 Hz, 2H), 7.44 (d, *J* = 8.5 Hz, 2H), 6.99 – 6.90 (m, 2H), 6.90 – 6.82 (m, 2H), 3.91 (s, 3H), 3.62 (s, 2H), 3.13 (t, *J* = 5.0 Hz, 4H), 2.66 – 2.62 (t, *J* = 5.0 Hz, 4H); ^{13}C NMR (101 MHz, Chloroform-*d*) δ 167.1, 158.4, 156.0, 148.0, 148.0, 143.4, 129.7, 129.2, 129.0, 117.9, 117.9, 115.7, 115.4, 62.6, 53.2, 52.1, 50.2; ^{19}F NMR (376 MHz, Chloroform-*d*) δ -124.62; HRMS (ESI) *m/z* calcd for $C_{19}H_{21}FN_2O_2$ $[M+H]^+$ 329.1660, found 329.1663.

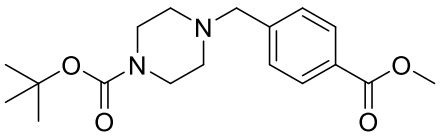

***tert*-Butyl 4-{[4-(methoxycarbonyl)phenyl]methyl}piperazine-1-carboxylate (4.1d)**

Isolated as a white solid, (92%).

^{1}H NMR (400 MHz, Chloroform-*d*) δ 7.96 (d, *J* = 8.3 Hz, 2H), 7.38 (d, *J* = 8.4 Hz, 2H), 3.88 (s, 3H), 3.53 (s, 2H), 3.41 (t, *J* = 5.0 Hz, 4H), 2.36 (t, *J* = 5.0 Hz, 4H), 1.43 (s, 9H); ^{13}C NMR (101 MHz, Chloroform-*d*) δ 167.0, 154.8, 143.3, 129.6, 129.1, 128.9, 79.6, 62.6, 52.9, 52.1, 28.4; HRMS (ESI) *m/z* calcd for $C_{18}H_{26}N_2O_4$ $[M+H]^+$ 335.1966, found 335.1958.

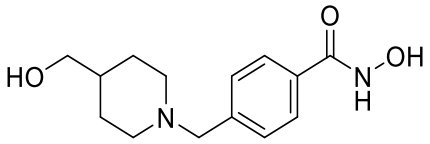

***N*-hydroxy-4-{[4-(hydroxymethyl)piperidin-1-yl]methyl}benzamide (4.2a).**

Isolated as colourless solid, (54%).

^{1}H NMR (400 MHz, Methanol-d_4) δ 7.71 (d, *J* = 8.3 Hz, 2H), 7.43 (d, *J* = 8.6 Hz, 2H), 3.57 (s, 2H), 3.39 (d, *J* = 6.4 Hz, 2H), 2.90 (brd-d, *J* = 11.6 Hz, 2H), 2.03 (td, *J* = 11.8, 2.6 Hz, 2H), 1.72 (d, *J* = 12.8 Hz, 2H), 1.54 – 1.40 (m, 1H), 1.26 (qd, *J* = 12.3, 3.8 Hz, 2H); ^{13}C NMR (101 MHz, Methanol-d_4) δ 167.9, 142.7, 132.6, 130.8, 128.0, 67.8, 63.8, 54.4, 39.5, 29.6; HRMS (ESI) *m/z* calcd for $C_{14}H_{20}N_2O_3$ $[M+H]^+$ 265.1547, found 265.1545.

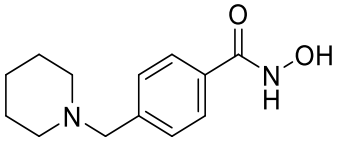

***N*-hydroxy-4-[(piperidin-1-yl)methyl]benzamide (4.2b).**

Isolated as a white solid, (40%).

IR (cm^{-1}) 3184, 2935, 2843, 2430, 1638; ^{1}H NMR (400 MHz, DMSO-d_6) δ 11.09 (brd-s, 1H), 9.07 (brd-s, 1H), 7.69 (d, *J* = 8.2 Hz, 2H), 7.35 (d, *J* = 8.3 Hz, 2H), 3.44 (s, 2H), 2.30 (brd-s, 4H), 1.48 (p, *J* = 5.5 Hz, 4H), 1.43 – 1.32 (m, 2H); ^{13}C NMR (101 MHz, DMSO-d_6) δ 164.1, 142.0, 131.3, 128.5, 126.7, 62.4, 53.9, 25.5, 23.9; HRMS (ESI) *m/z* calcd for $C_{13}H_{18}N_2O_2$ $[M+H]^+$ 235.1441, found 235.1437.

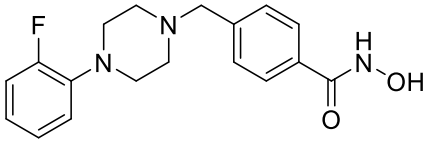

4-{[4-(2-fluorophenyl)piperazin-1-yl]methyl}-*N*-hydroxybenzamide (4.2d).

Isolated as a white solid, (48 %)

IR (cm^{-1}) 3479, 3354, 2951, 2851, 1657; ^{1}H NMR (400 MHz, Methanol-d_4) δ 7.73 (d, *J* = 8.3 Hz, 2H), 7.48 (d, *J* = 8.3 Hz, 2H), 7.11 – 6.91 (m, 4H), 3.65 (s, 2H), 3.10 (t, *J* = 4.9 Hz, 4H), 2.65 (t, *J* = 4.9 Hz, 4H); ^{13}C NMR (101 MHz, Methanol-d_4) δ 158.5, 148.8, 146.4, 133.3, 131.8, 131.7, 123.1, 121.2, 118.6, 116.2, 116.2, 114.4, 114.3, 110.8, 110.7, 107.5, 107.3, 53.9, 44.7, 42.0, 42.0; ^{19}F NMR (376 MHz, Methanol-d_4) δ -124.74; HRMS (ESI) *m/z* calcd for $C_{18}H_{20}FN_3O_2$ $[M+H]^+$ 330.1613, found 330.1605.

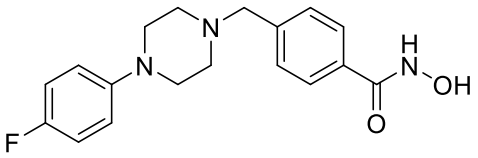

4-{[4-(4-fluorophenyl)piperazin-1-yl]methyl}-*N*-hydroxybenzamide (4.2c).

Isolated as a white solid, (11%)

IR (cm^{-1}) 3091, 2960, 2883, 2828, 1650; ^{1}H NMR (400 MHz, Methanol-d_4) δ 7.73 (d, J = 8.3 Hz, 2H), 7.48 (d, J = 8.3 Hz, 2H), 6.96 (d, J = 6.5 Hz, 4H), 3.64 (s, 2H), 3.15 – 3.09 (m, 4H), 2.66 – 2.59 (m, 4H); ^{13}C NMR (101 MHz, DMSO-d_6) δ 164.1, 157.1, 154.8, 147.9, 141.4, 131.5, 128.7, 126.8, 117.1, 117.0, 115.3, 115.1, 61.5, 52.5, 48.9; ^{19}F NMR (376 MHz, DMSO-d_6) δ -125.68; HRMS (ESI) *m/z* calcd for $C_{18}H_{20}FN_3O_2$ $[M+H]^+$ 330.1612, found 330.1625.

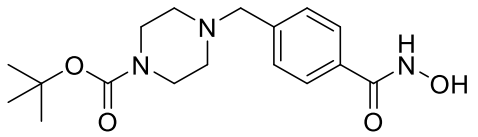

***tert*-Butyl 4-{[4-(hydroxycarbamoyl)phenyl]methyl}piperazine-1-carboxylate (4.2e).**

Isolated as a white solid, (77%).

IR (cm^{-1}) 3202, 2976, 2929, 2814, 1689, 1619; ^{1}H NMR (400 MHz, DMSO-d_6) δ 11.16 (s, 1H), 9.00 (s, 1H), 7.71 (d, J = 8.3 Hz, 2H), 7.37 (d, J = 8.4 Hz, 2H), 3.51 (s, 2H), 3.31 (t, J = 5.0 Hz, 4H), 2.30 (t, J = 5.0 Hz, 4H), 1.38 (s, 9H); ^{13}C NMR (101 MHz, DMSO-d_6) δ 164.1, 153.7, 141.2, 131.5, 128.7, 126.8, 78.7, 61.4, 52.3, 28.0; HRMS (ESI) *m/z* calcd for $C_{17}H_{25}N_3O_4$ $[M+H]^+$ 336.1918, found 336.1913.

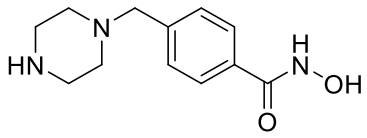

***N*-hydroxy-4-[(piperazin-1-yl)methyl]benzamide (4.2f).**

Isolated as a white solid, (quant)

IR (cm^{-1}) 3476, 2963, 2686, 2570, 2451, 1713, 1637; ^{1}H NMR (400 MHz, DMSO-d_6) δ 7.81 (d, *J* = 8.3 Hz, 2H), 7.66 (d, *J* = 8.3 Hz, 2H), 4.55 (s, 2H), 3.70 – 3.58 (m, 8H); ^{13}C NMR (101 MHz, DMSO-d_6) δ 163.3, 133.6, 131.6, 129.5, 127.2, 57.9, 47.3, 27.9; HRMS (ESI) *m/z* calcd for $C_{12}H_{17}N_3O_2$ $[M+H]^+$ 236.1394, found 236.1379.

4.6.5. *Meta*-series

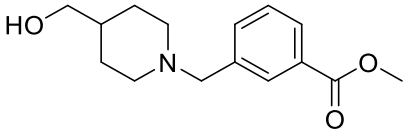

Methyl 3-{[4-(hydroxymethyl)piperidin-1-yl]methyl}benzoate (4.3a).

Isolated as a yellow oil, (72%).

IR (cm^{-1}) 3348, 2916, 2801, 2759, 1719; ^{1}H NMR (400 MHz, Chloroform-*d*) δ 7.95 (s, 1H), 7.91 (d, *J* = 7.7 Hz, 1H), 7.53 (d, *J* = 7.4 Hz, 1H), 7.37 (t, *J* = 7.7 Hz, 1H), 3.90 (s, 3H), 3.52 (s, 2H), 3.47 (s, 2H), 2.87 (d, *J* = 11.3 Hz, 2H), 1.97 (t, *J* = 11.6 Hz, 2H), 1.69 (d, *J* = 12.7 Hz, 2H), 1.55 – 1.42 (m, 1H), 1.27 (qd, *J* = 12.2, 3.2 Hz, 2H); ^{13}C NMR (101 MHz, Chloroform-*d*) δ 167.3, 139.0, 133.8, 130.3, 130.1, 128.4, 67.9, 63.0, 53.5, 52.2, 38.6, 28.8; HRMS (ESI) *m/z* calcd for $C_{15}H_{21}NO_3$ $[M+H]^+$ 264.1594, found 264.1584.

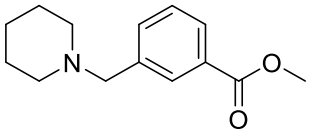

Methyl 3-[(piperidin-1-yl)methyl]benzoate (4.3b).

Isolated as a colourless oil, (76%).

IR (cm^{-1}) 2933, 2852, 2794, 2755, 1721; ^{1}H NMR (400 MHz, Chloroform-*d*) δ 7.96 (s, 1H), 7.90 (dt, *J* = 7.7, 1.4 Hz, 1H), 7.53 (dt, *J* = 7.6, 1.6 Hz, 1H), 7.36 (t, *J* = 7.7 Hz, 1H), 3.90 (s, 3H), 3.49 (s, 2H), 2.36 (t, *J* = 5.5 Hz, 4H), 1.60 – 1.51 (m, 4H), 1.46 – 1.37 (m, 2H); ^{13}C NMR (101 MHz, Chloroform-*d*) δ 167.3, 139.2, 133.8, 130.3, 130.1, 128.3, 128.2, 63.5, 54.5, 52.1, 26.0, 24.4; HRMS (ESI) *m/z* calcd for $C_{14}H_{19}NO_2$ $[M+H]^+$ 234.1489, found 234.1479.

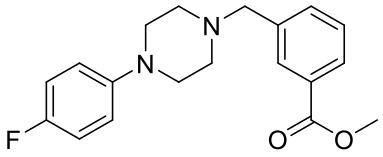

Methyl 3-{[4-(4-fluorophenyl)piperazin-1-yl]methyl}benzoate (4.3c).

Isolated as a yellow oil, (75%).

IR (cm^{-1}) 2948, 2814, 2770, 1718; ^{1}H NMR (400 MHz, Chloroform-*d*) δ 8.03 – 8.00 (m, 1H), 7.95 (dt, *J* = 7.7, 1.4 Hz, 1H), 7.58 (d, *J* = 7.6 Hz, 1H), 7.41 (t, *J* = 7.7 Hz, 1H), 6.99 – 6.91 (m, 2H), 6.89 – 6.83 (m, 2H), 3.92 (s, 3H), 3.62 (s, 2H), 3.16 – 3.09 (m, 4H), 2.65 – 2.59 (m, 4H); ^{13}C NMR (101 MHz, Chloroform-*d*) δ 167.2, 158.4, 156.1, 148.1, 148.0, 133.8, 130.3, 130.3, 128.6, 128.5, 117.9, 117.9, 115.7, 115.5, 62.6, 53.1, 52.2, 50.2; ^{19}F NMR (376 MHz, Chloroform-*d*) δ -124.63; HRMS (ESI) *m/z* calcd for $C_{19}H_{21}FN_2O_2$ $[M+H]^+$ 329.1660, found 329.1658.

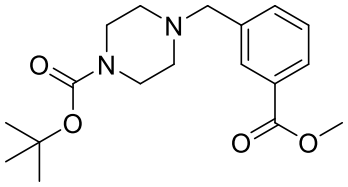

***tert*-Butyl 4-{[3-(methoxycarbonyl)phenyl]methyl}piperazine-1-carboxylate (4.3d).**

Isolated as a yellow gel, (78%).

IR (cm^{-1}) 2975, 2950, 2807, 1721, 1690; ^{1}H NMR (400 MHz, Chloroform-*d*) δ 7.94 (s, 1H), 7.90 (d, *J* = 7.7 Hz, 1H), 7.50 (d, *J* = 7.6 Hz, 1H), 7.36 (t, *J* = 7.6 Hz, 1H), 3.88 (d, *J* = 0.8 Hz, 3H), 3.52 (s, 2H), 3.40 (t, *J* = 5.0 Hz, 4H), 2.36 (t, *J* = 5.0 Hz, 4H), 1.42 (s, 9H); ^{13}C NMR (101 MHz, Chloroform-*d*) δ 167.1, 154.7, 138.3, 133.7, 130.2, 130.2, 128.5, 128.4, 79.6, 62.5, 52.8, 52.1, 43.6, 28.4; HRMS (ESI) *m/z* calcd for $C_{18}H_{26}N_2O_4$ $[M+H]^+$ 335.1965, found 335.1963.

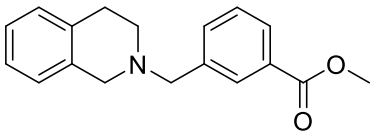

Methyl 3-[(3,4-dihydroisoquinolin-2(1*H*)-yl)methyl]benzoate (4.3e).

Isolated as a yellow oil, (74%).

IR (cm^{-1}) 3022, 2948, 2915, 2797, 2756, 1718; ^{1}H NMR (400 MHz, Chloroform-*d*) δ 8.07 (s, 1H), 7.97 (d, *J* = 7.8 Hz, 1H), 7.64 (d, *J* = 7.2 Hz, 1H), 7.42 (t, *J* = 7.7 Hz, 1H), 7.19 – 7.07 (m, 3H), 7.03 – 6.95 (m, 1H), 3.93 (s, 3H), 3.74 (s, 2H), 3.65 (s, 2H), 2.92 (t, *J* = 5.9 Hz, 2H), 2.76 (t, *J* = 5.9 Hz, 2H); ^{13}C NMR (101 MHz, Chloroform-*d*) δ 167.2, 139.0, 134.8, 134.4, 133.7, 130.3, 130.2, 128.8, 128.5, 128.5, 126.6, 126.2, 125.7, 62.4, 56.1, 52.1, 50.7, 29.2; HRMS (ESI) *m/z* calcd for $C_{18}H_{19}NO_2$ $[M+H]^+$ 282.1489, found 282.1484.

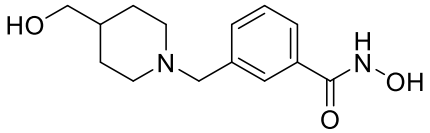

***N*-hydroxy-3-{[4-(hydroxymethyl)piperidin-1-yl]methyl}benzamide (4.4a)**

Isolated as a yellow oil, (67%).

IR (cm^{-1}) 3176, 2934, 2870, 1639; ^{1}H NMR (500 MHz, Methanol-d_4) δ 8.00 (s, 1H), 7.84 (d, *J* = 7.9 Hz, 1H), 7.80 (d, *J* = 7.8 Hz, 1H), 7.57 (t, *J* = 7.8 Hz, 1H), 4.43 (s, 2H), 3.50 (d, *J* = 12.3 Hz, 2H), 3.45 (d, *J* = 6.2 Hz, 2H), 3.11 (t, *J* = 13.6 Hz, 2H), 1.97 (d, *J* = 12.9 Hz, 2H), 1.87 – 1.75 (m, 1H), 1.61 (q, *J* = 11.5 Hz, 2H); ^{13}C NMR (126 MHz, Methanol-d_4) δ 167.1, 135.7, 134.2, 131.2, 131.2, 130.5, 129.5, 66.3, 60.8, 53.2, 37.1, 26.8; HRMS (ESI) *m/z* calcd for $C_{14}H_{20}N_2O_3$ $[M+H]^+$ 265.1547, found 265.1541.

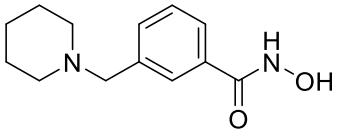

***N*-hydroxy-3-[(piperidin-1-yl)methyl]benzamide (4.4b).**

Isolated as a yellow oil, (89%)

IR (cm^{-1}) 2945, 2677, 1644; ^{1}H NMR (400 MHz, DMSO-d_6) δ 7.95 (s, 1H), 7.78 (t, *J* = 7.0 Hz, 2H), 7.49 (t, *J* = 7.7 Hz, 1H), 4.21 (s, 2H), 2.97 (s, 4H), 1.81 – 1.68 (m, 4H), 1.54 – 1.40 (m, 2H); ^{13}C NMR (101 MHz, DMSO-d_6) δ 167.9, 134.3, 133.6, 131.3, 130.5, 129.1, 127.8, 59.4, 52.2, 22.8, 22.1; HRMS (ESI) *m/z* calcd for $C_{13}H_{18}N_2O_2$ $[M+H]^+$ 235.1441, found 235.1433.

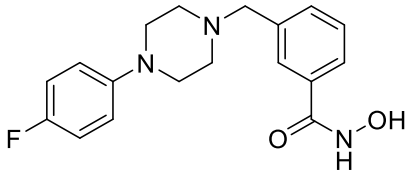

3-{[4-(4-fluorophenyl)piperazin-1-yl]methyl}-*N*-hydroxybenzamide (4.4c).

Isolated as a pale yellow solid, (25%).

IR (cm^{-1}) 2819, 1634; ^{1}H NMR (400 MHz, Methanol-d_4) δ 7.76 (t, *J* = 1.8 Hz, 1H), 7.67 (dt, *J* = 7.8, 1.5 Hz, 1H), 7.53 (dt, *J* = 7.7, 1.5 Hz, 1H), 7.42 (t, *J* = 7.7 Hz, 1H), 6.99 – 6.87 (m, 4H), 3.60 (s, 2H), 3.13 – 3.02 (m, 4H), 2.65 – 2.54 (m, 4H); ^{13}C NMR (101 MHz, Methanol-d_4) δ 167.9, 159.8, 157.4, 149.3, 149.2, 139.1, 133.9, 133.6, 129.6, 129.3, 127.1, 119.2, 119.1, 119.1, 116.3, 116.1, 63.3, 53.9, 50.9; ^{19}F NMR (376 MHz, Methanol-d_4) δ -126.29; HRMS (ESI) *m/z* calcd for $C_{18}H_{20}FN_3O_2$ $[M^+H]^+$ 330.1612, found 330.1603.

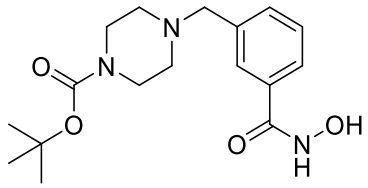

***tert*-Butyl 4-{[3-(hydroxycarbamoyl)phenyl]methyl}piperazine-1-carboxylate (4.4d).**

Isolated as a white solid, (58%).

IR (cm^{-1}) 280, 1651; ^{1}H NMR (400 MHz, DMSO-d_6) δ 11.20 (brd-s, 1H), 9.02 (brd-s, 1H), 7.69 (s, 1H), 7.63 (dt, *J* = 7.4, 1.6 Hz, 1H), 7.46 – 7.36 (m, 2H), 3.50 (s, 2H), 3.31 (s, 4H), 2.31 (t, *J* = 5.0 Hz, 4H), 1.38 (s, 9H); ^{13}C NMR (101 MHz, DMSO-d_6) δ 164.2, 153.8, 138.2, 132.8, 131.6, 128.2, 127.4, 125.5, 78.7, 61.6, 52.3, 43.2, 28.0; HRMS (ESI) *m/z* calcd for $C_{17}H_{25}N_3O_4$ $[M^+H]^+$ 336.1918, found 336.1911.

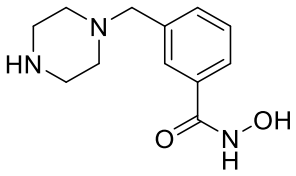

***N*-hydroxy-3-[(piperazin-1-yl)methyl]benzamide (4.4f).**

Isolated as a white solid, (63 %)

IR (cm^{-1}) 3004, 2408, 1663; ^{1}H NMR (400 MHz, DMSO-d_6) δ 8.01 (s, 1H), 7.84 (d, J = 7.7 Hz, 1H), 7.80 (d, J = 7.8 Hz, 1H), 7.53 (t, J = 7.7 Hz, 1H), 4.47 (s, 2H), 3.47 (brd-s, 8H); ^{13}C NMR (101 MHz, DMSO-d_6) δ 163.7, 134.3, 133.3, 130.6, 129.1, 128.9, 127.9, 58.1, 47.2; HRMS (ESI) *m/z* calcd for $C_{12}H_{17}N_3O_2$ $[M^+H]^+$ 236.1394, found 236.1378.

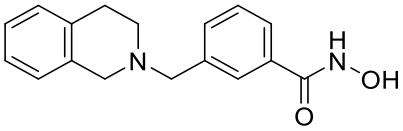

3-[(3,4-dihydroisoquinolin-2(1*H*)-yl)methyl]-*N*-hydroxybenzamide (4.4e).

Isolated as a yellow solid, (62 %).

IR (cm^{-1}) 2800, 1634; ^{1}H NMR (400 MHz, DMSO-d_6) δ 11.23 (brd-s, 1H), 9.04 (brd-s, 1H), 7.77 (s, 1H), 7.66 (dt, *J* = 7.6, 1.5 Hz, 1H), 7.51 (dt, *J* = 7.6, 1.5 Hz, 1H), 7.42 (t, *J* = 7.6 Hz, 1H), 7.12 – 7.05 (m, 3H), 7.00 (dt, *J* = 6.3, 1.7 Hz, 1H), 3.71 (s, 2H), 3.57 (s, 2H), 2.82 (t, *J* = 5.9 Hz, 2H), 2.71 (t, *J* = 5.9 Hz, 2H); ^{13}C NMR (101 MHz, DMSO-d_6) δ 164.2, 138.4, 134.4, 133.9, 132.8, 131.5, 128.4, 128.3, 127.4, 126.3, 126.0, 125.5, 125.5, 61.4, 55.2, 50.1, 28.5; HRMS (ESI) *m/z* calcd for $C_{17}H_{18}N_2O_2$ $[M^+H]^+$ 283.1441, found 283.1450.

4.6.6. *Ortho*-series

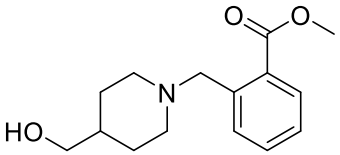

Methyl 2-{[4-(hydroxymethyl)piperidin-1-yl]methyl}benzoate (4.5a).

Isolated as a yellow oil, (98%).

IR (cm^{-1}) 3383, 2938, 2803, 2759, 1716; ^{1}H NMR (400 MHz, Chloroform-*d*) δ 7.69 – 7.65 (m, 1H), 7.46 – 7.35 (m, 2H), 7.27 (td, *J* = 7.5, 1.6 Hz, 1H), 3.86 (s, 3H), 3.73 (s, 2H), 3.45 (t, *J* = 5.9 Hz, 2H), 2.80 (d, *J* = 11.5 Hz, 2H), 1.99 (t, *J* = 10.7 Hz, 2H), 1.76 (t, *J* = 5.4 Hz, 1H), 1.65 (d, *J* = 13.6 Hz, 2H), 1.54 – 1.40 (m, 1H), 1.20 (qd, *J* = 12.1, 3.9 Hz, 2H); ^{13}C NMR (101 MHz, Chloroform-*d*) δ 169.4, 139.8, 131.6, 131.0, 129.9, 129.6, 126.9, 67.9, 60.8, 53.4, 52.0, 38.6, 29.0; HRMS (ESI) *m/z* calcd for $C_{15}H_{21}NO_3$ $[M^+H]^+$ 264.1594, found 264.1584.

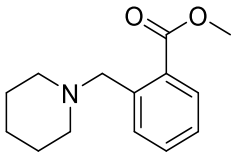

Methyl 2-[(piperidin-1-yl)methyl]benzoate (4.5b).

Isolated as a yellow oil, (91%).

IR (cm^{-1}) 2933, 2851, 2797, 2724, 1722; ^{1}H NMR (400 MHz, Chloroform-*d*) δ 7.68 (dd, *J* = 7.6, 1.2 Hz, 1H), 7.49 – 7.37 (m, 2H), 7.29 (td, *J* = 7.5, 1.6 Hz, 1H), 3.89 (s, 3H), 3.71 (s, 2H), 2.36 (brd-s, 4H), 1.54 (p, *J* = 5.5 Hz, 4H), 1.43 (q, *J* = 6.0 Hz, 2H); ^{13}C NMR (101 MHz, Chloroform-*d*) δ 169.5, 140.0, 131.7, 130.9, 129.8, 129.5, 126.8, 61.3, 54.5, 51.9, 26.2, 24.4; HRMS (ESI) *m/z* calcd for $C_{14}H_{19}NO_2$ $[M^+H]^+$ 234.1489, found 234.1482.

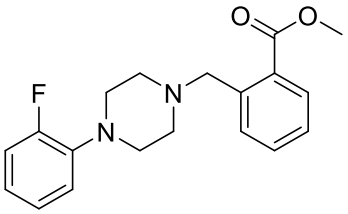

Methyl 2-{[4-(2-fluorophenyl)piperazin-1-yl]methyl}benzoate (4.5d).

Isolated as a yellow solid (53%).

IR (cm^{-1}) 3025, 3065, 2946, 2880, 2824, 1720; ^{1}H NMR (400 MHz, Chloroform-*d*) δ 7.71 (dd, *J* = 7.7, 0.9 Hz, 1H), 7.48 – 7.39 (m, 2H), 7.31 (td, *J* = 7.5, 1.8 Hz, 1H), 7.07 – 6.87 (m, 4H), 3.89 (s, 3H), 3.83 (s, 2H), 3.06 (t, *J* = 4.8 Hz, 4H), 2.65 – 2.57 (m, 4H); ^{13}C NMR (101 MHz, Chloroform-*d*) δ 169.3, 157.0, 154.5, 140.3, 140.2, 139.2, 131.8, 131.0, 130.0, 129.7, 127.1, 124.5, 124.4, 122.4, 122.3, 118.9, 118.9, 116.2, 116.0, 60.6, 53.1, 52.0, 50.7, 50.7; ^{19}F NMR (376 MHz, Chloroform-*d*) δ -122.58; HRMS (ESI) *m/z* calcd for $C_{19}H_{21}FN_2O_2$ $[M^+H]^+$ 329.1660, found 329.1655.

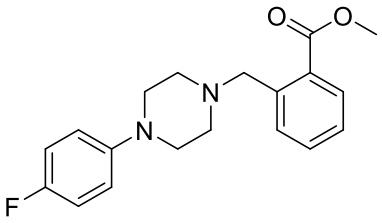

Methyl 2-{[4-(4-fluorophenyl)piperazin-1-yl]methyl}benzoate (4.5c)

Isolated as a yellow solid, (58%).

IR (cm^{-1}) 2948, 2834, 2779, 1721; ^{1}H NMR (400 MHz, Chloroform-*d*) δ 7.71 (dd, *J* = 7.6, 1.1 Hz, 1H), 7.49 – 7.39 (m, 2H), 7.31 (td, *J* = 7.5, 1.7 Hz, 1H), 6.99 – 6.90 (m, 2H), 6.88 – 6.81 (m, 2H), 3.88 (s, 3H), 3.83 (s, 2H), 3.09 – 3.04 (m, 4H), 2.62 – 2.56 (m, 4H); ^{13}C NMR (101 MHz, Chloroform-*d*) δ 169.2, 158.3, 155.9, 148.1, 148.1, 139.1, 131.7, 131.1, 130.0, 129.7, 127.1, 117.8, 117.7, 115.6, 115.4, 60.5, 53.0, 52.0, 50.3; ^{19}F NMR (376 MHz, Chloroform-*d*) δ -124.76; HRMS (ESI) *m/z* calcd for $C_{19}H_{21}FN_2O_2$ $[M^+H]^+$ 329.1660, found 329.1656.

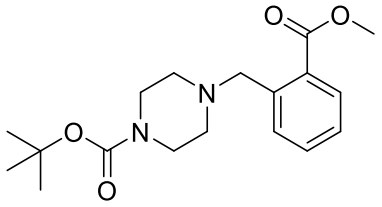

***tert*-Butyl 4-{[2-(methoxycarbonyl)phenyl]methyl}piperazine-1-carboxylate (4.5e).**

Isolated as a colourless oil, (89%).

IR (cm^{-1}) 2975, 2946, 2810, 1723, 1691; ^{1}H NMR (400 MHz, Chloroform-*d*) δ 7.69 (d, *J* = 7.5 Hz, 1H), 7.44 – 7.38 (m, 2H), 7.33 – 7.26 (m, 1H), 3.87 (s, 3H), 3.77 (s, 2H), 3.37 (t, *J* = 5.0 Hz, 4H), 2.36 (t, *J* = 5.0 Hz, 4H), 1.44 (s, 9H); ^{13}C NMR (101 MHz, Chloroform-*d*) δ 169.1, 154.8, 138.9, 131.6, 131.1, 129.9, 129.7, 127.1, 79.5, 60.5, 52.8, 52.0, 43.7, 28.4; HRMS (ESI) *m/z* calcd for $C_{18}H_{26}N_2O_4$ $[M^+H]^+$ 335.1965, found 335.1960.

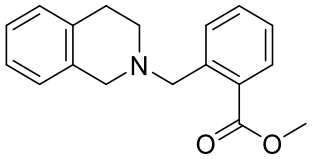

Methyl 2-[(3,4-dihydroisoquinolin-2(1*H*)-yl)methyl]benzoate (4.5f).

Isolated as an orange solid, (95%).

IR (cm^{-1}) 3021, 2997, 2939, 2792, 2747, 2721, 1711, ^{1}H NMR (400 MHz, Chloroform-*d*) δ 7.77 (dd, *J* = 7.7, 1.3 Hz, 1H), 7.58 (d, *J* = 7.7 Hz, 1H), 7.46 (td, *J* = 7.5, 1.5 Hz, 1H), 7.33 (td, *J* = 7.5, 1.4 Hz, 1H), 7.17 – 7.08 (m, 3H), 7.03 – 6.97 (m, 1H), 3.99 (s, 2H), 3.82 (s, 3H), 3.68 (s, 2H), 2.88 (t, *J* = 5.9 Hz, 2H), 2.74 (t, *J* = 5.9 Hz, 2H); ^{13}C NMR (101 MHz, Chloroform-*d*) δ 169.0, 139.8, 135.0, 134.5, 131.4, 131.3, 129.8, 128.7, 127.0, 126.5, 126.1, 125.5, 60.2, 56.1, 52.0, 50.6, 29.3; HRMS (ESI) *m/z* calcd for $C_{18}H_{19}NO_2$ $[M^+H]^+$ 282.1489, found 282.1477.

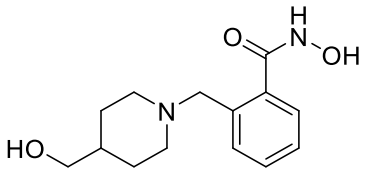

***N*-hydroxy-2-{[4-(hydroxymethyl)piperidin-1-yl]methyl}benzamide (4.6a)**

Isolated as a colourless solid, (93%).

IR (cm^{-1}) 3399, 3315, 3147, 3027, 2961, 2840, 1625; ^{1}H NMR (400 MHz, Methanol-d_4) δ 7.75 – 7.42 (m, 4H), 4.38 (s, 2H), 3.47 (d, *J* = 6.0 Hz, 4H), 3.13 (t, *J* = 13.7 Hz, 2H), 2.01 (d, *J* = 15.7 Hz, 2H), 1.91 – 1.76 (m, 1H), 1.53 (q, *J* = 10.8 Hz, 2H); ^{13}C NMR (101 MHz, Methanol-d_4) δ 168.6, 134.8, 134.8, 133.1, 131.7, 130.7, 130.0, 66.3, 52.9, 49.8, 37.3, 27.4; HRMS (ESI) *m/z* calcd for $C_{14}H_{20}N_2O_3$ $[M^+H]^+$ 265.1547, found 265.1540.

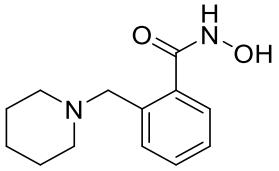

***N*-hydroxy-2-[(piperidin-1-yl)methyl]benzamide (4.6b).**

Isolated as a white solid, (25%).

IR (cm^{-1}) 3191, 2931, 2848, 1653; ^{1}H NMR (400 MHz, DMSO-d_6) δ 7.56 (dd, J = 7.4, 1.7 Hz, 1H), 7.45 – 7.32 (m, 3H), 3.49 (s, 2H), 2.38 (s, 4H), 1.49 (p, J = 5.1 Hz, 4H), 1.45 – 1.36 (m, 2H); ^{13}C NMR (101 MHz, DMSO-d_6) δ 165.3, 135.1, 134.8, 131.0, 129.6, 129.1, 127.5, 60.5, 52.9, 25.4, 23.7; HRMS (ESI) *m/z* calcd for $C_{13}H_{18}N_2O_2$ $[M^+H]^+$ 235.1441, found 235.1431.

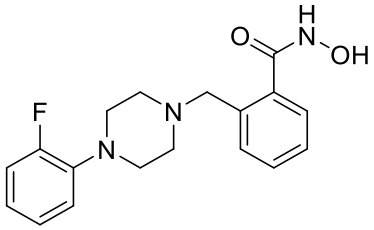

2-{[4-(2-fluorophenyl)piperazin-1-yl]methyl}-*N*-hydroxybenzamide (4.6d).

Isolated as a yellow solid, (19%).

IR (cm^{-1}) 2816, 1650; ^{1}H NMR (400 MHz, Methanol-d_4) δ 7.72 (dd, J = 7.3, 1.6 Hz, 1H), 7.50 – 7.37 (m 3H), 7.10 – 6.92 (m, 4H), 3.70 (s, 2H), 3.10 (brd-s, 4H), 2.72 (brd-s, 4H); ^{13}C NMR (101 MHz, Methanol-d_4) δ 168.8, 158.3, 155.9, 141.1, 141.0, 135.6, 135.5, 133.1, 131.7, 130.8, 129.4, 125.7, 125.7, 124.0, 124.0, 120.3, 120.3, 117.0, 116.8, 61.8, 53.2, 51.6, 51.6; ^{19}F NMR (376 MHz, Methanol-d_4) δ -124.81; HRMS (ESI) *m/z* calcd for $C_{18}H_{20}FN_3O_2$ $[M^+H]^+$ 330.1613, found 330.1601.

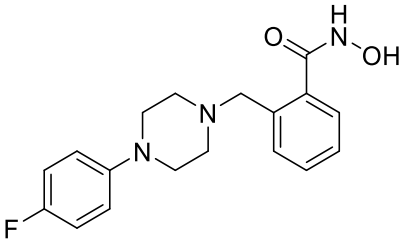

2-{[4-(4-fluorophenyl)piperazin-1-yl]methyl}-*N*-hydroxybenzamide (4.6c).

Isolated as a yellow solid, (71%).

IR (cm^{-1}) 2992, 2837, 2667, 1632;

^{1}H NMR (400 MHz, Methanol-d_4) δ 7.75 – 7.59 (m, 4H), 7.10 – 6.97 (m, 4H), 4.52 (s, 2H), 3.81 – 3.68 (m, 2H), 3.61 – 3.50 (m, 2H), 3.46 – 3.36 (m, 2H), 3.18 – 3.00 (m, 2H); ^{13}C NMR (101 MHz, Methanol-d_4) δ 167.1, 159.3, 156.9, 146.3, 146.3, 133.5, 133.4, 131.8, 130.5, 128.8, 128.6, 118.9, 118.8, 115.4, 115.1, 58.9, 51.1; ^{19}F NMR (376 MHz, Methanol-d_4) δ -124.49; HRMS (ESI) *m/z* calcd for $C_{18}H_{20}FN_3O_2$ $[M^+H]^+$ 330.1613, found 330.1603.

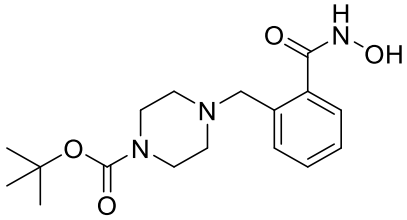

***tert*-Butyl 4-{[2-(hydroxycarbamoyl)phenyl]methyl}piperazine-1-carboxylate (4.6e).**

Isolated as a pale orange solid, (73%).

IR (cm^{-1}) 2818, 1689, 1646; ^{1}H NMR (400 MHz, DMSO-d_6) δ 11.34 (brd-s, 1H), 9.03 (brd-s, 1H), 7.45 – 7.37 (m, 3H), 7.37 – 7.30 (m, 1H), 3.57 (s, 2H), 3.30 (t, *J* = 5.0 Hz, 4H), 2.33 (t, *J* = 5.0 Hz, 4H), 1.39 (s, 9H); ^{13}C NMR (101 MHz, DMSO-d_6) δ 165.7, 153.8, 135.3, 135.1, 130.2, 129.5, 128.3, 127.2, 78.8, 59.2, 51.9, 43.2, 28.0; HRMS (ESI) *m/z* calcd for $C_{17}H_{25}N_3O_4$ $[M^+H]^+$ 336.1918, found 336.1918.

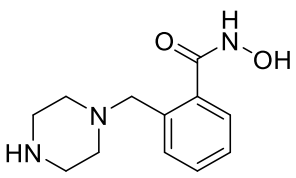

***N*-hydroxy-2-[(piperazin-1-yl)methyl]benzamide (4.6g).**

Isolated as a pale pink solid, (quant).

IR (cm^{-1}) 1644; ^{1}H NMR (400 MHz, DMSO-d_6) δ 11.40 (brd-s, 1H), 10.08 (brd-s, 1H), 7.94 (d, *J* = 7.4 Hz, 1H), 7.63 – 7.45 (m, 3H), 4.50 (s, 2H), 3.48 (brd-s, 8H); ^{13}C NMR (101 MHz, DMSO-d_6) δ 165.2, 135.1, 133.1, 130.7, 129.9, 128.3, 127.8, 56.4, 47.7, 39.7; HRMS (ESI) *m/z* calcd for $C_{12}H_{17}N_3O_2$ $[M^+H]^+$ 236.1394, found 236.1372.

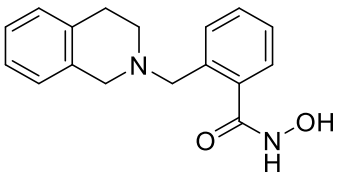

2-[(3,4-dihydroisoquinolin-2(1*H*)-yl)methyl]-*N*-hydroxybenzamide (4.6f).

Isolated as an orange solid, (48%).

IR (cm^{-1}) 3113, 2857, 1631; ^{1}H NMR (400 MHz, DMSO-d_6) δ 11.70 (brd-s, 1H), 9.05 (brd-s, 1H), 7.53 – 7.41 (m, 3H), 7.37 (td, *J* = 7.3, 1.6 Hz, 1H), 7.15 – 7.06 (m, 3H), 7.01 (d, *J* = 6.3 Hz, 1H), 3.74 (s, 2H), 3.58 (s, 2H), 2.82 (t, *J* = 5.6 Hz, 2H), 2.72 (t, *J* = 5.7 Hz, 2H); ^{13}C NMR (101 MHz, DMSO-d_6) δ 165.5, 135.3, 135.0, 134.2, 133.8, 130.5, 129.7, 128.6, 128.5, 127.4, 126.4, 126.1, 125.5, 59.3, 54.7, 49.7, 28.5; HRMS (ESI) *m/z* calcd for $C_{17}H_{18}N_2O_2$ $[M^+H]^+$ 283.1441, found 283.1429.

4.6.7. Alkene-series

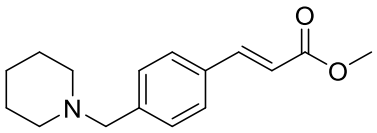

Methyl (2*E*)-3-{4-[(piperidin-1-yl)methyl]phenyl}prop-2-enoate (4.7a).

Isolated as a white solid, (61 %)

^{1}H NMR (400 MHz, Chloroform-*d*) δ 7.68 (d, *J* = 16.0 Hz, 1H), 7.47 (d, *J* = 8.1 Hz, 2H), 7.34 (d, *J* = 8.2 Hz, 2H), 6.42 (d, *J* = 16.0 Hz, 1H), 3.80 (s, 3H), 3.48 (s, 2H), 2.38 (t, *J* = 5.4 Hz, 4H), 1.58 (p, *J* = 5.6 Hz, 4H), 1.48 – 1.39 (m, 2H); ^{13}C NMR (101 MHz, Chloroform-*d*) δ 167.6, 144.9, 141.5, 133.2, 129.7, 128.0, 117.3, 63.5, 54.6, 51.8, 26.0, 24.4; HRMS (ESI) *m/z* calcd for $C_{16}H_{21}NO_2$ $[M^+H]^+$ 260.1645, found 260.1633.

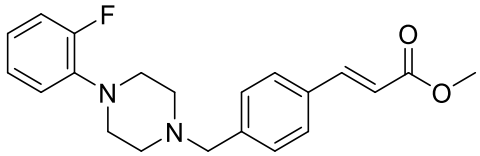

Methyl (2*E*)-3-(4-{[4-(2-fluorophenyl)piperazin-1-yl]methyl}phenyl)prop-2-enoate (4.7c).

Isolated as a white solid, (23%).

IR (cm^{-1}) 2933, 2826, 1707, 1635, 1609; ^{1}H NMR (400 MHz, Chloroform-*d*) δ 7.69 (d, *J* = 16.0 Hz, 1H), 7.50 (d, *J* = 8.2 Hz,21H), 7.41 (d, *J* = 7.9 Hz, 2H), 7.09 – 6.89 (m, 4H), 6.44 (d, *J* = 16.0 Hz, 1H), 3.81 (s, 3H), 3.63 (s, 2H), 3.14 (brd-s, 4H), 2.68 (brd-s, 4H); ^{13}C NMR (101 MHz, Chloroform-*d*) δ 167.6, 157.0, 154.6, 144.6, 129.9, 128.2, 124.6, 124.5, 119.1, 117.7, 116.3, 116.1, 62.7, 53.5, 53.2, 51.8, 50.4; ^{19}F NMR (376 MHz, Chloroform-*d*) δ -122.79; HRMS (ESI) *m/z* calcd for $C_{21}H_{23}FN_2O_2$ $[M^+H]^+$ 355.1817, found 355.1826.

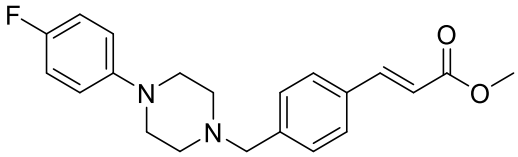

Methyl (2*E*)-3-(4-{[4-(4-fluorophenyl)piperazin-1-yl]methyl}phenyl)prop-2-enoate (4.7b).

Isolated as a white solid, (55%).

IR (cm^{-1}) 2947, 2824, 1703, 1631, 1607; ^{1}H NMR (400 MHz, Chloroform-*d*) δ 7.69 (d, *J* = 16.0 Hz, 1H), 7.50 (d, *J* = 8.2 Hz, 2H), 7.38 (d, *J* = 8.1 Hz, 2H), 6.98 – 6.91 (m, 2H), 6.90 – 6.83 (m, 2H), 6.44 (d, *J* = 16.0 Hz, 1H), 3.81 (s, 3H), 3.58 (s, 2H), 3.15 – 3.08 (m, 4H), 2.66 – 2.57 (m, 4H); ^{13}C NMR (101 MHz, Chloroform-*d*) δ 167.6, 158.5, 156.1, 148.1, 148.0, 144.7, 133.5, 129.7, 128.2, 118.0, 117.9, 117.6, 115.7, 115.5, 62.7, 53.2, 51.8, 50.2; ^{19}F NMR (376 MHz, Chloroform-*d*) δ -124.60; HRMS (ESI) *m/z* calcd for $C_{21}H_{23}FN_2O_2$ $[M^+H]^+$ 355.1817, found 355.1814.

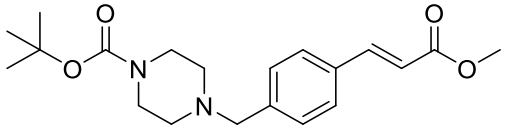

***tert*-Butyl 4-({4-[(1*E*)-3-methoxy-3-oxoprop-1-en-1-yl]phenyl}methyl) piperazine-1-carboxylate (4.7d).**

Isolated as a white solid, (84%).

IR (cm^{-1}) 2973, 2953, 2918, 1751, 1712, 1697, 1686, 1607; ^{1}H NMR (400 MHz, Chloroform-*d*) δ 7.67 (d, *J* = 16.0 Hz, 1H), 7.47 (d, *J* = 8.2 Hz, 2H), 7.33 (d, *J* = 8.2 Hz, 2H), 6.41 (d, *J* = 16.0 Hz, 1H), 3.79 (s, 3H), 3.51 (s, 2H), 3.42 (t, *J* = 5.0 Hz, 4H), 2.38 (t, *J* = 5.1 Hz, 4H), 1.44 (s, 9H); ^{13}C NMR (101 MHz, Chloroform-*d*) δ 167.5, 154.8, 144.6, 140.6, 133.5, 129.6, 128.1, 117.6, 79.7, 62.7, 52.9, 51.7, 43.6, 28.5; HRMS (ESI) *m/z* calcd for $C_{20}H_{28}N_2O_4$ $[M^+H]^+$ 361.2122, found 361.2123.

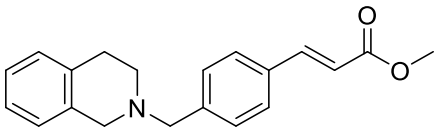

Methyl (2*E*)-3-{4-[(3,4-dihydroisoquinolin-2(1*H*)-yl)methyl]phenyl}prop-2-enoate (4.7e).

Isolated as a yellow solid, (56%).

IR (cm^{-1}) 3397, 3019, 2932, 2802, 2760, 1703, 1634, 1606; ^{1}H NMR (400 MHz, Chloroform-*d*) δ 7.71 (d, *J* = 16.0 Hz, 1H), 7.50 (d, *J* = 8.3 Hz, 2H), 7.43 (d, *J* = 8.2 Hz, 2H), 7.16 – 7.07 (m, 3H), 7.01 – 6.95 (m, 1H), 6.44 (d, *J* = 16.1 Hz, 1H), 3.81 (s, 3H), 3.70 (s, 2H), 3.64 (s, 2H), 2.91 (t, *J* = 5.9 Hz, 2H), 2.76 (t, *J* = 5.9 Hz, 2H); ^{13}C NMR (101 MHz, Chloroform-*d*) δ 167.6, 144.8, 141.1, 134.7, 134.3, 133.4, 129.6, 128.8, 128.2, 126.7, 126.3, 125.7, 117.5, 62.4, 56.2, 51.8, 50.8, 29.1; HRMS (ESI) *m/z* calcd for $C_{20}H_{21}NO_2$ $[M^+H]^+$ 308.1645, found 308.1647.

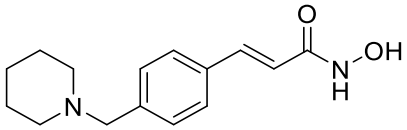

(2*E*)-*N*-hydroxy-3-{4-[(piperidin-1-yl)methyl]phenyl}prop-2-enamide (4.8a).

Isolated as a yellow solid, (50%).

IR (cm^{-1}) 2932, 1653, 1608; ^{1}H NMR (400 MHz, Methanol-d_4) δ 7.59 (d, *J* = 8.2 Hz, 1H), 7.56 (d, *J* = 15.8 Hz, 1H), 7.53 (d, *J* = 8.2 Hz, 1H), 7.37 (d, *J* = 8.1 Hz, 2H), 6.46 (d, *J* = 15.8 Hz, 1H), 3.53 (s, 2H), 2.45 (brd-s, 4H), 1.61 (p, *J* = 5.6 Hz, 4H), 1.51 – 1.42 (m, 2H); ^{13}C NMR (101 MHz, Methanol-d_4) δ 166.3, 141.2, 140.1, 135.4, 131.4, 128.6, 118.3, 64.2, 55.3, 26.4, 25.0; HRMS (ESI) *m/z* calcd for $C_{15}H_{20}N_2O_2$ $[M^+H]^+$ 261.1598, found 261.1596.

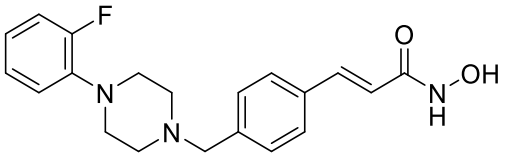

(2*E*)-3-(4-{[4-(2-fluorophenyl)piperazin-1-yl]methyl}phenyl)-*N*-hydroxyprop-2-enamide (4.8c).

Isolated as an orange solid, (15%).

IR (cm^{-1}) 3125, 2984, 2833, 1650, 1607; ^{1}H NMR (400 MHz, Methanol-d_4) δ 7.57 (d, J = 15.8 Hz, 1H), 7.53 (d, J = 7.9 Hz, 2H), 7.40 (d, J = 7.8 Hz, 2H), 7.10 – 6.90 (m, 4H), 6.48 (d, J = 15.8 Hz, 1H), 3.61 (s, 2H), 3.08 (t, J = 4.8 Hz, 4H), 2.65 (t, J = 4.8 Hz, 4H); ^{13}C NMR (101 MHz, Methanol-d_4) δ 166.2, 158.3, 155.9, 141.2, 141.1, 141.0, 140.0, 135.5, 131.3, 131.1, 128.8, 127.5, 125.7, 125.7, 124.0, 123.9, 120.3, 120.2, 118.4, 117.0, 116.8, 63.4, 54.1, 51.3, 51.3; ^{19}F NMR (376 MHz, Methanol-d_4) δ -124.67; HRMS (ESI) *m/z* calcd for $C_{20}H_{22}FN_3O_2$ $[M^+H]^+$ 356.1769, found 356.1761.

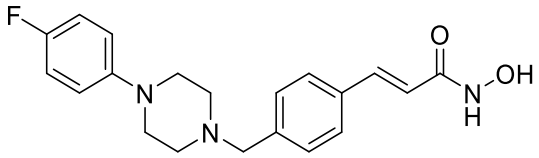

(2*E*)-3-(4-{[4-(4-fluorophenyl)piperazin-1-yl]methyl}phenyl)-*N*-hydroxyprop-2-enamide (4.8b).

Isolated as an orange solid, (5%).

IR (cm^{-1}) 2921, 2836, 2460, 1689, 1629; ^{1}H NMR (400 MHz, Methanol-d_4) δ 7.64 (d, J = 16.3 Hz, 1H), 7.61 (d, J = 8.4 Hz, 2H), 7.45 (d, J = 8.1 Hz, 2H), 6.97 (d, J = 6.5 Hz, 4H), 6.50 (d, J = 16.0 Hz, 1H), 3.76 (s, 2H), 3.21 – 3.12 (m, 4H), 2.82 – 2.75 (m, 4H); ^{13}C NMR (101 MHz, Methanol-d_4) δ 165.7, 160.6, 158.2, 147.7, 140.3, 138.1, 133.1, 131.3, 129.5, 120.3, 120.1, 120.1, 116.7, 116.5, 60.9, 52.9; ^{19}F NMR (376 MHz, Methanol-d_4) δ -124.58; HRMS (ESI) *m/z* calcd for $C_{20}H_{22}FN_3O_2$ $[M^+H]^+$ 356.1769, found 356.1766.

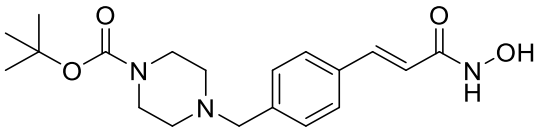

***tert*-Butyl 4-({4-[(1*E*)-3-(hydroxyamino)-3-oxoprop-1-en-1-yl]phenyl} methyl)piperazine-1-carboxylate (4.8d).**

Isolated as a white solid, (23%).

IR (cm^{-1}) 3172, 2976, 2818, 1690, 1651, 1611; ^{1}H NMR (400 MHz, Methanol-d_4) δ 7.57 (d, J = 15.8 Hz, 1H), 7.53 (d, J = 8.1 Hz, 2H), 7.38 (d, J = 8.1 Hz, 2H), 6.46 (d, J = 15.8 Hz, 1H), 3.55 (s, 2H), 3.43 (t, J = 5.1 Hz, 4H), 2.41 (t, J = 5.1 Hz, 4H), 1.45 (s, 9H); ^{13}C NMR (101 MHz, Methanol-d_4) δ 166.3, 156.4, 141.3, 140.7, 135.4, 131.0, 128.7, 118.2, 81.2, 63.4, 53.8, 28.6; HRMS (ESI) *m/z* calcd for $C_{19}H_{27}N_3O_4$ $[M^+H]^+$ 362.2074, found 362.2080.

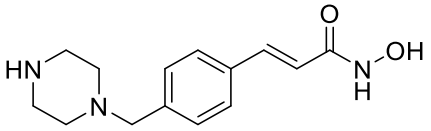

(2*E*)-*N*-hydroxy-3-{4-[(piperazin-1-yl)methyl]phenyl}prop-2-enamide (4.8f).

Isolated as an off-white solid, (65%).

IR (cm^{-1}) 2682, 2443, 1659, 1638; ^{1}H NMR (400 MHz, D_2O) δ 7.68 (d, J = 7.9 Hz, 2H), 7.55 (d, J = 8.0 Hz, 2H), 7.47 (d, J = 15.9 Hz, 1H), 6.51 (d, J = 15.9 Hz, 1H), 4.51 (s, 2H), 3.63 (s, 8H); ^{13}C NMR (101 MHz, D_2O) δ 165.7, 140.0, 136.3, 131.8, 128.8, 128.6, 118.0, 60.2, 47.9, 40.6; HRMS (ESI) *m/z* calcd for $C_{14}H_{19}N_3O_2$ $[M^+H]^+$ 262.1550, found 262.1545.

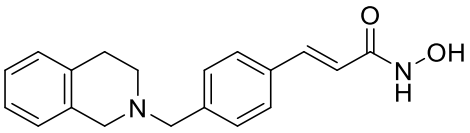

(2*E*)-3-{4-[(3,4-dihydroisoquinolin-2(1*H*)-yl)methyl]phenyl}-*N*-hydroxyprop-2-enamide (4.8e).

Isolated as a white solid, (62%).

IR (cm^{-1}) 2796, 1653, 1606; ^{1}H NMR (400 MHz, Methanol-d_4) δ 7.59 (d, J = 15.2 Hz, 1H), 7.45 (d, J = 8.0 Hz, 2H), 7.14 – 7.05 (m, 3H), 7.02 – 6.96 (m, 1H), 6.48 (d, J = 15.8 Hz, 1H), 3.74 (s, 2H), 3.65 (s, 2H), 2.91 (t, J = 6.0 Hz, 2H), 2.79 (t, J = 6.0 Hz, 2H); ^{13}C NMR (101 MHz, Methanol-d_4) δ 141.2, 140.4, 135.5, 135.2, 135.0, 131.2, 129.6, 128.8, 127.5, 127.5, 126.8, 118.4, 109.5, 63.2, 56.9, 51.7, 29.5; HRMS (ESI) *m/z* calcd for $C_{19}H_{20}N_2O_2$ $[M^+H]^+$ 309.1598, found 309.1589.

Chapter Five

5. The design and synthesis of a novel HDAC inhibitor with a carboxylic acid ZBG.

5.1. Introduction

HDAC inhibitors can be broadly defined as fitting into one of five structural classes based on their protein-ligand binding interactions; hydroxamates, cyclic tetrapeptides, benzamides, electrophilic ketones and carboxylic acids. Examples of each have been discussed in this thesis and in particular the hydroxamates. Hydroxamates are by far the most popular choice of ZBG for inhibitors of the zinc dependent HDACs due to the strong binding interaction between the hydroxamate group and the Zn^{2+} cation. This strong binding interaction however comes at a price. More than 300 enzymes are known to rely on zinc for their function[143] and hence, the strong binding affinity of the hydroxamate group for zinc inevitably leads to a number of off-target effects.[144] These high levels of toxicity are tolerated in the field of oncology but if the HDACs are to be targeted in the treatment of other less life-threatening conditions then much more targeted inhibitors are required.

Carboxylic acids are an interesting alternative ZBG. The binding interaction between the HDAC Zn^{2+} cofactor and the carboxylic acid functional group is much weaker than that between Zn^{2+} and hydroxamates. This means that there is less chance of off-target effects. However, it also means that it is much more of a challenge to achieve high levels of potency. Indeed, inhibitors of HDACs containing a carboxylic acid ZBG are relatively rare and with IC_{50} values in the milli-molar range.

To date, the most studied HDAC inhibitors containing containing a carboxylic acid ZBG are the short chain fatty acids valproic acid, butyric acid and phenylbutyrate (Figure 1.18). Valproic acid is an old drug used for the treatment of seizures,[145] butyric acid plays a role in the therapy of gastrointestinal diseases[146] and phenylbutyrate is a prodrug approved for use in the treatment of hyperammonemia.[147] All have since been identified as inhibitors of the HDACs, albeit in high doses.[148–150] However, as mentioned these are old drugs and there

is very little activity around the development of novel HDAC inhibitors with a carboxylic acid functional group. As such, this chapter will present the synthesis of a novel HDAC inhibitor (**5.6a**) comprising a carboxylic acid ZBG, with low μM levels of potency. In addition, a series of analogues are also presented with the aim of determining which groups are important for binding interactions between **5.6a** and the HDAC active site as well as investigating if these changes lead to an increase in potency/isoform selectivity.

5.2. The synthesis of a HDAC inhibitor comprising a carboxylic acid ZBG.

Previous work in our group comprised the development of a series of novel irreversible LSD1 inhibitors with nano-molar levels of potency and included compound **5.8** (Scheme 5.1).[151] Following this, we subsequently worked on a way to increase the specificity of **5.8** through *N*-alkylation, with the aim of reducing affinity for MAO. During that work we modified the synthetic route in order to reduce the number of steps and increase yield. It is that work that led to the discovery of a novel HDAC inhibitor with a carboxylic acid ZBG.

The existing pathway comprised two pinch points, the creation of the cyclopropyl group from an alkene via a Johnson-Corey-Chaykovsky (JCC) reaction (Scheme 5.1, Step 2) and the conversion of a carboxylic acid to an amide via Curtius rearrangement (Scheme 5.1, Step 4). A literature search turned up a general method, described by Barluenga *et al.* for the metal free cyclopropanation of alkenes using tosylhydrozones.[152] This method allows the direct synthesis of **5.3** in a two-step, one-pot process in which benzaldehyde **5.1** is converted to the appropriate cyclopropane **5.3**, via the tosylhydrazone intermediate **5.9** (Scheme 5.2). Benzaldehyde **5.1** is heated at 70 °C with tosylhydrazine for one hour before the addition of *tert*-butyl acrylate and an appropriate base then heating at 110 °C for a further six hours. Following an aqueous workup and purification by column chromatography, *trans*-**5.3** is afforded in around 25% yield.

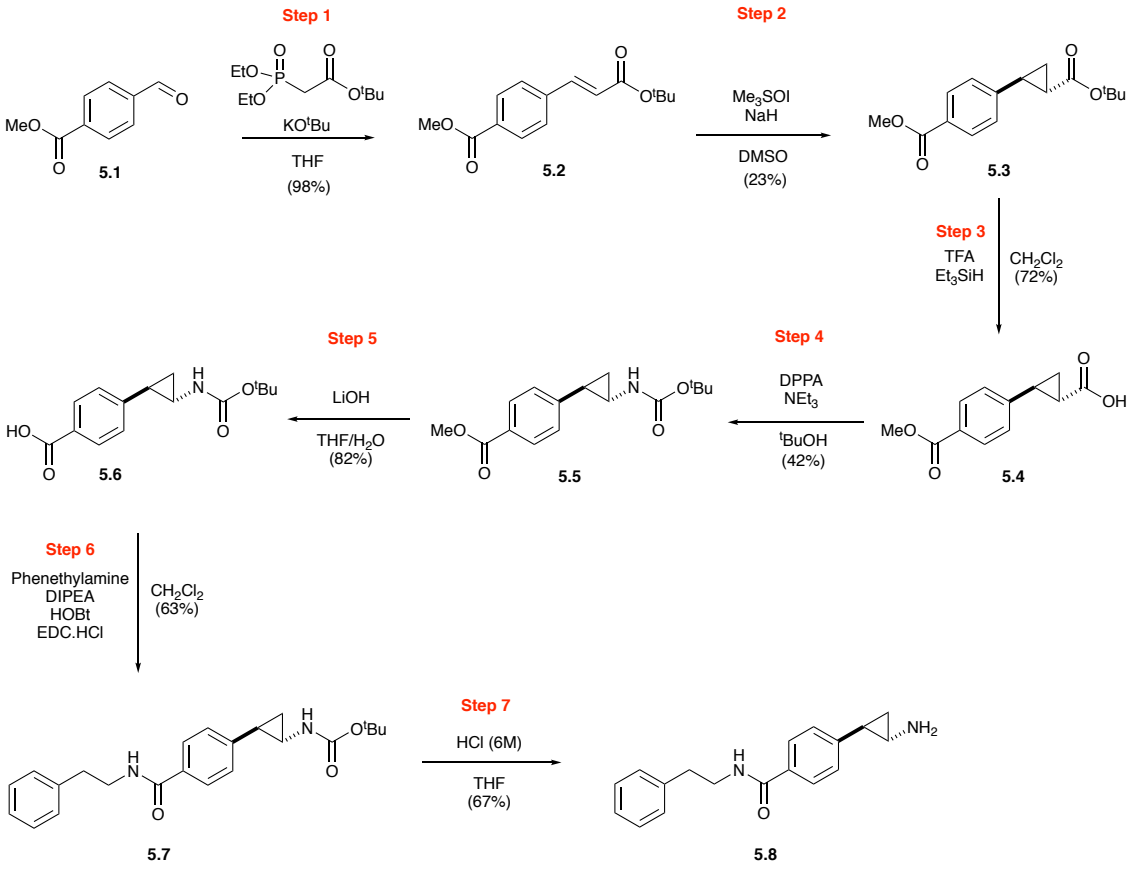

Scheme 5.1. *Original synthesis of the LSD1 inhibitor **5.8** by Borrello et al.*[151]

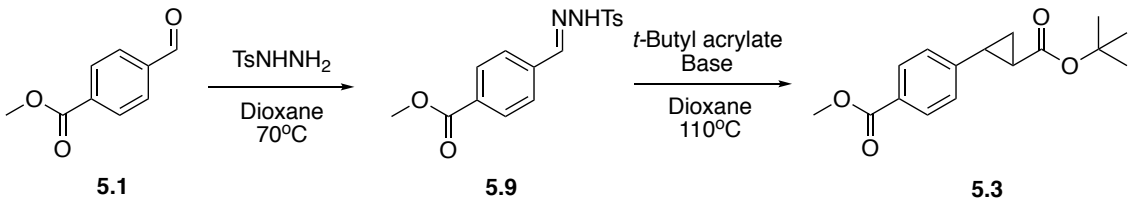

Scheme 5.2. *Alternative tosylhydrazone method of cyclopropane ring formation.*

The yield was comparable to that originally reported for the synthesis of compound **5.3** using the JCC method however, unlike the JCC method, it results in a mixture of both *cis* and *trans* diastereoisomers. The *cis:trans* ratio appeared to be low at around 0.34:1 as determined by the *tert*-butyl ^{1}H NMR peaks (Figure 5.1) and it was thought that it may be possible to decrease this ratio further by exploiting the acidic proton on the cyclopropyl ring of **5.3**. In principle this should create an equilibrium which would favour the less sterically hindered *trans* isomer

(Scheme 5.3). To test this a *cis/trans* mixture of **5.3** was dissolved in deuterated methanol in the presence of NaOMe. Proton NMR spectra were then taken periodically over several days but no change in the *tert*-butyl peak ratio was observed, thus suggesting an unchanged diastereomeric ratio. Further to this, K_2CO_3 was substituted for NaOMe in the original reaction in order to see if the higher temperatures would help facilitate the equilibrium. This resulted in a slightly higher yield (~28%) but with no change in the diastereomeric ratio.

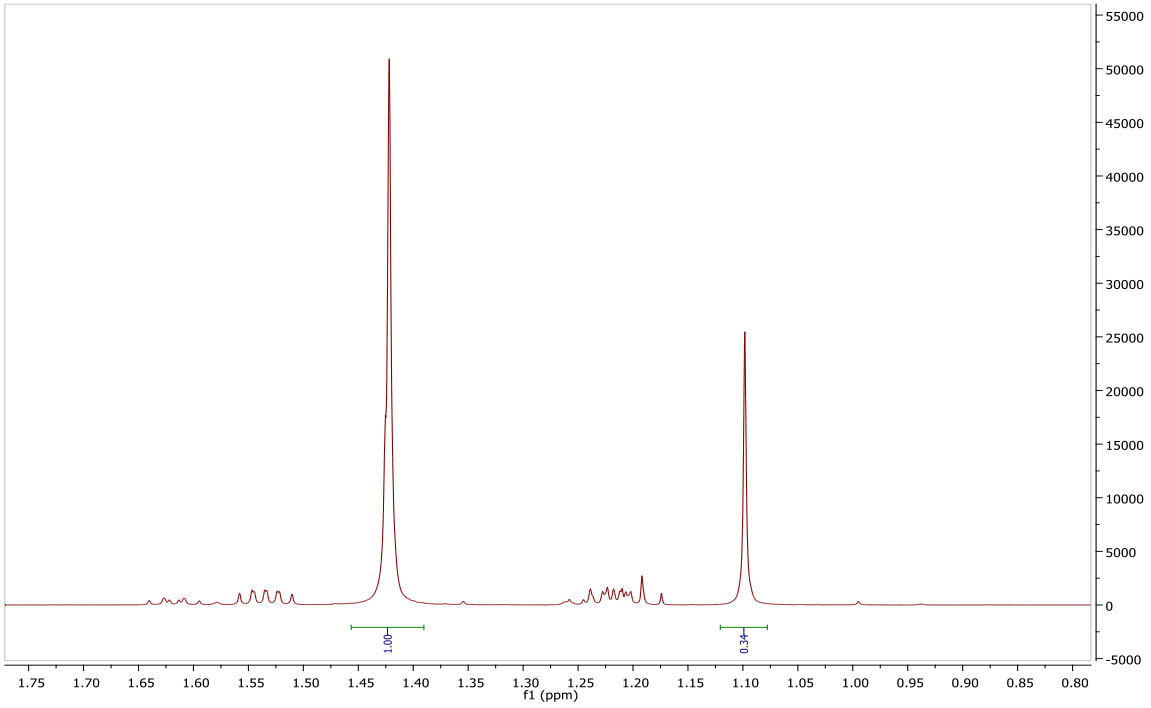

Figure 5.1. *The tert-butyl peak ratio, as determined by NMR, from a diastereomeric mixture of compound 5.3 following synthesis via the tosylhydrazone method.*

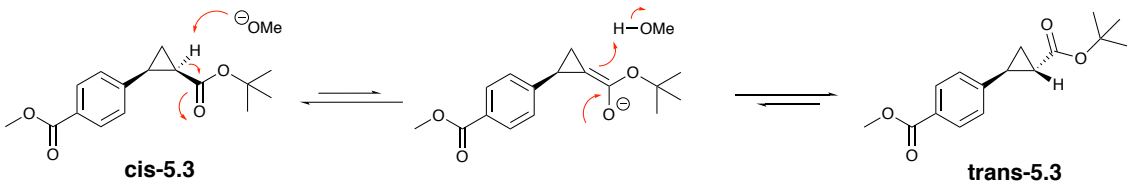

Scheme 5.3. *The anticipated, but unobserved, cis/trans equilibration of **5.3** under basic conditions.*

The lack of an increase in yield and relative difficulty of separating the *cis/trans* diastereoisomers led to us sticking with the JCC method for this reaction. As stated, the JCC reaction exclusively gives the desired *trans* diastereomers. This

is down to both the reversibility of the initial addition reaction and the ease of bond rotation of the resulting betaine to the more favourable *trans*-conformation to allow backside attack on the sulfonium (Scheme 5.4).[153]

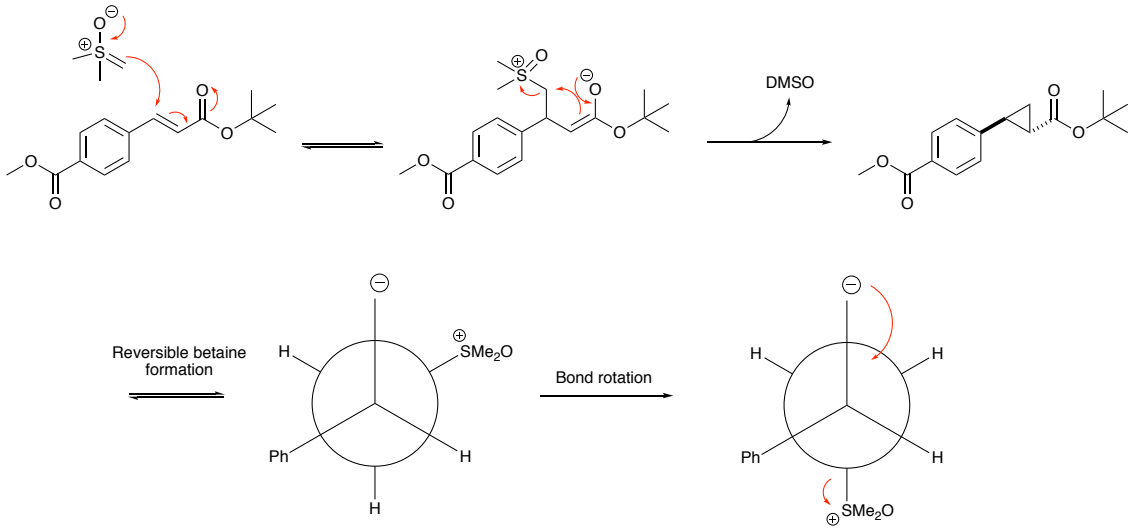

Scheme 5.4. *The conversion of alkene **5.2** to cyclopropane **5.3** via the stereospecific JCC reaction.*

The low yield of the JCC reaction was still a problem however. Given that we believed the proton on the cyclopropyl ring to be acidic, using a strong base such as sodium hydride may have been contributing to this by breaking open the cyclopropyl ring upon formation. This was supported by the isolation of by-product **5.10** following workup. It is believed that irreversible deprotonation leads to ring opening and the resulting anion quenched during the aqueous workup to give **5.10** (Scheme 5.5). Subsequently, we switched the base to potassium *tert*-butoxide. This had good effect and yields more than doubled from around 25% to over 50%. By-product **5.10** was still observed in yields of around 9%.

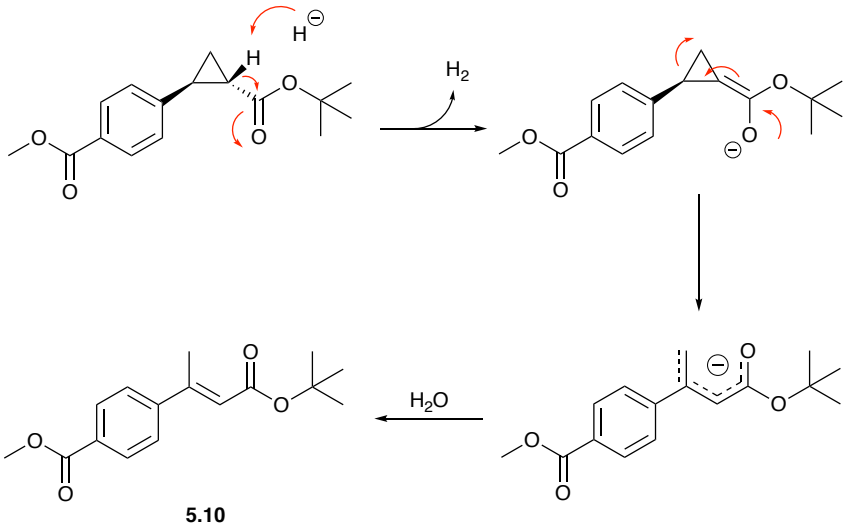

Scheme 5.5. *The proposed mechanism of the alkene by-product **5.10** during the JCC reaction.*

The second pinch point in Borrello's synthetic route was the Curtius rearrangement of carboxylic acid **5.4** to amide **5.5** in 42% yield (Scheme 5.1, Step 4). Borrello *et al.* chose to carry out the rearrangement at step 4 as they were creating a series of analogues in which a number of different amines were coupled to the carboxylic acid at position 4 of the benzene ring (Scheme 5.1, Step 6). It therefore made sense to have the variable step at the end of the synthesis. We only needed to make one of these analogues and so were able to swap the amide coupling step with the Curtius rearrangement step. This allows the overall synthesis of **5.8** to be reduced from seven steps to six by allowing the moderately yielding Curtius rearrangement to be modified so as to give the primary amine in place of the Boc-protected amine (Scheme 5.7). This also helped to improve the yield. To get the Boc-protected amine the reaction is carried out in anhydrous *tert*-butanol. Any water has an adverse effect as it acts as a nucleophile, attacking the isocyanate intermediate and giving the carbamate. The carbamate subsequently breaks down through the loss of carbon dioxide to give the primary amine. This is not a problem if the protected amine is not required and following the formation of the isocyanate, the reaction is continued in the presence of aqueous acid.

It was this modified synthetic route that produced intermediate carboxylic acid **5.13a** (Scheme 5.7).

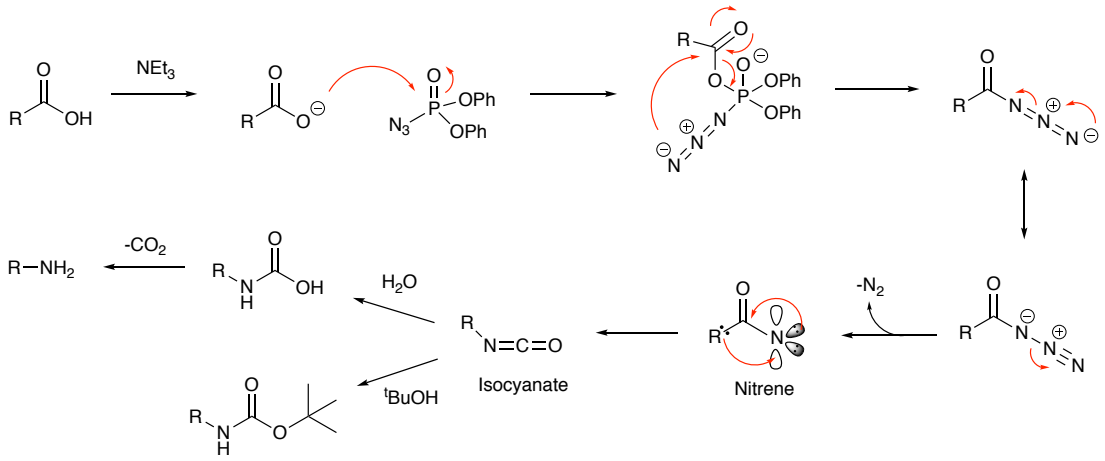

Scheme 5.6. *The mechanism of the Curtius rearrangement in both the presence and absence of water.*

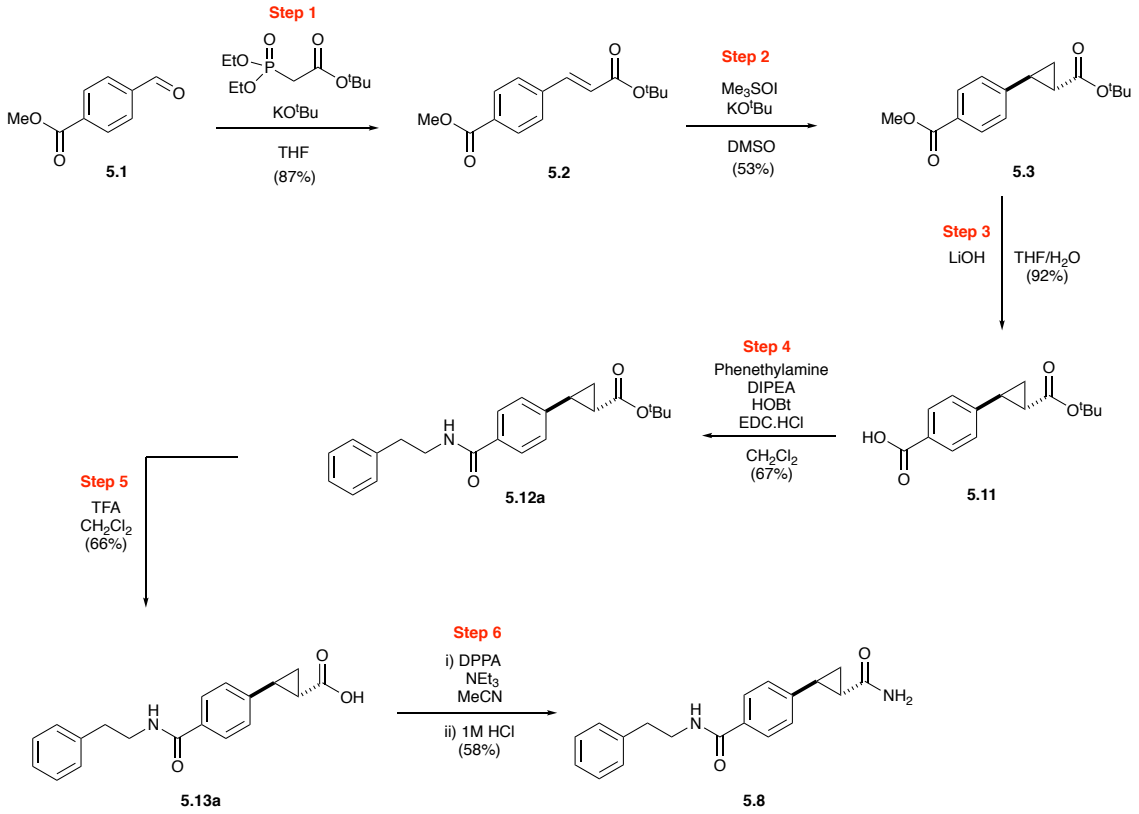

Scheme 5.7. *The modified Borrello synthesis used in this work.*

5.3. The enzymatic evaluation of 5.13a.

Compound **5.13a** was analysed for inhibitory activity against HDAC1, 3, 6 and 8 using a HDAC-Glo™ I/II Assay from Promega in collaboration with Dusan Ruzic of the University of Belgrade, carried out at the Fraunhofer Institute, Freiburg. Compounds were measured at a concentration range of 100 - 0.10 μM, the half maximal inhibitory concentration (IC_{50}) determined via a dose-response experiment and the data analysed using GraphPad Prism software.
Results were relatively consistent across all isoforms suggesting that **5.13a** is acting as a pan-HDAC inhibitor. Further testing across all other isoforms is required to determine if it is a true pan inhibitor or predominantly class I selective. **5.13a** inhibited all tested HDAC isoforms with IC_{50} values of around 20-25 μM (pIC_{50}: 4.59–4.69). For a compound with a carboxylic acid ZBG this is an exciting result and gives the basis for further optimisation to improve potency further.

	pIC50 ± Std. Error			
Compound	**HDAC1**	**HDAC3**	**HDAC6**	**HDAC8**
5.13a	4.69±0.04	4.59±0.08	4.60±0.05	4.63±0.03

Table 5.1. Results of the HDAC assays carried out on compound **5.13a**.

Data given as pIC_{50} ± SE, n=3.
Data generated by Ruzic et al., University of Belgrade (unpublished).

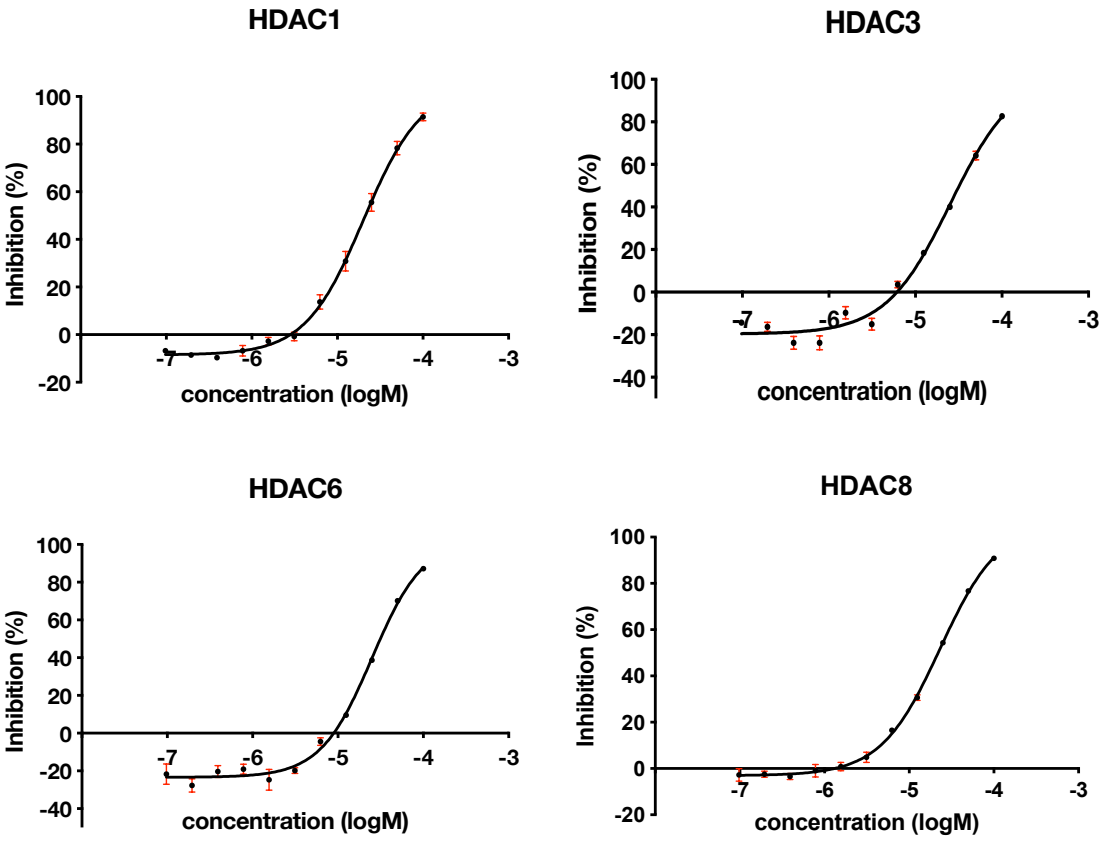

Figure 5.2. Graphical representation of the HDAC inhibition data presented in Table 5.1.

Data shown as % inhibition ± Std. Error, n=3.

Data generated by Ruzic et al., University of Belgrade (unpublished).

5.4. The synthesis of further analogues of 5.13a.

To investigate which features of **5.13a** are important for affinity to HDACs, several analogues were created which incorporated changes to both the cap and the linker, whist leaving the ZBG unchanged (Figure 5.3).

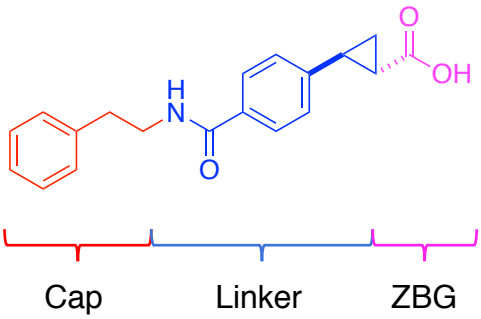

Figure 5.3. *Compound 5.13a showing the cap, linker and ZBG sections of the molecule.*

The cap was changed by varying the length of the carbon chain from two carbons to three and by changing the cap group completely from a phenethyl group to a 1-(4-Fluorophenyl)piperazine group. The linker was changed by replacing the cyclopropane ring with both an unsubstituted *trans*-alkene and a methyl substituted *trans*-alkene (Scheme 5.8).

The unsubstituted alkene **5.19** is synthesised as for **5.13a** but with the omission of the cyclopropanation step. The methyl substituted alkene **5.16**, adopted the first two steps of the synthesis as **5.13a**, a Horner-Wadsworth-Emmons (HWE) reaction followed by JCC reaction of the resulting alkene **5.2**. As discussed, the JCC reaction created both the cyclopropane **5.3a** as the major product along with the substituted alkene **5.3b** as the minor product. The synthesis of the minor product **5.3b** was taken advantage of to create a product with a minimal change to the linker and along with **5.19**, will allow us to investigate if it is the cyclopropane ring itself that is important or if it is the length/rigidity of the linker that matters. The major product **5.3a** was used to create two products in which the cap group is altered (Scheme 5.8, **5.13b** and **5.13c**).

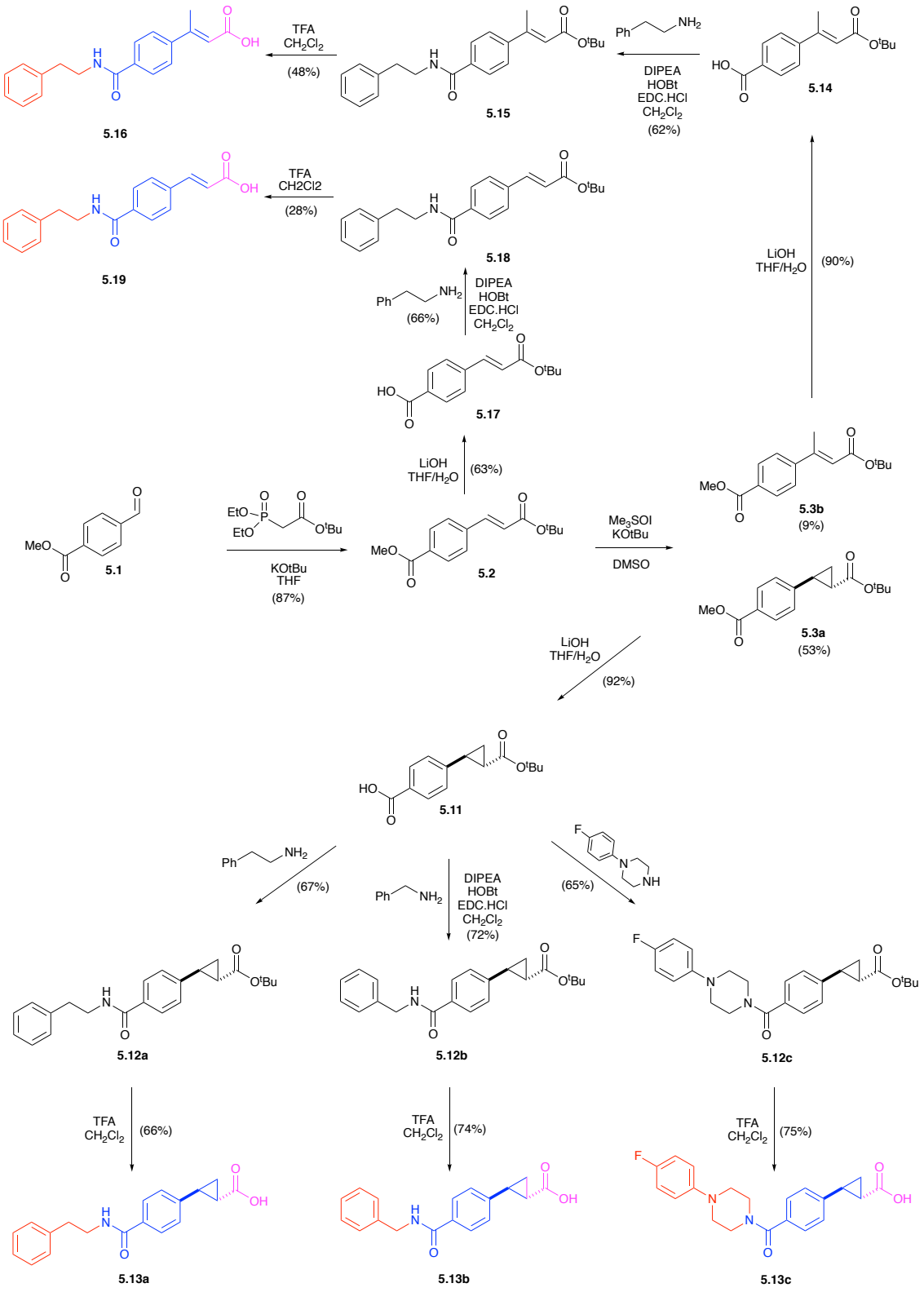

Scheme 5.8. *The synthetic route of **5.13a** along with analogues **5.13b**, **5.13c**, **5.16** and **5.19**.*

5.5. Conclusion and future works.

A novel HDAC inhibitor (**5.13a**) comprising a carboxylic ZBG was synthesised in five steps. **5.13a** was tested in a cell free HDAC inhibition assay for activity in HDAC1, 3, 6 and 8, and found to consistently inhibit all isoforms at around IC_{50}: 20-25 μM (pIC_{50}: 4.59-4.63) suggesting that **5.13a** may be a pan-HDAC inhibitor. To investigate which features of **5.13a** are important for its affinity to HDACs a small series of analogues were developed comprising changes to both the cap and linker sections of the inhibitor.

Future work should extend HDAC assay testing of **5.13a** to the remaining seven zinc dependent isoforms to determine if **5.13a** is a true pan inhibitor or just class I selective. In addition, in cell assays should be performed to determine if activity extends to pharmacological effects beyond cell-free assays.

Finally, all analogues require testing in HDAC1, 3 6 and 8 as a minimum so as to compare activity with **5.13a** and establish the effects of the changes made.

5.6. Chapter five experimental.

5.6.1. Experimental procedures

All experimental procedures are the same as for those described in Chapter two, section 2.7.1.

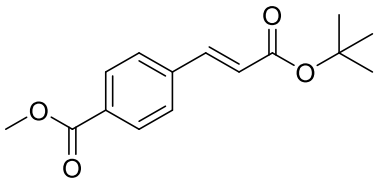

(*E*)-methyl-4-(3-(*tert*-butoxy)-3-oxyprop-1-en-1-yl)benzoate (5.2).

Potassium *tert*-butoxide (4.28 g, 38.1 mmol) was dissolved in THF (30 ml) and cooled to -5 ºC. *tert*-Butyl diethylphoshonacetate (8.9 ml, 37.91 mmol) was slowly added and the resulting mixture stirred at -5ºC for 40 minutes. **5.1** (5.63 g, 34.32 mmol) was dissolved in THF (40 ml) and added dropwise to the mixture with vigorous stirring at -5ºC over a period of 20 minutes before warming to room temperature. Stirring under a nitrogen atmosphere was continued for 16hrs before adding water (100 ml) and EtOAc (100 ml). The organic layer was separated, and the aqueous layer further extracted with EtOAc (2 x 100 ml). The combined organic layers were then washed with water (150 ml) and brine (150 ml), dried over $MgSO_4$, filtered and concentrated. The concentrate was purified on silica, eluting with a gradient of 0-5 % EtOAc in hexane to give **5.2** (7.82 g, 87 %) as a white solid. Mp 63-64°C; ^{1}H NMR (400 MHz, Chloroform-*d*) δ 8.03 (d, *J* = 8.3 Hz, 0H), 7.59 (d, *J* = 16.0 Hz, 0H), 7.56 (d, *J* = 8.5 Hz, 1H), 6.44 (d, *J* = 16.0 Hz, 0H), 3.92 (s, 0H), 1.53 (s, 1H); ^{13}C NMR (101 MHz, Chloroform-*d*) δ 166.6, 165.9, 142.2, 139.0, 131.2, 130.1, 127.9, 122.7, 81.0, 52.3, 28.3; No HRMS was obtained for this compound.

These data are consistent with that reported in the literature.[151]

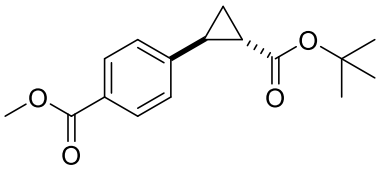

Methyl 4-[2-(*tert*-butoxycarbonyl)cyclopropyl]benzoate (5.3a).

A flame dried flask was charged with Potassium *tert*-butoxide (0.49 g, 4.37 mmol) and trimethylsufoxonium iodide (0.92 g, 4.18 mmol). DMSO (25 ml) was then added before stirring under a nitrogen atmosphere for 30 minutes. **5.2**, (1.00 g, 3.81 mmol) was then dissolved in DMSO (15 ml) before adding dropwise over 30 minutes. The mixture was stirred at ambient temperature under a nitrogen atmosphere for 16hrs. Water (50 ml) and EtOAc (50 ml) were then added and the organic layer separated. The aqueous layer was extracted a further 4 times with EtOAc (50 ml) before drying the combined organic extracts over $MgSO_4$ and concentrating. Purification by silica column chromatography gave **5.3a** as a white solid (0.56 g, 53 %). Mp 39-41 °C; ^{1}H NMR (400 MHz, Chloroform-*d*) δ 7.93 (d, *J* = 8.5 Hz, 2H), 7.13 (d, *J* = 8.1 Hz, 2H), 3.89 (s, 3H), 2.47 (ddd, *J* = 9.2, 6.3, 4.1 Hz, 1H), 1.89 (ddd, *J* = 8.5, 5.4, 4.1 Hz, 1H), 1.58 (ddd, *J* = 9.1, 5.4, 4.5 Hz, 1H), 1.47 (s, 9H), 1.27 (ddd, *J* = 8.5, 6.3, 4.6 Hz, 1H); ^{13}C NMR (101 MHz, Chloroform-*d*) δ 172.2, 167.0, 146.2, 129.8, 128.3, 126.0, 81.0, 52.1, 28.2, 25.9, 25.7, 17.6; HMRS (ESI) *m/z* calcd for $C_{16}H_{20}O_4$ $[M+NH4]^+$ 294.1700, found 294.1703, calcd for $[M+Na]^+$ 299.1254, found 299.1257.

These data are consistent with that reported in the literature.[151]

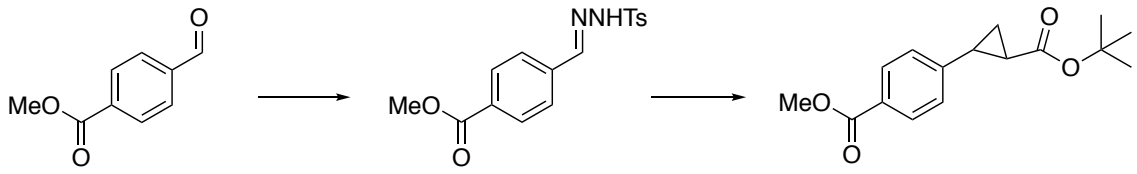

Methyl 4-[2-(*tert*-butoxycarbonyl)cyclopropyl]benzoate (5.3a). Alternative method.

Methyl-4-formylbenzoate (**5.1**) (0.51 g, 3.09 mmol) was added to a flame dried round bottom flask. *p*-Toluenesulfonhydrazide (0.63 g, 3.37 mmol) was added along with anhydrous dioxane (10 ml) and the mixture heated to 70 ºC and stirred under a nitrogen atmosphere for 1 hr. *tert*-Butyl acrylate (0.9 ml, 6.14 mmol) and sodium methoxide (0.25 g, 4.68 mmol) were added before increasing the temperature to 100 ºC and stirring under nitrogen for a further 6 hrs. The flask was then allowed to cool to room temperature before adding water (20 ml) and EtOAc (10 ml). The organic layer was separated, and the aqueous layer extracted twice more with EtOAc. The combined organic layers were then dried over $MgSO_4$ and concentrated. The concentrate was then purified by silica column chromatography (2:8, EtOAc:PE) to give **5.3a** as a colourless oil (0.26 g, 30%). ^{1}H NMR (400MHz, Chloroform-*d*) δ 7.93 (d, *J* = 8.4Hz, 2H), 7.13 (d, *J* = 8.4Hz, 2H), 3.90 (s, 3H), 2.49-2.44 (m, 1H), 1.89 (ddd, *J* = 8.5, 5.4, 4.2Hz, 1H), 1.62-1.56 (m, 1H), 1.47 (s, 9H), 1.27 (ddd, *J* = 8.5, 6.3, 4.6Hz, 1H); ^{13}C NMR (101 MHz, Chloroform-*d*) δ 172.2, 167.1, 146.3, 130.0, 129.9, 128.7, 128.3, 126.1, 81.0, 52.2, 28.3, 26.0, 25.7, 17.7.

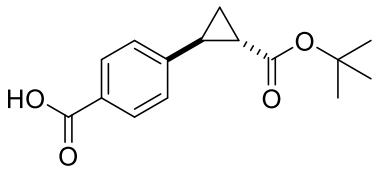

4-[2-(tert-butoxycarbonyl)cyclopropyl]benzoic acid (5.11).

To a solution of **5.3a**, (3.45 g, 11.84 mmol) in a 3:1 mixture of THF:H_2O (30 ml) was added lithium hydroxide (0.81 g, 36.76 mmol) and the resulting mixture stirred at 50 ºC for 24 hrs. The mixture was then cooled to room temperature and diluted with water (30 ml) before acidifying with $KHSO_4$ to pH 1–2. The mixture was extracted three times with EtOAc (30 ml) and the combined organic layers dried over MgSO4, filtered and the solvent removed in *vacuo* to give **5.11** as a white solid (3.02 g, 92 %). ^{1}H NMR (400 MHz, Chloroform-*d*) δ 8.01 (d, *J* = 8.4 Hz, 2H), 7.17 (d, *J* = 8.4 Hz, 2H), 2.50 (ddd, *J* = 9.2, 6.3, 4.1 Hz, 1H), 1.92 (ddd, *J* = 8.5, 5.5, 4.1 Hz, 1H), 1.61 (ddd, *J* = 9.1, 5.4, 4.6 Hz, 1H), 1.48 (s, 9H), 1.29 (ddd, *J* = 8.5, 6.3, 4.6 Hz, 1H); ^{13}C NMR (101 MHz, Chloroform-*d*) δ 172.1, 171.5, 147.3, 130.5, 127.3, 126.2, 81.1, 28.3, 26.0, 25.8, 17.81; HRMS (ESI) *m/z* calcd for $C_{15}H_{18}O_4$ $[M-H]^-$ 261.1132, found 261.1135.

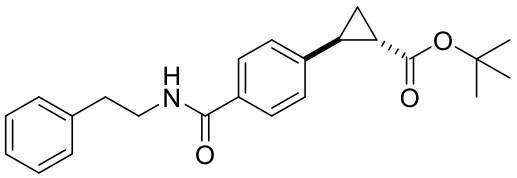

***tert*-Butyl 2-{4-[(2-phenylethyl)carbamoyl]phenyl}cyclopropane-1-carboxylate (5.12a).**

To a suspension of **5.11** (2.15 g, 8.20 mmol) in dichloromethane (30 ml) was added DIPEA (2.8 ml) and stirred until clear. HOBt monohydrate (0.25 g, 1.63 mmol) was then added followed by EDC hydrochloride (2.40 g, 12.5 mmol), and the resulting solution stirred at room temperature for 30 mins. Phenethylamine (1.3 ml, 10.3 mmol) was then added via syringe in one portion and the mixture stirred at room temperature under a nitrogen atmosphere overnight. The mixture was then diluted with dichloromethane (50 ml) and washed with 2M HCl (100 ml), 1M NaOH (50 ml), 1M $NaHCO_3$ (50 ml), H_2O (100 ml) and brine (100 ml). The organic phase was then dried over $MgSO_4$, filtered and concentrated. The concentrate was purified on silica, eluting with a gradient of 0-30 % EtOAc in hexane to give **5.12a** (2.02 g, 67 %) as a white solid. ^{1}H NMR (400 MHz, Chloroform-*d*) δ 7.59 (d, *J* = 8.4 Hz, 2H), 7.33 (tt, *J* = 7.0, 1.0 Hz, 2H), 7.28 – 7.20

(m, 3H), 7.11 (d, *J* = 8.4 Hz, 2H), 6.05 (brd-s, 1H), 3.76 – 3.68 (q, *J* = 6.8 Hz, 2H), 2.93 (t, *J* = 6.9 Hz, 2H), 2.45 (ddd, *J* = 9.1, 6.4, 4.1 Hz, 1H), 1.85 (ddd, *J* = 8.5, 5.4, 4.2 Hz, 1H), 1.60 – 1.53 (m, 1H), 1.47 (s, 9H), 1.24 (ddd, *J* = 8.5, 6.4, 4.5 Hz, 1H); ^{13}C NMR (101 MHz, Chloroform-*d*) δ 172.2, 167.1, 144.5, 139.0, 132.7, 128.9, 128.8, 127.1, 126.7, 126.3, 81.0, 41.2, 35.8, 28.2, 25.7, 25.5, 17.5; LC-ToF (ESI) *m/z* calcd for $C_{23}H_{27}NO_3$ $[M+H]^+$ 366.21, found 366.21.

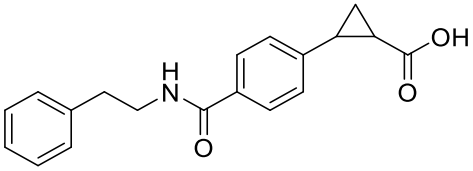

2-{4-[(2-phenylethyl)carbamoyl]phenyl}cyclopropane-1-carboxylic acid (5.13a).

5.12a (0.30 g, 0.82 mmol) was dissolved in dichloromethane (10 ml) and trifluoroacetic acid (0.6 ml, 7.84 mmol) added in one portion. The resulting solution was stirred at room temperature in air overnight. The solution was diluted with dichloromethane (20 ml) and water was added (20 ml). 4M NaOH was added until the mixture was pH 12-14. The organic layer was removed, and the aqueous layer acidified with 2M HCl until pH 2 before extracting with dichloromethane (3 x 30 ml). The combined organic layers were washed with brine and the solvent removed under reduced pressure to give **5.13a** (0.17 g, 66 %) as a fluffy white solid. ^{1}H NMR (400 MHz, Methanol-d_4) δ 7.70 (d, *J* = 8.4 Hz, 2H), 7.32 – 7.16 (m, 7H), 3.58 (t, *J* = 7.3 Hz, 2H), 2.91 (t, *J* = 7.8 Hz, 2H), 2.51 (ddd, *J* = 9.2, 6.5, 4.1 Hz, 1H), 1.90 (ddd, *J* = 8.4, 5.4, 4.1 Hz, 1H), 1.58 (ddd, *J* = 9.2, 5.4, 4.6 Hz, 1H), 1.41 (ddd, *J* = 8.5, 6.4, 4.5 Hz, 1H); ^{13}C NMR (101 MHz, Methanol-d_4) δ 176.5, 169.9, 145.6, 140.6, 133.8, 129.8, 129.4, 128.5, 127.3, 127.1, 42.6, 36.5, 26.8, 25.4, 17.7; HRMS (ESI) *m/z* calcd for $C_{19}H_{19}NO_3$ $[M+H]^+$ 310.1438, found 310.1426.

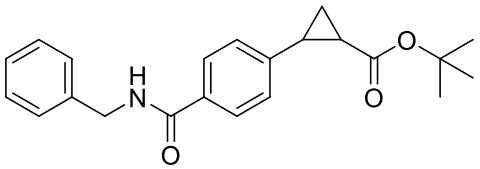

***tert*-Butyl 2-[4-(benzylcarbamoyl)phenyl]cyclopropane-1-carboxylate (5.12b).**

Isolated as a white solid, (130 mg, 72 %).

Synthesised using the procedure for compound **5.12a**.

^{1}H NMR (400 MHz, Chloroform-*d*) δ 7.70 (d, *J* = 8.3 Hz, 2H), 7.38 – 7.27 (m, 5H), 7.12 (d, *J* = 8.3 Hz, 2H), 6.39 (t, *J* = 5.0 Hz, 1H), 4.64 (d, *J* = 5.7 Hz, 2H), 2.46 (ddd, *J* = 9.2, 6.4, 4.1 Hz, 1H), 1.86 (ddd, *J* = 8.5, 5.4, 4.1 Hz, 1H), 1.57 (ddd, *J* = 9.1, 5.4, 4.5 Hz, 1H), 1.47 (s, 9H), 1.28 – 1.21 (m, 1H); ^{13}C NMR (101 MHz, Chloroform-*d*) δ 172.2, 167.0, 144.7, 138.3, 132.4, 128.9, 128.0, 127.7, 127.2, 126.3, 81.0, 44.2, 28.2, 25.8, 25.5, 17.5; HRMS (ESI) *m/z* calcd for $C_{22}H_{25}NO_3$ $[M+H]^+$ 352.1907, found 352.1906.

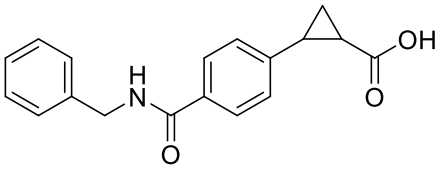

2-[4-(benzylcarbamoyl)phenyl]cyclopropane-1-carboxylic acid (5.13b).

Isolated as a white solid, (81 mg, 74 %).

Synthesised using the procedure for compound **5.13a**.

^{1}H NMR (400 MHz, DMSO-d_6) δ 12.35 (s, 1H), 8.98 (t, *J* = 6.0 Hz, 1H), 7.81 (d, *J* = 8.4 Hz, 2H), 7.35 – 7.20 (m, 7H), 4.47 (d, *J* = 6.0 Hz, 2H), 2.45 (ddd, *J* = 9.1, 6.3, 4.1 Hz, 1H), 1.88 (ddd, *J* = 8.4, 5.3, 4.1 Hz, 1H), 1.47 (ddd, *J* = 9.3, 5.4, 4.3 Hz, 1H), 1.39 (ddd, *J* = 8.4, 6.4, 4.3 Hz, 1H); ^{13}C NMR (101 MHz, DMSO-d_6) δ 173.7, 165.8, 143.8, 139.7, 132.1, 128.2, 127.3, 127.1, 126.6, 125.7, 42.5, 25.1, 24.5, 17.0; HRMS (ESI) *m/z* calcd for $C_{18}H_{17}NO_3$ $[M+H]^+$ 296.1281, found 296.1288.

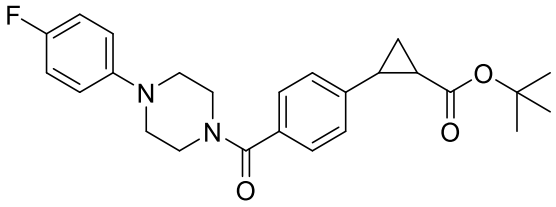

***tert*-Butyl-2-{4-[4-(4-fluorophenyl)piperazine-1-carbonyl]phenyl} cyclopropane-1-carboxylate (5.12c).**

Isolated as a yellow solid, (529 mg, 65 %).

Synthesised using the procedure for compound **5.12a**.

^{1}H NMR (400 MHz, Chloroform-*d*) δ 7.35 (d, *J* = 8.4 Hz, 2H), 7.13 (d, *J* = 8.2 Hz, 2H), 7.01 – 6.93 (m, 2H), 6.91 – 6.84 (m, 2H), 3.75 (brd-d, *J* = 108.4 Hz, 4H), 3.08 (brd-s, 4H), 2.46 (ddd, *J* = 9.2, 6.4, 4.1 Hz, 1H), 1.85 (ddd, *J* = 8.5, 5.4, 4.2 Hz, 1H), 1.56 (ddd, *J* = 9.2, 5.4, 4.5 Hz, 1H), 1.47 (s, 9H), 1.28 – 1.20 (m, 1H); ^{13}C NMR (101 MHz, Chloroform-*d*) δ 172.2, 170.2, 158.9, 156.5, 147.6, 142.8, 133.5, 127.5, 126.2, 118.8, 118.7, 115.9, 115.7, 80.9, 50.9, 28.2, 25.6, 25.5, 17.3; ^{19}F NMR (376 MHz, Chloroform-*d*) δ -123.14; HRMS (ESI) *m/z* calcd for $C_{25}H_{29}FN_2O_3$ $[M+H]^+$ 425.2235, found 425.2251.

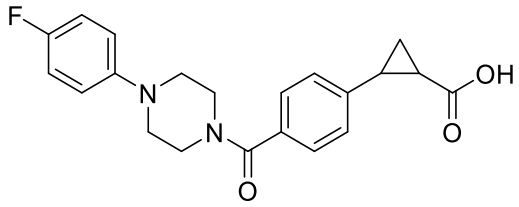

2-{4-[4-(4-fluorophenyl)piperazine-1-carbonyl]phenyl}cyclopropane-1-carboxylic acid (5.13c).

Isolated as a white solid, (289 mg, 75 %).

Synthesised using the general procedure for compound **5.13a**.

^{1}H NMR (400 MHz, DMSO-d_6) δ 12.34 (brd-s, 1H), 7.34 (d, *J* = 8.3 Hz, 2H), 7.24 (d, *J* = 8.3 Hz, 2H), 7.10 – 7.02 (m, 2H), 7.00 – 6.93 (m, 2H), 3.59 (brd-d, *J* = 83.9 Hz, 4H), 3.09 (s, 4H), 2.45 (ddd, *J* = 9.2, 6.4, 4.1 Hz, 1H), 1.87 (ddd, *J* = 8.4, 5.4, 4.1 Hz, 1H), 1.46 (ddd, *J* = 9.4, 5.4, 4.4 Hz, 1H), 1.39 (ddd, *J* = 8.3, 6.4, 4.3 Hz, 1H); ^{13}C NMR (101 MHz, DMSO-d_6) δ 173.7, 168.8, 157.4, 155.1, 147.6, 147.6, 142.0, 133.6, 127.2, 125.9, 117.8, 117.7, 115.4, 115.2, 49.3, 25.0, 24.4, 16.8; ^{19}F NMR (376 MHz, DMSO-d_6) δ -124.79; HRMS (ESI) *m/z* calcd for $C_{21}H_{21}FN_2O_3$ $[M+H]^+$ 369.1609, found 369.1608.

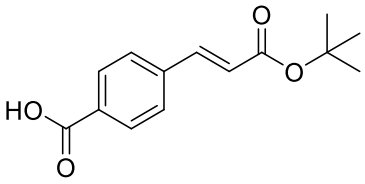

4-[(1E)-3-tert-butoxy-3-oxoprop-1-en-1-yl]benzoic acid (5.17).

Isolated as a white solid, (905 mg, 63 %).

Synthesised using the procedure for compound **5.11**.

^{1}H NMR (400 MHz, DMSO-d_6) δ 13.03 (s, 1H), 7.94 (d, J = 8.4 Hz, 2H), 7.80 (d, J = 8.1 Hz, 2H), 7.60 (d, J = 16.0 Hz, 1H), 6.63 (d, J = 16.0 Hz, 1H), 1.48 (s, 9H); ^{13}C NMR (101 MHz, DMSO-d_6) δ 166.7, 165.2, 142.2, 138.2, 131.8, 129.7, 128.3, 122.1, 80.2, 27.8; HRMS (ESI) m/z calcd for $C_{14}H_{16}O_4$ $[M+H]^+$ 247.0976 found 247.0980.

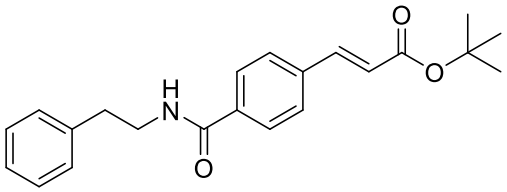

tert-Butyl (2E)-3-{4-[(2-phenylethyl)carbamoyl]phenyl}prop-2-enoate (5.18).

Isolated as a white solid, (704 mg, 66 %).

Synthesised using the procedure for compound **5.12a**.

^{1}H NMR (400 MHz, Chloroform-*d*) δ 7.71 (d, J = 8.3 Hz, 2H), 7.58 (d, J = 16.0 Hz, 1H), 7.54 (d, J = 8.2 Hz, 2H), 7.39 – 7.31 (m, 2H), 7.31 – 7.22 (m, 3H), 6.42 (d, J = 16.0 Hz, 1H), 6.29 (brd-t, J = 5.9 Hz, 1H), 3.74 (td, J = 6.9, 5.8 Hz, 2H), 2.96 (t, J = 6.9 Hz, 2H), 1.56 (s, 1H); ^{13}C NMR (101 MHz, Chloroform-*d*) δ 166.8, 166.0, 142.2, 138.9, 137.6, 135.7, 128.9, 128.8, 128.1, 127.4, 126.7, 122.1, 80.9, 41.3, 35.7, 28.2; HRMS (ESI) m/z calcd for $C_{22}H_{25}NO_3$ $[M+H]^+$ 352.1907 found 352.1911.

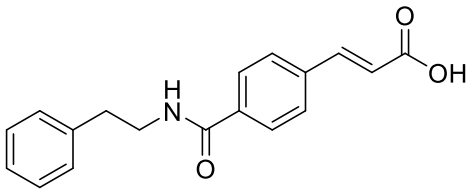

(2E)-3-{4-[(2-phenylethyl)carbamoyl]phenyl}prop-2-enoic acid (5.19).

Isolated as a white solid, (133 mg, 28 %).

Synthesised using the procedure for compound **5.13a**.

^{1}H NMR (500 MHz, DMSO-d_6) δ 12.50 (brd-s, 1H), 8.64 (t, J = 5.6 Hz, 1H), 7.84 (d, J = 8.5 Hz, 2H), 7.77 (d, J = 8.5 Hz, 2H), 7.62 (d, J = 16.0 Hz, 1H), 7.32 – 7.27 (m, 2H), 7.26 – 7.22 (m, 2H), 7.22 – 7.18 (m, 1H), 6.62 (d, J = 16.1 Hz, 1H), 3.52 – 3.46 (m, 2H), 2.85 (t, J = 7.4 Hz, 2H); ^{13}C NMR (126 MHz, DMSO-d_6) δ 167.4, 165.4, 142.8, 139.5, 136.7, 135.6, 128.6, 128.3, 128.0, 127.6, 126.1, 120.8, 40.9, 35.0; HRMS (ESI) m/z calcd for $C_{18}H_{17}NO_3$ $[M+H]^+$ 296.1281 found 296.1288.

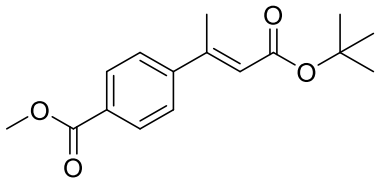

Methyl 4-[(2E)-4-tert-butoxy-4-oxobut-2-en-2-yl]benzoate (5.3b).

Isolated as a white solid.

Recovered as a by-product during the synthesis of compound **5.3a**.

^{1}H NMR (400 MHz, Chloroform-*d*) δ 8.02 (d, J = 8.8 Hz, 2H), 7.51 (d, J = 8.8 Hz, 2H), 6.09 (q, J = 1.3 Hz, 1H), 3.92 (s, 3H), 2.54 (d, J = 1.4 Hz, 3H), 1.52 (s, 9H); ^{13}C NMR (101 MHz, Chloroform-*d*) δ 166.8, 166.1, 152.8, 147.1, 130.3, 129.8, 126.4, 120.8, 80.5, 52.3, 28.4, 17.8. No HRMS was obtained for this compound.

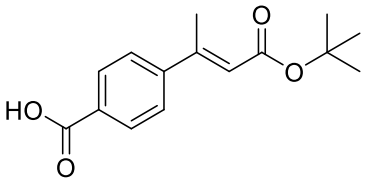

4-[(2E)-4-tert-butoxy-4-oxobut-2-en-2-yl]benzoic acid (5.14).

Isolated as a white solid, (1.50 g, 90 %).

Synthesised using the procedure for compound **5.11**.

^{1}H NMR (400 MHz, DMSO-d_6) δ 13.00 (s, 1H), 7.94 (d, J = 8.6 Hz, 2H), 7.64 (d, J = 8.6 Hz, 2H), 6.10 (q, J = 1.3 Hz, 1H), 2.47 (d, J = 1.4 Hz, 3H), 1.47 (s, 9H); ^{13}C NMR (101 MHz, DMSO-d_6) δ 166.8, 165.2, 152.2, 145.5, 131.0, 129.5, 126.4, 119.6, 79.8, 27.8, 17.1; HRMS (ESI) m/z calcd for $C_{15}H_{18}O_4$ $[M-H]^-$ 261.1132 found 261.1124.

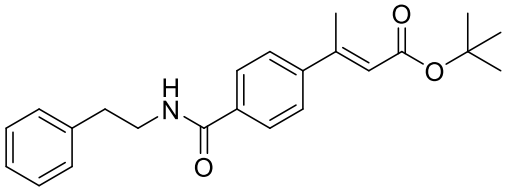

***tert*-Butyl (2E)-3-{4-[(2-phenylethyl)carbamoyl]phenyl}but-2-enoate (5.15).**

Isolated as a white solid, (1.15g, 62 %).

Synthesised using the procedure for compound **5.12a**.

^{1}H NMR (400 MHz, Chloroform-*d*) δ 7.60 (d, J = 8.6 Hz, 2H), 7.40 (d, J = 8.6 Hz, 2H), 7.28 – 7.22 (m, 2H), 7.20 – 7.13 (m, 3H), 6.14 (t, J = 5.4 Hz, 1H), 5.99 (q, J = 1.4 Hz, 1H), 3.65 (td, J = 6.9, 5.8 Hz, 2H), 2.86 (t, J = 6.9 Hz, 2H), 2.44 (d, J = 1.4 Hz, 3H), 1.45 (s, 9H); ^{13}C NMR (101 MHz, Chloroform-*d*) δ 166.9, 166.1, 152.7, 145.6, 138.9, 134.7, 128.9, 128.8, 127.1, 126.7, 126.6, 120.4, 80.4, 41.2, 35.8, 28.4, 17.7; HRMS (ESI) m/z calcd for $C_{23}H_{27}NO_3$ $[M+H]^+$ 366.2064 found 366.2060.

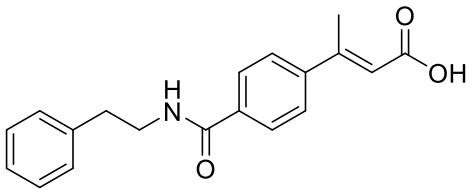

(2E)-3-{4-[(2-phenylethyl)carbamoyl]phenyl}but-2-enoic acid (5.16).

Isolated as a white solid, (400 mg, 48%).

Synthesised using the procedure for compound **5.13a**.

^{1}H NMR (400 MHz, Acetone-d_6) δ 7.90 (d, J = 8.6 Hz, 2H), 7.64 (d, J = 8.6 Hz, 2H), 7.32 – 7.25 (m, 4H), 7.23 – 7.17 (m, 1H), 6.21 (q, J = 1.4 Hz, 1H), 3.69 – 3.60 (m, 2H), 2.97 – 2.90 (m, 2H), 2.57 (d, J = 1.4 Hz, 3H); ^{13}C NMR (101 MHz, DMSO-d_6) δ 167.4, 165.5, 152.6, 143.8, 139.5, 134.8, 128.6, 128.3, 127.3, 126.1, 126.0, 118.5, 40.8, 35.0, 17.1; HRMS (ESI) m/z calcd for $C_{19}H_{19}NO_3$ $[M+H]^+$ 310.1438 found 310.1426.

Appendix

Chapter two NMR.

2.10a

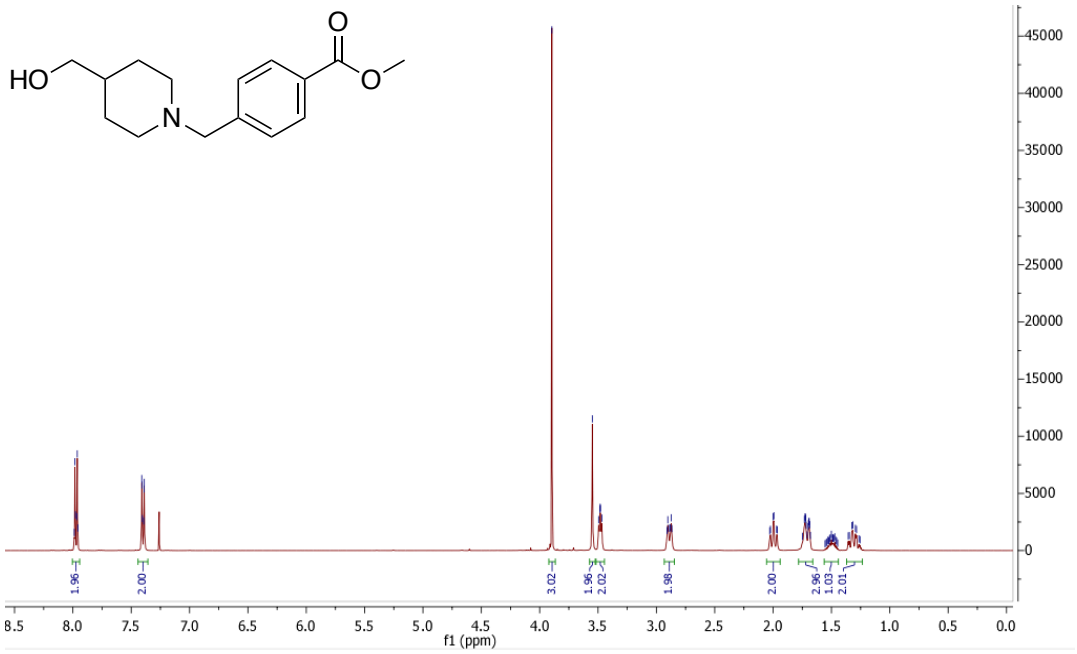

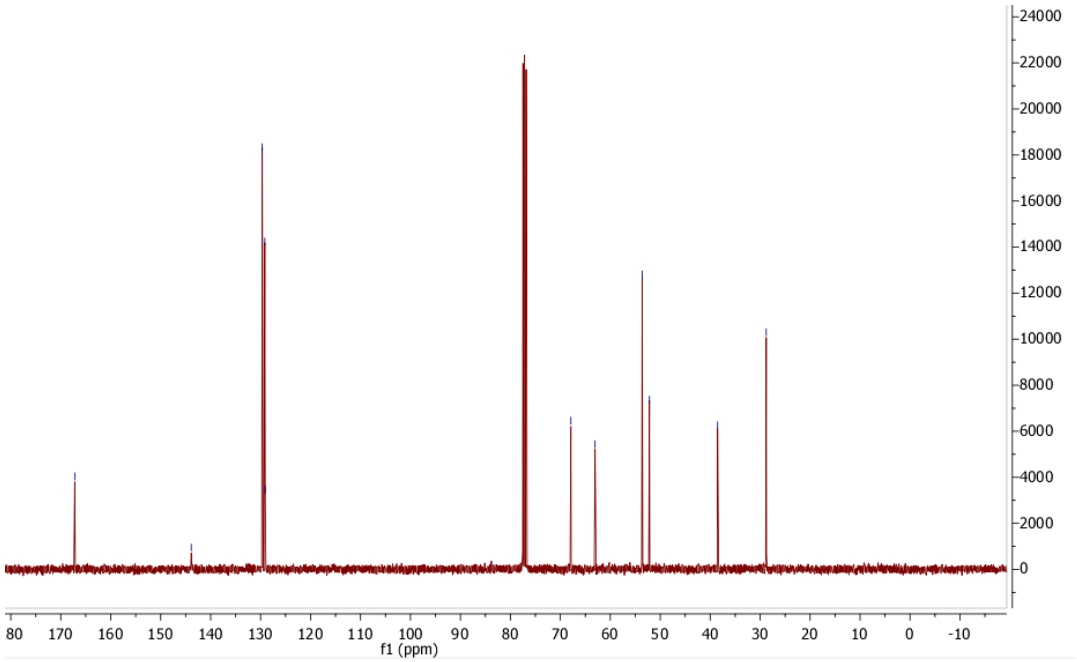

2.10b

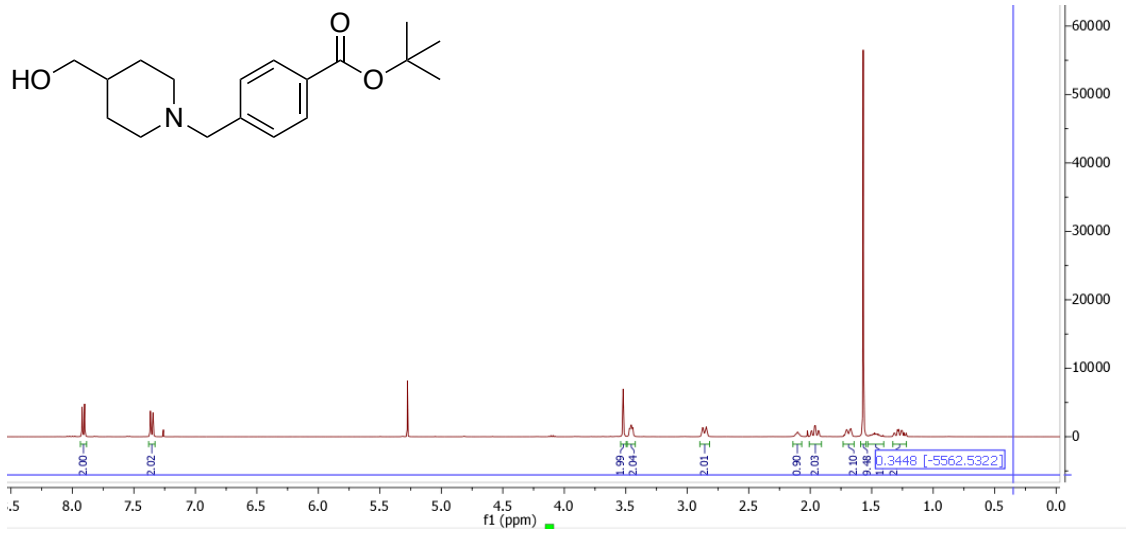
HO
N
O
O
60000
50000
40000
30000
20000
10000
0
0.3448 [-5562.5322]
f1 (ppm)

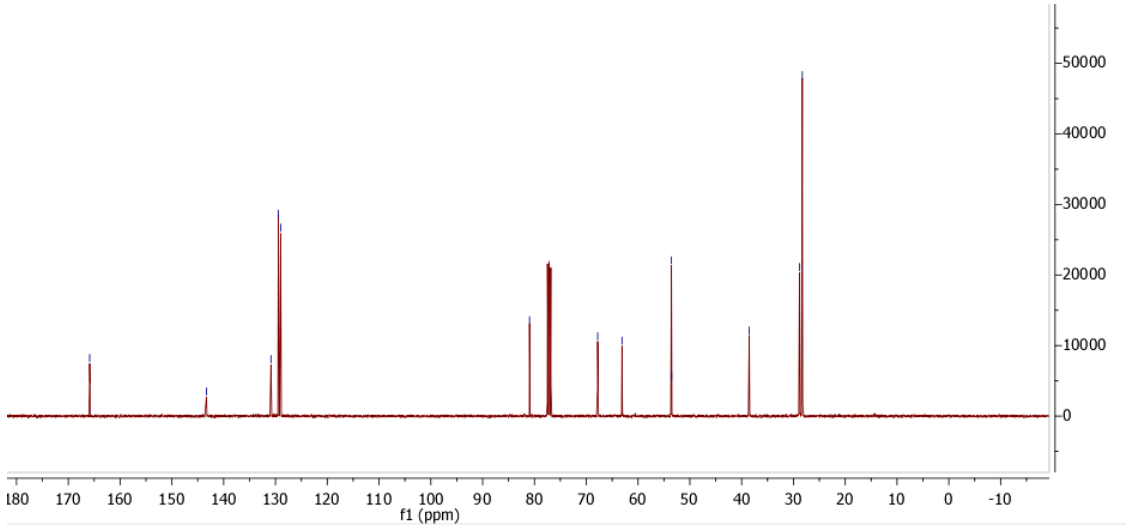
50000
40000
30000
20000
10000
0
f1 (ppm)

2.11a

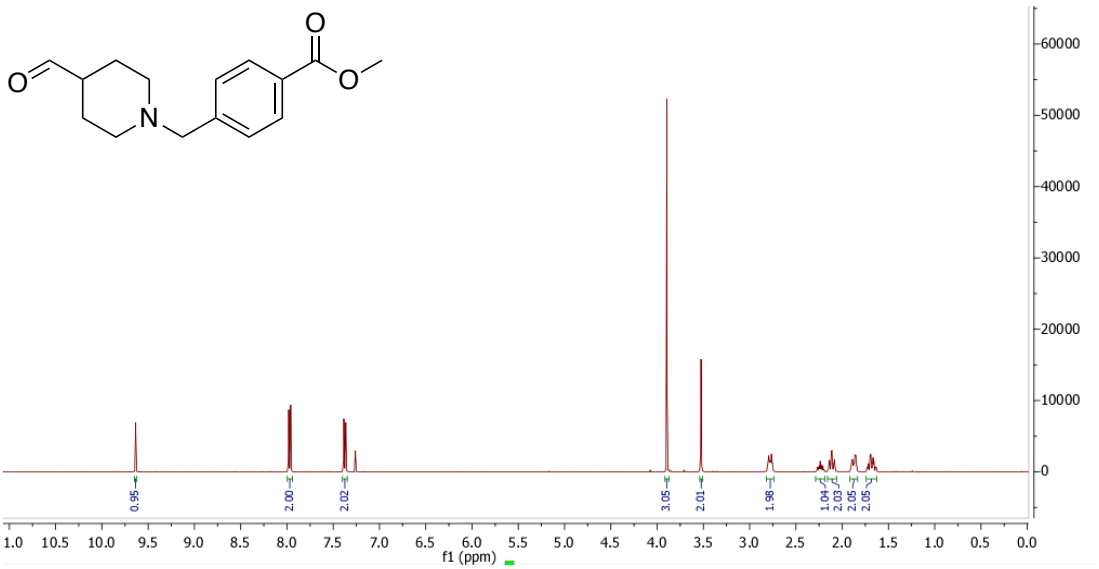
O
O
O
N
60000
50000
40000
30000
20000
10000
0
0.95
2.00
2.02
3.05
2.01
1.98
1.04
2.03
2.05
2.05
1.0 10.5 10.0 9.5 9.0 8.5 8.0 7.5 7.0 6.5 6.0 5.5 5.0 4.5 4.0 3.5 3.0 2.5 2.0 1.5 1.0 0.5 0.0
f1 (ppm)

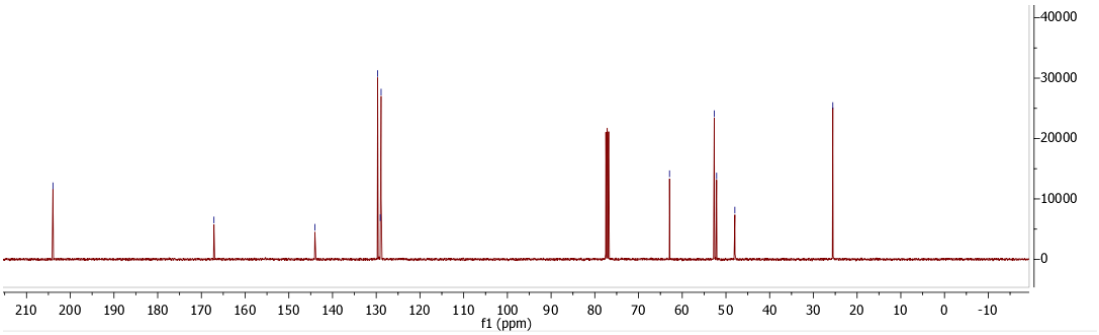
40000
30000
20000
10000
0
210 200 190 180 170 160 150 140 130 120 110 100 90 80 70 60 50 40 30 20 10 0 -10
f1 (ppm)

2.11b

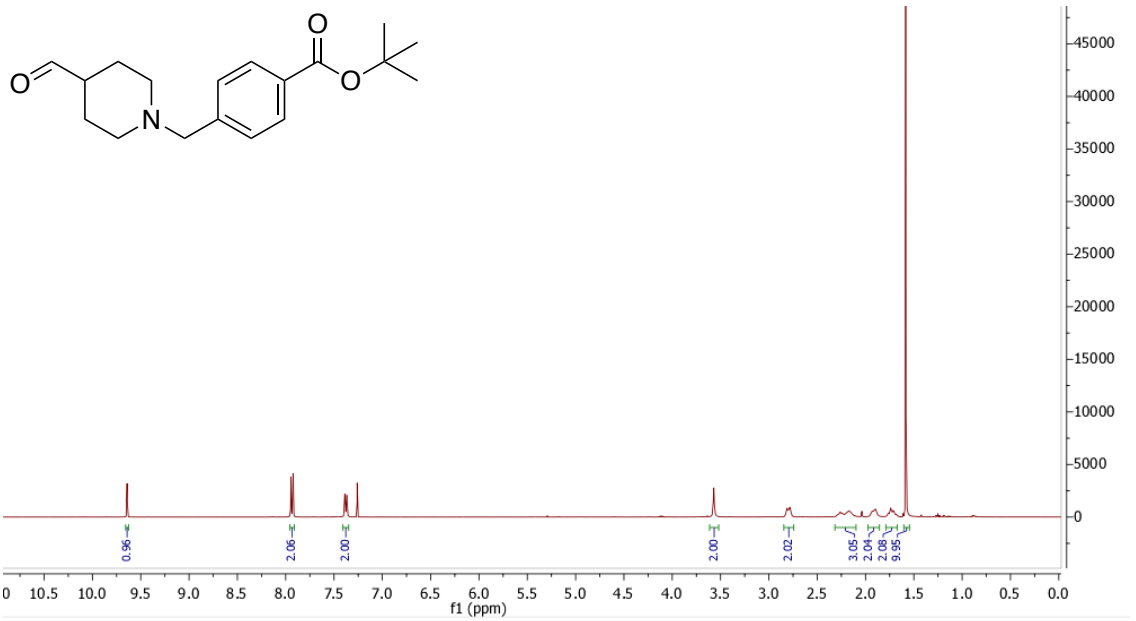
O
O
O
N
45000
40000
35000
30000
25000
20000
15000
10000
5000
0
0.96
2.06
2.00
2.00
2.02
3.05
2.04
2.08
9.95
0 10.5 10.0 9.5 9.0 8.5 8.0 7.5 7.0 6.5 6.0 5.5 5.0 4.5 4.0 3.5 3.0 2.5 2.0 1.5 1.0 0.5 0.0
f1 (ppm)

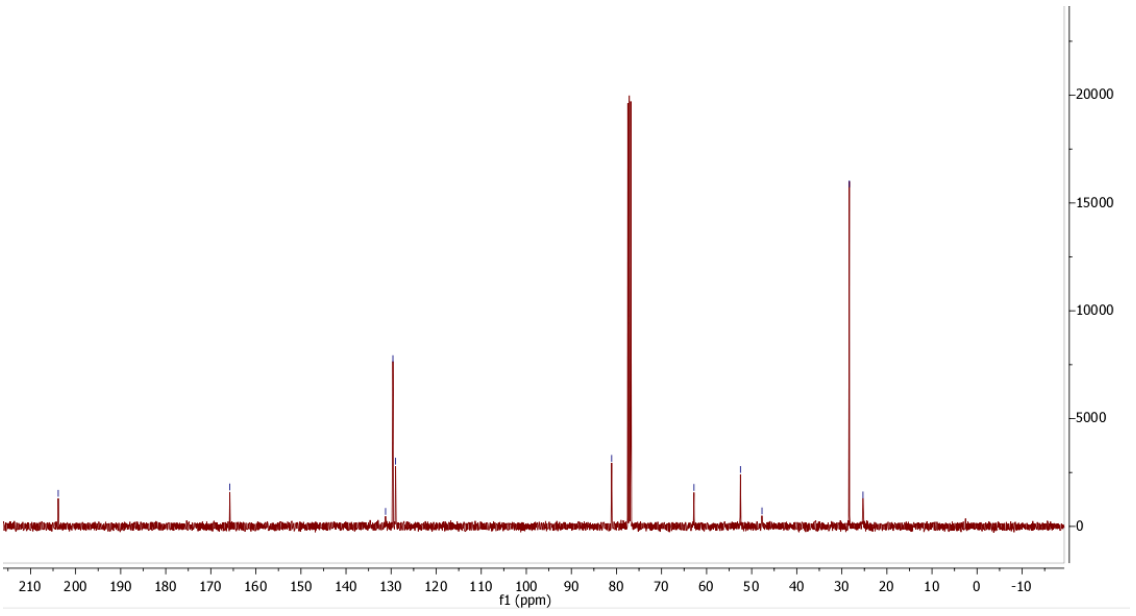
20000
15000
10000
5000
0
210 200 190 180 170 160 150 140 130 120 110 100 90 80 70 60 50 40 30 20 10 0 -10
f1 (ppm)

2.7a

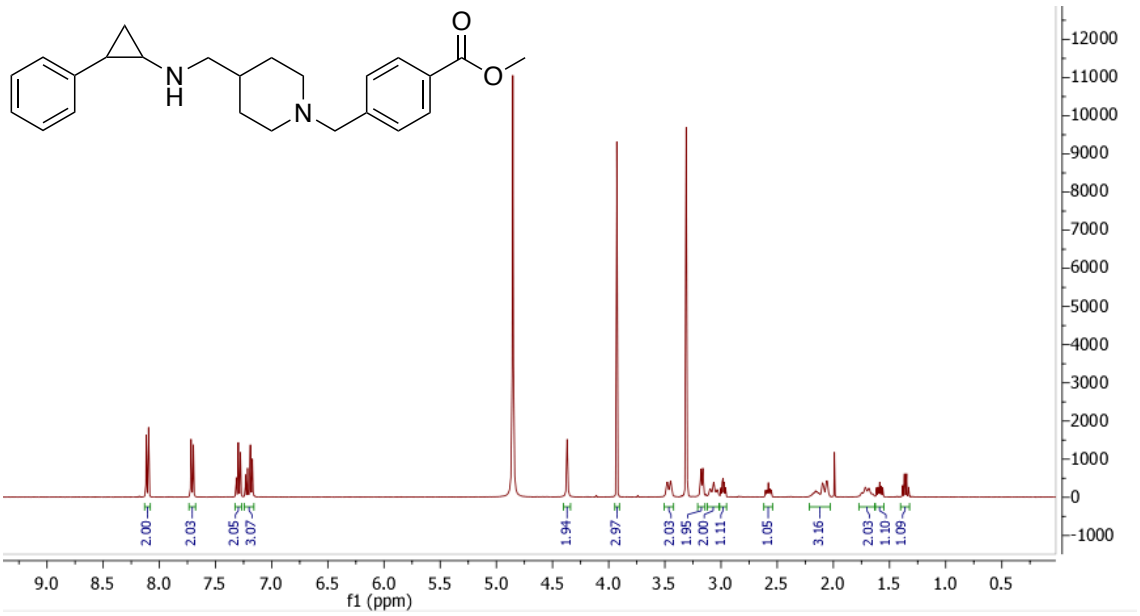
O
N
H
N
O
12000
11000
10000
9000
8000
7000
6000
5000
4000
3000
2000
1000
0
-1000
2.00
2.03
2.05
3.07
1.94
2.97
2.03
1.95
2.00
1.11
1.05
3.16
2.03
1.10
1.09
9.0
8.5
8.0
7.5
7.0
6.5
6.0
5.5
5.0
4.5
4.0
3.5
3.0
2.5
2.0
1.5
1.0
0.5
f1 (ppm)

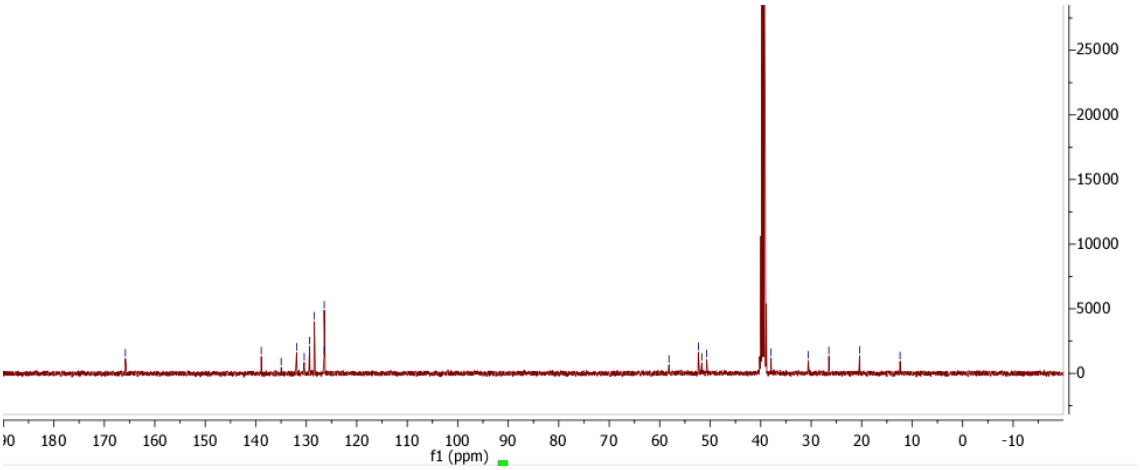
25000
20000
15000
10000
5000
0
180
170
160
150
140
130
120
110
100
90
80
70
60
50
40
30
20
10
0
-10
f1 (ppm)

2.7b

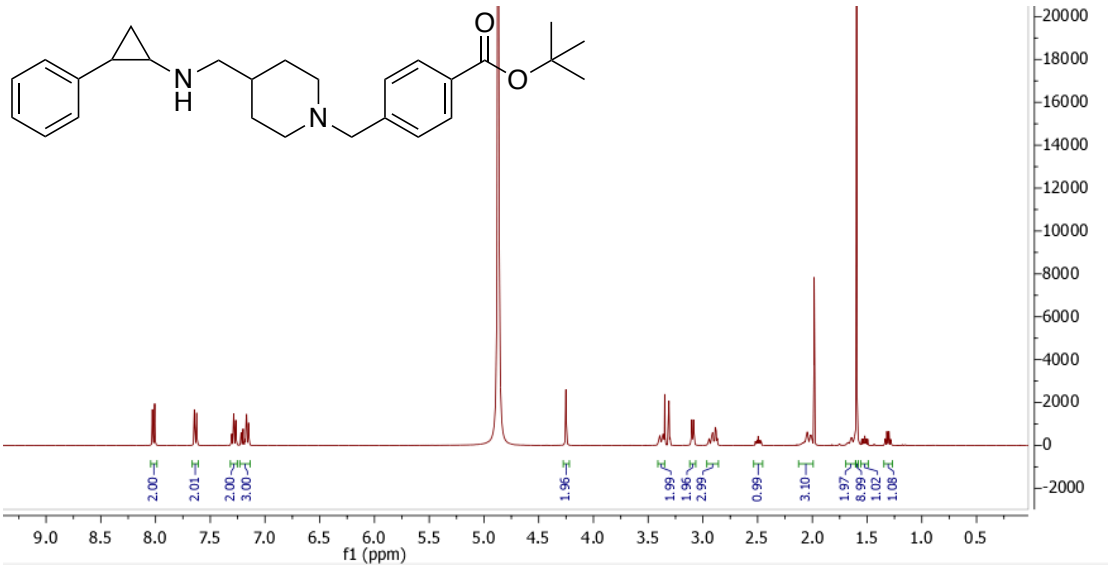
O
N
H
N
O
20000
18000
16000
14000
12000
10000
8000
6000
4000
2000
0
-2000
2.00
2.01
2.00
3.00
1.96
1.99
1.96
2.99
0.99
3.10
1.97
8.99
1.02
1.08
9.0 8.5 8.0 7.5 7.0 6.5 6.0 5.5 5.0 4.5 4.0 3.5 3.0 2.5 2.0 1.5 1.0 0.5
f1 (ppm)

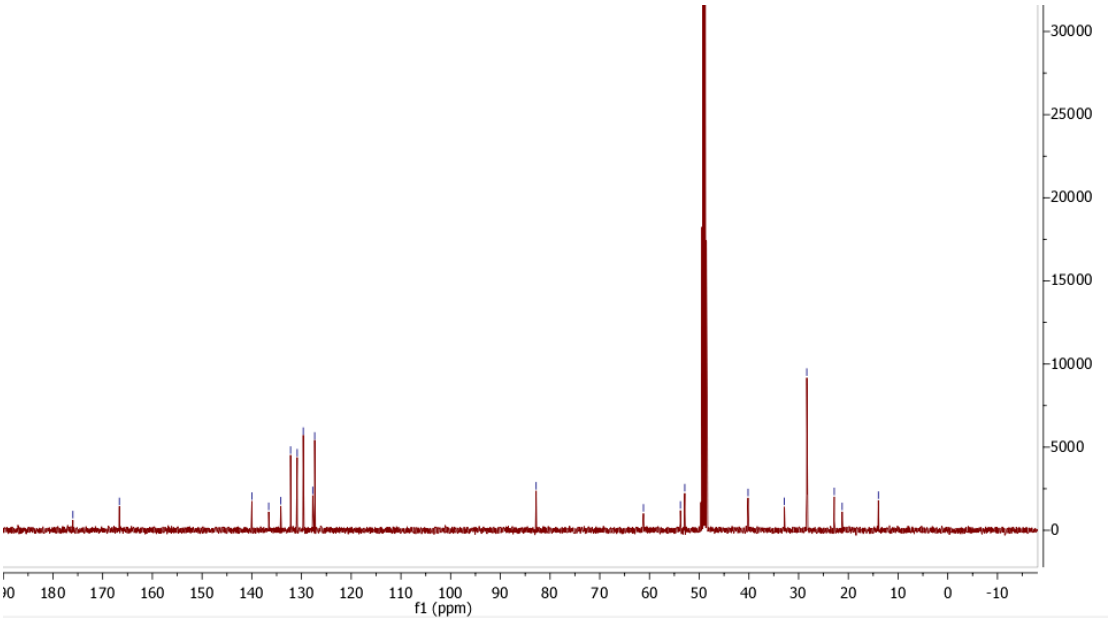
30000
25000
20000
15000
10000
5000
0
180 170 160 150 140 130 120 110 100 90 80 70 60 50 40 30 20 10 0 -10
f1 (ppm)

1.35

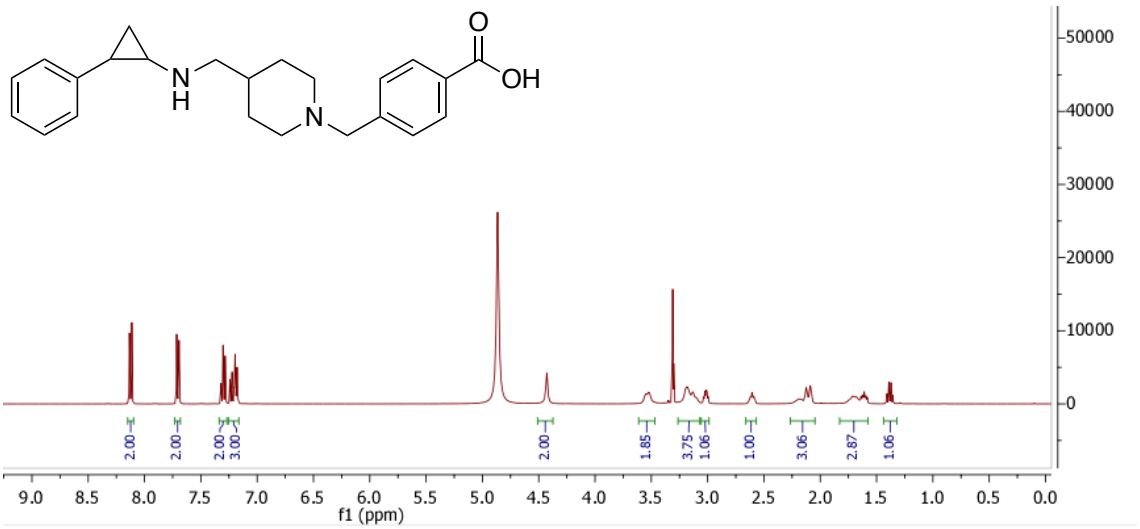
O
OH
N
H
N
50000
40000
30000
20000
10000
0
2.00
2.00
2.00
3.00
2.00
1.85
3.75
1.06
1.00
3.06
2.87
1.06
9.0 8.5 8.0 7.5 7.0 6.5 6.0 5.5 5.0 4.5 4.0 3.5 3.0 2.5 2.0 1.5 1.0 0.5 0.0
f1 (ppm)

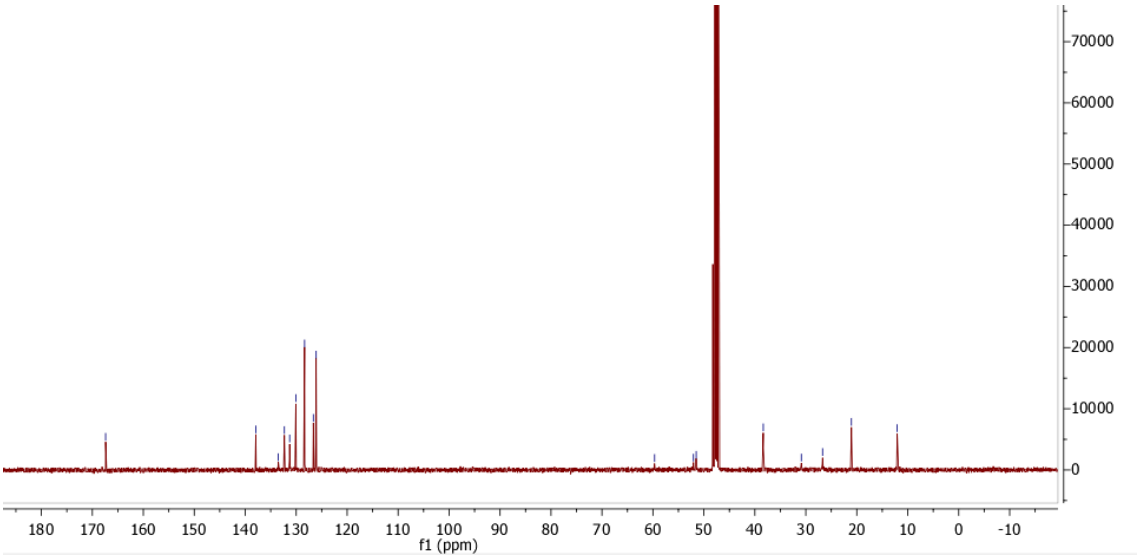
70000
60000
50000
40000
30000
20000
10000
0
180 170 160 150 140 130 120 110 100 90 80 70 60 50 40 30 20 10 0 -10
f1 (ppm)

2.8a

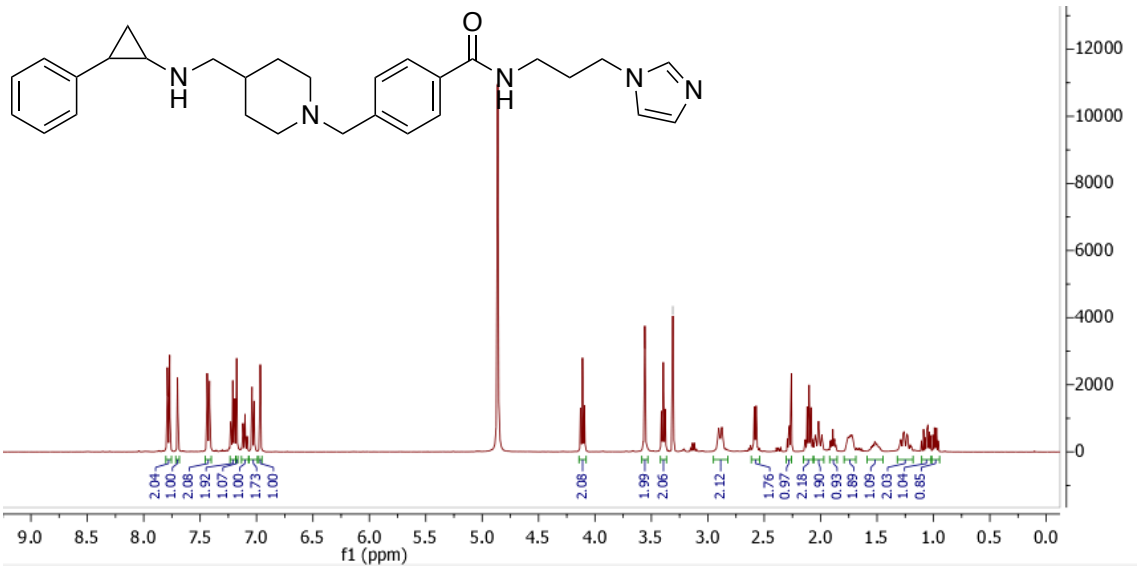
O
N
H
N
N
H
N
N
12000
10000
8000
6000
4000
2000
0
2.04
1.00
2.08
1.92
1.07
1.00
1.73
1.00
2.08
1.99
2.06
2.12
1.76
0.97
2.18
1.90
0.93
1.89
1.09
2.03
1.04
0.85
9.0
8.5
8.0
7.5
7.0
6.5
6.0
5.5
5.0
4.5
4.0
3.5
3.0
2.5
2.0
1.5
1.0
0.5
0.0
f1 (ppm)

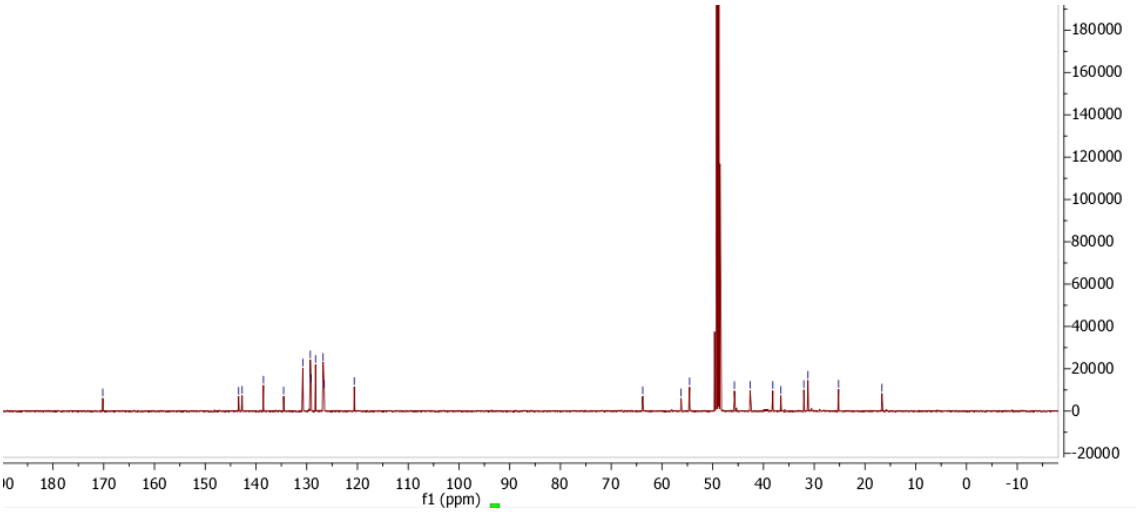
180000
160000
140000
120000
100000
80000
60000
40000
20000
0
-20000
180
170
160
150
140
130
120
110
100
90
80
70
60
50
40
30
20
10
0
-10
f1 (ppm)

2.8b

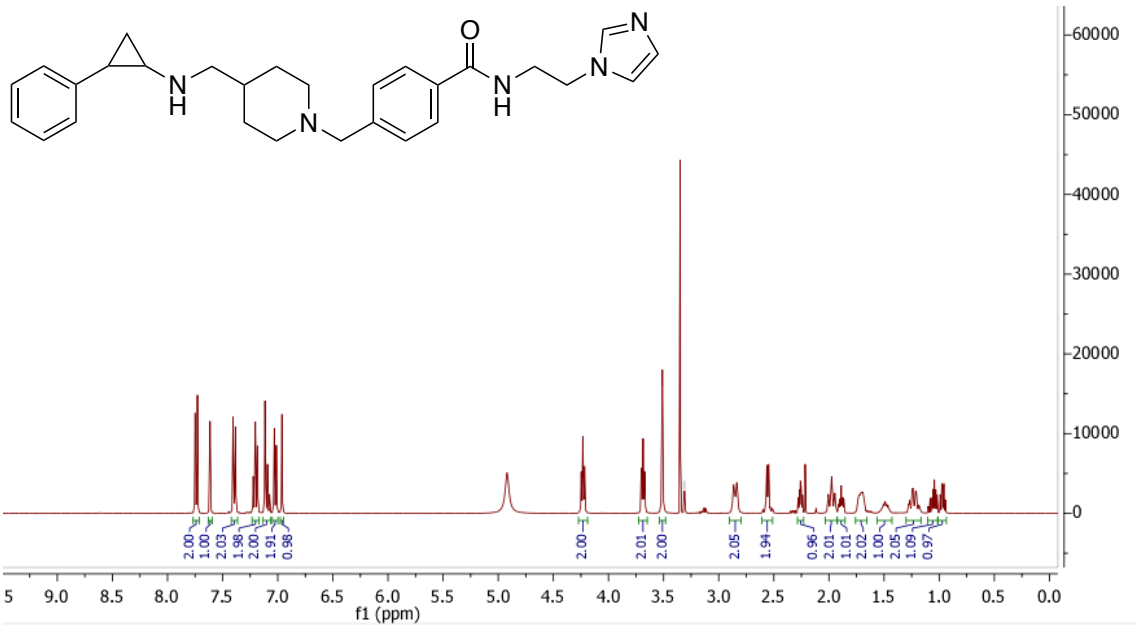
O
N
H
N
N
N
H
60000
50000
40000
30000
20000
10000
0
2.00
1.00
2.03
1.98
2.00
1.91
0.98
2.00
2.01
2.00
2.05
1.94
0.96
2.01
1.01
2.02
1.00
2.05
1.09
0.97
9.0
8.5
8.0
7.5
7.0
6.5
6.0
5.5
5.0
4.5
4.0
3.5
3.0
2.5
2.0
1.5
1.0
0.5
0.0
f1 (ppm)

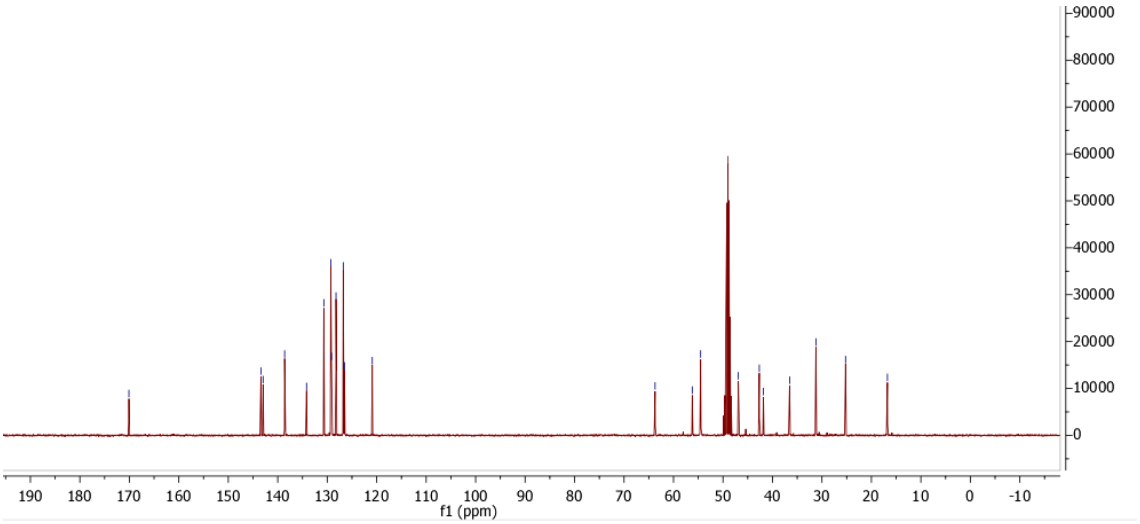
90000
80000
70000
60000
50000
40000
30000
20000
10000
0
190
180
170
160
150
140
130
120
110
100
90
80
70
60
50
40
30
20
10
0
-10
f1 (ppm)

2.8c

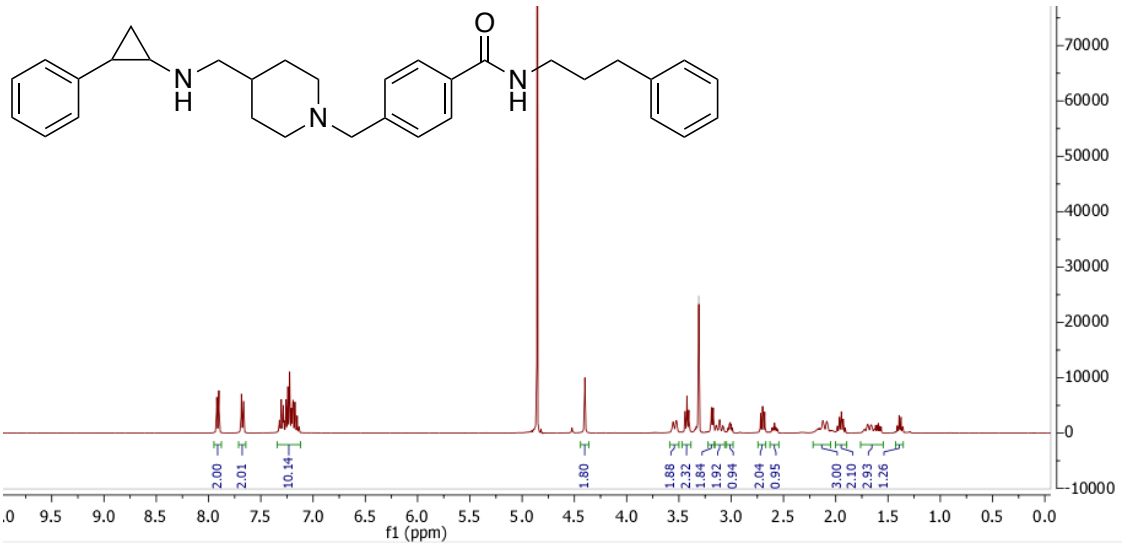
O
N
H
N
N
H
2.00
2.01
10.14
1.80
1.88
2.32
1.84
1.92
0.94
2.04
0.95
3.00
2.10
2.93
1.26
f1 (ppm)

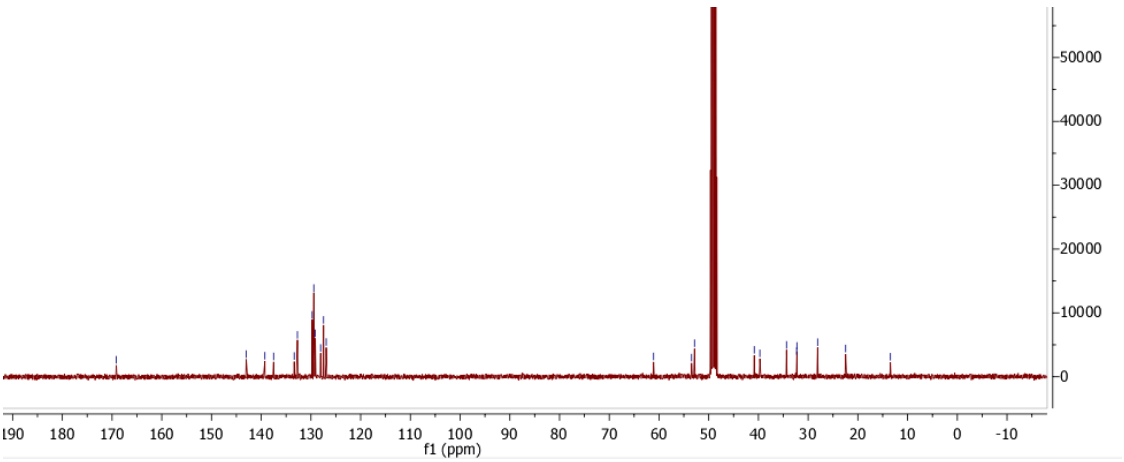
f1 (ppm)

2.8d

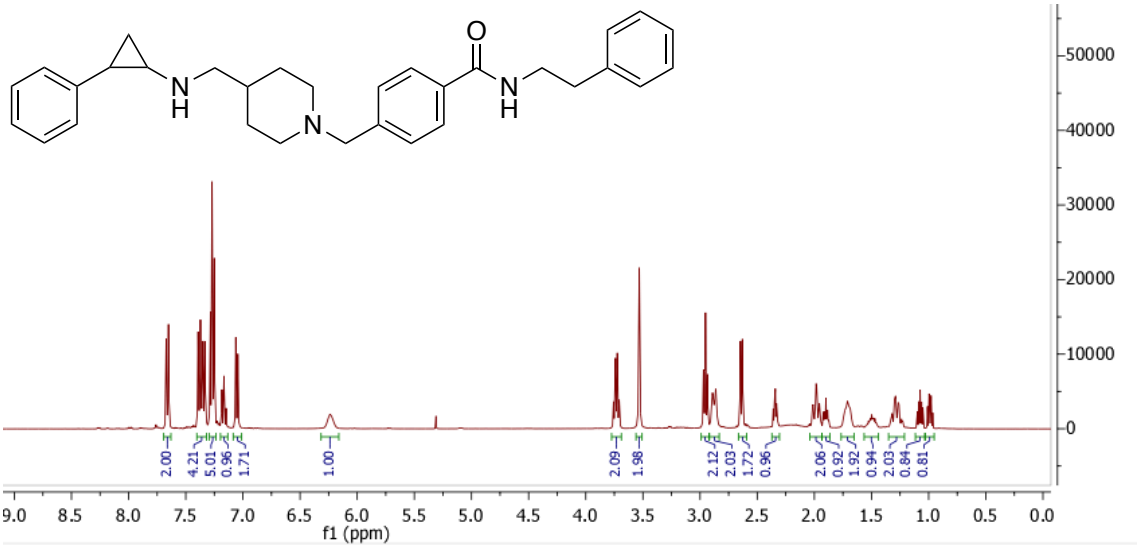
O
N
H
N
N
H
50000
40000
30000
20000
10000
0
2.00
4.21
5.01
0.96
1.71
1.00
2.09
1.98
2.12
2.03
1.72
0.96
2.06
0.92
1.92
0.94
2.03
0.84
0.81
9.0 8.5 8.0 7.5 7.0 6.5 6.0 5.5 5.0 4.5 4.0 3.5 3.0 2.5 2.0 1.5 1.0 0.5 0.0
f1 (ppm)

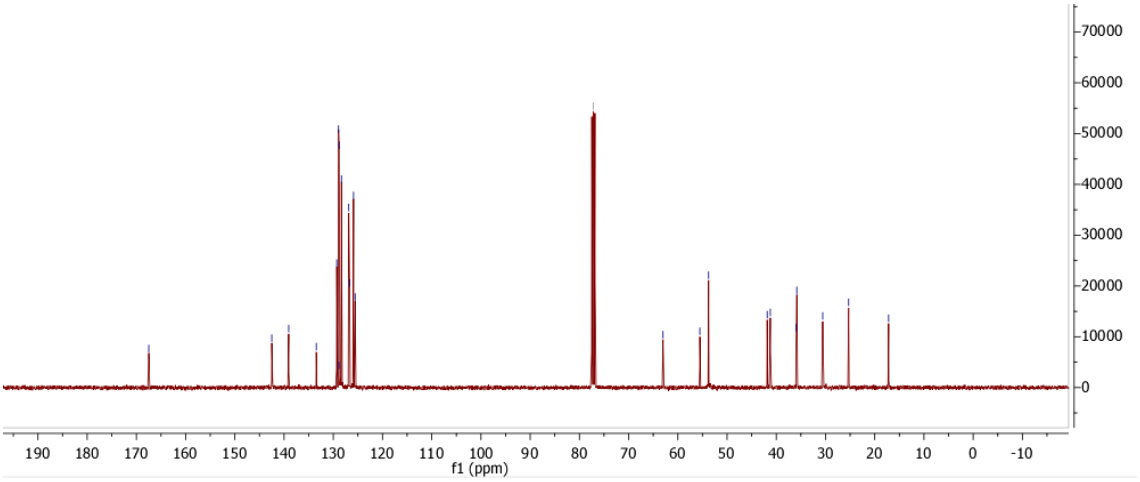
70000
60000
50000
40000
30000
20000
10000
0
190 180 170 160 150 140 130 120 110 100 90 80 70 60 50 40 30 20 10 0 -10
f1 (ppm)

2.8e

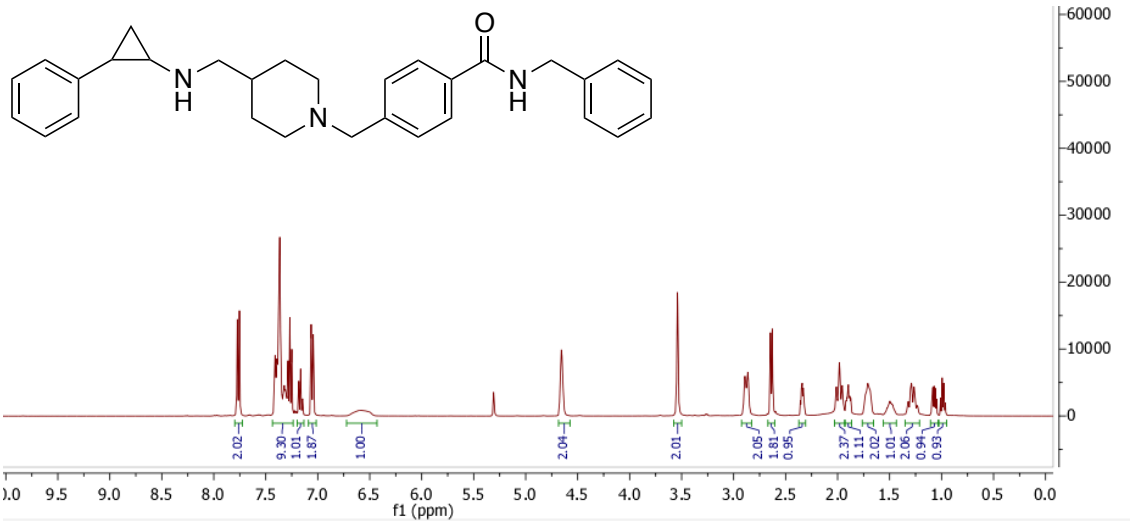
O
N
H
N
N
H
60000
50000
40000
30000
20000
10000
0
2.02
9.30
1.01
1.87
1.00
2.04
2.01
2.05
1.81
0.95
2.37
1.11
2.02
1.01
2.06
0.94
0.93
9.5
9.0
8.5
8.0
7.5
7.0
6.5
6.0
5.5
5.0
4.5
4.0
3.5
3.0
2.5
2.0
1.5
1.0
0.5
0.0
f1 (ppm)

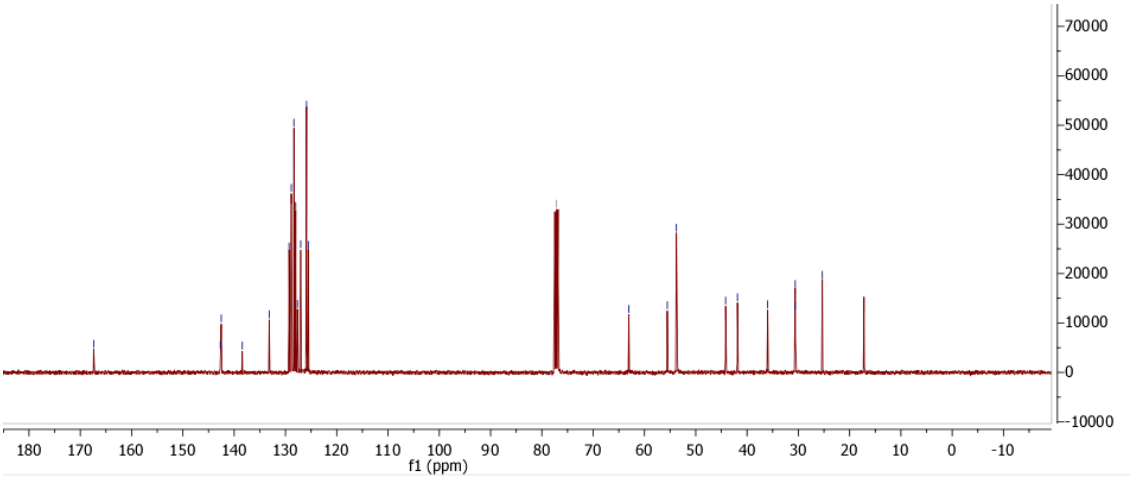
70000
60000
50000
40000
30000
20000
10000
0
-10000
180
170
160
150
140
130
120
110
100
90
80
70
60
50
40
30
20
10
0
-10
f1 (ppm)

2.8f

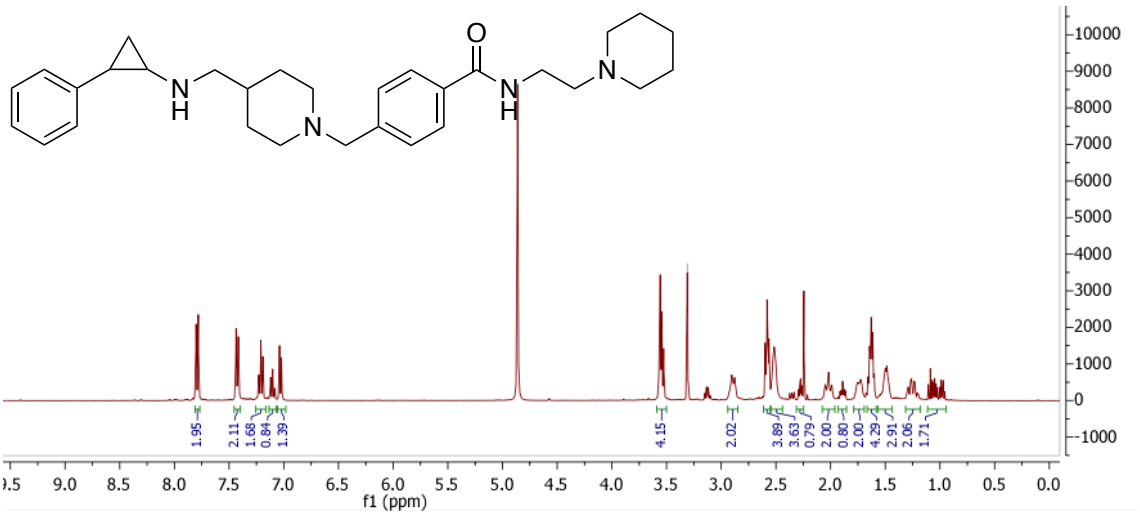
O
N
H
N
N
H
N
1.95
2.11
1.68
0.84
1.39
4.15
2.02
3.89
3.63
0.79
2.00
0.80
2.00
4.29
2.91
2.06
1.71
f1 (ppm)

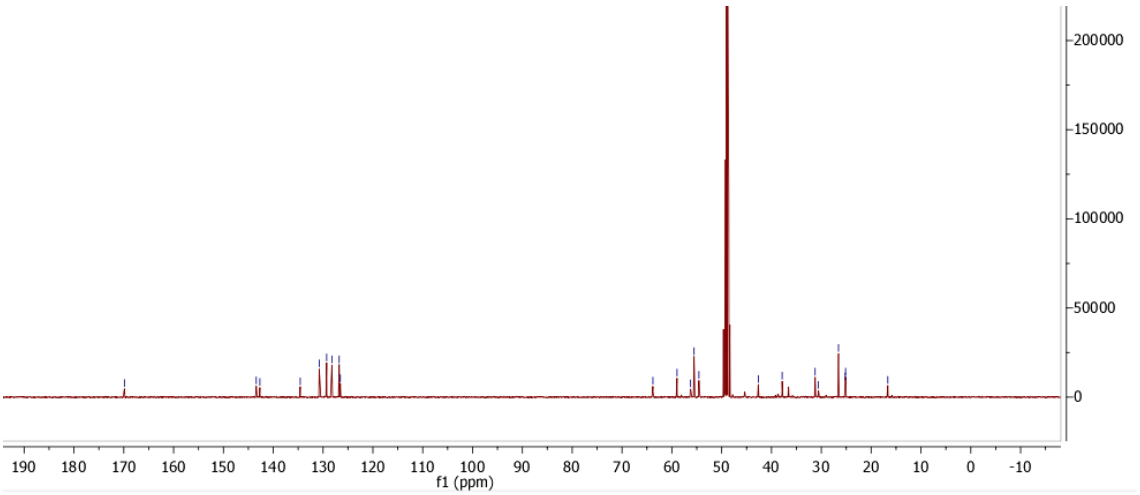
f1 (ppm)

2.8g

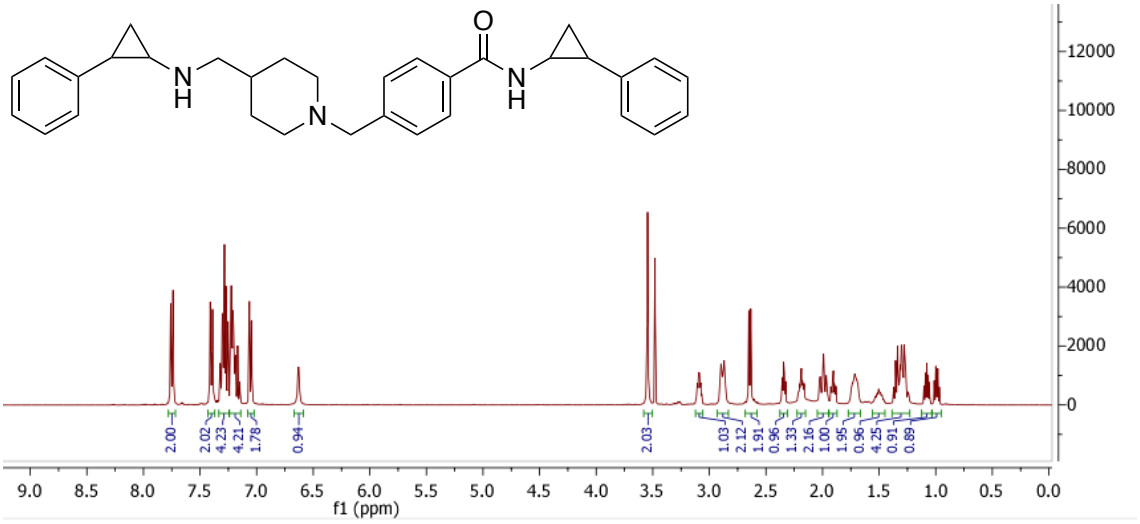
O
N
H
N
N
H
12000
10000
8000
6000
4000
2000
0
2.00
2.02
4.23
4.21
1.78
0.94
2.03
1.03
2.12
1.91
0.96
1.33
2.16
1.00
1.95
0.96
4.25
0.91
0.89
9.0 8.5 8.0 7.5 7.0 6.5 6.0 5.5 5.0 4.5 4.0 3.5 3.0 2.5 2.0 1.5 1.0 0.5 0.0
f1 (ppm)

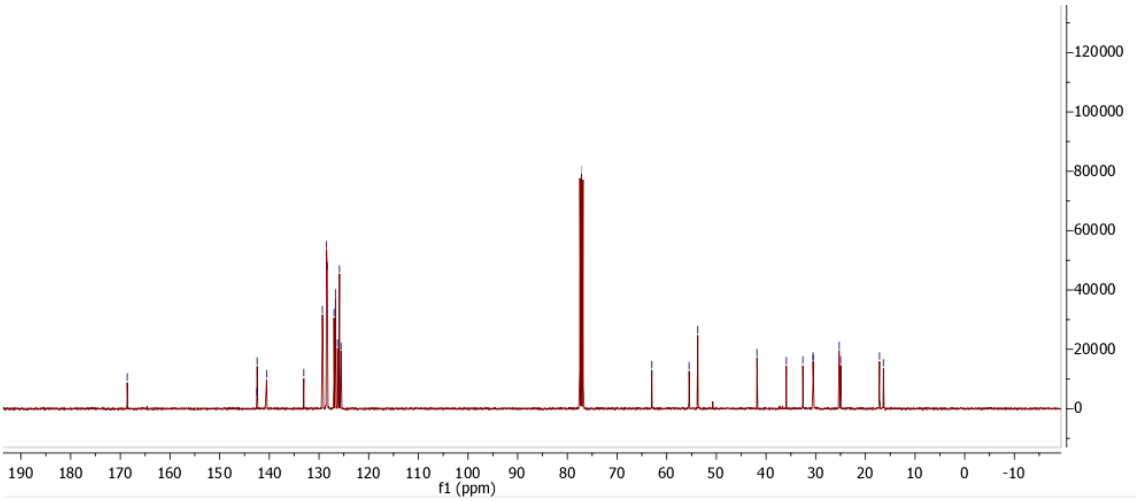
120000
100000
80000
60000
40000
20000
0
190 180 170 160 150 140 130 120 110 100 90 80 70 60 50 40 30 20 10 0 -10
f1 (ppm)

Chapter two HPLC data

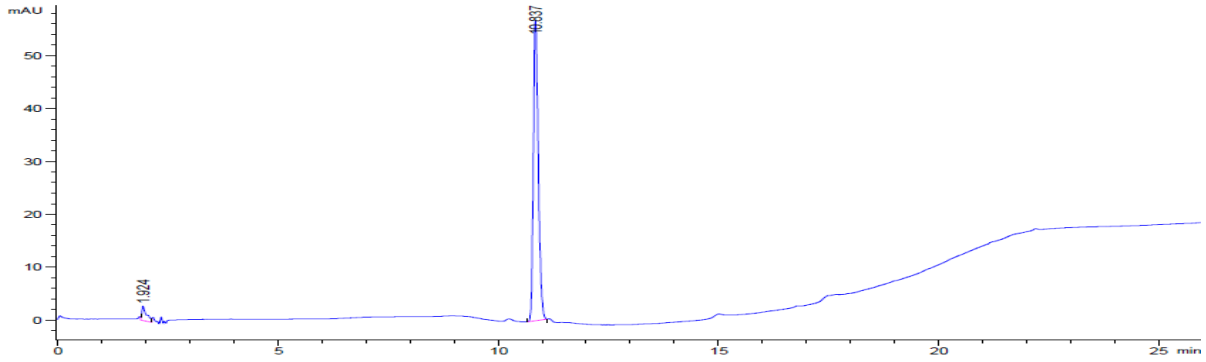

Compound	2.8a
λ (nm)	254
Retention time (min)	10.8
% Area	95.6

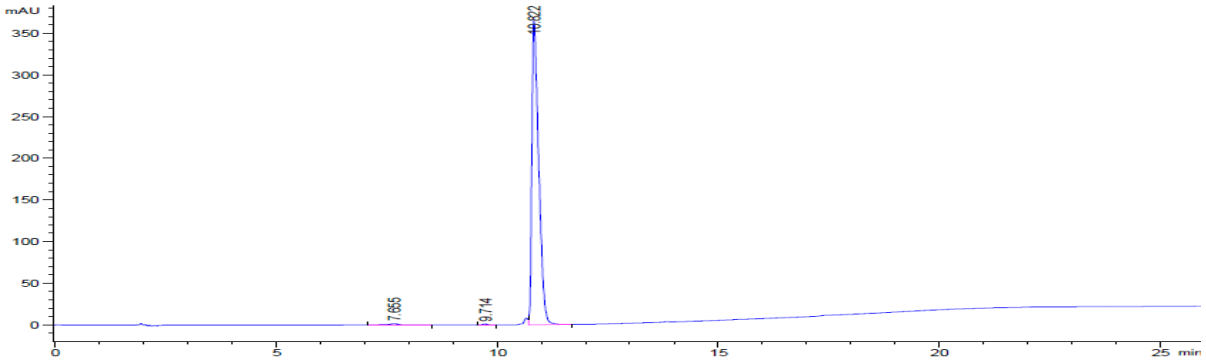

Compound	2.8b
λ (nm)	254
Retention time (min)	10.8
% Area	99.2

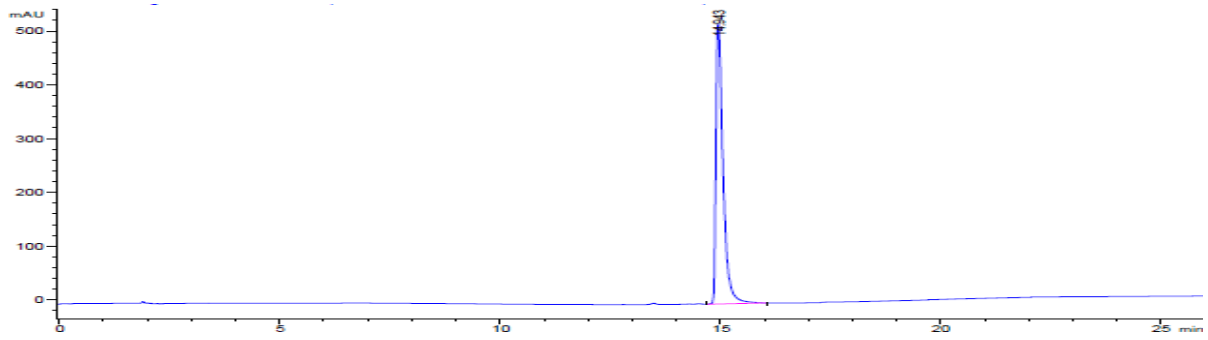

Compound	2.8c
λ (nm)	254
Retention time (min)	14.9
% Area	100

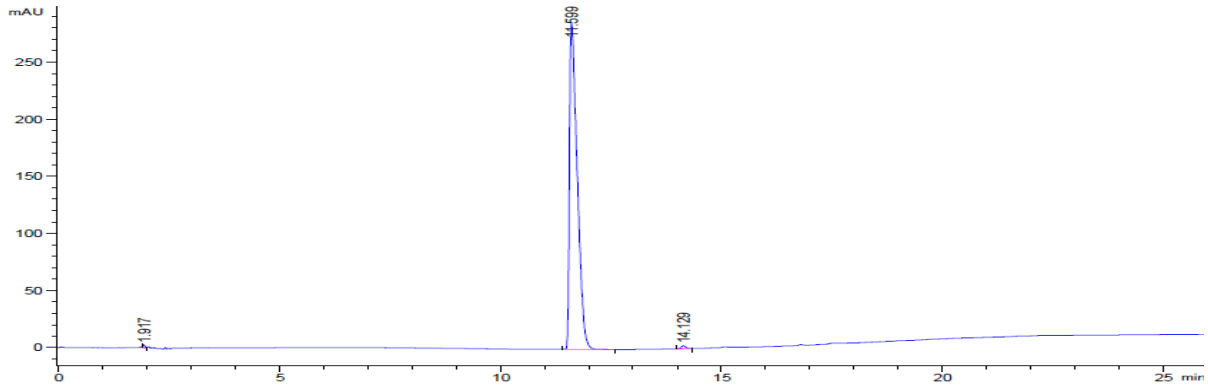

Compound	2.8d
λ (nm)	254
Retention time (min)	11.6
% Area	99.2

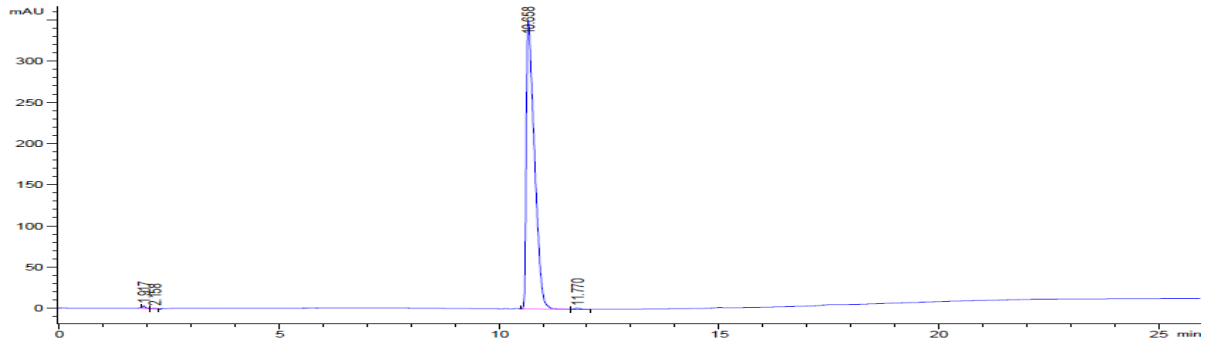

Compound	2.8e
λ (nm)	254
Retention time (min)	10.6
% Area	99.2

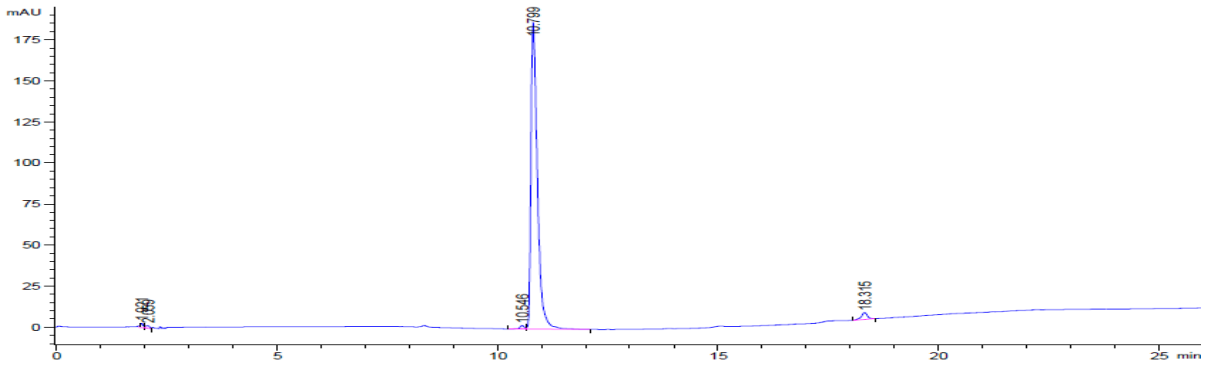

Compound	2.8f
λ (nm)	254
Retention time (min)	10.8
% Area	96.1

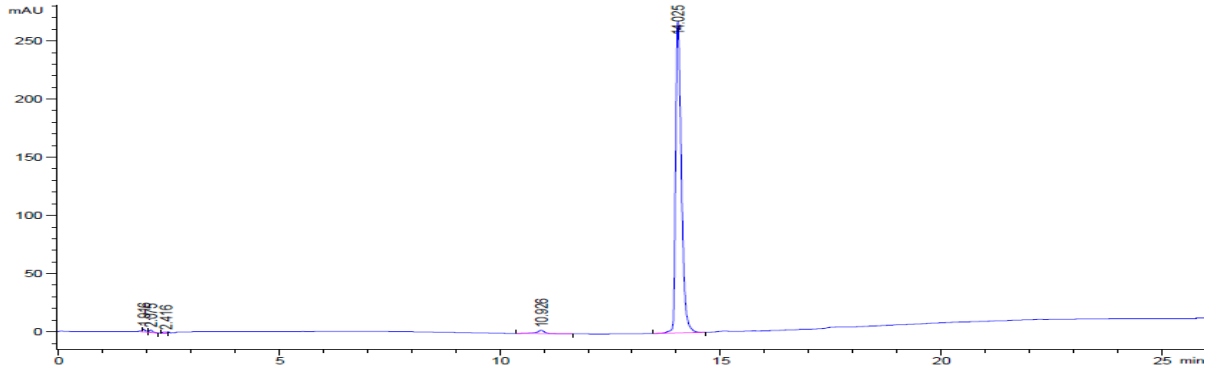

Compound	2.8g
λ (nm)	254
Retention time (min)	14.0
% Area	97.1

Chapter three NMR

3.8

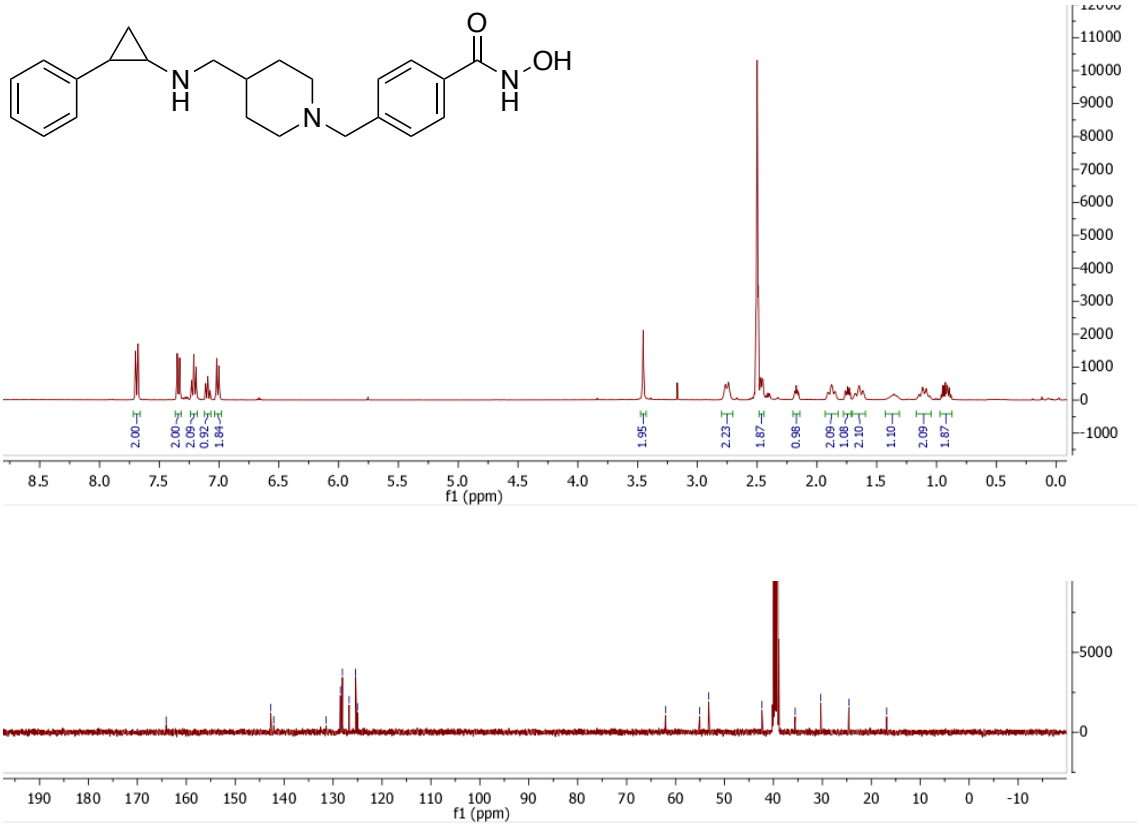

3.15

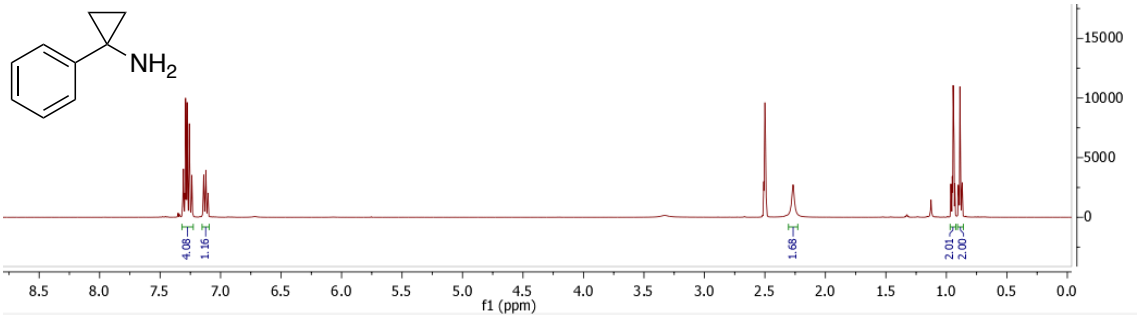
NH2
15000
10000
5000
0
4.08
1.16
1.68
2.01
2.00
8.5 8.0 7.5 7.0 6.5 6.0 5.5 5.0 4.5 4.0 3.5 3.0 2.5 2.0 1.5 1.0 0.5 0.0
f1 (ppm)

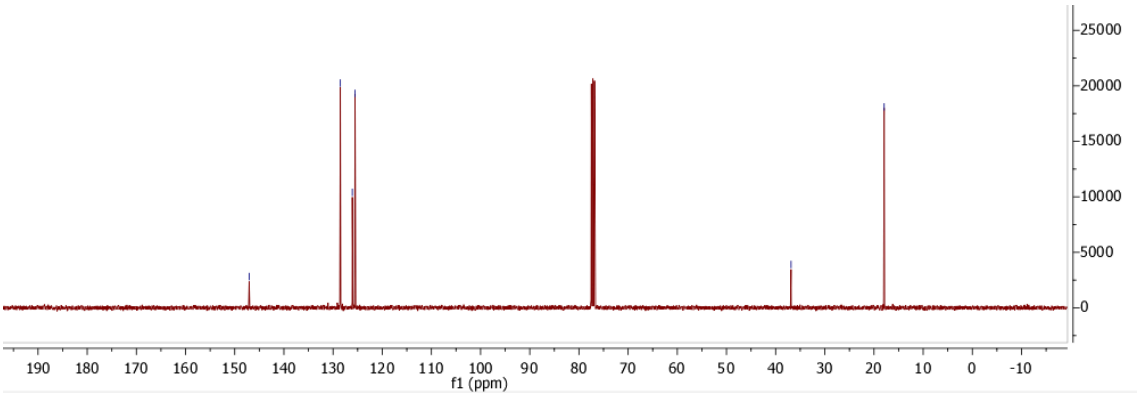
25000
20000
15000
10000
5000
0
190 180 170 160 150 140 130 120 110 100 90 80 70 60 50 40 30 20 10 0 -10
f1 (ppm)

3.16

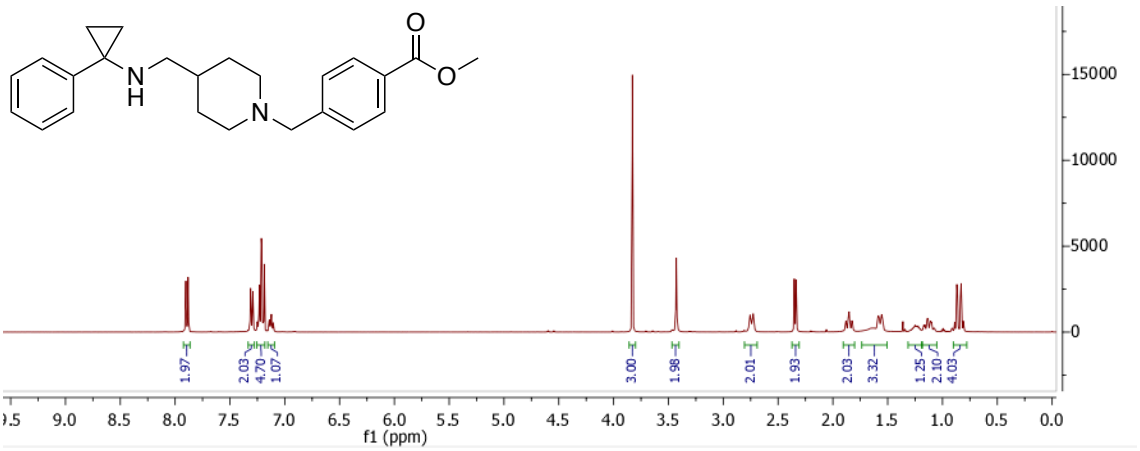
O
N
H
N
O
15000
10000
5000
0
1.97
2.03
4.70
1.07
3.00
1.98
2.01
1.93
2.03
3.32
1.25
2.10
4.03
9.0
8.5
8.0
7.5
7.0
6.5
6.0
5.5
5.0
4.5
4.0
3.5
3.0
2.5
2.0
1.5
1.0
0.5
0.0
f1 (ppm)

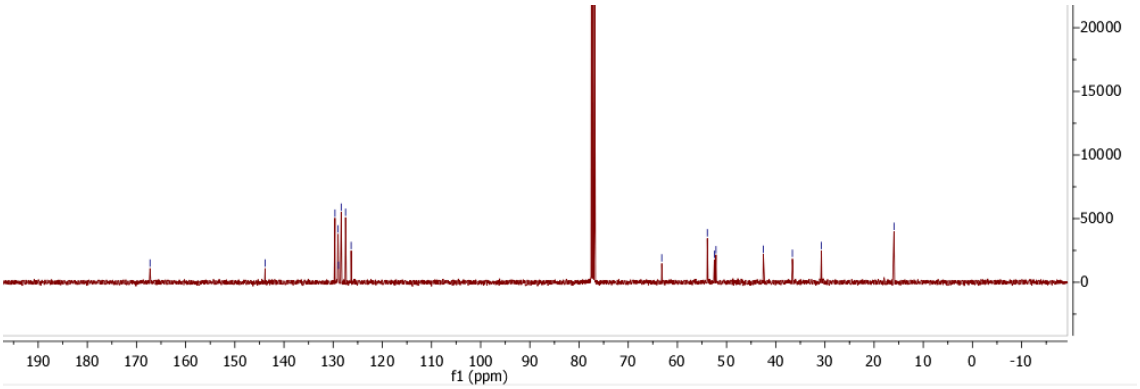
20000
15000
10000
5000
0
190
180
170
160
150
140
130
120
110
100
90
80
70
60
50
40
30
20
10
0
-10
f1 (ppm)

3.13

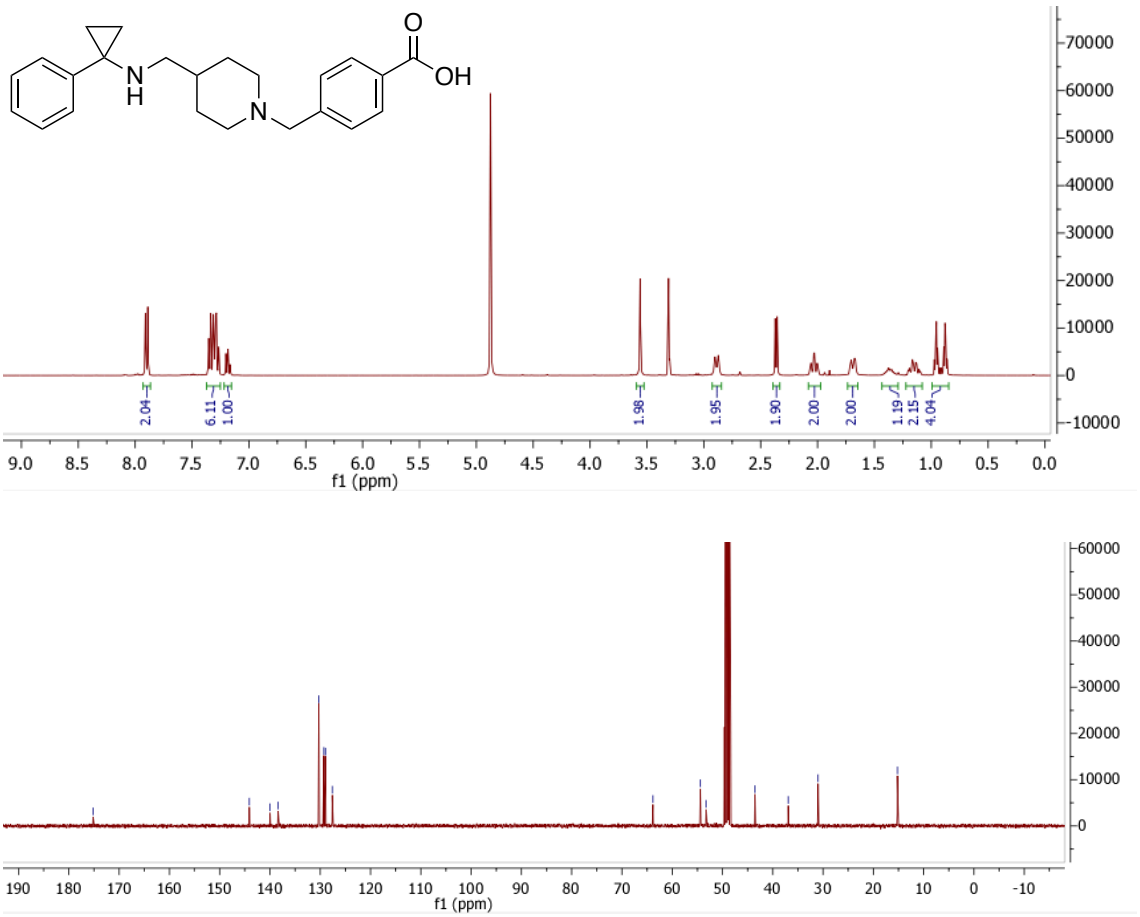

3.12

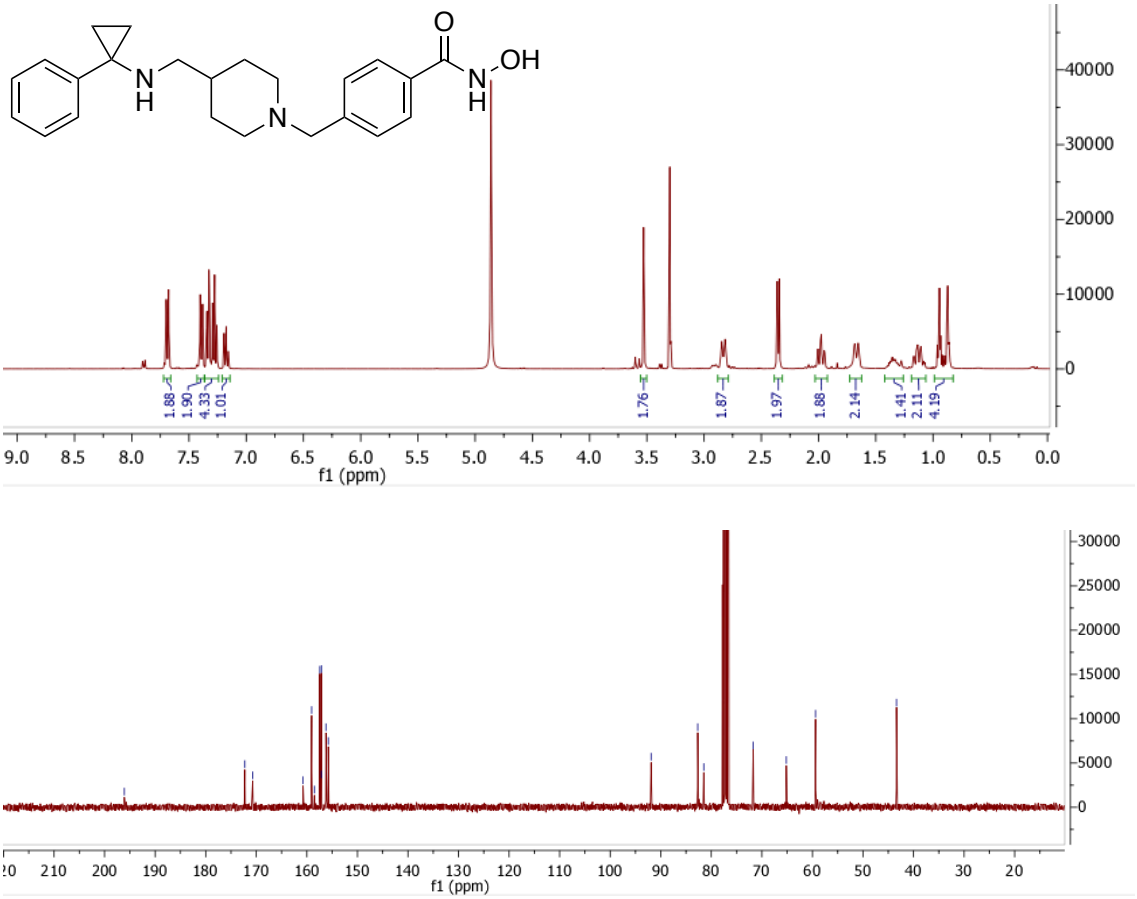
O
N
H
OH
N
N
H
40000
30000
20000
10000
0
1.88
1.90
4.33
1.01
1.76
1.87
1.97
1.88
2.14
1.41
2.11
4.19
9.0 8.5 8.0 7.5 7.0 6.5 6.0 5.5 5.0 4.5 4.0 3.5 3.0 2.5 2.0 1.5 1.0 0.5 0.0
f1 (ppm)
30000
25000
20000
15000
10000
5000
0
210 200 190 180 170 160 150 140 130 120 110 100 90 80 70 60 50 40 30 20
f1 (ppm)

Chapter three HPLC data

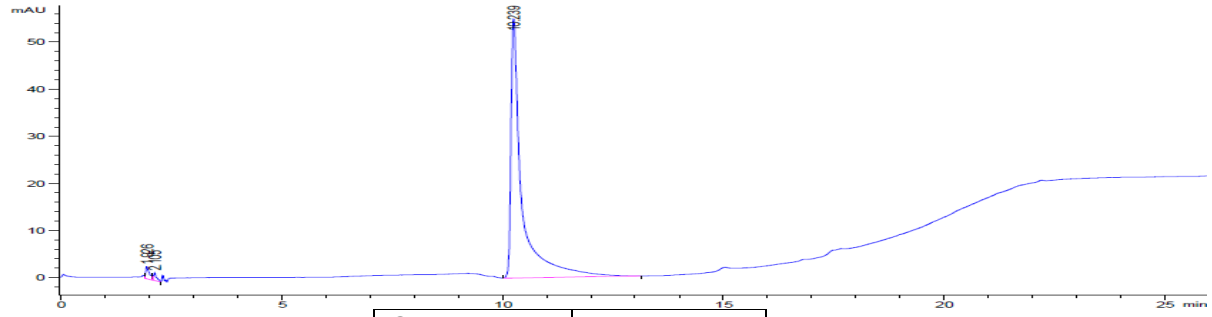

Compound	3.8
λ (nm)	254
Retention time (min)	10.2
% Area	97.5

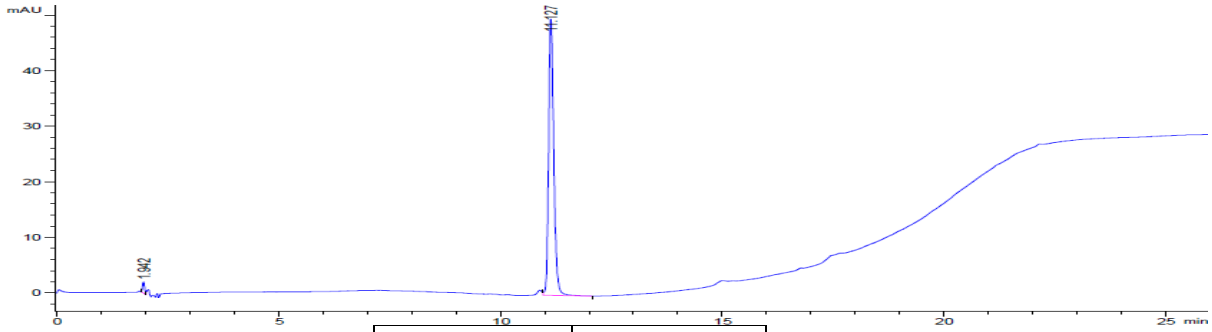

Compound	3.13
λ (nm)	214
Retention time (min)	11.1
% Area	98.3

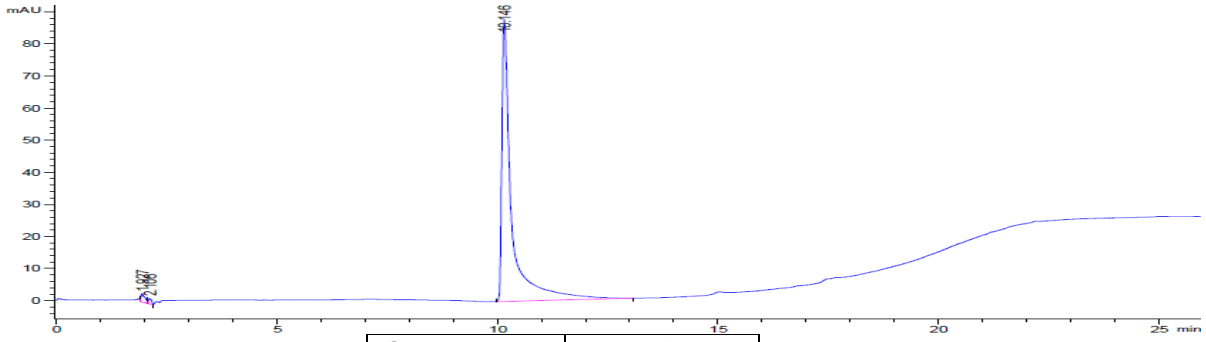

Compound	**3.12**
λ (nm)	254
Retention time (min)	10.1
% Area	98.1

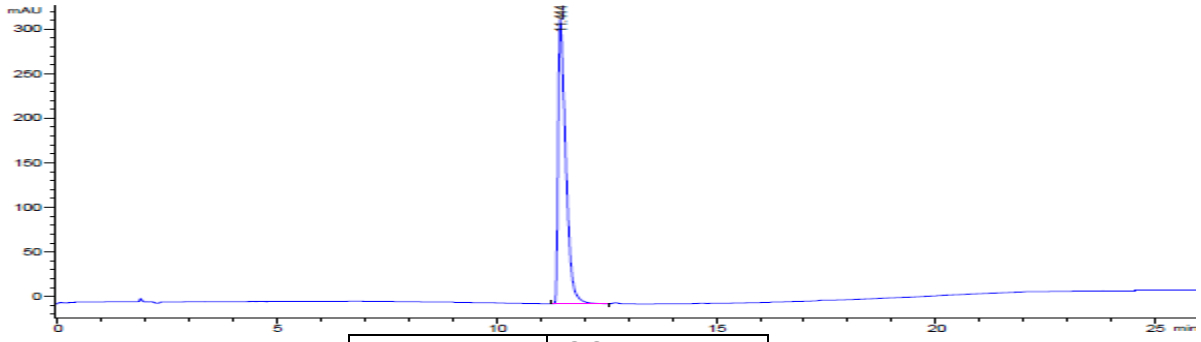

Compound	GSK2879552 (**1.35**)
λ (nm)	254
Retention time (min)	11.4
% Area	100

Chapter four NMR.

Para series

2.10a

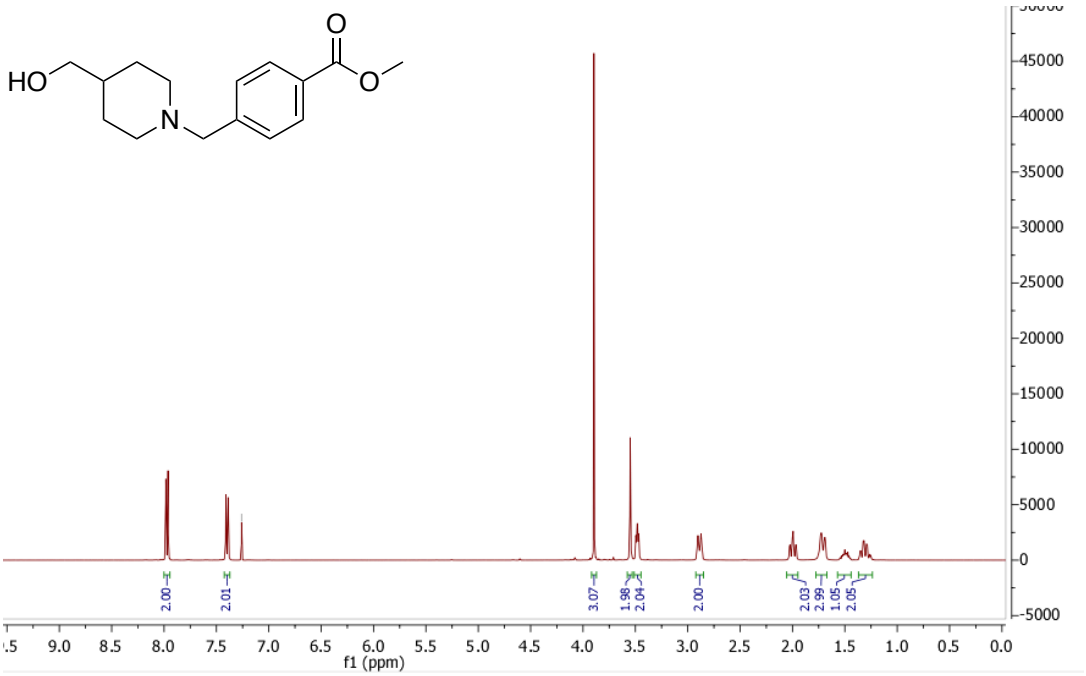

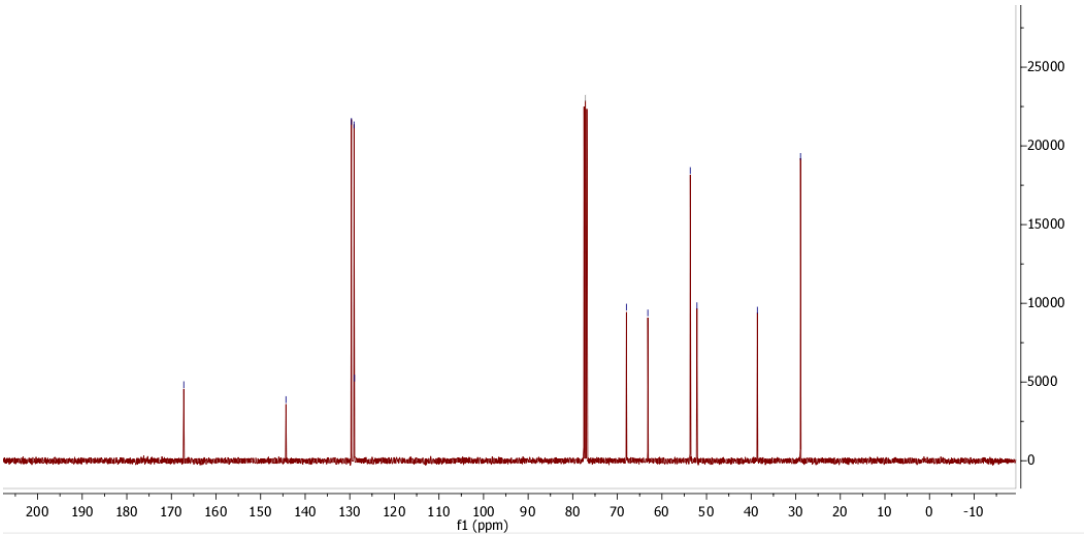

4.2a

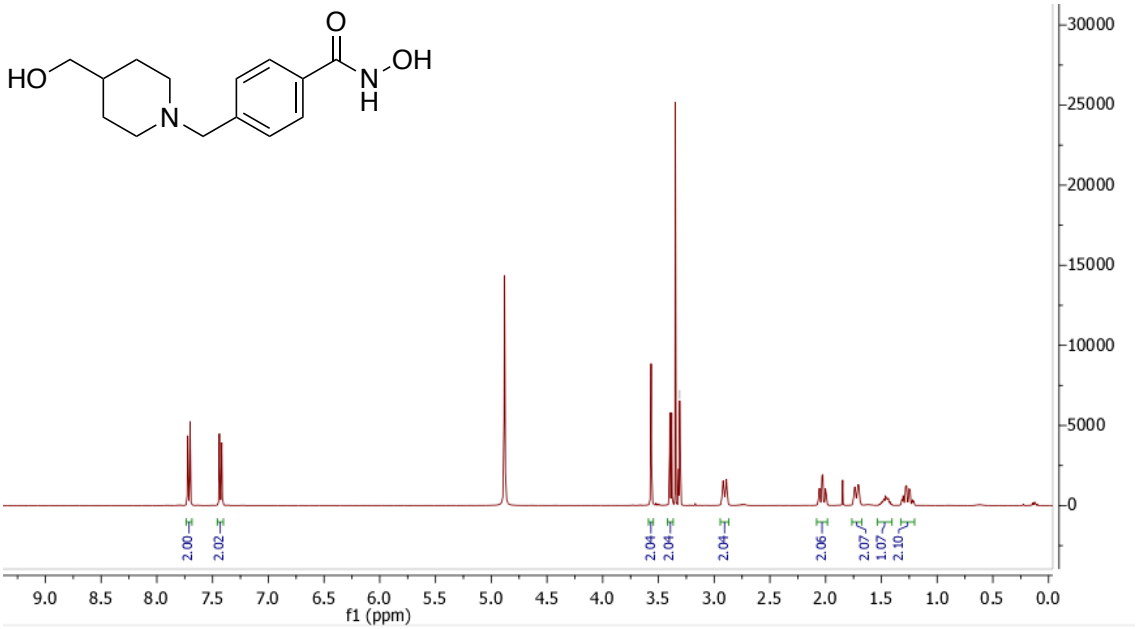
HO
N
O
N
H
OH
30000
25000
20000
15000
10000
5000
0
2.00
2.02
2.04
2.04
2.04
2.06
2.07
1.07
2.10
9.0 8.5 8.0 7.5 7.0 6.5 6.0 5.5 5.0 4.5 4.0 3.5 3.0 2.5 2.0 1.5 1.0 0.5 0.0
f1 (ppm)

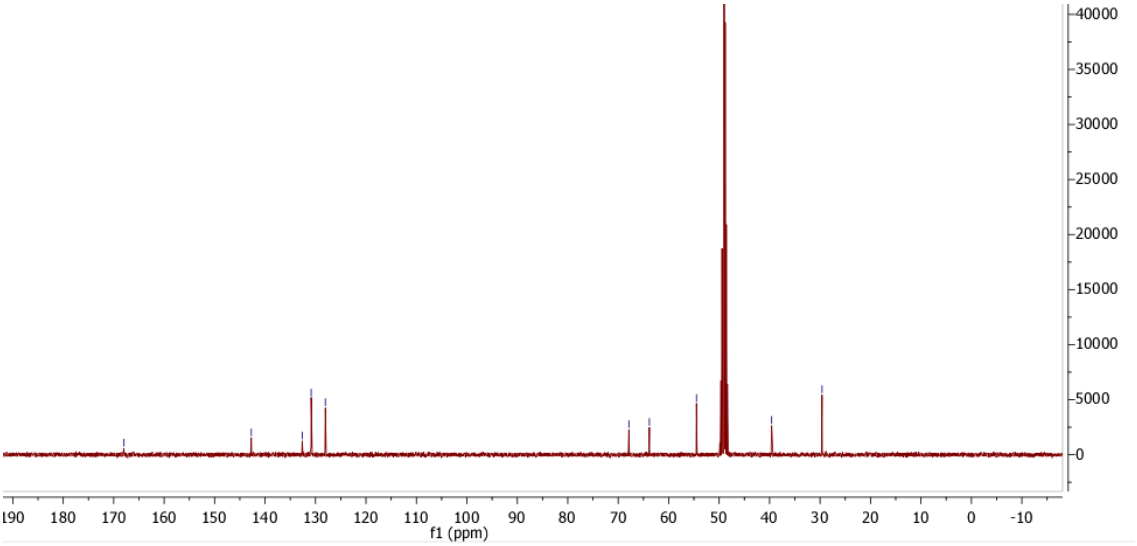
40000
35000
30000
25000
20000
15000
10000
5000
0
190 180 170 160 150 140 130 120 110 100 90 80 70 60 50 40 30 20 10 0 -10
f1 (ppm)

4.1a

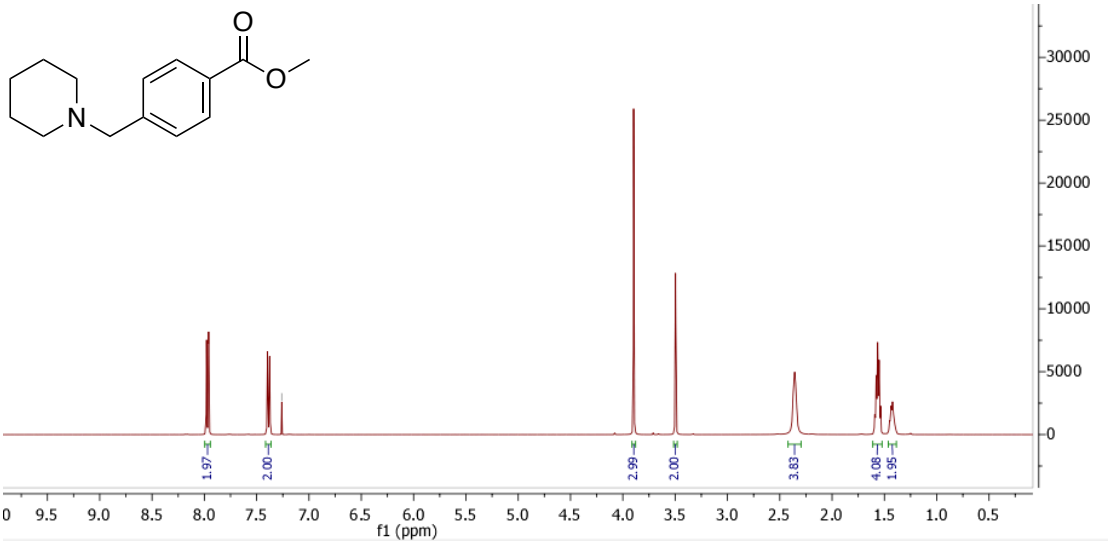
O
O
N
30000
25000
20000
15000
10000
5000
0
1.97
2.00
2.99
2.00
3.83
4.08
1.95
0 9.5 9.0 8.5 8.0 7.5 7.0 6.5 6.0 5.5 5.0 4.5 4.0 3.5 3.0 2.5 2.0 1.5 1.0 0.5
f1 (ppm)

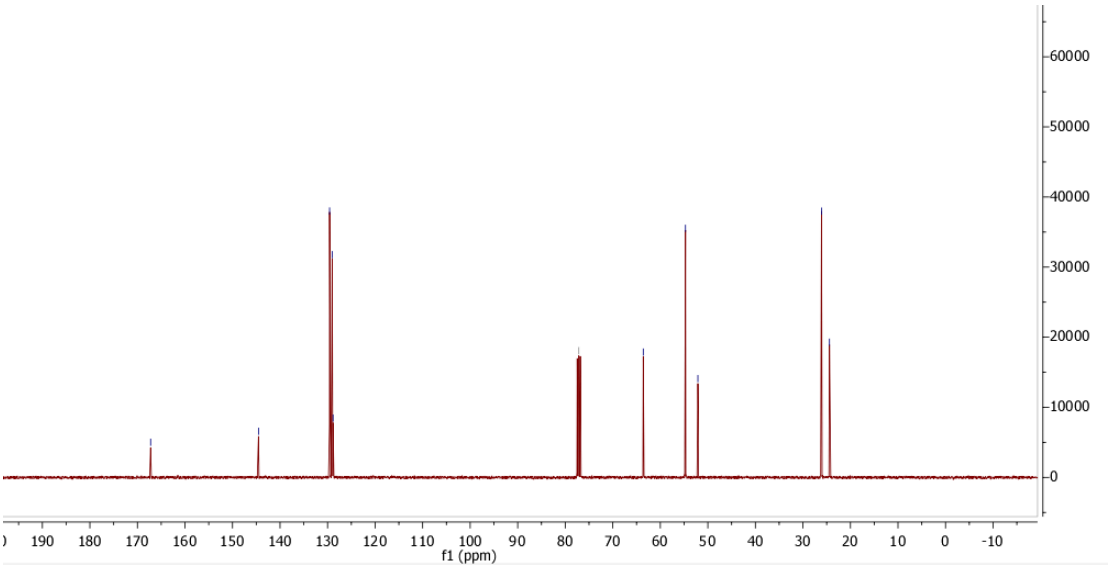
60000
50000
40000
30000
20000
10000
0
190 180 170 160 150 140 130 120 110 100 90 80 70 60 50 40 30 20 10 0 -10
f1 (ppm)

4.2b

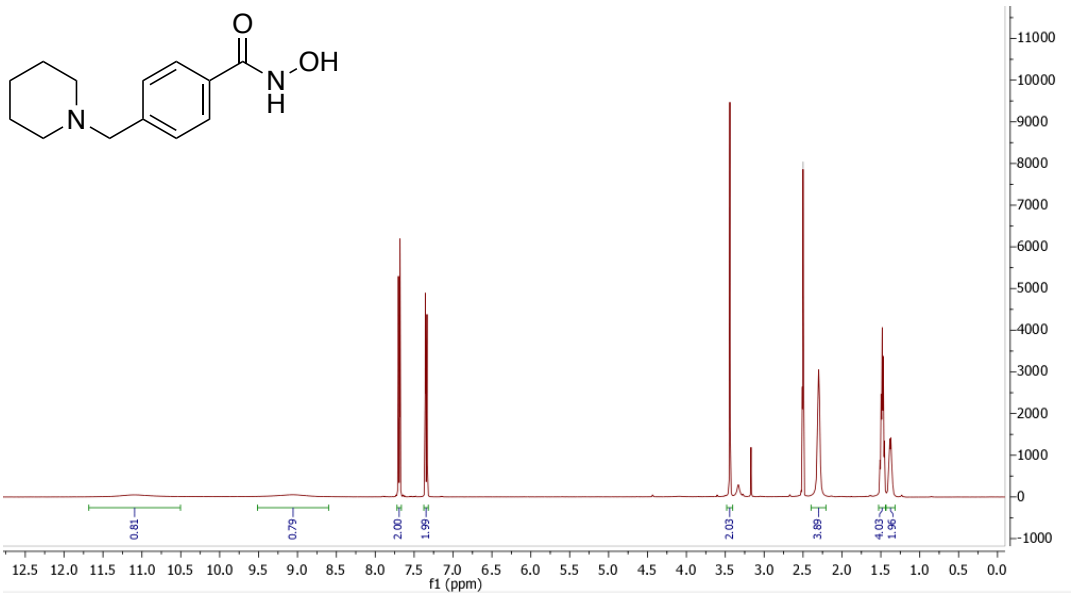

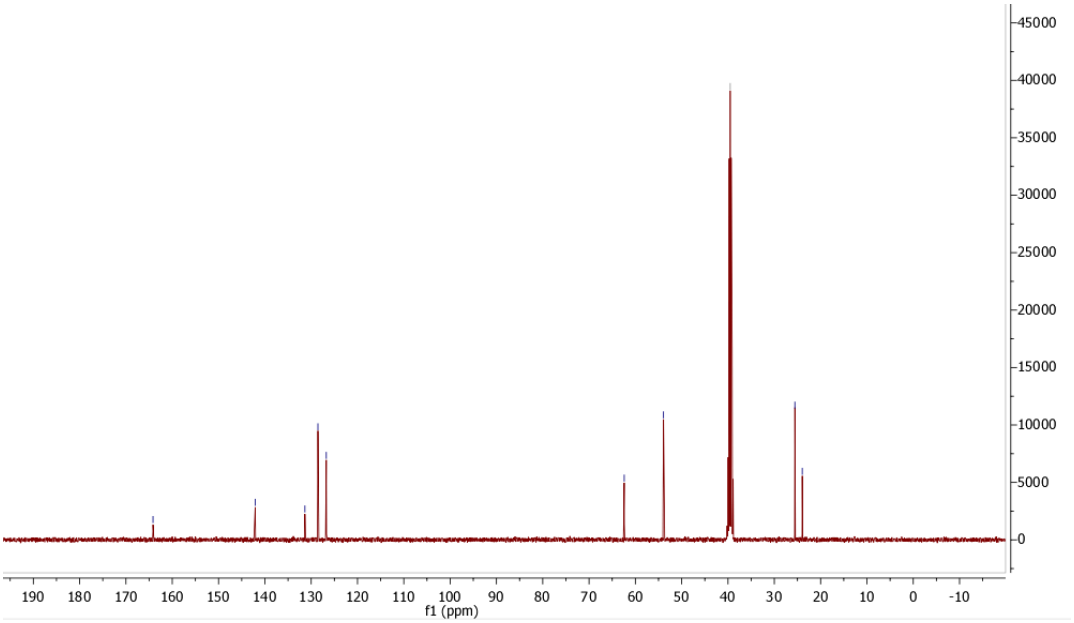

4.1b

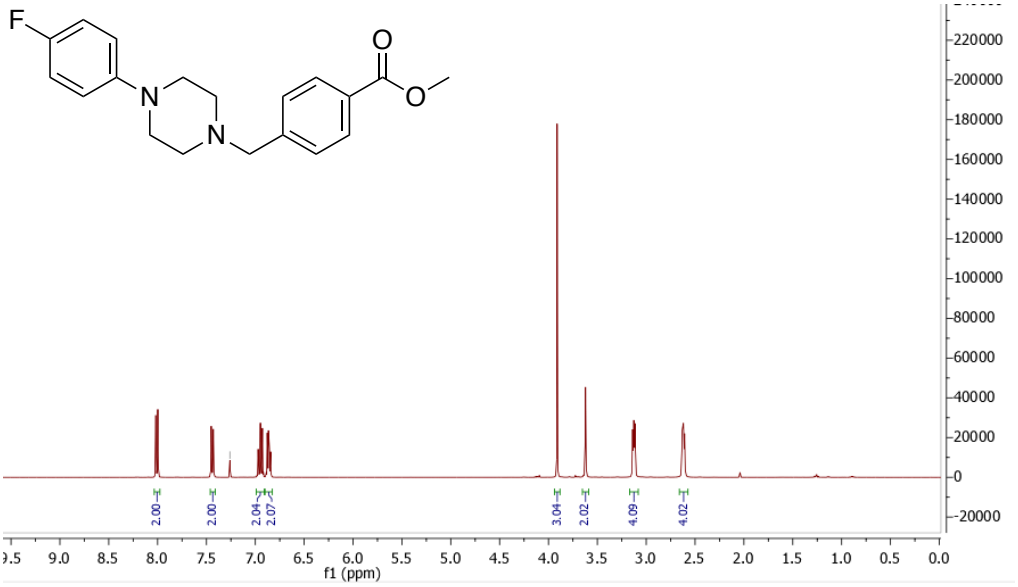

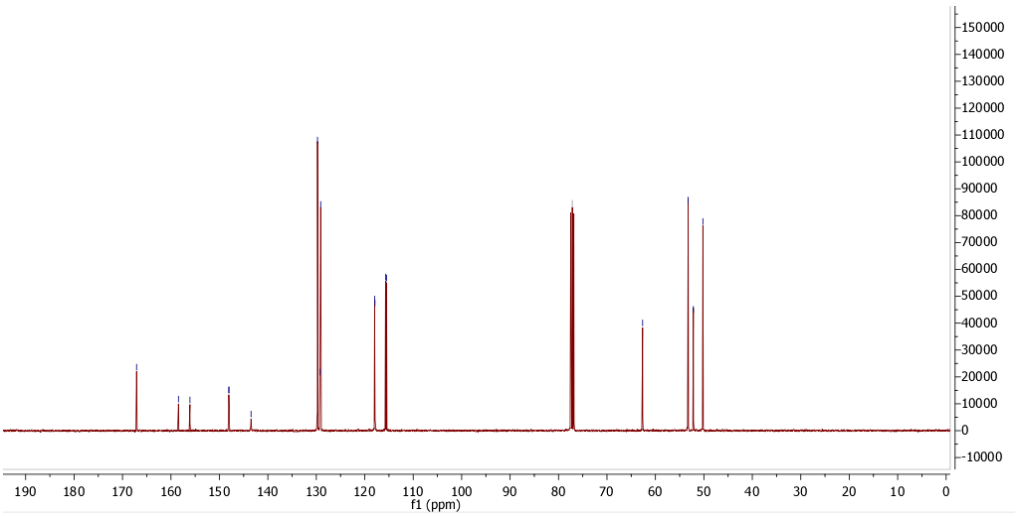

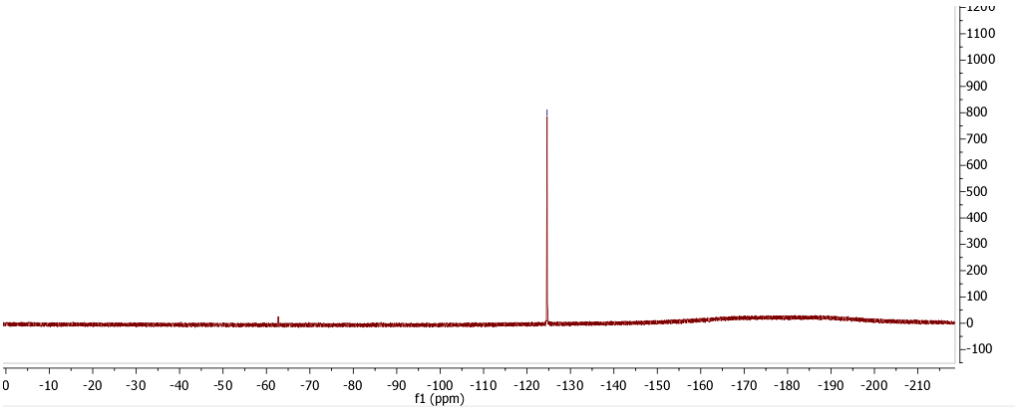

4.2c

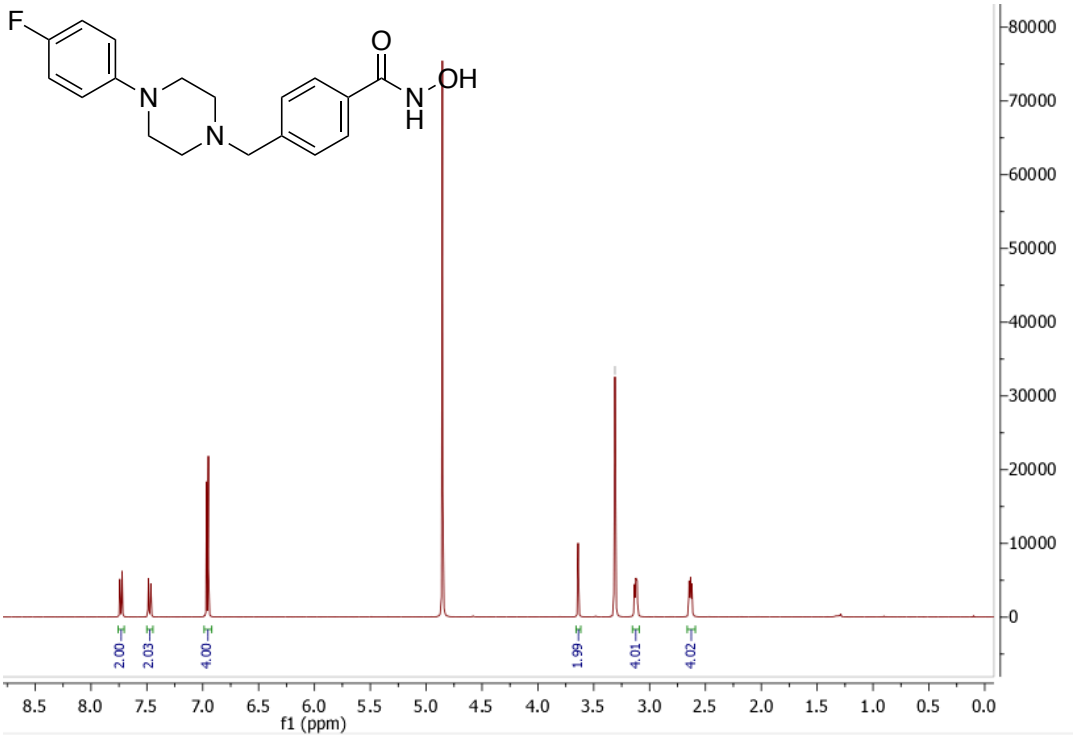

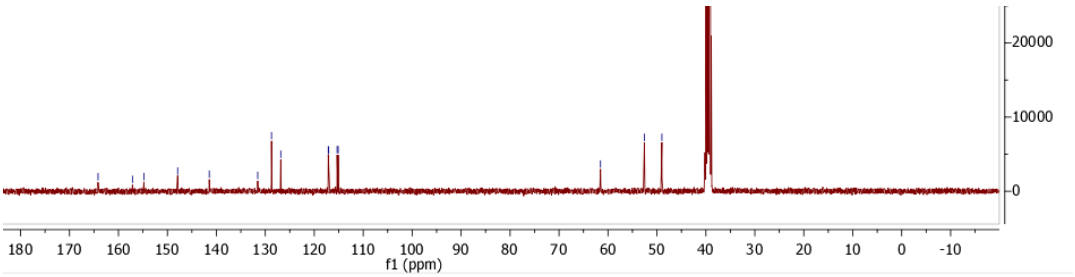

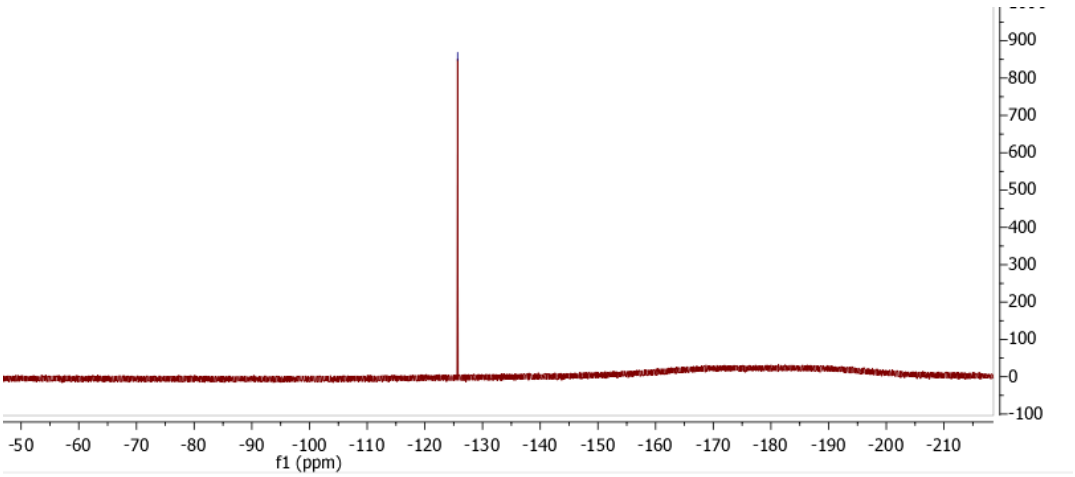

4.1c

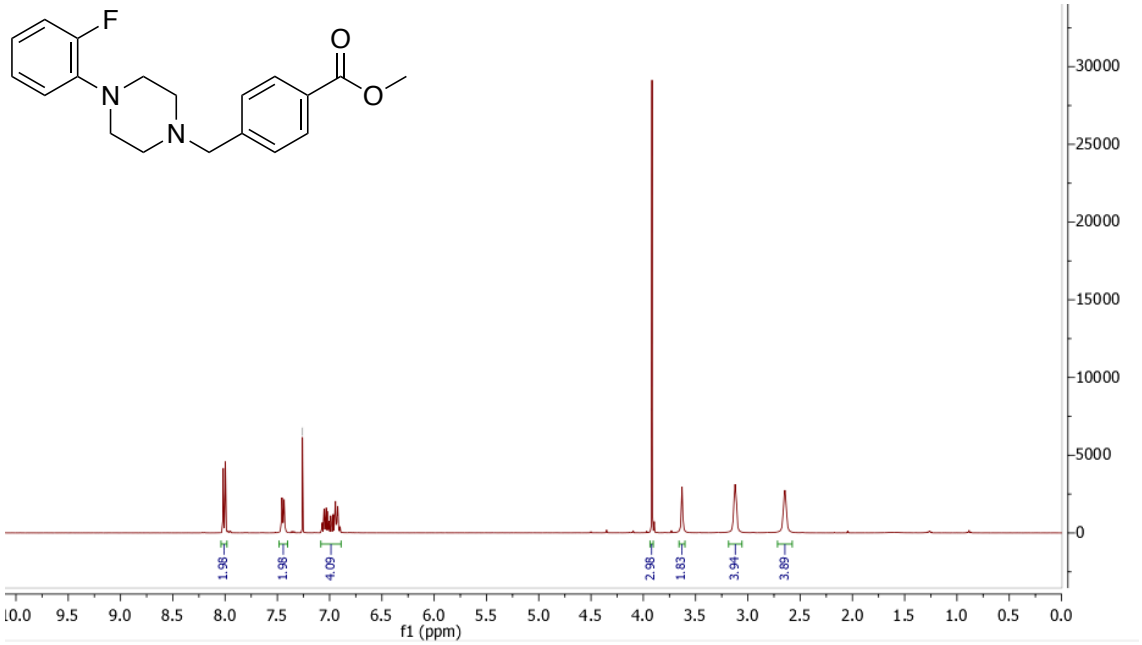

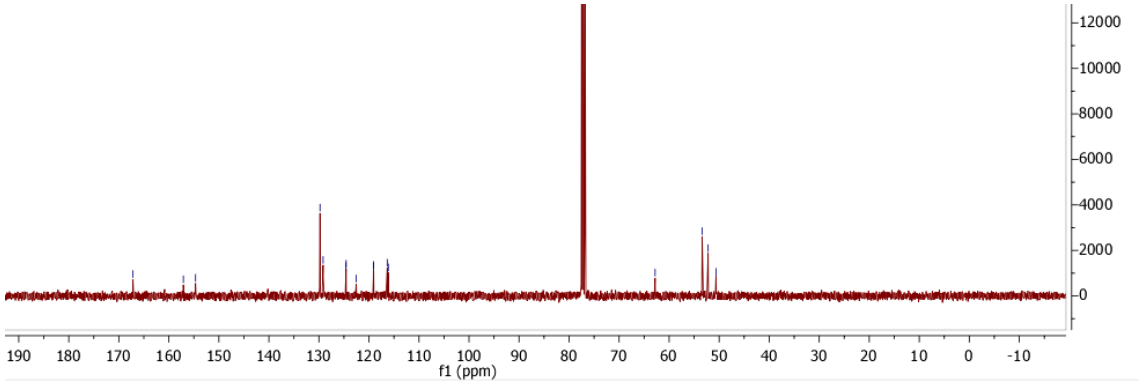

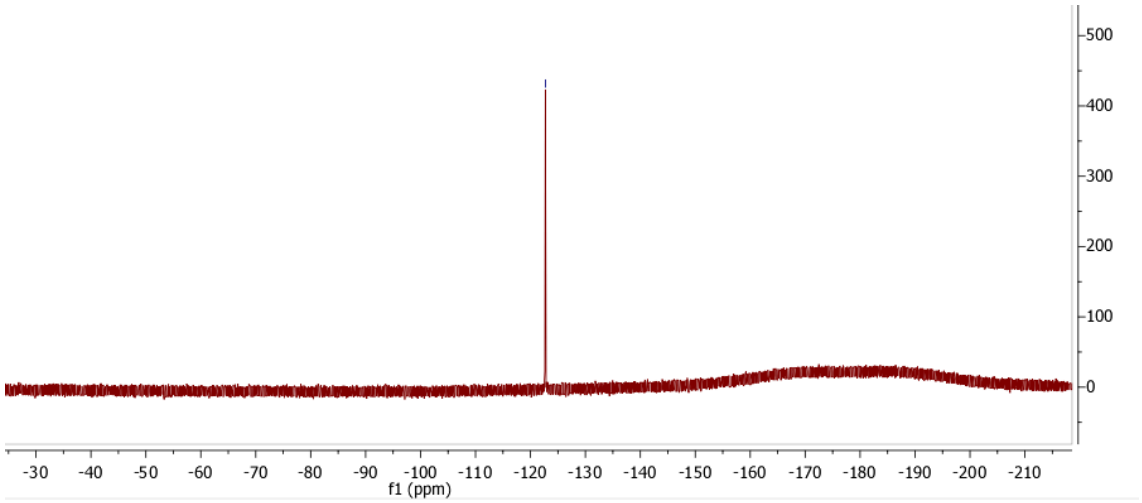

4.2d

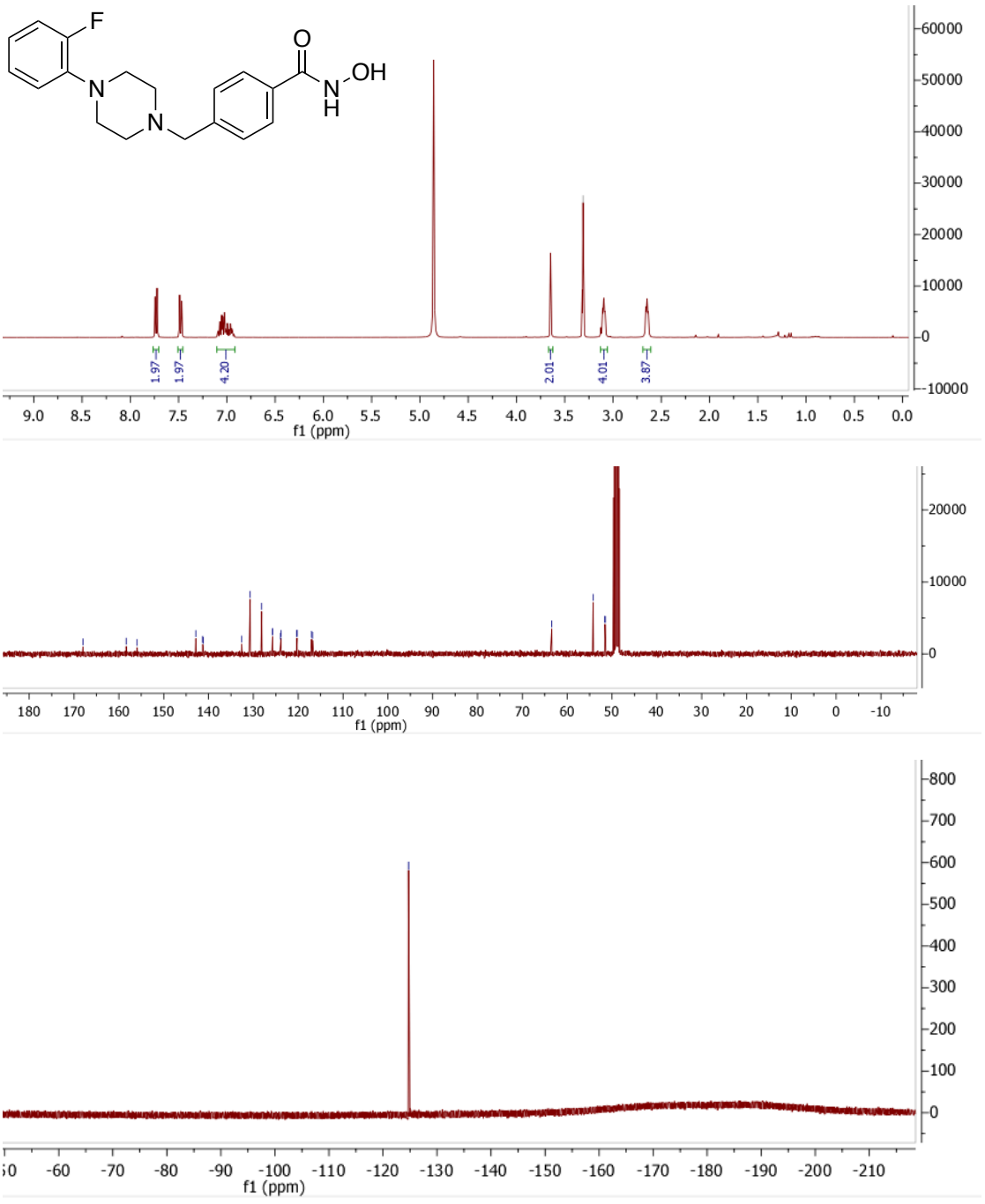

4.1d

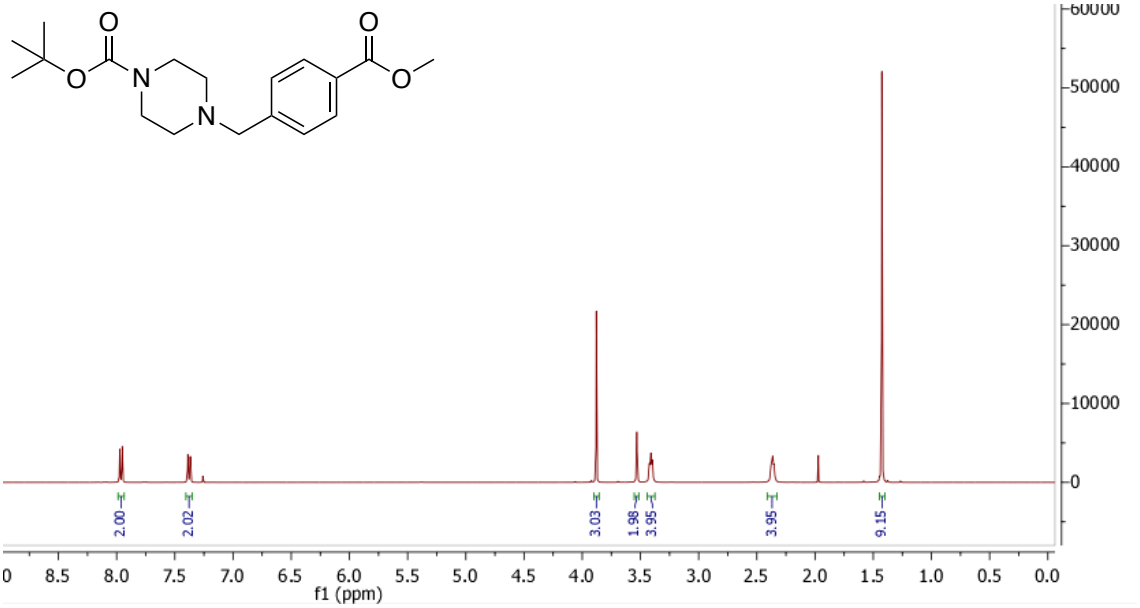

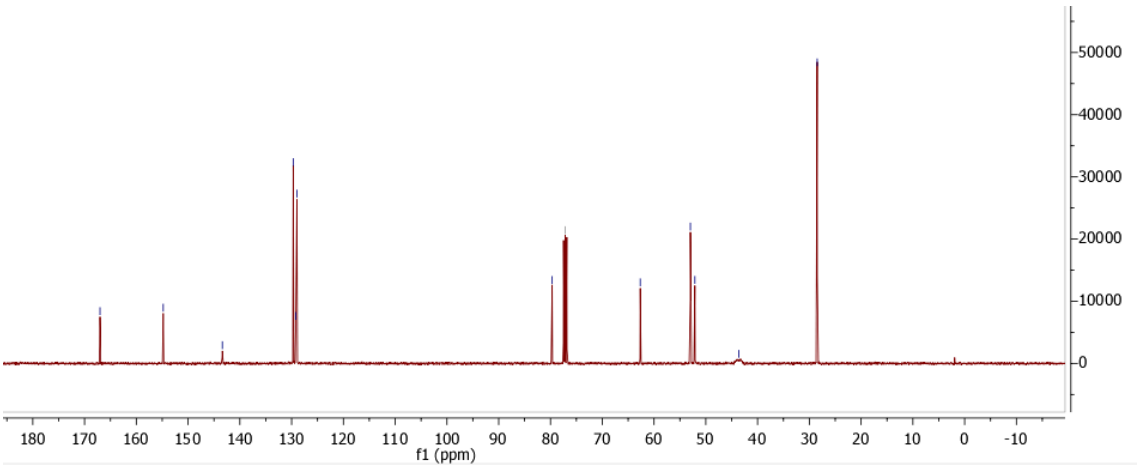

4.2e

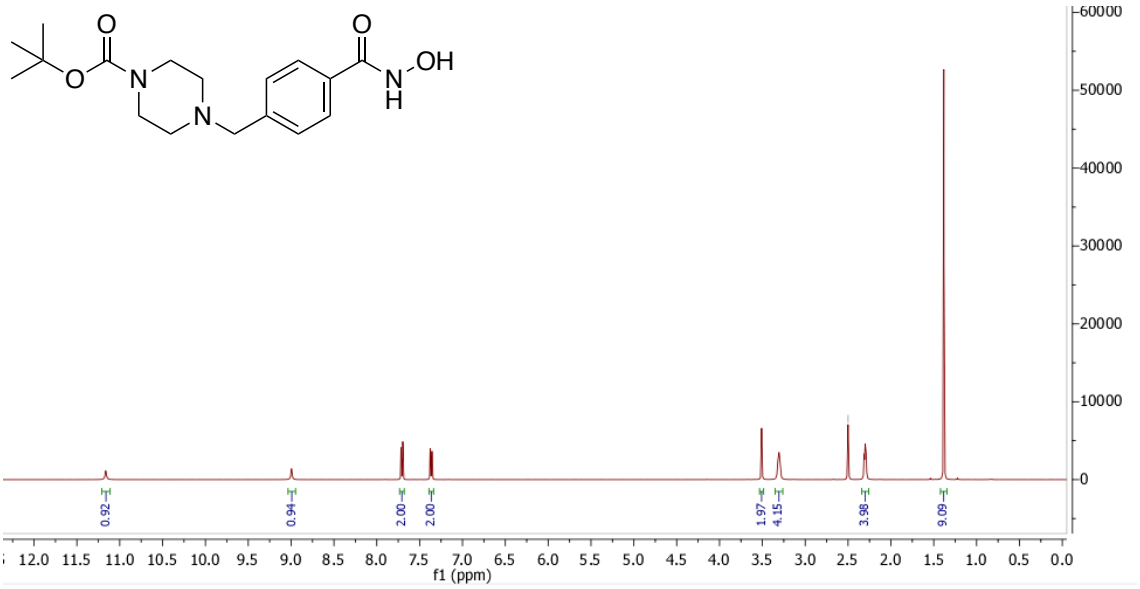
O
O
N
N
O
N
H
OH
60000
50000
40000
30000
20000
10000
0
0.92
0.94
2.00
2.00
1.97
4.15
3.98
9.09
12.0 11.5 11.0 10.5 10.0 9.5 9.0 8.5 8.0 7.5 7.0 6.5 6.0 5.5 5.0 4.5 4.0 3.5 3.0 2.5 2.0 1.5 1.0 0.5 0.0
f1 (ppm)

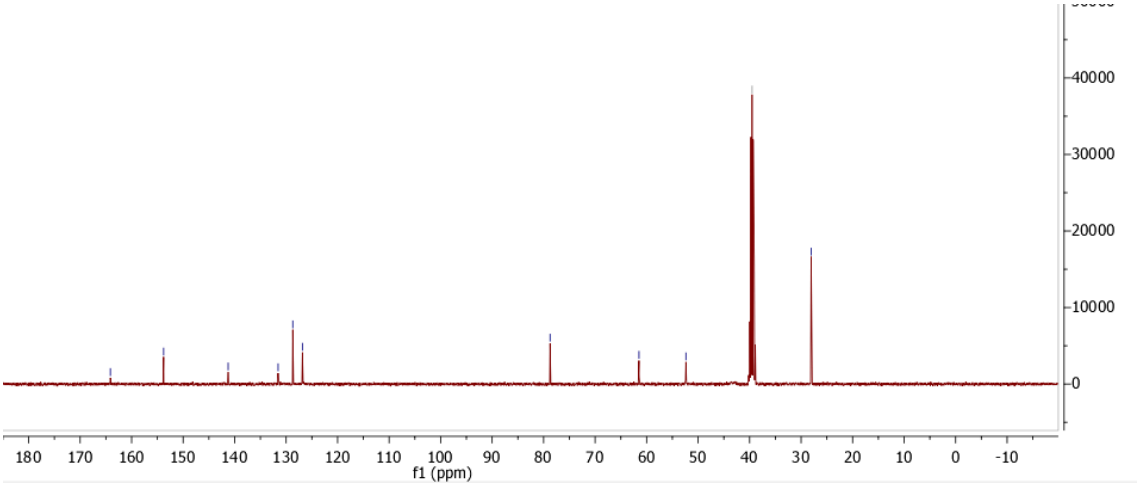
40000
30000
20000
10000
0
180 170 160 150 140 130 120 110 100 90 80 70 60 50 40 30 20 10 0 -10
f1 (ppm)

4.2f

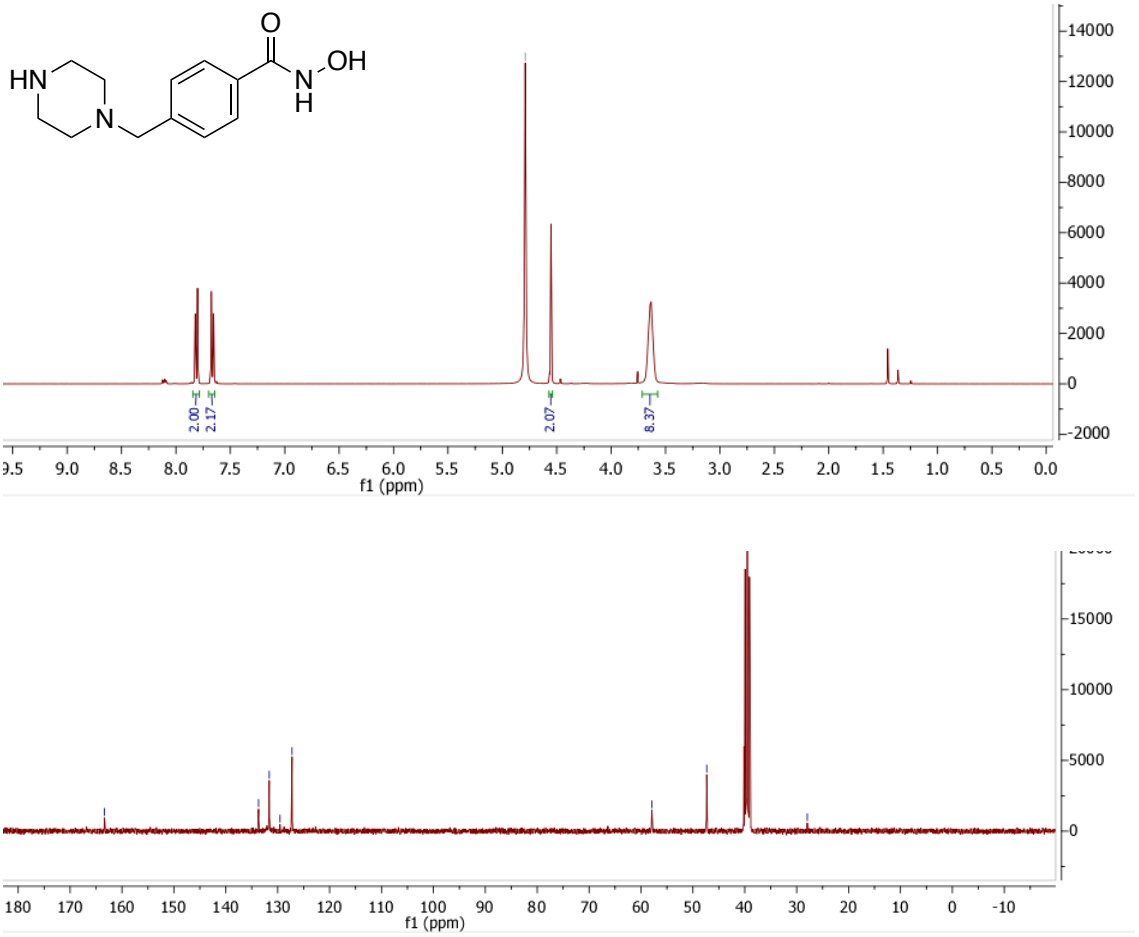

Meta series.

4.3a

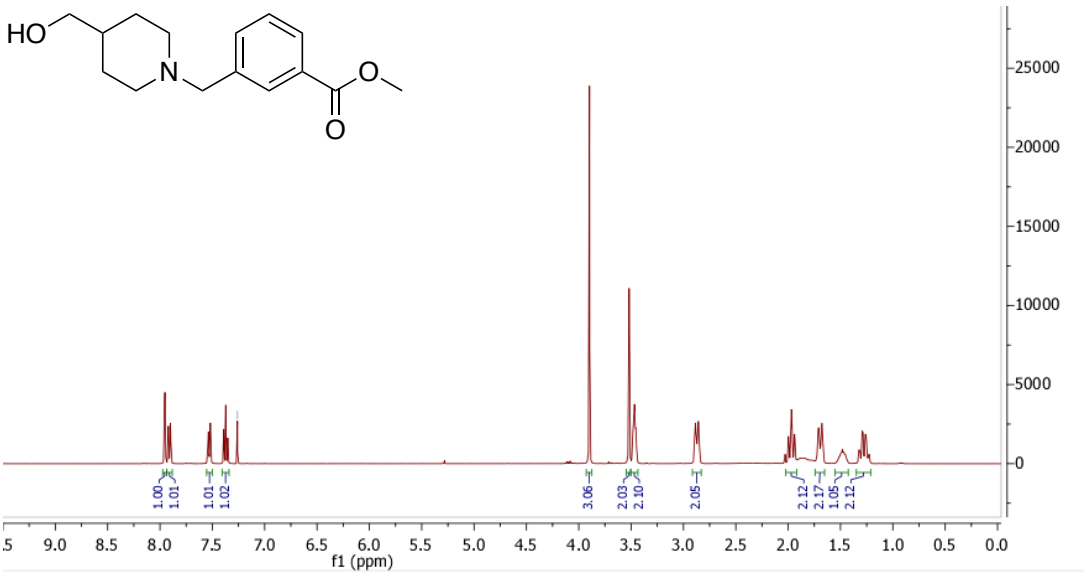

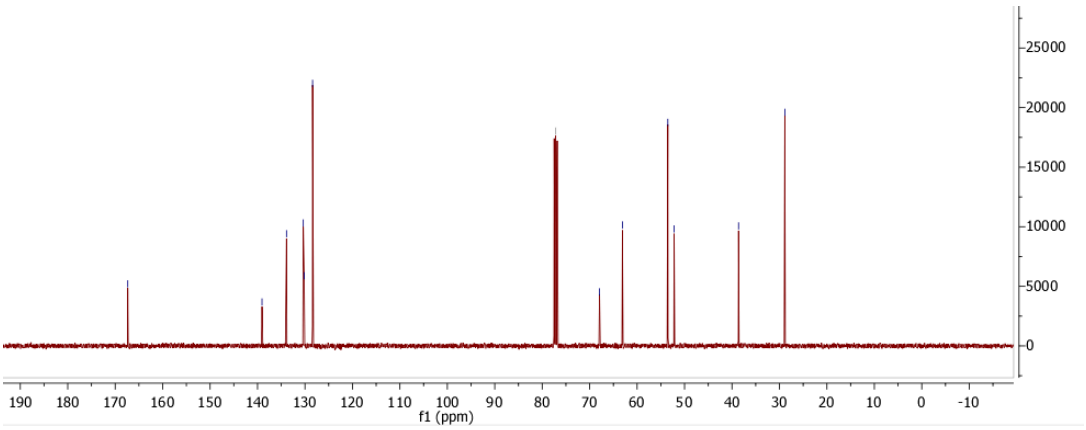

4.3b

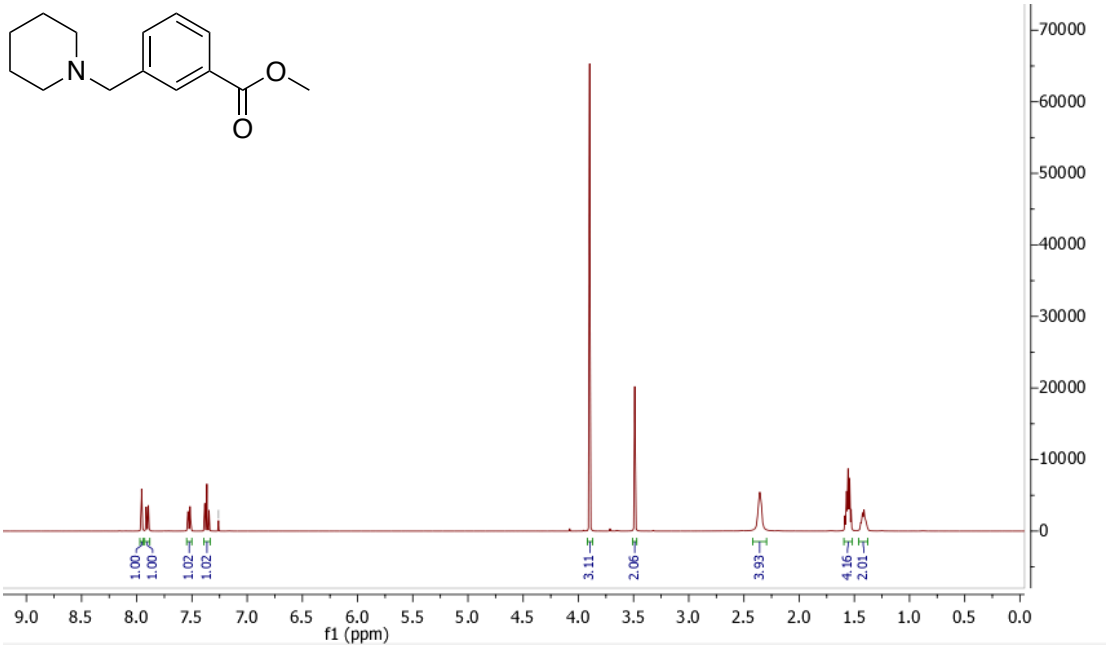
N
O
O
70000
60000
50000
40000
30000
20000
10000
0
1.00
1.00
1.02
1.02
3.11
2.06
3.93
4.16
2.01
9.0 8.5 8.0 7.5 7.0 6.5 6.0 5.5 5.0 4.5 4.0 3.5 3.0 2.5 2.0 1.5 1.0 0.5 0.0
f1 (ppm)

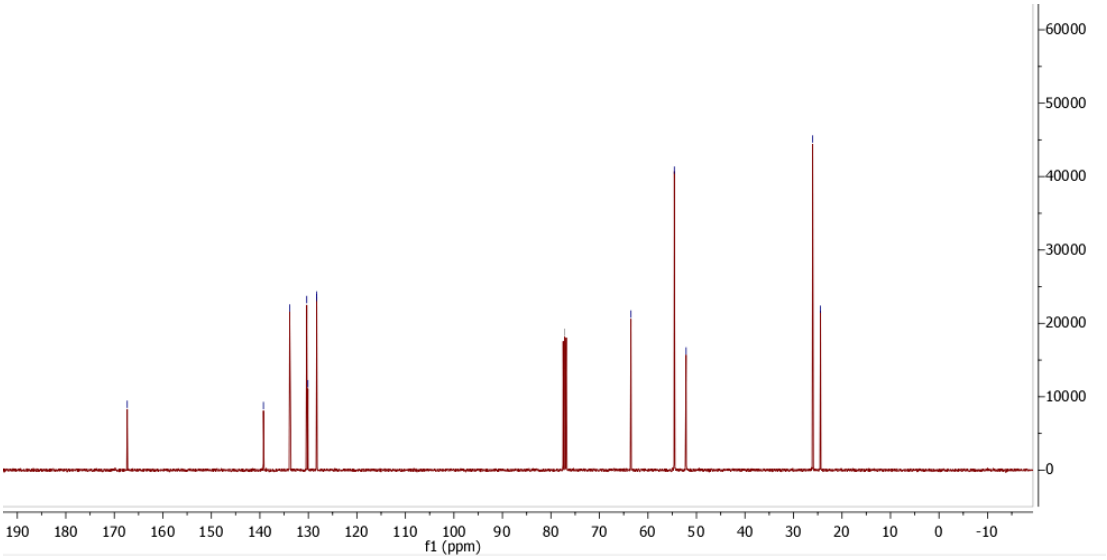
60000
50000
40000
30000
20000
10000
0
190 180 170 160 150 140 130 120 110 100 90 80 70 60 50 40 30 20 10 0 -10
f1 (ppm)

4.3c

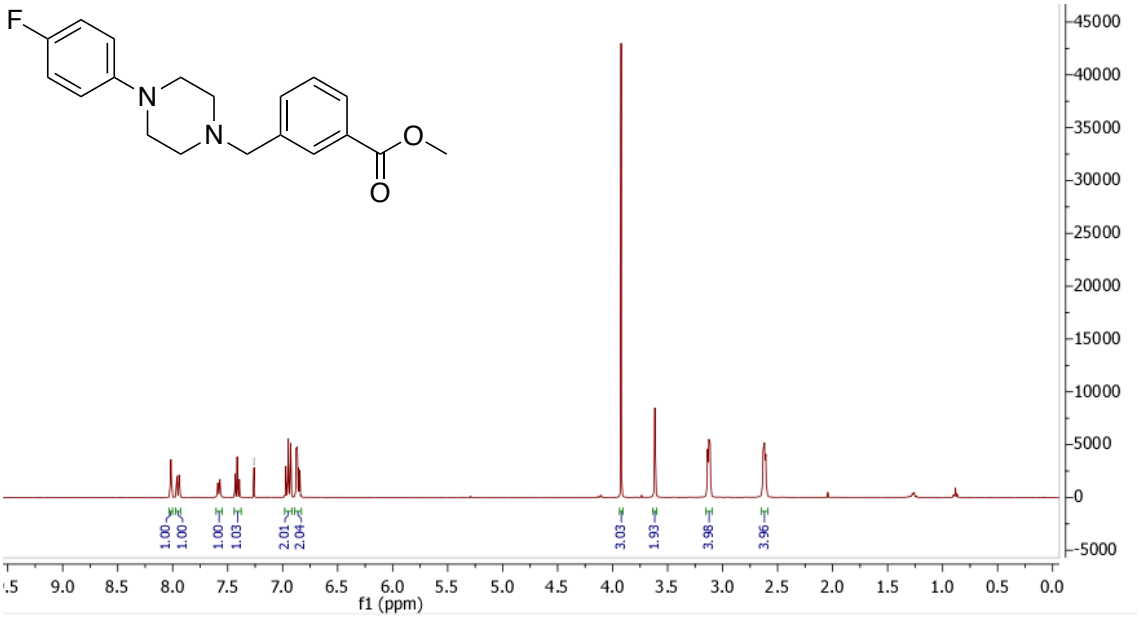
F
N
N
O
O
1.00
1.00
1.00
1.03
2.01
2.04
3.03
1.93
3.98
3.96
f1 (ppm)

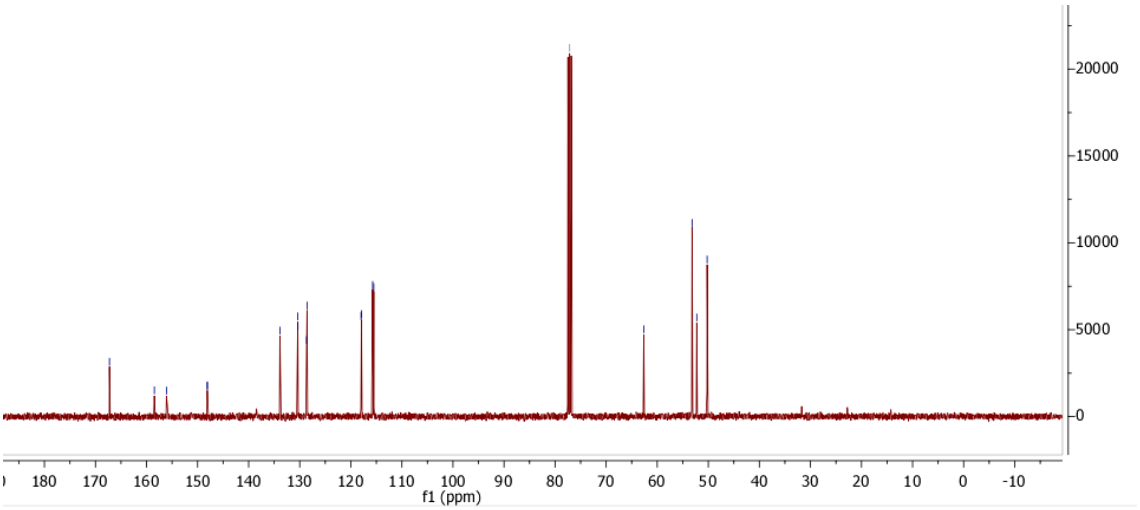
f1 (ppm)

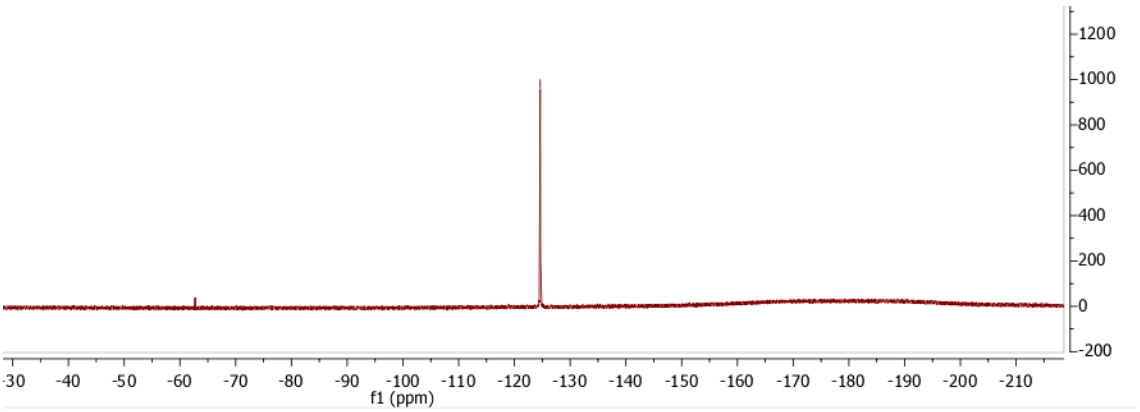
f1 (ppm)

4.3d

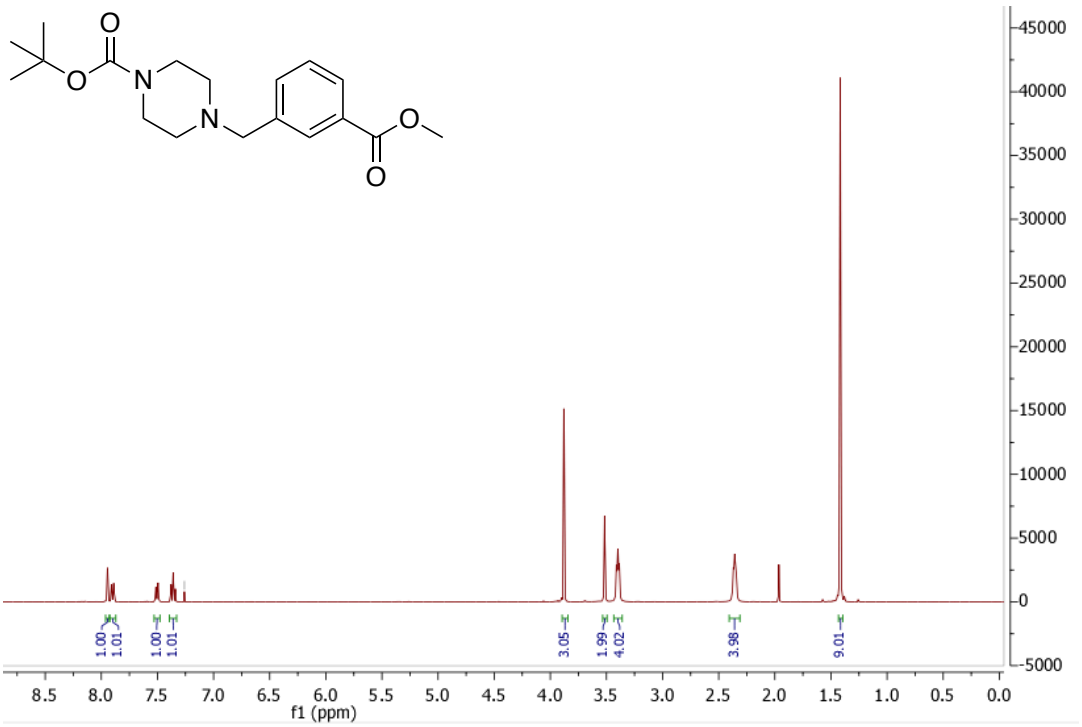

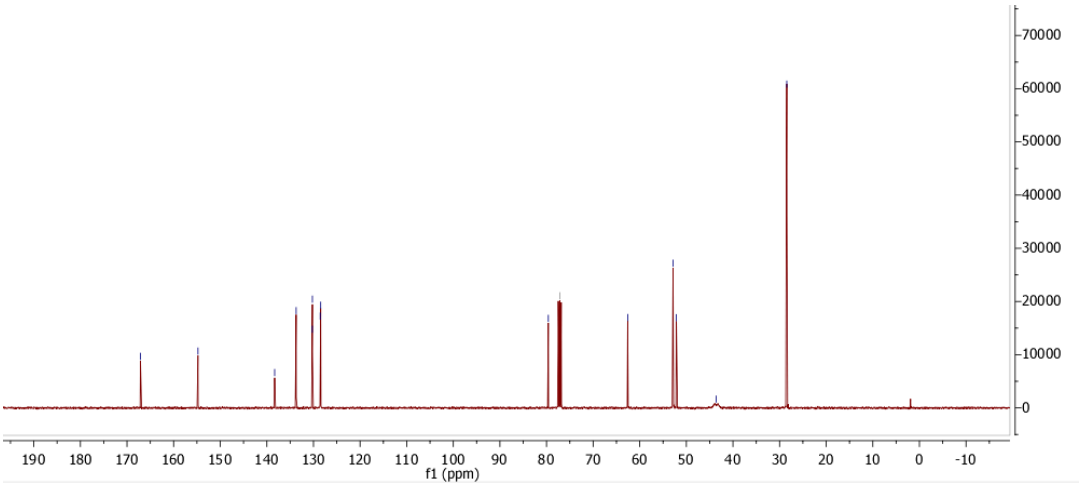

4.3e

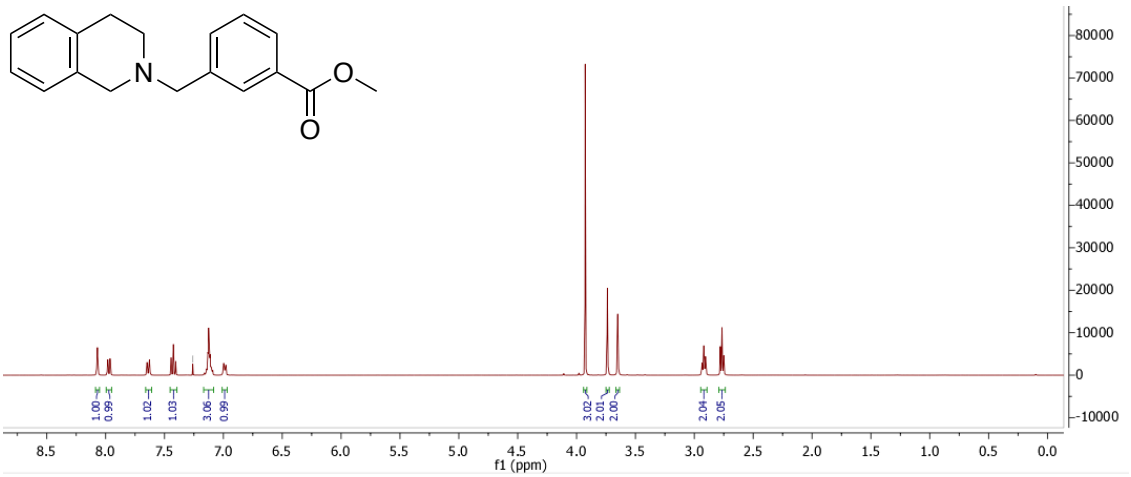

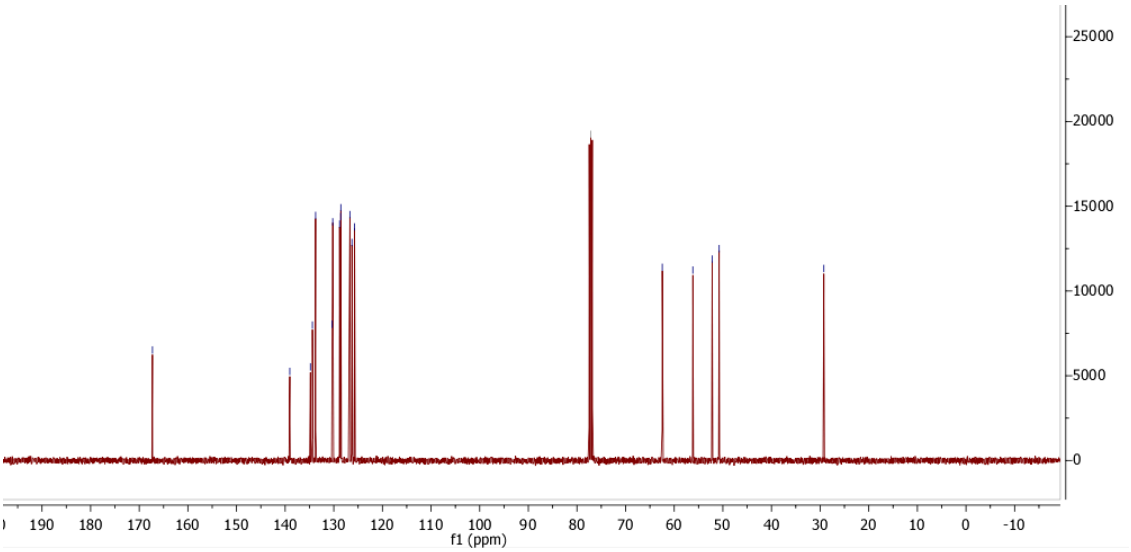

4.4a

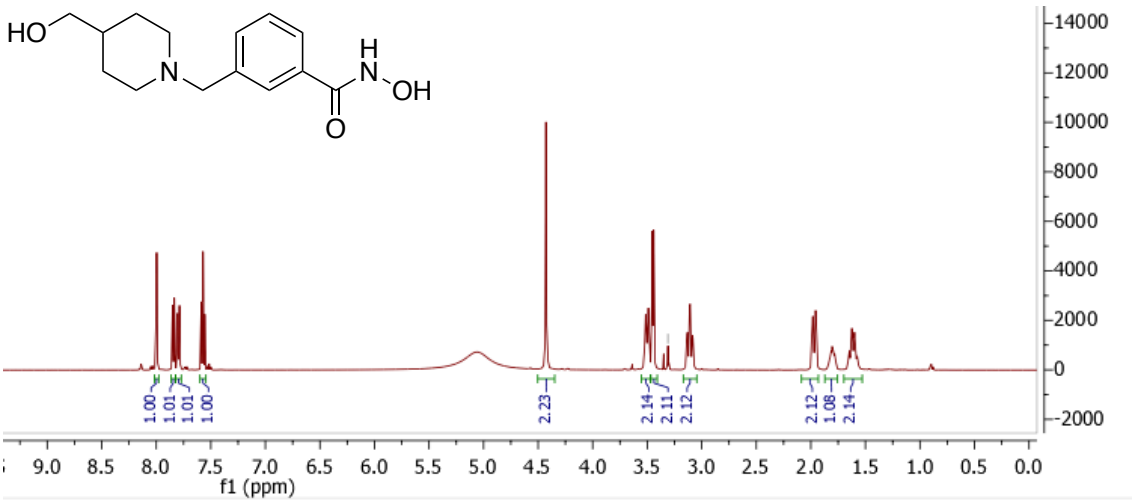
HO
N
H
N
OH
O
1.00
1.01
1.01
1.00
2.23
2.14
2.11
2.12
2.12
1.08
2.14
f1 (ppm)

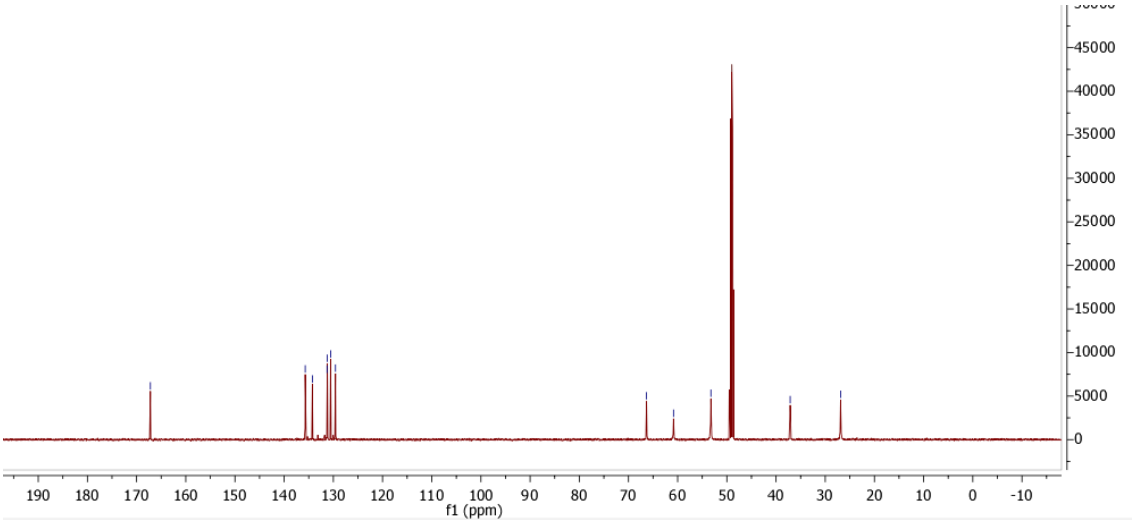
f1 (ppm)

4.4b

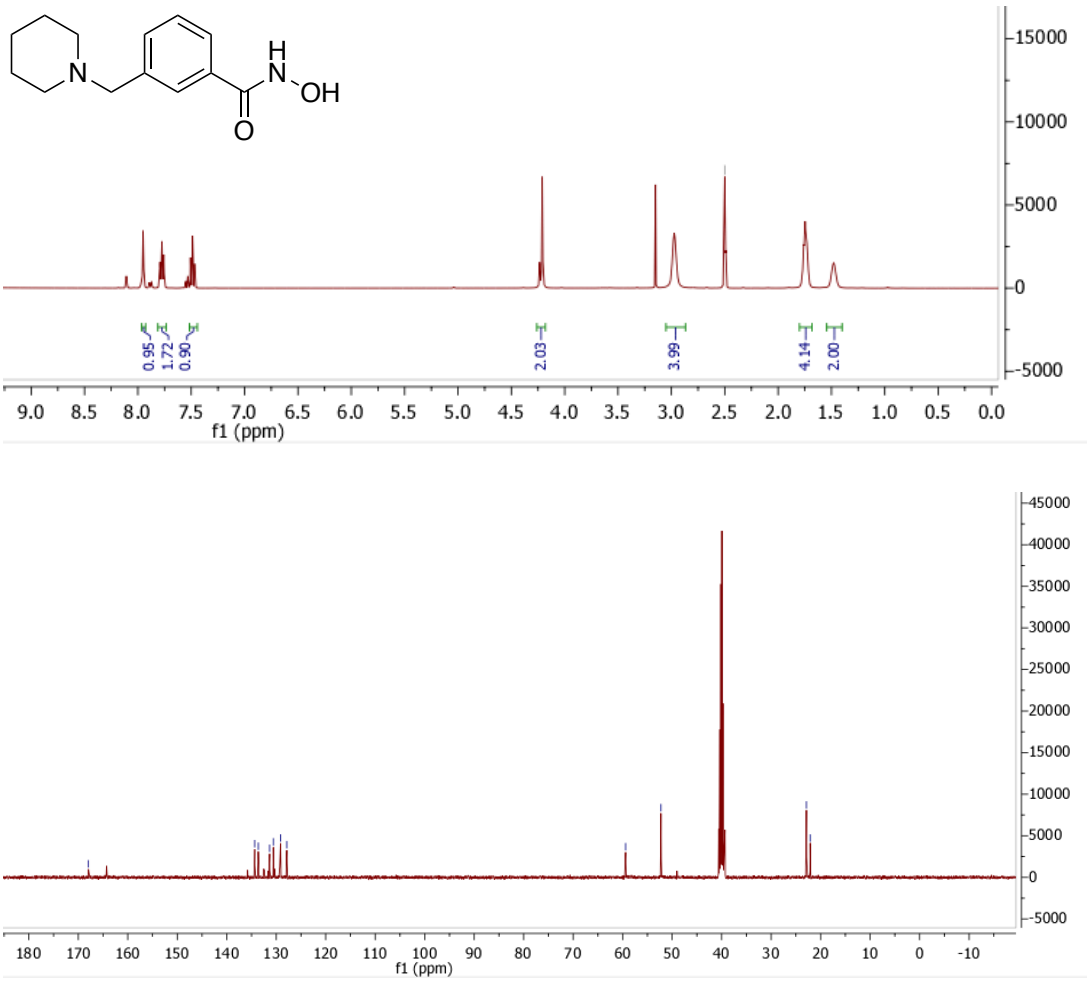
N
H
N
OH
O
15000
10000
5000
0
-5000
0.95
1.72
0.90
2.03
3.99
4.14
2.00
9.0 8.5 8.0 7.5 7.0 6.5 6.0 5.5 5.0 4.5 4.0 3.5 3.0 2.5 2.0 1.5 1.0 0.5 0.0
f1 (ppm)
45000
40000
35000
30000
25000
20000
15000
10000
5000
0
-5000
180 170 160 150 140 130 120 110 100 90 80 70 60 50 40 30 20 10 0 -10
f1 (ppm)

4.4c

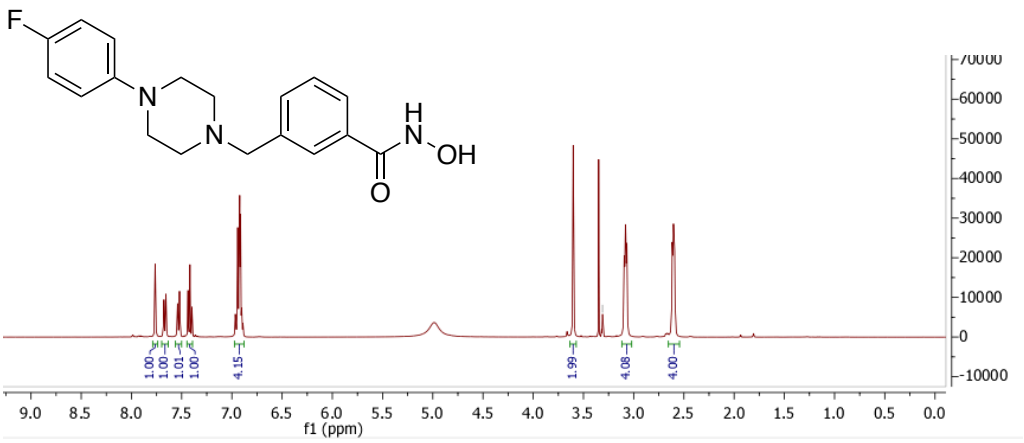

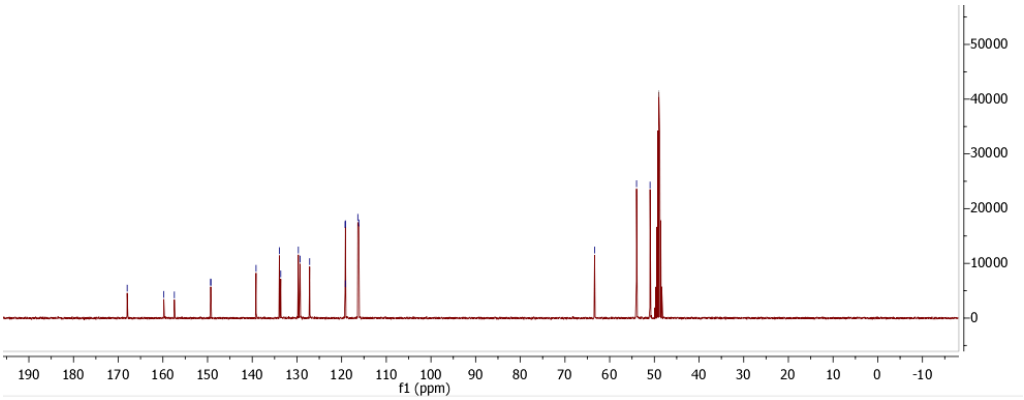

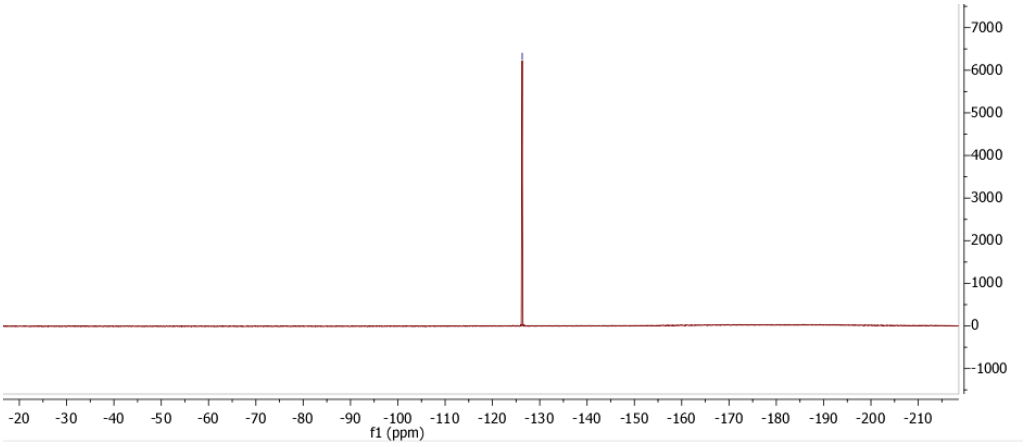

4.4d

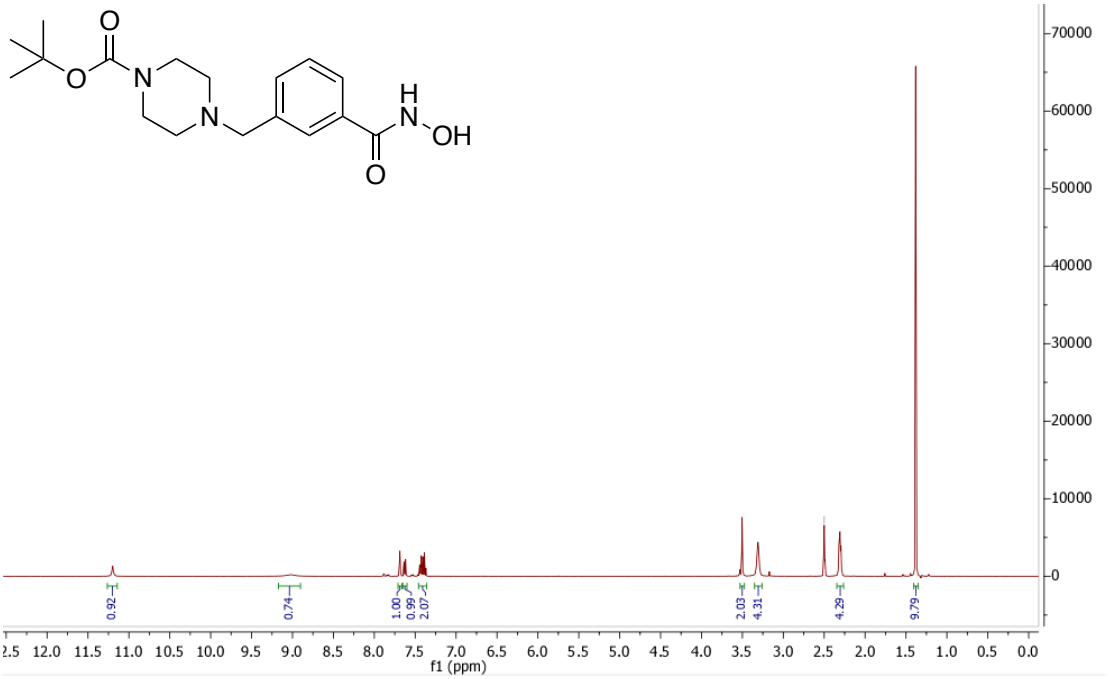

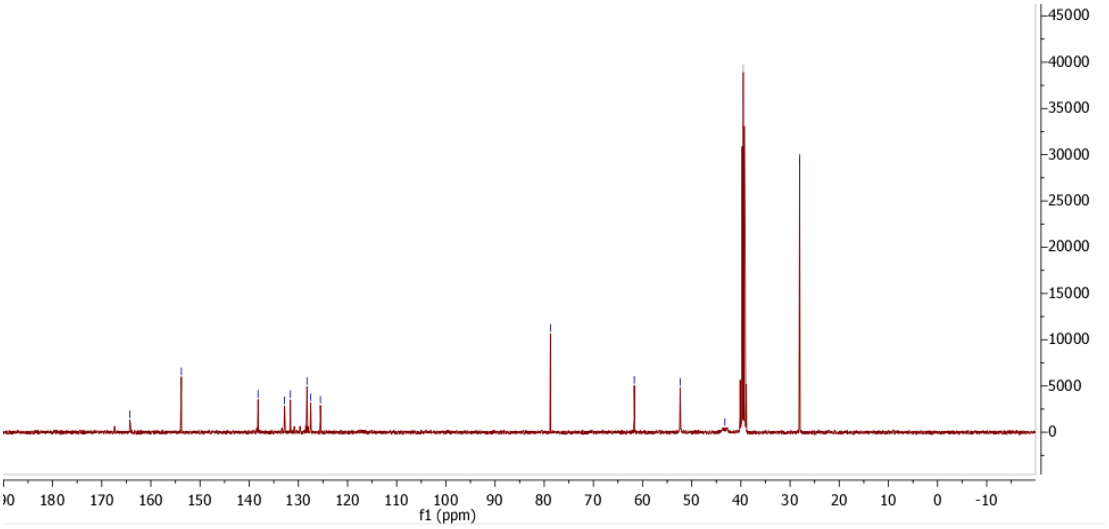

4.4e

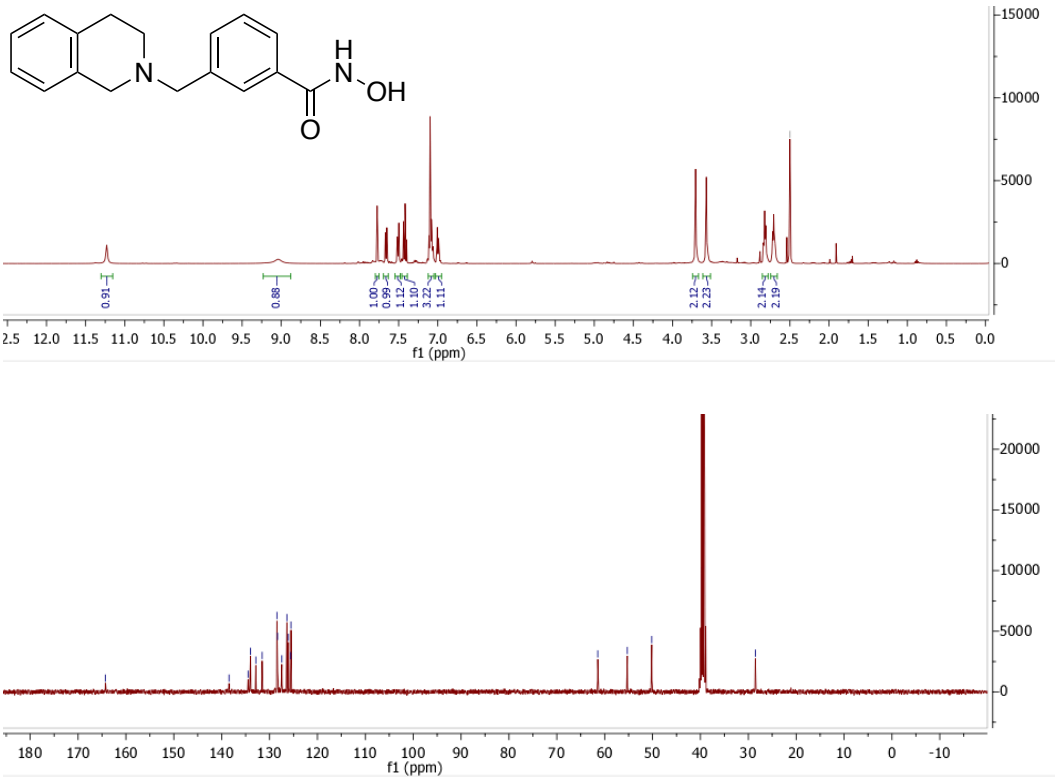
H
N
OH
O
15000
10000
5000
0
0.91
0.88
1.00
0.99
1.12
1.10
3.21
1.11
2.12
2.23
2.14
2.19
2.5 12.0 11.5 11.0 10.5 10.0 9.5 9.0 8.5 8.0 7.5 7.0 6.5 6.0 5.5 5.0 4.5 4.0 3.5 3.0 2.5 2.0 1.5 1.0 0.5 0.0
f1 (ppm)
20000
15000
10000
5000
0
180 170 160 150 140 130 120 110 100 90 80 70 60 50 40 30 20 10 0 -10
f1 (ppm)

4.4f

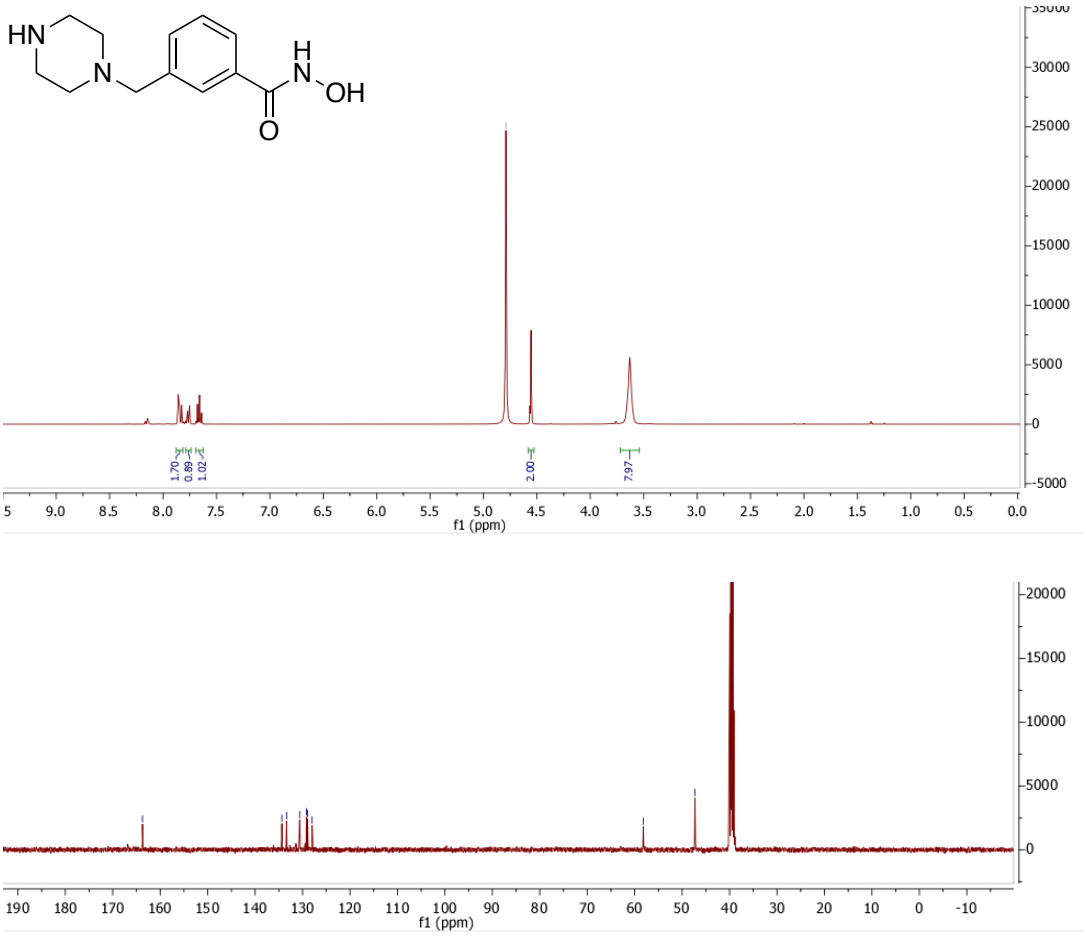

Ortho series

4.5a

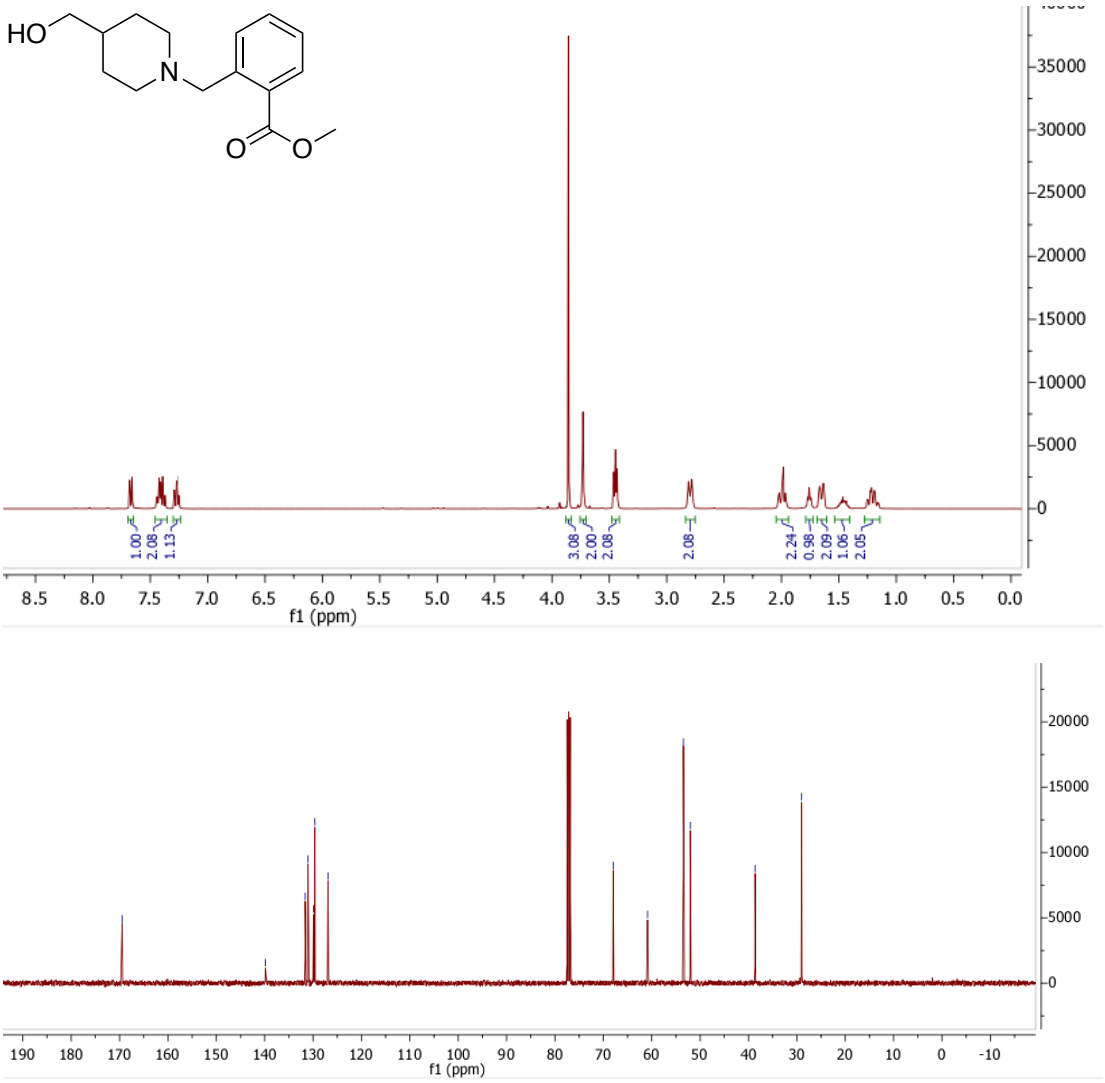

4.5b

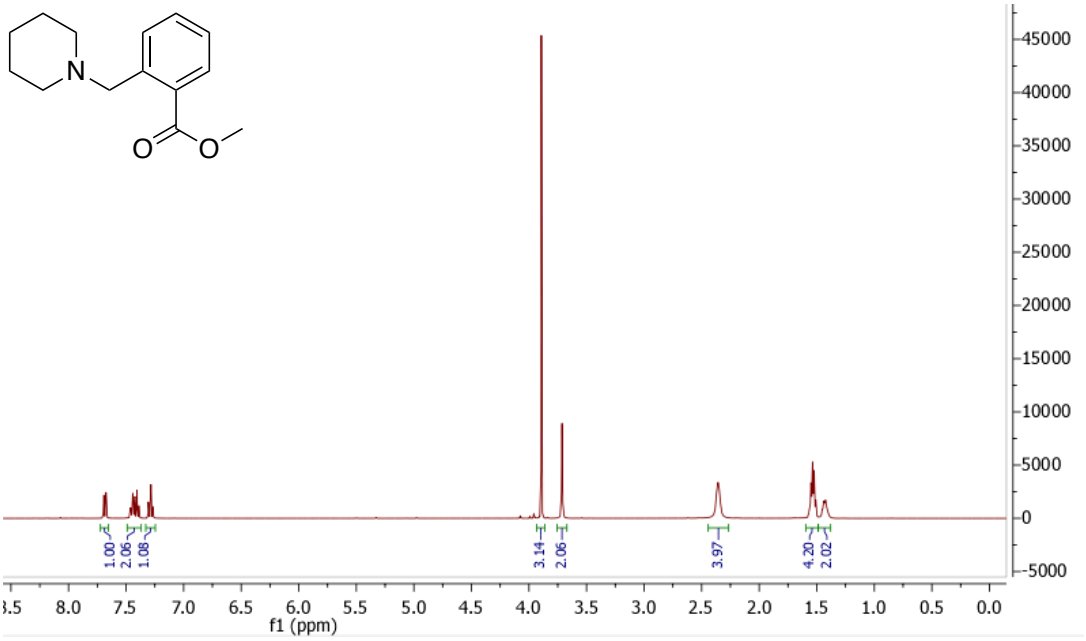
N
O
O
45000
40000
35000
30000
25000
20000
15000
10000
5000
0
-5000
1.00
2.06
1.08
3.14
2.06
3.97
4.20
2.02
8.0
7.5
7.0
6.5
6.0
5.5
5.0
4.5
4.0
3.5
3.0
2.5
2.0
1.5
1.0
0.5
0.0
f1 (ppm)

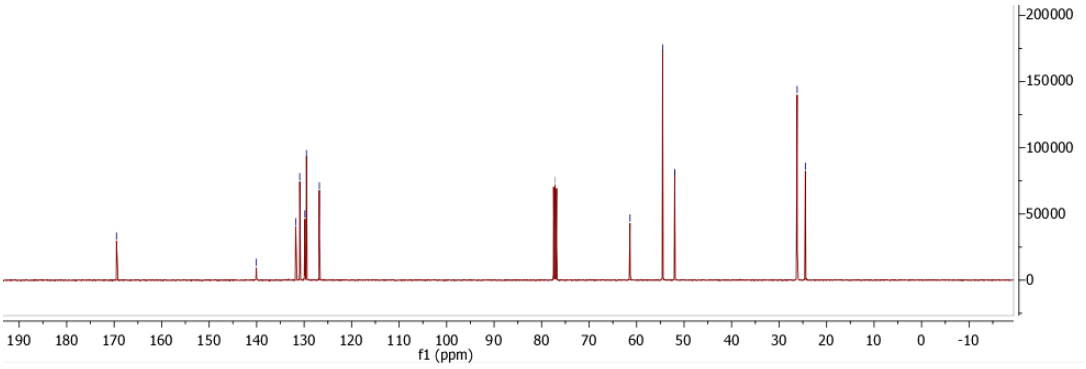
200000
150000
100000
50000
0
190
180
170
160
150
140
130
120
110
100
90
80
70
60
50
40
30
20
10
0
-10
f1 (ppm)

4.5c

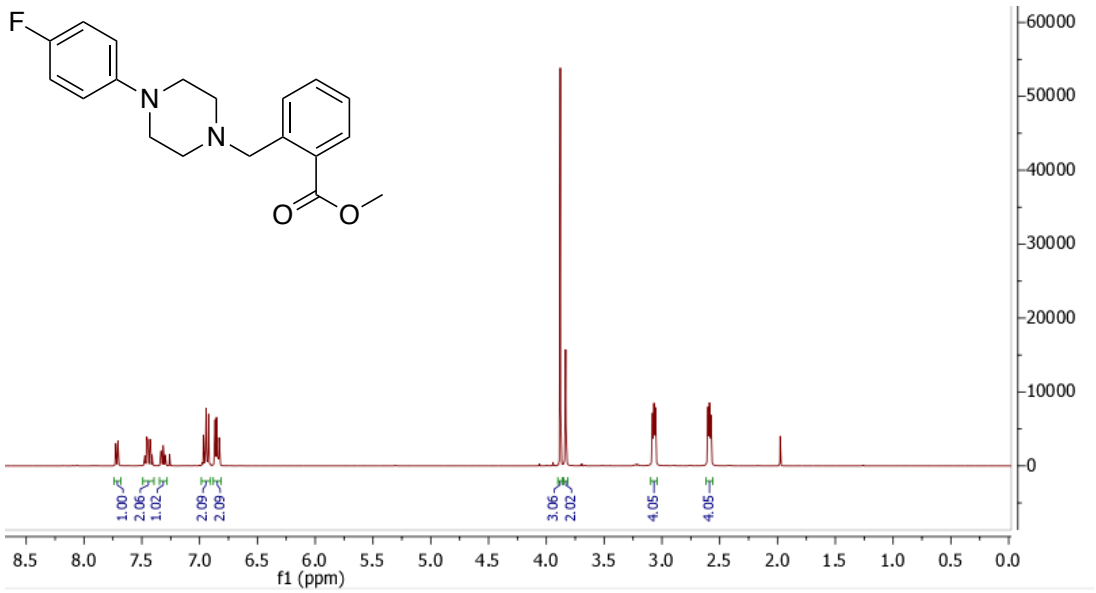

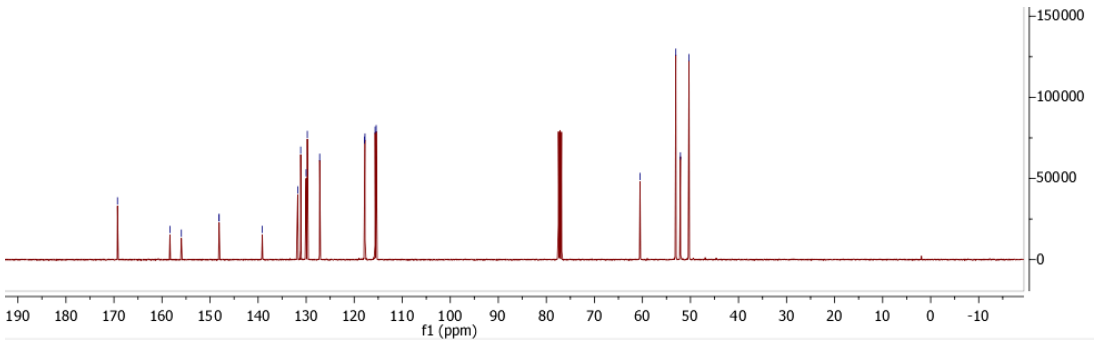

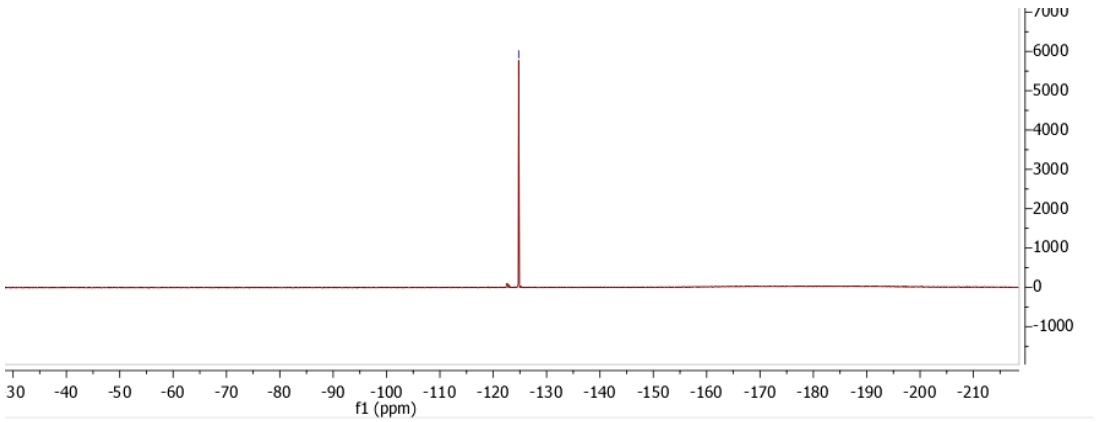

4.5d

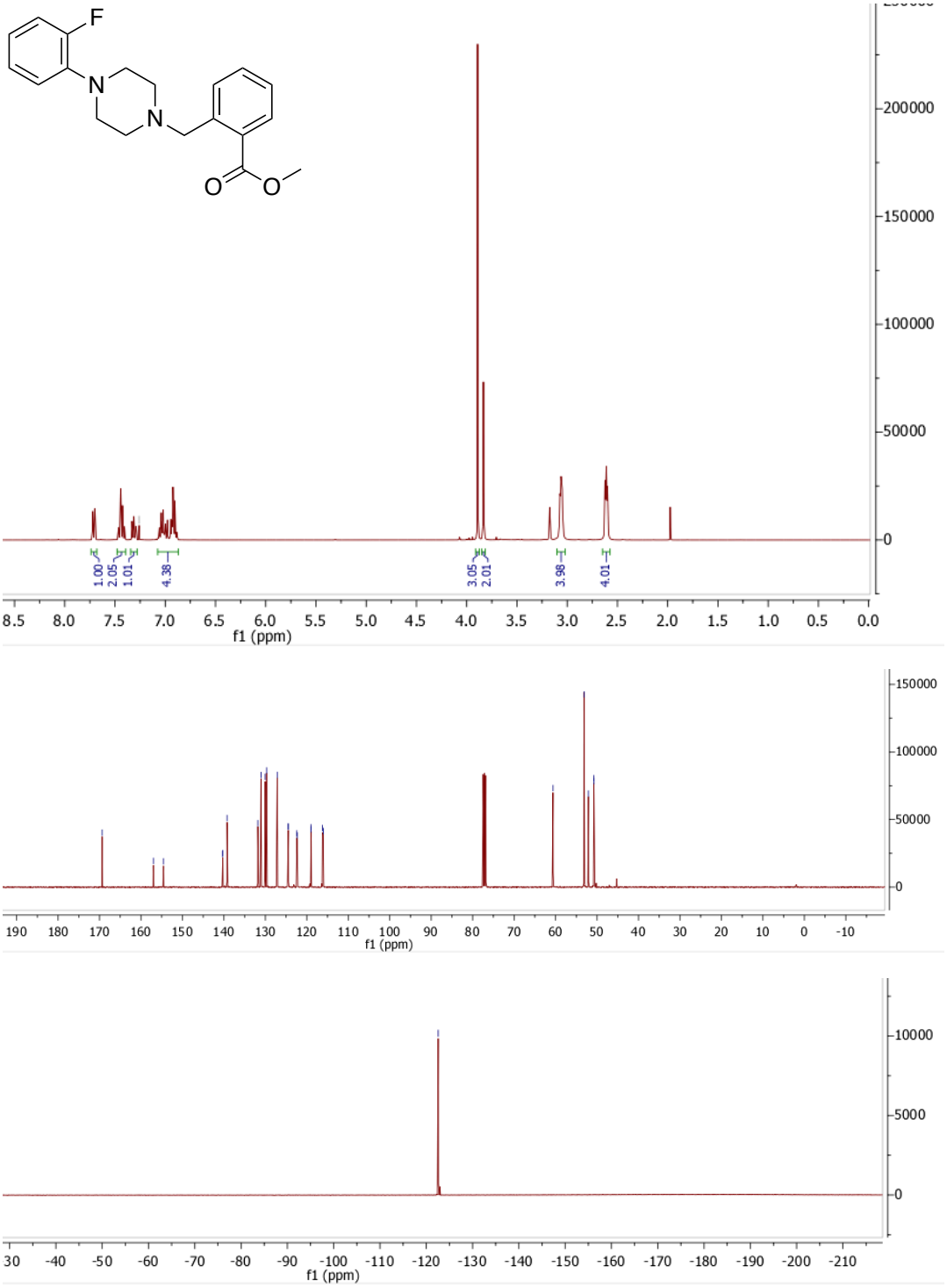

4.5e

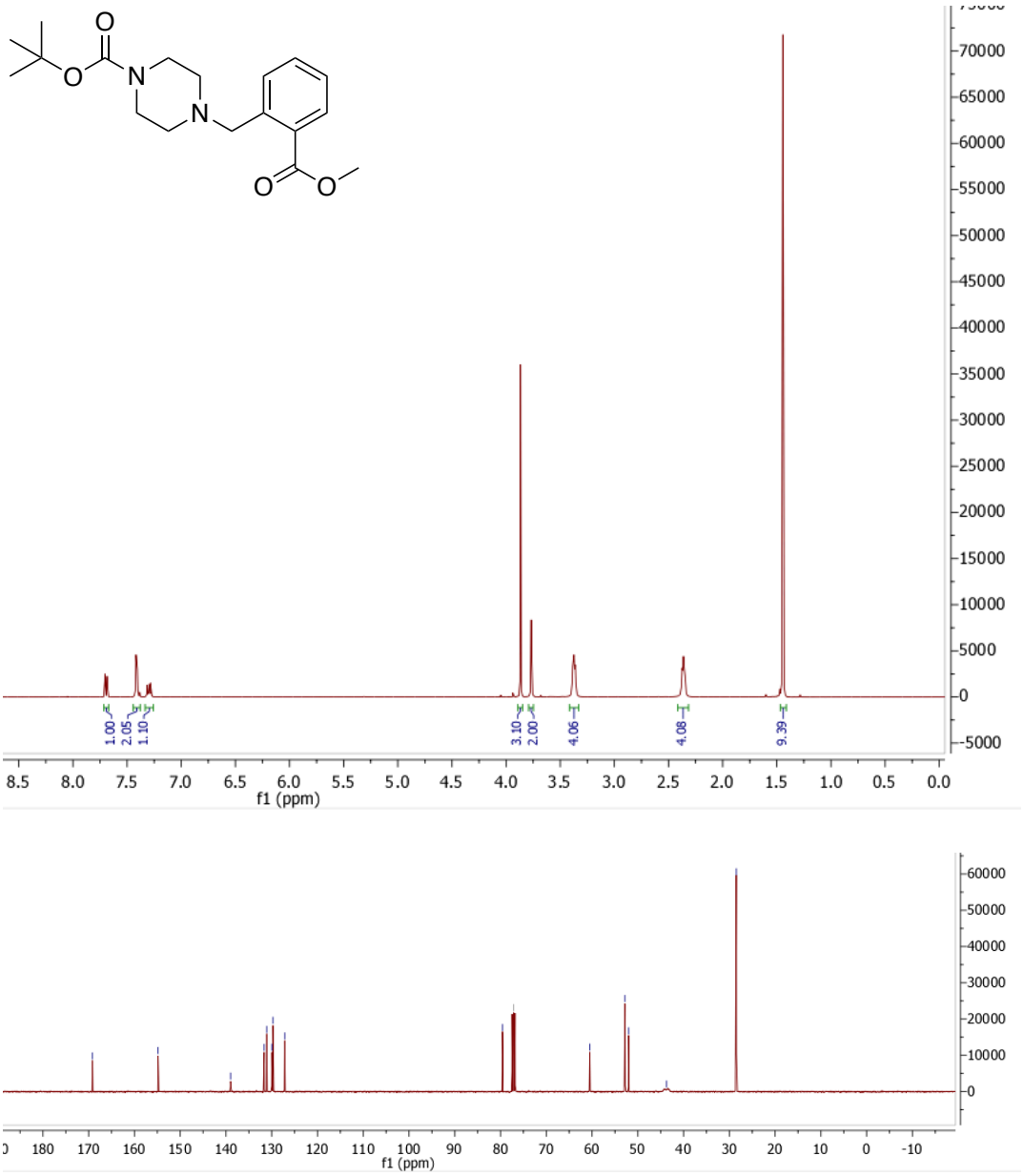

4.5f

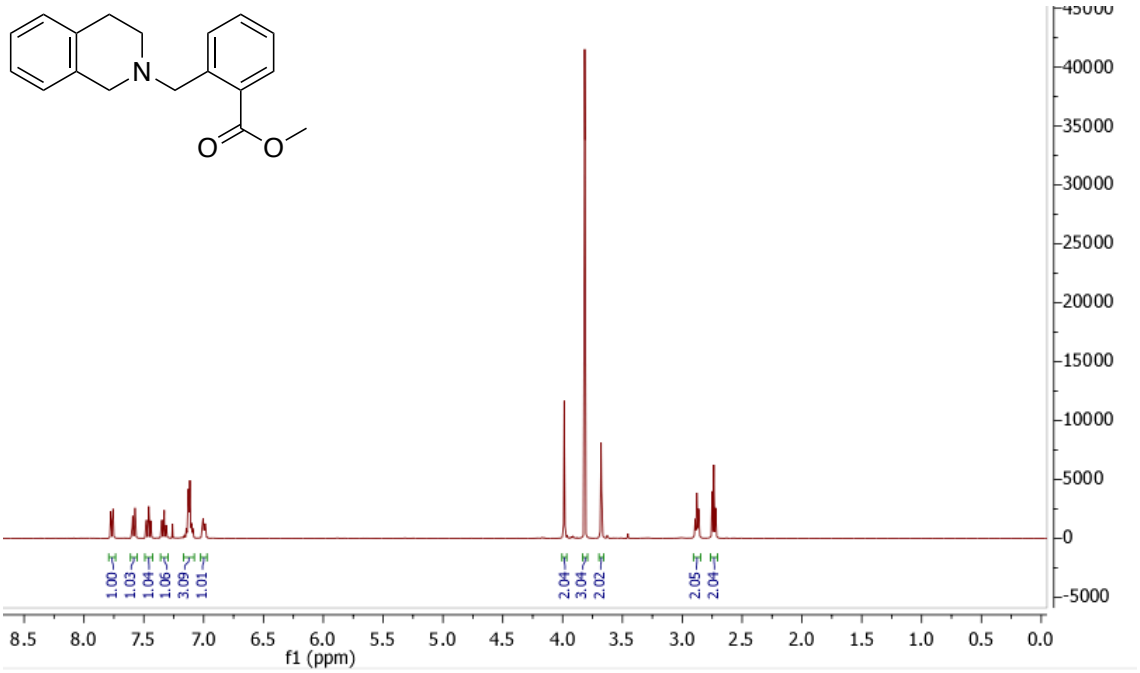

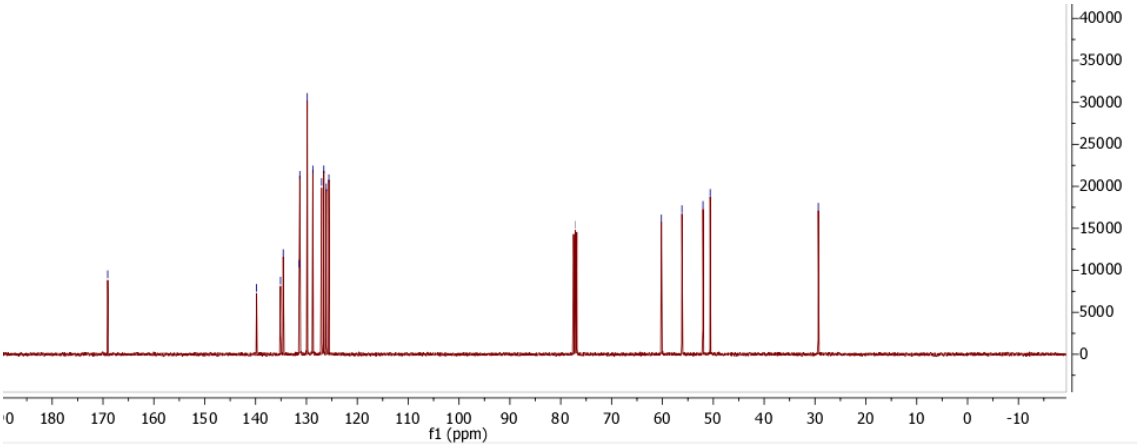

4.6a

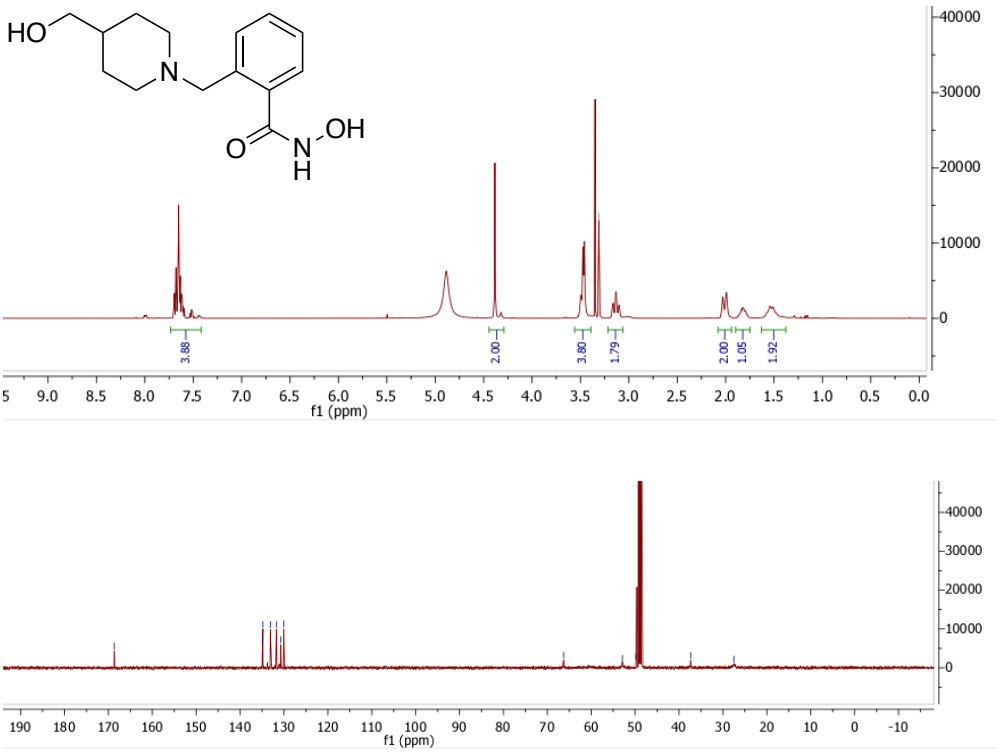
HO
N
O
N
H
OH
40000
30000
20000
10000
0
3.88
2.00
3.80
1.79
2.00
1.05
1.92
f1 (ppm)

4.6b

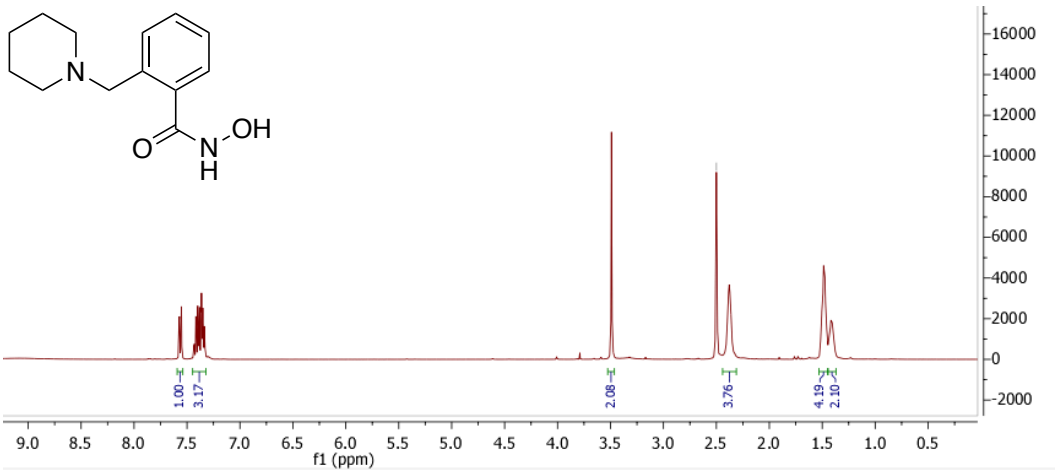
N
O
N
H
OH
16000
14000
12000
10000
8000
6000
4000
2000
0
-2000
1.00
3.17
2.08
3.76
4.19
2.10
9.0 8.5 8.0 7.5 7.0 6.5 6.0 5.5 5.0 4.5 4.0 3.5 3.0 2.5 2.0 1.5 1.0 0.5
f1 (ppm)

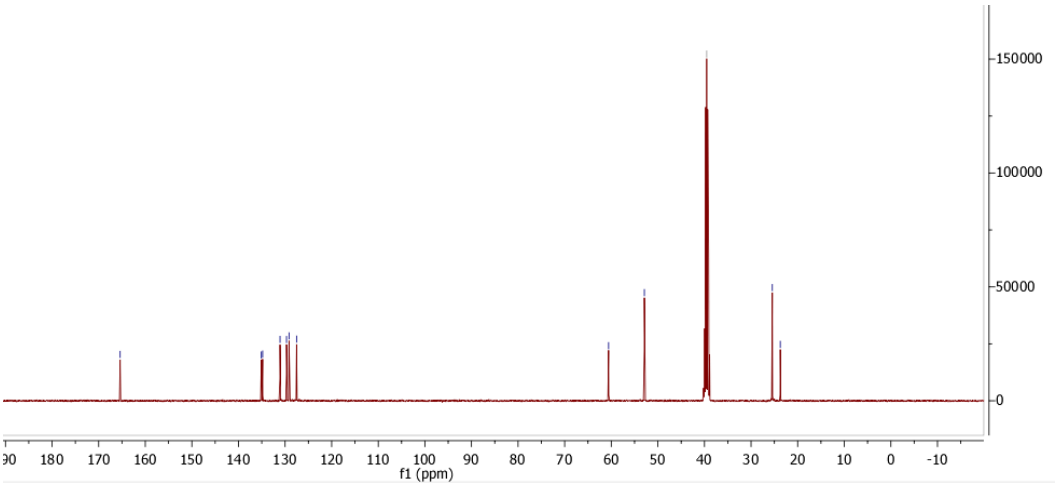
150000
100000
50000
0
90 180 170 160 150 140 130 120 110 100 90 80 70 60 50 40 30 20 10 0 -10
f1 (ppm)

4.6c

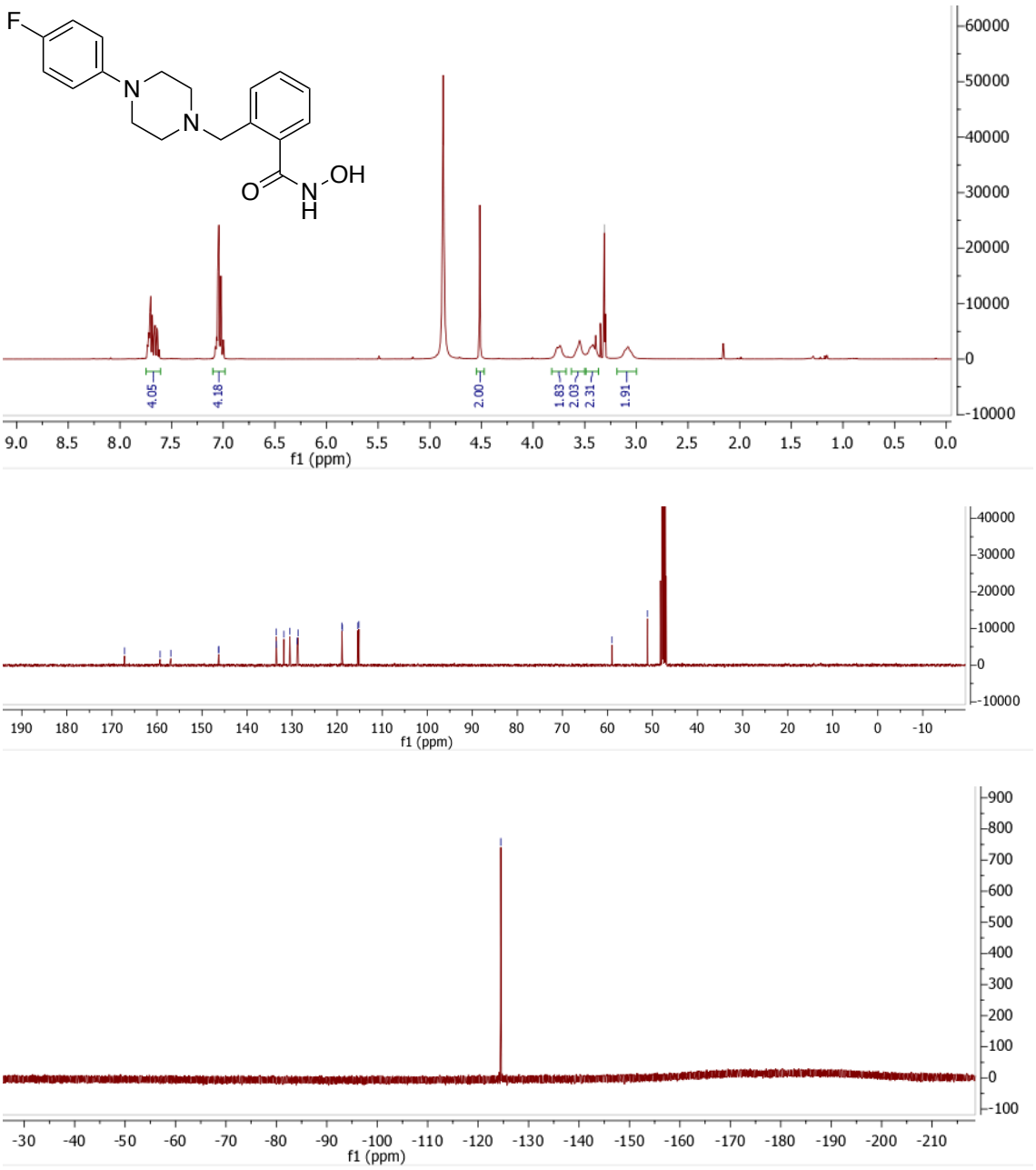

4.6d

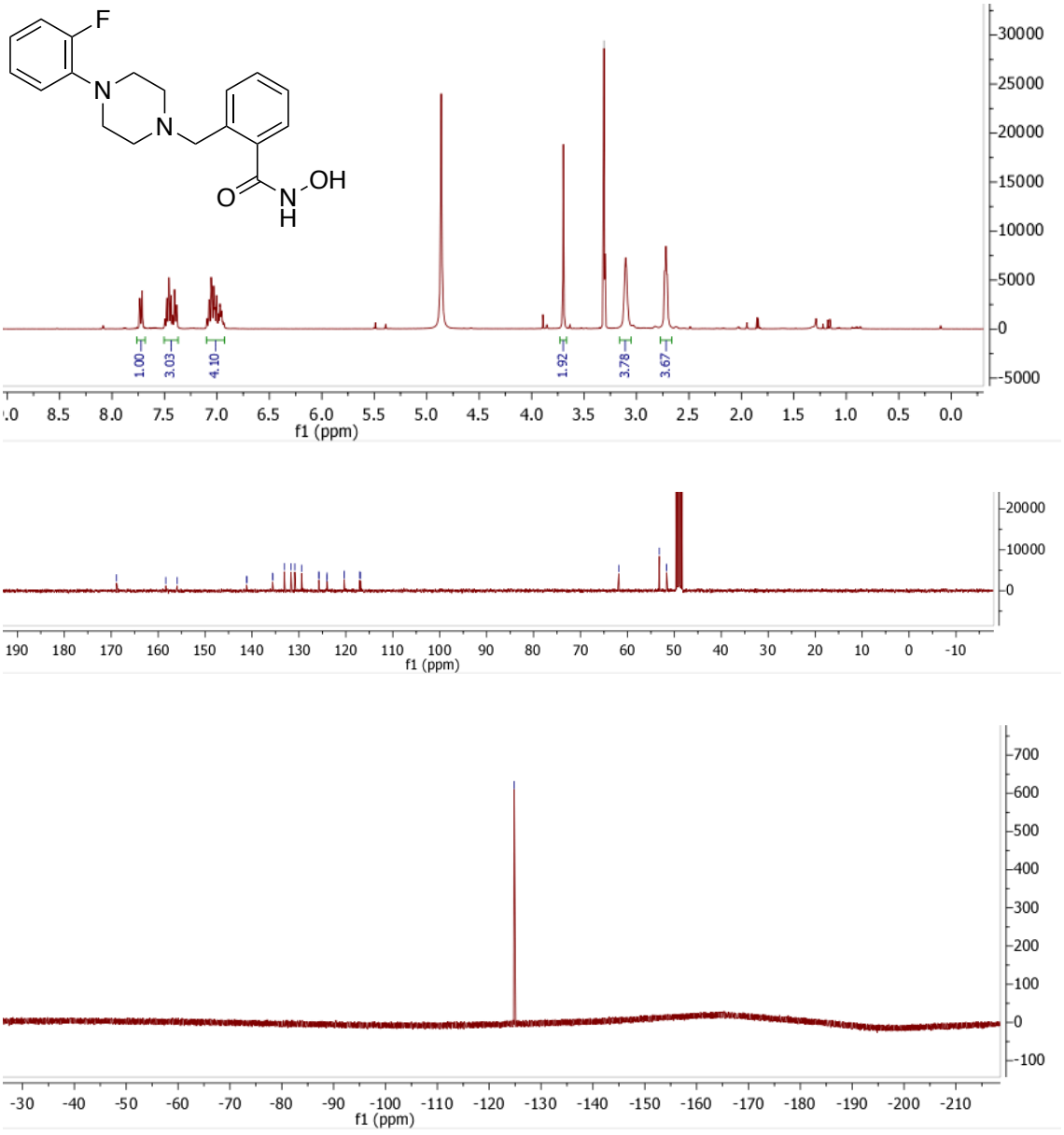

4.6e

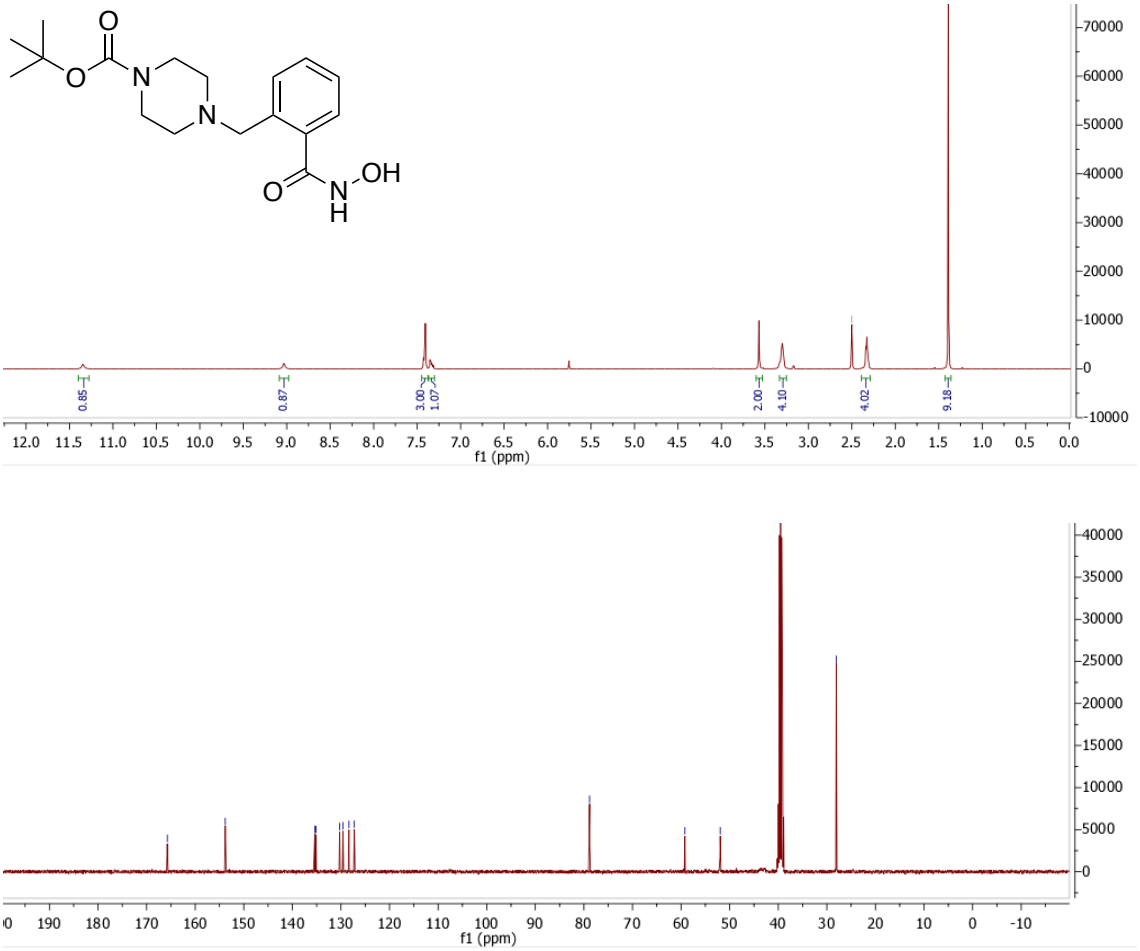

4.6f

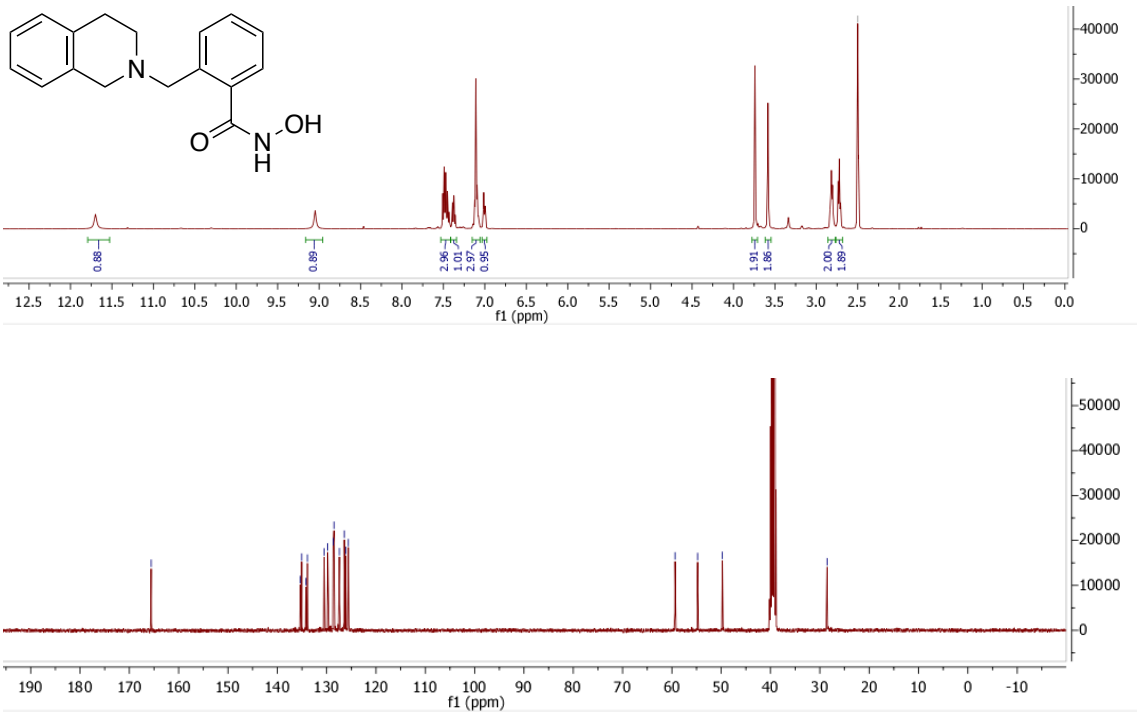

4.6g

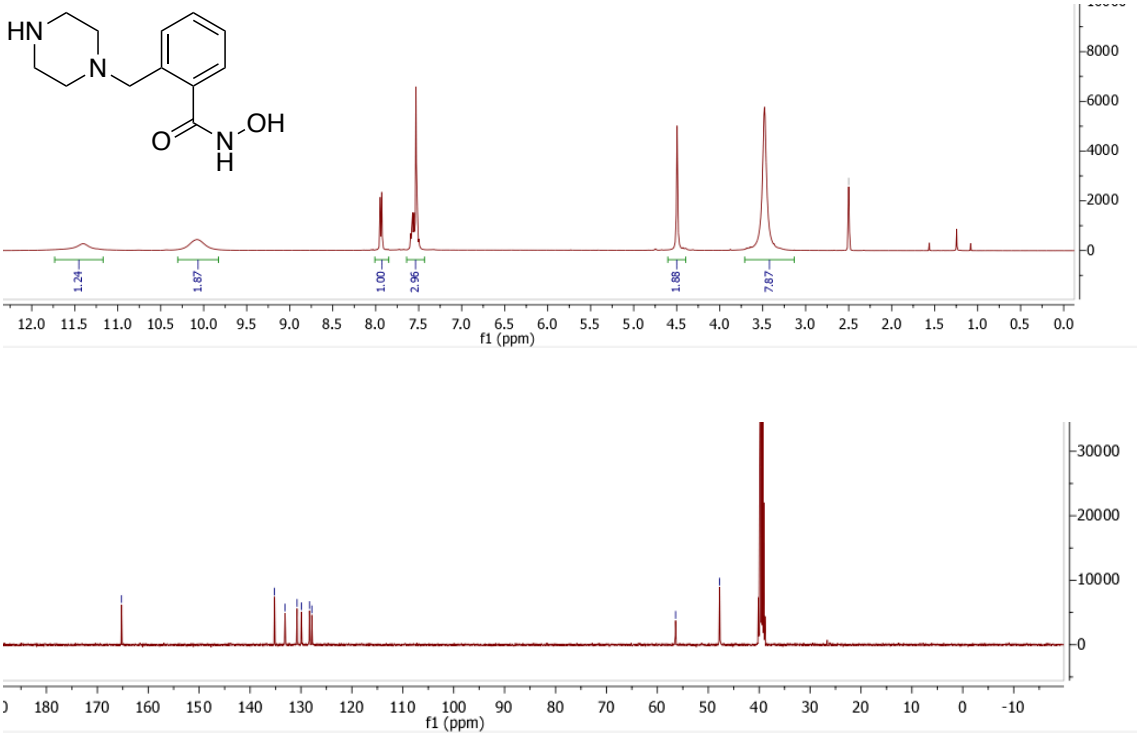

Alkene series

4.7a

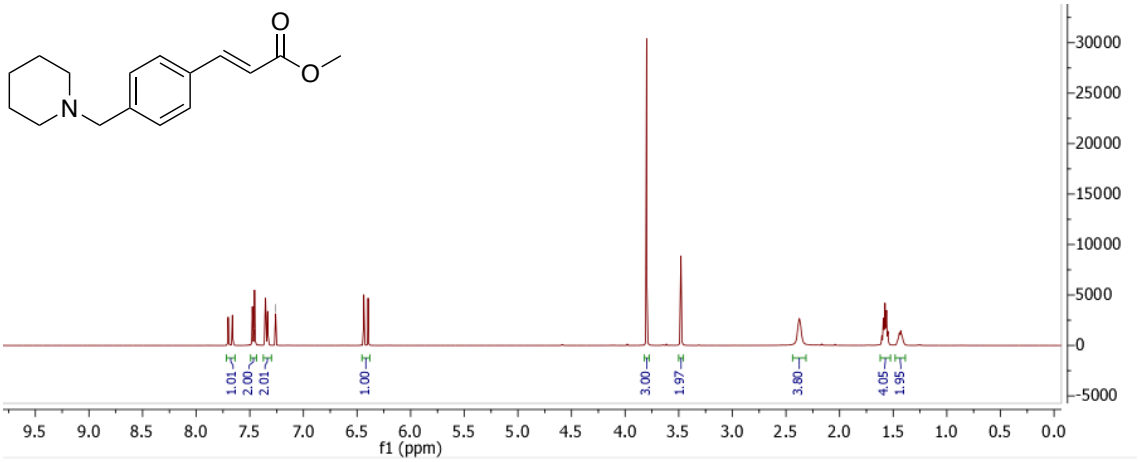

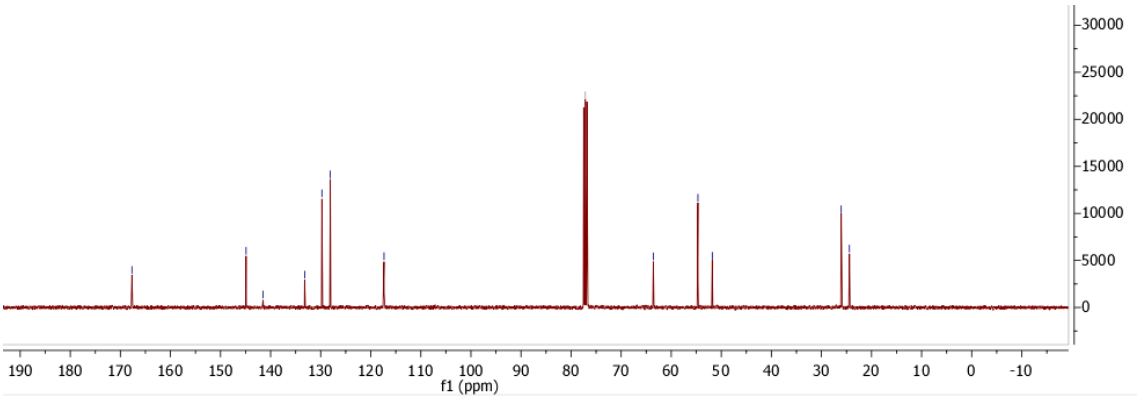

4.7b

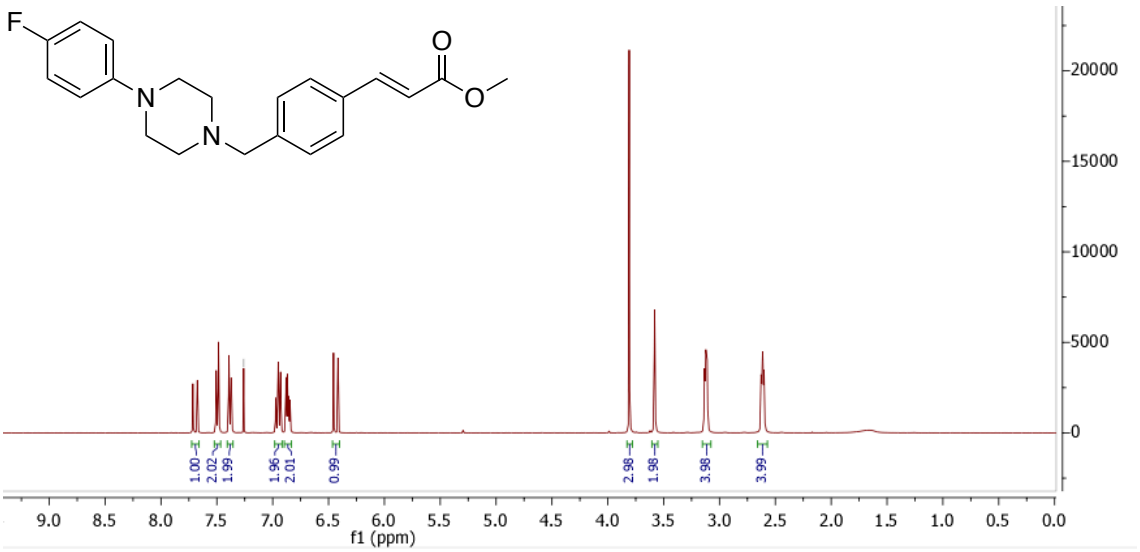
F
N
N
O
O
1.00
2.02
1.99
1.96
2.01
0.99
2.98
1.98
3.98
3.99
f1 (ppm)

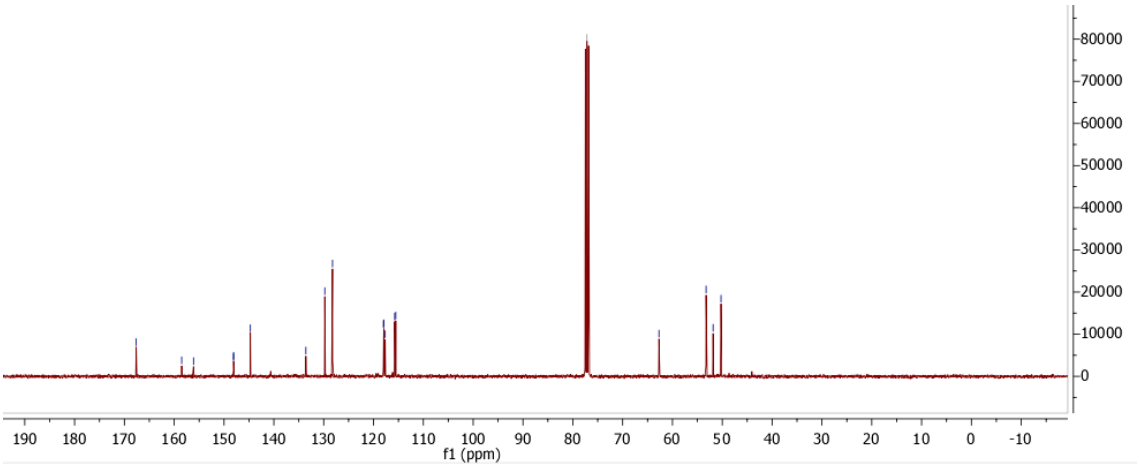
f1 (ppm)

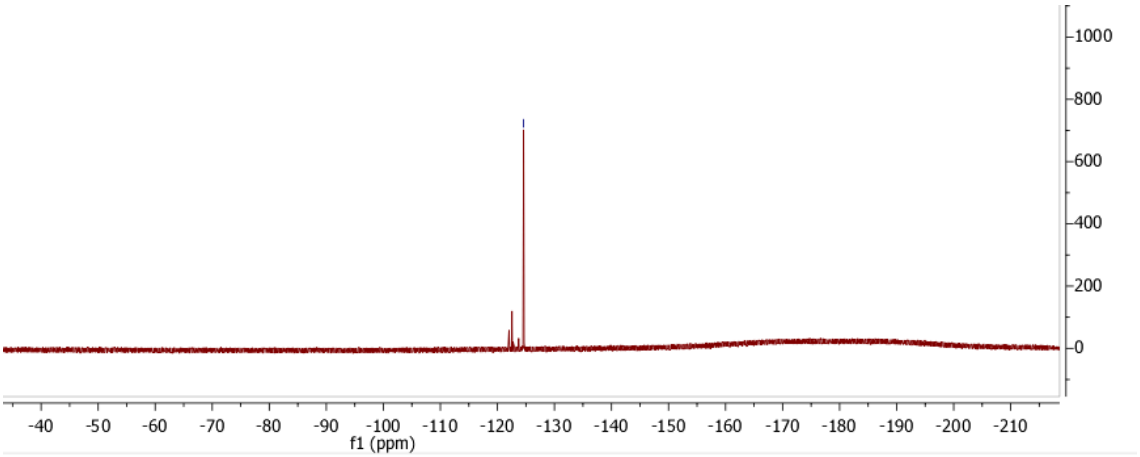
f1 (ppm)

4.7c

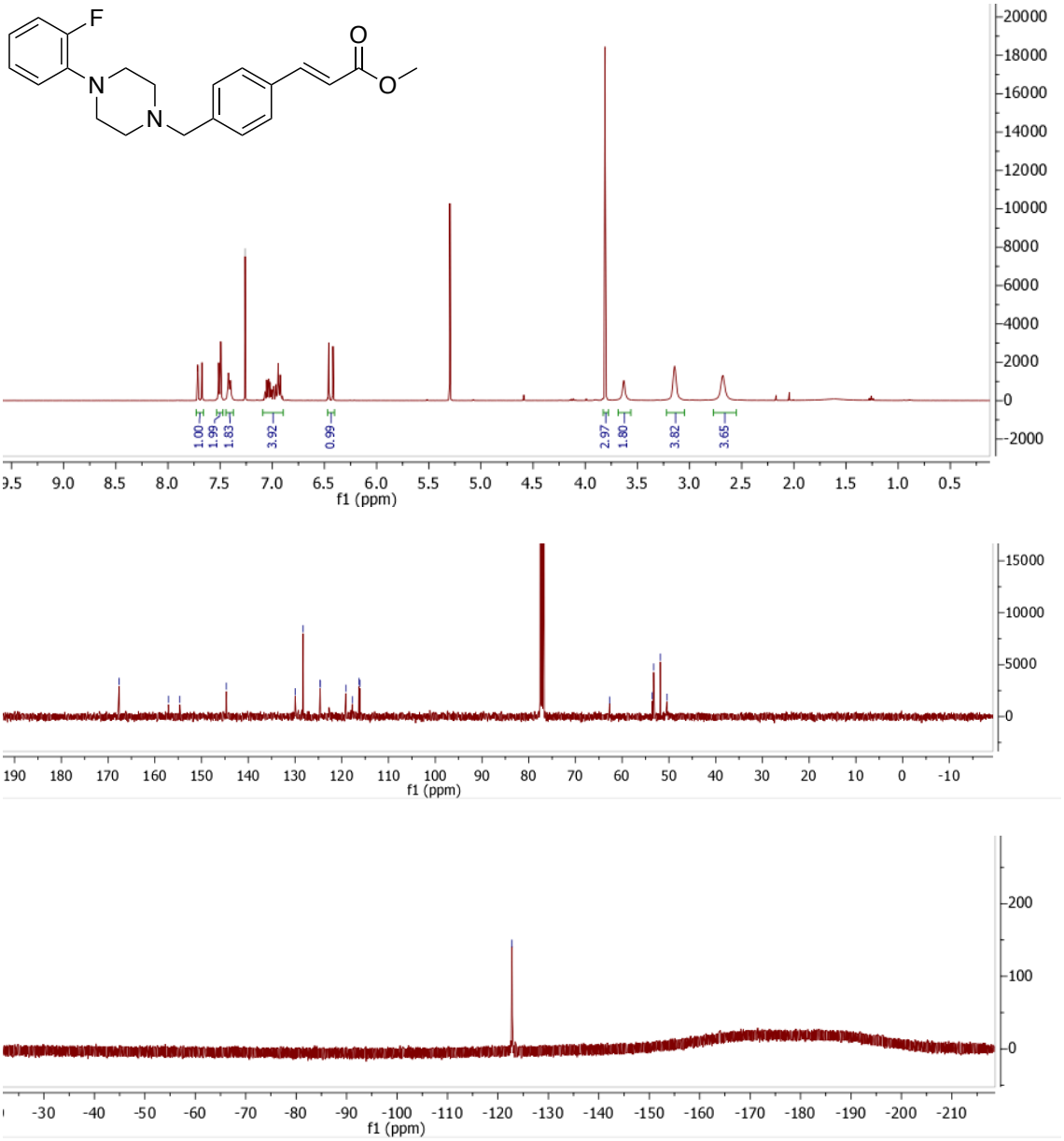

4.7d

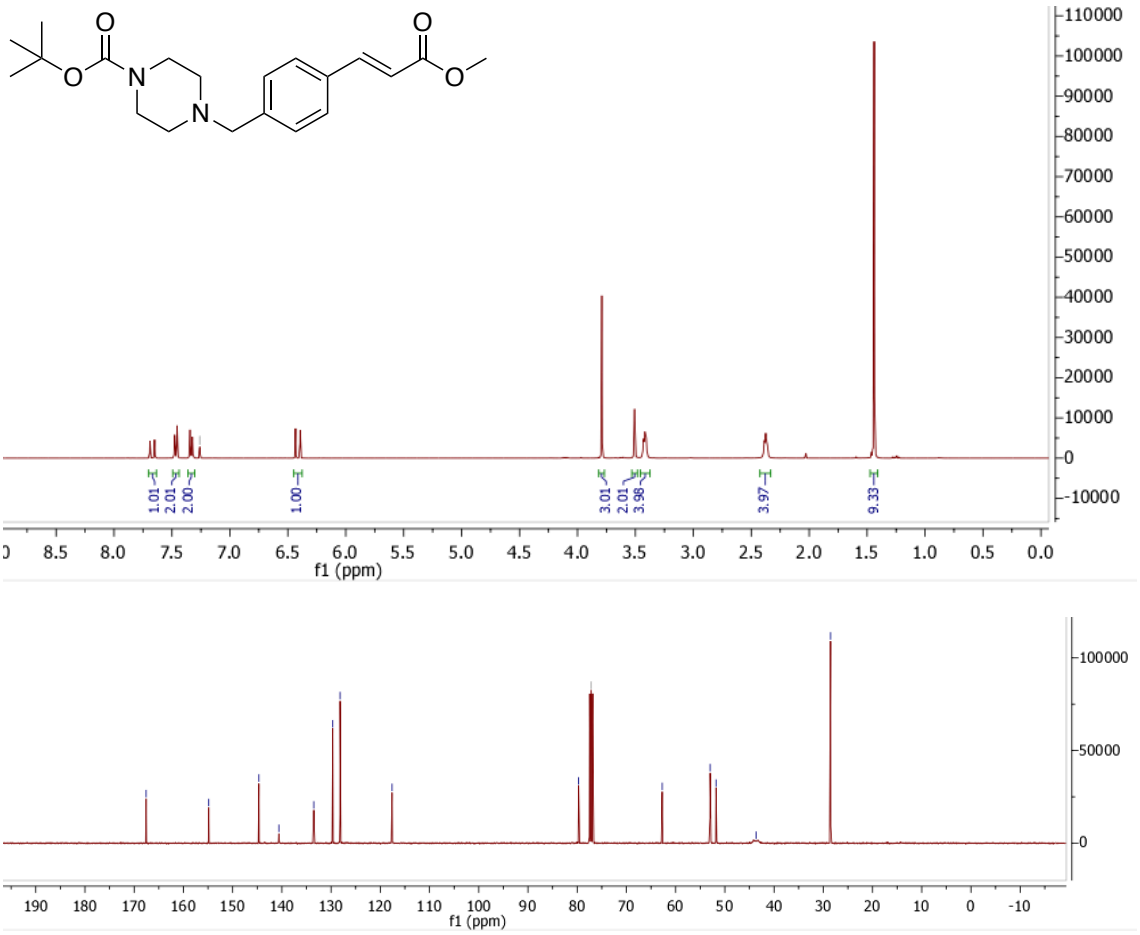

4.7e

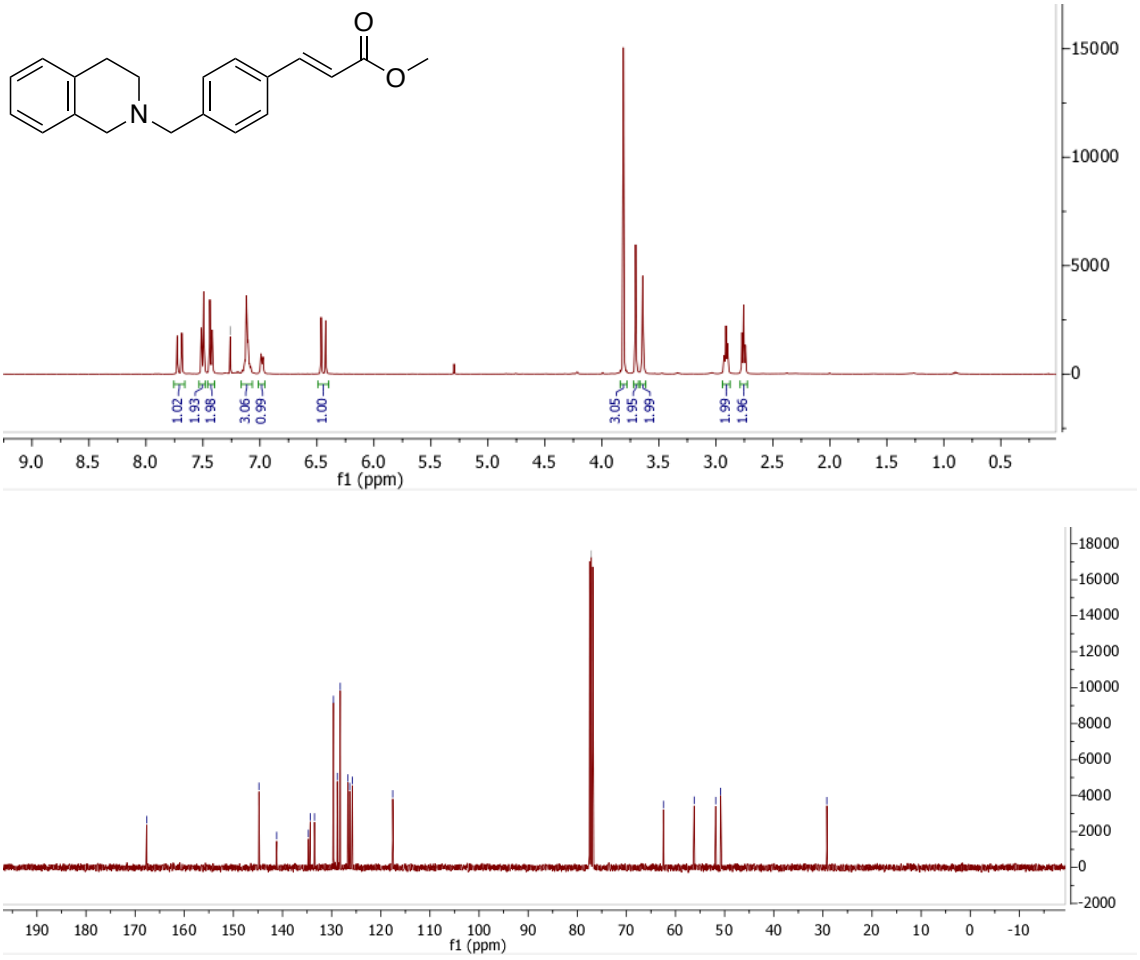
O
O
N
15000
10000
5000
0
1.02
1.93
1.98
3.06
0.99
1.00
3.05
1.95
1.99
1.99
1.96
9.0 8.5 8.0 7.5 7.0 6.5 6.0 5.5 5.0 4.5 4.0 3.5 3.0 2.5 2.0 1.5 1.0 0.5
f1 (ppm)
18000
16000
14000
12000
10000
8000
6000
4000
2000
0
-2000
190 180 170 160 150 140 130 120 110 100 90 80 70 60 50 40 30 20 10 0 -10
f1 (ppm)

4.8a

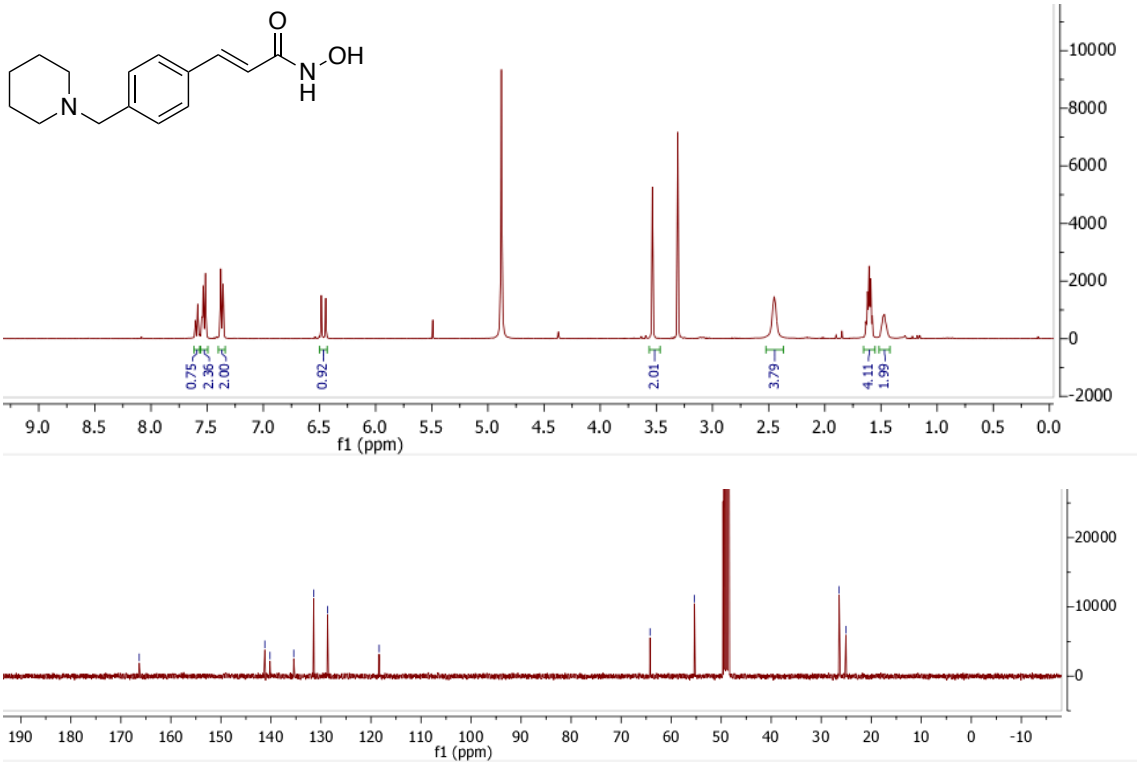

4.8b

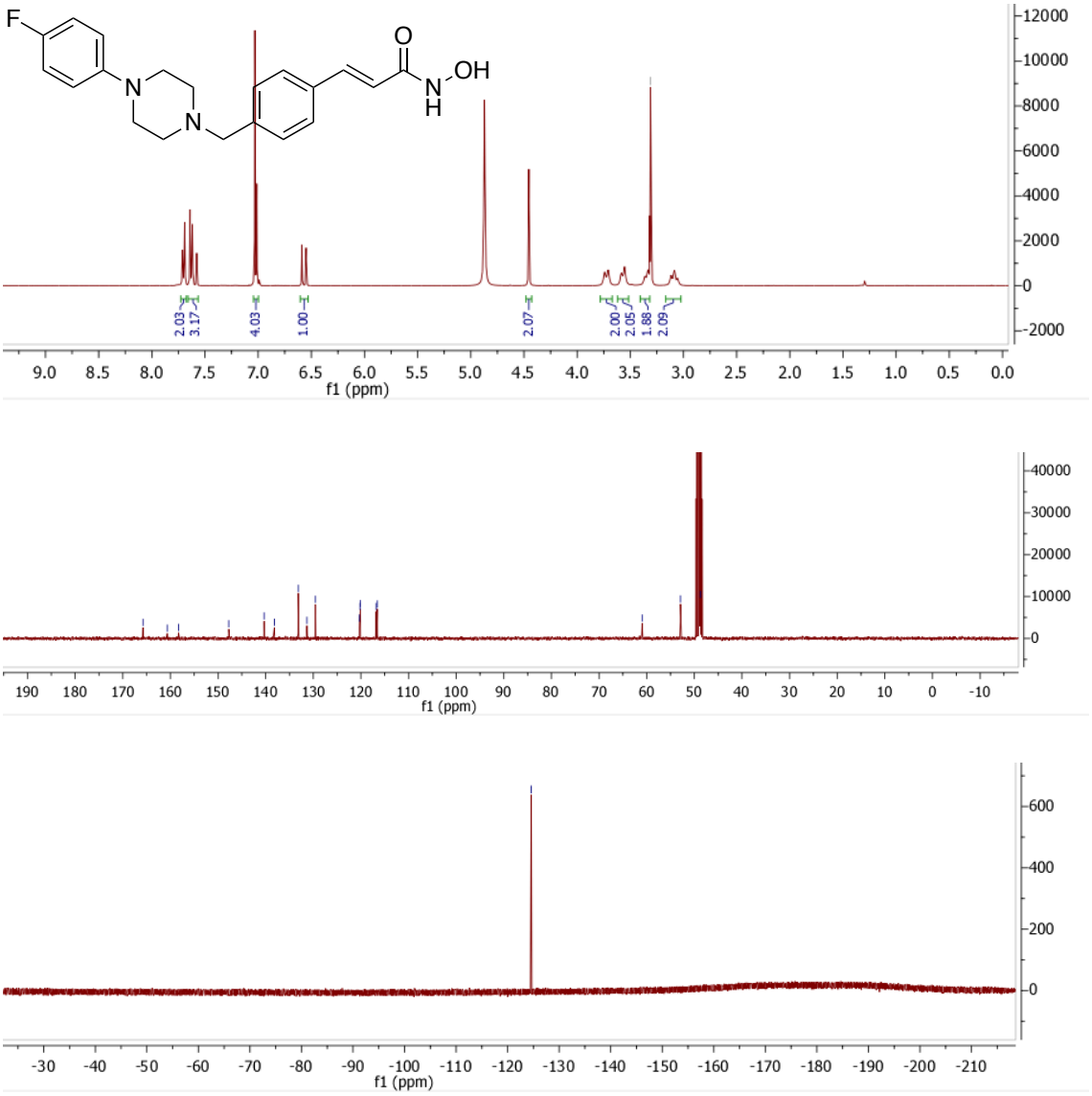
F
N
N
O
N
H
OH
2.03
3.17
4.03
1.00
2.07
2.00
2.05
1.88
2.09
f1 (ppm)
f1 (ppm)
f1 (ppm)

4.8c

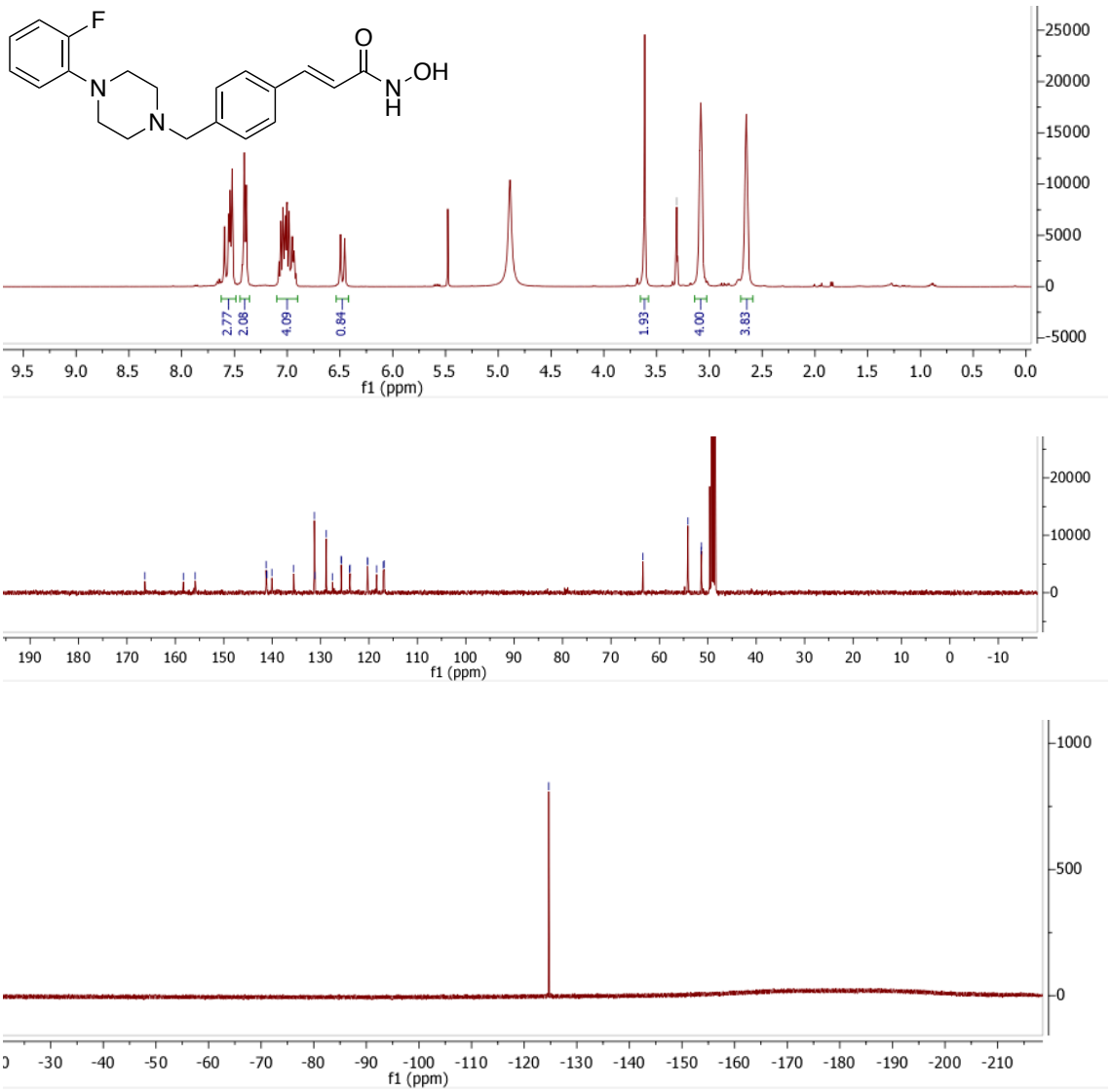

4.8d

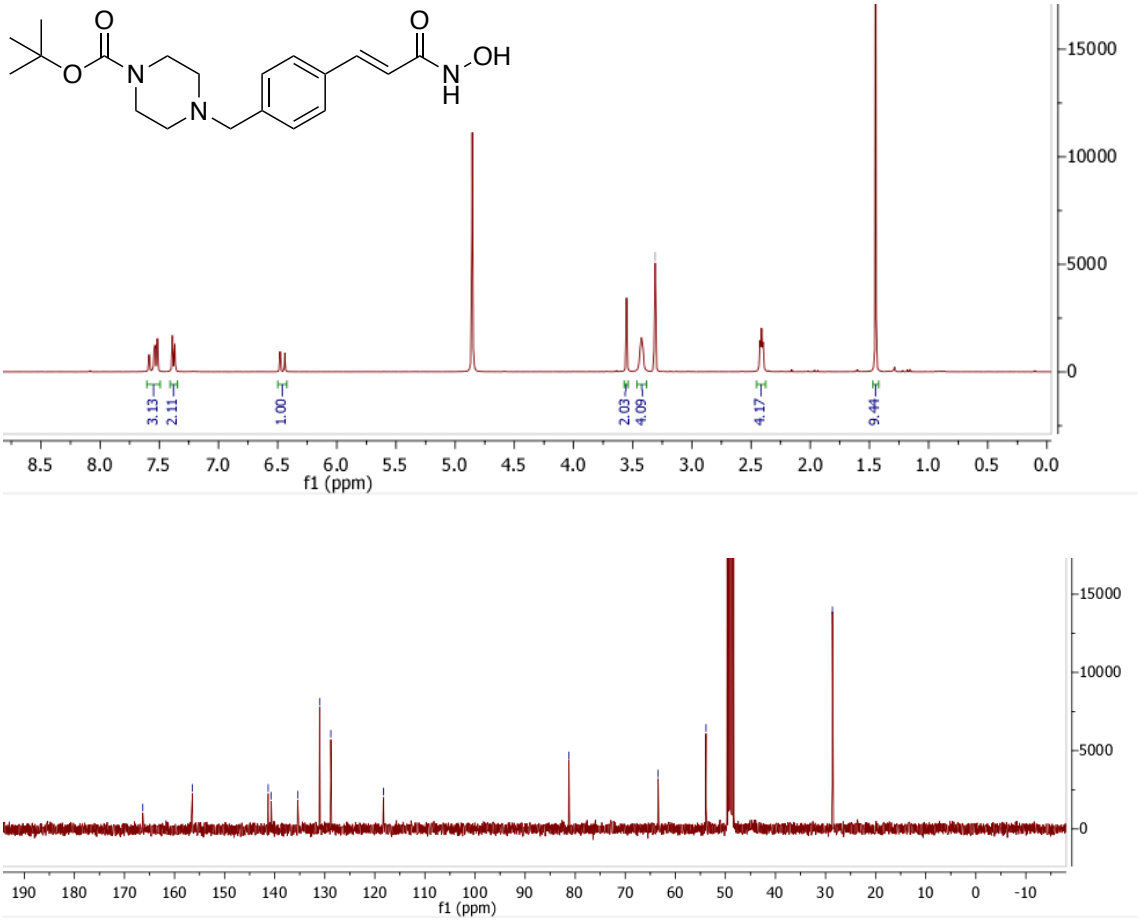
O
O
N
N
O
N
H
OH
15000
10000
5000
0
3.13
2.11
1.00
2.03
4.09
4.17
9.44
8.5 8.0 7.5 7.0 6.5 6.0 5.5 5.0 4.5 4.0 3.5 3.0 2.5 2.0 1.5 1.0 0.5 0.0
f1 (ppm)
15000
10000
5000
0
190 180 170 160 150 140 130 120 110 100 90 80 70 60 50 40 30 20 10 0 -10
f1 (ppm)

4.8e

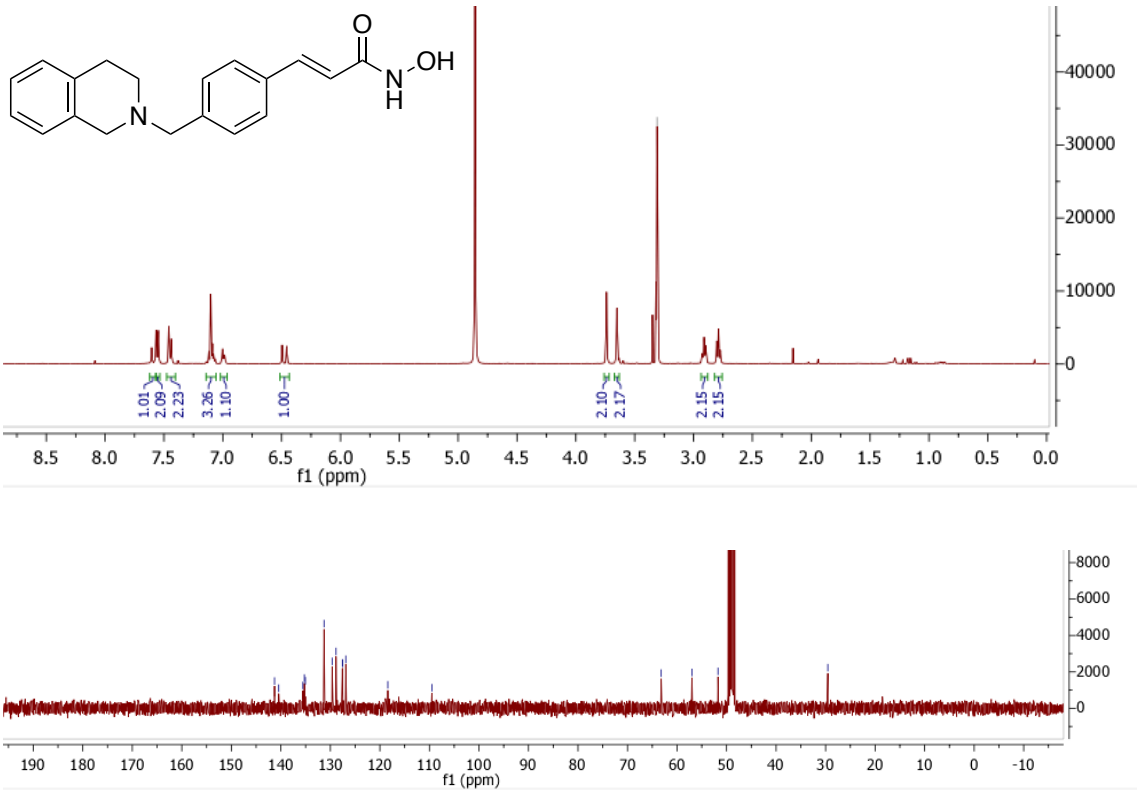
O
N
OH
H
N
40000
30000
20000
10000
0
1.01
2.09
2.23
3.26
1.10
1.00
2.10
2.17
2.15
2.15
8.5 8.0 7.5 7.0 6.5 6.0 5.5 5.0 4.5 4.0 3.5 3.0 2.5 2.0 1.5 1.0 0.5 0.0
f1 (ppm)
8000
6000
4000
2000
0
190 180 170 160 150 140 130 120 110 100 90 80 70 60 50 40 30 20 10 0 -10
f1 (ppm)

4.8f

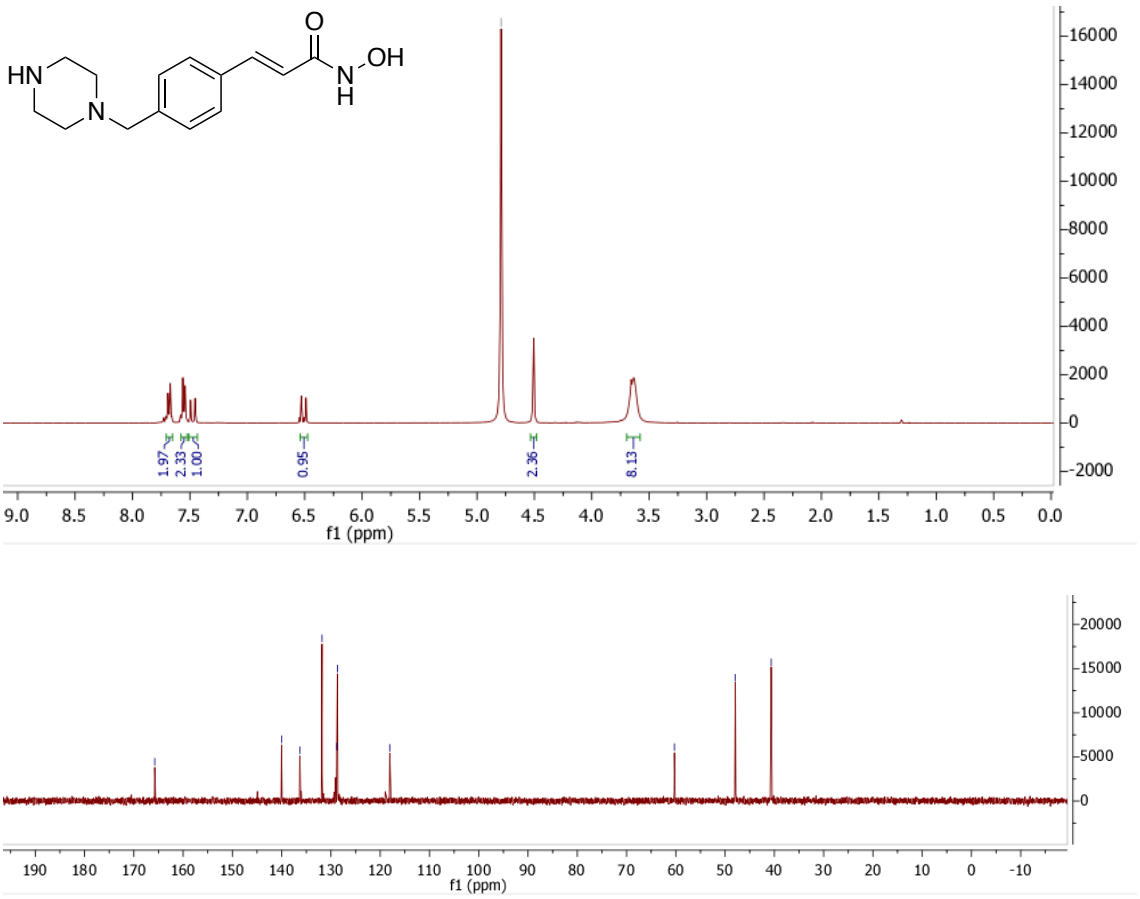

Chapter five NMR

5.2

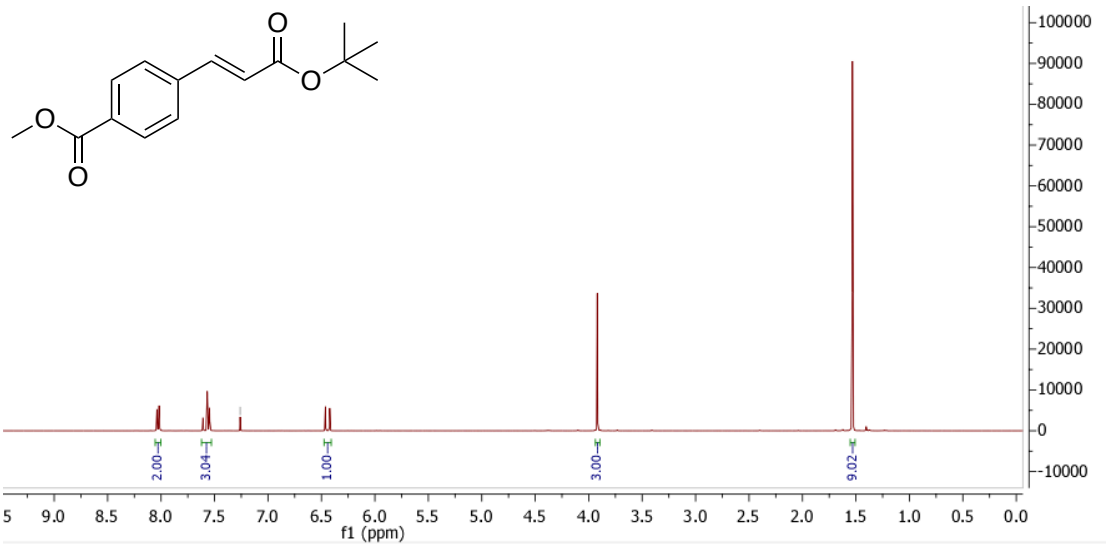

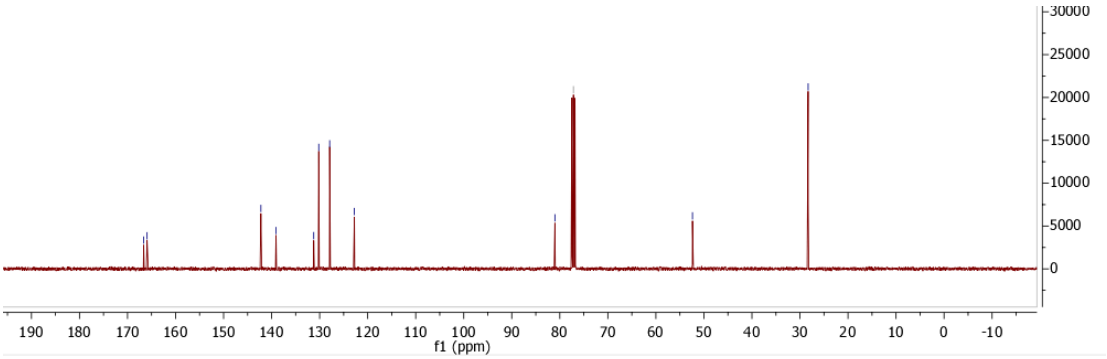

5.3

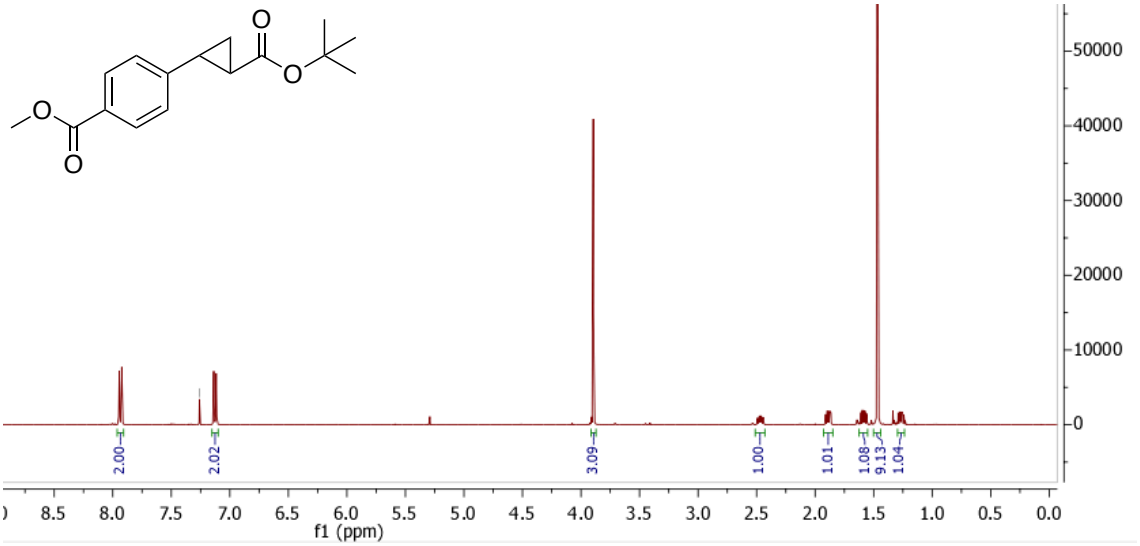
O
O
O
O
50000
40000
30000
20000
10000
0
2.00
2.02
3.09
1.00
1.01
1.08
9.13
1.04
8.5
8.0
7.5
7.0
6.5
6.0
5.5
5.0
4.5
4.0
3.5
3.0
2.5
2.0
1.5
1.0
0.5
0.0
f1 (ppm)

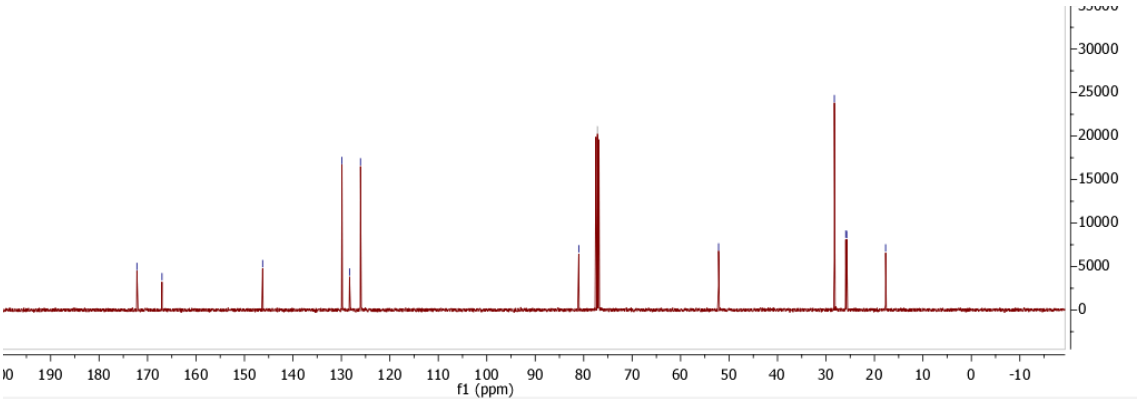
30000
25000
20000
15000
10000
5000
0
190
180
170
160
150
140
130
120
110
100
90
80
70
60
50
40
30
20
10
0
-10
f1 (ppm)

5.11

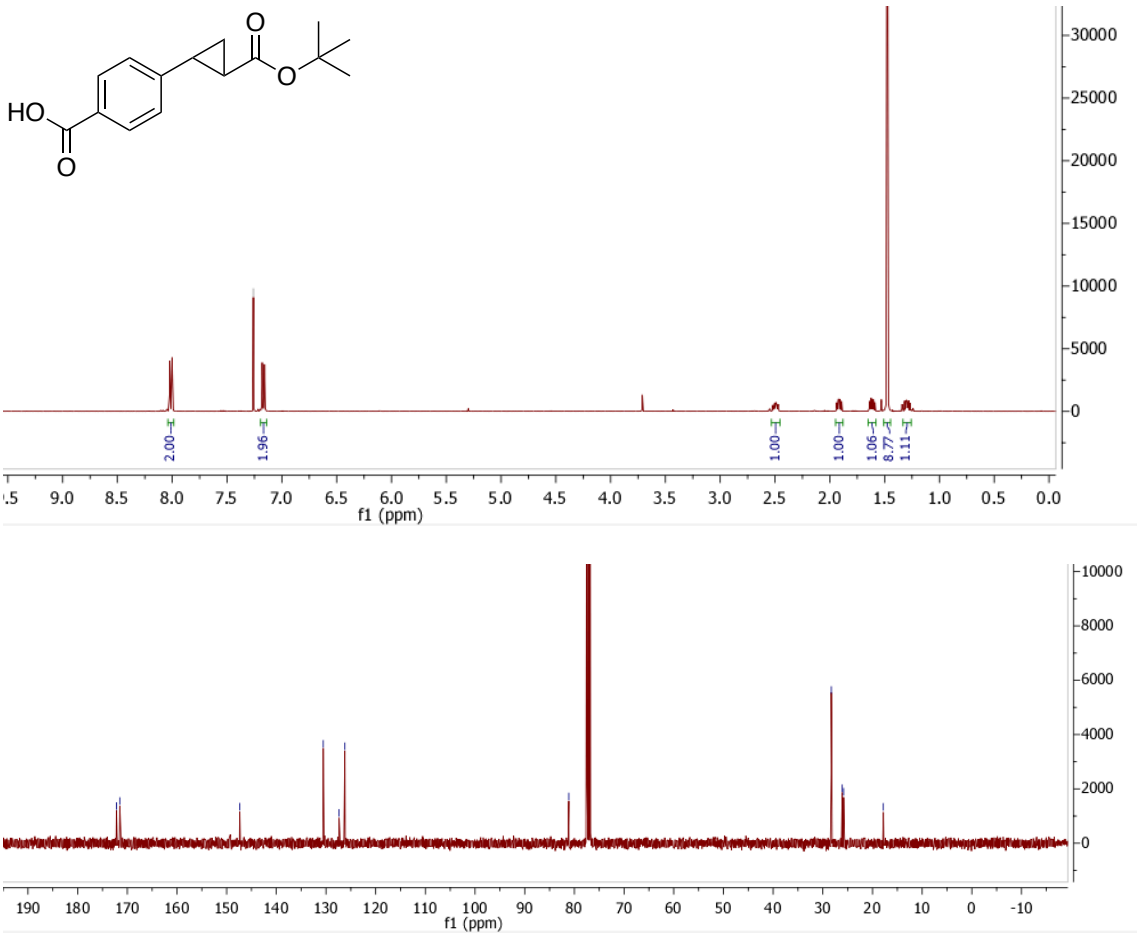

5.12a

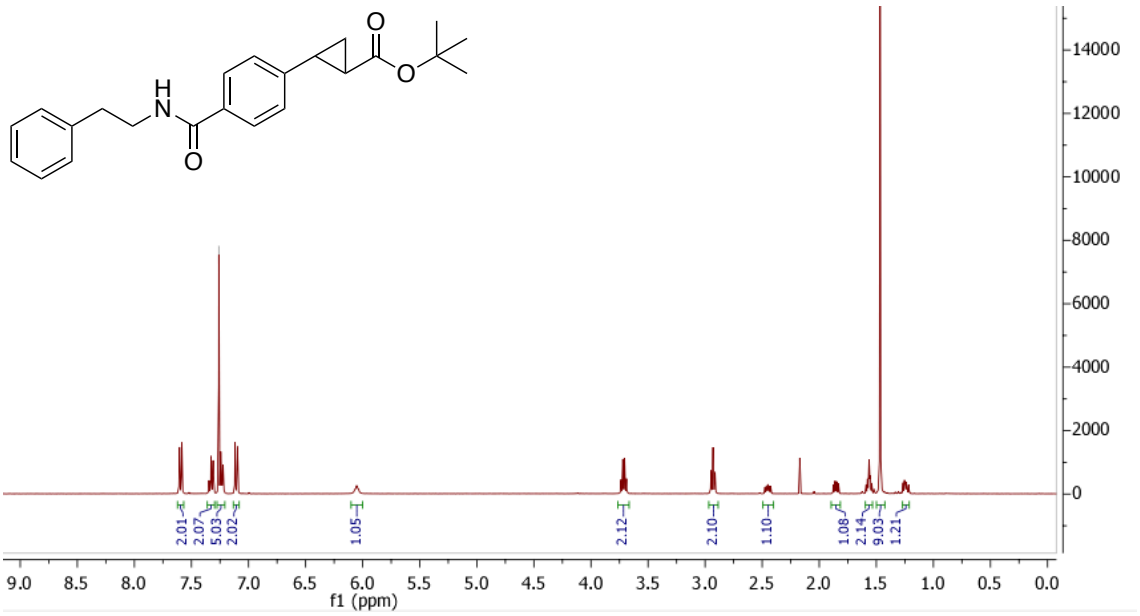
O
O
H
N
O
14000
12000
10000
8000
6000
4000
2000
0
2.01
2.07
5.03
2.02
1.05
2.12
2.10
1.10
1.08
2.14
9.03
1.21
9.0 8.5 8.0 7.5 7.0 6.5 6.0 5.5 5.0 4.5 4.0 3.5 3.0 2.5 2.0 1.5 1.0 0.5 0.0
f1 (ppm)

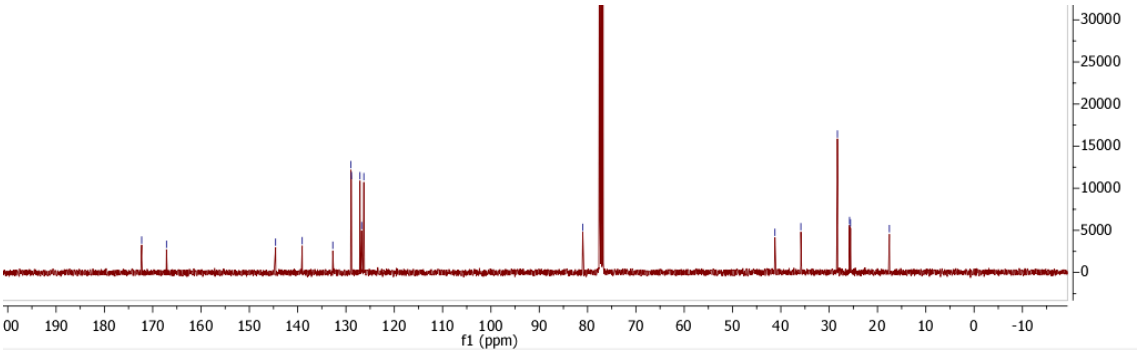
30000
25000
20000
15000
10000
5000
0
00 190 180 170 160 150 140 130 120 110 100 90 80 70 60 50 40 30 20 10 0 -10
f1 (ppm)

5.13a

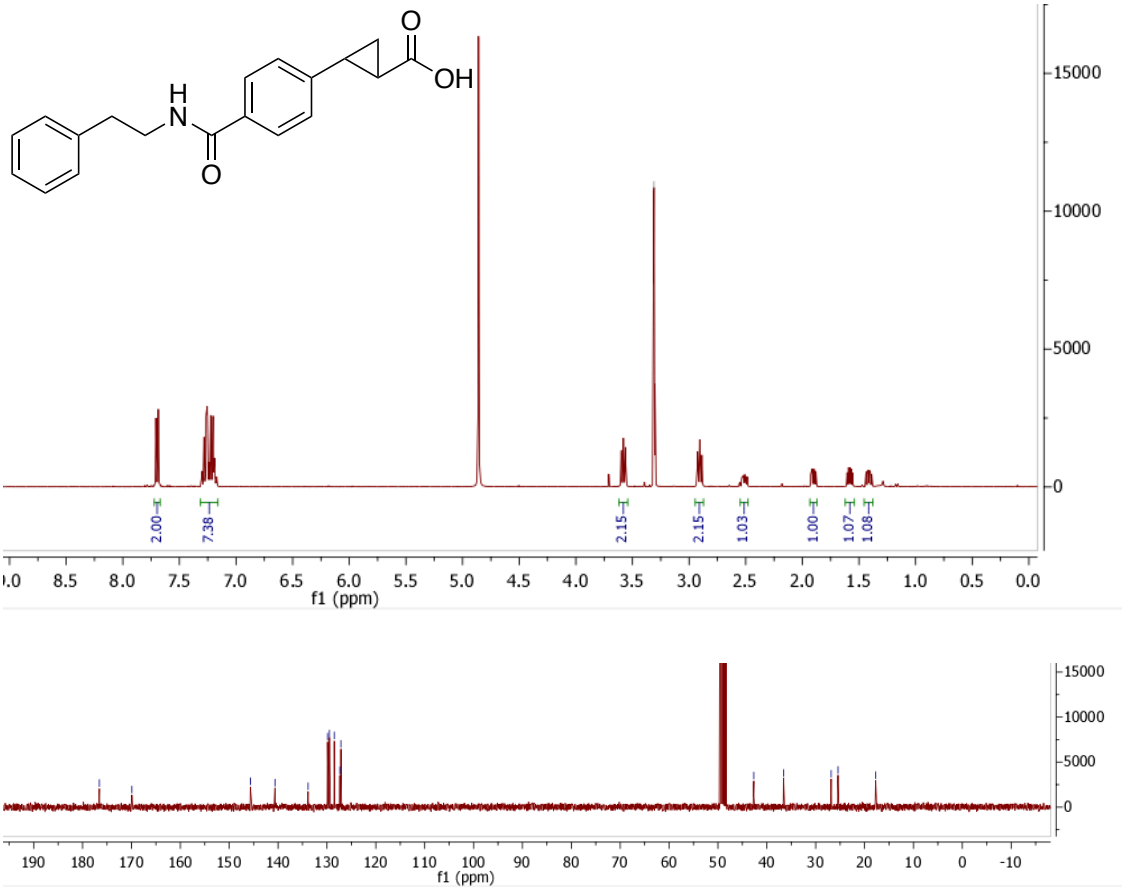
O
OH
H
N
O
15000
10000
5000
0
2.00
7.38
2.15
2.15
1.03
1.00
1.07
1.08
f1 (ppm)
15000
10000
5000
0
f1 (ppm)

5.12b

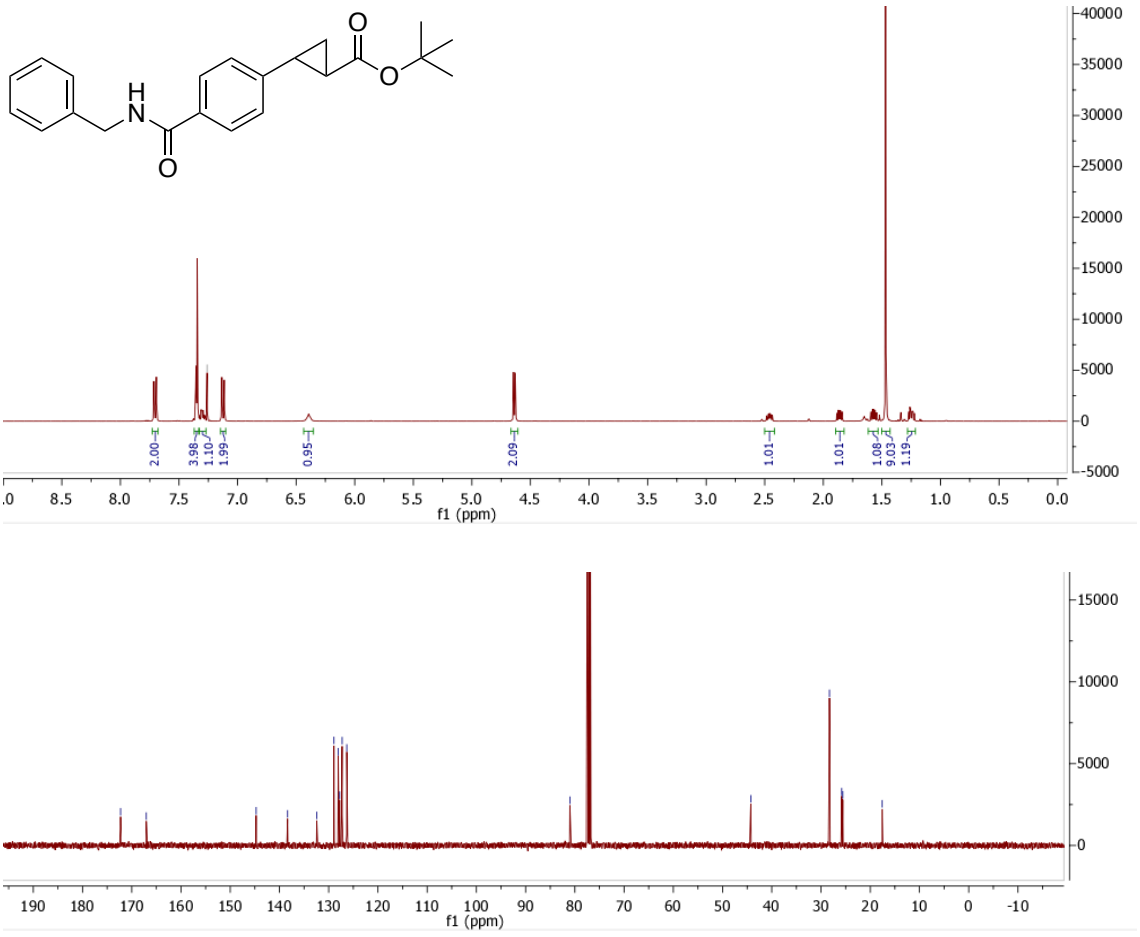

5.13b

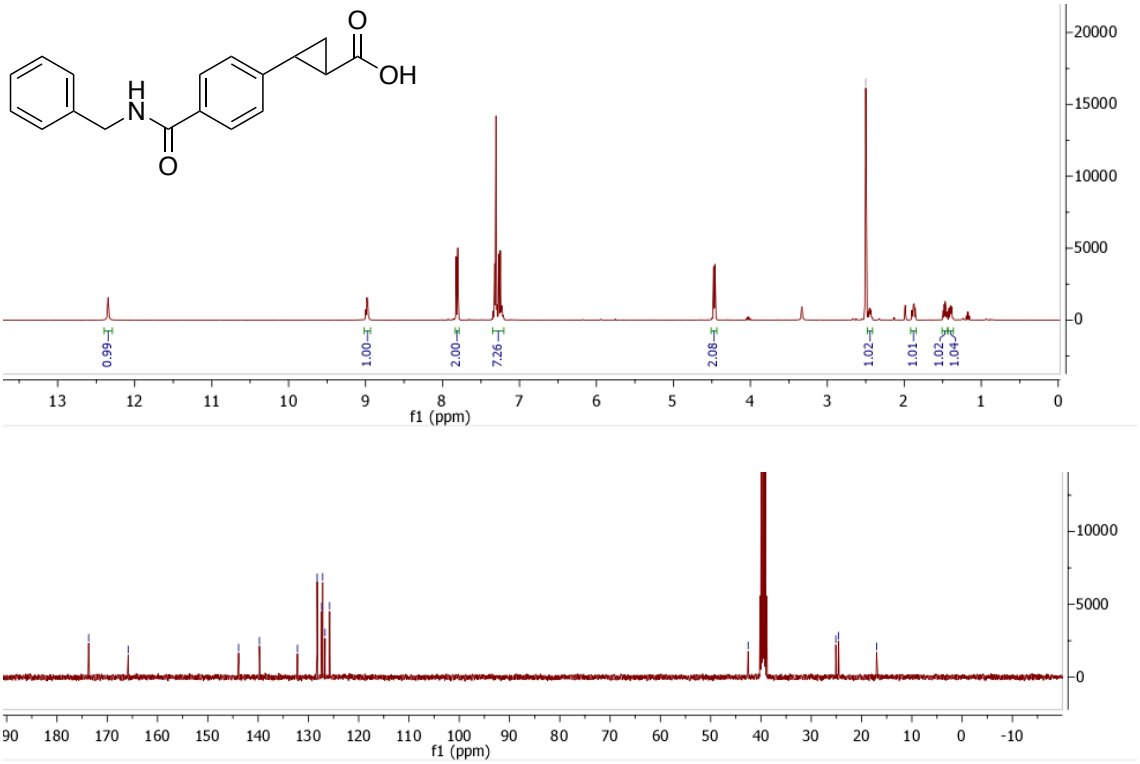

5.12c

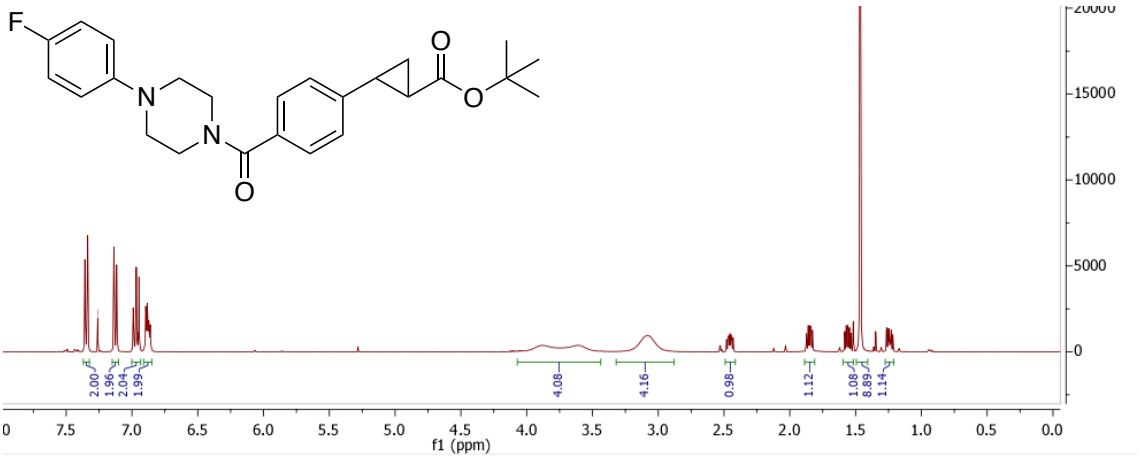
F
N
N
O
O
O
2.00
1.96
2.04
1.99
4.08
4.16
0.98
1.12
1.08
8.89
1.14
f1 (ppm)

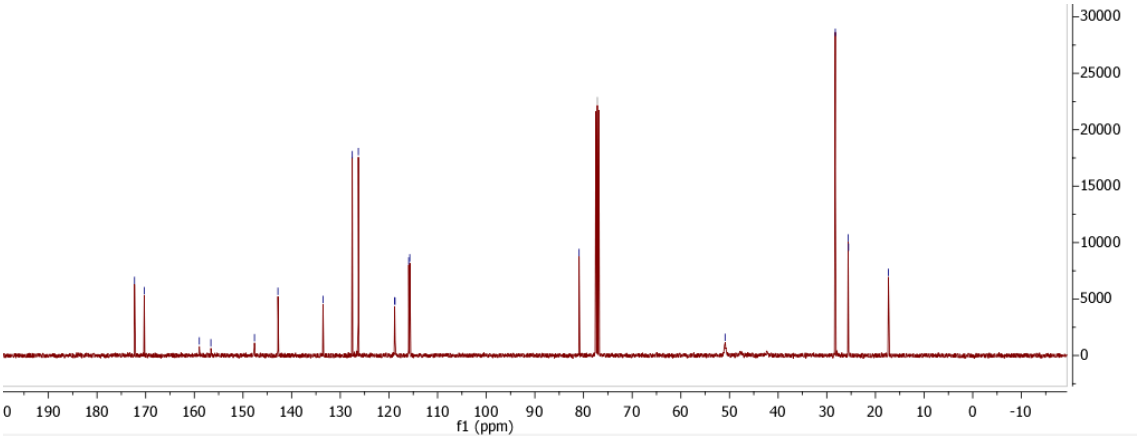
f1 (ppm)

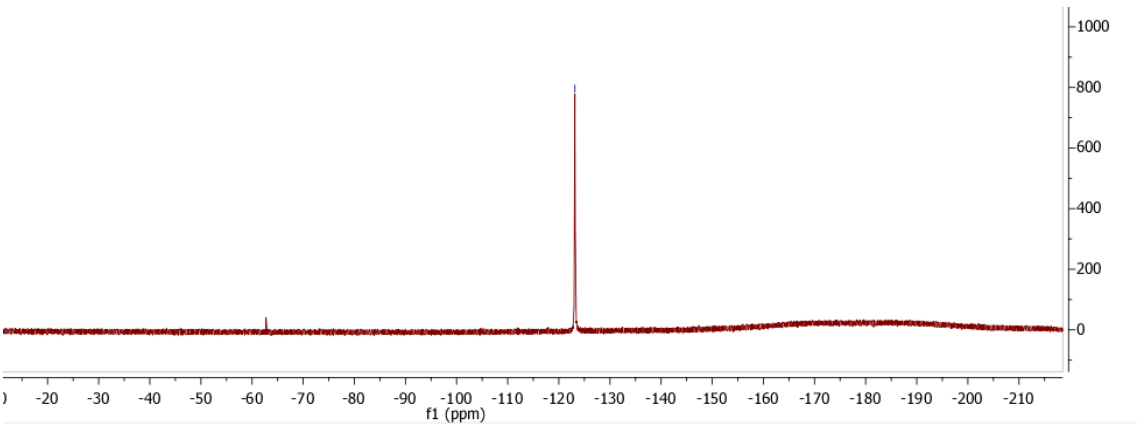
f1 (ppm)

5.13c

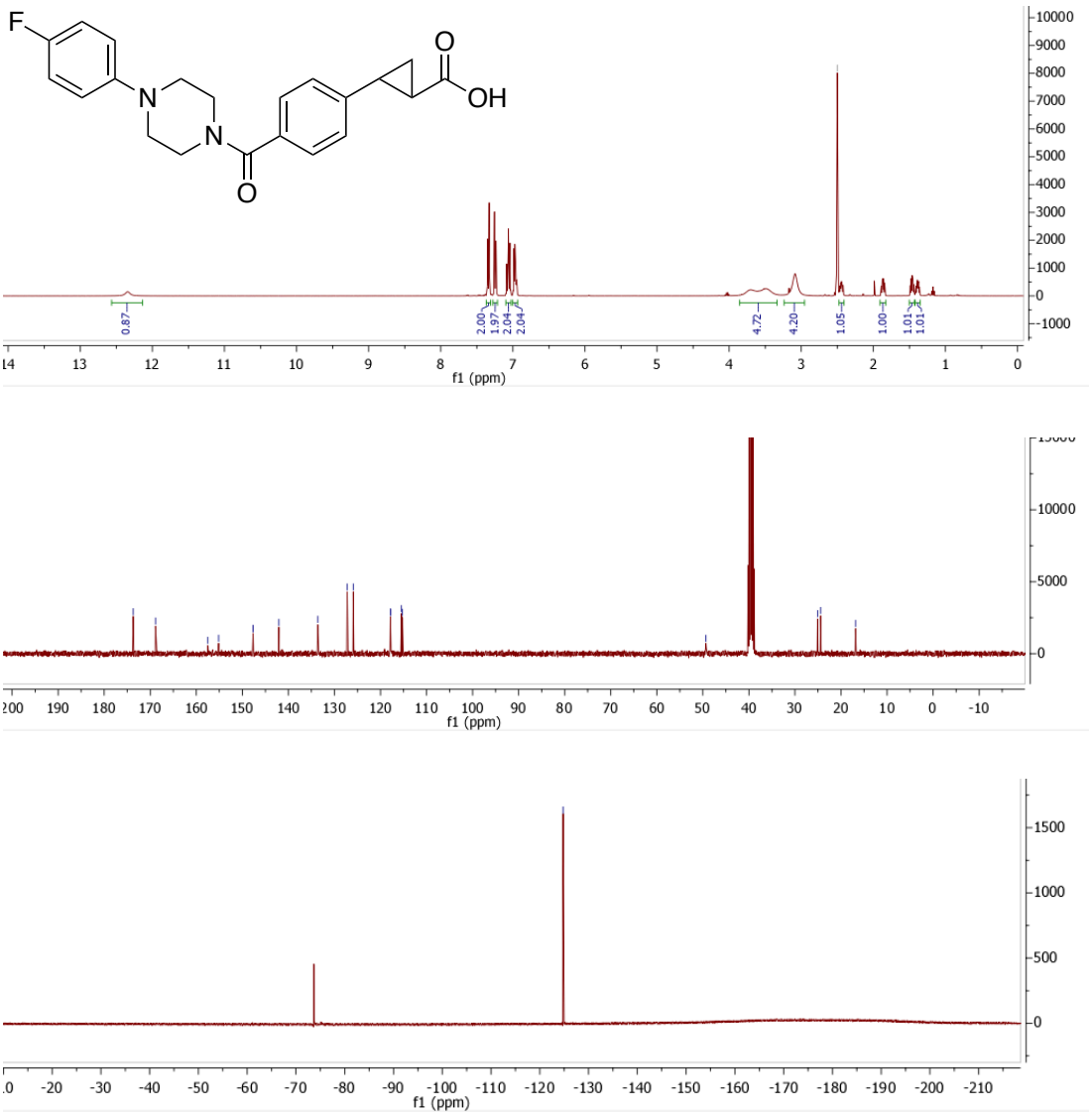

5.17

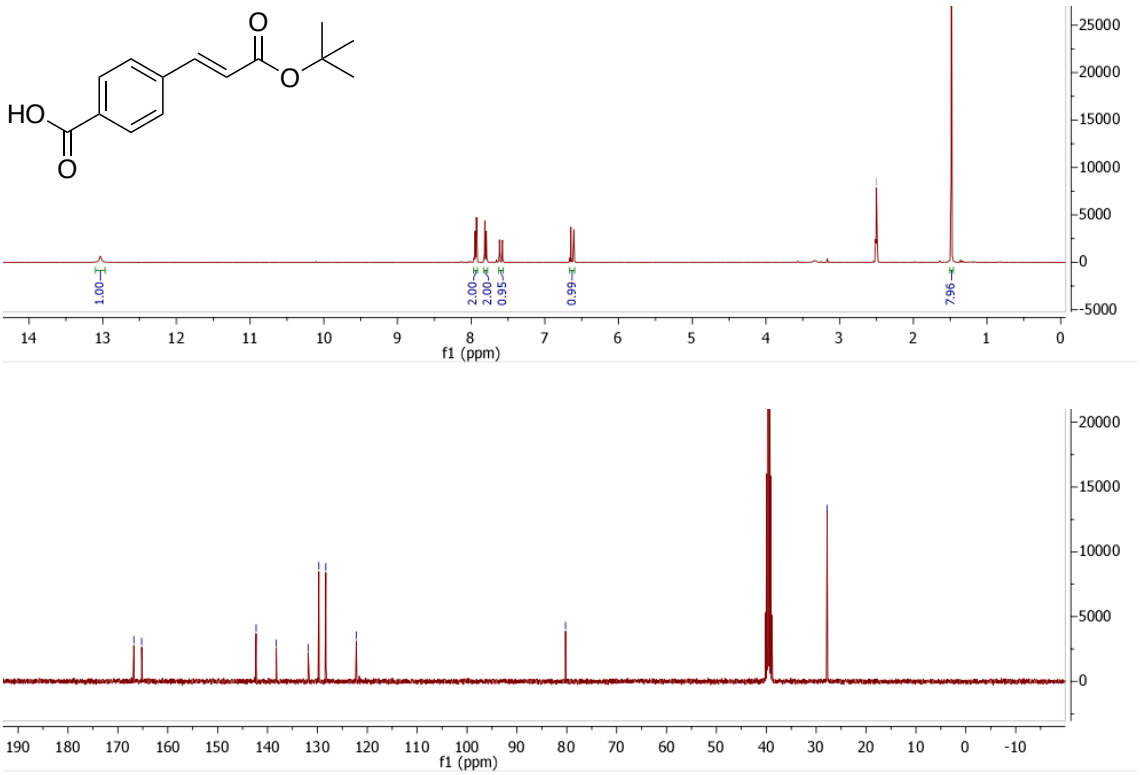

5.18

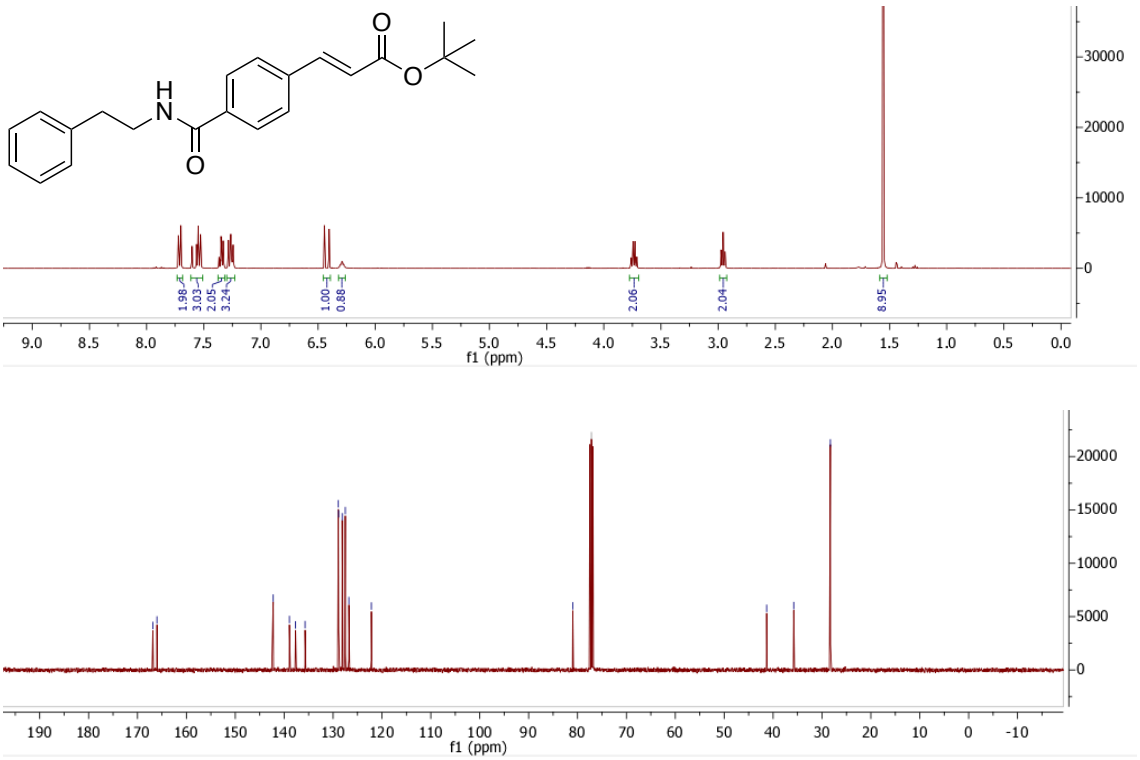
O
O
H
N
O
30000
20000
10000
0
1.98
3.03
2.05
3.24
1.00
0.88
2.06
2.04
8.95
9.0 8.5 8.0 7.5 7.0 6.5 6.0 5.5 5.0 4.5 4.0 3.5 3.0 2.5 2.0 1.5 1.0 0.5 0.0
f1 (ppm)

20000
15000
10000
5000
0
190 180 170 160 150 140 130 120 110 100 90 80 70 60 50 40 30 20 10 0 -10
f1 (ppm)

5.19

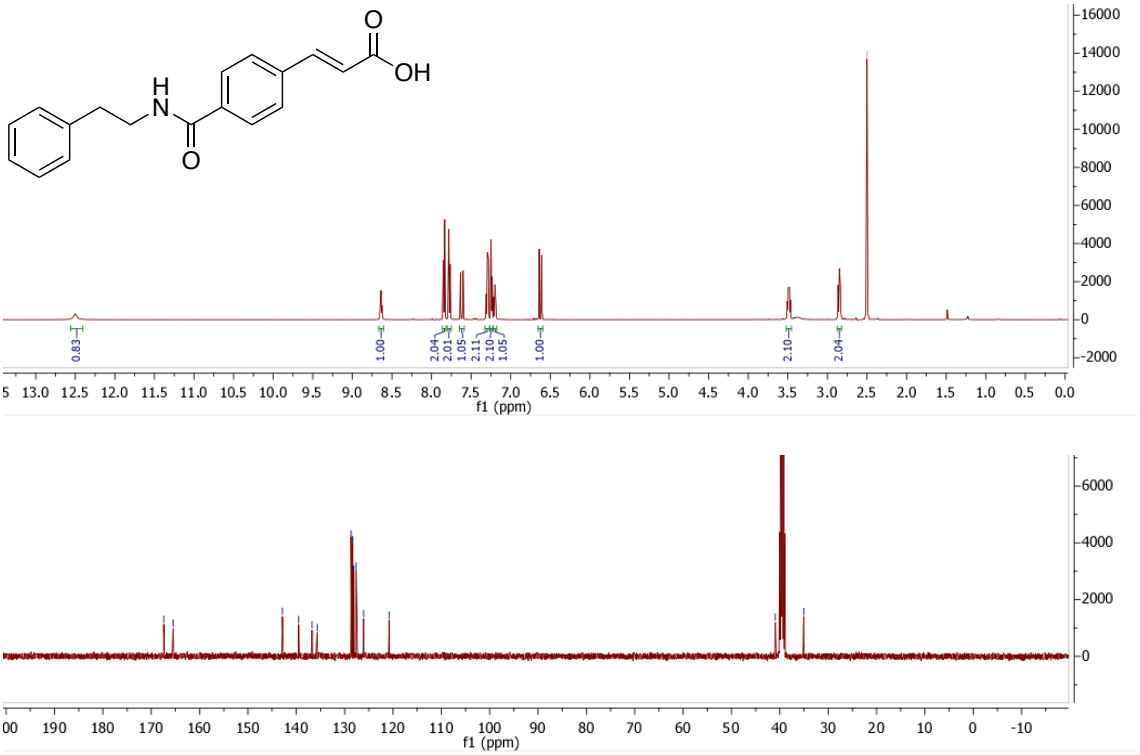
O
OH
H
N
O
16000
14000
12000
10000
8000
6000
4000
2000
0
-2000
0.83
1.00
2.04
2.01
1.05
2.11
2.10
1.05
1.00
2.10
2.04
f1 (ppm)
6000
4000
2000
0
f1 (ppm)

5.3b

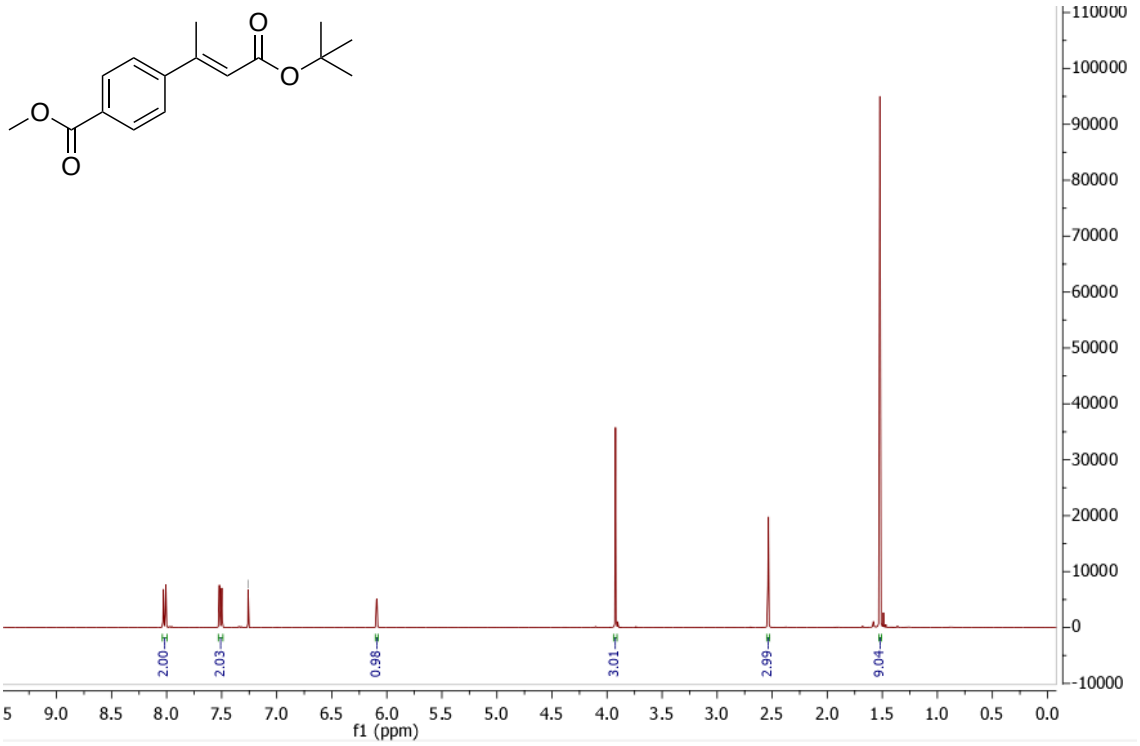

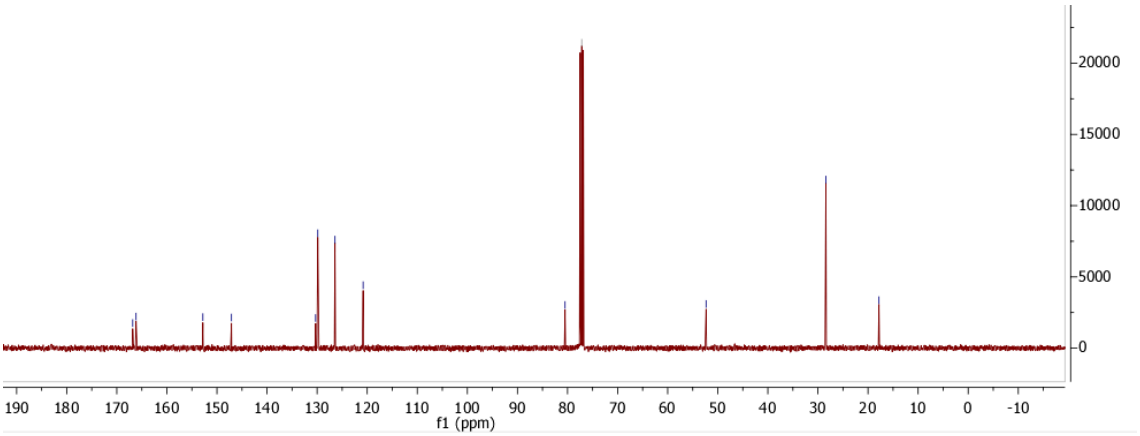

5.14

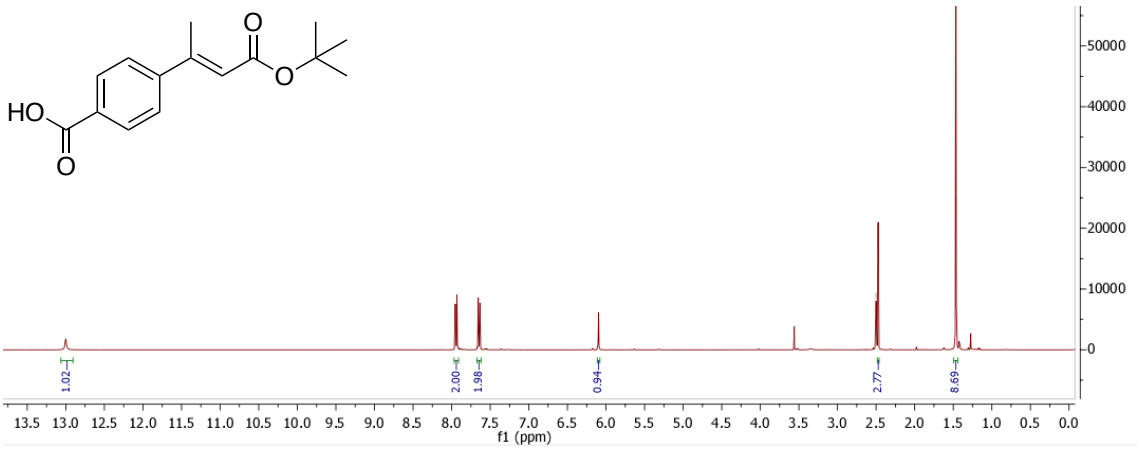
HO
O
O
O
50000
40000
30000
20000
10000
0
1.02
2.00
1.98
0.94
2.77
8.69
13.5 13.0 12.5 12.0 11.5 11.0 10.5 10.0 9.5 9.0 8.5 8.0 7.5 7.0 6.5 6.0 5.5 5.0 4.5 4.0 3.5 3.0 2.5 2.0 1.5 1.0 0.5 0.0
f1 (ppm)

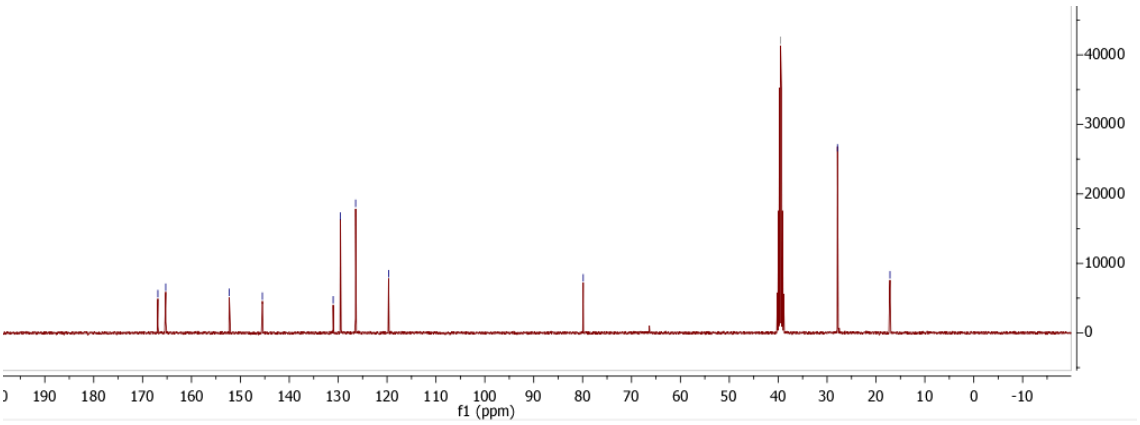
40000
30000
20000
10000
0
190 180 170 160 150 140 130 120 110 100 90 80 70 60 50 40 30 20 10 0 -10
f1 (ppm)

5.15

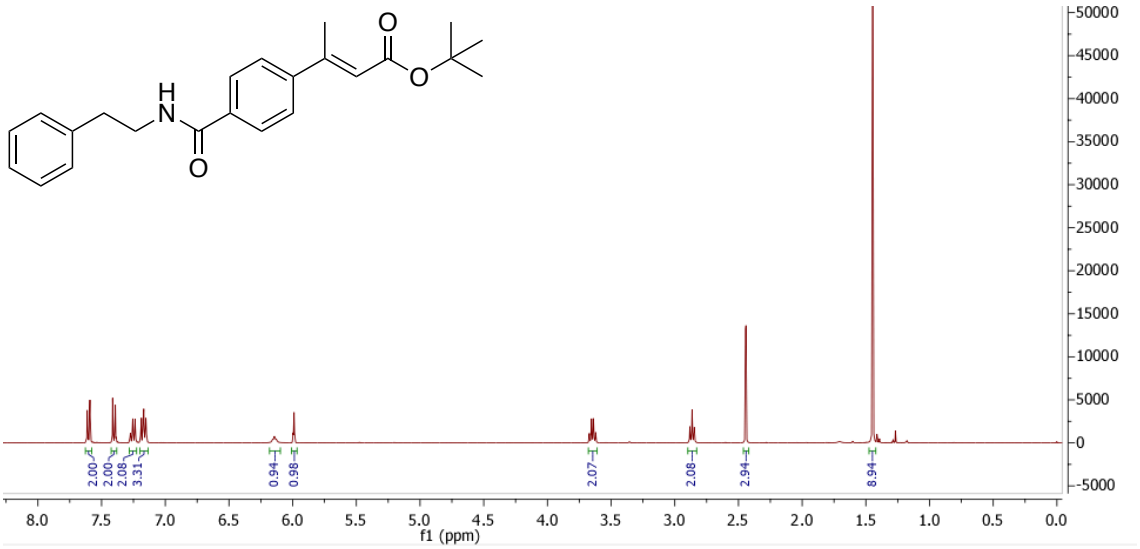
O
O
H
N
O
2.00
2.00
2.08
3.31
0.94
0.98
2.07
2.08
2.94
8.94
50000
45000
40000
35000
30000
25000
20000
15000
10000
5000
0
-5000
8.0
7.5
7.0
6.5
6.0
5.5
5.0
4.5
4.0
3.5
3.0
2.5
2.0
1.5
1.0
0.5
0.0
f1 (ppm)

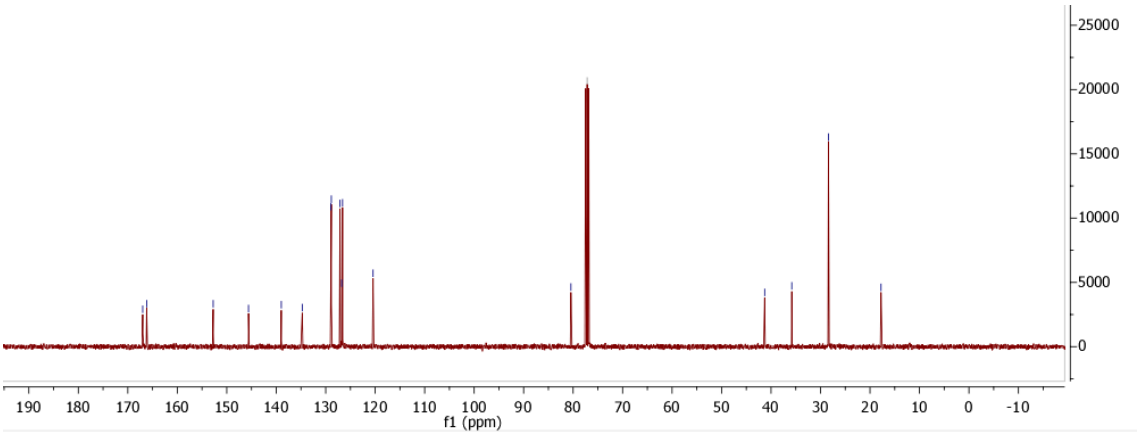
25000
20000
15000
10000
5000
0
190
180
170
160
150
140
130
120
110
100
90
80
70
60
50
40
30
20
10
0
-10
f1 (ppm)

5.16

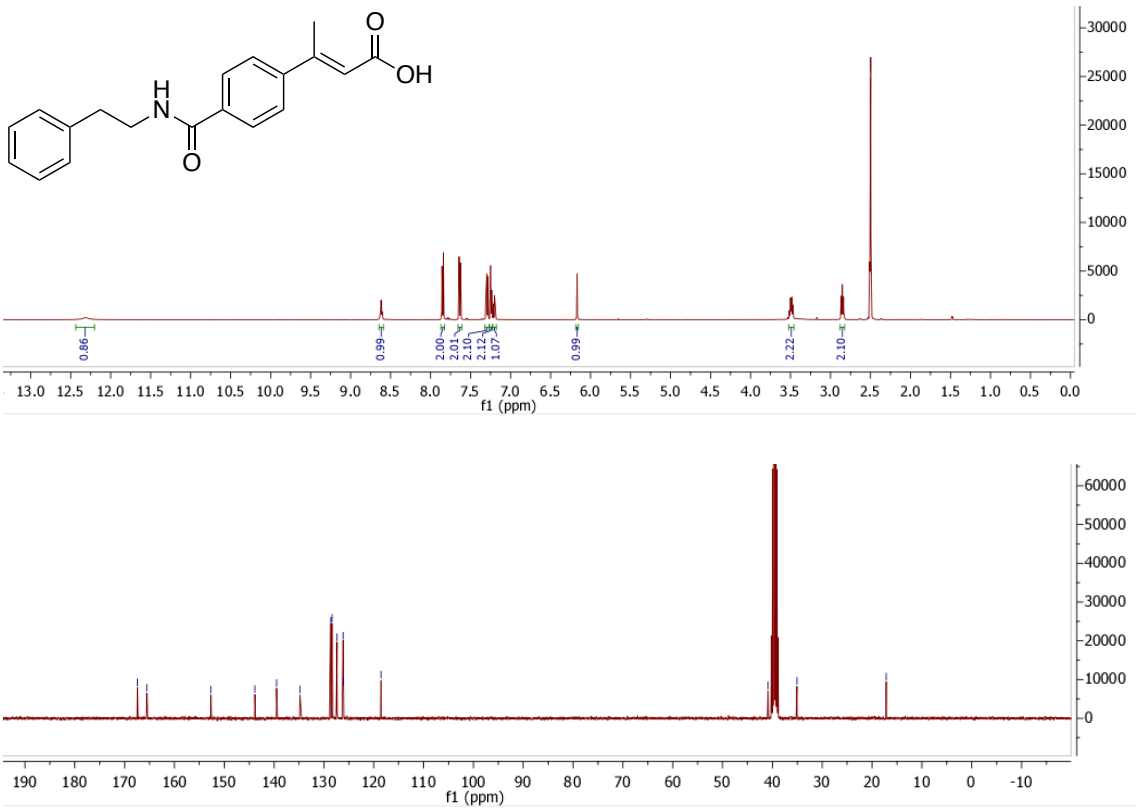

References

(1) Landman, O. E. Inheritance of Characteristics Revisited Acquired Heritable Changes in Traits ,. *Bioscience* **1993**, *43* (10), 696–705.

(2) Turner, B. M. Lamarck and the Nucleosome: Evolution and Environment across 200 Years. *Front. Life Sci.* **2013**, *7* (1–2), 2–11.

(3) Waddington, C. H. *An Introduction to Modern Genetics*; New York, The Macmillan Company, 1939.

(4) Waddington, C. H. Canalization of Development and the Inheritance of Acquired Characters. *Nature* **1942**, *150* (3811), 563–565.

(5) Waddington, C. H. The Strategy of the Genes. Allen and Unwin 1957, p 29.

(6) Nanney, D. L. Epigenetic Control Systems. *Proc. Natl. Acad. Sci. U. S. A.* **1958**, *44* (7), 712–717.

(7) Haig, D. Weismann Rules! OK? Epigenetics and the Lamarckian Temptation. *Biol. Philos.* **2007**, *22* (3), 415–428.

(8) Hunt, J.; Ingram, V. Allelomorphism and the Chemical Differences of the Human Haemoglobins A, S and C. *Nature* **1958**, *181* (4615), 1062–1063.

(9) D.N. Cooper, E.V. Ball, P.D. Stenson, A.D. Phillips, K. Evans, S. Heywood, M.J. Hayden, M. E. M. and M. H. The Human Gene Mutation Database http://www.hgmd.cf.ac.uk/ac/search.php.

(10) Kornberg, R. D.; Lorch, Y. Twenty-Five Years of the Nucleosome, Fundamental Particle of the Eukaryote Chromosome. *Cell* **1999**, *98* (3), 285–294.

(11) Goll, M. G.; Kirpekar, F.; Maggert, K. A.; Yoder, J. A.; Hsieh, C.-L.; Zhang, X.; Golic, K. G.; Jacobsen, S. E.; Bestor, T. H. Methylation of TRNAAsp by the DNA Methyltransferase Homolog Dnmt2. *Science* **2006**, *311* (5759), 395–398.

(12) Zangi, R.; Arrieta, A.; Cossío, F. P. Mechanism of DNA Methylation: The Double Role of DNA as a Substrate and as a Cofactor. *J. Mol. Biol.* **2010**, *400* (3), 632–644.

(13) Bird, A. P.; Wolffe, A. P. Methylation-Induced Repression— Belts, Braces, and Chromatin. *Cell* **1999**, *99* (5), 451–454.

(14) El-Maarri, O. DNA Methylation and Human Disease. *Nat. Rev. Genet.* **2003**, *544* (8), 135–144.

(15) Feinberg, A. P.; Tycko, B. The History of Cancer Epigenetics. *Nat. Rev. Cancer* **2004**, *4* (2), 143–153.

(16) Flanagan, J. F.; Mi, L.-Z.; Chruszcz, M.; Cymborowski, M.; Clines, K. L.; Kim, Y.; Minor, W.; Rastinejad, F.; Khorasanizadeh, S. Double Chromodomains Cooperate to Recognize the Methylated Histone H3 Tail. *Nature* **2005**, *438* (7071), 1181–1185.

(17) Nishioka, K.; Chuikov, S.; Sarma, K.; Erdjument-Bromage, H.; Allis, C. D.; Tempst, P.; Reinberg, D. Set9, a Novel Histone H3 Methyltransferase That Facilitates Transcription by Precluding Histone Tail Modifications Required for Heterochromatin Formation. *Genes Dev.* **2002**, *16* (4), 479–489.

(18) Shi, Y.; Lan, F.; Matson, C.; Mulligan, P.; Whetstine, J. R.; Cole, P. A.; Casero, R. A.; Shi, Y. Histone Demethylation Mediated by the Nuclear Amine Oxidase Homolog LSD1. *Cell* **2004**, *119* (7), 941–953.

(19) Tan, J. Z.; Yan, Y.; Wang, X. X.; Jiang, Y.; Xu, H. E. EZH2: Biology, Disease, and Structure-Based Drug Discovery. *Acta Pharmacol Sin* **2014**, *35* (2), 161–174.

(20) Cao, R.; Wang, L.; Wang, H.; Xia, L.; Erdjument-Bromage, H.; Tempst, P.; Jones, R. S.; Zhang, Y. Role of Histone H3 Lysine 27 Methylation in Polycomb-Group Silencing. *Science* **2002**, *298* (5595), 1039–1043.

(21) Ding, X.; Wang, X.; Sontag, S.; Qin, J.; Wanek, P.; Lin, Q.; Zenke, M. The Polycomb Protein Ezh2 Impacts on Induced Pluripotent Stem Cell Generation. *Stem Cells Dev.* **2014**, *00* (00), 19–24.

(22) Simon, J. A.; Lange, C. A. Roles of the EZH2 Histone Methyltransferase in Cancer Epigenetics. *Mutat. Res. - Fundam. Mol. Mech. Mutagen.* **2008**, *647* (1–2), 21–29.

(23) Kipp, D. R.; Quinn, C. M.; Fortin, P. D. Enzyme-Dependent Lysine Deprotonation in EZH2 Catalysis. *Biochemistry* **2013**, *52* (39), 6866–6878.

(24) Cloos, P. A. C.; Christensen, J.; Agger, K.; Helin, K. Erasing the Methyl

Mark: Histone Demethylases at the Center of Cellular Differentiation and Disease. *Genes Dev.* **2008**, *22* (9), 1115–1140.

(25) Speranzini, V.; Rotili, D.; Ciossani, G.; Pilotto, S.; Marrocco, B.; Forgione, M.; Lucidi, A.; Forneris, F.; Mehdipour, P.; Velankar, S.; et al. Polymyxins and Quinazolines Are LSD1/KDM1A Inhibitors with Unusual Structural Features. *Sci. Adv.* **2016**, *2* (9), e1601017.

(26) Yi-Chao Zheng, JinlianMa, ZhiruWang, Jinfeng Li, Bailing Jiang, Wenjuan Zhou, Xiaojing Shi, Xixin Wang,Wen Zhao, and H.-M. L. A Systematic Review of Histone Lysine-Specific Demethylase 1 and Its Inhibitors. *Med. Res. Rev.* **2015**, *35* (5), 1032–1071.

(27) Hou, H.; Yu, H. Structural Insights into Histone Lysine Demethylation. *Curr. Opin. Struct. Biol.* **2010**, *20* (6), 739–748.

(28) Hino, S.; Kohrogi, K.; Nakao, M. Histone Demethylase LSD1 Controls the Phenotypic Plasticity of Cancer Cells. *Cancer Sci.* **2016**, *107* (9), 1187–1192.

(29) Huang, J.; Sengupta, R.; Espejo, A. B.; Lee, M. G.; Dorsey, J. A.; Richter, M.; Opravil, S.; Shiekhattar, R.; Bedford, M. T.; Jenuwein, T.; et al. P53 Is Regulated by the Lysine Demethylase LSD1. *Nature* **2007**, *449* (7158), 105–108.

(30) Tsai, W.-W.; Nguyen, T. T.; Shi, Y.; Barton, M. C. P53-Targeted LSD1 Functions in Repression of Chromatin Structure and Transcription in Vivo. *Mol. Cell. Biol.* **2008**, *28* (17), 5139–5146.

(31) Nicholson, T. B.; Chen, T. LSD1 Demethylates Histone and Non-Histone Proteins. *Epigenetics* **2009**, *4* (3), 129–132.

(32) Wang, J.; Hevi, S.; Kurash, J. K.; Lei, H.; Gay, F.; Bajko, J.; Su, H.; Sun, W.; Chang, H.; Xu, G.; et al. The Lysine Demethylase LSD1 (KDM1) Is Required for Maintenance of Global DNA Methylation. *Nat. Genet.* **2009**, *41* (1), 125–129.

(33) Kontaki, H.; Talianidis, I. Lysine Methylation Regulates E2F1-Induced Cell Death. *Mol. Cell* **2010**, *39* (1), 152–160.

(34) Cho, H. S.; Suzuki, T.; Dohmae, N.; Hayami, S.; Unoki, M.; Yoshimatsu, M.; Toyokawa, G.; Takawa, M.; Chen, T.; Kurash, J. K.; et al.

Demethylation of RB Regulator MYPT1 by Histone Demethylase LSD1 Promotes Cell Cycle Progression in Cancer Cells. *Cancer Res.* **2011**, *71* (3), 655–660.

(35) Yang, J.; Huang, J.; Dasgupta, M.; Sears, N.; Miyagi, M.; Wang, B.; Chance, M. R.; Chen, X.; Du, Y.; Wang, Y.; et al. Reversible Methylation of Promoter-Bound STAT3 by Histone-Modifying Enzymes. *Proc. Natl. Acad. Sci. U. S. A.* **2010**, *107* (50), 21499–21504.

(36) Abu-Farha, M.; Lanouette, S.; Elisma, F.; Tremblay, V.; Butson, J.; Figeys, D.; Couture, J. F. Proteomic Analyses of the SMYD Family Interactomes Identify HSP90 as a Novel Target for SMYD2. *J. Mol. Cell Biol.* **2011**, *3* (5), 301–308.

(37) Sakane, N.; Kwon, H. S.; Pagans, S.; Kaehlcke, K.; Mizusawa, Y.; Kamada, M.; Lassen, K. G.; Chan, J.; Greene, W. C.; Schnoelzer, M.; et al. Activation of Hiv Transcription by the Viral Tat Protein Requires a Demethylation Step Mediated by Lysine-Specific Demethylase 1

(38) Nair, S. S.; Li, D. Q.; Kumar, R. A Core Chromatin Remodeling Factor Instructs Global Chromatin Signaling through Multivalent Reading of Nucleosome Codes. *Mol. Cell* **2013**, *49* (4), 704–718.

(39) Zhang, X.; Tanaka, K.; Yan, J.; Li, J.; Peng, D.; Jiang, Y.; Yang, Z.; Barton, M. C.; Wen, H.; Shi, X. Regulation of Estrogen Receptor α by Histone Methyltransferase SMYD2-Mediated Protein Methylation. *Proc. Natl. Acad. Sci. U. S. A.* **2013**, *110* (43), 17284–17289.

(40) Lee, A.; Borrello, M. T.; Ganesan, A. *LSD (Lysine-Specific Demethylase): A Decade-Long Trip from Discovery to Clinical Trials*; Sippl, W., Jung, M., Eds.; © 2019 Wiley-VCH Verlag GmbH & Co. KGaA, 2019.

(41) Kerenyi, M. A.; Shao, Z.; Hsu, Y.-J.; Guo, G.; Luc, S.; O'Brien, K.; Fujiwara, Y.; Peng, C.; Nguyen, M.; Orkin, S. H. Histone Demethylase Lsd1 Represses Hematopoietic Stem and Progenitor Cell Signatures during Blood Cell Maturation. *Elife* **2013**, *2*, e00633.

(42) Pollock, J. A.; Larrea, M. D.; Jasper, J. S.; McDonnell, D. P.; McCafferty, D. G. Lysine-Specific Histone Demethylase 1 Inhibitors Control Breast Cancer Proliferation in ER-Dependent and Independent Manners. *ACS*

Chem. Biol. **2012**, *7* (7), 1221–1231.

(43) Prusevich, P.; Kalin, J. H.; Ming, S. A.; Basso, M.; Givens, J.; Li, X.; Hu, J.; Taylor, M. S.; Cieniewicz, A. M.; Hsiao, P. Y.; et al. A Selective Phenelzine Analogue Inhibitor of Histone Demethylase LSD1. *ACS Chem. Biol.* **2014**, *9* (6), 1284–1293.

(44) Shih, J. C.; Chen, K.; Ridd, M. J. MONOAMINE OXIDASE: From Genes to Behavior. *Annu. Rev. Neurosci.* **1999**, *22* (1), 197–217.

(45) Ruthenburg, A. J.; Allis, C. D.; Wysocka, J. Methylation of Lysine 4 on Histone H3: Intricacy of Writing and Reading a Single Epigenetic Mark. *Mol. Cell* **2007**, *25* (1), 15–30.

(46) Binda, C.; Valente, S.; Romanenghi, M.; Pilotto, S.; Cirilli, R.; Karytinos, A.; Ciossani, G.; Botrugno, O. A.; Forneris, F.; Tardugno, M.; et al. Biochemical, Structural, and Biological Evaluation of Tranylcypromine Derivatives as Inhibitors of Histone Demethylases LSD1 and LSD2. *J. Am. Chem. Soc.* **2010**, *132* (19), 6827–6833.

(47) Kang, G. Il; Hong, S. K. Quantitative Structure-Activity Relationships in MAO-Inhibitory 2-Phenylcyclopropylamines: Insights into the Topography of MAO-A and MAO-B. *Arch. Pharm. Res.* **1990**, *13* (1), 82–96.

(48) Karytinos, A.; Forneris, F.; Profumo, A.; Ciossani, G.; Battaglioli, E.; Binda, C.; Mattevi, A. A Novel Mammalian Flavin-Dependent Histone Demethylase. *J. Biol. Chem.* **2009**, *284* (26), 17775–17782.

(49) Ueda, R.; Suzuki, T.; Mino, K.; Tsumoto, H.; Nakagawa, H.; Hasegawa, M.; Sasaki, R.; Mizukami, T.; Miyata, N. Identification of Cell-Active Lysine Specific Demethylase 1-Selective Inhibitors. *J. Am. Chem. Soc.* **2009**, *131* (48), 17536–17537.

(50) Schmidt, D. M. Z.; McCafferty, D. G. Trans-2-Phenylcyclopropylamine Is a Mechanism-Based Inactivator of the Histone Demethylase LSD1. *Biochemistry* **2007**, *46* (14), 4408–4416.

(51) Mohammad, H. P.; Smitheman, K. N.; Kamat, C. D.; Soong, D.; Federowicz, K. E.; VanAller, G. S.; Schneck, J. L.; Carson, J. D.; Liu, Y.; Butticello, M.; et al. A DNA Hypomethylation Signature Predicts

Antitumor Activity of LSD1 Inhibitors in SCLC. *Cancer Cell* **2015**, *28* (1), 57–69.

(52) Ulrich, S.; Ricken, R.; Adli, M. Tranylcypromine in Mind (Part I): Review of Pharmacology. *Eur. Neuropsychopharmacol.* **2017**, *27* (8), 697–713.

(53) Benelkebir, H.; Hodgkinson, C.; Duriez, P. J.; Hayden, A. L.; Bulleid, R. A.; Crabb, S. J.; Packham, G.; Ganesan, A. Enantioselective Synthesis of Tranylcypromine Analogues as Lysine Demethylase (LSD1) Inhibitors. *Bioorganic Med. Chem.* **2011**, *19* (12), 3709–3716.

(54) Ahmed Khan, M. N.; Tsumoto, H.; Itoh, Y.; Ota, Y.; Suzuki, M.; Ogasawara, D.; Nakagawa, H.; Mizukami, T.; Miyata, N.; Suzuki, T. Design, Synthesis, and Biological Activity of N-Alkylated Analogue of NCL1, a Selective Inhibitor of Lysine-Specific Demethylase 1. *Med. Chem. Commun.* **2015**, *6* (3), 407–412.

(55) Burg, J. M.; Link, J. E.; Morgan, B. S.; Heller, F. J.; Hargrove, A. E.; McCafferty, D. G. KDM1 Class Flavin-dependent Protein Lysine Demethylases. *Pept. Sci.* **2015**, *104* (4), 213–246.

(56) A., J.; J.N., A. Histone Lysine Demethylase Inhibitors. *Cold Spring Harb. Perspect. Med.* **2017**, *7* (1), 1–26.

(57) Vianello, P.; Botrugno, O. A.; Cappa, A.; Ciossani, G.; Dessanti, P.; Mai, A.; Mattevi, A.; Meroni, G.; Minucci, S.; Thaler, F.; et al. Synthesis, Biological Activity and Mechanistic Insights of 1-Substituted Cyclopropylamine Derivatives: A Novel Class of Irreversible Inhibitors of Histone Demethylase KDM1A. *Eur. J. Med. Chem.* **2014**, *86*, 352–363.

(58) Borrello, M. T.; Schinor, B.; Bartels, K.; Benelkebir, H.; Pereira, S.; Al-Jamal, W. T.; Douglas, L.; Duriez, P. J.; Packham, G.; Haufe, G.; et al. Fluorinated Tranylcypromine Analogues as Inhibitors of Lysine-Specific Demethylase 1 (LSD1, KDM1A). *Bioorganic Med. Chem. Lett.* **2017**, *27* (10), 2099–2101.

(59) Shi, Y.; Wu, Y. R.; Su, M. B.; Shen, D. H.; Gunosewoyo, H.; Yang, F.; Li, J.; Tang, J.; Zhou, Y. B.; Yu, L. F. Novel Spirocyclic Tranylcypromine Derivatives as Lysine-Specific Demethylase 1 (LSD1) Inhibitors. *RSC Adv.* **2018**, *8* (3), 1666–1676.

(60) Schenk, T.; Stengel, S.; Zelent, A. Unlocking the Potential of Retinoic Acid in Anticancer Therapy. *Br. J. Cancer* **2014**, *111* (11), 2039–2045.

(61) Altucci, L.; Gronemeyer, H. The Promise of Retinoids to Fight against Cancer. *Nat. Rev. Cancer* **2001**, *1* (3), 181–193.

(62) Yang, G. J.; Lei, P. M.; Wong, S. Y.; Ma, D. L.; Leung, C. H. Pharmacological Inhibition of LSD1 for Cancer Treatment. *Molecules* **2018**, *23* (12), 1–20.

(63) Maes, T.; Mascaró, C.; Tirapu, I.; Estiarte, A.; Ciceri, F.; Lunardi, S.; Guibourt, N.; Perdones, A.; Lufino, M. M. P.; Somervaille, T. C. P.; et al. ORY-1001, a Potent and Selective Covalent KDM1A Inhibitor, for the Treatment of Acute Leukemia. *Cancer Cell* **2018**, *33* (3), 495-511.e12.

(64) Fang, Y.; Liao, G.; Yu, B. LSD1/KDM1A Inhibitors in Clinical Trials: Advances and Prospects. *J. Hematol. Oncol.* **2019**, *12* (1), 129.

(65) Maes, T.; Mascaró, C.; Rotllant, D.; Cavalcanti, F.; Carceller, E.; Ortega, A.; Molinero, C.; Buesa, C. Ory-2001: An Epigenetic Drug for the Treatment of Cognition Defects in Alzheimer'S Disease and Other Neurodegenerative Disorders. *Alzheimer's Dement.* **2016**, *12* (7), P1192.

(66) Maes, T.; Mascaró, C.; Ortega, A.; Lunardi, S.; Ciceri, F.; P Somervaille, T. C.; Buesa, C. KDM1 Histone Lysine Demethylases as Targets for Treatments of Oncological and Neurodegenerative Disease. *Epigenomics* **2015**, *7* (4), 609–626.

(67) Lee, S. H.; Liu, X. M.; Diamond, M.; Dostalik, V.; Favata, M.; He, C.; Wu, L.; Wynn, R.; Yao, W.; Hollis, G.; et al. Abstract 4704: The Evaluation of INCB059872, an FAD-Directed Inhibitor of LSD1, in Preclinical Models of Human Small Cell Lung Cancer. *Cancer Res.* **2016**, *76* (14 Supplement), 4704 LP – 4704.

(68) MATSUMOTO, S.; HATTORI, Y.; TOYOFUKU, M.; DAINI, M.; KOJIMA, T.; KAKU, T.; ITO, M. Cyclopropylamine Compound and Use Thereof. World Patent WO 2015/156417. W O 2015/156417 A l, 2015.

(69) Allfrey, G.; Faulkner, R.; Mirsky, A. E. Possible Role in the Regulation of Rna Synthesis *. *Biochemistry* **1964**, *315* (1938), 786–794.

(70) Gallwitz, D.; Sekeris, C. E. The Acetylation of Histones of Rat Liver Nuclei

in Vitro by Acetyl-CoA. *Hoppe. Seylers. Z. Physiol. Chem.* **1969**, *350* (1), 150–154.

(71) Inoue, A.; Fujimoto, D. Enzymatic Deacetylation of Histone. *Biochem. Biophys. Res. Commun.* **1969**, *36* (1), 146–150.

(72) Leipe, D. D.; Landsman, D. Histone Deacetylases, Acetoin Utilization Proteins and Acetylpolyamine Amidohydrolases Are Members of an Ancient Protein Superfamily. *Nucleic Acids Res.* **1997**, *25* (18), 3693–3697.

(73) Durrington, P. N. What Every Doctor Wants to Know about Cholesterol: Answers to Some Difficult Questions. *Postgrad. Med. J.* **1992**, *68* (805), 867–883.

(74) Suraweera, A.; O'Byrne, K. J.; Richard, D. J. Combination Therapy with Histone Deacetylase Inhibitors (HDACi) for the Treatment of Cancer: Achieving the Full Therapeutic Potential of HDACi. *Front. Oncol.* **2018**, *8* (MAR), 1–15.

(75) Finnin, M. S.; Donigian, J. R.; Cohen, A.; Richon, V. M.; Rifkind, R. A.; Marks, P. A.; Breslow, R.; Pavletich, N. P. Structures of TSA and SAHA. *Nature* **1999**, *401* (SEPTEMBER), 188–193.

(76) Vanommeslaeghe, K.; De Proft, F.; Loverix, S.; Tourwé, D.; Geerlings, P. Theoretical Study Revealing the Functioning of a Novel Combination of Catalytic Motifs in Histone Deacetylase. *Bioorganic Med. Chem.* **2005**, *13* (12), 3987–3992.

(77) Corminboeuf, C.; Hu, P.; Tuckerman, M. E.; Zhang, Y. Unexpected Deacetylation Mechanism Suggested by a Density Functional Theory QM/MM Study of Histone-Deacetylase-like Protein. *J. Am. Chem. Soc.* **2006**, *128* (14), 4530–4531.

(78) Bertrand, P. Inside HDAC with HDAC Inhibitors. *Eur. J. Med. Chem.* **2010**, *45* (6), 2095–2116.

(79) Roche, J.; Bertrand, P. Inside HDACs with More Selective HDAC Inhibitors. *Eur. J. Med. Chem.* **2016**, *121*, 451–483.

(80) Chen, K.; Zhang, X.; Wu, Y. D.; Wiest, O. Inhibition and Mechanism of HDAC8 Revisited. *J. Am. Chem. Soc.* **2014**, *136* (33), 11636–11643.

(81) Gantt, S. M. L.; Decroos, C.; Lee, M. S.; Gullett, L. E.; Bowman, C. M.; Christianson, D. W.; Fierke, C. A. General Base-General Acid Catalysis in Human Histone Deacetylase 8. *Biochemistry* **2016**, *55* (5), 820–832.

(82) Benedetti, R.; Conte, M.; Altucci, L. Targeting Histone Deacetylases in Diseases: Where Are We? *Antioxidants Redox Signal.* **2015**, *23* (1), 99–126.

(83) Haggarty, S. J.; Koeller, K. M.; Wong, J. C.; Grozinger, C. M.; Schreiber, S. L. Domain-Selective Small-Molecule Inhibitor of Histone Deacetylase 6 (HDAC6)-Mediated Tubulin Deacetylation. *Proc. Natl. Acad. Sci. U. S. A.* **2003**, *100* (8), 4389–4394.

(84) Wagner, F. F.; Weyiwer, M.; Lewis, M. C.; Holson, E. B. Small Molecule Inhibitors of Zinc-Dependent Histone Deacetylases. *Neurotherapeutics* **2013**, *10* (4), 589–604.

(85) Santo, L.; Hideshima, T.; Kung, A. L.; Tseng, J. C.; Tamang, D.; Yang, M.; Jarpe, M.; Van Duzer, J. H.; Mazitschek, R.; Ogier, W. C.; et al. Preclinical Activity, Pharmacodynamic, and Pharmacokinetic Properties of a Selective HDAC6 Inhibitor, ACY-1215, in Combination with Bortezomib in Multiple Myeloma. *Blood* **2012**, *119* (11), 2579–2589.

(86) Balasubramanian, S.; Ramos, J.; Luo, W.; Sirisawad, M.; Verner, E.; Buggy, J. J. A Novel Histone Deacetylase 8 (HDAC8)-Specific Inhibitor PCI-34051 Induces Apoptosis in T-Cell Lymphomas. *Leukemia* **2008**, *22* (5), 1026–1034.

(87) Atadja, P.; Perez, L. Discovery and Development of Farydak (NVPLBH589, Panobinostat) as an Anticancer Drug. In *Successful Drug Discovery*; Fischer, J., Childers, W. E., Eds.; Wiley-VCH, 2016; pp 59–88.

(88) Ganesan, A. *Macrocyclic Inhibitors of Zinc-Dependent Histone Deacetylases (HDACs)*; Levin, J., Ed.; 2015.

(89) Ning, Z. Q.; Li, Z. Bin; Newman, M. J.; Shan, S.; Wang, X. H.; Pan, D. S.; Zhang, J.; Dong, M.; Du, X.; Lu, X. P. Chidamide (CS055/HBI-8000): A New Histone Deacetylase Inhibitor of the Benzamide Class with Antitumor Activity and the Ability to Enhance Immune Cell-Mediated Tumor Cell Cytotoxicity. *Cancer Chemother. Pharmacol.* **2012**, *69* (4),

901–909.

(90) Gurvich, N.; Tsygankova, O. M.; Meinkoth, J. L.; Klein, P. S. Histone Deacetylase Is a Target of Valproic Acid-Mediated Cellular Differentiation. *Cancer Res.* **2004**, *64* (3), 1079–1086.

(91) Suzuki, T.; Kouketsu, A.; Matsuura, A.; Kohara, A.; Ninomiya, S. I.; Kohda, K.; Miyata, N. Thiol-Based SAHA Analogues as Potent Histone Deacetylase Inhibitors. *Bioorganic Med. Chem. Lett.* **2004**, *14* (12), 3313–3317.

(92) Wen, J.; Bao, Y.; Niu, Q.; Yang, J.; Fan, Y.; Li, J.; Jing, Y.; Zhao, L.; Liu, D. Identification of N-(6-Mercaptohexyl)-3-(4-Pyridyl)-1 H-Pyrazole-5-Carboxamide and Its Disulfide Prodrug as Potent Histone Deacetylase Inhibitors with in Vitro and in Vivo Anti-Tumor Efficacy. *Eur. J. Med. Chem.* **2016**, *109*, 350–359.

(93) Xu, Q.; Yu, S.; Cai, Y.; Yang, J.; Zhao, L.; Liu, D. Design, Synthesis and Biological Evaluation of Novel Selective Thiol-Based Histone Deacetylase(HDAC) VI Inhibitors Bearing Indeno[1,2-c]Pyrazole or Benzoindazole Scaffold. *Chem. Res. Chinese Univ.* **2018**, *34* (1), 75–83.

(94) Ueda, H.; Nakajima, H.; Hori, Y.; Fujita, T.; Nishimura, M.; Goto, T.; Okuhara, M. FR901228, A Novel Antitumor Bicyclic Depsipeptide Produced by Chromobacterium Violaceum No. 968. *J. Antibiot. (Tokyo).* **1994**, *47* (3), 301–310.

(95) Nakajima, H.; Kim, Y. B.; Terano, H.; Yoshida, M.; Horinouchi, S. FR901228, a Potent Antitumor Antibiotic, Is a Novel Histone Deacetylase Inhibitor. *Exp. Cell Res.* **1998**, *241* (1), 126–133.

(96) Cole, K. E.; Dowling, D. P.; Boone, M. A.; Phillips, A. J.; Christianson, D. W. Structural Basis of the Antiproliferative Activity of Largazole, a Depsipeptide Inhibitor of the Histone Deacetylases. *J. Am. Chem. Soc.* **2011**, *133* (32), 12474–12477.

(97) Bowers, A. A.; West, N.; Newkirk, T. L.; Troutman-Youngman, A. E.; Schreiber, S. L.; Wiest, O.; Bradner, J. E.; Williams, R. M. Synthesis and Histone Deacetylase Inhibitory Activity of Largazole Analogs: Alteration of the Zinc-Binding Domain and Macrocyclic Scaffold. *Org. Lett.* **2009**, *11*

(6), 1301–1304.

(98) Poli, G.; Di Fabio, R.; Ferrante, L.; Summa, V.; Botta, M. Largazole Analogues as Histone Deacetylase Inhibitors and Anticancer Agents: An Overview of Structure–Activity Relationships. *ChemMedChem* **2017**, *12* (23), 1917–1926.

(99) Kim, S. W.; Hooker, J. M.; Otto, N.; Win, K.; Muench, L.; Shea, C.; Carter, P.; King, P.; Reid, A. E.; Volkow, N. D.; et al. Whole-Body Pharmacokinetics of HDAC Inhibitor Drugs, Butyric Acid, Valproic Acid and 4-Phenylbutyric Acid Measured with Carbon-11 Labeled Analogs by PET. *Nucl. Med. Biol.* **2013**, *40* (7), 912–918.

(100) Bora-Tatar, G.; Dayangaç-Erden, D.; Demir, A. S.; Dalkara, S.; Yelekçi, K.; Erdem-Yurter, H. Molecular Modifications on Carboxylic Acid Derivatives as Potent Histone Deacetylase Inhibitors: Activity and Docking Studies. *Bioorganic Med. Chem.* **2009**, *17* (14), 5219–5228.

(101) Chen, Y.; Yang, Y.; Wang, F.; Wan, K.; Yamane, K.; Zhang, Y.; Lei, M. Crystal Structure of Human Histone Lysine-Specific Demethylase 1 (LSD1). *Proc. Natl. Acad. Sci. U. S. A.* **2006**, *103* (38), 13956–13961.

(102) Johnson, N. W.; Kasparec, J.; Miller, W. H.; Rouse, M. B.; Suarez, D.; Tian, X. Cyclopropylamines as LSD1 Inhinbitors. World Patent WO 2012/135113, 2012.

(103) Bhattacharyya, S. Titanium(IV) Isopropoxide and Sodium Borohydride : A Reagent of Choice for Reductive Amination. *Tetrahedron Lett.* **1994**, *35* (15), 2401–2404.

(104) Valeur, E.; Bradley, M. Amide Bond Formation: Beyond the Myth of Coupling Reagents. *Chem. Soc. Rev.* **2009**, *38* (2), 606–631.

(105) Molina, D. M.; Jafari, R.; Ignatushchenko, M.; Seki, T.; Larsson, E. A.; Dan, C.; Sreekumar, L.; Cao, Y.; Nordlund, P. Monitoring Drug Target Engagement in Cells and Tissues Using the Cellular Thermal Shift Assay. *Science (80-.).* **2013**, *341* (6141), 84–87.

(106) Nakamura, T.; Mori, T.; Tada, S.; Krajewski, W.; Rozovskaia, T.; Wassell, R.; Dubois, G.; Mazo, A.; Croce, C. M.; Canaani, E. ALL-1 Is a Histone Methyltransferase That Assembles a Supercomplex of Proteins Involved

in Transcriptional Regulation. *Mol. Cell* **2002**, *10* (5), 1119–1128.

(107) Biswas, D.; Milne, T. A.; Basrur, V.; Kim, J.; Elenitoba-Johnson, K. S. J.; Allis, C. D.; Roeder, R. G. Function of Leukemogenic Mixed Lineage Leukemia 1 (MLL) Fusion Proteins through Distinct Partner Protein Complexes. *Proc. Natl. Acad. Sci. U. S. A.* **2011**, *108* (38), 15751–15756.

(108) Harris, W. J.; Huang, X.; Lynch, J. T.; Spencer, G. J.; Hitchin, J. R.; Li, Y.; Ciceri, F.; Blaser, J. G.; Greystoke, B. F.; Jordan, A. M.; et al. The Histone Demethylase KDM1A Sustains the Oncogenic Potential of MLL-AF9 Leukemia Stem Cells. *Cancer Cell* **2012**, *21* (4), 473–487.

(109) Lynch, J. T.; Cockerill, M. J.; Hitchin, J. R.; Wiseman, D. H.; Somervaille, T. C. P. CD86 Expression as a Surrogate Cellular Biomarker for Pharmacological Inhibition of the Histone Demethylase Lysine-Specific Demethylase. *Anal. Biochem.* **2013**, *442* (1), 104–106.

(110) Fang, J.; Ying, H.; Mao, T.; Fang, Y.; Lu, Y.; Wang, H.; Zang, I.; Wang, Z.; Lin, Y.; Zhao, M.; et al. Upregulation of CD11b and CD86 through LSD1 Inhibition Promotes Myeloid Differentiation and Suppresses Cell Proliferation in Human Monocytic Leukemia Cells. *Oncotarget* **2017**, *8* (49), 85085–85101. https://doi.org/10.18632/oncotarget.18564.

(111) Mokhtari, R. B.; Homayouni, T. S.; Baluch, N.; Morgatskaya, E.; Kumar, S.; Das, B.; Yeger, H. Combination Therapy in Combating Cancer. *Oncotarget* **2017**, *8* (23), 38022–38043.

(112) Sugahara, K. N.; Teesalu, T.; Prakash Karmali, P.; Ramana Kotamraju, V.; Agemy, L.; Greenwald, D. R.; Ruoslahti, E. Coadministration of a Tumor-Penetrating Peptide Enhances the Efficacy of Cancer Drugs. *Science (80-.).* **2010**, *328* (5981), 1031–1035.

(113) Blagosklonny, M. V. Overcoming Limitations of Natural Anticancer Drugs by Combining with Artificial Agents. *Trends Pharmacol. Sci.* **2005**, *26* (2), 77–81.

(114) Baselga, J. Current and Planned Clinical Trials with Trastuzumab (Herceptin). *Semin. Oncol.* **2000**, *27*, 27–32.

(115) Kerr, J. F. R.; Wyllie, A. H.; Currie, A. R. Apoptosis: A Basic Biological Phenomenon with Wide-Ranging Implications in Human Disease. *Br. J.*

Cancer **1972**, *26*, 239–257.

(116) Green, D. R. Apoptotic Pathways. *Cell* **1998**, *94* (6), 695–698.

(117) Schutte, B.; Nuydens, R.; Geerts, H.; Ramaekers, F. Annexin V Binding Assay as a Tool to Measure Apoptosis in Differentiated Neuronal Cells. *J. Neurosci. Methods* **1998**, *86* (1), 63–69.

(118) Hanahan, D.; Weinberg, R. A. Hallmarks of Cancer: The next Generation. *Cell* **2011**, *144* (5), 646–674.

(119) Aubel-Sadron, G.; Londos-Gagliardi, D. Daunorubicin and Doxorubicin, Anthracycline Antibiotics, a Physicochemical and Biological Review. *Biochimie* **1984**, *66* (5), 333–352.

(120) Arcamone, F.; Franoeschi, G.; Pence, S.; Farmitalia, I. R.; Selva, A. Adriamycin, A Novel Antitumor Antibiotic. *Tetrahedron Lett.* **1969**, *13* (13), 1007–1010.

(121) Wang, J. C. Cellular Roles of DNA Topoisomerases: A Molecular Perspective. *Nat. Rev. Mol. Cell Biol.* **2002**, *3* (6), 430–440.

(122) Marinello, J.; Delcuratolo, M.; Capranico, G. Anthracyclines as Topoisomerase II Poisons: From Early Studies to New Perspectives. *Int. J. Mol. Sci.* **2018**, *19* (11).

(123) Kinner, A.; Wu, W.; Staudt, C.; Iliakis, G. Gamma-H2AX in Recognition and Signaling of DNA Double-Strand Breaks in the Context of Chromatin. *Nucleic Acids Res.* **2008**, *36* (17), 5678–5694.

(124) Podhorecka, M.; Skladanowski, A.; Bozko, P. H2AX Phosphorylation: Its Role in DNA Damage Response and Cancer Therapy. *J. Nucleic Acids* **2010**, *2010*.

(125) Schaupp, C. M.; White, C. C.; Merril, G. F.; Kavanagh, T. J. Metabolism of Doxorubicin to the Cardiotoxic Metabolite Doxorubicinol Is Increased in a Mouse Model of Chronic Glutathione Deficiency: A Potential Role for Carbonyl Reductase 3. *Chem Biol Interact* **2015**, *234*, 154–161.

(126) Salvatorelli, E.; Guarnieri, S.; Menna, P.; Liberi, G.; Calafiore, A. M.; Mariggio, M. A.; Mordente, A.; Gianni, L.; Minotti, G. Defective One- or Two-Electron Reduction of the Anticancer Anthracycline Epirubicin in Human Heart: Relative Importance of Vesicular Sequestration and

Impaired Efficiency of Electron Addition. *J. Biol. Chem.* **2006**, *281* (16), 10990–11001.

(127) Forneris, F.; Binda, C.; Adamo, A.; Battaglioli, E.; Mattevi, A. Structural Basis of LSD1-CoREST Selectivity in Histone H3 Recognition. *J. Biol. Chem.* **2007**, *282* (28), 20070–20074.

(128) Albrecht, B. K.; Audia, J. E.; Duplessis, M.; Gehling, V. S.; Good, A. C.; Harmange, J.-C.; Leblanc, Y.; Nasveschuk, C. G.; Taylor, A. M.; Vaswani, R. G. Therapeutic Compound and Uses Thereof. World Patent - WO2016/123387., 2016.

(129) Burger, A.; Yost, W. L. Arylcycloalkylamines. I. 2-Phenylcyclopropylamine. *J. Am. Chem. Soc.* **1948**, *70* (6), 2198–2201.

(130) Li, Y. H.; Wang, P. P.; Li, X. X.; Yu, C. Y.; Yang, H.; Zhou, J.; Xue, W. W.; Tan, J.; Zhu, F. The Human Kinome Targeted by FDA Approved Multi-Target Drugs and Combination Products: A Comparative Study from the Drug-Target Interaction Network Perspective. *PLoS One* **2016**, *11* (11), 1–15.

(131) Shi, Y. J.; Matson, C.; Lan, F.; Iwase, S.; Baba, T.; Shi, Y. Regulation of LSD1 Histone Demethylase Activity by Its Associated Factors. *Mol. Cell* **2005**, *19* (6), 857–864.

(132) Wang, Y.; Zhang, H.; Chen, Y.; Sun, Y.; Yang, F.; Yu, W.; Liang, J.; Sun, L.; Yang, X.; Shi, L.; et al. LSD1 Is a Subunit of the NuRD Complex and Targets the Metastasis Programs in Breast Cancer. *Cell* **2009**, *138* (4), 660–672.

(133) Nalawansha, D. A.; Pflum, M. K. H. LSD1 Substrate Binding and Gene Expression Are Affected by HDAC1-Mediated Deacetylation. *ACS Chem. Biol.* **2017**, *12* (1), 254–264.

(134) Lee, M. G.; Wynder, C.; Bochar, D. A.; Hakimi, M.-A.; Cooch, N.; Shiekhattar, R. Functional Interplay between Histone Demethylase and Deacetylase Enzymes. *Mol. Cell. Biol.* **2006**, *26* (17), 6395–6402.

(135) Huang, P. H.; Chen, C. H.; Chou, C. C.; Sargeant, A. M.; Kulp, S. K.; Teng, C. M.; Byrd, J. C.; Chen, C. S. Histone Deacetylase Inhibitors Stimulate Histone H3 Lysine 4 Methylation in Part via Transcriptional

Repression of Histone H3 Lysine 4 Demethylases. *Mol. Pharmacol.* **2011**, *79* (1), 197–206.

(136) Singh, M. M.; Manton, C. A.; Bhat, K. P.; Tsai, W. W.; Aldape, K.; Barton, M. C.; Chandra, J. Inhibition of LSD1 Sensitizes Glioblastoma Cells to Histone Deacetylase Inhibitors. *Neuro. Oncol.* **2011**, *13* (8), 894–903.

(137) Duan, Y. C.; Ma, Y. C.; Qin, W. P.; Ding, L. N.; Zheng, Y. C.; Zhu, Y. L.; Zhai, X. Y.; Yang, J.; Ma, C. Y.; Guan, Y. Y. Design and Synthesis of Tranylcypromine Derivatives as Novel LSD1/HDACs Dual Inhibitors for Cancer Treatment. *Eur. J. Med. Chem.* **2017**, *140*, 392–402.

(138) Kalin, J. H.; Wu, M.; Gomez, A. V.; Song, Y.; Das, J.; Hayward, D.; Adejola, N.; Wu, M.; Panova, I.; Chung, H. J.; et al. Targeting the CoREST Complex with Dual Histone Deacetylase and Demethylase Inhibitors. *Nat. Commun.* **2018**, *9* (1).

(139) Amitai, G.; Gez, R.; Raveh, L.; Bar-Ner, N.; Grauer, E.; Chapman, S. Novel Bifunctional Hybrid Small Molecule Scavengers for Mitigating Nerve Agents Toxicity. *Chem. Biol. Interact.* **2016**, *259*, 187–204.

(140) Rajagopal, S.; Hallur, M. S.; Dewang, P.; Murugan, K.; Kumar, C. H.; Iyer, P.; Mulakala, C.; Sivanandhan, D.; Nair, S.; Zainuddin, M.; et al. Cyclopropyl-Amide Compounds as Dual LSD1/HDAC Inhibitors. World Patent. WO 2017/195216 A1., 2017.

(141) Baldwin, E. L.; Osheroff, N. Etoposide, Topoisomerase II and Cancer. *Curr. Med. Chem. - Anti-Cancer Agents* **2005**, *5* (4), 363–372.

(142) Porter, N. J.; Mahendran, A.; Breslow, R.; Christianson, D. W. Unusual Zinc-Binding Mode of HDAC6-Selective Hydroxamate Inhibitors. *Proc. Natl. Acad. Sci. U. S. A.* **2017**, *114* (51), 13459–13464.

(143) Hambidge, M. Zinc and Health: Current Status and Future Directions. *J. Nutr.* **2000**, *130*, 1344S-1349S.

(144) Shen, S.; Kozikowski, A. P. Why Hydroxamates May Not Be the Best Histone Deacetylase Inhibitors - What Some May Have Forgotten or Would Rather Forget? *ChemMedChem* **2016**, *11* (1), 15–21.

(145) Mattson, R. H.; Cramer, J. A.; Williamson, P. D.; Novelly, R. A. Valproic Acid in Epilepsy: Clinical and Pharmacological Effects. *Ann. Neurol.*

1978, *3* (1), 20–25.

(146) Borycka-Kiciak, K.; Banasiewicz, T.; Rydzewska, G. Butyric Acid-a Well-Known Molecule Revisited. *Prz. Gastroenterol.* **2017**, *12* (2), 83–89.

(147) Brusilow, S. W. Phenylacetylglutamine May Replace Urea as a Vehicle for Waste Nitrogen Excretion. *Pediatr. Res.* **1991**, *29* (2), 147–150.

(148) Iannitti, T.; Palmieri, B. Clinical and Experimental Applications of Sodium Phenylbutyrate. *Drugs R D* **2011**, *11* (3), 227–249.

(149) Göttlicher, M.; Minucci, S.; Zhu, P.; Krämer, O. H.; Schimpf, A.; Giavara, S.; Sleeman, J. P.; Lo Coco, F.; Nervi, C.; Pelicci, P. G.; et al. Valproic Acid Defines a Novel Class of HDAC Inhibitors Inducing Differentiation of Transformed Cells. *EMBO J.* **2001**, *20* (24), 6969–6978.

(150) Candido, E. P. M.; Reeves, R.; Davie, J. R. Sodium Butyrate Inhibits Histone Deacetylation in Cultured Cells. *Cell* **1978**, *14* (1), 105–113.

(151) Borrello, M. T. PhD Thesis, University of East Anglia, 2016.

(152) Barluenga, J.; Quiñones, N.; Tomás-Gamasa, M.; Cabal, M. P. Intermolecular Metal-Free Cyclopropanation of Alkenes Using Tosylhydrazones. *European J. Org. Chem.* **2012**, No. 12, 2312–2317.

(153) Aggarwal, V. K.; Richardson, J. The Complexity of Catalysis: Origins of Enantio- and Diastereocontrol in Sulfur Ylide Mediated Epoxidation Reactions. *Chem. Commun.* **2003**, *44* (21), 2644–2651.